Oxidative Medicine and Cellular Longevity

MicroRNA Regulation of Oxidative Stress

Lead Guest Editor: Jaideep Banerjee
Guest Editors: Savita Khanna and Akash Bhattacharya

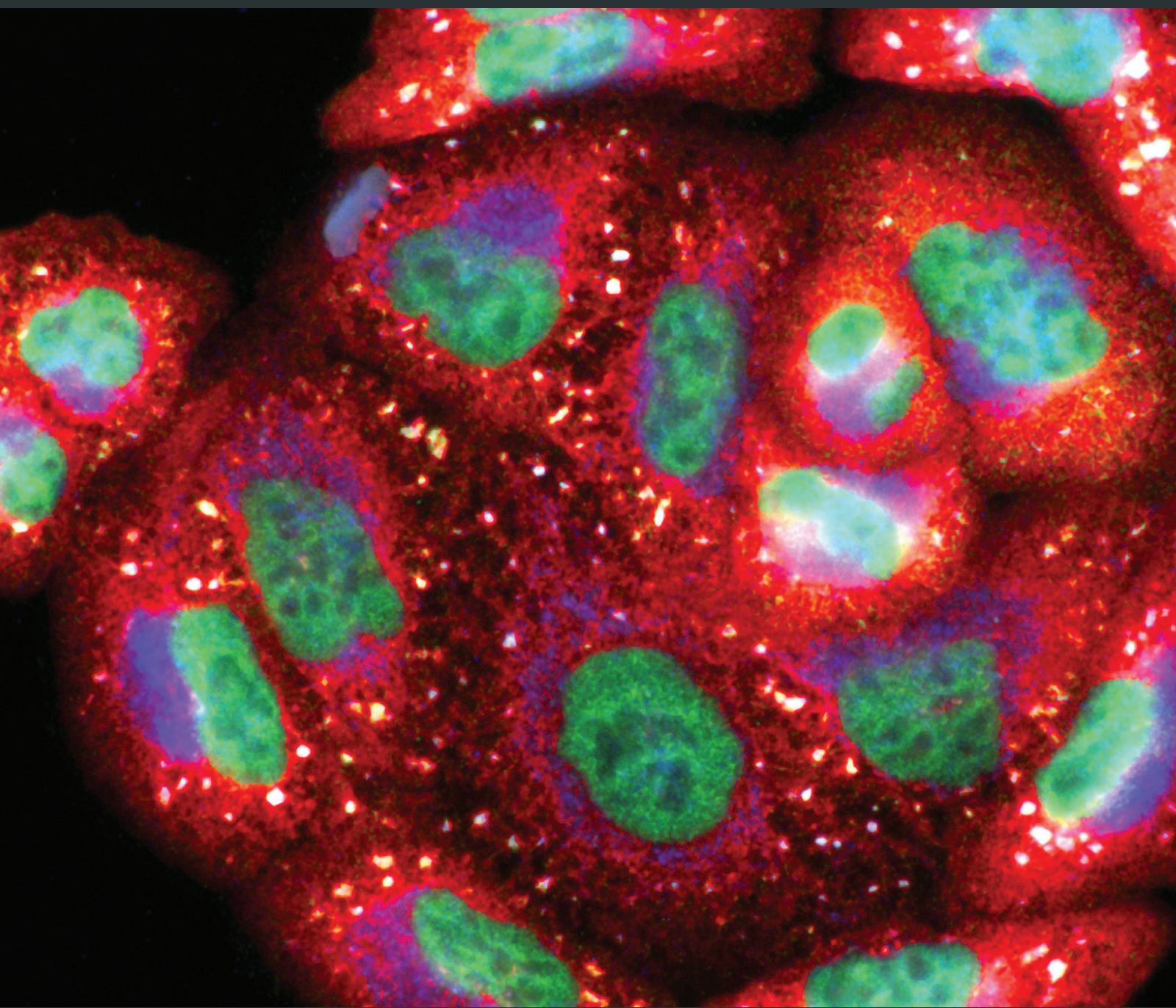

MicroRNA Regulation of Oxidative Stress

Oxidative Medicine and Cellular Longevity

MicroRNA Regulation of Oxidative Stress

Lead Guest Editor: Jaideep Banerjee
Guest Editors: Savita Khanna and Akash Bhattacharya

Editorial Board

Contents

Hindawi
Oxidative Medicine and Cellular Longevity
Volume 2017, Article ID 2872156, 3 pages
https://doi.org/10.1155/2017/2872156

Editorial

MicroRNA Regulation of Oxidative Stress

Jaideep Banerjee,[1] Savita Khanna,[2] and Akash Bhattacharya[3]

[1]*George Washington University, Washington, DC, USA*
[2]*The Ohio State University, Columbus, OH, USA*
[3]*University of Texas Health Science Center, San Antonio, TX, USA*

Correspondence should be addressed to Jaideep Banerjee; banerjee.42@osu.edu

Received 28 September 2017; Accepted 28 September 2017; Published 31 October 2017

MicroRNAs (miRNAs) as a biomarker of pathology and regulators of gene expression have been well established through numerous publications over the last 10 years. Oxidative stress-related tissue damage is an important component of many diseases, and more and more studies are focused on discovering the signature of the regulatory interactions between redox signaling and specific miRNAs attributing to the disease. Reactive oxygen species has two faces—the good ROS and the bad ROS. Sustained high levels of ROS can cause intracellular damage while oxidants are also important intracellular signaling molecules, and multiple studies over the last two decades have implicated redox-dependent signaling as essential to a host of cellular decisions including differentiation, growth, cell death, and senescence. This makes it all the more important for a well-regulated cellular ROS level, and miRNAs fill in the role of maintaining this homeostasis. A dysregulation of normal physiological miRNA levels can thus lead to oxidative damage and development of disease.

This special issue on microRNA regulation of oxidative stress encompasses cutting edge articles that focus on the role of microRNAs in regulating redox biology in several pathological conditions.

(i) Atherosclerosis. Endothelial cell apoptosis under oxidative stress plays a critical role in the initiation and progression of atherosclerosis. T. Li et al. have discovered the role of miRNA-210 in protecting human umbilical vein endothelial cells against oxidative stress-induced apoptosis. miRNA-210 is one of the most well-characterized hypoxamiRs. The authors discovered that overexpression of miRNA-210 inhibited apoptosis and reduced ROS level in HUVECs treated with H_2O_2 and downregulated caspase levels. Thus, miRNA-210 has a prosurvival and antiapoptotic effect on HUVECs under oxidative stress.

(ii) Vascular diseases. Endothelial cell dysfunction is implicated in various vascular diseases. Intracellular exchange of miRNAs can happen through packaging and releasing through exosomes. H. Liu et al., in their article, describe a unique cross-talk between neural progenitor cells (NPCs) and endothelial cells interacting through direct physical contact or through paracrine mechanisms and illustrate that miRNA-210 is the key player in the protective effects of NPC-EXs on attenuating Ang II-induced ROS overproduction and dysfunction in endothelial cells, majorly through the Nox2/ROS and VEGF/VEGFR2 signals.

(iii) Myocardial infarction. Cardiomyocytes are exposed to oxidative stress during ischemia/reperfusion and often undergo apoptosis. Y.-C. Fang and C.-H. Yeh explore the role of miRNAs in influencing cardiomyocyte apoptosis resulting from ischemia-induced myocardial infarction. The authors determined that miRNA-302 expression is elevated by hypoxia/reoxygenation injury, and this increase in miRNA-302 expression aggravated cardiomyocyte apoptosis by inhibiting antiapoptotic Mcl-1

expression, thereby activating proapoptotic molecules. These findings suggested that elevated miRNA-302 levels can be detrimental to cells, whereas decreased miRNA-302 levels are beneficial and can lead to an effective therapeutic intervention.

Nrf2 and MAFG are two transcription factors shown to be highly involved in the regulation of numerous antioxidant and detoxifying genes. In form of heterodimer, the complex Nrf2:MAFG binds to and activates the transcription of antioxidant/xenobiotic genes harboring antioxidant responsive elements (ARE), located in their transcription regulatory sequences. R. Caggiano identified a new "redoximiR" and discovered that miRNA-128 directly targets MAFG and in the process influences stress responses mediated by ARE-dependent genes. This work highlights a potential new prognostic and/or diagnostic marker for skeletal muscle diseases and cardiovascular ischemic diseases.

(iv) Hodgkin lymphomas (HL). HL is a cancer that starts in the lymphocytes. In their paper, P. Karihtala et al., for the first time, assessed the microRNAs that regulate antioxidant enzymes in HL. In a group of 41 HL patients, quantification of the miRNA levels from freshly frozen lymph node samples revealed that miRNA-23b correlated inversely with CD3 and CD20 expressions and miRNA-144 with CD3, CD20, and CD30. High MnSOD mRNA levels associated with poor HL-specific outcome in the patients with advanced disease, and high miRNA-122 levels associated with worse HL-specific survival in the whole patient population. When standardized according to the CD30 expression, high miRNA-212 and miRNA-510 levels predicted worse relapse-free survival. The authors therefore successfully identified novel biomarkers for HL.

(v) Type 2 diabetes mellitus (T2DM). T2DM is characterized by inflammatory and oxidant status. L. Sun et al. studied the effect of a fruit juice of *Actinidia chinensis Planch* (FJACP) on the antioxidant and anti-inflammatory status on 122 Type 2 diabetes mellitus (T2DM) patients. The authors found that the treatment resulted in higher levels of serum miRNA-424, which was positively related to Keap1 and Nrf2 levels, while Keap1 and Nrf2 levels were positively related to the levels of SOD and GSH and negatively related to proinflammatory IL-1 beta and IL-6. The authors thus concluded that FJACP treatment can be developed as a novel non-pharmaceutical intervention for T2DM patients.

(vi) Neurological disorders (stroke and dementia). J. Song et al. investigated whether miRNA-let7A controls the damage of brain endothelial cells in a hyperglycemic state. Hyperglycemia can trigger the disruption of blood-brain barrier (BBB), leading to diverse neurological diseases including stroke and dementia. The authors found that miRNA-let7A overexpression significantly prevented cell death and loss of tight junction proteins and attenuated proinflammatory response and nitrite production in the hyperglycemic cells and thus attenuated brain endothelial cell damage. Manipulation of miRNA-let7A may therefore provide a novel solution in controlling BBB disruption which is a major precursor of central nervous system diseases.

(vii) Cancer and aging. Hepatocellular carcinoma (HCC) is the fifth most common cancer and the third cause of cancer-related mortality worldwide. The study by Y. Wan identified miRNAs in hepatocellular carcinoma (HCC) cells which are involved in oxidative stress-response. An integrated analysis of miRNA expression signature revealed four miRNAs (miRNA-34a-5p, miRNA-1915-3p, miRNA-638, and miRNA-150-3p) elevated under oxidative stress and were found to play an important role in antiapoptosis process. The authors found that these four miRNAs were associated with patients' overall survival and thus may offer new strategies for HCC diagnosis and prognosis.

Wen Li et al., in their work, identified a direct relationship between ULK1 and miRNA-93 and suggested that autophagy may be important for sustaining the viability of the cancerous cell line during stressful hypoxia condition.

Cellular senescence or cell growth arrest drives the aging process and age-related disorders. Aging-induced dysregulation of miRNA biogenesis proteins is reported to promote aging and aging-associated pathologies. The comprehensive review article by H. Bu covers the importance of miRNAs in regulating oxidative stress in the context of aging and cellular senescence.

The findings reported in the article by J. Chao et al. reveal novel mechanisms of kallistatin in protection against senescence, aging, and cancer by modulating miR-34a and miR-21 levels and inhibiting oxidative stress. Kallistatin is an endogenous protein that regulates gene signaling via its active site and the heparin-binding domain. Through its heparin-binding site, kallistatin inhibits inflammation and oxidative stress by antagonizing TNF-α-induced NADPH oxidase activity and miR-21 expression, NF-κB activation, and inflammatory gene expression in endothelial cells. Through its active site, kallistatin inhibits miRNA-34a synthesis and stimulates eNOS and SIRT1 expressions in endothelial progenitor cells. Thus, by dual downregulation of miRNA-34a and miRNA-21 expressions, kallistatin

treatment attenuates oxidative damage and cellular senescence. Also, by silencing miRNA-21, kallistatin inhibits endothelial-mesenchymal transition that is a major contributor to organ fibrosis and tumor metastasis.

(viii) Hepatic steatosis: X.-Y. Guo studied a novel layer of epigenetic interaction between circRNA and miRNA and discovered a potential approach to the therapy of lipid peroxidative damage. Their findings reveal a circRNA-0046367/miR-34a/PPARα regulatory system underlying hepatic steatosis. Expression of circRNA-0046367, which is an endogenous modulator of miR-34a, is lost during hepatocellular steatosis resulting in miR-34a's inhibitory effect on peroxisome proliferator-activated receptor α (PPARα). PPARα restoration by circRNA-0046367 normalization led to the transcriptional activation of genes associated with lipid metabolism, including carnitine palmitoyltransferase 2 (CPT2) and acyl-CoA binding domain containing 3 (ACBD3), thus ameliorating lipoxidative stress and resulting in the steatosis resolution.

(ix) Chronic kidney disease. Renal tubulointerstitial fibrosis (TIF) is a prominent pathological feature of chronic kidney disease (CKD) leading to end-stage renal failure. Blocking or reversing TIF is one way to halt CKD progression. Y. Fang and his team studied the role of miRNA-382 in an obstructed kidney and reported that the abundance of miRNA-382 was associated with silencing of heat shock protein 60 (HSPD1) along with upregulation of 3-nitrotyrosine (3-NT) and downregulation of thioredoxin (Trx). Their work identifies a novel mechanism in which miRNA-382 contributes to the redox imbalance in the development of renal fibrosis.

Taken together, the articles in this special issue contributed by the experts in the fields of oxidative stress biology highlight the increasing importance of studying the role of redox-sensitive microRNAs to identify more effective biomarkers and develop better therapeutic targets for the plethora of oxidative stress-related diseases.

Jaideep Banerjee
Savita Khanna
Akash Bhattacharya

Hindawi
Oxidative Medicine and Cellular Longevity
Volume 2017, Article ID 2709053, 13 pages
https://doi.org/10.1155/2017/2709053

Research Article

MicroRNA-93 Regulates Hypoxia-Induced Autophagy by Targeting ULK1

Wen Li,[1,2] Yue Yang,[3] Zhaoyu Ba,[4] Shupeng Li,[5] Hao Chen,[5] Xiaoyan Hou,[5] Linlin Ma,[6] Pengcheng He,[7] Lei Jiang,[7] Longxuan Li,[8] Rongrong He,[2] Liangqing Zhang,[3] and Du Feng[1,5]

[1]*Key Laboratory of Protein Modification and Degradation, School of Basic Medical Sciences, Affiliated Cancer Hospital & Institute of Guangzhou Medical University, Guangzhou Medical University, Guangzhou 511436, China*
[2]*Anti-Stress and Health Research Center, College of Pharmacy, Jinan University, Guangzhou 510632, China*
[3]*Department of Anesthesiology, Guangdong Medical University, Zhanjiang 524001, China*
[4]*Department of Spine Surgery, Shanghai East Hospital, Tongji University School of Medicine, Tongji University, Shanghai 200120, China*
[5]*Institute of Neurology, Guangdong Key Laboratory of Age-Related Cardiac-Cerebral Vascular Disease, Affiliated Hospital of Guangdong Medical University, Zhanjiang, Guangdong 524001, China*
[6]*Department of Obstetrics and Gynecology, Beijing Hospital, National Center of Gerontology, Beijing 100730, China*
[7]*Department of Cardiology, Guangdong Cardiovascular Institute, Guangdong Provincial Key Laboratory of Coronary Heart Disease Prevention, Guangdong General Hospital, Guangdong Academy of Medical Sciences, Guangzhou, China*
[8]*Department of Neurology, Gongli Hospital, Pudong New Area, Shanghai 200135, China*

Correspondence should be addressed to Rongrong He; rongronghe66@163.com, Liangqing Zhang; zhanglq1970@163.com, and Du Feng; feng_du@foxmail.com

Received 30 January 2017; Revised 13 July 2017; Accepted 8 August 2017; Published 3 October 2017

Academic Editor: Savita Khanna

The expression of the core autophagy kinase, Unc51-like kinase 1 (ULK1), is regulated transcriptionally and translationally by starvation-induced autophagy. However, how ULK1 is regulated during hypoxia is not well understood. Previously, we showed that ULK1 expression is induced by hypoxia stress. Here, we report a new ULK1-modulating microRNA, miR-93; its transcription is negatively correlated with the translation of ULK1 under hypoxic condition. miR-93 targets ULK1 and reduces its protein levels under hypoxia condition. miR-93 also inhibits hypoxia-induced autophagy by preventing LC3-I to LC3-II transition and P62 degradation; these processes are reversed by the overexpression of an endogenous miR-93 inhibitor. Re-expression of ULK1 without miR-93 response elements restores the hypoxia-induced autophagy which is inhibited by miR-93. Finally, we detected the effects of miR-93 on cell viability and apoptosis in noncancer cell lines and cancer cells. We found that miR-93 sustains the viability of MEFs (mouse embryonic fibroblasts) and inhibits its apoptosis under hypoxia. Thus, we conclude that miR-93 is involved in hypoxia-induced autophagy by regulating ULK1. Our results provide a new angle to understand the complicated regulation of the key autophagy kinase ULK1 during different stress conditions.

1. Introduction

Autophagy is a regulated and highly conserved process that can develop double-membraned autophagosomes to degrade large protein aggregates and damaged organelles upon fusing with lysosomes [1, 2]. Autophagy can not only recycle intracellular energy resources when the cell is deficient in nutrients but also remove cytotoxic proteins and damaged organelles under a lot of stress conditions including pathogen invasion, hypoxia, and mitochondrial depolarization [3–5].

ULK1 is a mammalian homologue of yeast Atg1 [6, 7]. As an initiator of autophagy, ULK1 regulates autophagy through interaction of upstream mTOR and AMPK and then transduce signals to downstream mediators [8–13]. ULK1 protein level can be regulated by a variety of stimuli such as nutrient-depleted condition, energy deprivation, and hypoxia [14–16].

In the initial stage of nutrient-depletion condition, the elevated transcription of ULK1 is immediately induced, but after prolonged starvation, the ULK1 protein level is reduced because of the suppressed translation as well as the increased degradation of ULK1, which limits further autophagy induction [17–19]. ULK1 level is significantly increased in response to inhibition of mitochondrial respiratory complexes in cell treated with inhibitors of the mitochondrial complex I (rotenone), complex II (thenoyltrifluoroacetone/TTFA), or complex III (antimycin A or myxothiazol) [17]. Previously, we also found that ULK1 level is induced in cells subjected to 1% oxygen stress condition or by mitochondrial depolarized drug, FCCP, indicating that the ULK1 level is regulated at both transcriptional and translational levels and is more complicatedly controlled than previously thought [15, 16].

miRNAs are 17 ~ 22 nucleotide, noncoding and single-stranded RNA molecules playing a role in a variety of pathophysiologic processes including apoptosis, cell proliferation, and differentiation [20–22]. It targets multiple genes via blocking mRNA translation. Silencing Dicer1, a major component of the miRNA-silencing machinery, increases the levels of the Atg protein and the formation of autophagosomes in cells [23]. Kap1, also known as TRIM28 (tripartite motif protein 28), acts as a scaffold for a multimolecular complex that silences transcription through the formation of heterochromatin [24, 25]. Hematopoietic-restricted deletion of Kap1 fails to induce mitophagy (the process of removing damaged mitochondrial through autophagy)-associated genes [26, 27] and retains mitochondria due to lack of repression of a subset of microRNAs, which target mitophagy transcripts. We also found that hypoxia-responsive miR-137 regulates mitophagy by targeting two mitophagy receptors FUNDC1 and NIX. These findings indicate that miRNAs can regulate autophagy [28, 29]. Although several studies on microRNA regulation of ULK1 have been reported, those microRNAs do not respond to hypoxic environments [30–38].

miR-93 plays a variety of roles in regulating cellular homeostasis. For example, the expression of miR-93 causes hypersusceptibility to vesicular stomatitis virus infection in Dicer1-deficient mice [39]. miR-93 promotes the axon growth of spinal cord neurons by targeting to EphA4 [40]. In proliferation, miR-93 promotes the proliferation of osteosarcoma cells by targeting PTEN [41, 42].

Nevertheless, how microRNA-modulated key autophagic machinery is involved in hypoxic condition remains poorly understood. Here, we uncovered the regulating mechanism between miRNA-93, ULK1, and hypoxia-induced autophagy.

2. Materials and Methods

2.1. Reagents and Antibodies. DMEM (Gibco, C11965500BT), fetal bovine serum (Gibco, 16000044), EBSS (MACGENE, CC026), FITC Annexin V apoptosis detection kit I (BD Biosciences, 556547), cell counting kit (YEASEN, QF0026), lysis buffer (Beyotime, P0013), PVDF membranes (Millipore, ISEQ00010), albumin bovine V (Solarbio, A8020), lipofectamine 2000 (Invitrogen, 11668027), Dual-Luciferase® Reporter Assay System (Promega, E1910), and terminal deoxynucleotidyl transferase-mediated dUTP nick-end labeling (TUNEL) staining kit (Promega, G3250). Bafilomycin A1 was purchased from Sigma. The following antibodies were used: anti-ULK1 (Sigma-Aldrich, A7481), anti-P62 (MBL, PM045), anti-P62 (Abcam, ab56416), anti-LC3B (Sigma, L7543), anti-c-Myc monoclonal antibody (Sigma, C3956), anti-β-actin (Sino Biological, 100162-RP02-100), anti-Gapdh (Transgen, HC301), anti-ULK1 (Sigma, A7481), anti-ATG5 (Sigma, A0731), anti-ATG7 (Sigma, A2856), anti-Beclin1 (CST, 3738), anti-Tom20 (BD Biosciences, 612278), DAPI (CST, 4083), HRP Affinipure goat anti-mouse IgG (Earthox, E030110), and HRP Affinipure goat anti-rabbit IgG (Earthox, E030120). The following fluorescent secondary antibodies were used: Alexa Fluor 555-labeled donkey anti-mouse IgG antibodies (Invitrogen, A31570) and Alexa Fluor 488-labeled donkey anti-rabbit IgG antibodies (Invitrogen, A21206).

2.2. Cell Culture, Hypoxia, Starvation Treatment, and Transfection. The methods we used in the Materials and Methods were followed from our previous paper by Li et al. [43]. MEFs (mouse embryonic fibroblasts), CHO (Chinese hamster ovary cell), and HeLa cells were used in this study. Cells were cultured in Dulbecco's modified Eagle's medium supplemented with 10% FBS and 1% penicillin/streptomycin (Beyotime, referred to as complete medium) at 37°C and 5% CO_2. To determine the levels of autophagy, we starved cells for different times with EBSS. Hypoxic conditions were achieved with a hypoxia chamber (Billups-Rothenberg) flushed with a preanalyzed gas mixture of 1% O_2, 5% CO_2, and 94% N_2. Cell transfection was performed using lipofectamine 2000 according to protocols provided by manufacturers.

2.3. Plasmids. Myc-ULK1 constructs were described previously. The 3′ untranslated region (UTR) of ULK1 (NM_009469) was amplified from mouse cDNA. The primers used were as follows: 5′-GCGCTAGCCCAGGG GTCCCTTGCCCAC-3′ (UTR, F), 5′-GGTCTAGAGTAAA GTGTGGAAGTTGAGG-3′ (UTR, R). PCR products were cloned into pmirGLO dual-luciferase miRNA target expression vector (Promega) using NheI and XbaI restriction sites, named pmirGLO-ULK1. The corresponding binding site mutation was also cloned using the following primers: 5′-TTTGTAAGTCACCGGTAACTGCCATGCATACAGAGA CTGGA-3′ (M-UTR, F), 5′-TCCAGTCTCTGTATGCATG GCAGTTACCGGTGACTTACAAA-3′ (M-UTR, R). Mutation, named mutant pmirGLO-ULK1, was created by site-directed mutagenesis, changing "gcacttt" to "aactgcc." Q5® High-Fidelity DNA Polymerase (Bio Labs, M0491S) was used for PCR reaction. The plasmids were sequenced to verify the accuracy.

2.4. siRNAs and miRNAs. Five pairs of siRNAs were designed and synthesized as follows by GenePharma: si-ULK1-Mus-488 (sense: CCGUCAAAUGCAUUAACAATT, antisense: UUGUUAAUGCAUUUGACGGTT), si-ULK1-

Mus-2457 (sense: GCUGCUUAAGGCUGCAUUUTT, antisense: AAAUGCAGCCUUAAGCAGCTT), si-ULK1-Mus-3310 (sense: GCUGUGCAAAUGGUACAAUTT, antisense: AUUGUACCAUUUGCACAGCTT), and negative control (NC) and negative control FAM (sense: UUCUCCGAACG UGUCACGUTT, antisense: ACGUGACACGUUCGGAGA ATT). miR-93 mimics (93) and miR-93 inhibitor (IN-93) were synthesized by RiboBio (Guangzhou, China) with reference to miRNA's sequence information in miRbase. Meanwhile, NControl (NC) and inhibitor NControl (IN-NC) were also synthesized as a negative control.

2.5. Luciferase Assay. Cells were seeded in 24-well plates 1 day before transfection. For reporter assays, the cells were transiently cotransfected with 0.8 μg of reporter plasmid in the presence of 100 nM scramble NC (NC), miR-93 mimics (93), NC inhibitor (IN-NC), or miR-93 inhibitor (IN-93) using lipofectamine 2000. Firefly and Renilla luciferase activities were measured consecutively by using dual-luciferase reporter assay system according to the manufacturer's instructions. Independent experiments were performed in triplicate.

2.6. qRT-PCR. Total RNA was isolated with TRIzol (Life Technologies) followed by a DNase treatment to eliminate contaminating genomic DNA (Thermo, B43) and reverse transcription reaction (Thermo, K1622). Amplification and relative quantification of cDNA was carried out with SYBR® Premix Ex Taq™ (Tli RNaseH Plus) (TaKaRa, RR420A) according to the manufacturer's protocol. Relative quantitative PCRs for miRNAs were performed with SYBR PrimeScript miRNA RT-PCR Kit (TaKaRa, RR716) as described before. Fold changes were calculated using the $2^{-\triangle\triangle Ct}$ method with normalization to endogenous control. Primers used were as follows: 5′-CTCGCTTCGGCAGCACA-3′ (U6-F), 5′-AACGCTTCACGAATTTGCGT-3′ (U6-R). miR-93 qPCR primers were purchased from RiboBio (Guangzhou, China). 5′-CCAGGCAGACATTGAGAACA-3′ (ULK1-F), 5′-GTTGGCAGCAGGTAGTCAGG-3′ (ULK1-R), 5′-CCAC CCAGAAGACTGTGGAT-3′ (Gapdh-F), 5′-CACATTGGG GGTAGGAACAC-3′ (Gapdh-R). Independent experiments were performed in triplicate.

2.7. Western Blotting. Whole cell lysates used for immunoblotting were prepared in lysis buffer containing a phosphatase inhibitor (Roche, 4693116001) on ice. Lysates were mixed with SDS loading buffer and boiled for 10 min. Protein samples were separated on SDS-PAGE gels and then transferred to PVDF membrane. Membranes were blocked by 5% nonfat milk (dissolved in PBST) for 1 h at room temperature. Corresponding primary antibody was used for overnight incubation at 4°C, followed by HRP-labeled secondary antibodies' incubation at room temperature for 2 hrs. For loading controls, membranes were probed with the antibody against β-actin or Gapdh. Densitometric ratios were quantified by ImageJ software.

2.8. Immunofluorescence Microscopy. Cells were grown to 60% confluence on a coverslip. After treatment, the cells were washed in PBS and fixed with 4% paraformaldehyde for 20 mins. After washed twice in PBS, the cells were permeabilized with 0.1% Triton X-100 (in PBS). Coverslips were blocked in 1% albumin bovine V (in PBS) for 30 mins at room temperature and then were incubated with primary antibody diluted in PBS (0.01% Triton X-100) for 1 h at room temperature. After washed with PBS for 4×5 mins, secondary antibodies were applied. Cell images were captured with a TCS SPF5 II Leica confocal microscope and software (LAS-AF-Lite_2.2.0_4758, Germany).

2.9. CCK-8 Assay. Cell viability was measured using the CCK-8 kit. Briefly, 7×10^6 cells in the logarithmic growth phase were seeded into a 24-well plate and incubated in 500 μL complete medium overnight. MEFs and HeLa cells were transfected with scramble NC (NC), miR-93 mimics (93), NC inhibitor (IN-NC), or miR-93 inhibitor (IN-93) individually for 12 h, followed by the treatment of hypoxia for another 24 h. Moreover, MEFs were transfected with scramble NC (NC), miR-93 mimics (93), NC inhibitor (IN-NC), or miR-93 inhibitor (IN-93) individually for 24 h, followed by subjecting to starvation for another 1 h. The cell viability was detected according to the manufacturer's instructions. The optical density (OD) at 450 nm was measured using a microplate spectrophotometer (Biotek, Epoch). Cell viability was presented using the normal group as control.

2.10. Flow Cytometry. Cell apoptosis was also assessed by flow cytometry after Annexin V-FITC/PI staining as manufacturer's instructions. MEFs were transfected with scramble NC (NC), miR-93 mimics (93), NC inhibitor (IN-NC), or miR-93 inhibitor (IN-93) individually for 12 h, followed by the treatment of hypoxia for another 24 h. The normal group was set as control. Analyses were carried out with a COULTER EPICS XL-MCL™ flow cytometer (Beckman Coulter) equipped with Expo32 ADC analysis software. The cellular apoptosis rate was mapped by GraphPad Prism 5.

2.11. TUNEL Assay. Briefly, HeLa cells were transfected with scramble NC (NC), miR-93 mimics (93), NC inhibitor (IN-NC), or miR-93 inhibitor (IN-93) individually for 12 h, followed by the treatment of hypoxia for another 24 h. Analysis of apoptotic cells was performed using the TUNEL staining kit following the manufacturer's instruction, using normal group as control. Cell images were captured with an EVOS FL Auto Cell Imaging System (Thermo Fisher Scientific). The nuclei were counterstained with 4′,6-diamidino-2-phenylindole (DAPI) (blue). TUNEL-positive cells had a pyknotic nucleus with dark green fluorescent staining, indicative of apoptosis.

3. Results

3.1. miR-93 Targets ULK1 and Regulates Its Expression. ULK1 is the initiation factor of autophagy, which belongs to the family of serine/threonine kinases and is essential for the induction of autophagy [44, 45]. However, ULK1-modulating microRNAs are not well understood. In order to determine the miRNA that targets ULK1, we used DIANALAB to perform bioinformatics search. Interestingly, the

software showed that ULK1 is the target of miR-93. Prediction of the interaction between miR-93 and 3′ UTR of ULK1 was shown in Figure 1(a). ULK1 contains a miR-93 binding site in the 3′ UTR (302–309 nucleotides). We then used the dual luciferase carrier pmirGLO to verify whether the miR-93 can identify and bind the 3′ UTR of ULK1. The 3′ UTR of ULK1 was cloned and inserted into the downstream of the firefly luciferase of plasmid pmirGLO. 100 nM scramble NC (NC), miR-93 mimics (93), NC inhibitor (IN-NC), or miR-93 inhibitor (IN-93) and a reporter gene were cotransfected into MEFs, respectively. As shown in Figure 1(b), the expression of miR-93 inhibited the firefly luciferase enzyme activity. However, the IN-93 could restore the activity of luciferase, suggesting the strong inhibitory effect of endogenous miR-93. Real-time quantitative PCR (qPCR) was performed by using U6 and Gapdh as the benchmark to detect the expression of miR-93 and ULK1 in either MEFs or CHO cells. The results showed that overexpression of exogenous miR-93 mimics or miR-93 inhibitor group was successful. ULK1 and miR-93 were individually inhibited by 93 and IN-93 (Figures 1(c) and 1(d)). The NC, 93, IN-NC, and IN-93 were also transfected into the cells for 24 h to detect the protein expression of ULK1 to confirm the inhibitory effect of miR-93 by Western blotting. miR-93, respectively, decreased the expression of ULK1 by 32% (in MEFs) and 70% (in CHO cells). Nevertheless, miR-93 inhibitor increased the expression of ULK1 by 28% (in MEFs) and 32% (in CHO cells) (Figures 1(e) and 1(f)). In order to exclude the off-target effects of miR-93 and to monitor a time course of the inhibitory effect of miR-93 to ULK1, some other autophagy-related genes were also examined by Western blotting. The expression of ATG5, ATG7, Beclin1, or Tom20 did not change when exogenously overexpressed with miR-93 and did not increase while exogenously overexpressed with miR-93 inhibitor (IN-93) (Figures 1(g) and 1(h)).

3.2. miR-93 Suppresses Hypoxia-Induced Autophagy. In order to find out whether miR-93 regulates the expression of ULK1 under the condition of hypoxia, cells were divided into four groups according to the time of hypoxia. Similarly as before, the protein levels of ULK1, P62, and LC3 transition confirmed that hypoxia could induce autophagy (Figure 2(a)). In hypoxia groups, the expression levels of ULK1 and LC3-I to LC3-II transition were increased but the expression of P62 was reduced (Figure 2(a)). The transcriptional and translational levels of ULK1 were higher than those in the normal group (Figures 2(a) and 2(b)). In contrast, the expression of miR-93 decreased during hypoxia (Figure 2(b)). Based on the above findings, we hypothesized that miR-93 might play an important role in hypoxia-induced autophagy. We then transfected scramble NC (NC), miR-93 mimics (93), NC inhibitor (IN-NC), or miR-93 inhibitor (IN-93) to examine their roles in hypoxia-induced autophagy. We found that miR-93 caused the downregulation of ULK1 as well as upregulation of P62, and decreased the ratio of LC3-II to LC3-I under hypoxic condition (Figure 2(c)). In contrast, this effect could be reversed by the endogenously overexpressed IN-93 during hypoxia. The expression of ULK1 in miR-93 group was lower than that in NC group. Compared to IN-NC group, IN-93 group promoted the expressional level of ULK1 (Figure 2(c)). Lysosomal inhibitor Bafilomycin A1 (BAF1) prevented the transition of LC3 and P62 protein degradation under hypoxic condition, indicating that hypoxia promotes the improvement of autophagic flux. The densitometric ratios from the samples were quantified by using ImageJ (Figure 2(c)). The results were further examined by immunofluorescence. The samples were stained with anti-ULK1 (green) and anti-P62 (red) antibodies. miR-93 inhibited the expression of ULK1 as well as its puncta formation during hypoxia (Figure 2(d)). On the contrary, miR-93 increased the P62 puncta under the same condition. Conversely, this effect could be reversed by IN-93, an inhibitor of endogenous miR-93. Upon inhibition of endogenous miR-93, ULK1 puncta increased accompanied by decreased expressional level of P62 (Figure 2(d)).

3.3. The Knockdown of ULK1 by siRNA Suppressed Hypoxia-Induced Autophagy. From the above results, we knew that hypoxia could trigger the decrease of miR-93 and the increase of ULK1 expression and consequently induce autophagy. Therefore, the modulatory effect of miR-93 on ULK1 might become less relevant since the weakened expression of miR-93 under hypoxic condition. To determine the relevance of miR-93 in the regulation of ULK1, siRNA of ULK1 was used to reveal that if knocking down of ULK1 had the same effect similar to miR-93 in hypoxia-induced autophagy. It is clear that siRNA, a class of double-stranded RNA molecules, interferes with the expression of specific genes by degrading mRNA after transcription (via complementary nucleotide sequences), resulting in no translation [46, 47]. Four pairs of siRNAs (including negative control) were designed, synthesized, and transfected into MEFs and CHO cells. Fortunately, we found the most effective siRNA interference site (488) attributing to its interference efficiency in MEF cells (~40%) and CHO cells (~60%) (Figures 3(a) and 3(b)). We then transfected si-ULK1 (488) and negative control RNA (NC) to examine their roles in hypoxia-induced autophagy. We found that si-ULK1 caused the downregulation of ULK1 as well as upregulation of P62 and decreased the ratio of LC3-II/LC3-I under hypoxic condition. The expression of ULK1 in si-ULK1 group was lower than that in NC group. BAF1 prevented the transition of LC3 and P62 protein degradation under hypoxic condition. The densitometric ratios from the samples were quantified by using ImageJ (Figure 3(c)). The results were further examined by immunofluorescence. The samples were stained with anti-ULK1 (green) and anti-P62 (red) antibodies. si-ULK1 inhibited the expression of ULK1 as well as its puncta formation during hypoxia. On the contrary, si-ULK1 increased the P62 puncta under the same condition (Figure 3(d)).

3.4. Re-Expression of ULK1 without miR-93 Binding Elements Restores Autophagy Inhibited by miR-93. In order to verify that the inhibition of ULK1 is due to miR-93, we evaluated the expression of ULK1-Myc (CDS) which lacked the miR-93 recognition element so that it can resist miR-93-mediated inhibition. ULK1-Myc (CDS) transfection

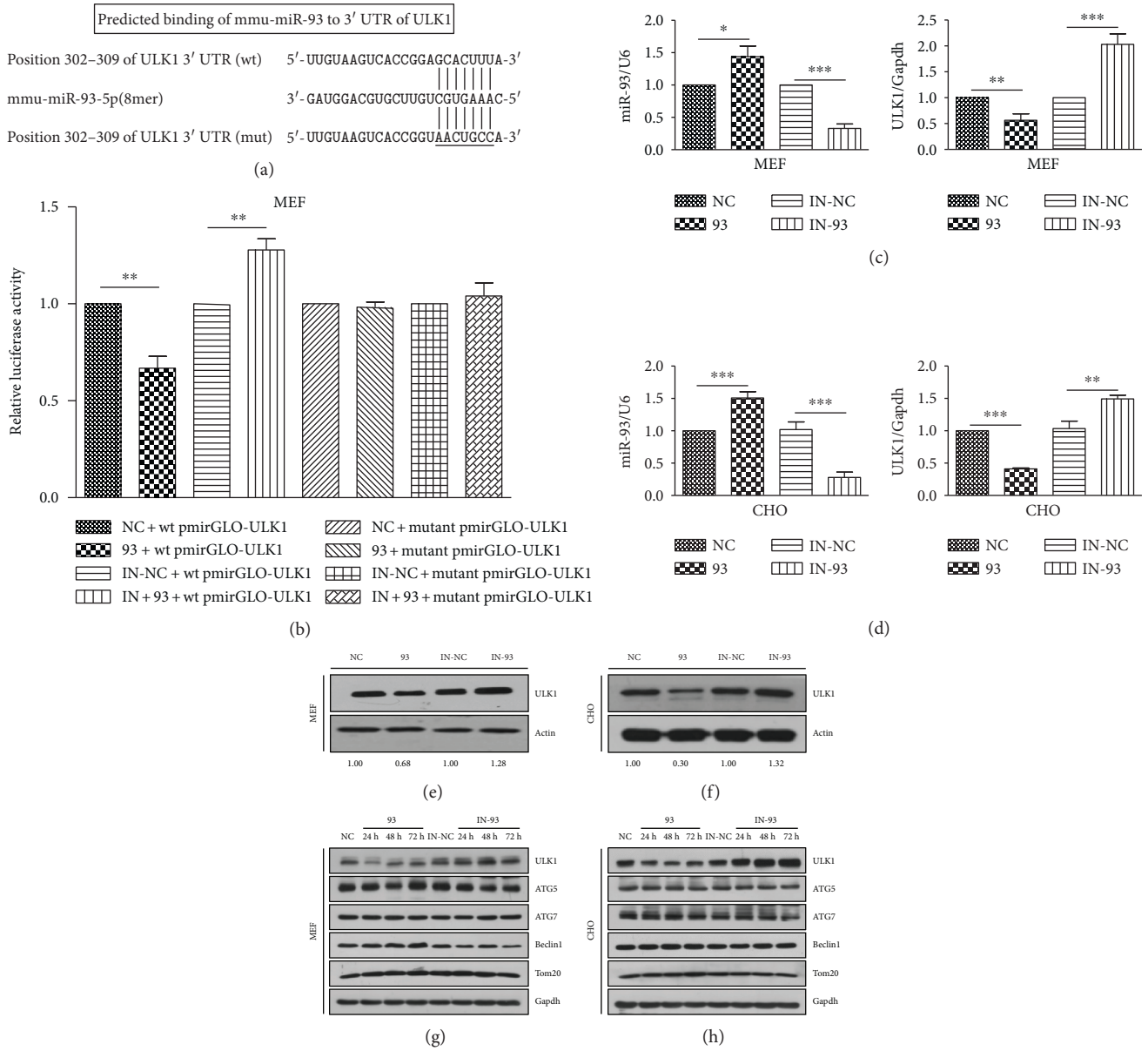

Figure 1: miR-93 targets ULK1 and regulates its expression. (a) Predicted binding sites of mmu-miR-93 to the 3′ UTR of ULK1. The short vertical lines indicate complementary paired bases of miR-93 and ULK1. The 302–309 nucleotides of ULK1 3′ UTR present the miRNA regulatory element (MRE). The underlined bases were mutant MRE. (b) Luciferase reporter assay by the interaction between miR-93 and the predicted MRE in MEFs. Each luciferase construct was cotransfected with scramble NC (NC), scramble IN-NC (IN-NC), miR-93 mimics (93), or miR-93 inhibitor (IN-93). At approximately 24 h after transfection, the luciferase activity was detected. The firefly luciferase activity was normalized to *Renilla*. Data were shown as the mean ± S.D. from three independent experiments. $^{**}P < 0.01$. (c) miR-93 represses the endogenous ULK1 expression in MEFs. NC, 93, IN-NC, and IN-93 were transfected into MEFs. At 24 h after transfection, qPCR was performed to detect the expression of miR-93 and ULK1. Data were from three independent experiments. $^{*}P < 0.05$; $^{**}P < 0.01$; $^{***}P < 0.001$. (d) miR-93 represses the endogenous ULK1 expression in CHO cells. NC, 93, IN-NC, and IN-93 were transfected into CHO cells. At 24 h after transfection, qPCR was performed to detect the expression of miR-93 and ULK1. Data were from three independent experiments. $^{**}P < 0.01$; $^{***}P < 0.001$. (e) Cell lysates in (c) were prepared and subjected to Western blot analysis by using anti-ULK1 and anti-β-actin antibody. The densitometric ratios of ULK1/actin from the samples were quantified by using ImageJ. Data were from three independent experiments. Representative data are shown. (f) Cell lysates in (d) were prepared and subjected to Western blot analysis by using anti-ULK1 and anti-β-actin antibody. The densitometric ratios of ULK1/actin from the samples were quantified by using ImageJ. Data were from three independent experiments. Representative data are shown. (g, h) MEFs and CHO cells were transfected with miR-93 (93) and miR-93 inhibitor (IN-93) for 24 h, 48 h, and 72 h, individually, setting group NC as a control. Cell lysates were prepared and subjected to Western blot analysis by using anti-ULK1, anti-ATG5, anti-ATG7, anti-Beclin1, anti-Tom20, and anti-Gapdh. Data were from three independent experiments. Representative data are shown.

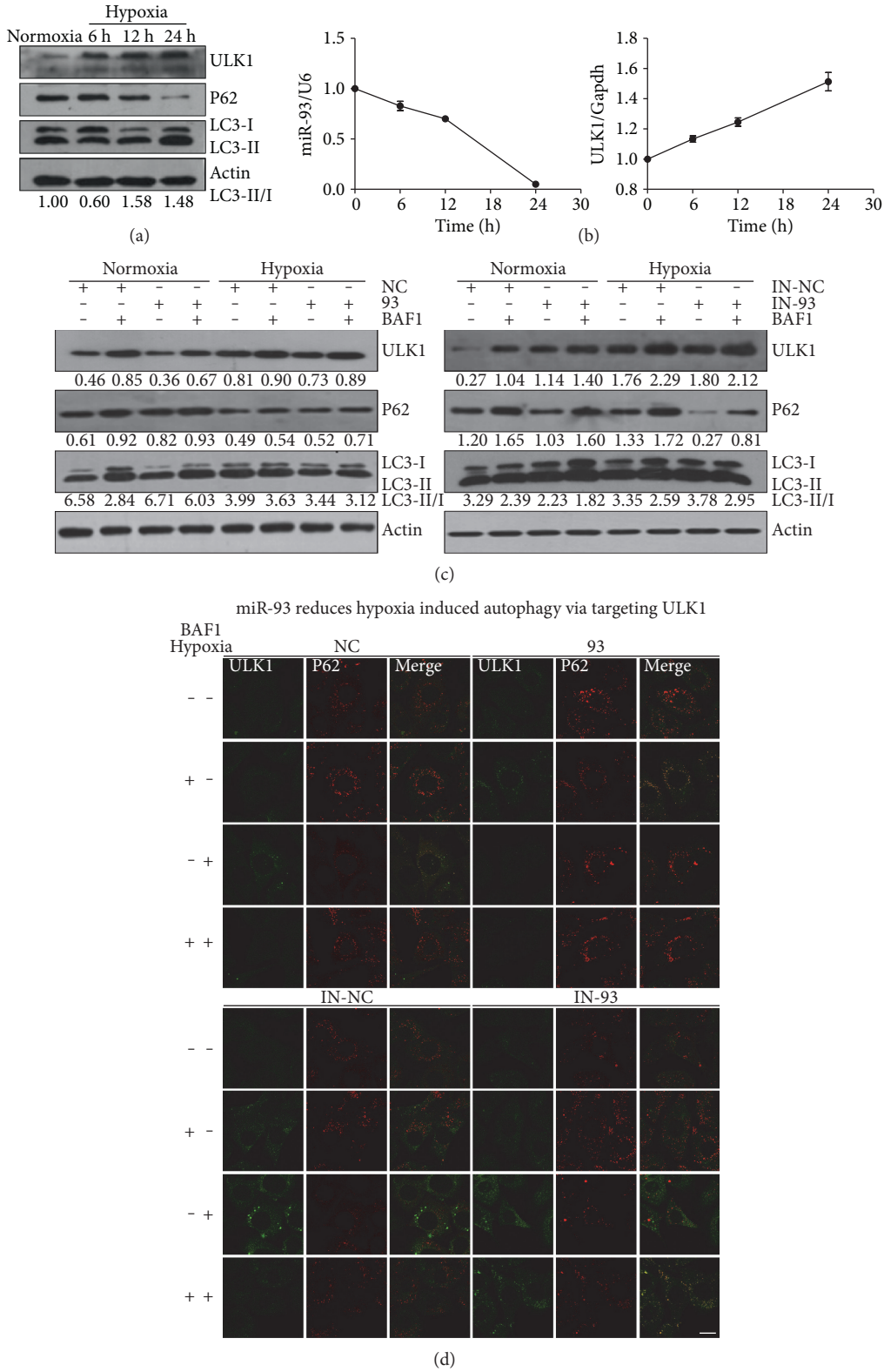

Figure 2: miR-93 inhibits hypoxia-induced autophagy. (a) The expression of ULK1 is induced by hypoxia. MEFs are subjected to hypoxia conditions for 0 h, 6 h, 12 h, and 24 h. Endogenous ULK1, P62, LC3, and β-actin were blotted by corresponding antibodies. Densitometric ratios of LC3-II/I from the samples were quantified by using ImageJ. (b) Expression levels of endogenous miR-93 and ULK1 in MEFs under hypoxia condition for 0 h, 6 h, 12 h, or 24 h by qPCR. (c) MEFs were transfected with scramble NC (NC), miR-93 mimics (93), scramble IN-NC (IN-NC), or miR-93 inhibitor (IN-93) for 12 h; afterward, MEFs were sealed in a hypoxic or normoxic condition for another 24 h with or without Bafilomycin A1 (BAF1). Samples were blotted with anti-ULK1, anti-P62, anti-LC3, and anti-β-actin antibodies. (d) MEFs were treated as the same as (c). Cells were fixed and immunostained with anti-ULK1 (green) and anti-P62 (red) antibodies. Scale bar, 20 μm.

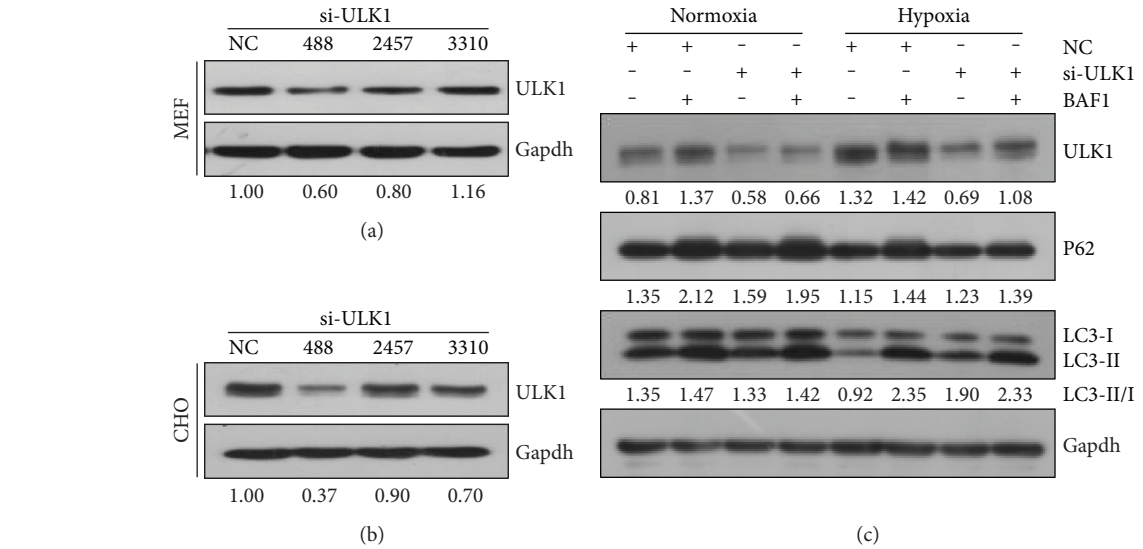

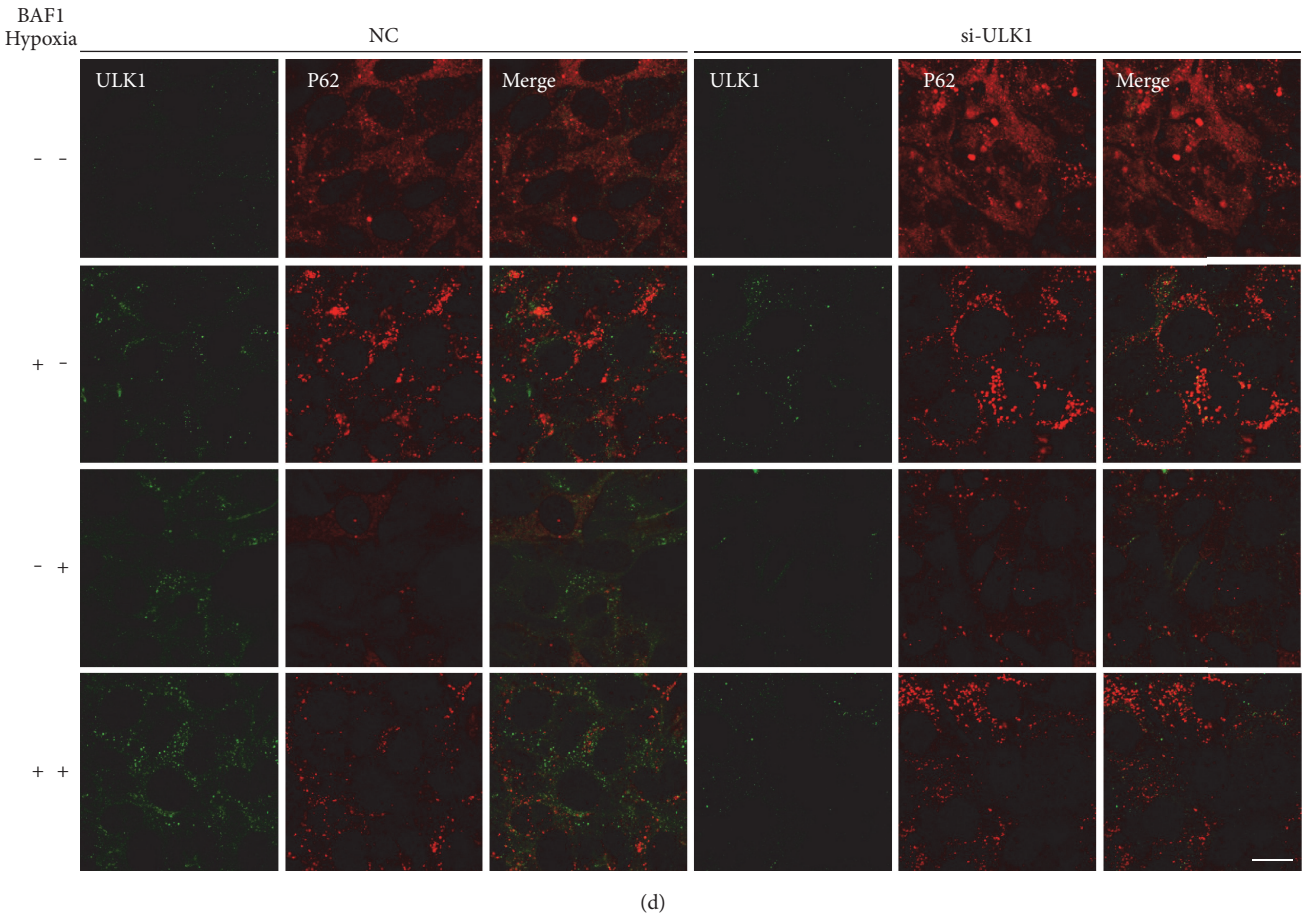

Figure 3: The knockdown of ULK1 by siRNA suppressed hypoxia-induced autophagy. (a, b) MEFs and CHO cells were transfected with three pairs of siRNAs to ULK for 24 h, respectively, si-ULK1 (488), si-ULK1 (2457), and si-ULK1 (3310), setting NC as a control. Cell lysates were prepared and subjected to Western blot analysis by using anti-ULK1 and anti-Gapdh. The densitometric ratios from the samples were quantified by using ImageJ. Data were from three independent experiments. Representative data are shown. (c) Si-ULK1 (488) was transfected into MEFs for 12 h, followed by hypoxic treatment or normoxic treatment for another 24 h. Cell lysates were analyzed by Western blot using anti-ULK1, anti-P62, anti-LC3, and anti-Gapdh. Densitometric ratios of the samples were quantified by using ImageJ. (d) MEFs were treated as the same as (c). Cells were fixed and immunostained by anti-ULK1 (green) and anti-P62 (red) antibodies. Scale bar, 20 μm.

effectively induced the P62 degradation and LC3-I to II transition even in the presence of miR-93 under hypoxia (Figure 4(a)). In order to distinguish the immunoreactivity-derived signal from the background staining, MEFs were fixed, permeabilized, and only stained with the second antibody donkey anti-rabbit 488 or donkey anti-mouse 555. As seen from Figure 4(b), there was no fluorescence signal of MEFs. Consistent with Figure 4(a), immunofluorescence results revealed that ULK1-Myc could effectively induce P62 degradation which was inhibited by exogenous overexpression of miR-93 under hypoxia as confirmed by WB (Figure 4(b)).

3.5. The Effects of miR-93 on Cell Viability and Apoptosis in Noncancer Cell Lines and Cancer Cells. Some genes involved in cell death are associated with the autophagy pathway. Excessive autophagy leads to cell death due to excessive digestion of essential intracellular proteins and organelles, which triggers the death signal [48–50]. Considering that miR-93 is involved in hypoxia by targeting key autophagy proteins, we assessed whether miR-93 is involved in cell viability in nutrient-depleted condition or during hypoxia. We used the cell counting kit to analyze and evaluate the cell viability during either condition. The cell viability of MEFs decreased to about 65%, in these conditions (Figures 5(a) and 5(b)). Upon starvation, the cell viability of MEFs did not change notably after the exogenous overexpression of miR-93 or miR-93 inhibitor, compared to NC or IN-NC group. Although the cell viability of MEFs between NC + starvation group and IN-NC + starvation group seemed to be different, there was no significant difference between the two groups ($P = 0.09$) (Figure 5(a)). Unlike starvation condition, in hypoxic condition, the miR-93 group recovered the cell viability from 65% to 136% (±6%) compared with NC group, while IN-93 further dampened the cell viability of MEFs to about 74% (±21%) during hypoxia, (Figure 5(b)). Although the cell viability of MEFs between NC + hypoxia group and IN-NC + hypoxia group seemed to vary, there was no significant difference between the two groups ($P = 0.21$) (Figure 5(b)). We subsequently examined whether miR-93 protected the cells from hypoxic stress by weakening cell apoptosis. Flow cytometry analysis revealed that miR-93 decreased hypoxia-induced cell apoptosis of MEFs, which was reversed by miR-93 inhibitor (IN-93) (Figure 5(c)). Given that autophagy and hypoxia are implicated to play an important role in cancer, we further investigated miR-93-based regulation of ULK1, and hypoxia-mediated modulation of miR-93 in human cancer cells. HeLa cells were used to take cell viability test and TUNEL assay. As shown in Figure 5(d), the cell viability of HeLa was dramatically reduced under hypoxic condition, compared with normal group. Interestingly, the exogenous overexpressed miR-93 (93) further accelerated the decrease of cell viability under the stress of hypoxia. By contrast, miR-93 inhibitor (IN-93) could reverse the cell viability by reducing the expression of endogenous miR-93. In view of the interesting experimental phenomena mentioned above, we did the TUNEL assay afterwards. Nevertheless, the overall apoptosis differences between groups were not significant (Figure 5(e)).

4. Discussion

Here, we found that the expression of ULK1 was upregulated but miR-93 level was declined under hypoxic condition. Their expression patterns showed a negative correlation (Figure 2). By using LAB DIANA, we uncovered a direct relationship of miR-93 and ULK1. The 3′ UTR of ULK1 had miR-93 pairing sites. The luciferase activity assay, quantitative RT-PCR, and Western blotting results showed that miR-93, when overexpressed, regulated ULK1 at the transcriptional and posttranscriptional levels. The inhibitory effect of miR-93 on ULK1 was also observed under hypoxic condition (Figure 2). Immunofluorescence showed that the expression of ULK1 was declined and the P62 level was increased by miR-93 (Figure 2). To determine the relevance of miR-93 in the regulation of ULK1, siRNA of ULK1 was used to reveal that knockdown of ULK1 had the same effect as compared to miR-93 in hypoxia-induced autophagy. Data showed that hypoxia induced autophagy was indeed suppressed after interference with ULK1 (Figure 3). This is consistent with the results from miR-93. In order to verify that the inhibition of ULK1 was caused by miR-93, we assessed whether the ULK1 plasmid lacking the miR-93 recognition element was able to resist miR-93-mediated inhibition. Immunofluorescence and Western blotting indicate that ULK1 plasmid that lacks miR-93 recognition element can rescue the autophagy inhibited by miR-93 (Figure 4).

Substantial progress helps us to understand the molecular mechanism of autophagy but there are still a lot of unknowns needed to be further clarified. Recent evidence that most autophagy genes can be regulated by miRNAs increases a more complicated cellular layer control of autophagy. Autophagy and microRNAs seem to have mutual communications with each other. On one hand, microRNAs regulate autophagy by directly targeting the autophagy genes including Beclin1 [51, 52], ATG3 [53], or ATG5 [54] as well as mitophagy genes, FUNDC1 and NIX [29]. On the other hand, autophagy activity modulates miRNA-mediated gene silencing and degrades the core miRISC component [55].

We found the negative correlation of miR-93 and ULK1. While ULK1 is induced and miR-93 is decreased under hypoxia. Interestingly, Hazarika et al. reported that hypoxia induced an increased expression of miR-93 [56], but Ke and colleagues observed a decreased level of miR-93 [41], which is consistent with our observations. We thought that the discrepancy may be due to the use of different cell types.

The cellular level of ULK1 is coordinately controlled by a variety of mechanisms. During early stages of autophagy, the E3 ligase complex AMBRA1–TRAF6 mediates K63-linked polyubiquitination of ULK1 to maintain its stability and kinase activity [57]. On the contrary, Cullin/KLHL20 catalyzes K48-linked polyubiquitination of ULK1 for proteasome degradation during prolonged nutrient starvation, thus providing negative feedback loop of the autophagy control [17]. Recently, Nazio et al. provide evidence that levels and activity of ULK1 are temporally controlled by NEDD4L-mediated degradation and mTOR-dependent de novo protein synthesis to modulate the duration of the autophagy response during prolonged starvation [19]. Similarly, the

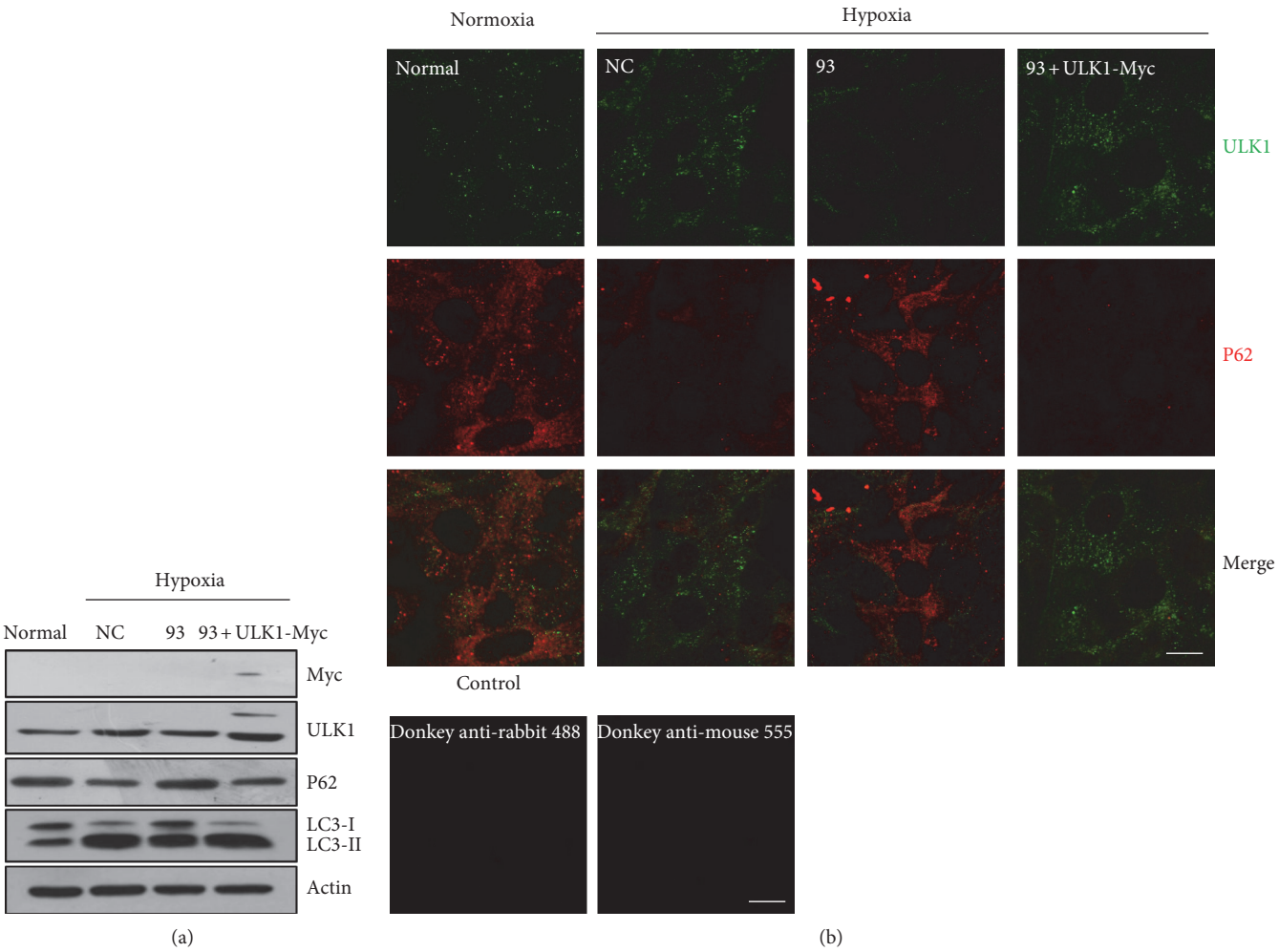

Figure 4: Re-expression of ULK1 without miR-93 response elements restores autophagy inhibited by miR-93. (a) MEFs were transfected with scramble NC (NC) and miR-93 mimics (93) or cotransfected miR-93 mimics (93) with the indicated constructs (ULK1-Myc) for 24 h by using the normal group as a control. Protein samples were collected and the expression of ULK1, Myc, LC3, and P62 was analyzed through Western blot. Actin was used as a loading control. (b) MEFs were fixed and immunostained by donkey anti-rabbit 488 or donkey anti-mouse 555. Scale bar, 20 μm. (c) MEFs were treated the same as (a). Cells were fixed and immunostained by anti-ULK1 (green) and anti-P62 (red) antibodies. Scale bar, 20 μm.

ULK1 expression is induced under hypoxia treatment. Our previous results demonstrate that the level of ULK1 is regulated by hypoxia from tens of minutes to 24 hours [15, 16]. But the expression of ULK1 declines if the hypoxic time is longer than 36 hours, indicating that the ULK1 expression is controlled by multiple cellular factors.

In this study, we have discovered that ULK1 is a new target gene of miR-93. Unlike the effect of miR-93 in nutrient-deprivation condition, our results show that miR-93 was able to recover the cell viability and lower the rate of apoptosis compared to the NC group under hypoxic condition in noncancerous MEFs, indicating that miR-93 might contribute some beneficial effects to this kind of cells under hypoxia. However, the effect of miR-93 in cancerous cell line HeLa is quite different. The cell viability of HeLa was dramatically reduced under hypoxic condition, compared with normal group. But, the exogenous overexpressed miR-93 (93) further accelerated the decrease of cell viability under the stress of hypoxia. By contrast, miR-93 inhibitor (IN-93) could revert the cell viability by reducing the expression of endogenous miR-93. The data suggests that autophagy might be more important for sustaining the viability of the cancerous cell line than noncancer cell lines during stressful hypoxia condition. Nevertheless, the overall apoptosis differences between groups were not significant (Figure 5). The different cell viability results of miR-93 in cancerous and noncancerous cell lines under hypoxia condition demonstrated a quite complex regulation of microRNA, autophagy, and cells that undergo hypoxic stress. This may be because of that the metabolism and oxygen consumption rate varies in cancerous and noncancerous cell lines. The detailed molecular mechanism needs to be further investigated.

We also observed that hypoxia substantially increases autophagy flux by upregulating the levels of ULK1 and suppresses the expression of miR-93 (Figure 2). This study provides a novel insight into how the oscillation level of

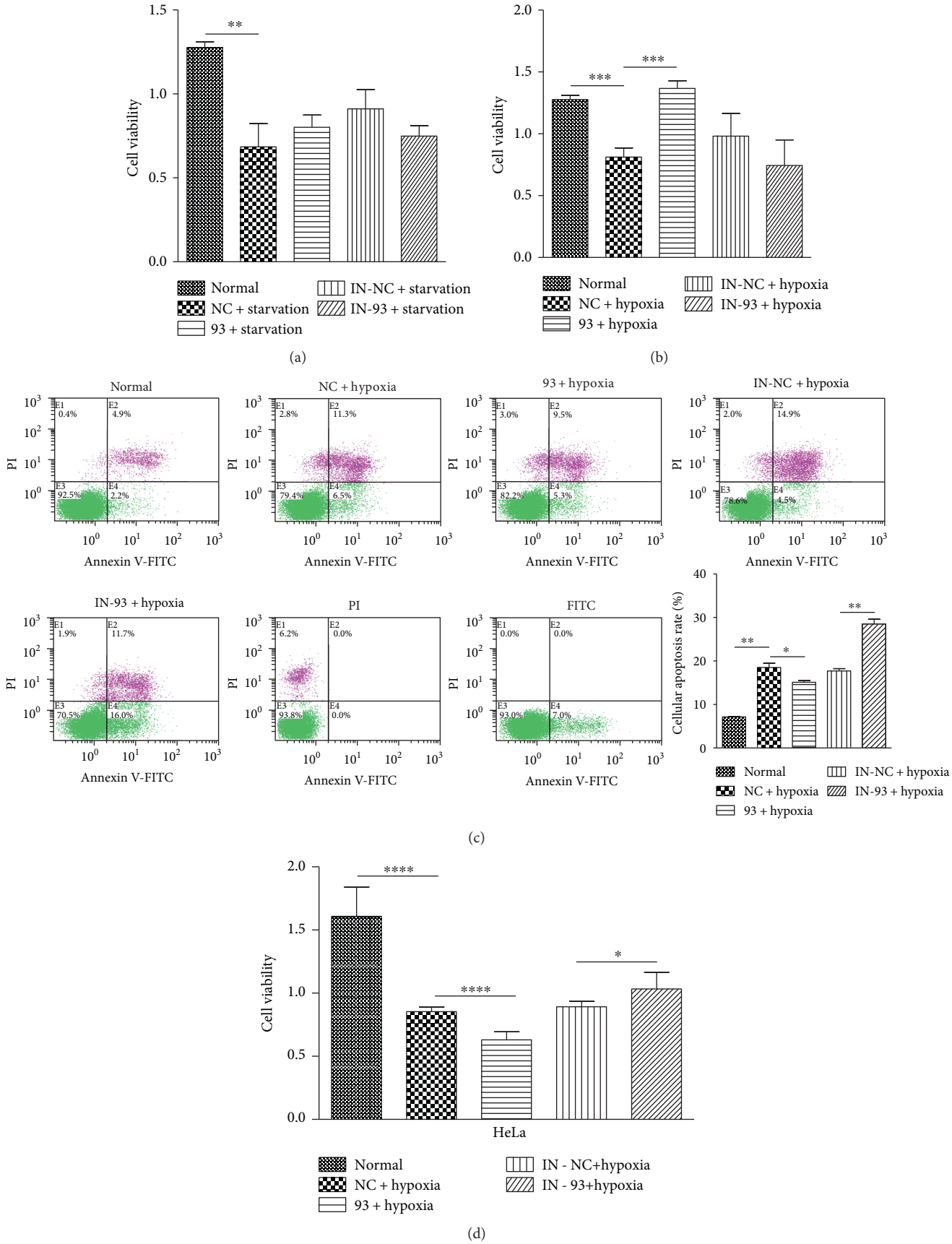

Figure 5: Continued.

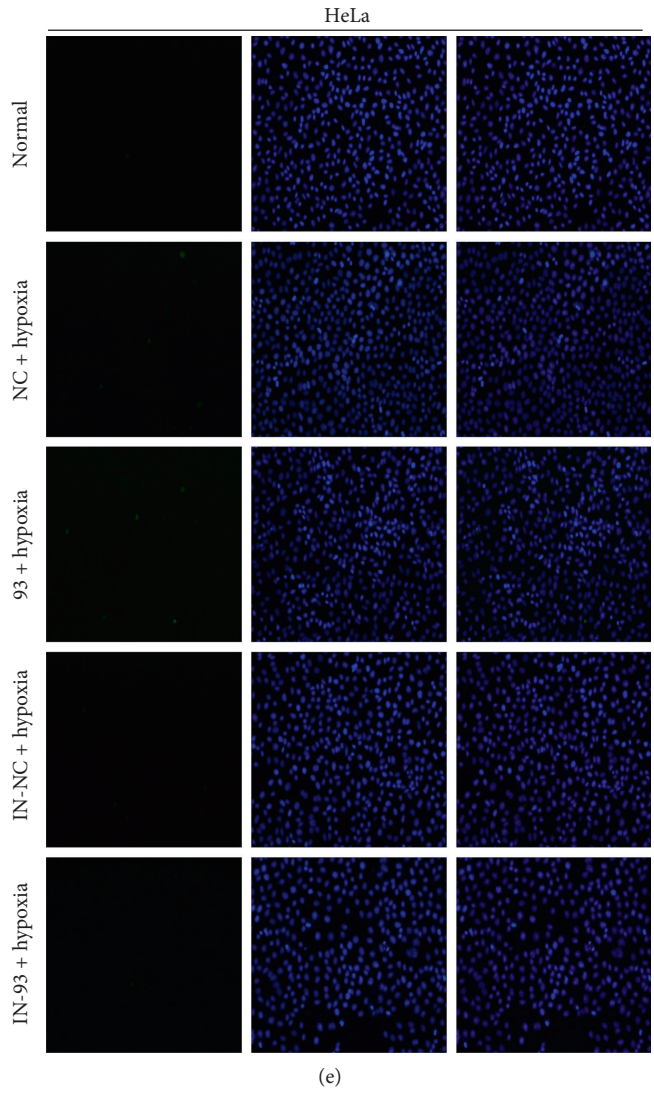

Figure 5: The effects of miR-93 on cell viability and apoptosis in noncancer cell lines and cancer cells. (a, b) CCK8 proliferation assays were performed on MEFs transfected with indicated RNA for 12 h. MEFs were exposed to starvation or hypoxic conditions for another 24 h. The graph represents the cell proliferation of three replicates with standard deviation represented by error bars. $^{**}P < 0.01$; $^{***}P < 0.001$. (c) MEFs were transfected with the indicated microRNAs or left untransfected for 12 h; the cells were exposed to hypoxic condition for another 24 h. The cell apoptosis rate was detected by flow cytometry. Cellular apoptosis rate was calculated by GraphPad Prism 5. (d) HeLa cells were transfected with scramble NC (NC), miR-93 mimics (93), scramble IN-NC (IN-NC), or miR-93 inhibitor (IN-93) for 12 h, followed by hypoxic treatment for another 24 h. Normal group was set as control. The CCK8 proliferation assays were detected. $^{*}P < 0.05$; $^{****}P < 0.0001$. (e) HeLa cells were treated as (d), then subjected to TUNEL staining. DAPI (blue), TUNEL-positive cells (green). Magnification, 20x.

ULK1 is maintained by miR-93, and miR-93-modulated key autophagic machinery involved in hypoxic microenvironment.

Conflicts of Interest

The authors declare that they have no conflict of interests.

Authors' Contributions

Du Feng conceived and supervised the work. Du Feng, Liangqing Zhang, Wen Li, and Yue Yang designed the experiments. Wen Li, Yue Yang, Zhaoyu Ba, Hao Chen, and Xiaoyan Hou performed the experiments with the help of other coauthors. Du Feng, Liangqing Zhang, Wen Li, Yue Yang, Zhaoyu Ba, Hao Chen, and Xiaoyan Hou analyzed the data. Wen Li, Yue Yang, and Du Feng wrote the paper. Wen Li, Yue Yang, Zhaoyu Ba, and Shupeng Li contributed equally to this work. Wen Li, Yue Yang, Zhaoyu Ba, Shupeng Li are the co-first author of the paper.

Acknowledgments

This work was supported by the NSFC (no. 31771531, no. 31401182, no. 81270196, and no. 81470405), by the National Basic Research Program of China (2013CB910100), by the Natural Science Foundation of Guangdong Province, China

(2014A030313533), by Yangfan Plan of Talents Recruitment Grant, Guangdong, China (Yue Cai Jiao [2015] 216), by the Science and Technology Planning Project of Guangdong Province (2016A020215152) to Du Feng, by the Key Specialty Construction Project of Shanghai Municipal Health Bureau (no. ZK2015B16) to Longxuan Li, and by the Key Discipline Construction Project of Shanghai East Hospital (YZX-2015-9).

References

[1] D. J. Klionsky, P. Codogno, A. M. Cuervo et al., "A comprehensive glossary of autophagy-related molecules and processes," *Autophagy*, vol. 6, pp. 438–448, 2010.

[2] D. J. Klionsky and Y. Ohsumi, "Vacuolar import of proteins and organelles from the cytoplasm," *Annual Review of Cell and Developmental Biology*, vol. 15, pp. 1–32, 1999.

[3] N. Mizushima, T. Yoshimori, and Y. Ohsumi, "The role of Atg proteins in autophagosome formation," *Annual Review of Cell and Developmental Biology*, vol. 27, pp. 107–132, 2011.

[4] N. Mizushima, B. Levine, A. M. Cuervo, and D. J. Klionsky, "Autophagy fights disease through cellular self-digestion," *Nature*, vol. 451, pp. 1069–1075, 2008.

[5] D. Feng, L. Liu, Y. Zhu, and Q. Chen, "Molecular signaling toward mitophagy and its physiological significance," *Experimental Cell Research*, vol. 319, pp. 1697–1705, 2013.

[6] J. Yan, H. Kuroyanagi, A. Kuroiwa et al., "Identification of mouse ULK1, a novel protein kinase structurally related to C. elegans UNC-51," *Biochemical and Biophysical Research Communications*, vol. 246, pp. 222–227, 1998.

[7] T. Hara and N. Mizushima, "Role of ULK-FIP200 complex in mammalian autophagy: FIP200, a counterpart of yeast Atg17?," *Autophagy*, vol. 5, pp. 85–87, 2009.

[8] L. Shang and X. Wang, "AMPK and mTOR coordinate the regulation of Ulk1 and mammalian autophagy initiation," *Autophagy*, vol. 7, pp. 924–926, 2011.

[9] A. S. Loffler, S. Alers, A. M. Dieterle et al., "Ulk1-mediated phosphorylation of AMPK constitutes a negative regulatory feedback loop," *Autophagy*, vol. 7, pp. 696–706, 2011.

[10] D. Egan, J. Kim, R. J. Shaw, and K. L. Guan, "The autophagy initiating kinase ULK1 is regulated via opposing phosphorylation by AMPK and mTOR," *Autophagy*, vol. 7, pp. 643-644, 2011.

[11] L. Shang, S. Chen, F. Du, S. Li, L. Zhao, and X. Wang, "Nutrient starvation elicits an acute autophagic response mediated by Ulk1 dephosphorylation and its subsequent dissociation from AMPK," *Proceedings of the National Academy of Sciences of the United States of America*, vol. 108, pp. 4788–4793, 2011.

[12] J. Kim, M. Kundu, B. Viollet, and K. L. Guan, "AMPK and mTOR regulate autophagy through direct phosphorylation of Ulk1," *Nature Cell Biology*, vol. 13, pp. 132–141, 2011.

[13] J. W. Lee, S. Park, Y. Takahashi, and H. G. Wang, "The association of AMPK with ULK1 regulates autophagy," *PLoS One*, vol. 5, article e15394, 2010.

[14] L. R. Pike, D. C. Singleton, F. Buffa et al., "Transcriptional up-regulation of ULK1 by ATF4 contributes to cancer cell survival," *The Biochemical Journal*, vol. 449, pp. 389–400, 2013.

[15] W. Wu, W. Tian, Z. Hu et al., "ULK1 translocates to mitochondria and phosphorylates FUNDC1 to regulate mitophagy," *EMBO Reports*, vol. 15, pp. 566–575, 2014.

[16] W. Tian, W. Li, Y. Chen et al., "Phosphorylation of ULK1 by AMPK regulates translocation of ULK1 to mitochondria and mitophagy," *FEBS Letters*, vol. 589, pp. 1847–1854, 2015.

[17] G. Allavena, C. Boyd, K. S. Oo, E. Maellaro, B. Zhivotovsky, and V. O. Kaminskyy, "Suppressed translation and ULK1 degradation as potential mechanisms of autophagy limitation under prolonged starvation," *Autophagy*, vol. 12, pp. 2085–2097, 2016.

[18] Y. G. Zhao and H. Zhang, "ULK1 cycling: the ups and downs of the autophagy response," *The Journal of Cell Biology*, vol. 215, pp. 757–759, 2016.

[19] F. Nazio, M. Carinci, C. Valacca et al., "Fine-tuning of ULK1 mRNA and protein levels is required for autophagy oscillation," *The Journal of Cell Biology*, vol. 215, pp. 841–856, 2016.

[20] M. Hesse and C. Arenz, "MicroRNA maturation and human disease," *Methods in Molecular Biology*, vol. 1095, pp. 11–25, 2014.

[21] Y. Y. Mo, "MicroRNA regulatory networks and human disease," *Cellular and Molecular Life Sciences*, vol. 69, pp. 3529–3531, 2012.

[22] V. S. Gomase and A. N. Parundekar, "microRNA: human disease and development," *International Journal of Bioinformatics Research and Applications*, vol. 5, pp. 479–500, 2009.

[23] D. Gibbings, S. Mostowy, F. Jay, Y. Schwab, P. Cossart, and O. Voinnet, "Selective autophagy degrades DICER and AGO2 and regulates miRNA activity," *Nature Cell Biology*, vol. 14, pp. 1314–1321, 2012.

[24] S. Quenneville, P. Turelli, K. Bojkowska et al., "The KRAB-ZFP/KAP1 system contributes to the early embryonic establishment of site-specific DNA methylation patterns maintained during development," *Cell Reports*, vol. 2, pp. 766–773, 2012.

[25] D. C. Schultz, K. Ayyanathan, D. Negorev, G. G. Maul, and F. J. Rauscher 3rd, "SETDB1: a novel KAP-1-associated histone H3, lysine 9-specific methyltransferase that contributes to HP1-mediated silencing of euchromatic genes by KRAB zinc-finger proteins," *Genes & Development*, vol. 16, pp. 919–932, 2002.

[26] L. Esteban-Martinez, E. Sierra-Filardi, R. S. McGreal et al., "Programmed mitophagy is essential for the glycolytic switch during cell differentiation," *The EMBO Journal*, vol. 36, pp. 1688–1706, 2017.

[27] W. Li, H. Chen, S. Li, G. Lin, and D. Feng, "Exploring microRNAs on NIX-dependent mitophagy," *Methods in Molecular Biology*, vol. 15, pp. 1–11, 2017.

[28] I. Barde, B. Rauwel, R. M. Marin-Florez et al., "A KRAB/KAP1-miRNA cascade regulates erythropoiesis through stage-specific control of mitophagy," *Science*, vol. 340, pp. 350–353, 2013.

[29] W. Li, X. Zhang, H. Zhuang et al., "MicroRNA-137 is a novel hypoxia-responsive microRNA that inhibits mitophagy via regulation of two mitophagy receptors FUNDC1 and NIX," *The Journal of Biological Chemistry*, vol. 289, pp. 10691–10701, 2014.

[30] F. Jin, Y. Wang, M. Li et al., "MiR-26 enhances chemosensitivity and promotes apoptosis of hepatocellular carcinoma cells through inhibiting autophagy," *Cell Death & Disease*, vol. 8, article e2540, 2017.

[31] Y. Lin, W. Deng, J. Pang et al., "The microRNA-99 family modulates hepatitis B virus replication by promoting IGF-1R/PI3K/Akt/mTOR/ULK1 signaling-induced autophagy," *Cellular Microbiology*, vol. 19, no. 5, 2017.

[32] S. I. Rothschild, O. Gautschi, J. Batliner, M. Gugger, M. F. Fey, and M. P. Tschan, "MicroRNA-106a targets autophagy and enhances sensitivity of lung cancer cells to Src inhibitors," *Lung Cancer*, vol. 107, pp. 73–83, 2017.

[33] S. D'Adamo, O. Alvarez-Garcia, Y. Muramatsu, F. Flamigni, and M. K. Lotz, "MicroRNA-155 suppresses autophagy in chondrocytes by modulating expression of autophagy proteins," *Osteoarthritis and Cartilage*, vol. 24, pp. 1082–1091, 2016.

[34] Y. Chen, S. Wang, L. Zhang et al., "Identification of ULK1 as a novel biomarker involved in miR-4487 and miR-595 regulation in neuroblastoma SH-SY5Y cell autophagy," *Scientific Reports*, vol. 5, article 11035, 2015.

[35] X. Duan, T. Zhang, S. Ding et al., "microRNA-17-5p modulates Bacille Calmette-Guerin growth in RAW264.7 cells by targeting ULK1," *PLoS One*, vol. 10, article e0138011, 2015.

[36] Z. Wang, N. Wang, P. Liu et al., "MicroRNA-25 regulates chemoresistance-associated autophagy in breast cancer cells, a process modulated by the natural autophagy inducer isoliquiritigenin," *Oncotarget*, vol. 5, pp. 7013–7026, 2014.

[37] H. Wu, F. Wang, S. Hu et al., "MiR-20a and miR-106b negatively regulate autophagy induced by leucine deprivation via suppression of ULK1 expression in C2C12 myoblasts," *Cellular Signalling*, vol. 24, pp. 2179–2186, 2012.

[38] Y. Chen, R. Liersch, and M. Detmar, "The miR-290-295 cluster suppresses autophagic cell death of melanoma cells," *Scientific Reports*, vol. 2, p. 808, 2012.

[39] M. Otsuka, Q. Jing, P. Georgel et al., "Hypersusceptibility to vesicular stomatitis virus infection in Dicer1-deficient mice is due to impaired miR24 and miR93 expression," *Immunity*, vol. 27, pp. 123–134, 2007.

[40] X. Chen, H. Yang, X. Zhou, L. Zhang, and X. Lu, "MiR-93 targeting EphA4 promotes neurite outgrowth from spinal cord neurons," *Journal of Molecular Neuroscience*, vol. 58, pp. 517–524, 2016.

[41] Z. P. Ke, P. Xu, Y. Shi, and A. M. Gao, "MicroRNA-93 inhibits ischemia-reperfusion induced cardiomyocyte apoptosis by targeting PTEN," *Oncotarget*, vol. 7, pp. 28796–28805, 2016.

[42] L. Jiang, C. Wang, F. Lei et al., "miR-93 promotes cell proliferation in gliomas through activation of PI3K/Akt signaling pathway," *Oncotarget*, vol. 6, pp. 8286–8299, 2015.

[43] W. Li, Y. Yang, X. Hou et al., "MicroRNA-495 regulates starvation-induced autophagy by targeting ATG3," *FEBS Letters*, vol. 590, pp. 726–738, 2016.

[44] D. Papinski and C. Kraft, "Atg1 kinase organizes autophagosome formation by phosphorylating Atg9," *Autophagy*, vol. 10, pp. 1338–1340, 2014.

[45] D. Papinski, M. Schuschnig, W. Reiter et al., "Early steps in autophagy depend on direct phosphorylation of Atg9 by the Atg1 kinase," *Molecular Cell*, vol. 53, pp. 471–483, 2014.

[46] N. Agrawal, P. V. Dasaradhi, A. Mohmmed, P. Malhotra, R. K. Bhatnagar, and S. K. Mukherjee, "RNA interference: biology, mechanism, and applications," *Microbiology and Molecular Biology Reviews*, vol. 67, pp. 657–685, 2003.

[47] S. M. Elbashir, J. Harborth, W. Lendeckel, A. Yalcin, K. Weber, and T. Tuschl, "Duplexes of 21-nucleotide RNAs mediate RNA interference in cultured mammalian cells," *Nature*, vol. 411, pp. 494–498, 2001.

[48] T. Yonekawa and A. Thorburn, "Autophagy and cell death," *Essays in Biochemistry*, vol. 55, pp. 105–117, 2013.

[49] K. M. Chung and S. W. Yu, "Interplay between autophagy and programmed cell death in mammalian neural stem cells," *BMB Reports*, vol. 46, pp. 383–390, 2013.

[50] R. L. Macintosh and K. M. Ryan, "Autophagy in tumour cell death," *Seminars in Cancer Biology*, vol. 23, pp. 344–351, 2013.

[51] Z. Zou, L. Wu, H. Ding et al., "MicroRNA-30a sensitizes tumor cells to cis-platinum via suppressing beclin 1-mediated autophagy," *The Journal of Biological Chemistry*, vol. 287, pp. 4148–4156, 2012.

[52] H. Zhu, H. Wu, X. Liu et al., "Regulation of autophagy by a beclin 1-targeted microRNA, miR-30a, in cancer cells," *Autophagy*, vol. 5, pp. 816–823, 2009.

[53] S. Comincini, G. Allavena, S. Palumbo et al., "microRNA-17 regulates the expression of ATG7 and modulates the autophagy process, improving the sensitivity to temozolomide and low-dose ionizing radiation treatments in human glioblastoma cells," *Cancer Biology & Therapy*, vol. 14, pp. 574–586, 2013.

[54] K. A. Tekirdag, G. Korkmaz, D. G. Ozturk, R. Agami, and D. Gozuacik, "MIR181A regulates starvation- and rapamycin-induced autophagy through targeting of ATG5," *Autophagy*, vol. 9, pp. 374–385, 2013.

[55] P. Zhang and H. Zhang, "Autophagy modulates miRNA-mediated gene silencing and selectively degrades AIN-1/GW182 in *C. elegans*," *EMBO Reports*, vol. 14, pp. 568–576, 2013.

[56] S. Hazarika, C. R. Farber, A. O. Dokun et al., "MicroRNA-93 controls perfusion recovery after hind-limb ischemia by modulating expression of multiple genes in the cell cycle pathway," *Circulation*, vol. 127, pp. 1818–1828, 2013.

[57] F. Nazio, F. Strappazzon, M. Antonioli et al., "mTOR inhibits autophagy by controlling ULK1 ubiquitylation, self-association and function through AMBRA1 and TRAF6," *Nature Cell Biology*, vol. 15, pp. 406–416, 2013.

Hindawi
Oxidative Medicine and Cellular Longevity
Volume 2017, Article ID 9308310, 13 pages
https://doi.org/10.1155/2017/9308310

Research Article

miR-128 Is Implicated in Stress Responses by Targeting MAFG in Skeletal Muscle Cells

Rocco Caggiano,[1] Fabio Cattaneo,[1,2] Ornella Moltedo,[3] Giovanni Esposito,[2] Cinzia Perrino,[2] Bruno Trimarco,[2] Rosario Ammendola,[1] and Raffaella Faraonio[1,4]

[1]*Dipartimento di Medicina Molecolare e Biotecnologie Mediche, Università di Napoli Federico II, Napoli, Italy*
[2]*Dipartimento di Scienze Biomediche Avanzate, Università di Napoli Federico II, Napoli, Italy*
[3]*Dipartimento di Farmacia, Università degli Studi di Salerno, Fisciano, Salerno, Italy*
[4]*CEINGE-Biotecnologie Avanzate s.c. a r.l, Napoli, Italy*

Correspondence should be addressed to Raffaella Faraonio; faraonio@dbbm.unina.it

Received 4 April 2017; Revised 30 June 2017; Accepted 18 July 2017; Published 12 September 2017

Academic Editor: Jaideep Banerjee

MAFG (v-Maf avian musculoaponeurotic fibrosarcoma oncogene homolog G) is a bZIP-type transcriptional regulator that belongs to the small MAF (sMAFs) protein family. By interacting with other bZIP transcription factors, sMAFs can form homo- and heterodimers governing either repressive or activating transcriptional functions. As heterodimeric partner of Nrf2, MAFG positively influences the ARE-dependent antioxidant/xenobiotic pathways, at least in condition of a correct MAFG:Nrf2 balance. MicroRNAs (miRs) participate to different regulatory networks being involved as fine-tuning regulators of gene expression. However, the connections between cellular surveillance to stresses mediated by MAFG:Nrf2 and miR regulations are not well understood. Here, we explored the impact of miR-128 in expression of genes related to stress response. Bioinformatic predictions coupled with functional analysis revealed the presence of miR-128 binding site in the 3′UTR of MAFG. Ectopic miR-128 expression correlated with reduced expression of endogenous MAFG-dependent genes and negatively affected ARE-mediated molecular phenotype based on Nrf2 activity. Indeed, miR-128 impairs redox-dependent pathways induced in response to oxidative stress. Moreover, in condition of hypoxia, MAFG induction correlated with reduced levels of miR-128. This lead to increased mRNA levels of HMOX-1 and x-CT for blunting stress. Overall, these findings identify MAFG as novel direct target of miR-128.

1. Introduction

In response to oxidative and xenobiotic stresses, cells activate numerous defense systems associated with both enzymatic and not enzymatic activities. The events underlying these redox-related responses are accomplished by a tight regulation of gene expression patterns involving multilayered regulatory mechanisms [1, 2]. Two transcription factors shown to be highly involved in the regulation of numerous antioxidant and detoxifying genes at transcriptional levels are Nrf2 [nuclear factor (erythroid-derived 2)-like 2] [3–5] and MAFG (v-Maf avian musculoaponeurotic fibrosarcoma oncogene homolog G) [6]. In particular, in the form of heterodimer, the complex Nrf2:MAFG binds to and activates the transcription of antioxidant/xenobiotic genes harboring antioxidant responsive elements (ARE)/electrophile responsive elements (core ARE: TGACNNNGC), located in their transcription regulatory sequences [7, 8].

The proteins of the MAF family, described for the first time as a viral oncogene in their prototype v-Maf, are transcription factors, which are widely known to participate in gene expression regulation [9]. The MAF family consists of 7 members, which are grouped into "large" (c-Maf, MafA, MafB, and Nrl) and "small" (MafG, MafK, and MafF) Maf subfamily, based on their size [6]. Each member of the MAF family harbors a basic-leucine zipper (b-ZIP) domain involved in DNA binding and in dimer formation, either with themselves or with different b-ZIP transcription factors, in particular Nrf2 [10, 11]. In addition to the b-ZIP domain, large Maf proteins also possess an acidic transcriptional

activation domain (TAD) that, on the contrary, is absent in the small Mafs (sMafs). For this reason, the regulatory activity of small Mafs on gene transcription can be positive or negative, depending on their specific partner and on the promoter context. In general, homodimers of sMafs lacking TAD (i.e., MafG:MafK) repress gene transcription by binding to the Maf recognition element (MARE: TGCTGACT CAGCA) [6, 12]. The heterodimers with cap 'n' collar (CNC) proteins such as p45 NF-E2 [13] or with NF-E2-related factors (Nrf1, Nrf2, and Nrf3) [14, 15] as well as with the Bach (BTB and CNC homology) factors (Bach1 and Bach2) [16], unlike homodimers, can either function as transcriptional activators or repressors [6]. Among these, as mentioned before, the Nrf2:sMaf heterodimers promote transcription and represent the most relevant means for adjusting a multitude of intracellular protein levels in response to oxidative/electrophilic stresses [5]. Under basal unstressed conditions, Nrf2 is polyubiquitinated and targeted to 26S proteasome by the Kelch-like ECH-associated protein 1(Keap1)-Cul3 E3 ligase complex [17]. Stresses provoke dissociation of Keap1 through modification of specific cysteine residues [18]. Thus, Nrf2 can migrate into the nucleus, where in association with sMaf, in particular MAFG, binds to the promoters of target genes harboring ARE sequences to activate their transcription [8].

sMafs also interact with HIF-1α to positively regulate hypoxic responses [19]. On the other hand, Bach1:sMaf heterodimers act as negative regulator of the HMOX-1 gene and its role is supported by genetic data [20]. In addition, Fang and colleagues recently demonstrated that high MAFG levels driven by BRAF (V600) recruit Bach1 as partner along with CHD8, a chromatin remodeling factor, and DNMT3B, a DNA methyltransferase, to trigger epigenetic silencing of genes frequently hypermethylated in melanoma and colorectal cancer [21].

In the last decades, microRNAs (miRs) have added a new layer of complexity to the regulatory mechanisms underlying gene expression [22, 23]. miRs are small endogenous noncoding RNAs that downmodulate protein expression at posttranscriptional level. By interacting with specific regions, generally localized in the 3′-untranslated regions (UTRs) of transcripts, miRs mediate repression of mRNA translation or stability [24, 25]. Given that each single miR could target multiple transcripts and often a miR regulates several targets of the same pathway, they supervise cellular signaling and networks involved in fundamental biological processes, including stress responses [26–28].

Numerous studies have shown that miR-128 is involved in different cellular processes such as differentiation, apoptosis, senescence, and metabolism [29–32]. Here, we investigated its role in the stress/antioxidant networks regulated by the heterodimeric complex Nrf2:MAFG. We demonstrated that miR-128 by targeting MAFG influences stress responses mediated by ARE-dependent genes.

2. Materials and Methods

2.1. Cell Cultures and Reagents. Human embryonic kidney HEK293 cells and mouse myogenic C2C12 cells were obtained from American Type Culture Collection (ATCC, Manassas, VA, USA). Cells were cultured in Dulbecco's modified Eagle's medium (DMEM) (Thermo Fisher SCIENTIFIC, Italia, Monza, Italy) supplemented with fetal bovine serum (FBS) (Invitrogen) at 10% for HEK293 and 20% for C2C12 cells. To induce differentiation of C2C12 cells, culture medium was replaced to near-confluent cultures (about 90%) with DMEM containing 2% horse serum (Thermo Fisher SCIENTIFIC).

Hypoxia (2% O_2) for 4 h was induced when C2C12 cells were at 85% confluence. After being washed three times with phosphate-buffered saline (PBS), cultures were transferred to a 37°C incubator within a hypoxic chamber (93% N_2, 5% CO_2, 2% O_2), and culture medium was replaced with a saline buffer that was prebubbled for five minutes with the same gas mix, to provide an average O_2 pressure (14.7 mmHg) equivalent to that in the ambient air of the chamber.

Treatments with diethylmaleate (DEM) (Sigma-Aldrich, Milan, Italy) were performed for 2 h (HEK293) or 4 h (C2C12) using a final concentration of 200 μM in complete culture medium.

2.2. Plasmid Constructs and Transfections. The plasmid expressing miR-128 (pCMV-miR-128) was obtained by cloning the human ARPP21 intronic region of 284 bp encompassing the pre-miR-128-2 sequence with 100 bp upstream and downstream flanking sequences into pRcCMVneo vector. This fragment was prepared from human IMR90 DNA by PCR using the following oligonucleotides: 5′-ACgTA AAAgCTTAAgAAggCTATTgACAATCCAg-3′ and 5′-CgA CATATCTAgATTTggTCAgCAggAATgaCAC harboring HindIII and XbaI restriction sites, respectively. The identity of the cloned region was established by digestion and confirmed by sequencing. The expression of mature miR-128 was evaluated by Northern blot (Supplementary Materials available online at https://doi.org/10.1155/2017/9308310) in HEK293 cells and miR-128 levels measured by reverse transcription-quantitative real-time PCR (RT-qPCR).

The luciferase constructs were produced by cloning the 3′ UTR regions with the miR-128 site/s of candidate genes into the pGL3-control vector, downstream the Firefly luciferase gene (Promega, Madison, WI, USA). The 3′UTR fragment of MAFG was amplified by PCR using human IMR90 DNA with primer pairs containing XbaI sites: 5′-ATCATTCTA GAGGATCCATGCAGGCATGCTGGCTCC-3′ and 5′-AT CATTCTAGATTCAAGCTACTATCAGACAATGT-3′. The 3′UTR of Nrf2 was obtained from the full length cDNA (I.M.A.G.E.: 4548874) by using the following primers with Xba sites: 5′-ACGTACTCAGATTTAGGAGGATTTGAC CT-3′ and 5′-ACGTACTCAGATAACAGTCATAATAAT CCTTTATTA-3′. The orientation of the cloned fragments was established by digestion and confirmed by sequencing. The pGL3 constructs with the reverse orientation were used as negative controls. All the plasmids bearing the 3′UTR fragments were transfected in HEK293 cells with Lipofectamine 2000 Reagent (Thermo Fisher SCIENTIFIC) in 24-well plates (40.000 cells/well), according to the manufacturer's instructions, and cotransfected with synthetic pre-miR-128 (ID:

PM1176) or pre-miR-negative control number 1 (100 nM) (Thermo Fisher SCIENTIFIC) as well as with pCMV-miR-128 or pCMVneo (ratio 1 : 5). Transfections of cells with synthetic pre-miR-128 or pre-miR negative control were performed as previously described [33].

The plasmid expressing the FLAG-tagged Nrf2 and the plasmids GSTA1-LUC, x-CT-LUC, and NQO1-LUC bearing the promoters of the respective genes driving the expression of luciferase reporter gene have been described previously [34, 35].

2.3. Luciferase Reporter Assay. The pGL3-3′UTR constructs (100 ng) were cotransfected with the Renilla luciferase reporter plasmid (20 ng) as an internal control using Lipofectamine 2000 (Thermo Fisher SCIENTIFIC) in HEK293 cells in the presence of miR-128 or negative control. Luciferase activity was measured at 24 h after transfection using a dual luciferase reporter assay (Promega) according to the manufacturer's instructions and performed on a $20/20^{n}$ Luminometer (Turner BioSystems, Sunnyvale, CA, USA). Relative luciferase activity was calculated by normalizing the Firefly luminescence to the Renilla luminescence and then calculated relative to the control. C2C12 cells plated in 24-well plates (30.000 cells/well) were cotransfected with the GSTA1-LUC, x-CT-LUC, and NQO1-LUC constructs (500 ng) and FLAG-Nrf2 or empty vector (60 ng) and simultaneously with miR-128 expressing plasmid or empty vector (500 ng) using Lipofectamine® LTX Reagent (Thermo Fisher SCIENTIFIC) according to the manufacturer's instructions. All the transfections also contained a Renilla luciferase construct (40 ng) for internal normalization. Cells were then harvested at 36 h after transfections, and luciferase activity was determined as described above.

2.4. Western Blotting. Total proteins were extracted from transfected cells/treated cells with a buffer containing 0.02 M HEPES (pH 7.9), 0.4 M NaCl, 0.1% NP-40, 10% *v*/*v* glycerol, 1 mM NaF, 1 mM Na_3VO4, and a protease inhibitor cocktail (Sigma-Aldrich). Cytoplasmic and nuclear proteins were fractionated as previously described [34], and cytosolic/nuclear fractions were evaluated by using the antibody of UCHL3 [36]. Cellular protein extracts were loaded on SDS-PAGE, followed by blotting to PVDF membranes. After blocking in nonfat milk solution, membranes were probed with specific primary antibodies (indicated below) and then incubated with horseradish peroxidase-conjugated secondary antibodies for 1 h. Protein bands were visualized using the ECL chemiluminescence system (Amersham, Buckinghamshire, UK).

Murine adductor muscles were homogenized using the program Protein_1 on a gentleMACS tissue Dissociator (Miltenyi Biotec) [37]. Briefly, tissues were lysated in a buffer containing 50 mM Tris-HCl (pH 7.4), 150 mM NaCl, 1% NP-40, 1 mM EDTA, 0.25% sodium deoxycholate, 10 mM NaF, 10 μM Na_3VO4, 1 mM PMSF, and protease inhibitor cocktail (10 g/mg aprotinin, 10 g/ml pepstatin, and 10 g/ml leupeptin). Lysates were centrifuged at 14,000 rpm for 15 min, and protein concentrations were measured using Bio-Rad assay kit (Bio-Rad) and immunoblotting was performed as described [38].

MAFG antibody was from GeneTex (GTX114541); HIF-1α antibody was from Novus Biologicals (NB100-105). Antibody of FLAG M2 was from Sigma-Aldrich. Antibodies of Nrf2 (number SC-13032), BMI-1 (number SC-390443), HMOX-1 (number SC-136960), tubulin (number SC-8035), UCHL3 (number SC-100340), and vinculin (number SC-7649) were from Santa Cruz Biotechnology Inc., Santa Cruz, CA, USA.

2.5. Reverse Transcription-Quantitative Real-Time PCR (RT-qPCR). Total RNA was extracted using TRIzol reagent (Thermo Fisher SCIENTIFIC), and cDNA was synthesized from one μg of RNA using random primers and iScript cDNA synthesis kit (Bio-Rad Laboratories, Hercules, CA, USA). mRNA levels were quantified using IQ SYBR green supermix (Bio-Rad Laboratories) on the CFX96 real-time system instrument (Bio-Rad). Specific primers located in different exons of the same gene were designed to detect relative mRNA levels. The housekeeping β-2 microglobulin or c-ABL genes were used for internal normalization. All the PCR reactions were performed in triplicate, and PCR products were also visualized on agarose gels after ethidium bromide staining. The oligonucleotide sequences are reported in Supplemental Table S2. Relative fold variations were calculated using the $2^{-\Delta\Delta Ct}$ method by the formula: $2^{-(\text{sample}\Delta Ct - \text{control}\Delta Ct)}$, where ΔCt is the difference between the amplification fluorescent thresholds of the gene of interest and the internal reference gene/s used for normalization [39].

To detect the levels of mature miR-128, total RNA was prepared with TRIzol reagent (Thermo Fisher SCIENTIFIC) and miR amounts were evaluated by using the TaqMan miRNA assay kit (Thermo Fisher SCIENTIFIC). For normalization of RNA levels, the amounts of small nucleolar RNA RNU6 (Thermo Fisher SCIENTIFIC) were measured [39].

2.6. Animal Studies. All experiments involving animals were conforming to the Guide for the Care and Use of Laboratory Animals published by the US National Institutes of Health (NIH Publication 8th edition, update 2011) and were approved by the animal welfare regulation of the University of Naples Federico II, Italy. Wild-type C57BL/6 male mice (age 8 to 9 weeks) were included in the study and maintained under identical conditions of temperature (21 ± 1°C), humidity (60 ± 5%), and light/dark cycle and had free access to normal mouse chow.

2.7. Peripheral Ischemia Procedure. Mice were anesthetized with an intraperitoneal injection of 1 ml/kg (50 mg/kg) of a mixture of 50% tiletamine and 50% zolazepam (50 mg/ml tiletamine and 50 mg/ml di zolazepam, Zoletil 100) plus xylazine 5 mg/kg (Sigma-Aldrich). The adequacy of anaesthesia was confirmed by the absence of reflex response to foot squeeze. Hindlimb ischemia was induced as previously described (PI, $n = 7$) [40]. Briefly, the proximal and distal portions of the left femoral artery were ligated and arteriectomy was performed between these two sites. Mice were laid

on a heating pad (37°C) under anaesthesia, and their blood flow was measured by a laser Doppler perfusion imager (Perimed, Periscan, USA) in the ischemic and nonischemic limbs before and 0 and 4 hours after surgery, to confirm vascularization impairment after the procedure. SHAM-operated animals underwent the same procedure without femoral artery ligation (SHAM, $n = 4$). All SHAM-operated controls and all mice subjected to peripheral ischemia (PI) survived.

2.8. Statistical Analysis. For the statistical analyses, the Student's *t*-test was used; data were considered significant at a value of $p < 0.05$.

3. Results

3.1. MAFG Is a Novel Direct Target of miR-128. A previous study of Venkataraman et al. reports that miR-128 promotes intracellular ROS increases [31]. Given that Nrf2 signaling is the main driver of the transcriptional program inducing the expression of a wide range of antioxidant genes [3–5], we hypothesized that miR-128 would affect this regulatory pathway. Thus, we used in silico prediction programs to search for putative targets of miR-128 among the components of Nrf2 pathway. TargetScan, miRanda, and RNAhybrid algorithms predicted conserved seed region/s of miR-128 in the 3′UTRs of Nrf2 and MAFG as well as on the Nrf2-regulated gene x-CT (Supplemental Table S1). Since Nrf2 and MAFG are transcription factors and both implicated in the activation of ARE-dependent transcription [8], we performed further analyses on these genes. To assess whether Nrf2 and MAFG are direct targets of miR-128, the entire 3′UTR of Nrf2 and a region encompassing the mir-128 seed sequence of MAFG (250 bp) were cloned into the pGL3-vector downstream of the luciferase gene. Moreover, to validate specificity of miR-128 interaction with 3′UTRs, mutant reporter constructs (mut) harboring the same regions cloned in the opposite orientation were prepared. Figure 1(a) shows that ectopic expression of synthetic pre-miR-128 slightly decreases the luciferase activity of the construct harboring the 3′UTR region (wt) of Nrf2 in HEK293 cells. In the same conditions, miR-128 overexpression however significantly ($p < 0.05$) reduced the activity of the reporter construct bearing the wild-type 3′UTR (wt) of MAFG compared to miR-SCR-transfected cells (Figure 1(b)). Conversely, mutant MAFG reporter construct (mut) did not respond to miR-128 increases (Figure 1(b)).

To set up a more physiological miR-128 hyperexpression, we also prepared a construct (pCMV-miR-128) that drives miR-128 overexpression from the ARPP21 genomic region (see Materials and Methods). We confirmed that ectopic expression of miR-128 through pCMV-miR-128 (of about 100 folds at 24 h posttransfection, Supplemental Figure S1) in HEK293 cells indeed reduced the luciferase activity of the MAFG-3′UTR reporter construct while there was no effect on the Nrf2-3′UTR construct, very similar to the results obtained with synthetic pre-miR-128 (data not shown).

To validate the above results on the expression of endogenous MAFG protein, we next performed Western blotting analysis on extracts from HEK293 cells transfected for 24 h either with synthetic pre-miR-128 or with pCMV-miR-128. Figure 1(c) shows that endogenous protein levels of MAFG are significantly reduced in condition of miR-128 overexpression, compared to the negative control-transfected cells. In the same conditions, the downregulation of BMI-1 protein levels, a known miR-128 target, is also detected (Figure 1(c)).

We also observed that miR-128 hyperexpression correlates with MAFG downregulation (Supplemental Figure S2) in physiological/pathological conditions, like differentiation of mouse C2C12 myoblasts [41, 42] or atrophic stimulation of differentiated C2C12 [43]. Taken together, the above reported results suggest that miR-128 represses the expression of the MAFG protein.

3.2. miR-128 Influences the Basal Expression of Some MAFG-Regulated Genes. Following the observation that MAFG is negatively regulated by miR-128, we aimed to test the effects of miR-128 on MAFG-dependent transcriptional activity. To this end, we examined the mRNA levels of various MAFG-regulated genes [15, 44] such as AKR1D1, ALDH3, CCDC53, HMOX-1, Nrf2, PCBD2, and UCHL1 upon miR-128 hyperexpression (Figure 2(a)). The results show that in HEK293 cells, the basal expression of AKR1D1, ALDH3, and PCBD2 genes was reduced in conditions of miR-128 overexpression. These results further support a role of miR-128 in the regulation of a set of MAFG-dependent genes.

MAFG is a known basic leucine zipper (bZIP) protein that was shown to interact with other transcription factors, in particular with Nrf2 to activate the expression of numerous genes [7, 15]. Furthermore, MAFG could enhance nuclear retention of Nrf2 [45]. Therefore, we next determined whether the Nrf2 levels are influenced by miR-128 overexpression. Nrf2 is present at very low levels in the cells; thus to stabilize its levels, we exposed wild-type HEK293 and transfected HEK293 cells to low concentration of diethylmaleate (DEM), a glutathione depleting agent [46], for 2 h before harvesting. Western blotting analysis was used to detect the endogenous Nrf2 protein levels after exposure to DEM (Figure 2(b)). In HEK293 control cells, Nrf2 was found substantially increased in the cytosol and also weakly enhanced in the nucleus by DEM exposure. In the same conditions of treatments, cells transfected with miR-128 did not result in reduced accumulation/translocation of Nrf2 compared to cells transfected with empty vector. These results are also in line with the data obtained by 3′UTR luciferase assays that demonstrated that miR-128 is not involved in Nrf2 posttranscriptional regulation.

Since miR-128 has site/s in the 3′UTR of MAFG conserved among mammals (Supplemental Table 1) and since targets of miRNA are cell-type specific, we also examined the effect of miR-128 on the expression of endogenous mouse MAFG using the mouse myogenic C2C12 cell line. The results showed that ectopic expression of miR-128 also promotes downregulation of MAFG protein in the mouse context (Figure 2(c)). In the same conditions, as expected, BMI-1 protein levels were downregulated. In parallel, we evaluated whether the changes observed for MAFG-

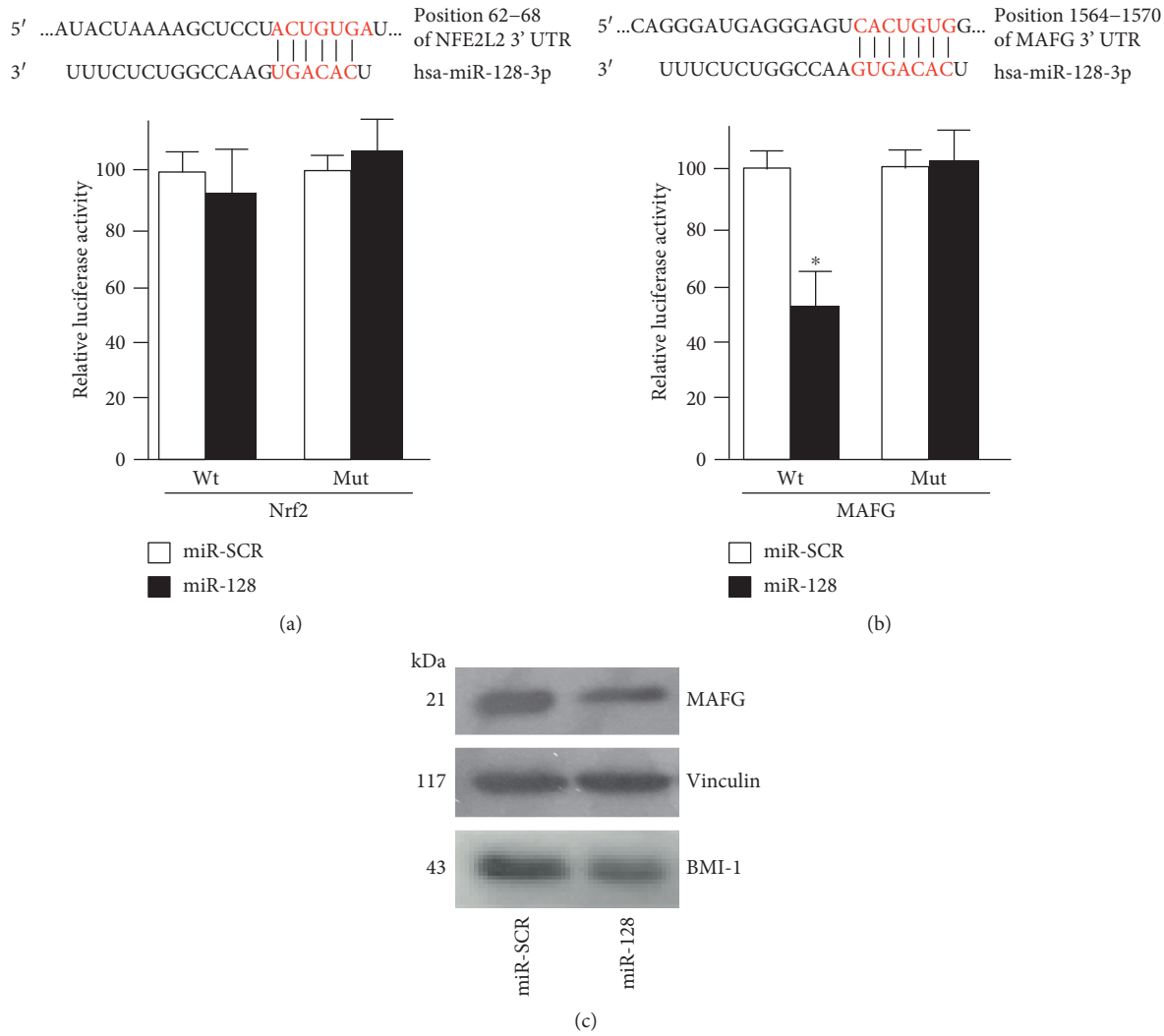

Figure 1: Validation of miR-128 targets by luciferase assay in HEK293 cells. (a) HEK293 cells were transiently transfected with the luciferase construct bearing wild-type (wt) or inverted (mut) 3′UTR fragment holding putative miR-128 target sites of human Nrf2. The alignment of miR-128 with Nrf2-3′UTR is indicated at the top. Cells were simultaneously transfected with either 100 nM of pre-miR-128 (miR-128) or pre-miR negative control (miR-SCR). The pRLSV40 encoding Renilla luciferase plasmid was used as an internal control. Dual luciferase assays were performed as described in the Materials and Methods. Transfections were performed in triplicate, and the ratio (±SD) Firefly/Renilla luciferase activity from three independent experiments were averaged and expressed as percentage of the respective transfections performed with miR-SCR control. $^{*}p < 0.05$. (b) Luciferase constructs containing wild-type (wt) or mutated (mut) 3′UTR of MAFG with predicted miR-128 site (indicated on the top) were cotransfected with either 100 nM of pre-miR-128 (miR-128) or pre-miR negative control (miR-SCR) in HEK293 cells and luciferase activity quantified as described in (a). $^{*}p < 0.05$. (c) Western blotting analysis of MAFG and BMI-1 levels on total proteins from HEK293 cells transfected for 24 h with either 100 nM of pre-miR-128 (miR-128) or pre-miR negative control (miR-SCR); vinculin was used as a loading control.

dependent genes in HEK293 are also present in mouse C2C12 after miR-128 overexpression. As shown in Figure 2(d), the basal mRNA levels of AKR1D1, ALDH3, and UCHL1 genes were reduced in conditions of miR-128 hyperexpression. These results support a role of miR-128 in the regulation of MAFG protein levels and of MAFG-dependent genes also in mouse contexts.

3.3. Ectopic Expression of miR-128 Influences the Expression of an Array of ARE-Dependent Genes. MAFG as bZIP protein interacts with Nrf2 to facilitate its binding to the ARE consensus within the regulatory regions of numerous cytoprotective genes. To determine whether MAFG down-regulation through miR-128 also affects the basal transcription of an array of genes that are typically regulated by the Nrf2:MAFG heterodimer [8, 11], we examined the mRNA levels of representative genes such as GCLC, GSTA-1, NQO1, x-CT, and SQSTM1 in C2C12 cells overexpressing miR-128. The mRNA levels of Nrf2 and $p21^{WAF1}$ were used as controls, since it has been demonstrated that these genes are not dependent on MAFG regulation [8]. As shown in Figure 3(a), the mRNA levels of GCLC, NQO1, and SQSTM1 were significantly ($p < 0.05$) downregulated in C2C12 cells, whereas other Nrf2 target genes such as x-CT and GSTA-1

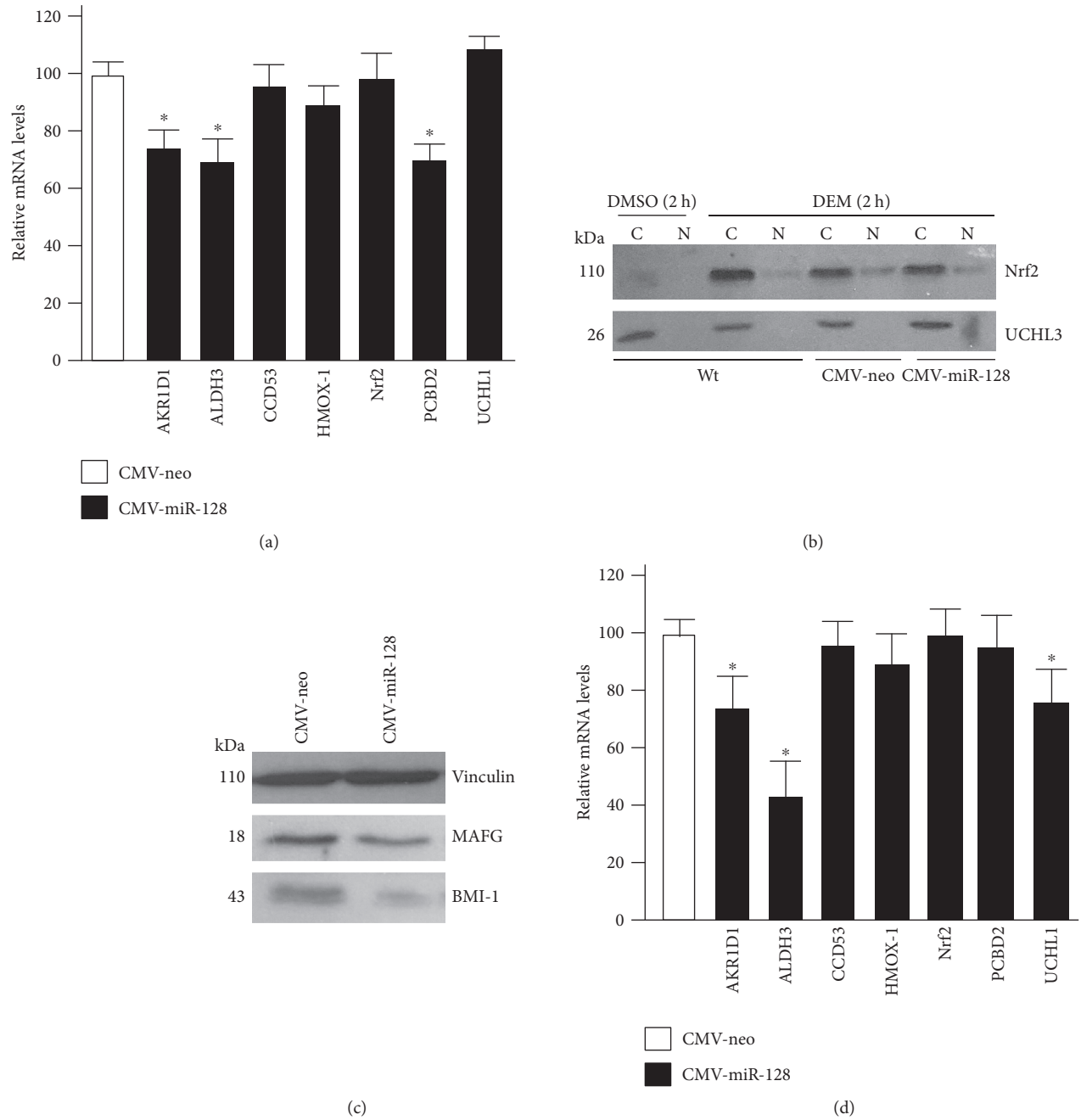

Figure 2: miR-128 downregulates the expression of MAFG and MAFG-regulated genes in human and mouse contexts. (a) HEK293 cells were transfected with either CMV-miR-128 construct or negative control vector (CMV-neo). After 24 h, total RNAs were isolated and the relative mRNA levels of the indicated genes were calculated through quantitative real-time PCR by comparing the levels associated to miR-128 expressing- versus CMV-neo control cells, after normalization with c-ABL. Data were reported as relative to the vector control, which was set equal to 100. Each column in the panel represents the mean ± SD of 3 independent experiments. $^*p < 0.05$. (b) HEK293 cells were transfected with either pre-CMV-miR-128 or negative control (CMV-neo). After 22 h, cells were treated for 2 h with 200 μM DEM. Untransfected HEK293 cells were used as positive control for DEM treatment. Nrf2 protein levels were determined by Western blotting on cytosolic [C] and nuclear [N] extracts. UCHL3 was used as a control of extract preparations. (c) CMV-neo or CMV-miR-128 were transiently transfected into C2C12 cells for 30 h, and Western blotting analysis of MAFG and BMI-1 was performed on total protein extracts; vinculin was used as a loading control. (d) mRNA levels of AKR1D1, ALDH3, CCDC53, HMOX-1, Nrf2, PCBD2, and UCHL1 genes were analyzed as described in (a) at 30 h after transfection in C2C12 cells. Each column in the panel represents the mean ± SD of at least 3 independent experiments. $^*p < 0.05$.

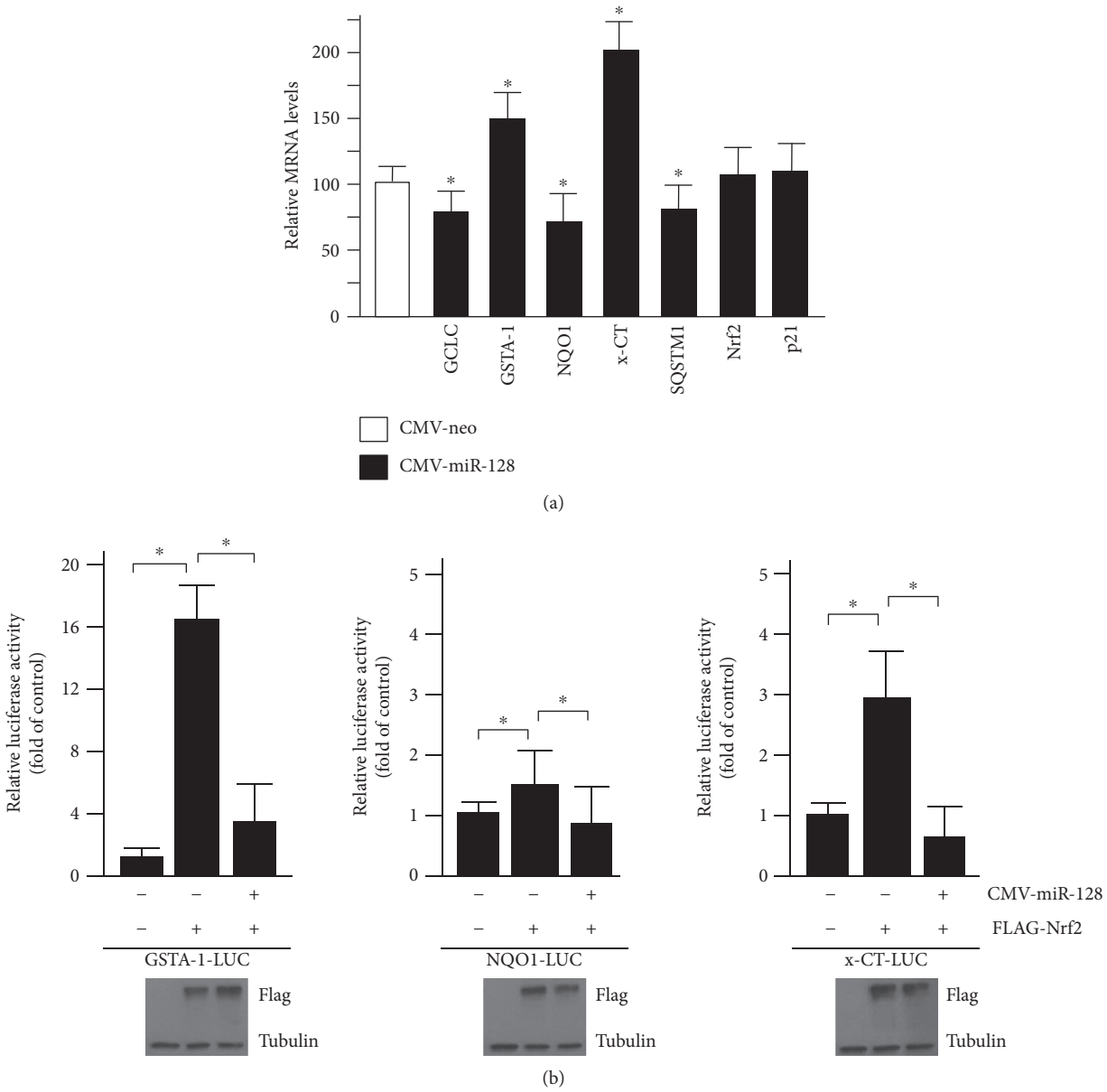

Figure 3: miR-128 provokes modifications of ARE-dependent genes at basal levels and impairs Nrf2 activity. (a) Analysis of GCLC, GSTA-1, NQO1, x-CT, SQSTM1, Nrf2, and p21WAF1 expression in C2C12 cells by RT-qPCR after miR-128 overexpression. mRNA levels in miR-128-transfected cells are expressed as percentage of the levels found in cells transfected with CMV-neo, after normalization with the c-ABL. Each column represents the mean ± SD of 3 independent experiments of transfections. $^{*}p < 0.05$. (b) The promoter regions of GSTA-1 (GSTA1-LUC) or NQO1 (NQO1-LUC) or x-CT (x-CT-LUC) containing ARE motifs cloned into PGL3 basic vector were transiently cotransfected with pRLSV40 encoding Renilla luciferase, in the presence or absence of miR-128 expressing vector. They were also cotransfected with FLAG-Nrf2 or with equivalent amount of empty plasmid, as indicated. 30 h after transfections, the Firefly/Renilla luciferase activities were assessed and the values were reported as relative to the luciferase activities obtained with the respective LUC construct, which were set equal to 1. The results are representative of three independent experiments, each performed in triplicate. $^{*}p < 0.05$. Representative Western blotting of FLAG-Nrf2 overexpression is also presented. Tubulin protein levels were used as loading controls.

were upregulated. These findings indicate that protein reduction of MAFG following miR-128 overexpression influences the basal expression of some ARE-dependent genes in C2C12 cells. The above results also suggest that lowered basal expression of GCLC and NQO1 after miR-128 overexpression could explain the ROS increase observed by other authors [31].

Increased levels of Nrf2:MAFG heterodimer activate the transcription of a wide variety of genes containing ARE sequences in their promoters [8]. Therefore, we analyzed the ability of miR-128 to influence the Nrf2 activity on ARE regulatory regions of selected genes. To this aim, we used luciferase reporter constructs, namely, GSTA1-LUC, NQO1-LUC, and x-CT-LUC [34, 35], that in conditions of Nrf2

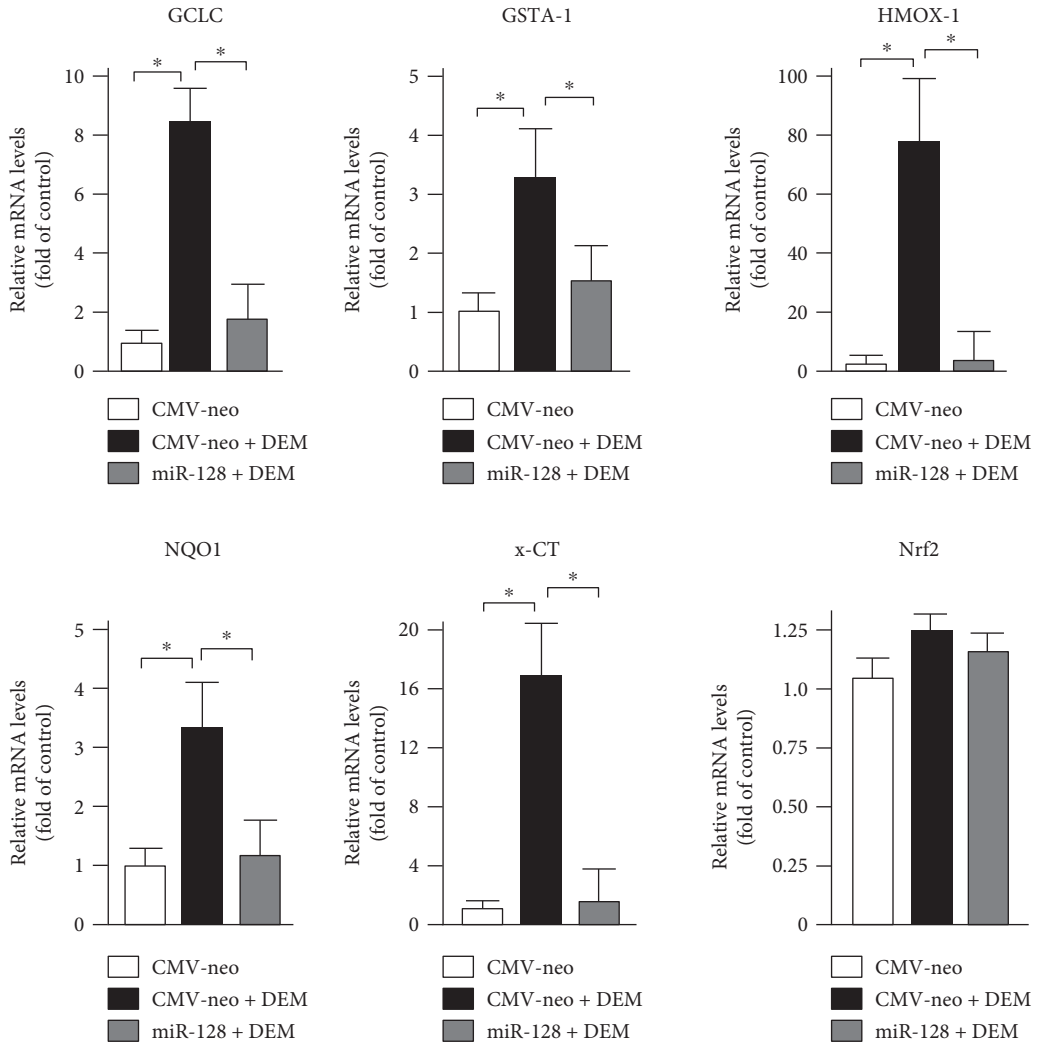

Figure 4: miR-128 interferes with the DEM-mediated induction of ARE-dependent genes. C2C12 cells were transiently transfected with miR-128 expressing construct or with an equivalent amount of empty plasmid. 36 h after transfections, the cells were treated for 3 h with 200 μM DEM and then harvested. The mRNA levels of GCLC, GSTA-1, HMOX-1, NQO1, x-CT, and Nrf2 genes were determined by RT-qPCR on total RNA after normalization with the c-ABL mRNA level. Data are expressed as relative to the values obtained upon transfection with CMV-neo control in the absence of DEM, which were set equal to 1. Each column in the panels represents the mean ± SD of 3 independent experiments. $^*p < 0.05$.

overexpression strongly induce luciferase activity [34, 35]. Thus, the above LUC constructs were cotransfected in C2C12 cells along with a construct expressing FLAG-Nrf2 or with empty vector, in the absence or presence of miR-128. As shown in Figure 3(b), the luciferase activity driven by the regulatory regions of x-CT and GSTA-1 genes is highly induced after ectopic expression of Nrf2, compared with the control vector, and these effects are completely abolished by the overexpression of miR-128. Even though the Nrf2-mediated activation of NQO1-LUC was less prominent, miR-128 significantly weakened this induction (Figure 3(b)). The expression of ectopic Nrf2 was validated by Western blotting analysis with anti-FLAG antibody.

These results suggested that miR-128 counteracts the Nrf2-mediated induction of ARE-dependent promoters through MAFG downmodulation. The differences observed between the ARE-responsive regions (Figure 3(b)) and the mRNA levels of endogenous GSTA-1 and x-CT (Figure 3(a)) genes could be due to the contributions of additional regulatory regions/transcription factors in the chromatin contexts.

3.4. miR-128 Interferes with the DEM-Mediated Induction of ARE-Dependent Genes. The effects described above led us to investigate whether a reduced expression of endogenous MAFG through miR-128 could result in dysregulation of endogenous stress responses. We selected a group of genes that are responsive to oxidative stress induced by DEM, a well-known inducer of ROS accumulation, by taking advantage of a published list of genes that are responsive to this agent in mouse context [8]. C2C12 cells were transfected with miR-128 or control vectors for 36 h and then exposed to DEM. RT-qPCR analysis was used to determine transcript levels of a small set of ARE-dependent genes,

namely, GCLC, GSTA-1, HMOX-1, NQO1, and x-CT. As shown in Figure 4, upon DEM treatments, the endogenous mRNA levels of these genes are strongly induced in C2C12 cells transfected with CMV-neo. In the same conditions of treatments, miR-128 overexpression significantly decreased the DEM-mediated induction of the above genes, when compared to control-transfected cells. In conclusion, miR-128 by downregulating MAFG antagonizes the expression of ARE-dependent genes. The mRNA levels of Nrf2 transcripts, used as control gene, were unaffected [8].

3.5. miR-128 Downmodulation Regulates MAFG Increase in Hypoxic Condition Both In Vitro and In Vivo. Given that MAFG regulates hypoxic responses by interacting with HIF-1α [19], we examined the involvement of miR-128-MAFG axis in C2C12 cell responses to hypoxia. First, we estimated the endogenous levels of miR-128 after exposure to hypoxia (2% O_2) for 4 h. RT-qPCR analysis for mature miR-128 amounts showed significant ($p < 0.05$) decreased levels of miR-128 after hypoxia in C2C12 (Figure 5(a)). To test whether the observed miR-128 changes influence, also MAFG protein levels, we performed Western blotting analysis of MAFG and HMOX-1, which is a common target of HIF-1α and Nrf2 transcription factors. The results show that the protein levels of HMOX-1, as expected, are induced following treatment of C2C12 cells within 4 h of low O_2. Importantly, at the same time, we observed an increase of MAFG protein, which correlates with an enhanced HIF-1α expression (Figure 5(b)).

Since hypoxia induces ROS production, we also measured the mRNA levels of selected ARE-regulated genes such as HMOX-1 and x-CT. In this condition, the mRNA levels of these genes are strongly induced after exposure of C2C12 cells to hypoxia (Figure 5(c)). These results indicate that miR-128 downregulation could be important for adjusting the MAFG levels necessary for both HIF-1α transactivation and ARE-dependent gene induction in hypoxic conditions *in vitro*.

Finally, we analyzed the role of miR-128-MAFG axis in the ischemic process in vivo. We induced peripheral ischemia (PI) by femoral artery ligation for 4 h in C57BL/6J mice ($n = 4$). Sham-operated animals ($n = 3$) underwent the same surgical procedures without ligation of femoral artery. Hindlimb blood flow was analyzed by ecolordoppler pre- and 4 h after surgical procedures (Figure 5(d)). Western blotting experiments show that MAFG protein levels are significantly induced in the hindlimb muscle lysates (Figure 5(e)). We also investigated whether the upregulated levels of MAFG are inversely correlated to miR-128 amounts. RT-qPCR analysis for mature miR-128 levels show a significant decrease of miR-128 levels (Figure 5(f)).

Overall, these results indicate that miR-128-MAFG axis is an important contributor for responses to hypoxia both *in vitro* and *in vivo*.

4. Discussion

miRs play crucial roles in the regulation of gene expression. miRs are considered primarily "fine-tuning" regulators of protein activities, and thus they could balance the antioxidant responses. Recent studies indeed indicate that many miRs called redoximiRs can be either direct or indirect effectors of redox-related pathways [47]. In particular, several evidences demonstrate that, on one hand, Nrf2 itself can be a direct target of miRs and that, on the other hand, Nrf2 modulators, such as Keap1 and Bach1, can be regulated by miRs [5, 48–51]. The transcription factor Nrf2 participates in the adaptive responses to oxidative stress by enhancing transcription of many genes encoding antioxidant/detoxification enzymes, and impaired Nrf2 functions decrease tolerance to oxidative/chemical insults [5].

Herein, we identified a new function of miR-128 as redoximiR, which has a direct role in suppressing MAFG expression. Based on complementary screening for MAFG-dependent genes as well as for ARE-dependent genes functioning through Nrf2:MAFG heterodimer or Nrf2-regulated genes, we demonstrate that miR-128 interferes with the induction of a group of selected genes, namely, GCLC, GSTA-1, HMOX-1, NQO1, and x-CT under oxidative stress. In fact, MAFG acts as positive partner of Nrf2 and its downmodulation by miR-128 consequently affects the Nrf2/ARE pathway.

Deregulated redox signaling and diminished antioxidant defenses represent a major cause of pathophysiological processes including cardiovascular and neurodegenerative diseases, cataracts, diabetes, and cancers, most of which are age related. Therefore, pharmacological/natural strategies addressed to an increase of Nrf2 activity could be beneficial for preventing oxidative stress-related diseases [52–55].

Hypoxia is known to produce ROS, suggesting a cross-talk between HIF-1α and the Nrf2 pathways [56]. Since MAFG is related to both of these signalings, we also analyzed the involvement of miR-128 in hypoxic responses. Our results indicate that miR-128-MAFG axis significantly contribute in responses to hypoxia in C2C12 cells and the decrease of miR-128 is parallel with MAFG induction, which consequently could affect MAFG-related genes such as HMOX-1 and x-CT. Of note, the responses observed *in vitro* are also observed during the ischemic process *in vivo*.

Several studies demonstrate the involvement of miR-128 in different cellular processes such as differentiation, apoptosis, senescence, and metabolism [29–32]. Furthermore, miR-128 is found downregulated under hypoxic conditions in human trophoblasts [57] and a recent study implicates a protective role *in vivo* of miR-128 inhibition during myocardial I/R injury [58]. We demonstrate that mir-128 is involved in the modulation of the antioxidant responses *in vitro* as well as in ischemic condition both *in vitro* and *in vivo*. Indeed, repression of miR-128 parallels with MAFG increases that consequently could affect MAFG-related genes such as HMOX-1 and x-CT. Our findings further suggest that downmodulation of miR-128 might contribute to the coordination of the adaptive hypoxic reprogramming that among many others involves genes that are dependent on MAFG, now considered a regulatory hub for numerous transcription factors [8, 15, 19].

Ischemic cardiovascular diseases are a leading cause of morbidity and mortality in developed countries [59]. Even though the detrimental role of ROS generated during ischemia

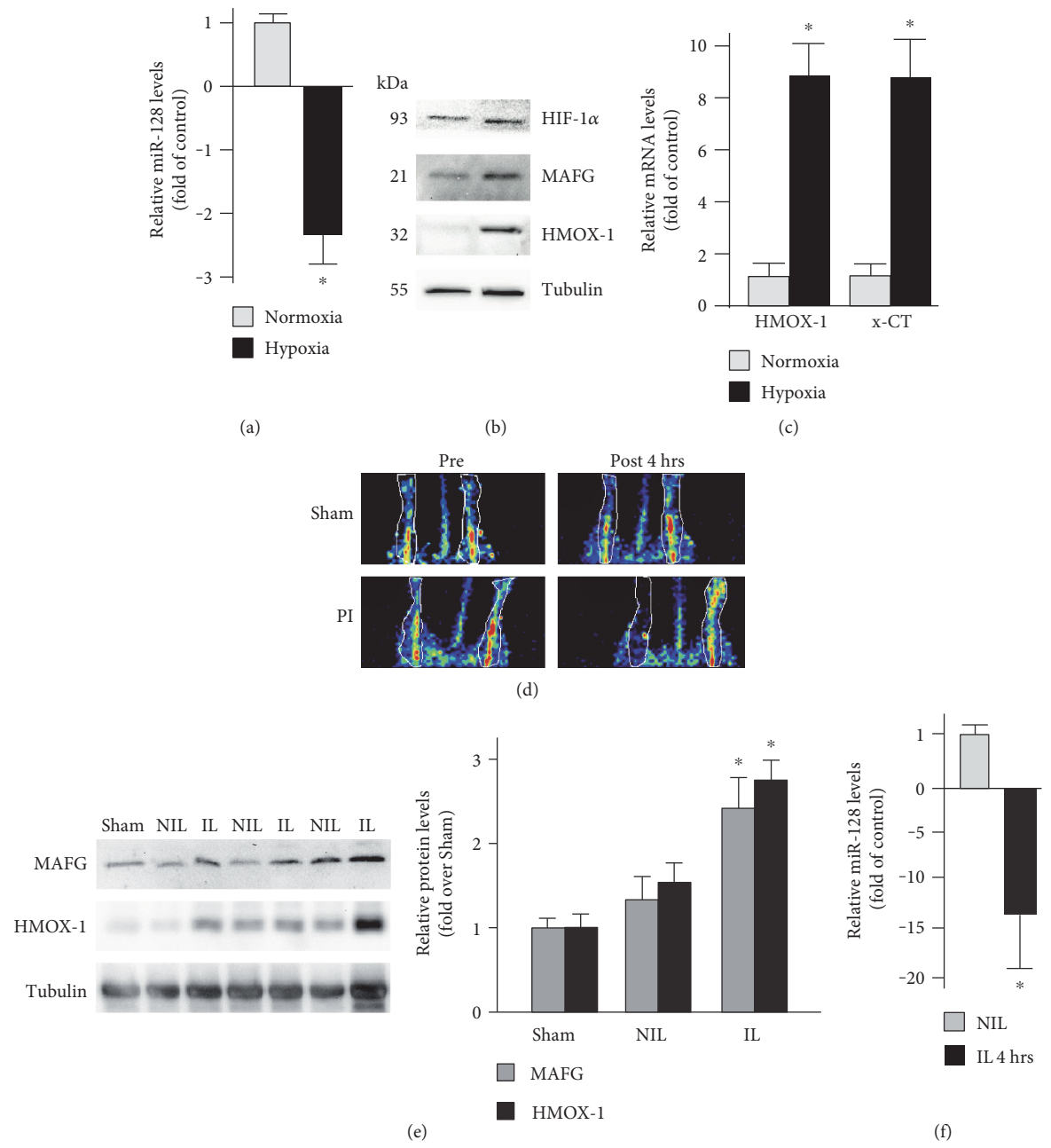

Figure 5: miR-128 downmodulation regulates MAFG increase in hypoxic condition both *in vitro* and *in vivo*. C2C12 cells were exposed to hypoxia (2% O2) for 4 h, and miR-128 levels (a) were determined by RT-qPCR on total RNAs after normalization with the small RNU6. Data are expressed as relative to the values obtained in untreated control which were set equal to 1. Each column in the panels represents the mean ± SD of 3 independent experiments. $^{*}p < 0.05$. Western blotting analysis (b) of HIF-1α, MAFG, and HMOX-1 was performed on total extracts from the same cells, as described in Materials and Methods. Tubulin was used as a loading control. mRNA levels of HMOX-1 and x-CT genes (c) were determined by RT-qPCR on total RNAs, and relative changes were calculated by comparing treated cells versus control, after normalization with c-ABL. Data were reported as relative to the values obtained in normoxia, which were set equal to 1. Each column in the panel represents the mean ± SD of 3 independent experiments. $^{*}p < 0.05$. Representative laser Doppler analysis (d) of blood flow before and 4 hours after (post 4 h) hindlimb ischemia procedure ($n = 3$-4 mice/group). Representative Western blot analysis and densitometric analysis (e) of MAFG and HMOX-1 protein levels performed on hindlimb muscle lysates from littermates after sham procedure (sham) or not-ischemic limb (NIL) and ischemic limb (IL) 4 h after femoral artieriectomy. Tubulin protein levels were used as loading controls ($^{*}p < 0.05$ versus sham; $n = 3$-4 hindlimb/group). miR-128 levels (f) were determined by RT-qPCR on total RNAs after normalization with the small RNU6. The values obtained in not-ischemic limb (NIL) were set equal to 1. The data are expressed as the mean ± standard error and are representative of 3 independent experiments. $^{*}p < 0.05$.

is well demonstrated, an effective antioxidant therapy is still far to be determined. Many studies indeed indicate that Nrf2 protects against cardiovascular diseases albeit reductive conditions also generate ROS (reviewed in [60, 61]). In this context, our work highlights a novel possibility to manage the activities of the Nrf2 signal by miR-128, alone or in combination with other pharmacologic strategies, that in future studies can be considered.

miR-128 has been detected in plasma and its levels are altered in various pathological conditions [62–64], but further studies are required to better clarify the potential role of mir-128 levels as new prognostic and/or diagnostic marker in cardiovascular ischemic diseases.

Abbreviations

ALDH1A1: Aldehyde dehydrogenase 1A1
ARE: Antioxidant-responsive element
AKR1D1: Aldo-keto reductase family 1, member D1
ALDH3A1: Aldehyde dehydrogenase 3 family member A1
CCDC53: Coiled-coil domain containing 53
HMOX-1/HO-1: Heme oxygenase-1
PCBD2: Pterin-4 alpha-carbinolamine dehydratase 2
BACH: BTB and CNC homology
bZIP: Basic-region leucine zipper
CHD8: Chromo-ATPase/helicase DNA-binding protein 8
CNC: Cap 'n' collar
DNMT3B: DNA methyltransferase 3 beta
EpRE: Electrophile-responsive element
GCLC: Glutamate-cysteine ligase catalytic
GST: Glutathione S-transferase
HIF-1α: Hypoxia inducible factor 1 alpha subunit
Keap1: Kelch-like ECH-associated protein 1
miR: MicroRNA
Nrf2/NF-E2: Nuclear factor-erythroid 2
NQO1: NAD(P):Quinone oxidoreductase 1
NRF: NF-E2 p45-related factor
PCR: Polymerase chain reaction
PVDF: Polyvinylidene difluoride
RT-qPCR: Reverse transcription-quantitative real-time PCR
ROS: Reactive oxygen species
sMaf: Small Maf (musculoaponeurotic fibrosarcoma retrovirus transforming gene)
UCHL1: Ubiquitin C-terminal hydrolase L1
UTR: Untranslated region.

Conflicts of Interest

The authors declare that they have no conflicts of interest.

Authors' Contributions

Rocco Caggiano and Fabio Cattaneo contributed equally to this work.

Acknowledgments

This study was supported by the Ministero dell'Università e della Ricerca Scientifica e Tecnologica (MiUR PRIN 2009).

References

[1] K. M. Holmstrom and T. Finkel, "Cellular mechanisms and physiological consequences of redox-dependent signalling," *Nature Reviews Molecular Cell Biology*, vol. 15, no. 6, pp. 411–421, 2014.

[2] Y. Mikhed, A. Görlach, U. G. Knaus, and A. Daiber, "Redox regulation of genome stability by effects on gene expression, epigenetic pathways and DNA damage/repair," *Redox Biology*, vol. 5, pp. 275–289, 2015.

[3] L. Baird and A. T. Dinkova-Kostova, "The cytoprotective role of the Keap1-Nrf2 pathway," *Archives of Toxicology*, vol. 85, no. 4, pp. 241–272, 2011.

[4] J. D. Hayes and A. T. Dinkova-Kostova, "The Nrf2 regulatory network provides an interface between redox and intermediary metabolism," *Trends in Biochemical Sciences*, vol. 39, no. 4, pp. 199–218, 2014.

[5] C. Espinosa-Diez, V. Miguel, D. Mennerich et al., "Antioxidant responses and cellular adjustments to oxidative stress," *Redox Biology*, vol. 6, pp. 183–197, 2015.

[6] F. Katsuoka and M. Yamamoto, "Small Maf proteins (MafF, MafG, MafK): history, structure and function," *Gene*, vol. 586, no. 2, pp. 197–205, 2016.

[7] F. Katsuoka, H. Motohashi, T. Ishii, H. Aburatani, J. D. Engel, and M. Yamamoto, "Genetic evidence that small maf proteins are essential for the activation of antioxidant response element-dependent genes," *Molecular and Cellular Biology*, vol. 25, no. 18, pp. 8044–8051, 2005.

[8] Y. Hirotsu, F. Katsuoka, R. Funayama et al., "Nrf2-MafG heterodimers contribute globally to antioxidant and metabolic networks," *Nucleic Acids Research*, vol. 40, no. 20, pp. 10228–10239, 2012.

[9] G. P. Sykiotis and D. Bohmann, "Stress-activated cap'n'collar transcription factors in aging and human disease," *Science Signaling*, vol. 3, no. 112, article re3, 2010.

[10] K. Itoh, T. Chiba, S. Takahashi et al., "An Nrf2/small Maf heterodimer mediates the induction of phase II detoxifying enzyme genes through antioxidant response elements," *Biochemical and Biophysical Research Communications*, vol. 236, no. 2, pp. 313–322, 1997.

[11] A. Otsuki, M. Suzuki, F. Katsuoka et al., "Unique cistrome defined as CsMBE is strictly required for Nrf2-sMaf heterodimer function in cytoprotection," *Free Radical Biology and Medicine*, vol. 91, pp. 45–57, 2016.

[12] T. Q. de Aguiar Vallim, E. J. Tarling, H. Ahn et al., "MAFG is a transcriptional repressor of bile acid synthesis and metabolism," *Cell Metabolism*, vol. 21, no. 2, pp. 298–310, 2015.

[13] R. Fujita, M. Takayama-Tsujimoto, H. Satoh et al., "NF-E2 p45 is important for establishing normal function of platelets," *Molecular and Cellular Biology*, vol. 33, no. 14, pp. 2659–2670, 2013.

[14] Y. Zhang and Y. Xiang, "Molecular and cellular basis for the unique functioning of Nrf1, an indispensable transcription factor for maintaining cell homoeostasis and organ integrity," *Biochemical Journal*, vol. 473, no. 8, pp. 961–1000, 2016.

[15] F. Katsuoka, H. Yamazaki, and M. Yamamoto, "Small Maf deficiency recapitulates the liver phenotypes of Nrf1- and Nrf2-deficient mice," *Genes to Cells*, vol. 21, no. 12, pp. 1309–1319, 2016.

[16] Y. Zhou, H. Wu, M. Zhao, C. Chang, and Q. Lu, "The Bach family of transcription factors: a comprehensive review," *Clinical Reviews in Allergy & Immunology*, vol. 50, no. 3, pp. 345–356, 2016.

[17] D. D. Zhang and M. Hannink, "Distinct cysteine residues in Keap1 are required for Keap1-dependent ubiquitination of Nrf2 and for stabilization of Nrf2 by chemopreventive agents and oxidative stress," *Molecular and Cellular Biology*, vol. 23, pp. 8137–8151, 2003.

[18] A. T. Dinkova-Kostova, R. V. Kostov, and P. Canning, "Keap1, the cysteine-based mammalian intracellular sensor for electrophiles and oxidants," *Archives of Biochemistry Biophysics*, vol. 617, pp. 84–93, 2017.

[19] K. Ueda, J. Xu, H. Morimoto, A. Kawabe, and S. Imaoka, "MafG controls the hypoxic response of cells by accumulating HIF-1alpha in the nuclei," *FEBS Letters*, vol. 582, no. 16, pp. 2357–2364, 2008.

[20] J. Sun, H. Hoshino, K. Takaku et al., "Hemoprotein Bach1 regulates enhancer availability of heme oxygenase-1 gene," *The EMBO Journal*, vol. 21, no. 19, pp. 5216–5224, 2002.

[21] M. Fang, L. Hutchinson, A. Deng, and M. R. Green, "Common BRAF(V600E)-directed pathway mediates widespread epigenetic silencing in colorectal cancer and melanoma," *Proceedings of the National Academy of Sciences of the United States of America*, vol. 113, no. 5, pp. 1250–1255, 2016.

[22] G. Stefani and F. J. Slack, "Small non-coding RNAs in animal development," *Nature Reviews Molecular Cell Biology*, vol. 9, no. 3, pp. 219–230, 2008.

[23] K. U. Tüfekci, M. G. Oner, R. L. Meuwissen, and S. Genç, "The role of microRNAs in human diseases," *Methods in Molecular Biology*, vol. 1107, pp. 33–50, 2014.

[24] D. P. Bartel, "MicroRNAs: target recognition and regulatory functions," *Cell*, vol. 136, no. 2, pp. 215–233, 2009.

[25] A. E. Pasquinelli, "MicroRNAs and their targets: recognition, regulation and an emerging reciprocal relationship," *Nature Reviews Genetics*, vol. 13, no. 4, pp. 271–282, 2012.

[26] A. K. Leung and P. A. Sharp, "MicroRNA functions in stress responses," *Molecular Cell*, vol. 40, no. 2, pp. 205–215, 2010.

[27] R. C. Siow and H. J. Forman, "Redox regulation of microRNAs in health and disease," *Free Radical Biology and Medicine*, vol. 64, pp. 1–3, 2013.

[28] D. Ayers, B. Baron, and T. Hunter, "miRNA influences in NRF2 pathway interactions within cancer models," *Journal of Nucleic Acids*, vol. 2015, Article ID 143636, 6 pages, 2015.

[29] A. M. Krichevsky, K. S. King, C. P. Donahue, K. Khrapko, and K. S. Kosik, "A microRNA array reveals extensive regulation of microRNAs during brain development," *RNA*, vol. 9, no. 10, pp. 1274–1281, 2003.

[30] J. Godlewski, M. O. Nowicki, A. Bronisz et al., "Targeting of the Bmi-1 oncogene/stem cell renewal factor by microRNA-128 inhibits glioma proliferation and self-renewal," *Cancer Research*, vol. 68, no. 22, pp. 9125–9130, 2008.

[31] S. Venkataraman, I. Alimova, R. Fan, P. Harris, N. Foreman, and R. Vibhakar, "MicroRNA 128a increases intracellular ROS level by targeting Bmi-1 and inhibits medulloblastoma cancer cell growth by promoting senescence," *PLoS One*, vol. 5, no. 6, article e10748, 2010.

[32] Y. K. Adlakha and N. Saini, "MicroRNA: a connecting road between apoptosis and cholesterol metabolism," *Tumour Biology*, vol. 37, no. 7, pp. 8529–8554, 2016.

[33] M. Comegna, M. Succoio, M. Napolitano et al., "Identification of miR-494 direct targets involved in senescence of human diploid fibroblasts," *FASEB Journal*, vol. 28, no. 8, pp. 3720–3733, 2014.

[34] R. Faraonio, P. Vergara, D. D. Marzo, M. Napolitano, T. Russo, and F. Cimino, "Transcription regulation in NIH3T3 cell clones resistant to diethylmaleate-induced oxidative stress and apoptosis," *Antioxidants & Redox Signaling*, vol. 8, no. 3-4, pp. 365–374, 2006.

[35] R. Faraonio, P. Vergara, D. Di Marzo et al., "p53 suppresses the Nrf2-dependent transcription of antioxidant response genes," *The Journal of Biological Chemistry*, vol. 281, no. 52, pp. 39776–39784, 2006.

[36] M. Succoio, M. Comegna, C. D'Ambrosio, A. Scaloni, F. Cimino, and R. Faraonio, "Proteomic analysis reveals novel common genes modulated in both replicative and stress-induced senescence," *Journal of Proteomics*, vol. 128, pp. 18–29, 2015.

[37] G. G. Schiattarella, F. Cattaneo, G. Pironti et al., "Akap1 deficiency promotes mitochondrial aberrations and exacerbates cardiac injury following permanent coronary ligation via enhanced mitophagy and apoptosis," *PLoS One*, vol. 11, no. 5, article e0154076, 2016.

[38] F. Cattaneo, M. Parisi, T. Fioretti, D. Sarnataro, G. Esposito, and R. Ammendola, "Nuclear localization of formyl-peptide receptor 2 in human cancer cells," *Archives of Biochemistry and Biophysics*, vol. 603, pp. 10–19, 2016.

[39] K. J. Livak and T. D. Schmittgen, "Analysis of relative gene expression data using real-time quantitative PCR and the 2(−delta delta C(T))," *Methods*, vol. 25, no. 4, pp. 402–408, 2001.

[40] G. Esposito, G. G. Schiattarella, C. Perrino et al., "Dermcidin: a skeletal muscle myokine modulating cardiomyocyte survival and infarct size after coronary artery ligation," *Cardiovascular Research*, vol. 107, no. 4, pp. 431–441, 2015.

[41] P. Siengdee, N. Trakooljul, E. Murani, M. Schwerin, K. Wimmers, and S. Ponsuksili, "MicroRNAs regulate cellular ATP levels by targeting mitochondrial energy metabolism genes during C2C12 myoblast differentiation," *PLoS One*, vol. 10, no. 5, article e0127850, 2015.

[42] L. Shi, B. Zhou, P. Li et al., "MicroRNA-128 targets myostatin at coding domain sequence to regulate myoblasts in skeletal muscle development," *Cellular Signalling*, vol. 27, no. 9, pp. 1895–1904, 2015.

[43] B. Bodega, F. Marasca, V. Ranzani et al., "A cytosolic Ezh1 isoform modulates a PRC2-Ezh1 epigenetic adaptive response in postmitotic cells," *Nature Structural & Molecular Biology*, vol. 24, no. 5, pp. 444–452, 2017.

[44] S. A. Agrawal, D. Anand, A. D. Siddam et al., "Compound mouse mutants of bZIP transcription factors Mafg and Mafk reveal a regulatory network of non-crystallin genes associated with cataract," *Human Genetics*, vol. 134, no. 7, pp. 717–735, 2015.

[45] W. Li, S. Yu, T. Liu et al., "Heterodimerization with small Maf proteins enhances nuclear retention of Nrf2 via masking the NESzip motif," *Biochimica et Biophysica Acta (BBA)-Proteins and Proteomics*, vol. 1783, no. 10, pp. 1847–1856, 2008.

[46] R. Faraonio, F. Pane, M. Intrieri, T. Russo, and F. Cimino, "*In vitro* acquired cellular senescence and aging-specific phenotype can be distinguished on the basis of specific mRNA expression," *Cell Death and Differentiation*, vol. 9, no. 8, pp. 862–864, 2002.

[47] X. Cheng, C. H. Ku, and R. C. Siow, "Regulation of the Nrf2 antioxidant pathway by microRNAs: new players in micromanaging redox homeostasis," *Free Radical Biology and Medicine*, vol. 64, pp. 4–11, 2013.

[48] S. Kurinna and S. Werner, "NRF2 and microRNAs: new but awaited relations," *Biochemical Society Transactions*, vol. 43, no. 4, pp. 595–601, 2015.

[49] C. Zhang, L. Shu, and A. N. Kong, "MicroRNAs: new players in cancer prevention targeting Nrf2, oxidative stress and inflammatory pathways," *Current Pharmacology Reports*, vol. 1, no. 1, pp. 21–30, 2015.

[50] Y. Guo, S. Yu, C. Zhang, and A. N. Kong, "Epigenetic regulation of Keap1-Nrf2 signaling," *Free Radical Biology and Medicine*, vol. 88, Part B, pp. 337–349, 2015.

[51] X. Sun, H. Zuo, C. Liu, and Y. Yang, "Overexpression of miR-200a protects cardiomyocytes against hypoxia-induced apoptosis by modulating the kelch-like ECH-associated protein 1-nuclear factor erythroid 2-related factor 2 signaling axis," *International Journal of Molecular Medicine*, vol. 38, no. 4, pp. 1303–1311, 2016.

[52] J. Y. Chan and S. H. Chan, "Activation of endogenous antioxidants as a common therapeutic strategy against cancer, neurodegeneration and cardiovascular diseases: a lesson learnt from DJ-1," *Pharmacology & Therapeutics*, vol. 156, pp. 69–74, 2015.

[53] K. Kanninen, R. Heikkinen, T. Malm et al., "Intrahippocampal injection of a lentiviral vector expressing Nrf2 improves spatial learning in a mouse model of Alzheimer's disease," *Proceedings of the National Academy of Sciences of the United States of America*, vol. 106, pp. 16505–16510, 2009.

[54] R. T. Kolamunne, I. H. Dias, A. B. Vernallis, M. M. Grant, and H. R. Griffiths, "Nrf2 activation supports cell survival during hypoxia and hypoxia/reoxygenation in cardiomyoblasts; the roles of reactive oxygen and nitrogen species," *Redox Biology*, vol. 1, pp. 418–426, 2013.

[55] K. J. Liang, K. T. Woodard, M. A. Weaver, J. P. Gaylor, E. R. Weiss, and R. J. Samulski, "AAV-Nrf2 promotes protection and recovery in animal models of oxidative stress," *Molecular Therapy*, vol. 25, no. 3, pp. 765–779, 2017.

[56] V. Malec, O. R. Gottschald, S. Li, F. Rose, W. Seeger, and J. Hänze, "HIF-1 alpha signaling is augmented during intermittent hypoxia by induction of the Nrf2 pathway in NOX1-expressing adenocarcinoma A549 cells," *Free Radical Biology and Medicine*, vol. 48, no. 12, pp. 1626–1635, 2010.

[57] R. B. Donker, J. F. Mouillet, D. M. Nelson, and Y. Sadovsky, "The expression of Argonaute2 and related microRNA biogenesis proteins in normal and hypoxic trophoblasts," *Molecular Human Reproduction*, vol. 13, pp. 273–279, 2007.

[58] X. C. Zeng, L. Li, H. Wen, and Q. Bi, "MicroRNA-128 inhibition attenuates myocardial ischemia/reperfusion injury-induced cardiomyocyte apoptosis by the targeted activation of peroxisome proliferator-activated receptor gamma," *Molecular Medicine Reports*, vol. 14, pp. 129–136, 2016.

[59] J. Loscalzo, *Harrison's Cardiovascular Medicine*, McGraw-Hill Medical, New York, 2010.

[60] Y. Huang, W. Li, Z. Y. Su, and A. N. Kong, "The complexity of the Nrf2 pathway: beyond the antioxidant response," *The Journal of Nutritional Biochemistry*, vol. 26, no. 12, pp. 1401–1413, 2015.

[61] D. E. Handy and J. Loscalzo, "Responses to reductive stress in the cardiovascular system," *Free Radical Biology and Medicine*, vol. 109, pp. 114–124, 2017.

[62] L. Zhuang, L. Xu, P. Wang, and Z. Meng, "Serum miR-128-2 serves as a prognostic marker for patients with hepatocellular carcinoma," *PLoS One*, vol. 10, no. 2, article e0117274, 2015.

[63] J. Sun, K. Liao, X. Wu, J. Huang, S. Zhang, and X. Lu, "Serum microRNA-128 as a biomarker for diagnosis of glioma," *International Journal of Clinical and Experimental Medicine*, vol. 8, no. 1, pp. 456–463, 2015.

[64] J. Vistbakka, I. Elovaara, T. Lehtimäki, and S. Hagman, "Circulating microRNAs as biomarkers in progressive multiple sclerosis," *Multiple Sclerosis Journal*, vol. 23, no. 3, pp. 403–412, 2017.

Hindawi
Oxidative Medicine and Cellular Longevity
Volume 2017, Article ID 3960197, 16 pages
https://doi.org/10.1155/2017/3960197

Research Article

circRNA_0046367 Prevents Hepatoxicity of Lipid Peroxidation: An Inhibitory Role against Hepatic Steatosis

Xing-Ya Guo,[1] Jian-Neng Chen,[2] Fang Sun,[1] Yu-Qin Wang,[1] Qin Pan,[1] and Jian-Gao Fan[1,3]

[1]*Department of Gastroenterology, Xinhua Hospital, Shanghai Jiao Tong University School of Medicine, Shanghai 200092, China*
[2]*Department of Hepatology, Zhengxing Hospital, Zhangzhou, Fujian 363000, China*
[3]*Shanghai Key Laboratory of Children's Digestion and Nutrition, Shanghai 200092, China*

Correspondence should be addressed to Qin Pan; panqin@xinhuamed.com.cn and Jian-Gao Fan; fanjiangao@xinhuamed.com.cn

Received 12 April 2017; Revised 26 June 2017; Accepted 6 July 2017; Published 5 September 2017

Academic Editor: Jaideep Banerjee

Hepatic steatosis reflects the miRNA-related pathological disorder with triglyceride accumulation and lipid peroxidation, which leads to nonalcoholic steatohepatitis, liver fibrosis/cirrhosis, and even hepatocellular carcinoma. Circular RNA (circRNA)/miRNA interaction reveals a novel layer of epigenetic regulation, yet the miRNA-targeting circRNA remains uncertain in hepatic steatosis. Here, we uncover circRNA_0046367 to be endogenous modulator of miR-34a that underlies hepatic steatosis. In contrast to its expression loss during the hepatocellular steatosis in vivo and in vitro, circRNA_0046367 normalization abolished miR-34a's inhibitory effect on peroxisome proliferator-activated receptor α (PPARα) via blocking the miRNA/mRNA interaction with miRNA response elements (MREs). PPARα restoration led to the transcriptional activation of genes associated with lipid metabolism, including carnitine palmitoyltransferase 2 (CPT2) and acyl-CoA binding domain containing 3 (ACBD3), and then resulted in the steatosis resolution. Hepatotoxicity of steatosis-related lipid peroxidation, being characterized by mitochondrial dysfunction, growth arrest, and apoptosis, is resultantly prevented after the circRNA_0046367 administration. These findings indicate a circRNA_0046367/miR-34a/PPARα regulatory system underlying hepatic steatosis. Normalized expression of circRNA_0046367 may ameliorate the lipoxidative stress on the basis of steatosis attenuation. circRNA_0046367, therefore, is suggested to be potential approach to the therapy of lipid peroxidative damage.

1. Introduction

Hepatic steatosis, an ever-growing pathological disorder associated with metabolic syndrome and other etiologies [1–5], displays characteristics of triglyceride (TG) accumulation, lipid peroxidation, and mitochondrial dysfunction [1]. This oxidation-based hepatocellular injury deeply involves in the disease progression with outcomes of nonalcoholic steatohepatitis, liver fibrosis/cirrhosis, and hepatocellular carcinoma [6]. In spite of its clinical importance, hepatic steatosis is still prevented from effective therapy, with the only exceptions of dietary control and physical activity, due to our limited understanding of the underlying mechanisms.

Nowadays, clinical and experimental studies have uncovered the critical roles of miRNAs during initiation, progression, and resolution of hepatic steatosis [7–14]. miR-199a-5p among these contributes to the impaired mitochondrial β-oxidation of fatty acid and aberrant lipid deposits [7]. miR-291b-3p promotes the hepatic lipogenesis by negative regulation of adenosine 5′-monophosphate-(AMP-) activated protein kinase α1 [8]. In contrast, miR-185 and miR-29 protect hepatocytes from steatosis by transcriptional repression of lipogenetic genes (fatty acid synthase, HMGCR, and SREBP-1c/2) and physiological lipid distribution away from the liver, respectively [9, 10]. Dramatically, accumulating evidences demonstrate a fundamental link between miR-34a and hepatic steatosis [11–14]. The inhibitory effect of miR-34a on peroxisome proliferator-activated receptor α (PPARα), which functions to diminish the intake of fatty acid and facilitate lipoxidation, indicates it to be an important inducer of hepatocyte steatogenesis.

Circular RNA (circRNA) reflects a class of noncoding RNAs with the connection of 3′ and 5′ ends [15]. ciRS-7, a brain-specific circRNA, serves as the natural sponge of

miRNA-7 by ~70 tandem anti-miRNA sequences [16]. The ciRS-7 deficiency in neocortex (Brodmann A22) and hippocampal CA1 has been recognized to misregulate ciRS-7-miRNA-7-UBE2A circuit and then results in sporadic Alzheimer's disease [16]. In colorectal cancer (CRC), hsa_circ_001569 acts as the positive regulator of cell proliferation and invasion via "sponging event" of miR-145, which upregulates functional targets of E2F5, BAG4, and FMNL2 [17]. Physiologically, chondrocytic circRNA-CER modulates the MMP13 expression on a basis of competing with miR-136. Loss-of-function and rescue experiments further confirm the determinant action of CER in cartilage-related extracellular matrix degradation [18]. circRNA, therefore, qualifies itself for a pivotal part in the miRNA regulation. However, circRNAs targeting steatosis-related miRNAs, especially miR-34a, remain uncertain.

Integrating databases of noncoding RNA (circBase, miRBase) and their algorithms, circRNA_0046367 is filtered to be potential endogenous modulator of miR-34a, mainly by the high-complementary activity between miRNA response elements (MREs) of circRNA and "seed sequence" of miRNA [19, 20]. To reveal this circRNA-dependent regulatory action underlying hepatic steatosis, the relationships of circRNA_0046367, miR-34a, and its key target (PPARα) were analyzed in vivo and in vitro. Both circRNA_0046367/miR-34a and miR-34a/PPARα interactions were then validated by luciferase reporter assay. Furthermore, circRNA_0046367 expression was subjected to normalization in HepG2 cells with high-fat-induced steatosis, exhibiting its effect on miR-34a/PPARα regulatory system and downstream genes associated with lipid metabolism. Hepatocellular steatosis, lipid peroxidation, and oxidative hepatotoxication were subsequently investigated so as to highlight the results of circRNA_0046367 regulation.

2. Materials and Methods

2.1. Study Subjects. Five patients with biopsy-proven hepatic steatosis (5 of nonalcoholic fatty liver disease (NAFLD), age: 51.60 ± 12.10; male/female: 3/2) and 3 nonsteatosis controls (2 of chronic hepatitis B (CHB), 1 of primary biliary cirrhosis (PBC), age: 55.00 ± 18.19; male/female: 1/2) were enrolled from Xinhua Hospital (Shanghai, China). Subjects with type 2 diabetes, high alcohol intake (>30 g/d for men and >20 g/d for women), chronic hepatitis C (CHC), and current or previous treatment associated with hepatocyte steatosis were excluded [21–23]. This study was approved by the Ethics Committee of Xinhua Hospital and conducted according to the principles of the Helsinki Declaration.

2.2. Hepatic Pathology. Liver tissues of patients with hepatic steatosis were obtained by needle biopsy after informed consent. Samples were then fixed in 10% buffered formalin, embedded in paraffin, and sliced for further evaluation. The percentage of hepatic steatosis was finally subjected to evaluation on a basis of hematoxylin-eosin (HE) staining by 2 pathologists who were not aware of the experiments [24].

2.3. Induction of Hepatic Steatosis by High-Fat Stimulation. HepG2 cells from the Cell Bank of Type Culture Collection (Shanghai, China) were randomized into groups of normal ($n = 9$) and steatosis ($n = 9$). To establish the in vitro model of hepatic steatosis, the steatosis group was cocultured with oleic and palmitic acids (Sigma-Aldrich, St. Louis, USA) at a final concentration of 0.5 mM (oleate : palmitate = 2 : 1) for 24 hours [25].

Oil red-O staining reflected the hepatosteatogenesis induced by high-fat stimulation. In detail, formaldehyde-fixed HepG2 cell was administrated by 0.5% oil red-O in isopropyl alcohol for 20 minutes and counterstained with hematoxylin for 1 minute. TG levels of both groups were enzymatically measured by TG assay kit (Applygen Technologies Inc., Shanghai, China) against the protein content [26].

2.4. Bioinformatic Analysis. miRNAs targeted by has-circRNA_0046367 were investigated using miRNA target prediction software (Arraystar Inc., USA) on the basis of MRE-based circRNA/microRNA complementation [27, 28]. The sets of circRNA_0046367-targeting miRNAs and hepatosteatosis-related miRNAs were intersected so as to reveal the critical miRNAs that mediate circRNA_0046367's effect on hepatic steatosis [29].

2.5. Luciferase Reporter Assays. In order to reveal the circRNA-miRNA interaction, has-circRNA_0046367 (circBase, Rajewsky lab, Berlin, Germany) sequence containing the putative target sites for miR-34a was synthesized and cloned into the pMIR-REPORT™ reporter vector (Thermo Fisher Scientific Inc., Waltham, USA) downstream to the firefly luciferase (pMIR-REPORT-circRNA_0046367-wildtype). Mutant version of circRNA_0046367 (pMIR-REPORT-circRNA_0046367-mutant) was also generated with the deletion of complementary sites. After the cotransfection of reporter vector (pMIR-REPORT-circRNA_0046367-wildtype or pMIR-REPORT-circRNA_0046367 -mutant) and oligonucleotides (miR-34a mimics or negative control) in 293T cells, firefly luciferase activity was subjected to measurement by dual-luciferase assay kit (Promega, Madison, USA) against that of renilla luciferase [30]. Similarly, the complementarity between miR-34a and 3′-untranslated region (3′-UTR) of PPARα was evaluated by the methods mentioned above. Each assay was repeated in 5 independent experiments.

2.6. circRNA_0046367 Treatment. Exponentially growing HepG2 cells cultured in 6-well plates (2×10^5 cells/well) were randomly divided into groups of normal, steatosis, control, circRNA, circRNA + mimics, and circRNA + mimic NC ($n = 9$ for each group), respectively. Except for those without circRNA_0046367 regulation (normal, steatosis, and control groups), HepG2 cells were exposed to 12-hour treatment of pcDNA3.1(+)-GFP-circRNA_0046367 (circRNA group), pcDNA3.1(+)-GFP-circRNA_0046367 + miR-34a mimics (circRNA + mimics group), and pcDNA3.1(+)-GFP-circRNA_0046367 + miR-34a mimics, negative control (circRNA + mimic NC group), respectively [31]. The control group was contrastively treated

Table 1: Primers for real-time PCR.

Gene	Primer sequence (5′-3′)		Product (nt)
hsa_circ_000367	F: CTCGCTTCGGCAGCACA	R: AACGCTTCACGAATTTGCGT	101
PPARα	F: CCCCTCCTCGGTGACTTATC	R: ATTCGTCCAAAACGAATCGCGT	297
CPT2	F: CAGCAGATGATGGTTGAGTGC	R: CAGCATACCCAACACCAAAGC	262
ACBD3	F: GCTGGGTCTTCCTTGCCTAC	R: CTCCTCGGCCCACTGTAATC	265
U6	F: ATTGGAACGATACAGAGAAGATT	R: GGAACGCTTCACGAATTTG	70
GAPDH	F: CTGAACGGGAAGCTCACTGG	R: AAAGTGGTCGTTGAGGGCAA	252

by blank plasmid of pcDNA3.1(+)-GFP. Thereafter, free fatty acid administration was applied to different groups for another 24 hours according to the previously described procedure, with the only exception of normal group. Both oil red-O staining and TG assay demonstrated the steatotic degeneration accordingly.

2.7. Real-Time PCR. Total RNA was extracted from liver samples and HepG2 cells of each group and treated by ExScript RT reagent kit (TAKARA, Kusatsu, Japan) for reverse transcription (RT). Real-time PCR was successively performed using SYBR Premix Ex Taq (TAKARA, Kusatsu, Japan) on the Applied Biosystems 7500 Real-Time PCR Detection Systems (Bio-Rad, CA, USA). Primer sequences for these reactions were exhibited in Table 1. The gene expression levels were calculated by the $2^{-\Delta\Delta Ct}$ method.

Nevertheless, divergent primers were designed for the circRNA-specific real-time PCR [32]. Mir-X miRNA First Strand Synthesis Kit (TAKARA, Kusatsu, Japan) was employed to generate the cDNA of miRNA, following the real-time PCR by primers specific to mature miR-34a (TAKARA, Kusatsu, Japan) [14]. Expression level of both circRNA_0046367 and miR-34a was evaluated against U6 in the abovementioned way.

2.8. Western Blotting. Total protein of each sample was prepared and quantified by the bicinchoninic acid method (Pierce, Rockford, USA). After their electrophoretical separation on 12% SDS-PAGE gels, these protein samples were transferred onto polyvinylidine difluoride membranes and blocked by 5% nonfat dry milk (NFDM). Membranes with protein sample subsequently reacted to anti-PPARα (HepG2, 1 : 500, Santa Cruz, USA; liver: 1 : 1000, Santa Cruz, USA), anti-CPT2 (HepG2, 1 : 1000, Santa Cruz, USA), anti-ACBD3 (HepG2, 1 : 1000, Santa Cruz, USA), anti-GAPDH (HepG2, 1 : 1000, Santa Cruz, USA), and β-actin (liver, 1 : 200, Boster, China) overnight at 4°C and then HRP-conjugated secondary antibody (1 : 1500; Jackson ImmunoResearch Laboratories, Inc., USA) for 1 hour at room temperature. Both chemiluminescent visualization by ECL detection system and densitometric analysis by Image Lab Software 5.1 (Bio-Rad Laboratories, USA) were carried out to assess the immune signals specific to immunoblots [33].

2.9. Lipid Peroxidation and Antioxidation. For the lipid peroxidation assay, cells of each group were administrated as follows: (1) cytolysis by cell lysis buffer, (2) centrifugation at 10,000 ×g for 10 min to remove the debris, (3) measurement of supernatant malondialdehyde (MDA) concentration by MDA assay kit (Jiancheng Bioengineering Institute, Nanjing, China) according to the protocol of manufacturer [34]. Total protein was measured to normalize the intracellular level of MDA. In contrast to the peroxidative agent, intracellular levels of superoxide dismutase (SOD), a crucial marker for antioxidation, were also assessed by SOD assay kit (Beyotime, Shanghai, China) in the method of WST-8 [35].

2.10. Mitochondrial Membrane Potential (MMP). After the steatosis induction and circRNA_0046367 regulation, MMP was investigated so as to uncover the hepatic toxicity resulted from oxidative stress. Methodically, cells were cultured with Rhodamine 123 at a final concentration of 0.5 μM for 2 hours. When quantified by the ImageJ 1.34 software (National Institutes of Health, Bethesda, USA), fluorescence intensity at 535 nm reflected the MMP of each group [36].

2.11. Cell Proliferation Assay. Being seeded onto 96-well plate at 4×10^3/well, cells of each group were incubated with 10 μl of CCK-8 solution for 4 hours using the Cell Counting Kit 8 (Dojindo, Kumamoto, Japan). Then, the proliferative activity of different groups was detected on the basis of their light absorbance at 450 nm [37].

2.12. Apoptosis Assay. At the end of a 48-hour administration, cells were harvested from different groups for apoptosis analysis. Briefly, suspended cells were dual-labeled with Annexin V-APC and 7-AAD using Annexin V-APC/7-AAD Apoptosis Detection kit (KeyGEN, Nanjing, China) at room temperature for 10 min. Flow cytometry was finally performed to detect apoptosis by determining the relative amount of cells positive to Annexin V-APC (FC500 Fluorescence-Activated Cell Sorter, Beckman Coulter Inc., Brea, USA) [38].

2.13. Statistics. Results are expressed as means ± standard deviation (SD) for the independent experiments. All groups were compared statistically by Student's t-test or one-way analysis of variance (ANOVA) with GraphPad Prism (GraphPad Software, Inc., USA) [39]. Differences with $P < 0.05$ were considered statistically significant.

3. Results

3.1. circRNA_0046367 Loss Characterized High-Fat-Induced Steatosis in HepG2 Cells. When compared to the normal group, steatosis group with FFA exposure showed an enrichment of cytoplamic lipid droplets. Their positive reaction to

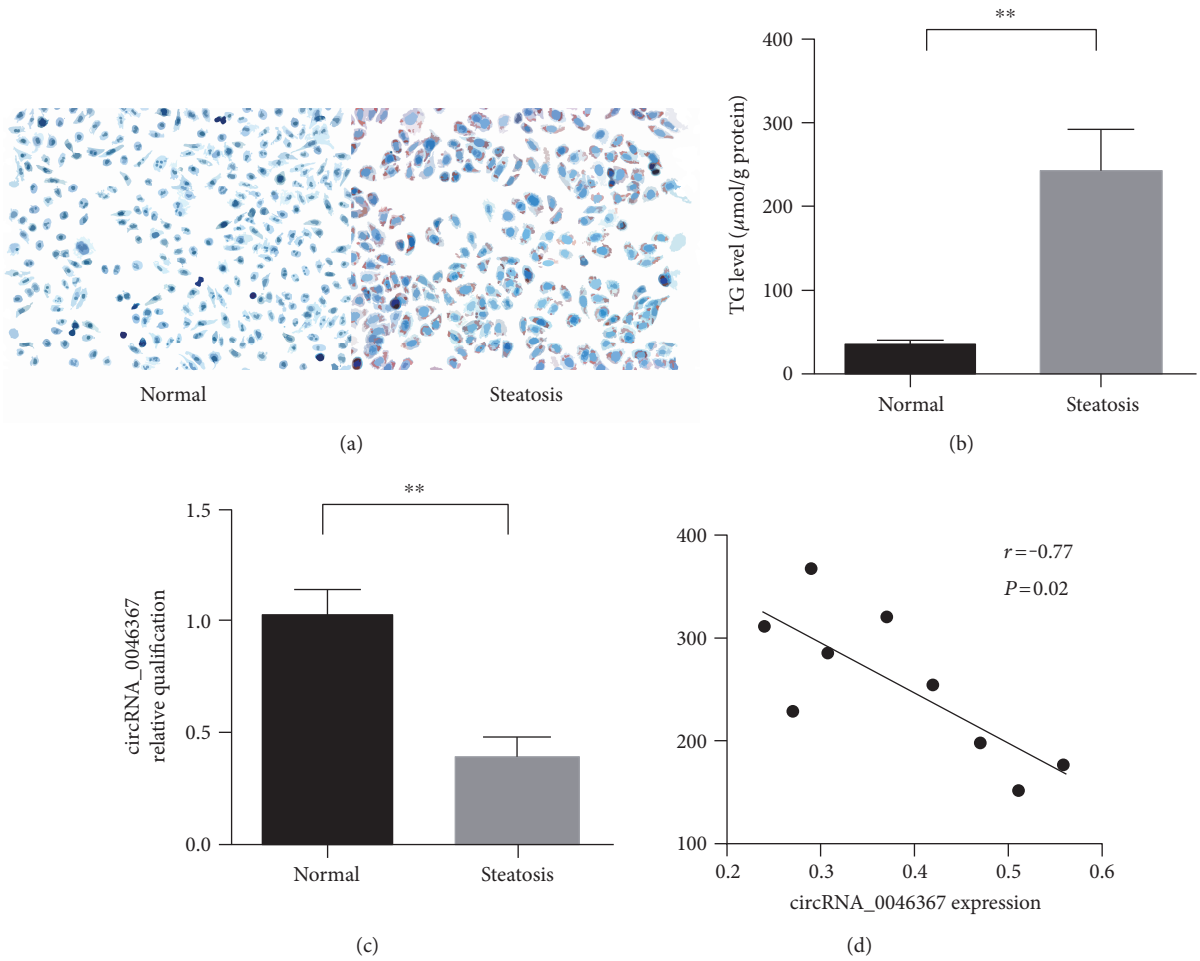

Figure 1: Expression loss of circRNA_0046367 characterizes the FFA-induced steatosis in HepG2 cells. (a) Oil red O staining identifies HepG2 cells with (steatosis group) or without FFA-induced steatosis (normal group), respectively (400x). (b) Enzymatical measurement demonstrates an upregulation of intracellular TG level in the steatosis group. (c) Quantitative assay for circRNA_0046367 reveals its decreased expression after hepatic steatosis. (d) circRNA_0046367 expression inversely correlates to TG level in the steatosis group. The presented results are expressed as means ± S.D. $^{**}P < 0.01$.

oil red-O reflected the neutral fat (TG) accumulation (Figure 1(a)). In parallel to these observations, enzymatical assay confirmed a significant upregulation of intracellular TG level in the steatosis group (Figure 1(b)).

Dramatically, cells with high-fat-induced steatosis (steatosis group) were characterized by the expression loss of circRNA_0046367 in comparison to those in the normal group (Figure 1(c)). Moreover, there was statistically inverse correlation between the TG level and circRNA_0046367 expression ($r = -0.77$, $P = 0.02$; Figure 1(d)), suggesting that it has an important role during the hepatosteatogenesis.

3.2. circRNA_0046367 Demonstrated Complementary Targeting to miR-34a. To reveal its effect underlying hepatic steatosis, circRNA_0046367 was subjected to target prediction depending on the principle of base complementation. According to the algorithms of circBase, complementary binding between MRE of circRNA and "seed sequence" of miRNA identified 20 targets of circRNA_0046367 (miR-1, miR-10b, miR-21, miR-24, miR-27, miR-27a, miR-27b, miR-30c, miR-33a, miR-33b, miR-34a, miR-107, miR-122, miR-128–2, miR-130a-3p, miR-155, miR-206, miR-217, miR-613, and miR-758) (Figure 2(a)). Dramatically, miR-34a was the only one of the circRNA_0046367's targets that intersected with the set of hepatosteatosis-related miRNAs (miR-15a-5p, miR-15b-5p, miR-16-5p, miR-24-3p, miR-27a-3p, miR-27b-3p, miR-34a-5p, miR-103a-3p, miR-195-5p, miR-205-5p, miR-214-3p, miR-326, miR-328-3p, miR-330-5p, miR-338-3p, miR-370-3p, miR-424-5p, miR-449a, miR-449b-5p, miR-485-5p, miR-497-5p, miR-503-5p, miR-544a, miR-761, miR-3619-5p, miR-3666) (Figure 2(a)).

Dual luciferase reporter assay further showed a significant decrease in the firefly luciferase activity when pMIR-REPORT-circRNA_0046367-wildtype was cotransfected with miR-34a mimics. This suppressive effect could be abrogated by deleting the perfectly complementary sequences in pMIR-REPORT-circRNA_0046367-mutant, which disrupted the interaction between circRNA_0046367 and miR-34a (Figures 2(b) and 2(c)). These demonstrations

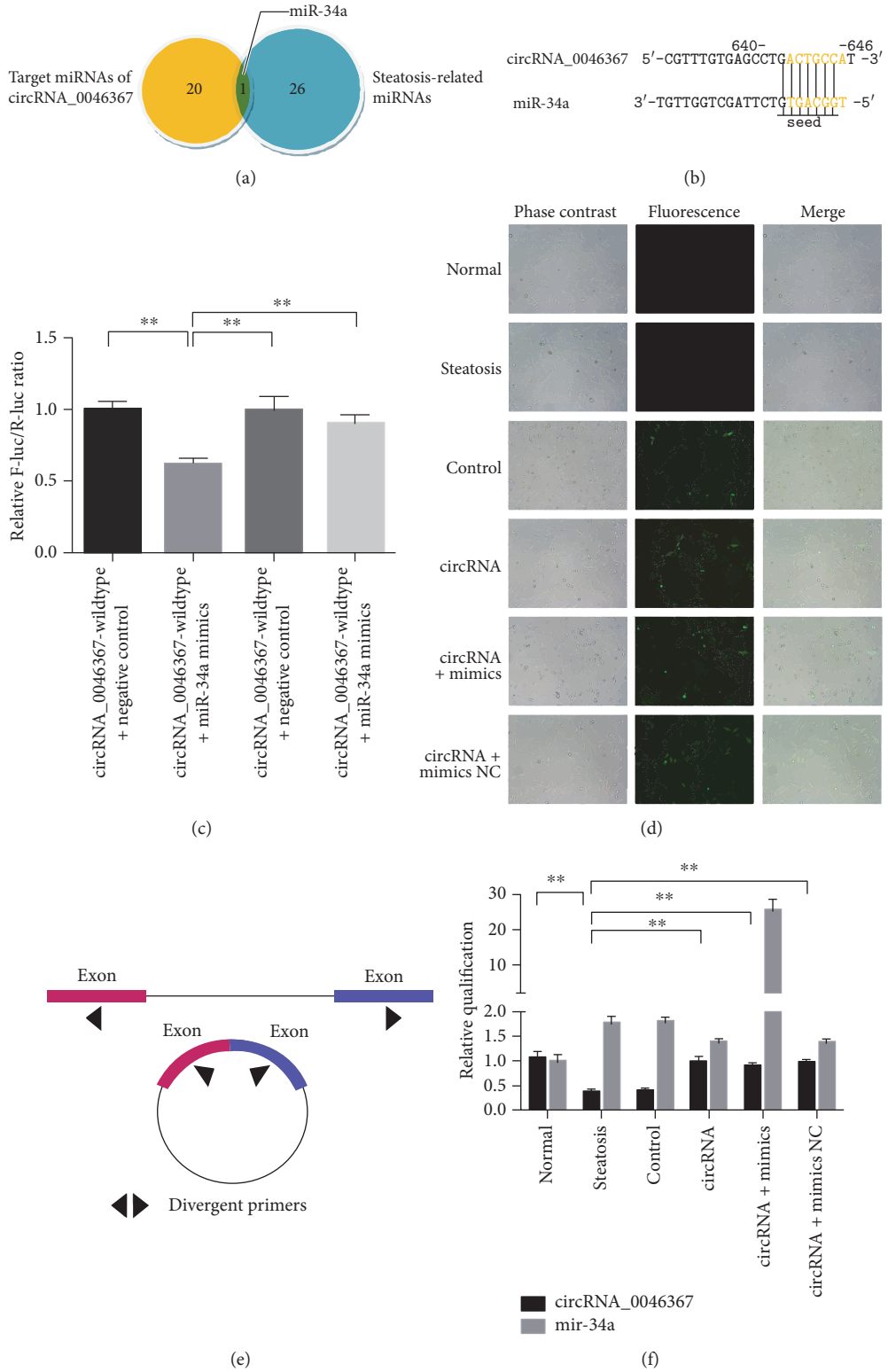

Figure 2: circRNA_0046367 exerts antagonizing effect on miR-34a. (a) Intersection of circRNA_0046367-targeting miRNAs and hepatosteatosis-related miRNAs. (b) Complementation between MRE of circRNA_0046367 and "seed sequence" of miR-34a predicts a circRNA_0046367/miR-34a interaction. (c) Dual luciferase reporter assay displays the complementary binding of circRNA_0046367 and miR-34a. (d) Phase contrast and fluorescent microscopy for the vector transfection in HepG2 cells with FFA-induced steatosis (400x). (e) Schematic diagram for the divergent primers that are employed to amplify the circRNA_0046367 transcripts. (f) Administration of circRNA-carrying vectors induces the circRNA_0046367 normalization to exert antagonizing impact on miR-34a. The presented results are expressed as means ± S.D. $^{**}P < 0.01$.

provided substantial evidence for a direct, high-affinitive targeting of miR-34a by circRNA_0046367.

3.3. Restoration of circRNA_0046367 Abolished the Inhibitory Effect of miR-34a on PPARα. In contrast to the decreased level of circRNA_0046367 in steatotic groups (steatosis and control group), its expression loss was statistically prevented in the circRNA and circRNA + mimic NC groups via transfection of overexpression vectors (Figures 2(d), 2(e), and 2(f)).

Both circRNA_0046367 and PPARα mRNA, which was proved to be the target of miR-34a by dual luciferase reporter assay (Figures 3(a) and 3(b)), shared the complementary sequences with miR-34a. Therefore, circRNA_0046367 is suggested to serve as the endogenous sponge of miR-34a and then abrogates its inhibitory effect on PPARα by means of competitive binding. As expected, the circRNA_0046367 restoration resulted in a significant upregulation of PPARα, at both transcription and translation levels, in the circRNA and circRNA + mimic NC groups (Figures 3(c), 3(d), and 3(e)), whereas the PPARα expression could not be rescued on condition of the saturated binding between circRNA_0046367 and miR-34a in the circRNA + mimic group (Figures 3(c), 3(d), and 3(e)).

3.4. PPARα Normalization Improved Hepatocellular Steatosis by Regulating Genes Associated with Lipid Metabolism. Resulting from circRNA_0046367 deficiency and miR-34a activation, PPARα inhibition represented one of the most important characteristics of groups with FFA-induced steatosis. Lack of hepatic PPARα prevented it from nuclear translocation and then reduced the transcriptional activation of multiple genes involved in lipid metabolism, including carnitine palmitoyltransferase 2 (CPT2) and acyl-CoA binding domain containing 3 (ACBD3) (Figures 4(a), 4(b), and 4(c)). Resultantly, the lipometabolic disorder led to TG-dominated steatosis (Figures 4(d) and 4(e)).

As compared to the decreased CPT2 and ACBD3 in steatotic cells (steatosis, control, and circRNA + mimic groups), circRNA_0046367 restoration stimulated their expression by PPARα-based transcriptional promotion (circRNA and circRNA + mimic NC groups), mainly on a basis of abolishing the miR-34a's inhibitory effect on PPARα (Figures 4(a), 4(b), and 4(c)). In the present experiments, the normalized expression of lipometabolic genes, which exhibited levels in similar to those of the normal group, gave rise to a great downregulation in the intracellular TG level (steatosis group versus circRNA group: $332.90 \pm 41.51\ \mu$mol/g protein versus $207.50 \pm 18.67\ \mu$mol/g protein, $P < 0.01$; steatosis group versus circRNA + mimic NC group: $332.90 \pm 41.51\ \mu$mol/g protein versus $201.10 \pm 17.23\ \mu$mol/g protein, $P < 0.01$) (Figure 4(d)). Amelioration of hepatic steatosis finally occurred in both circRNA and circRNA + mimic NC groups (Figure 4(e)).

3.5. Improvement of Hepatocellular Steatosis Attenuated Lipid Peroxidation and Mitochondrial Injury. FFA-induced TG accumulation (steatosis) introduced the serious burden of lipid oxidation. The ascending concentration of peroxidative product (MDA) and reduced level of antioxidative enzyme (SOD), both of which correlated to the circRNA_0046367 expression in opposite patterns (Figures 5(a) and 5(b)), demonstrated the unbalance of lipid peroxidation/antioxidation in the steatosis, control, and circRNA + mimic groups (Figures 5(c) and 5(d)). On the contrary, circRNA and circRNA + mimic NC groups were featured by the improved indexes of both MDA (steatosis group versus circRNA group: $3.19 \pm 0.47\ \mu$mol/g protein versus $2.14 \pm 0.18\ \mu$mol/g protein, $P < 0.05$; steatosis group versus circRNA + mimic NC group: $3.19 \pm 0.47\ \mu$mol/g protein versus $1.89 \pm 0.16\ \mu$mol/g protein, $P < 0.05$) and SOD (steatosis group versus circRNA group: 48.60 ± 2.69 U/mg protein versus 71.40 ± 6.91 U/mg protein, $P < 0.01$; steatosis group versus circRNA + mimic NC group: 48.60 ± 2.69 U/mg protein versus 68.73 ± 5.55 U/mg protein, $P < 0.01$) (Figures 5(c) and 5(d)), indicating the regaining of peroxidation/antioxidation balance. These observations qualified circRNA_0046367 to be a protective agent against the unlimited oxidative stress of hepatocelluar steatosis.

Lipid peroxidative stress takes a critical step in the steatosis-related hit to hepatocellular viability, with the major characteristics of mitochondrial dysfunction. Being assessed by the fluorescent intensity of Rhodamine 123 dyeing, there was great decrease in the MMP, an indicator of mitochondrial injury, of steatosis, control, and circRNA + mimic groups (Figures 5(e) and 5(f)). Interestingly, opposing results could be obtained in the groups of circRNA and circRNA + mimic NC, respectively, with statistical significance (Figures 5(e) and 5(f)). The antiperoxidative actions of circRNA_0046367, therefore, attenuate the mitochondria-based hepatotoxication.

3.6. Amelioration of Oxidative Impairment Exerts Proliferative and Antiapoptotic Effects. Cell viability has been well described to underlie its biological behaviors, especially the proliferative activity and apoptosis sensitivity. By cell proliferation assay, steatosis, control, and circRNA + mimic groups with mitochondrial injury suffered from proliferative inhibition (Figure 6(a)). In the circRNA group, mitochondria-specific amelioration of peroxidative injury accelerated the cell proliferation (steatosis group versus circRNA group: 0.63 ± 0.04 versus 0.73 ± 0.04, $P < 0.05$) (Figure 6(a)).

Similar phenomena took place in the hepatocellular apoptosis. In spite of its limited level in the normal group, apoptosis rate elevated statistically in the steatosis, control, and circRNA + mimic groups (Figures 6(b) and 6(c)). But apoptosis repression could be verified in the circRNA (steatosis group versus circRNA group: $7.35\% \pm 0.69\%$ versus $3.08\% \pm 0.51\%$, $P < 0.01$) and circRNA + mimic NC (steatosis group versus circRNA + mimic NC group: $7.35\% \pm 0.69\%$ versus $3.77\% \pm 0.68\%$, $P < 0.01$) instead of other groups (Figures 6(b) and 6(c)).

3.7. Characteristics of circRNA_0046367/miR-34a/PPARα Regulatory System in Patients with Hepatic Steatosis. Being compared to that of nonsteatosis controls (control group), NAFLD patients with hepatocyte steatosis (steatosis group)

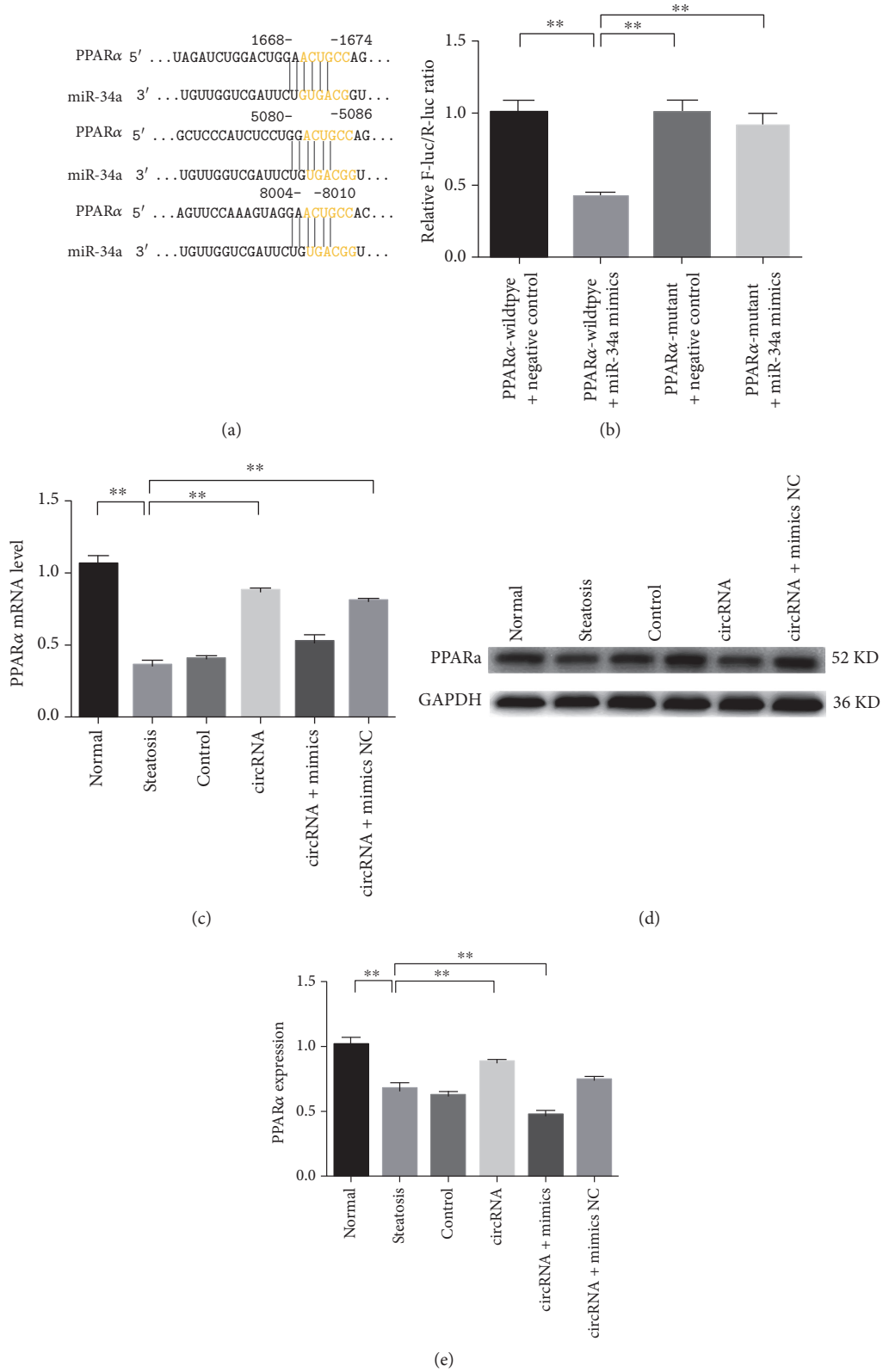

Figure 3: circRNA_0046367 normalization abolishes the miR-34a-induced inhibition of PPARα. (a) Complementation between "seed sequence" of miR-34a and 3′-UTR of PPARα predicts a miR-34a/PPARα interaction. (b) Dual luciferase reporter assay exhibits the inhibitory effect of miR-34a on PPARα. (c) circRNA_0046367 normalization restores the mRNA level of PPARα by miR-34a inactivation. (d), (e) Western blot (d) with quantification against GAPDH (e) shows the significant upregulation of PPARα in groups with normalized circRNA_0046367. The presented results are expressed as means ± S.D. $^{**}P < 0.01$.

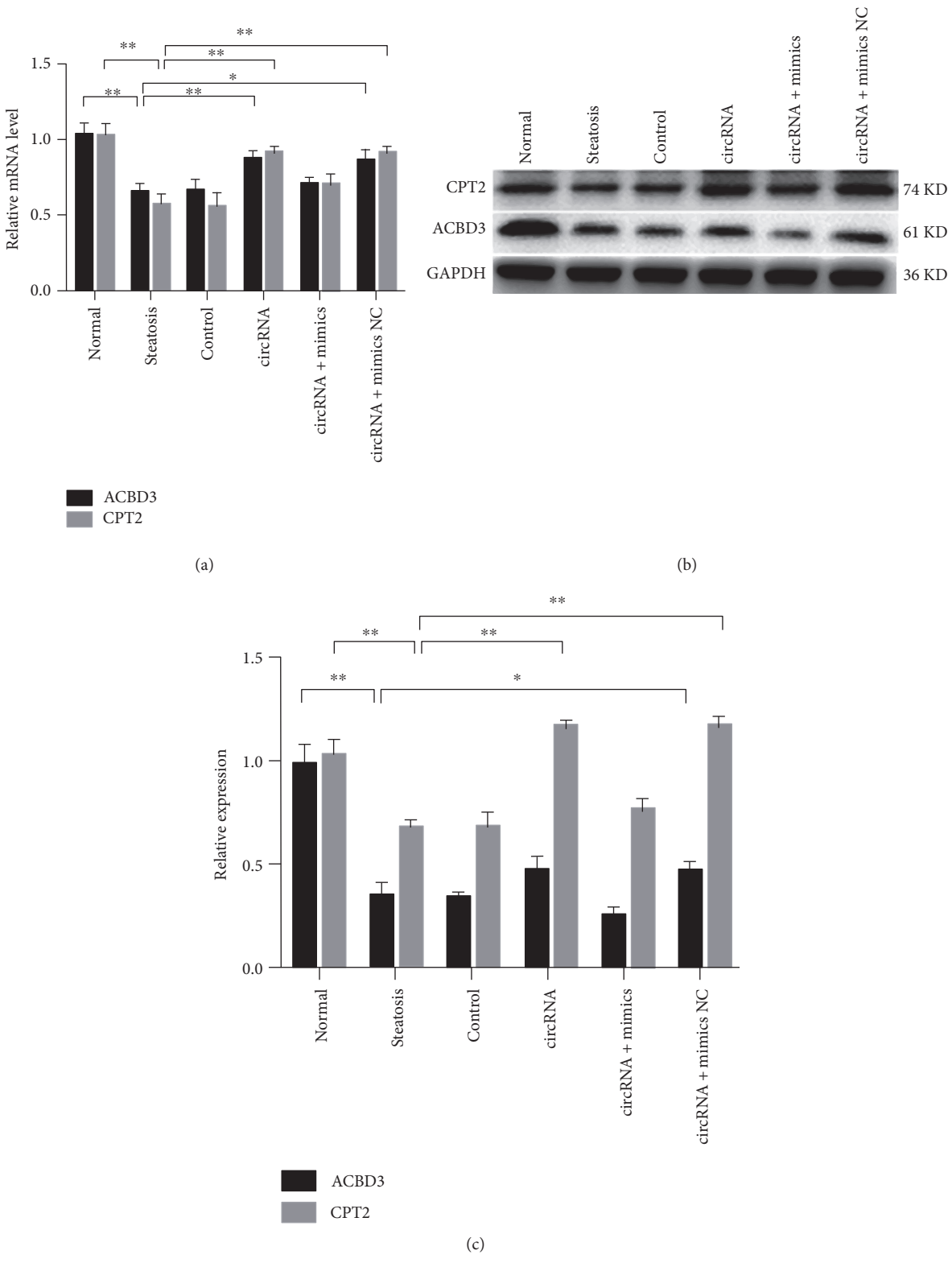

Figure 4: Continued.

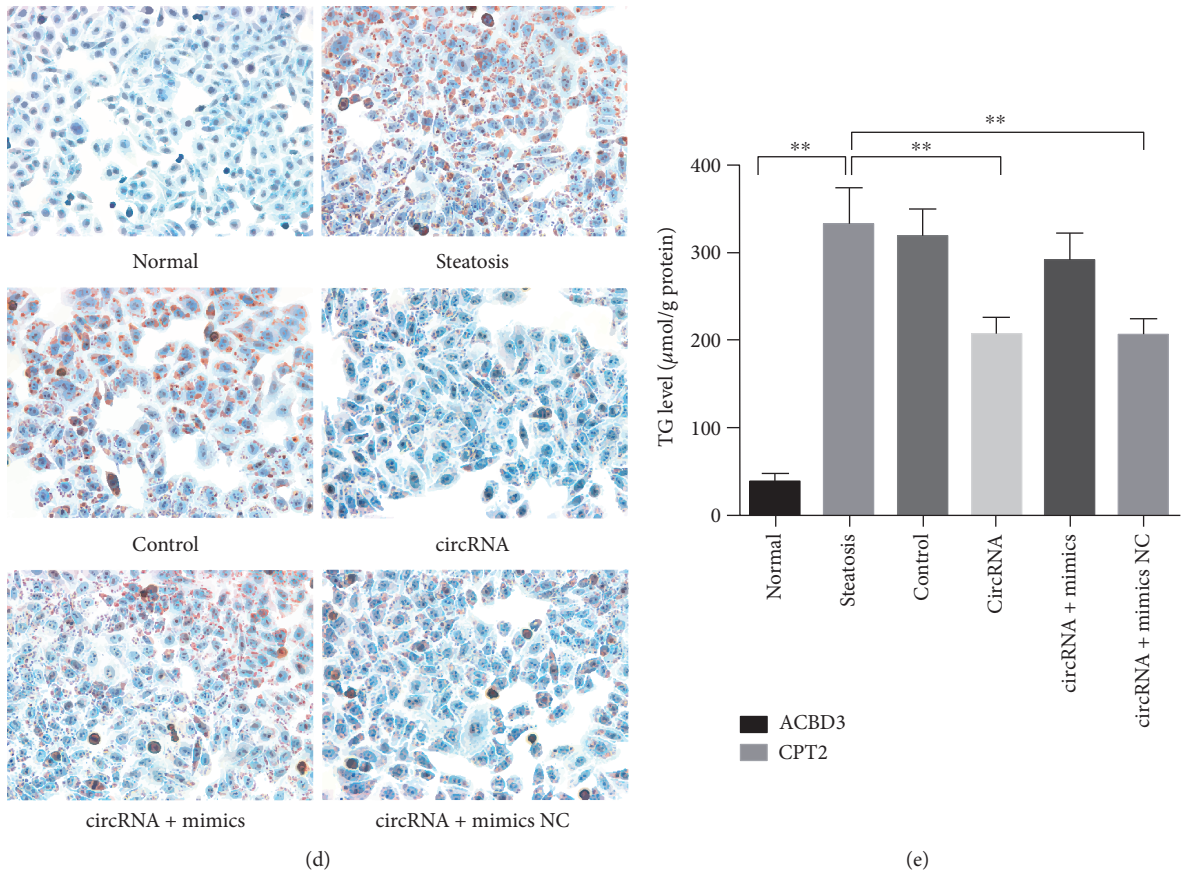

Figure 4: PPARα restoration improves hepatocellular steatosis by regulating genes associated with lipid metabolism. (a) PPARα restoration by circRNA_0046367 promotes the expression of CPT2 and ACBD3 at transcriptional level. (b), (c) Transcriptional activation of both CPT2 and ACBD3 results in their expressive upregulation (b) with statistical significance (c). (d), (e) Increased expression of lipometabolic genes leads to the reduction of TG level (d) and attenuation of hepatocellular steatosis (e) (200x), respectively. The presented results are expressed as means ± S.D. $^{*}P < 0.05$, $^{**}P < 0.01$.

were characterized by significant downregulation of hepatic circRNA_0046367 (Figures 7(a) and 7(b)). In contrast, there was statistical increased miR-34a level in their liver tissue (control group versus steatosis group, $P < 0.01$) (Figure 7(c)). The inconsistent levels of circRNA_0046367 and miR-34a prevented their complementary interaction and resultantly promoted the inhibitory effect of miR-34a on PPARα. Dramatically, PPARα repression indeed occurred in the steatosis group with statistical significance at both transcriptional and translational levels (Figures 7(d), 7(e), and 7(f)), indicating an impact on the circRNA_0046367/miR-34a/PPARα regulatory system with steatosis-inducing characteristics.

4. Discussion

Being verified by growing evidences, circRNA/miRNA/mRNA regulatory system represents a novel, yet important, layer of epigenetic control over gene expression in physiological (cartilage degradation, insulin secretion, etc.) [18, 40] and pathological processes (cancer, sporadic AD, cerebral ischemia-reperfusion injury, heart failure, etc.) [16, 17, 32, 41, 42]. In our experiments, circRNA_0046367 experienced expression loss during hepatic steatosis *in vivo* and *in vitro*. The circRNA_0046367 level even inversely correlated to both steatotic degree and intracellular TG content with statistical significance, suggesting a circRNA-dependent regulatory action throughout steatogenesis.

circRNA, with the characteristics of tissue- and pathology-specific expression, has now been well described to effect in a manner of circRNA-miRNA interaction [15]. To investigate the miRNA-related role of circRNA_0046367 and underlying mechanisms, both circBase (http://www.circbase.org/) and miRBase (http://microrna.sanger.ac.uk/) were subjected to integration and transdatabase iterative search [19, 20, 43]. Bioinformatically, miR-34a was recognized to be the only target of circRNA_0046367 that correlated to hepatic steaosis. miR-34a influences the expression of multiple genes within steatosis-inducing signaling pathways, especially PPAR signaling pathway (rno03320) [44, 45]. Most of these PPAR signaling members (i.e., SCD1, ACSL1, ACSL4, and PCK1) could be transcriptionally activated by PPARα [46–49], which is then qualified for the key target gene of miR-34a. Except for the circRNA_0046367/miR-34a interaction, there were also algorithm-based proofs for the complementation between "seed sequence" of miR-34a and 3′ untranslated region (3′ UTR) of PPARα in the present experiments. Thus, hepatic steaosis was proposed to be

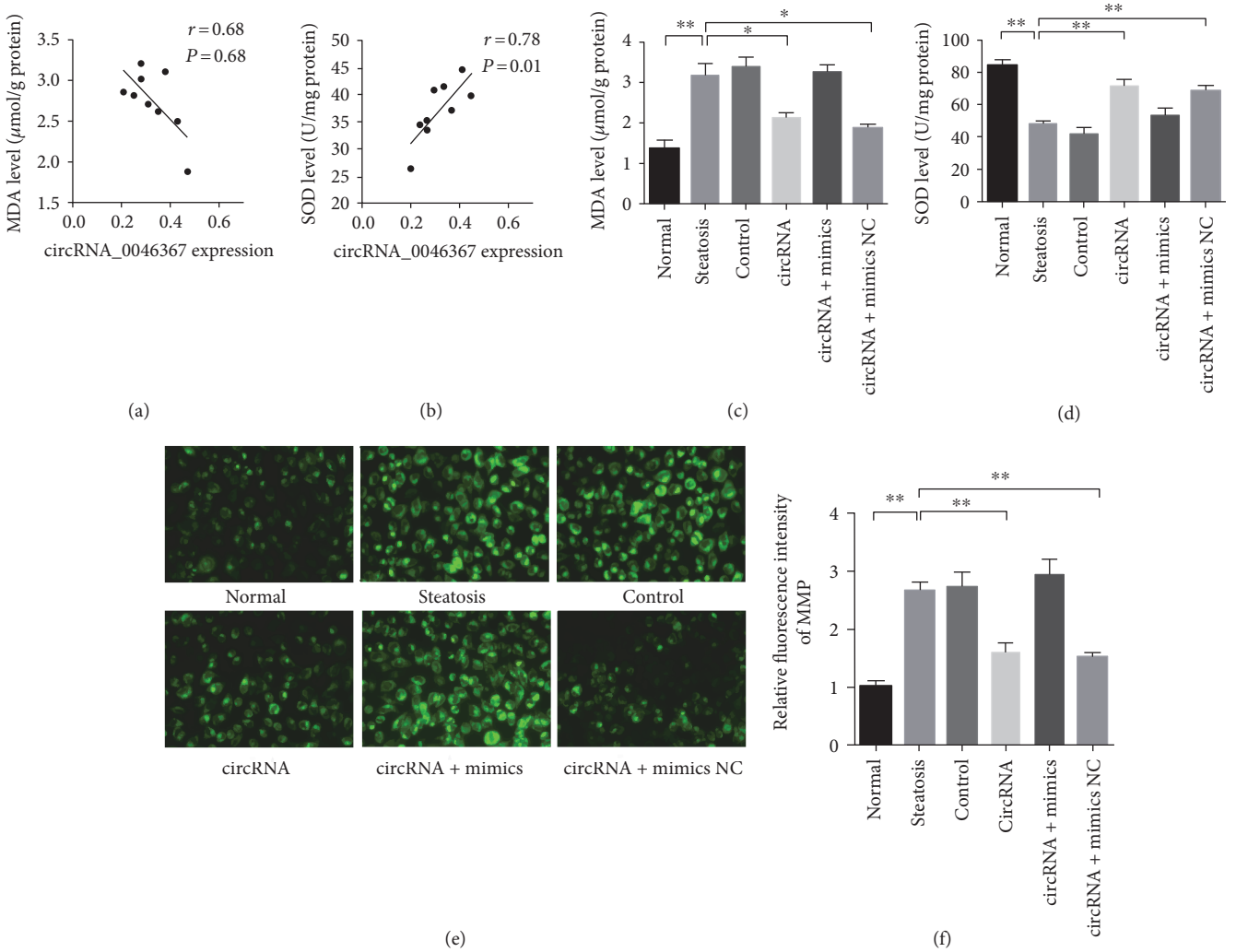

Figure 5: circRNA_0046367-dependent attenuation of hepatocellular steatosis ameliorates lipid peroxidation and mitochondrial dysfunction. (a), (b) circRNA_0046367 expression correlates to MDA (a) and SOD (b) levels of the steatosis group in negative and positive manner, respectively. (c), (d) circRNA_0046367 treatment reduces the indicator of lipid peroxidation (MDA) (c), whereas increases the antioxidative enzyme (SOD) (d) on a basis of steatosis improvement. (e), (f) Fluorescent assay for MMP represents the alleviated mitochondrial injury (e) (400x), with statistical significance (f), resulting from circRNA_0046367-dependent mitigation of lipid peroxidation. The presented results are expressed as means ± S.D. $^{*}P < 0.05$, $^{**}P < 0.01$.

associated with the abnormalities in circRNA_0046367/miR-34a/PPARα signaling.

Dual luciferase reporter assays in this study provided further verification that miR-34a mimics exerted complementary effect on both wild-type circRNA_0046367 and PPARα. In contrast, cotransfection of miR-34a and reporter vectors with mutant circRNA_0046367 and mutant PPARα, respectively, led to no decrease of firefly luciferase activity. circRNA_0046367, therefore, was indicated to serve as the miR-34a sponge and competing endogenous RNA (ceRNA) for PPARα. Its complementary binding to miR-34a prevented the miR-34a-PPARα interaction and then protected hepatocellular PPARα from transcriptional repression. PPARα, a ligand-activated transcription factor, belongs to the NR1C nuclear receptor subfamily. Multiple target genes of PPARα have been identified to underlie the fatty acid metabolism in tissues with high oxidative rates (liver, muscle, heart, etc.) [50]. PPARα downregulation, which further upregulates the SREBP-1c/PPARα ratio, predisposes obese patients to insulin resistance and hepatic steatogenesis [51]. Deductively, the impact of circRNA_0046367 on miR-34a/PPARα signaling is likely to ameliorate hepatocellular steatosis by the improvement in PPARα-mediated lipid metabolism.

In liver tissue of NAFLD patients and HepG2 cells with FFA-induced steatosis, PPARα expression indeed correlated to the level of circRNA_0046367 and miR-34a in positive and negative manner, respectively. Deficiency of CPT2 and ACBD3, both of which represent key target genes of PPARα, was detected in these steatotic cells characterized by lowered level of PPARα. When compared to that of the steatosis group, the circRNA group showed a dramatic increase in PPARα expression at both transcription and translation levels. The expression of lipometabolic genes increased

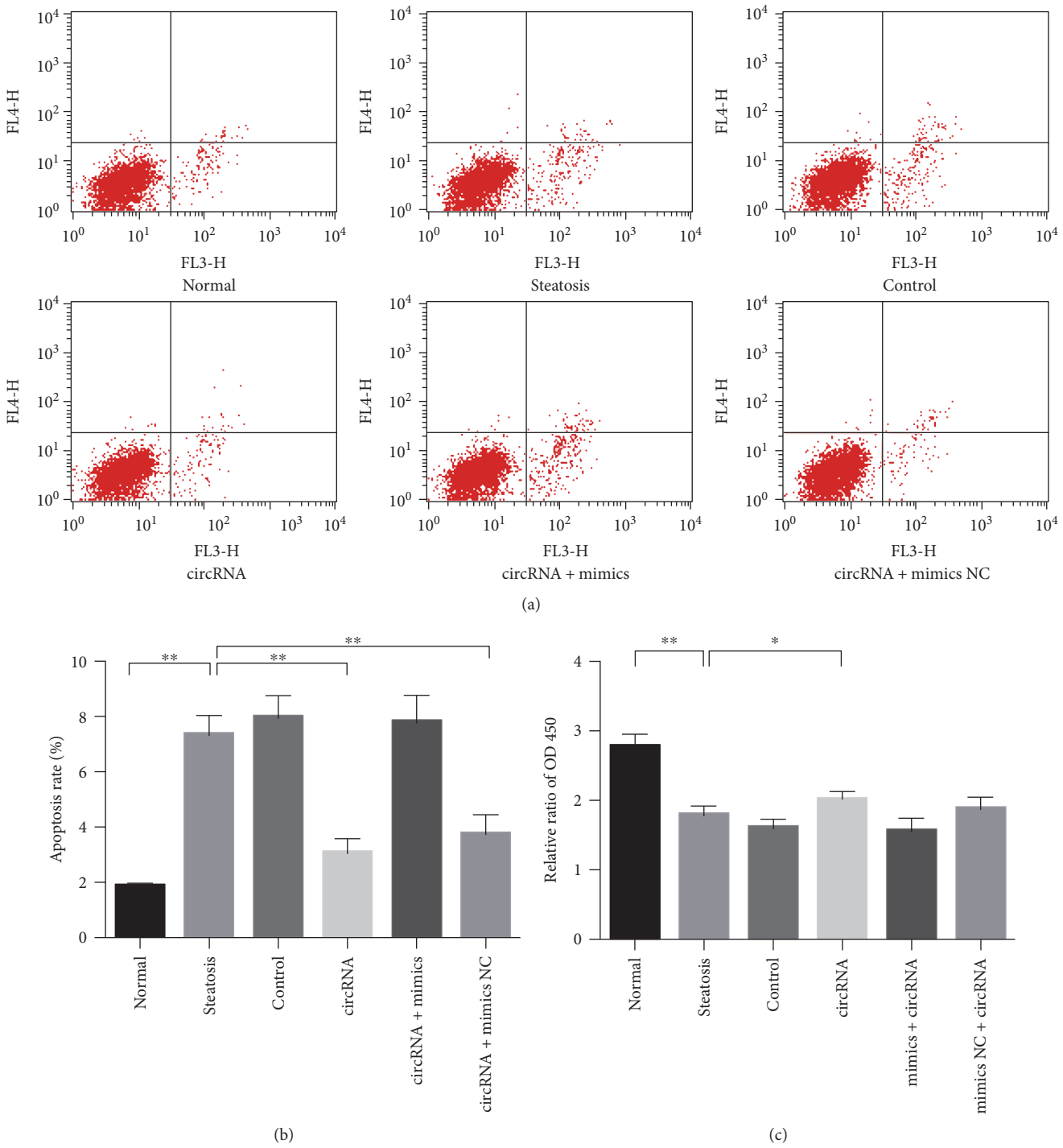

Figure 6: Improvement in proliferation and apoptosis reflects the protective effect of circRNA_0046367 against oxidative damage. (a) Dual-labeling flow cytometry presents ascending apoptosis rate in the groups exposed to FFA stimulation, yet decreasing apoptosis characterizes the effect of circRNA_0046367 intervention. (b) Quantitative assessment validates circRNA_0046367's impact on hepatocellular apoptosis. (c) Cell proliferation assay demonstrates the cytoprotective action of circRNA_0046367 against lipoxidative toxication. The presented results are expressed as means ± S.D. $^{*}P < 0.05$, $^{**}P < 0.01$.

simultaneously, in parallel to the levels of normal group. CPT2, one of the key enzymes in carnitine shuttle system, promotes mitochondrial β-oxidation in a process of long-chain fatty acid inflow [52, 53]. Nevertheless, ACBD3 takes the central place of an interaction network that composed of multiple genes involving steroid and cholesterol synthesis, including STAR, SCP2, NR0B1, acyl coenzyme-related ACBD1 and BACH, BLZF1, lipid degradation protein (AZGP1, alpha-2-glycoprotein 1, zinc-binding), and several p24 family members [54]. ACBD3 is then suggested to

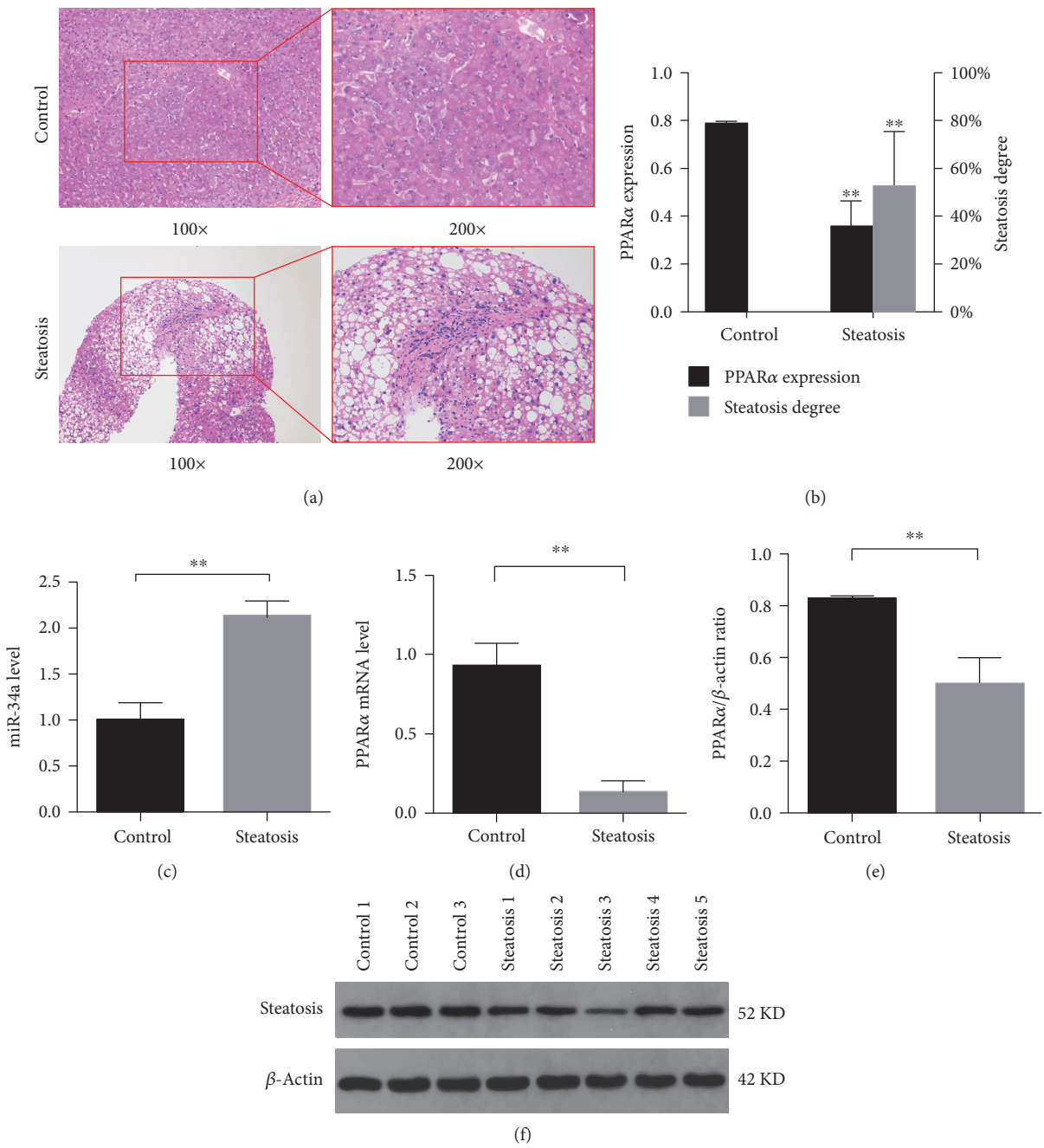

Figure 7: Characteristics of circRNA_0046367/miR-34a/PPARα regulatory system in hepatic steatosis. (a) HE staining identifies patients with (steatosis group) or without hepatic steatosis (control group), respectively. (b) Expression level of circRNA_0046367 and degree of hepatic steatosis (b). (c), (d) mRNA levels of hepatic miR-34a (c) and PPARα (d), respectively, in groups of control and steatosis. (e), (f) Western blot for the hepatic expression of PPARα (e) with relative quantification against β-actin (f) in different groups. The presented results are expressed as means ± S.D. Control group versus steatosis group: $^{**}P < 0.01$.

function as an A-kinase anchoring protein (AKAP) in the mitochondrial cholesterol transport and regulator of cAMP-dependent steroidogenesis [54, 55]. In consistent with their facilitatory role in lipid degradation [14], circRNA_0046367-induced normalization of both CPT2 and ACBD3 resultantly attenuated the hepatic steatosis by statistical downregulation of TG content.

Hepatic steatosis is accompanied by the impaired mitochondrial respiratory chain, which acts as a major source of reactive oxygen species (ROS) [56, 57]. Vice versa, the NOX2-generated oxidation appears to be deteriorated with the severity of hepatic steatosis in NAFLD patients, thereby results in the mitochondrial oxidative stress [58, 59]. Interestingly, the FFA-induced hepatic steatosis in our study demonstrated characteristics of increased MDA concentration and reduced level of SOD. MDA has been considered an important cytotoxic product of lipid peroxidation [60], whereas SOD catalyzes the dismutation from peroxide to

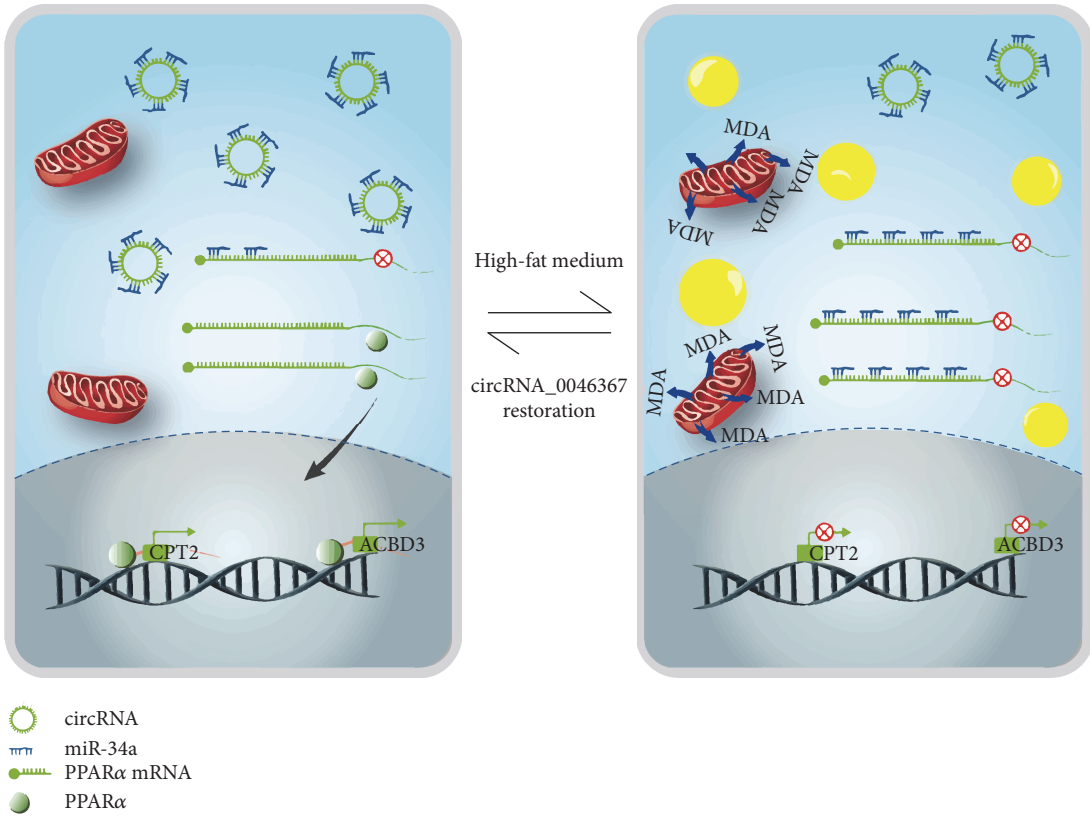

Figure 8: Schematic representation depicts the circRNA_0046367/miR-34a/PPARα regulatory system that underlies hepatic steatosis and lipoxidative damage. Expression loss of circRNA_0046367 characterizes the hepatic steatosis induced by high-fat stimulation. In contrast, circRNA_0046367 normalization abolishes miR-34a's inhibitory effect on PPARα via blocking the miRNA/mRNA interaction. Restored level of PPARα attenuates hepatic steatosis by the transcriptional activation of genes associated with lipid metabolism. Hepatotoxicity related to lipid peroxidation is resultantly resolved.

hydrogen peroxide [61]. These indicators for ROS-derived lipid peroxidation and antioxidative system, respectively, reflected an imbalance of prooxidant/antioxidant that occurred in mitochondrial oxidative stress after hepatosteatosis. On the contrary, circRNA_0046367 administration significantly downregulated the supernatant MDA on a basis of steatosis resolution. Its improvemental effect on SOD further restored the antioxidative process.

Impaired mitochondrial respiratory chain and β-oxidation in the hepatic steatosis induces ROS overproduction and lipid peroxidation and finally triggers a vicious circle that leads to mitochondrial oxidative stress [56]. Chronic oxidative stress is one of the critical factors responsible for lethal hepatocyte damage and disease progression in NAFLD [57, 62, 63], predominantly by the mitochondrial dysfunction [64, 65]. As evaluated by the abnormal MMP resulted from oxidative stress, groups with hepatic steatosis and circRNA_0046367 loss suffered from mitochondrial dysfunction in our experiments. Cell growth arrest and apoptosis took place in response to the progressive mitochondrial injury. Fortunately, circRNA_0046367 treatment abrogated the oxidation-dependent antiproliferative and proapoptotic actions with elevated MMP.

Because of their spatiotemporal expression, circRNAs have been uncovered to serve as diagnostic biomarkers for malignant (i.e., primary and metastatic ovarian carcinoma, acute myeloid leukemia, non-small-cell lung cancer, and colorectal cancer) [66–70] and nonmalignant disorders (i.e., major depressive disorder) [71]. Moreover, circRNA regulation demonstrates its potential role in the clinical interference of various diseases, such as colon cancer and hypertrophy-dependent heart failure [32, 72]. Methodologically, circCCDC66 knockdown is capable of inhibiting the tumor growth and cancer invasion in xenograft and orthotopic mouse models [72]. Enforced expression of heart-related circRNA (HRCR) *in vivo* and *in vitro* exhibits attenuated hypertrophic responses in cardiomyocytes [32]. According to its expressive lacking during hepatic steatosis, circRNA_0046367 normalization by intrahepatic overexpression may shed light on the clinical application of our findings. This circRNA-based gene therapy is proposed to induce the resolution of hepatic steatosis and lipid peroxidation in NAFLD patients via an impact on circRNA_0046367/miR-34a/PPARα axis.

5. Conclusions

circRNA_0046367/miR-34a/PPARα regulatory system represents a novel epigenetic mechanism underlying hepatic steatosis and related oxidative stress (Figure 8). In contrast

to its expression loss during steatogenesis, circRNA_0046367 normalization abolishes the miR-34a-induced PPARα inhibition and hepatic steatosis. The hepatotoxication by lipid peroxidation, with characteristics of mitochondrial dysfunction, growth arrest, and apoptosis, is resultantly improved. Therefore, circRNA_0046367 may be qualified for a potential approach to the therapy of lipoxidative toxication.

Conflicts of Interest

The authors declare no conflict of interests regarding the publication of this paper.

Authors' Contributions

Xing-Ya Guo and Jian-Neng Chen contributed equally to this paper.

Acknowledgments

The work is supported by the State Key Development Program for Basic Research of China, no. 2012CB517501; National Natural Science Foundation of China (81270492, 81470859, 81070346, 81270491, and 81470840); 100 Talents Program, no. XBR2011007h; and Program of the Committee of Science and Technology, no. 09140903500.

References

[1] F. S. Wang, J. G. Fan, Z. Zhang, B. Gao, and H. Y. Wang, "The global burden of liver disease: the major impact of China," *Hepatology*, vol. 60, no. 6, pp. 2099–2108, 2014.

[2] R. Jinjuvadia, F. Antaki, P. Lohia, and S. Liangpunsakul, "The association between nonalcoholic fatty liver disease and metabolic abnormalities in the United States population," *Journal of Clinical Gastroenterology*, vol. 51, no. 2, pp. 160–166, 2017.

[3] N. S. Choudhary, A. Duseja, N. Kalra, A. Das, R. K. Dhiman, and Y. K. Chawla, "Correlation of adipose tissue with liver histology in Asian Indian patients with nonalcoholic fatty liver disease (NAFLD)," *Annals of Hepatology*, vol. 11, no. 4, pp. 478–486, 2012.

[4] J. M. Navarro-Jarabo, E. Ubiña-Aznar, L. Tapia-Ceballos et al., "Hepatic steatosis and severity-related factors in obese children," *Journal of Gastroenterology and Hepatology*, vol. 28, no. 9, pp. 1532–1538, 2013.

[5] V. W. Wong, W. C. Chu, G. L. Wong et al., "Prevalence of nonalcoholic fatty liver disease and advanced fibrosis in Hong Kong Chinese: a population study using proton-magnetic resonance spectroscopy and transient elastography," *Gut*, vol. 61, no. 3, pp. 409–441, 2012.

[6] L. A. Adams, J. F. Lymp, J. St Sauver et al., "The natural history of nonalcoholic fatty liver disease: a population-based cohort study," *Gastroenterology*, vol. 129, no. 1, pp. 113–121, 2005.

[7] B. Li, Z. Zhang, H. Zhang et al., "Aberrant miR199a-5p/caveolin1/PPARα axis in hepatic steatosis," *Journal of Molecular Endocrinology*, vol. 53, no. 3, pp. 393–403, 2014.

[8] X. Meng, J. Guo, W. Fang et al., "Liver microRNA-291b-3p promotes hepatic lipogenesis through negative regulation of adenosine 5′-monophosphate (AMP)-activated protein kinase α1," *The Journal of Biological Chemistry*, vol. 291, no. 20, pp. 10625–10634, 2016.

[9] X. C. Wang, X. R. Zhan, X. Y. Li, J. J. Yu, and X. M. Liu, "MicroRNA-185 regulates expression of lipid metabolism genes and improves insulin sensitivity in mice with nonalcoholic fatty liver disease," *World Journal of Gastroenterology*, vol. 20, no. 47, pp. 17914–17923, 2014.

[10] A. N. Mattis, G. Wong, K. Hitchner et al., "A screen in mice uncovers repression of lipoprotein lipase by microRNA-29a as a mechanism for lipid distribution away from the liver," *Hepatology*, vol. 61, no. 1, pp. 141–152, 2015.

[11] X. Li, F. Lian, C. Liu, K. Q. Hu, and X. D. Wang, "Isocaloric pair-fed high-carbohydrate diet induced more hepatic steatosis and inflammation than high-fat diet mediated by miR-34a/SIRT1 axis in mice," *Scientific Reports*, vol. 5, p. 16774, 2015.

[12] R. E. Castro, D. M. Ferreira, M. B. Afonso et al., "miR-34a/SIRT1/p53 is suppressed by ursodeoxycholic acid in the rat liver and activated by disease severity in human nonalcoholic fatty liver disease," *Journal of Hepatology*, vol. 58, no. 1, pp. 119–125, 2013.

[13] W. Shan, L. Gao, W. Zeng et al., "Activation of the SIRT1/p66shc antiapoptosis pathway via carnosic acid-induced inhibition of miR-34a protects rats against nonalcoholic fatty liver disease," *Cell Death & Disease*, vol. 6, article e1833, 2015.

[14] J. Ding, M. Li, X. Wan et al., "Effect of miR-34a in regulating steatosis by targeting PPARα expression in nonalcoholic fatty liver disease," *Scientific Reports*, vol. 5, article 13729, 2015.

[15] T. B. Hansen, T. I. Jensen, B. H. Clausen et al., "Natural RNA circles function as efficient microRNA sponges," *Nature*, vol. 495, no. 7441, pp. 384–388, 2013.

[16] Y. Zhao, P. N. Alexandrov, V. Jaber, and W. J. Lukiw, "Deficiency in the ubiquitin conjugating enzyme UBE2A in Alzheimer's disease (AD) is linked to deficits in a natural circular miRNA-7 sponge (circRNA; ciRS-7)," *Genes*, vol. 7, no. 12, article E116, 2016.

[17] H. Xie, X. Ren, S. Xin et al., "Emerging roles of circRNA_001569 targeting miR-145 in the proliferation and invasion of colorectal cancer," *Oncotarget*, vol. 7, no. 18, pp. 26680–26691, 2016.

[18] Q. Liu, X. Zhang, X. Hu et al., "Circular RNA related to the chondrocyte ECM regulates MMP13 expression by functioning as a MiR-136 'Sponge' in human cartilage degradation," *Scientific Reports*, vol. 6, article 22572, 2016.

[19] P. Glažar, P. Papavasileiou, and N. Rajewsky, "circBase: a database for circular RNAs," *RNA*, vol. 20, no. 11, pp. 1666–1670, 2014.

[20] S. Griffiths-Jones, R. J. Grocock, S. van Dongen, A. Bateman, and A. J. Enright, "miRBase: microRNA sequences, targets and gene nomenclature," *Nucleic Acids Research*, vol. 34, Database issue, pp. D140–D144, 2006.

[21] A. L. Birkenfeld and G. I. Shulman, "Nonalcoholic fatty liver disease, hepatic insulin resistance, and type 2 diabetes," *Hepatology*, vol. 59, no. 2, pp. 713–723, 2014.

[22] P. Roingeard, "Hepatitis C virus diversity and hepatic steatosis," *Journal of Viral Hepatitis*, vol. 20, no. 2, pp. 77–84, 2013.

[23] J. Rehm, A. V. Samokhvalov, and K. D. Shield, "Global burden of alcoholic liver diseases," *Journal of Hepatology*, vol. 59, no. 1, pp. 160–168, 2013.

[24] G. C. Farrel, S. Chitturi, G. K. Lau, J. D. Sollano, and Asia-Pacific Working Party on NAFLD, "Guidelines for the assessment and management of non-alcoholic fatty liver disease in the Asia-Pacific region: executive summary," *Journal*

of Gastroenterology and Hepatology, vol. 22, no. 6, pp. 775–777, 2007.

[25] M. J. Gomez-Lechon, M. T. Donato, A. Martinez-Romero, N. Jimenez, J. V. Castell, and J. E. O'Connor, "A human hepatocellular in vitro model to investigate steatosis," *Chemico-Biological Interactions*, vol. 165, no. 2, pp. 106–116, 2007.

[26] X. Q. Zhang, Y. Pan, C. H. Yu et al., "PDIA3 knockdown exacerbates free fatty acid-induced hepatocyte steatosis and apoptosis," *PLoS One*, vol. 10, no. 7, article e0133882, 2015.

[27] Y. G. Zhang, H. L. Yang, Y. Long, and W. L. Li, "Circular RNA in blood corpuscles combined with plasma protein factor for early prediction of pre-eclampsia," *BJOG*, vol. 123, no. 13, pp. 2113–2118, 2016.

[28] X. Shang, G. Li, H. Liu et al., "Comprehensive circular RNA profiling reveals that hsa_circ_0005075, a new circular RNA biomarker, is involved in hepatocellular carcinoma development," *Medicine*, vol. 95, no. 22, article e3811, 2016.

[29] C. Sobolewski, N. Calo, D. Portius, and M. Foti, "MicroRNAs in fatty liver disease," *Seminars in Liver Disease*, vol. 35, no. 1, pp. 12–25, 2015.

[30] H. M. Yang, H. J. Do, D. K. Kim et al., "Transcriptional regulation of human Oct-4 by steroidogenic factor-1," *Journal of Cellular Biochemistry*, vol. 101, no. 5, pp. 1198–1209, 2007.

[31] H. Wu, M. Huang, M. Lu et al., "Regulation of microtubule-associated protein tau (MAPT) by miR-34c-5p determines the chemosensitivity of gastric cancer to paclitaxel," *Cancer Chemotherapy and Pharmacology*, vol. 71, no. 5, pp. 1159–1171, 2013.

[32] K. Wang, B. Long, F. Liu et al., "A circular RNA protects the heart from pathological hypertrophy and heart failure by targeting miR-223," *European Heart Journal*, vol. 37, no. 33, pp. 2602–2611, 2016.

[33] T. O. Crișan, T. S. Plantinga, F. L. van de Veerdonk et al., "Inflammasome-independent modulation of cytokine response by autophagy in human cells," *PLoS One*, vol. 6, no. 4, article e18666, 2011.

[34] J. Wang, P. Sun, Y. Bao, J. Liu, and L. An, "Cytotoxicity of single-walled carbon nanotubes on PC12 cells," *Toxicology In Vitro*, vol. 25, no. 1, pp. 242–250, 2011.

[35] J. Lin, Y. Zou, K. Cao, C. Ma, and Z. Chen, "The impact of heterologous catalase expression and superoxide dismutase overexpression on enhancing the oxidative resistance in Lactobacillus casei," *Journal of Industrial Microbiology & Biotechnology*, vol. 43, no. 5, pp. 703–711, 2016.

[36] M. Zeng, F. Xiao, X. Zhong et al., "Reactive oxygen species play a central role in hexavalent chromium-induced apoptosis in Hep3B cells without the functional roles of p53 and caspase-3," *Cellular Physiology and Biochemistry*, vol. 32, no. 2, pp. 279–290, 2013.

[37] C. J. Guo, Q. Pan, B. Jiang, G. Y. Chen, and D. G. Li, "Effects of upregulated expression of microRNA-16 on biological properties of culture-activated hepatic stellate cells," *Apoptosis*, vol. 14, no. 11, pp. 1331–1340, 2009.

[38] L. Liu, P. Huang, Z. Wang et al., "Inhibition of eEF-2 kinase sensitizes human nasopharyngeal carcinoma cells to lapatinib-induced apoptosis through the Src and Erk pathways," *BMC Cancer*, vol. 16, no. 1, p. 813, 2016.

[39] D. Upreti, A. Pathak, and S. K. Kung, "Development of a standardized flow cytometric method to conduct longitudinal analyses of intracellular CD3ζ expression in patients with head and neck cancer," *Oncology Letters*, vol. 11, no. 3, pp. 2199–2206, 2016.

[40] H. Xu, S. Guo, W. Li, and P. Yu, "The circular RNA Cdr1as, via miR-7 and its targets, regulates insulin transcription and secretion in islet cells," *Scientific Reports*, vol. 5, article 12453, 2015.

[41] Q. Zheng, C. Bao, W. Guo et al., "Circular RNA profiling reveals an abundant circHIPK3 that regulates cell growth by sponging multiple miRNAs," *Nature Communications*, vol. 7, article 11215, 2016.

[42] S. P. Lin, S. Ye, Y. Long et al., "Circular RNA expression alterations are involved in OGD/R-induced neuron injury," *Biochemical and Biophysical Research Communications*, vol. 471, no. 1, pp. 52–56, 2016.

[43] Q. Pan, C. Guo, C. Sun, J. Fan, and C. Fang, "Integrative analysis of the transcriptome and targetome identifies the regulatory network of miR-16: an inhibitory role against the activation of hepatic stellate cells," *Bio-Medical Materials and Engineering*, vol. 24, no. 6, pp. 3863–3871, 2014.

[44] Y. Chen, S. Cao, P. Xu et al., "Changes in the expression of miR-34a and its target genes following spinal cord injury in rats," *Medical Science Monitor*, vol. 22, pp. 3981–3993, 2016.

[45] Q. Su, C. Baker, P. Christian et al., "Hepatic mitochondrial and ER stress induced by defective PPARα signaling in the pathogenesis of hepatic steatosis," *American Journal of Physiology. Endocrinology and Metabolism*, vol. 306, no. 11, pp. E1264–E1273, 2014.

[46] H. I. Lee and M. K. Lee, "Coordinated regulation of scopoletin at adipose tissue-liver axis improved alcohol-induced lipid dysmetabolism and inflammation in rats," *Toxicology Letters*, vol. 237, no. 3, pp. 210–218, 2015.

[47] Q. Deng, X. Li, S. Fu et al., "SREBP-1c gene silencing can decrease lipid deposits in bovine hepatocytes cultured in vitro," *Cellular Physiology and Biochemistry*, vol. 33, no. 5, pp. 1568–1578, 2014.

[48] C. W. Miller and J. M. Ntambi, "Peroxisome proliferators induce mouse liver stearoyl-CoA desaturase 1 gene expression," *Proceedings of the National Academy of Sciences of the United States of America*, vol. 93, no. 18, pp. 9443–9448, 1996.

[49] J. S. Osorio, C. B. Jacometo, Z. Zhou, D. Luchini, F. C. Cardoso, and J. J. Loor, "Hepatic global DNA and peroxisome proliferator-activated receptor alpha promoter methylation are altered in peripartal dairy cows fed rumen-protected methionine," *Journal of Dairy Science*, vol. 99, no. 1, pp. 234–244, 2016.

[50] M. Pawlak, P. Lefebvre, and B. Staels, "Molecular mechanism of PPARα action and its impact on lipid metabolism, inflammation and fibrosis in non-alcoholic fatty liver disease," *Journal of Hepatology*, vol. 62, no. 3, pp. 720–733, 2015.

[51] P. Pettinelli, T. D. Pozo, J. Araya et al., "Enhancement in liver SREBP-1c/PPAR-alpha ratio and steatosis in obese patients: correlations with insulin resistance and n-3 long-chain polyunsaturated fatty acid depletion," *Biochimica et Biophysica Acta*, vol. 1792, no. 11, p. 1080, 2009.

[52] J. P. Bonnefont, F. Djouadi, C. Prip-Buus, S. Gobin, A. Munnich, and J. Bastin, "Carnitine palmitoyltransferases 1 and 2: biochemical, molecular and medical aspects," *Molecular Aspects of Medicine*, vol. 25, no. 5-6, pp. 495–520, 2004.

[53] M. Joshi, J. Eagan, N. K. Desai et al., "A compound heterozygous mutation in GPD1 causes hepatomegaly, steatohepatitis, and hypertriglyceridemia," *European Journal of Human Genetics*, vol. 22, no. 10, pp. 1229–1232, 2014.

[54] S. Ferdinandusse, G. Jimenez-Sanchez, J. Koster et al., "A novel bile acid biosynthesis defect due to a deficiency of peroxisomal ABCD3," *Human Molecular Genetics*, vol. 24, no. 2, pp. 361–370, 2015.

[55] E. Jarnaess, A. Ruppelt, A. J. Stokka, B. Lygren, J. D. Scott, and K. Tasken, "Dual specificity A-kinase anchoring proteins (AKAPs) contain an additional binding region that enhances targeting of protein kinase A type I," *The Journal of Biological Chemistry*, vol. 283, no. 48, pp. 33708–33718, 2008.

[56] X. Liu, J. Zhang, Y. Ming, X. Chen, M. Zeng, and Y. Mao, "The aggravation of mitochondrial dysfunction in nonalcoholic fatty liver disease accompanied with type 2 diabetes mellitus," *Scandinavian Journal of Gastroenterology*, vol. 50, no. 9, pp. 1152–1159, 2015.

[57] G. Paradies, V. Paradies, F. M. Ruggiero, and G. Petrosillo, "Oxidative stress, cardiolipin and mitochondrial dysfunction in nonalcoholic fatty liver disease," *World Journal of Gastroenterology*, vol. 20, no. 39, pp. 14205–14218, 2014.

[58] M. D. Ben, L. Polimeni, R. Carnevale et al., "NOX2-generated oxidative stress is associated with severity of ultrasound liver steatosis in patients with non-alcoholic fatty liver disease," *BMC Gastroenterology*, vol. 14, p. 81, 2014.

[59] M. A. Lanaspa, L. G. Sanchez-Lozada, Y. J. Choi et al., "Uric acid induces hepatic steatosis by generation of mitochondrial oxidative stress: potential role in fructose-dependent and -independent fatty liver," *The Journal of Biological Chemistry*, vol. 287, no. 48, pp. 40732–40449, 2012.

[60] G. Leonarduzzi, A. Scavazza, F. Biasi et al., "The lipid peroxidation end product 4-hydroxy-2,3-nonenal up-regulates transforming growth factor beta1 expression in the macrophage lineage: a link between oxidative injury and fibrosclerosis," *The FASEB Journal*, vol. 11, no. 11, pp. 851–857, 1997.

[61] M. Koruk, S. Taysi, M. C. Savas, O. Yilmaz, F. Akcay, and M. Karakok, "Oxidative stress and enzymatic antioxidant status in patients with nonalcoholic steatohepatitis," *Annals of Clinical and Laboratory Science*, vol. 34, no. 1, pp. 57–62, 2004.

[62] C. Xie, Z. Chen, C. Zhang et al., "Dihydromyricetin ameliorates oleic acid-induced lipid accumulation in L02 and HepG2 cells by inhibiting lipogenesis and oxidative stress," *Life Sciences*, vol. 157, pp. 131–139, 2016.

[63] E. Radi, P. Formichi, C. Battisti, and A. Federico, "Apoptosis and oxidative stress in neurodegenerative diseases," *Journal of Alzheimer's Disease*, vol. 42, Supplement 3, pp. S125–S152, 2014.

[64] B. Barnwal, H. Karlberg, A. Mirazimi, and Y. J. Tan, "The non-structural protein of Crimean-Congo hemorrhagic fever virus disrupts the mitochondrial membrane potential and induces apoptosis," *The Journal of Biological Chemistry*, vol. 291, no. 2, pp. 582–592, 2016.

[65] M. A. Esmekaya, N. Seyhan, H. Kayhan, M. Z. Tuysuz, A. C. Kurşun, and M. Yağcı, "Investigation of the effects of 2.1 GHz microwave radiation on mitochondrial membrane potential ($\Delta\Psi$m), apoptotic activity and cell viability in human breast fibroblast cells," *Cell Biochemistry and Biophysics*, vol. 67, no. 3, pp. 1371–1378, 2013.

[66] M. T. Venø, T. B. Hansen, S. T. Venø et al., "Spatio-temporal regulation of circular RNA expression during porcine embryonic brain development," *Genome Biology*, vol. 16, p. 245, 2015.

[67] I. Ahmed, T. Karedath, S. S. Andrews et al., "Altered expression pattern of circular RNAs in primary and metastatic sites of epithelial ovarian carcinoma," *Oncotarget*, vol. 7, no. 24, pp. 36366–36381, 2016.

[68] W. Li, C. Zhong, J. Jiao et al., "Characterization of hsa_circ_0004277 as a new biomarker for acute myeloid leukemia via circular RNA profile and bioinformatics analysis," *International Journal of Molecular Sciences*, vol. 18, no. 3, article E597, 2017.

[69] J. T. Yao, S. H. Zhao, Q. P. Liu et al., "Over-expression of CircRNA_100876 in non-small cell lung cancer and its prognostic value," *Pathology, Research and Practice*, vol. 213, no. 5, pp. 453–456, 2017.

[70] X. Wang, Y. Zhang, L. Huang et al., "Decreased expression of hsa_circ_001988 in colorectal cancer and its clinical significances," *International Journal of Clinical and Experimental Pathology*, vol. 8, no. 12, pp. 16020–16025, 2015.

[71] X. Cui, W. Niu, L. Kong et al., "hsa_circRNA_103636: potential novel diagnostic and therapeutic biomarker in major depressive disorder," *Biomarkers in Medicine*, vol. 10, no. 9, pp. 943–952, 2016.

[72] K. Y. Hsiao, Y. C. Lin, S. K. Gupta et al., "Noncoding effects of circular RNA CCDC66 promote colon cancer growth and metastasis," *Cancer Research*, vol. 77, no. 9, pp. 2339–2350, 2017.

Hindawi
Oxidative Medicine and Cellular Longevity
Volume 2017, Article ID 5189138, 12 pages
https://doi.org/10.1155/2017/5189138

Research Article

Identification of Four Oxidative Stress-Responsive MicroRNAs, miR-34a-5p, miR-1915-3p, miR-638, and miR-150-3p, in Hepatocellular Carcinoma

Yong Wan,[1] Ruixia Cui,[2] Jingxian Gu,[2] Xing Zhang,[2] Xiaohong Xiang,[2] Chang Liu,[2] Kai Qu,[2] and Ting Lin[2,3]

[1]*Department of Geriatric Surgery, The First Affiliated Hospital of Xi'an Jiaotong University, Xi'an 710061, China*
[2]*Department of Hepatobiliary Surgery, The First Affiliated Hospital of Xi'an Jiaotong University, Xi'an 710061, China*
[3]*Department of Surgical Intensive Care Units, The First Affiliated Hospital of Xi'an Jiaotong University, Xi'an 710061, China*

Correspondence should be addressed to Ting Lin; 947119451@qq.com

Received 30 January 2017; Accepted 20 April 2017; Published 24 July 2017

Academic Editor: Jaideep Banerjee

Increasing evidence suggests that oxidative stress plays an essential role during carcinogenesis. However, the underlying mechanism between oxidative stress and carcinogenesis remains unknown. Recently, microRNAs (miRNAs) are revealed to be involved in oxidative stress response and carcinogenesis. This study aims to identify miRNAs in hepatocellular carcinoma (HCC) cells which might involve in oxidative stress response. An integrated analysis of miRNA expression signature was performed by employing robust rank aggregation (RRA) method, and four miRNAs (miR-34a-5p, miR-1915-3p, miR-638, and miR-150-3p) were identified as the oxidative stress-responsive miRNAs. Pathway enrichment analysis suggested that these four miRNAs played an important role in antiapoptosis process. Our data also revealed miR-34a-5p and miR-1915-3p, but not miR-150-3p and miR-638, were regulated by p53 in HCC cell lines under oxidative stress. In addition, clinical investigation revealed that these four miRNAs might be involved in oxidative stress response by targeting oxidative stress-related genes in HCC tissues. Kaplan-Meier analysis showed that these four miRNAs were associated with patients' overall survival. In conclusion, we identified four oxidative stress-responsive miRNAs, which were regulated by p53-dependent (miR-34a-5p and miR-1915-3p) and p53-independent pathway (miR-150-3p and miR-638). These four miRNAs may offer new strategy for HCC diagnosis and prognosis.

1. Introduction

Hepatocellular carcinoma (HCC) is the fifth most common cancer and the third cause of cancer-related mortality worldwide [1]. It is established that hepatitis virus infection, as well as environmental carcinogens such as aflatoxin or chemical carcinogens, is associated with the development of HCC [2]. Although the carcinogenic mechanism of above risk factors varies, the common pathological process affected by those risk factors is hepatic chronic inflammation. Recruitment of inflammatory cells in hepatic environment and chemical mediator release, such as cytokines, chemokines, and reactive oxygen species (ROS), are considered to play a vital pathogenic role during hepatic carcinogenesis [3].

ROS are a group of chemically reactive molecules containing oxygen, which are mainly derived from cellular oxidative metabolism and play essential roles in the regulation of multiple cellular processes. During the development of many diseases, including malignant diseases, increasing ROS levels might lead to the imbalance of the pro-oxidant/antioxidant equilibrium and subsequently induce changes of intracellular molecules, including lipids, proteins, and nuclear acids [4]. Thus, the exploration of the intracellular molecules responsible for oxidative stress might enrich our understanding of molecular hepatic carcinogenesis.

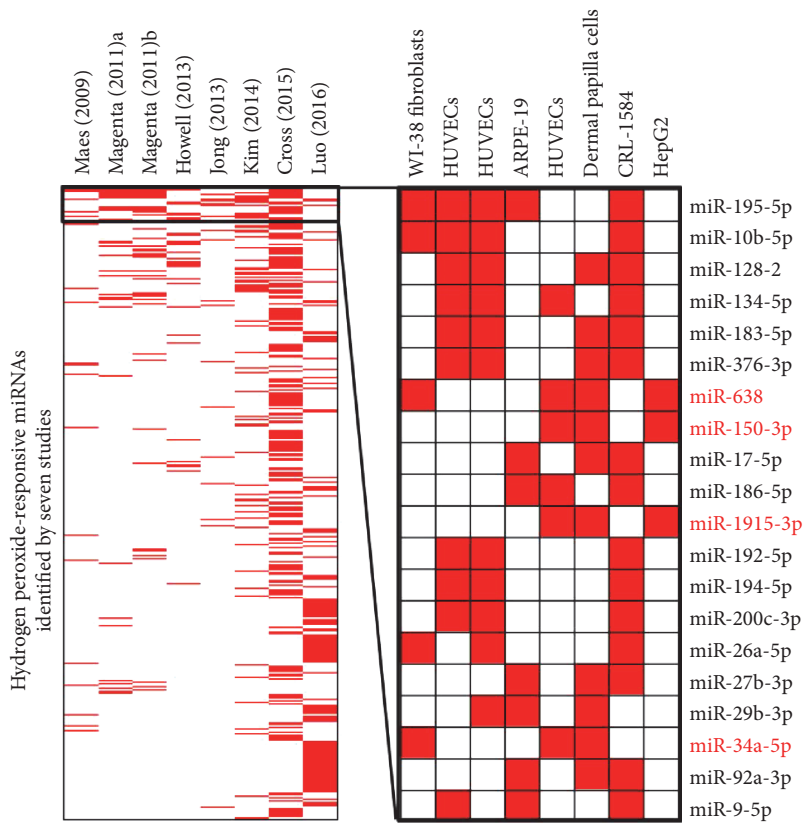

FIGURE 1: Heatmap of miRNAs reported by nine miRnome profiling studies. One selected miRNA was presented as red or white according to whether it was report by one study or not.

Recently, accumulating evidences suggest that a series of small noncoding RNAs (microRNA) can be induced by oxidative stress. Several studies have examined the changes of the microRNA (miRNAs) expression profiles in varying cells upon treatment with hydrogen peroxide (H_2O_2) [5–14]. Unfortunately, inconsistent conclusion was made from those miRNome profiling studies. Confounding factors may include employment of different cell origins, various detection platforms, and application of different statistical methods.

To overcome those limitations, in the present study, we integrated these published relevant studies and performed a meta-analysis applying the rank aggregation method. We identified four common oxidative stress-responsive microRNAs in H_2O_2-treated cells. Moreover, we also evaluated the association between those oxidative stress-responsive microRNAs and p53, a key oxidative stress-responsive mediator in HCC cell lines. Finally, we validated the expression of identified miRNAs and their target genes in HCC tissues.

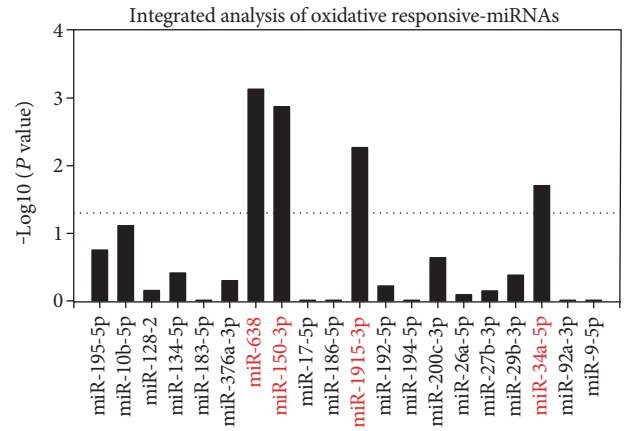

FIGURE 2: Integrated analysis of oxidative responsive-miRNAs by RRA method. The column was presented according to $-\text{Log}_{10}$ (P value) of each miRNA which was calculated by RRA method.

2. Materials and Methods

2.1. Literature Search and Inclusion Criteria. We performed a literature search in PubMed, Embase, and Web of Knowledge databases using search term combination of (miRNA* or microRNA* or mir-*) and profil* and (oxidati* or hydrogen peroxide) and (cell* or cell line*). We firstly screened all abstracts and selected potential abstracts for further full text evaluation. Only the original experimental studies that explored miRNA profile using a high-throughput miRNA expression profiling methods such as second-generation sequencing, polymerase chain reaction (PCR),

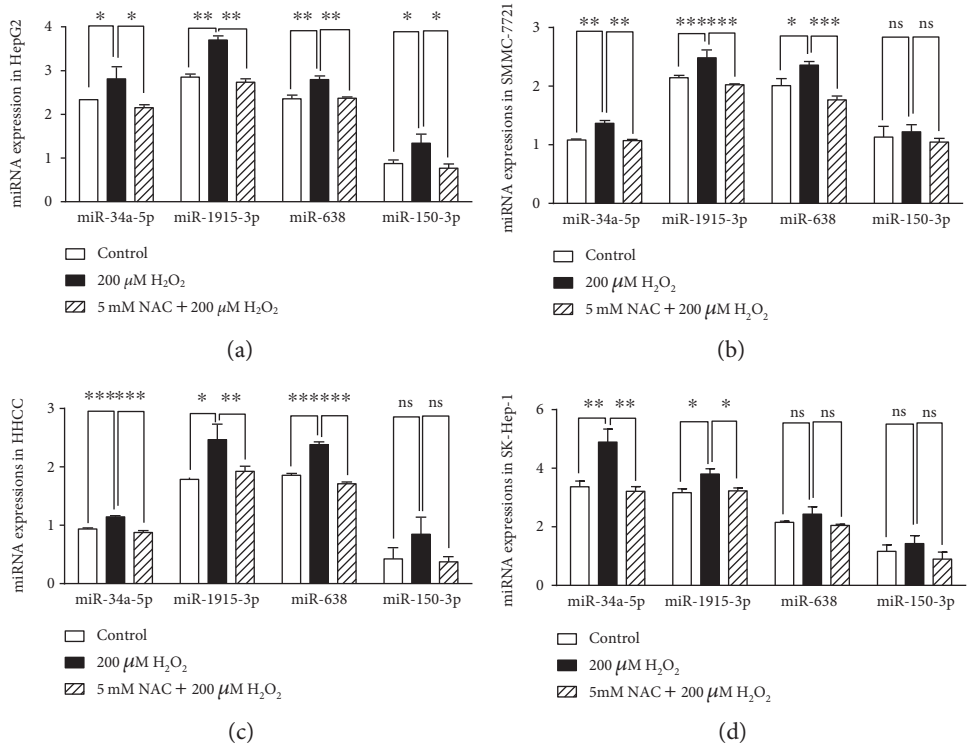

Figure 3: Expression of four oxidative stress-responsive miRNAs in different HCC cell lines. The expressions of miR-34a-5p, miR-1915-3p, miR-638, and miR-150-3p were measured by qRT-PCR method in HepG2 (a), SMMC-7721 (b), HHCC (c), and SK-Hep-1 (d). All HCC cell lines were treated with saline, 200 μM H_2O_2 or 5 mM NAC + 200 μM H_2O_2, respectively. All these experiments were conducted in triplicate. $^*P < 0.05$; $^{**}P < 0.01$; $^{***}P < 0.001$; ns, no significant.

or microarray-based high-throughput methods in H_2O_2-treated cells were included.

2.2. Data Extraction and Rank Aggregation Analysis. Rank lists of up- or downregulated miRNAs were extracted from the included studies. All included miRNA names were firstly standardized using miRBase (release 21.0). Rank aggregation method was implemented using an R package "Robust Rank Aggreg." This method analyzed miRNAs that are ranked consistently better than expected and assigns a P value for each miRNA.

2.3. Pathway Enrichment Analysis. We firstly collected validated targets of each miRNA using miRTarBase database (http://mirtarbase.mbc.nctu.edu.tw/). Gene ontology (GO) biological process enrichment of those validated targets was performed using Database for Annotation, Visualization and Integrated Discovery (DAVID) v6.8 (https://david.ncifcrf.gov/). Fisher's exact test was used to identify the significant pathway terms. Heatmap was presented by log-transformed P value. Moreover, the combinatorial pathway enrichment analysis of multiple miRNAs was analyzed using "miRPath" algorithm (http://www.microrna.gr/miRPathv2).

2.4. miRNA-Gene Interaction Network Analysis. We firstly performed target prediction by using Targetscan website (http://www.targetscan.org/), and only cumulative-weighted context++ score< −0.4 was selected for further analysis. The interaction between miRNA and their predicted target networks was constructed using the Cytoscape software. In the validation group, the miRNA-gene interaction was presented based on their Pearson's correlation coefficient.

2.5. HCC Cell Line Culture. Four *TP53* wild-type HCC cell lines, including HepG2, SMMC-7721, HHCC, and SK-Hep-1, were selected for experimental validation. All cell lines were cultured using Dulbecco minimum essential medium (DMEM) supplemented with heat-inactivated 10% fetal bovine serum (FBS), 100 U/ml penicillin, and 100 μg/ml streptomycin. Cells were incubated at 37°C and 5% CO_2 in a HF100 chamber (Heal Force, Hong Kong, China).

2.6. Pro- and Antioxidant Treatment. For pro-oxidant treatment, HCC cell lines were firstly synchronized by serum starvation overnight and then treated with 200 μM of H_2O_2 for 24 h. For antioxidant treatment, cells were preincubated with N-acetylcysteine (NAC, 5 mM) for 6 hours before exposure to H_2O_2. Following treatment, cells were harvested for further analysis.

2.7. Transfection of siRNA. RNA interference mediated by duplexes of 21-nucleotide RNA was performed in HCC cell lines. siRNA-*TP53* (5′-CUGGAAGACUCCAGUG GUA-3) and control-siRNA were synthesized by GenePharma (Shanghai, China). Transfection of siRNA

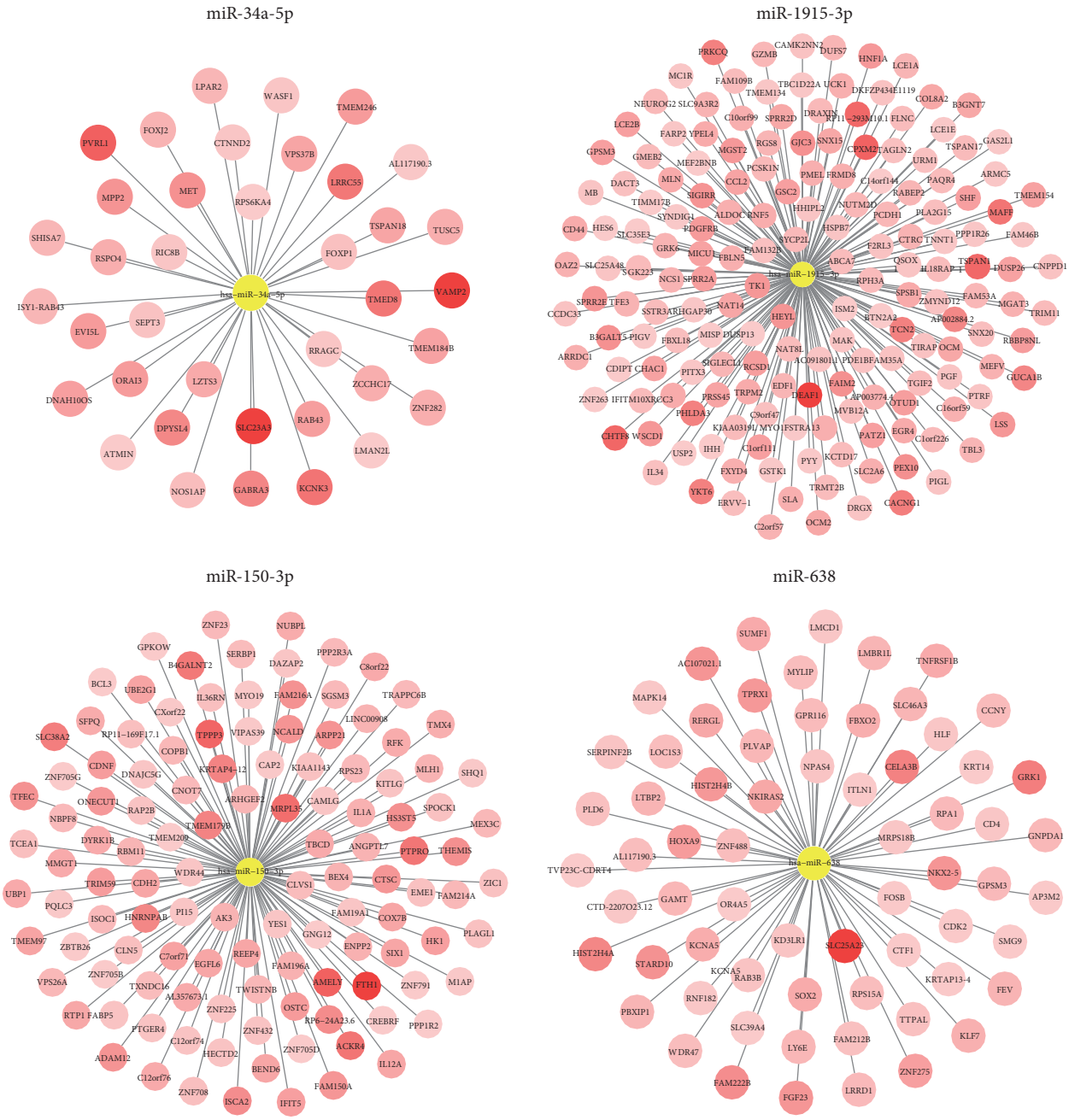

Figure 4: The interaction network between four miRNAs and their predicted targets.

(100 nM) was carried out with Lipofectamine 2000 (Invitrogen, Carlsbad, CA, USA) according to the manufacturer's protocols.

2.8. Quantitative Reverse Transcription-Polymerase Chain Reaction (qRT-PCR). Total RNA was extracted from cultured cells using Trizol reagent (Invitrogen, Carlsbad, CA, USA). qRT-PCR was performed using the SYBR® PrimeScript™ miRNA RT-PCR Kit and SYBR Premix Ex Taq™ (TaKaRa Biotechnology, Dalian, China). All primers of selective miRNAs were also synthesized by TaKaRa. The miRNA expression was assayed in triplicate and normalized to U6. The relative miRNA expression was calculated using the comparative-Ct (△△Ct) method.

2.9. Public Datasets for Validation. To validate the expression of miRNAs and their targets in HCC tissues, we used public datasets containing 100 paired HCC tissue samples (GSE62007 and GSE62043). GSE62007 dataset was conducted on miRXplore Microarray platform, and GSE62043 dataset was conducted on Agilent-014850 Whole Human Genome Microarray platform. For hepatocellular carcinoma, The Cancer Genome Atlas (TCGA) dataset were used to explore the prognosis

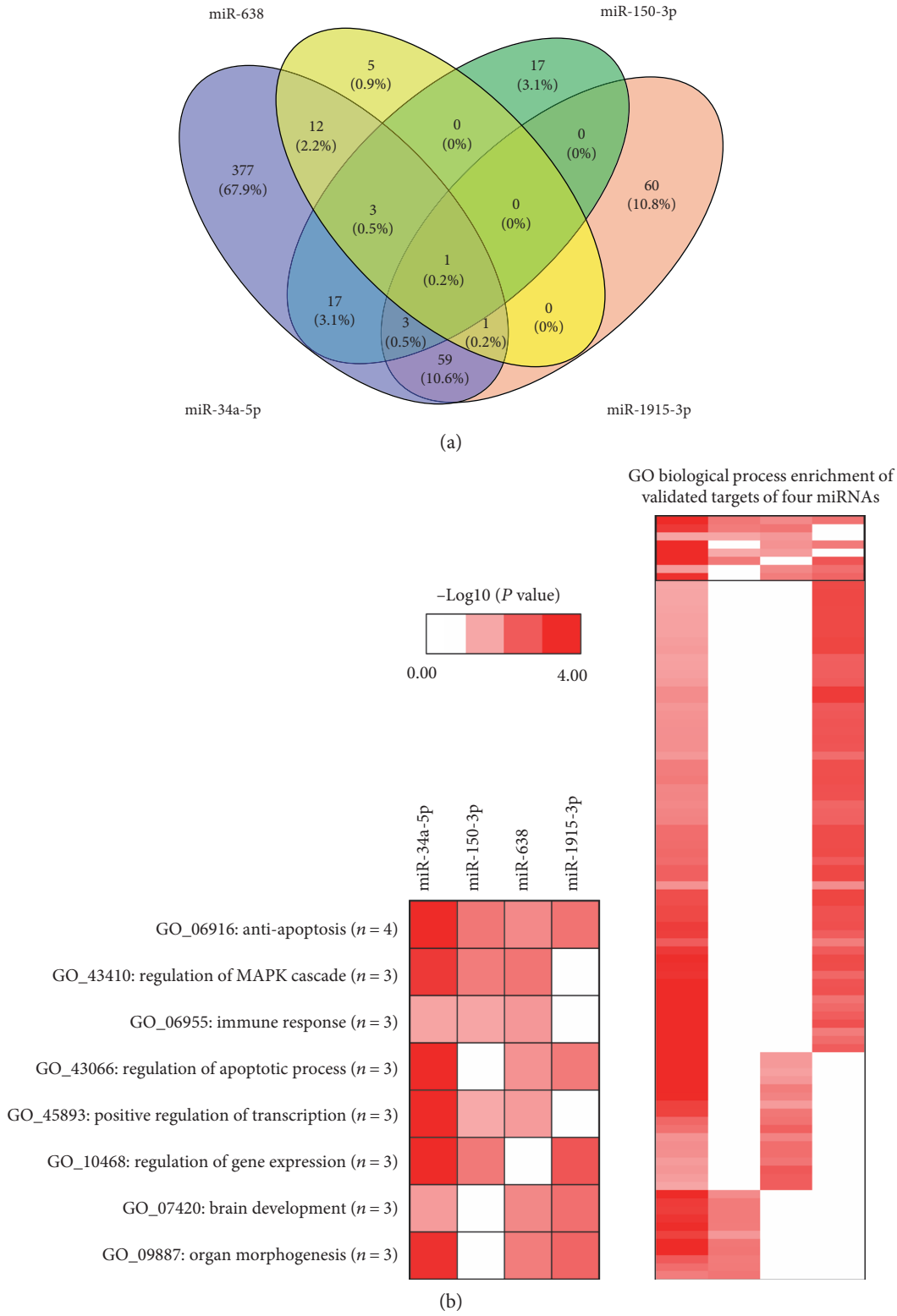

Figure 5: Pathway enrichment analysis of four oxidative stress-responsive miRNAs. (a) Venn diagram of pathways of four oxidative stress-responsive miRNAs. (b) Heatmap of pathways of four oxidative stress-responsive miRNAs. Range of colors (white to deep red) shows the $-\text{Log}_{10}$ (P value of pathway enrichment analysis) (low to high).

values of four miRNAs in HCC. The data were obtained from SurvMicro web tool (http://bioinformatica.mty.itesm.mx/SurvMicro).

2.10. Statistical Analysis. All data in this study were analyzed by SPSS 11.0 software (SPSS Inc., Chicago, IL, USA) and expressed as mean ± standard error of measurement (SEM).

Analysis of continuous variables was performed using a Student t-test. Expression correlation between variables was tested by Pearson's correlation analysis. $P < 0.05$ was considered statistically significant.

3. Results

3.1. Identification of Oxidative Stress-Responsive miRNAs. A total of 11 studies from 10 published articles were screened [5–14], and 8 studies were based on human cells [6, 7, 10–14], which were selected for further analysis. In summary, 504 aberrantly expressed miRNAs were recorded, including 404 upregulated and 99 downregulated miRNAs. Among them, twenty upregulated miRNAs were reported by more than three studies (Figure 1). By applying a rank aggregation analysis, we identified four oxidative stress-responsive miRNAs which were significant upregulated under H_2O_2 treatment, including miR-638, miR-150-3p, miR-1915-3p, and miR-34a-5p (Figure 2).

3.2. Validation of Oxidative Stress-Responsive miRNAs in HCC Cell Lines. To further explore the expression changes of identified miRNAs in oxidative stress response in HCC, we treated four *TP53* wild-type HCC cell lines with 200 μM H_2O_2 (the most widely used concertation) for 24 h and measured expression levels of four miRNAs (miR-34a-5p, miR-1915-3p, miR-638, and miR-150-3p). Our data revealed that the expressions of four miRNAs were all significantly increased after H_2O_2 treatment. By contrast, when preincubation with 5 mM NAC for 6 h, the upregulated expressions of miR-34a-5p, miR-1915-3p, miR-638, and miR-150-3p caused by H_2O_2 treatment were abrogated (Figure 3). The above results provide evidence that the expressions of miR-34a-5p, miR-1915-3p, miR-638, and miR-150-3p were tightly associated with intracellular oxidative stress status in HCC cell lines.

3.3. Function Prediction of Oxidative Stress-Responsive miRNAs. We firstly performed target prediction by using Targetscan web tool, and the miRNA-target interaction was visualized in Figure 4. To further evaluate biological functions of four miRNAs, we selected their experimental validated targets for GO pathway enrichment analysis. The number of enriched GO biological process of each miRNA ranged from 22 to 474 (Figure 5(a)). By conducting a heatmap of P values derived from Fisher's exact test, four miRNAs were shown to be all closely related to antiapoptosis pathways (Figure 5(b)). Furthermore, combinatorial pathway enrichment analysis revealed that those four oxidative stress-responsive miRNAs were related to p53 signaling pathway (Table 1). Previous studies had clearly demonstrated the closely association between p53 signaling pathway and oxidative stress [15, 16], suggesting a critical role of four miRNAs (miR-34a-5p, miR-1915-3p, miR-638, and miR-150-3p) in oxidative stress response.

3.4. miR-34a-5p and miR-1915-3p Are Regulated by p53 under Oxidative Stress. Since our data suggested an association between oxidative stress-responsive miRNAs and p53 signaling pathway, we wondered whether the expressions of these miRNAs in oxidative stress response are regulated by p53. Evidences from our [17, 18] and other groups [19] suggested that p53 was upregulated in response to oxidative stress in HCC. Thus, by employing four HCC cell line data, we quantified the correlation coefficient between p53 and four oxidative stress-responsive miRNAs expression. We found that p53 gene (*TP53*) was statistically positively correlated to the expressions of miR-34a-5p and miR-1915-3p ($P < 0.05$), but not miR-638 and miR-150-3p ($P > 0.05$) (Figure 6), indicating that p53 might regulate the miR-34a-5p and miR-1915-3p function in oxidative stress response. To further verify this hypothesis, we then examined the miR-34a-5p and miR-1915-3p expressions in siRNA-*TP53*-transfected HCC cells. As shown in Figures 7(a) and 7(c), the miR-34a-5p and miR-1915-3p expression levels were significantly decreased by knocking down of *TP53* (all $P < 0.05$). Furthermore, knocking down of *TP53* was shown to be able to attenuate the increased expression of miR-34a-5p and miR-1915-3p induced by H_2O_2 treatment, providing solid evidence for the regulatory roles of p53 in miR-34a-5p and miR-1915-3p in oxidative stress response (Figures 7(b) and 7(d)).

Table 1: The signaling pathway enrichments of validated targets of four miRNAs.

KEGG signaling pathways	P value
KEGG_04115: p53 signaling pathway	$2.24E-10$
KEGG_04310: Wnt signaling pathway	$4.83E-09$
KEGG_04330: notch signaling pathway	$1.34E-06$
KEGG_04630: Jak-STAT signaling pathway	$3.83E-04$
KEGG_04722: neurotrophin signaling pathway	$1.73E-03$
KEGG_04340: hedgehog signaling pathway	$1.89E-03$
KEGG_04010: MAPK signaling pathway	$3.33E-03$
KEGG_04370: VEGF signaling pathway	$4.06E-03$
KEGG_04350: TGF-beta signaling pathway	$4.98E-03$
KEGG_04660: T cell receptor signaling pathway	$9.59E-03$
KEGG_04150: mTOR signaling pathway	$2.14E-02$
KEGG_04920: adipocytokine signaling pathway	$3.27E-02$
KEGG_03320: PPAR signaling pathway	$3.36E-02$

3.5. Clinical Values of Four Oxidative Stress-Responsive miRNAs in HCC. To gain insight into clinical values of four oxidative stress-responsive miRNAs in HCC, we firstly obtained 4 miRNAs and 90 oxidative stress-related gene profiling data based on 100 paired HCC samples (GSE62007 and GSE62043) from Gene Expression Omnibus (GEO, http://www.ncbi.nlm.nih.gov/geo/) (Figure 8(a)). By calculating the expression correlations between each miRNA and oxidative stress-related gene, we conducted a miRNA-gene interaction network (Figure 8(b)). Our data showed that miR-150-3p and miR-1915-3p were negatively correlated with more than half of oxidative stress-related genes (54/90 and 50/90, resp.). miR-34a-5p was negatively correlated with 44 out of 90 oxidative stress-

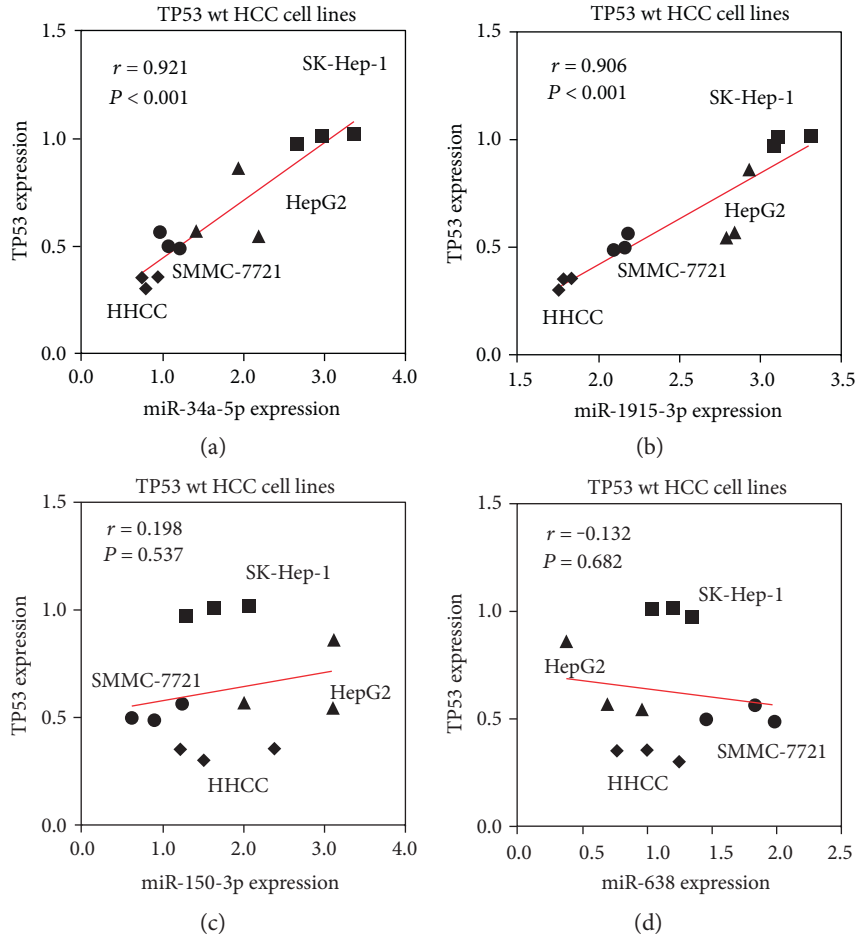

Figure 6: The expression correlation between four miRNAs and *TP53*. (a) miR-34a-5p, (b) miR-1915-3p, (c) miR-150-3p, and (d) miR-638.

related genes. Meanwhile, miR-638 was only negatively correlated with the least number of oxidative stress-related genes (38/90), which was partially consistent with previous study [20]. Moreover, tissue expression pattern also validated the positively correlation between p53 and miR-34a/miR-1915-3p with correlation coefficients of 0.13 and 0.16, respectively.

Next, we explored the prognosis values of four oxidative stress-responsive miRNAs in HCC patients. We obtained HCC TCGA data by using SurvMicro web tool (http://bioinformatica.mty.itesm.mx/SurvMicro) and conducted Kaplan-Meier analysis of HCC patients with different miRNA expression levels. We found that HCC patients with lower miR-34a and miR-1915-3p expression levels had shorter overall survival time, although we did not get a statistically significant *P* value which might due to a small sample size (Figures 9(a) and 9(b)). Similarly, we also found that miR-638 and miR-150-3p could predict HCC patients' survival time, with a *P* value of 0.042 (Figure 9(c)). It should be pointed out that the expression level of miR-638 in high-risk group was slightly higher than that in low risk group, with a nonsignificant *P* value (Figure 9(d)), which may warrant future larger study to confirm or refuse it.

4. Discussion

For decades, oxidative stress has been reported to impact carcinogenesis. However, the underlying interaction among oxidative stress and carcinogenesis remains unknown. Recently, increasing evidence suggested that some intracellular miRNAs play critical roles in oxidative stress response and carcinogenesis. Therefore, in the current study, we aim to identify several oxidative stress-responsive miRNAs which might involve in liver carcinogenesis. We firstly performed a comprehensive analysis by employing a recently published rank aggregation analysis method [21], to identify oxidative stress-responsive miRNAs. Based on miRNA profiling data, four miRNAs (miR-34a-5p, miR-1915-3p, miR-638, and miR-150-3p) were identified as the common upregulated miRNAs under oxidative stress. Next, we also validated these four oxidative stress-responsive miRNAs in four different HCC cell lines. Specifically, we found that the upregulation of miR-34a-5p and miR-1915-3p, but not miR-638 and miR-150-3p, was depended on p53 status in oxidative stress (Figure 10). Finally, our data also provide clinical evidences for the possible negative regulation of oxidative stress-related genes by these four miRNAs in HCC tissues. We found that the expression levels

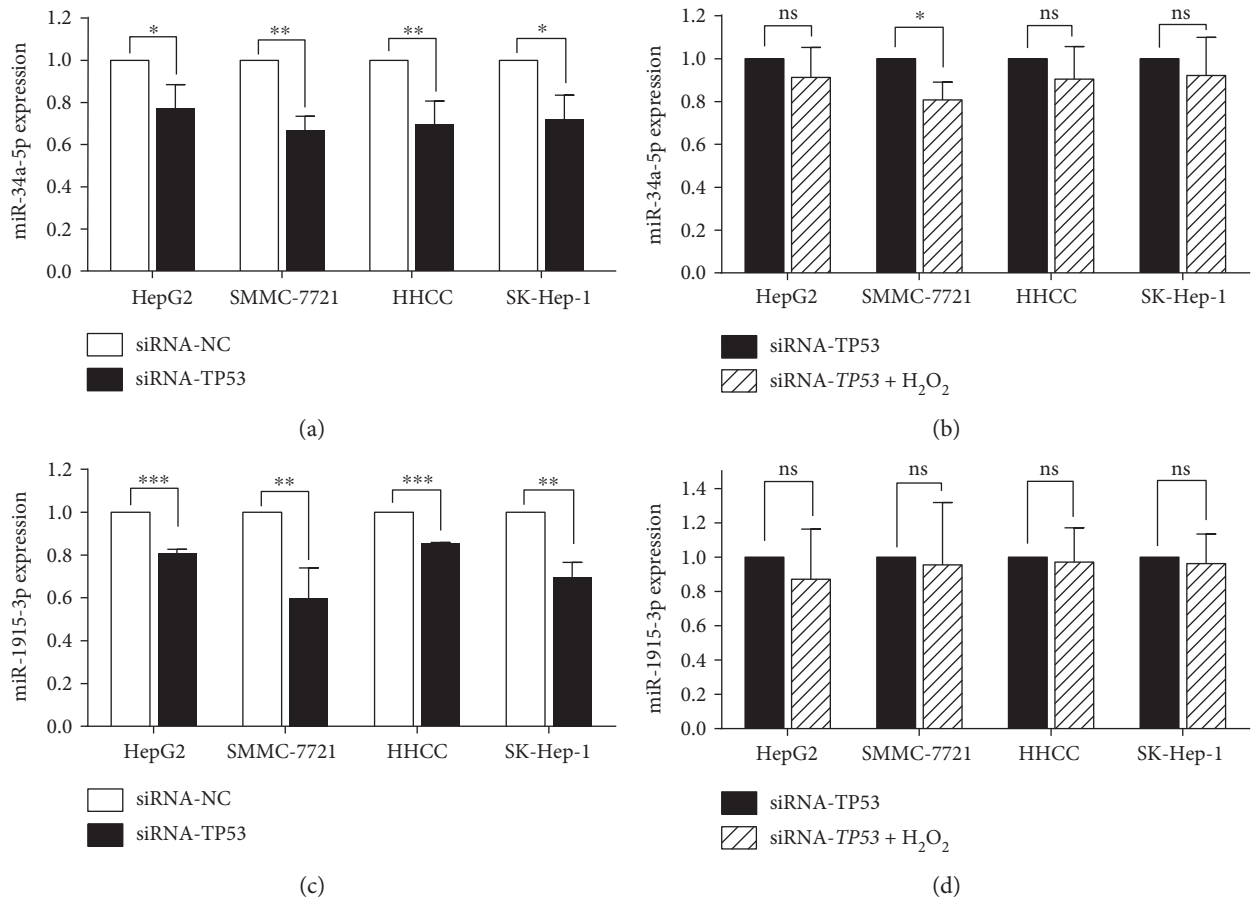

Figure 7: miR-1915-3p and miR-34a-5p are regulated by p53. (a, c) After transfection of siRNA-*TP53*, the expression of miR-34a-5p and miR-1915-3p was analyzed by qRT-PCR. (b, d) After transfection of siRNA-*TP53*, the expression of miR-34a-5p and miR-1915-3p was measured with or without H_2O_2 treatment. $^*P < 0.05$; $^{**}P < 0.01$; $^{***}P < 0.001$; ns, no significant.

of those four miRNAs were associated with overall survival time in HCC patients.

miR-34a-5p is one of the most explored miRNAs in carcinogenesis [22]. Although comparatively low levels of miR-34a-5p expression were reported in several cancers [23, 24], discrepancies emerged in HCC. Researchers found that the expression of miR-34a was downregulated during methyl-deficient diet-induced liver carcinogenesis [25]. By contrast, in a chemical-induced HCC model, miR-34a-5p was found to be upregulated [26]. We speculate that miR-34a-5p might be regulated by different mechanisms during liver carcinogenesis. It has been widely accepted that chemotherapeutic agents exhibited anticancer effects by producing ROS in the target tissue. We observed the ROS generation in HCC cells with cisplatin treatment [17]. Bai et al. also found that miR-34a-5p suppressed mitochondrial antioxidative enzymes with a concomitant increase in intracellular ROS level [27]. All above evidences suggested the miR-34-5p expression might be related to ROS level in HCC cells. In the present study, by conducting an oxidative stress model in four HCC cell lines, we confirmed that miR-34a-5p was related to intracellular oxidative stress status. Furthermore, we also found miR-34a-5p was involved in the p53-dependent pathway, which was consistent with previous results [22, 28].

miR-1915-3p was another dysregulated miRNA in various types of cancer, such as prostate cancer, renal cell carcinoma, breast cancer, lung cancer, and colorectal cancer [29–33]. However, the function of miR-1915-3p remains unknown in HCC. The present study revealed for the first time that miR-1915-3p was upregulated by oxidative stress, depending on p53 status in HCC. Recently, a study based on colorectal cancer cells also confirmed our results [32]. The authors [32] reported that miR-1915-3p was involved in response to chemotherapeutic drug-induced DNA damage by targeting *Bcl-2*, the latter of which was an important regulator of oxidative stress [34]. Additionally, they also found that p53 induced the processing of pri-miR-1915-3p to pre-miR-1915-3p, which promote overexpression of mature miR-1915-3p in. These data suggested that, differing from miR-34a-5p, miR-1915-3p expression was regulated by p53 in a transcription-independent way. When focusing on the genes potentially affect oxidative stress, we found that many oxidative stress-related genes might be potential targets of miR-1915-3p. These evidences suggest that by targeting oxidative stress-related genes, miR-

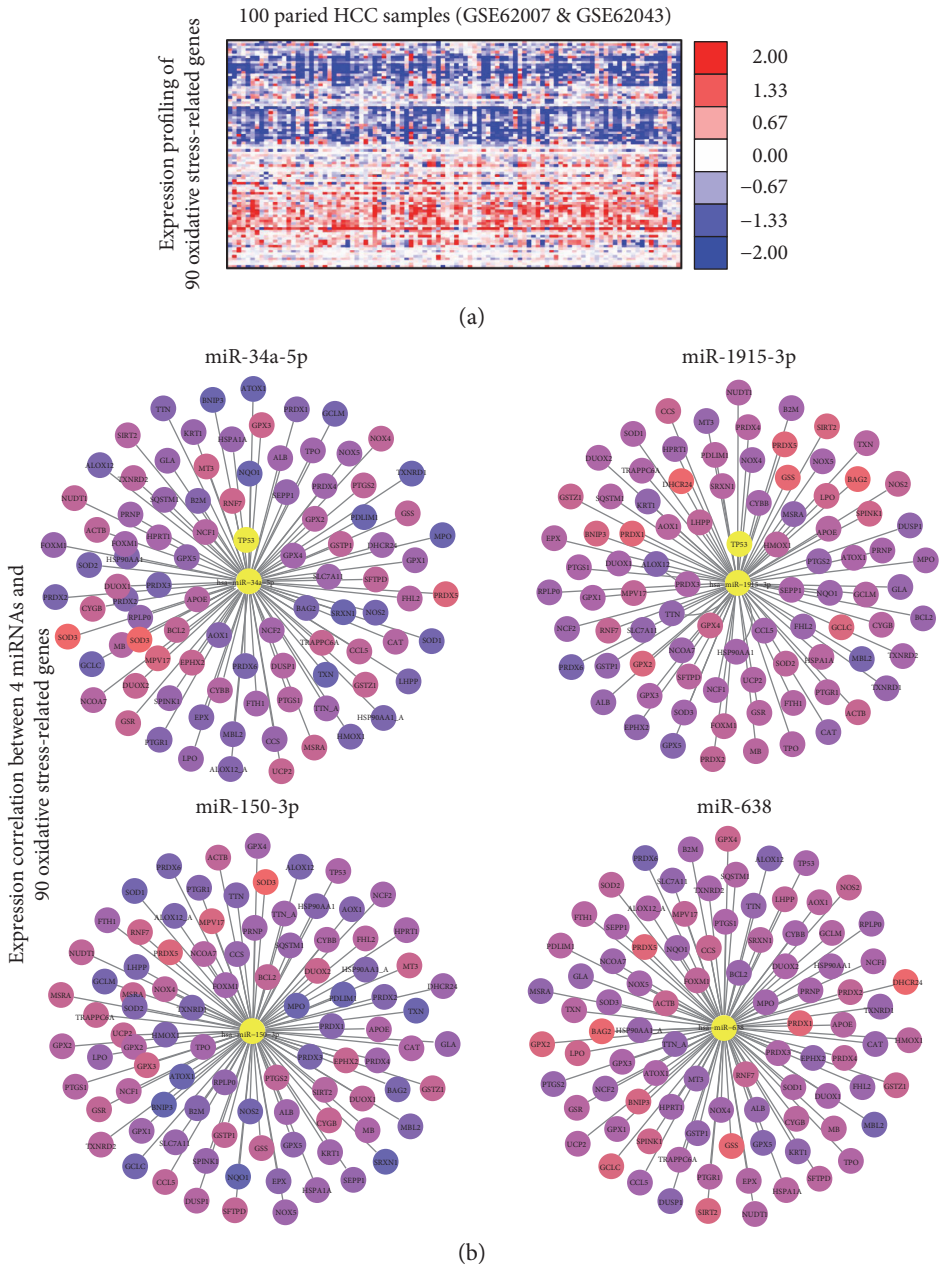

Figure 8: Four miRNAs and oxidative stress-related genes in HCC. (a) Heatmap of 90 oxidative stress-related gene expressions in HCC tissues with different miR-1915-3p status. (b) The expression correlation between four miRNAs and 90 oxidative stress-related genes. Range of colors (blue to red) was represented according to Pearson's correlation coefficient (low to high).

1915-3p might possess a significant role in the regulation of oxidative stress response.

miR-638 was previously reported to be associated with cellular senescence [6] and DNA damage [35]. In 2013, Christenson et al. [20] screened the gene expression in miR-638-inhibited fibroblasts and suggested that miR-638 might involve in oxidative stress response. In the present study, we, for the first time, identified miR-638 as an oxidative stress-induced miRNA in HCC cell lines. We found that the elevated expression of miR-638 was not induced by p53. However, the regulation mechanisms of miR-638 during oxidative stress have hardly been investigated. Tay et al. found that miR-638 was encoded by Dnm2 locus and demonstrated that both two components, miR-638 and its host gene Dnm2, were overexpressed in tumorigenesis [36]. Moreover, it was also reported that Dnm2 could be upregulated by radiation-induced oxidative stress [37]. Therefore, we hypothesized that oxidative stress might promote transcription of host gene Dnm2 and miR-638 was cooperatively upregulated. Furthermore, our data also showed that HCC patients with high risk had a higher expression level of miR-638 than low risk group. However, the association between miR-638 and cancer prognosis was inconsistent. Some studies showed that the

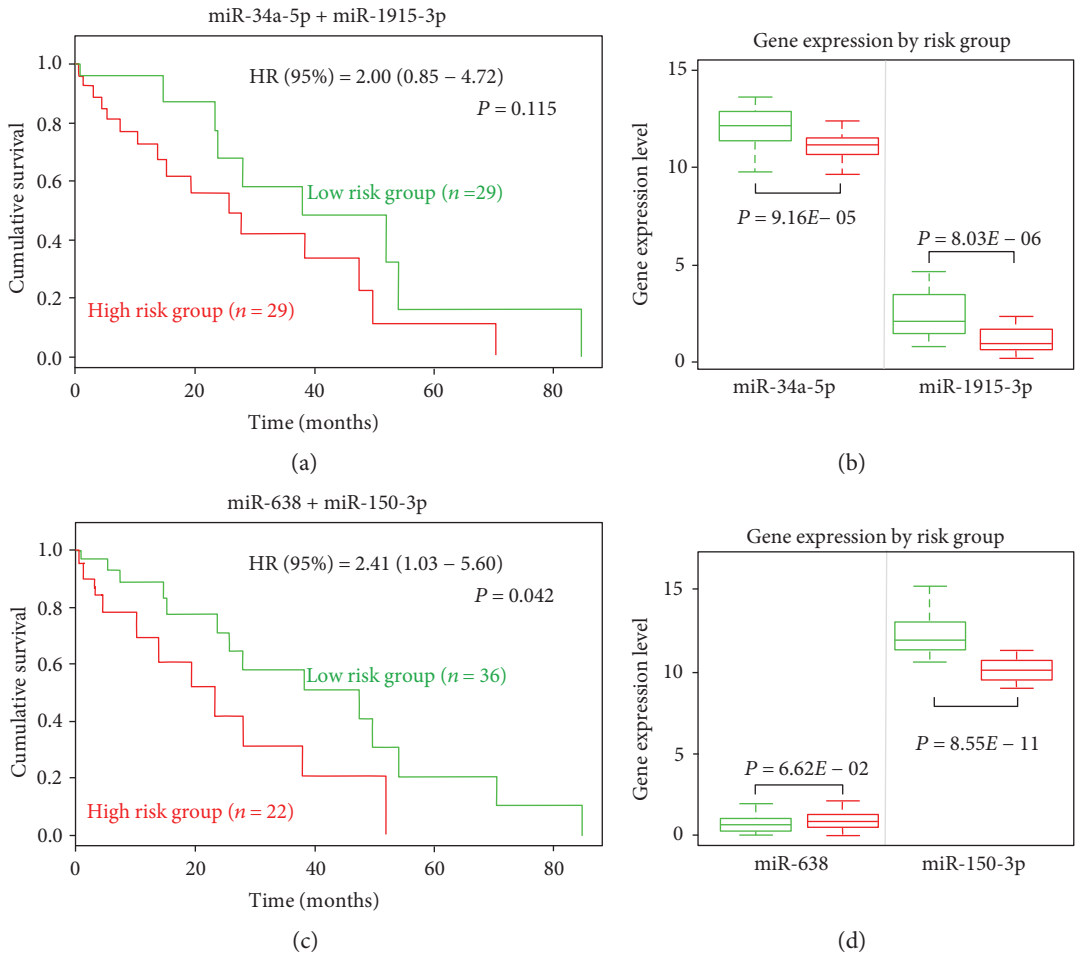

Figure 9: Prognosis values of four miRNAs in HCC. (a) Kaplan-Meier curve of overall survival for patients with different risk groups identified by miR-34a-5p and miR-1915-3p. (b) The expression levels of miR-34a-5p and miR-1915-3p in different risk groups. (c) Kaplan-Meier curve of overall survival for patients with different risk groups identified by miR-150-3p and miR-638. (d) The expression levels of miR-150-3p and miR-638 in different risk groups.

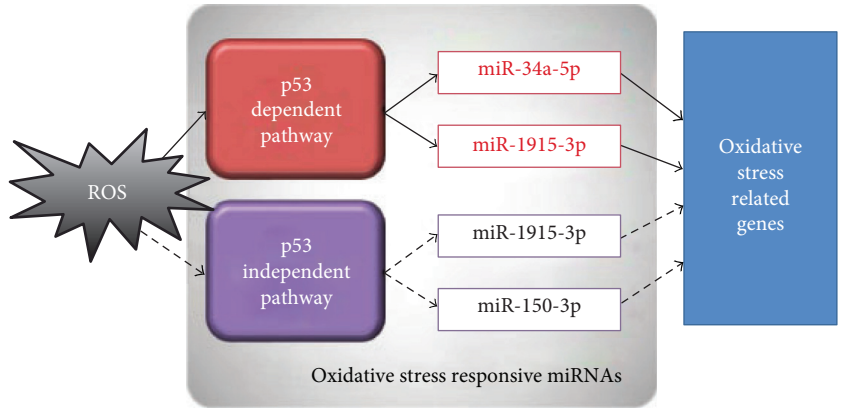

Figure 10: Overview of oxidative stress-responsive miRNAs mechanism in HCC. Oxidative stress-induced miRNA by p53-dependent (miR-34a-5p and miR-1915-3p) or p53-independent (miR-638 and miR-150-3p) pathways. All those oxidative stress-responsive miRNAs inhibit translation of their target genes and involve in oxidative stress process.

downregulation of miR-638 was involved in malignant phenotypes of osteosarcoma, gastric carcinoma, and colorectal carcinoma [38–40]. By contrast, Bhattacharya et al. [41] reported that miR-638 promoted melanoma progression. Besides, Ren et al. [42] also found that miR-638 acts as an oncogene and promotes cell proliferation and metastasis in esophageal squamous cell carcinoma and breast cancer cells. Considering our data did not get a statistically significant

P value, the jury must refrain from drawing a firm conclusion until a well-designed clinical study confirms or refutes the above findings.

Additionally, we also observed that miR-150-3p was induced by oxidative stress and was not depended on p53 overexpression. However, its functions in oxidative response and liver carcinogenesis have yet to be unravelled. It was reported that miR-150-3p could be induced by NF-kB activation [43]. Considering the important roles of NF-kB pathway in oxidative stress response and inflammation [44], investigating the underlying interaction between NF-kB and miR-150-3p will be of particular interest to study the molecular mechanisms of oxidative stress response in liver carcinogenesis.

Taken together, we identified four oxidative stress-responsive miRNAs (miR-34a-5p and miR-1915-3p, but not miR-638 and miR-150-3p) and further demonstrated p53-dependent and p53-independent mechanisms of miRNA expression regulation in HCC. Given a critical role for oxidative stress in carcinogenesis, our present findings have significant clinical implications. These miRNAs might offer new potential strategy for cancer diagnosis and prognosis.

Conflicts of Interest

The authors declare that they have no conflict of interests.

Authors' Contributions

Kai Qu and Chang Liu designed the research and wrote the paper; Yong Wan, Ting Lin, Ruixia Cui, Jingxian Gu, and Xing Zhang participated in the research work; Ting Lin and Xiaohong Xiang collected and analyzed the data; Yong Wan constructed the figures; and Kai Qu drafted and revised the manuscript.

Acknowledgments

This work was supported by the National Science Foundation of China (nos. 81071876, 81472247, and 81201549); the Project of Innovative Research Team for Key Science and Technology in Xi'an Jiaotong University, the Program for Innovative Research Team of Shaanxi Province (no. 2013KCJ-23); the Fundamental Research Funds for the Central Universities (no. 2016qngz05); the Clinical Research Award of the First Affiliated Hospital of Xi'an Jiaotong University, China (no. XJTU1AF-CRF-2015-011); and the Hospital Fund of the First Affiliated Hospital of Xi'an Jiaotong University (nos. 2014YK11 and 2016QN-23).

References

[1] A. Jemal, F. Bray, M. M. Center, J. Ferlay, E. Ward, and D. Forman, "Global cancer statistics," *CA: A Cancer Journal for Clinicians*, vol. 61, no. 2, pp. 69–90, 2011.

[2] H. B. El-Serag, "Epidemiology of viral hepatitis and hepatocellular carcinoma," *Gastroenterology*, vol. 142, no. 6, article e1261, pp. 1264–1273, 2012.

[3] J. K. Stauffer, A. J. Scarzello, Q. Jiang, and R. H. Wiltrout, "Chronic inflammation, immune escape, and oncogenesis in the liver: a unique neighborhood for novel intersections," *Hepatology*, vol. 56, no. 4, pp. 1567–1574, 2012.

[4] R. Cardin, M. Piciocchi, M. Bortolami et al., "Oxidative damage in the progression of chronic liver disease to hepatocellular carcinoma: an intricate pathway," *World Journal of Gastroenterology*, vol. 20, no. 12, pp. 3078–3086, 2014.

[5] Y. Lin, X. Liu, Y. Cheng, J. Yang, Y. Huo, and C. Zhang, "Involvement of MicroRNAs in hydrogen peroxide-mediated gene regulation and cellular injury response in vascular smooth muscle cells," *The Journal of Biological Chemistry*, vol. 284, no. 12, pp. 7903–7913, 2009.

[6] O. C. Maes, H. Sarojini, and E. Wang, "Stepwise up-regulation of microRNA expression levels from replicating to reversible and irreversible growth arrest states in WI-38 human fibroblasts," *Journal of Cellular Physiology*, vol. 221, no. 1, pp. 109–119, 2009.

[7] A. Magenta, C. Cencioni, P. Fasanaro et al., "miR-200c is upregulated by oxidative stress and induces endothelial cell apoptosis and senescence via ZEB1 inhibition," *Cell Death and Differentiation*, vol. 18, no. 10, pp. 1628–1639, 2011.

[8] B. Mateescu, L. Batista, M. Cardon et al., "miR-141 and miR-200a act on ovarian tumorigenesis by controlling oxidative stress response," *Nature Medicine*, vol. 17, no. 12, pp. 1627–1635, 2011.

[9] S. Xu, R. Zhang, J. Niu et al., "Oxidative stress mediated-alterations of the microRNA expression profile in mouse hippocampal neurons," *International Journal of Molecular Sciences*, vol. 13, no. 12, pp. 16945–16960, 2012.

[10] J. C. Howell, E. Chun, A. N. Farrell et al., "Global microRNA expression profiling: curcumin (diferuloylmethane) alters oxidative stress-responsive microRNAs in human ARPE-19 cells," *Molecular Vision*, vol. 19, pp. 544–560, 2013.

[11] H. L. Jong, M. R. Mustafa, P. M. Vanhoutte, S. AbuBakar, and P. F. Wong, "MicroRNA 299-3p modulates replicative senescence in endothelial cells," *Physiological Genomics*, vol. 45, no. 7, pp. 256–267, 2013.

[12] O. Y. Kim, H. J. Cha, K. J. Ahn, I. S. An, S. An, and S. Bae, "Identification of microRNAs involved in growth arrest and cell death in hydrogen peroxide-treated human dermal papilla cells," *Molecular Medicine Reports*, vol. 10, no. 1, pp. 145–154, 2014.

[13] C. E. Cross, M. F. Tolba, C. M. Rondelli, M. Xu, and S. Z. Abdel-Rahman, "Oxidative stress alters miRNA and gene expression profiles in villous first trimester trophoblasts," *BioMed Research International*, vol. 2015, Article ID 257090, 2015.

[14] Y. W. X. Luo, L. Wang, J. Gao et al., "Identification of microRNAs involved in growth arrest and apoptosis in hydrogen peroxide-treated human hepatocellular carcinoma cell line HepG2," *Oxidative Medicine and Cellular Longevity*, vol. 2016, Article ID 7530853, 2016.

[15] J. Pflaum, S. Schlosser, and M. Muller, "p53 family and cellular stress responses in cancer," *Frontiers in Oncology*, vol. 4, p. 285, 2014.

[16] A. V. Budanov, "The role of tumor suppressor p53 in the antioxidant defense and metabolism," *Sub-Cellular Biochemistry*, vol. 85, pp. 337–358, 2014.

[17] K. Qu, T. Lin, Z. Wang et al., "Reactive oxygen species generation is essential for cisplatin-induced accelerated senescence

in hepatocellular carcinoma," *Frontiers of Medicine*, vol. 8, no. 2, pp. 227–235, 2014.

[18] K. Qu, T. Lin, J. Wei et al., "Cisplatin induces cell cycle arrest and senescence via upregulating P53 and P21 expression in HepG2 cells," *Nan Fang Yi Ke da Xue Xue Bao = Journal of Southern Medical University*, vol. 33, no. 9, pp. 1253–1259, 2013.

[19] J. Zhao, J. Chen, B. Lu et al., "TIP30 induces apoptosis under oxidative stress through stabilization of p53 messenger RNA in human hepatocellular carcinoma," *Cancer Research*, vol. 68, no. 11, pp. 4133–4141, 2008.

[20] S. A. Christenson, C. A. Brandsma, J. D. Campbell et al., "miR-638 regulates gene expression networks associated with emphysematous lung destruction," *Genome Medicine*, vol. 5, no. 12, p. 114, 2013.

[21] U. Vosa, R. Kolde, J. Vilo, A. Metspalu, and T. Annilo, "Comprehensive meta-analysis of microRNA expression using a robust rank aggregation approach," *Methods in Molecular Biology (Clifton, NJ)*, vol. 1182, pp. 361–373, 2014.

[22] X. Xu, W. Chen, R. Miao et al., "miR-34a induces cellular senescence via modulation of telomerase activity in human hepatocellular carcinoma by targeting FoxM1/c-Myc pathway," *Oncotarget*, vol. 6, no. 6, pp. 3988–4004, 2015.

[23] H. Tazawa, N. Tsuchiya, M. Izumiya, and H. Nakagama, "Tumor-suppressive miR-34a induces senescence-like growth arrest through modulation of the E2F pathway in human colon cancer cells," *Proceedings of the National Academy of Sciences of the United States of America*, vol. 104, no. 39, pp. 15472–15477, 2007.

[24] C. Welch, Y. Chen, and R. L. Stallings, "MicroRNA-34a functions as a potential tumor suppressor by inducing apoptosis in neuroblastoma cells," *Oncogene*, vol. 26, no. 34, pp. 5017–5022, 2007.

[25] V. P. Tryndyak, S. A. Ross, F. A. Beland, and I. P. Pogribny, "Down-regulation of the microRNAs miR-34a, miR-127, and miR-200b in rat liver during hepatocarcinogenesis induced by a methyl-deficient diet," *Molecular Carcinogenesis*, vol. 48, no. 6, pp. 479–487, 2009.

[26] T. Sukata, K. Sumida, M. Kushida et al., "Circulating microRNAs, possible indicators of progress of rat hepatocarcinogenesis from early stages," *Toxicology Letters*, vol. 200, no. 1-2, pp. 46–52, 2011.

[27] X. Y. Bai, Y. Ma, R. Ding, B. Fu, S. Shi, and X. M. Chen, "miR-335 and miR-34a promote renal senescence by suppressing mitochondrial antioxidative enzymes," *Journal of the American Society of Nephrology: JASN*, vol. 22, no. 7, pp. 1252–1261, 2011.

[28] K. Kumamoto, E. A. Spillare, K. Fujita et al., "Nutlin-3a activates p53 to both down-regulate inhibitor of growth 2 and up-regulate mir-34a, mir-34b, and mir-34c expression, and induce senescence," *Cancer Research*, vol. 68, no. 9, pp. 3193–3203, 2008.

[29] H. C. He, Z. D. Han, Q. S. Dai et al., "Global analysis of the differentially expressed miRNAs of prostate cancer in Chinese patients," *BMC Genomics*, vol. 14, p. 757, 2013.

[30] L. Chen, Y. Li, Y. Fu et al., "Role of deregulated microRNAs in breast cancer progression using FFPE tissue," *PLoS One*, vol. 8, no. 1, article e54213, 2013.

[31] N. M. White, H. W. Khella, J. Grigull et al., "miRNA profiling in metastatic renal cell carcinoma reveals a tumour-suppressor effect for miR-215," *British Journal of Cancer*, vol. 105, no. 11, pp. 1741–1749, 2011.

[32] K. Nakazawa, N. Dashzeveg, and K. Yoshida, "Tumor suppressor p53 induces miR-1915 processing to inhibit Bcl-2 in the apoptotic response to DNA damage," *The FEBS Journal*, vol. 281, no. 13, pp. 2937–2944, 2014.

[33] C. Xu, H. Li, L. Zhang, T. Jia, L. Duan, and C. Lu, "MicroRNA19153p prevents the apoptosis of lung cancer cells by downregulating DRG2 and PBX2," *Molecular Medicine Reports*, vol. 13, no. 1, pp. 505–512, 2016.

[34] N. Susnow, L. Zeng, D. Margineantu, and D. M. Hockenbery, "Bcl-2 family proteins as regulators of oxidative stress," *Seminars in Cancer Biology*, vol. 19, no. 1, pp. 42–49, 2009.

[35] D. Li, Q. Wang, C. Liu et al., "Aberrant expression of miR-638 contributes to benzo(a)pyrene-induced human cell transformation," *Toxicological Sciences: An Official Journal of the Society of Toxicology*, vol. 125, no. 2, pp. 382–391, 2012.

[36] Y. Tay, S. M. Tan, F. A. Karreth, J. Lieberman, and P. P. Pandolfi, "Characterization of dual PTEN and p53-targeting microRNAs identifies microRNA-638/Dnm2 as a two-hit oncogenic locus," *Cell Reports*, vol. 8, no. 3, pp. 714–722, 2014.

[37] D. S. Gridley, T. L. Freeman, A. Y. Makinde et al., "Comparison of proton and electron radiation effects on biological responses in liver, spleen and blood," *International Journal of Radiation Biology*, vol. 87, no. 12, pp. 1173–1181, 2011.

[38] X. X. Wang, J. Liu, Y. M. Tang, L. Hong, Z. Zeng, and G. H. Tan, "MicroRNA-638 inhibits cell proliferation by targeting suppress PIM1 expression in human osteosarcoma," *Tumour Biology: The Journal of the International Society for Oncodevelopmental Biology and Medicine*, vol. 37, no. 12, pp. 16367–16375, 2016.

[39] J. Zhang, Z. Bian, J. Zhou et al., "MicroRNA-638 inhibits cell proliferation by targeting phospholipase D1 in human gastric carcinoma," *Protein & Cell*, vol. 6, no. 9, pp. 680–688, 2015.

[40] J. Zhang, B. Fei, Q. Wang et al., "MicroRNA-638 inhibits cell proliferation, invasion and regulates cell cycle by targeting tetraspanin 1 in human colorectal carcinoma," *Oncotarget*, vol. 5, no. 23, pp. 12083–12096, 2014.

[41] A. Bhattacharya, U. Schmitz, Y. Raatz et al., "miR-638 promotes melanoma metastasis and protects melanoma cells from apoptosis and autophagy," *Oncotarget*, vol. 6, no. 5, pp. 2966–2980, 2015.

[42] Y. Ren, Y. Chen, X. Liang, Y. Lu, W. Pan, and M. Yang, "MiRNA-638 promotes autophagy and malignant phenotypes of cancer cells via directly suppressing DACT3," *Cancer Letters*, vol. 390, pp. 126–136, 2017.

[43] N. Wang, Z. Zhou, T. Wu et al., "TNF-alpha-induced NF-kappaB activation upregulates microRNA-150-3p and inhibits osteogenesis of mesenchymal stem cells by targeting beta-catenin," *Open Biology*, vol. 6, no. 3, 2016.

[44] M. P. Borgohain, M. Lahkar, S. Ahmed et al., "Small molecule inhibiting nuclear factor-kB ameliorates oxidative stress and suppresses renal inflammation in early stage of alloxan-induced diabetic nephropathy in rat," *Basic & Clinical Pharmacology & Toxicology*, vol. 120, no. 5, pp. 442–449, 2017.

Hindawi
Oxidative Medicine and Cellular Longevity
Volume 2017, Article ID 5025610, 7 pages
https://doi.org/10.1155/2017/5025610

Review Article

Role of Kallistatin Treatment in Aging and Cancer by Modulating miR-34a and miR-21 Expression

Julie Chao, Youming Guo, Pengfei Li, and Lee Chao

Department of Biochemistry and Molecular Biology, Medical University of South Carolina, Charleston, SC, USA

Correspondence should be addressed to Julie Chao; chaoj@musc.edu

Received 6 April 2017; Accepted 17 May 2017; Published 28 June 2017

Academic Editor: Jaideep Banerjee

Kallistatin is an endogenous protein that regulates differential signaling pathways and a wide spectrum of biological activities via its two structural elements: an active site and a heparin-binding domain. Kallistatin via its heparin-binding site inhibits vascular inflammation and oxidative stress by antagonizing TNF-α-induced NADPH oxidase activity, NF-κB activation, and inflammatory gene expression in endothelial cells. Moreover, kallistatin via its active site inhibits microRNA-34a (miR-34a) synthesis and stimulates eNOS and SIRT1 expression in endothelial progenitor cells, whereas its heparin-binding site is crucial for blocking TNF-α-induced miR-21 expression and oxidative stress, thus reducing cellular senescence. By downregulating miR-34a and miR-21 expression, kallistatin treatment attenuates oxidative damage and aortic senescence in streptozotocin-induced diabetic mice and extends *Caenorhabditis elegans* lifespan under stress conditions. Likewise, kallistatin through the heparin-binding site inhibits TGF-β-induced miR-21 synthesis and oxidative stress in endothelial cells, resulting in inhibition of endothelial-mesenchymal transition, a process contributing to fibrosis and cancer. Furthermore, kallistatin's active site is essential for stimulating miR-34a and p53 expression and inhibiting the miR-21-Akt-Bcl-2 signaling pathway, thus inducing apoptosis in breast cancer cells. These findings reveal novel mechanisms of kallistatin in protection against senescence, aging, and cancer development by modulating miR-34a and miR-21 levels and inhibiting oxidative stress.

1. Introduction

Aging, characterized by the deterioration of human physiological functions, is the dominant risk factor for the development of cardiovascular disease and cancer [1]. Aging and cancer share common origins, as increased production of reactive oxygen species (ROS) plays a critical role in oxidative damage in aged cells and tumor progression [2, 3]. Thus, identifying new antioxidant agents to delay aging and reduce cancer development is imperative in pharmacological intervention. Moreover, microRNAs (miRNAs) negatively regulate the expression of target genes at the posttranscriptional level and play a pivotal role in cellular senescence and tumor progression [4, 5]. Among miRNAs, miR-21 has a widely described oncogenic function by targeting multiple signaling pathways in regulating cancer cell apoptosis, migration, invasion, proliferation, and angiogenesis [6, 7]. Conversely, miR-34a inhibits cancer cell survival, proliferation, invasion, and metastasis formation [8, 9]. Thus, miR-21 functions as an oncogene, while miR-34a acts as a tumor suppressor. However, both miR-34a and miR-21 promote cellular senescence and are crucial players in the regulation of aging and cancer development.

miR-21 promotes tumor progression by stimulating ROS production through downregulation of superoxide dismutase (SOD2/SOD3) [10]. Besides its association with oxidative stress, miR-21 has a potential role in fibrosis, as inhibition of miR-21 attenuates fibrosis in the heart, kidney, and lungs [11–13]. Transforming growth factor- (TGF-) β1, via stimulation of ROS formation, induces upregulation of miR-21, leading to organ fibrosis [14]. Moreover, miR-21 plays an important role in TGF-β-induced endothelial-to-mesenchymal transition (EndMT), a process that contributes to carcinoma-associated fibrosis and fibrotic disease [15]. Therefore, miR-21 exhibits a functional interplay with oxidative stress during tumorigenesis and fibrosis. Furthermore, miR-21 promotes cellular senescence by suppressing high-mobility group A2 in endothelial progenitor cells

(EPCs) [16]. Conversely, miR-34a exerts controversial functions in cancer development and the aging process, as it functions as a tumor suppressor and a senescence inducer [17, 18]. miR-34a inhibits cancer progression by inhibiting cancer cell survival, proliferation, invasion, and metastasis formation [8, 9], while it promotes renal cell senescence by inhibiting antioxidant enzymes [19]. miR-34a induces cellular senescence through suppression of the longevity gene sirtuin 1 (SIRT1) in endothelial cells [18]. Overexpression of miR-34a induces premature senescence of young mesangial cells via downregulation of SOD2, leading to an increase in ROS generation, while antisense miR-34a inhibits senescence of old mesangial cells via upregulation of SOD2 and a decrease in ROS [19]. Collectively, these findings indicate that miR-21 and miR-34a are pivotal players in aging and tumor progression.

Kallistatin was first identified in human plasma as a tissue kallikrein inhibitor and a serine proteinase inhibitor [20–23]. Kallistatin is widely distributed in tissues relevant to cardiovascular function, including those of the kidney, heart, and blood vessels [24–26]. Kallistatin contains two structural elements: an active site and a heparin-binding domain [27–29]. The active site of kallistatin is a key for inhibiting tissue kallikrein activity and stimulating endothelial nitric oxide synthase (eNOS) and SIRT1 expression [30, 31]. Kallistatin via its heparin-binding site interacts with cell surface heparan sulfate proteoglycans, thus antagonizing signaling pathways mediated by vascular endothelial growth factor (VEGF), tumor necrosis factor- (TNF-) α, high-mobility group box-1 (HMGB1), TGF-β, and epidermal growth factor (EGF) [31–35]. Kallistatin administration exhibits pleiotropic effects, including reduction in blood pressure and inhibition of oxidative stress, inflammation, angiogenesis, apoptosis, hypertrophy, and fibrosis in animal models [33, 36–42]. Kallistatin inhibits TNF-α-induced ROS production, nuclear factor- (NF-) κB activation, and inflammatory gene expression in endothelial cells [33, 42]. In addition, kallistatin reduces TNF-α-induced endothelial senescence and delays stress-induced aging by inhibiting miR-34a, miR-21, and oxidative stress and upregulating the expression of the antioxidant enzymes eNOS, SIRT1, catalase, and SOD3 in cultured EPCs, streptozotocin- (STZ-) induced diabetic mice, and *Caenorhabditis elegans* (*C. elegans*). Moreover, kallistatin treatment prevents TGF-β-induced EndMT by reducing ROS formation and miR-21 synthesis [31]. Furthermore, kallistatin induces apoptosis by stimulating miR-34a and suppressing miR-21 synthesis in breast cancer cells [43]. This review focuses on the protective role of kallistatin in cellular senescence, aging, and tumor progression by inhibiting oxidative stress and regulating miR-34a and miR-21 levels.

2. Kallistatin Inhibits Oxidative Stress and Inflammation

Oxidative stress stimulates inflammatory pathways, which promotes cellular senescence and aging [44]. Besides superoxide radical (O_2^-), NF-κB activation also links to accelerated aging in systemic inflammatory responses [45]. Oxidative stress and activation of NF-κB have been shown to be associated with senescence of cultured endothelial cells, and pharmacological inhibition of NF-κB signaling prevents age-associated features in mouse models [46]. Reduced kallistatin levels are correlated with increased oxidative stress, inflammation, and organ damage in animal models of hypertension, cardiovascular, and renal damage [22, 35, 40, 42]. Kallistatin treatment reduces ROS generation, inflammation, and organ damage associated with increased eNOS and NO levels in several animal models, including acute and chronic myocardial damage, salt-induced hypertension, and sepsis [34, 39, 40, 42]. On the other hand, depletion of endogenous kallistatin by neutralizing antibody injection further increases oxidative stress, inflammation, and fibrosis and augments cardiovascular and renal damage in salt-induced hypertensive rats [47]. These findings indicate that kallistatin has a protective role in cardiovascular and renal dysfunction by inhibition of oxidative stress and inflammation.

Kallistatin is an antioxidant as its heparin-binding site is essential for blocking TNF-α-induced NADPH oxidase activity and expression in endothelial cells [33, 42]. In addition, kallistatin's active site is a key for stimulating the expression of the antioxidant enzymes eNOS, SIRT1, and catalase in endothelial cells and EPCs [31, 48]. Kallistatin inhibits NAD(P)H oxidase activity and ROS formation, partly by NO formation in cardiomyocytes [39]. Kallistatin attenuates vascular inflammation by antagonizing TNF-α- and HMGB1-mediated NF-κB activation and expression of proinflammatory genes in endothelial cells [33, 34]. Moreover, kallistatin stimulates eNOS expression by interacting with the transcription factor Kruppel-like factor 4 and increases eNOS activity and NO generation by activating the phosphoinositide 3-kinase- (PI3K-) Akt signaling pathway [41]. Kallistatin not only stimulates eNOS expression but also prevents TNF-α-mediated inhibition of eNOS synthesis in endothelial cells [31]. NO production can inhibit inflammatory gene expression by preventing activation of NF-κB [49]. These findings indicate that kallistatin, through its antioxidative and anti-inflammatory effects, protects against multiorgan damage and accelerated aging.

3. Kallistatin Reduces Vascular Senescence and Aging by Downregulating miR-34a and miR-21 Synthesis

miR-34a and miR-21 have emerged as important regulators of cellular senescence and aging [50]. miR-34a functions as a main senescence promoter by inhibiting the expression of SIRT1, a conservative longevity gene, through a miR-34a-binding site within the 3′-UTR of SIRT1 [51]. Likewise, miR-21 is involved in accelerating cellular senescence in EPCs [16]. Moreover, oxidative stress induces vascular injury and endothelial senescence, with the inflammatory cytokine TNF-α being the main contributor to ROS production [52]. SIRT1 accounts for vascular homeostasis by activating many antioxidant enzymes, such as eNOS, catalase, and manganese superoxide dismutase (MnSOD), to diminish ROS [53]. Upregulation of antioxidant proteins, such as eNOS, SIRT1, catalase, and MnSOD, protects against oxidative stress-

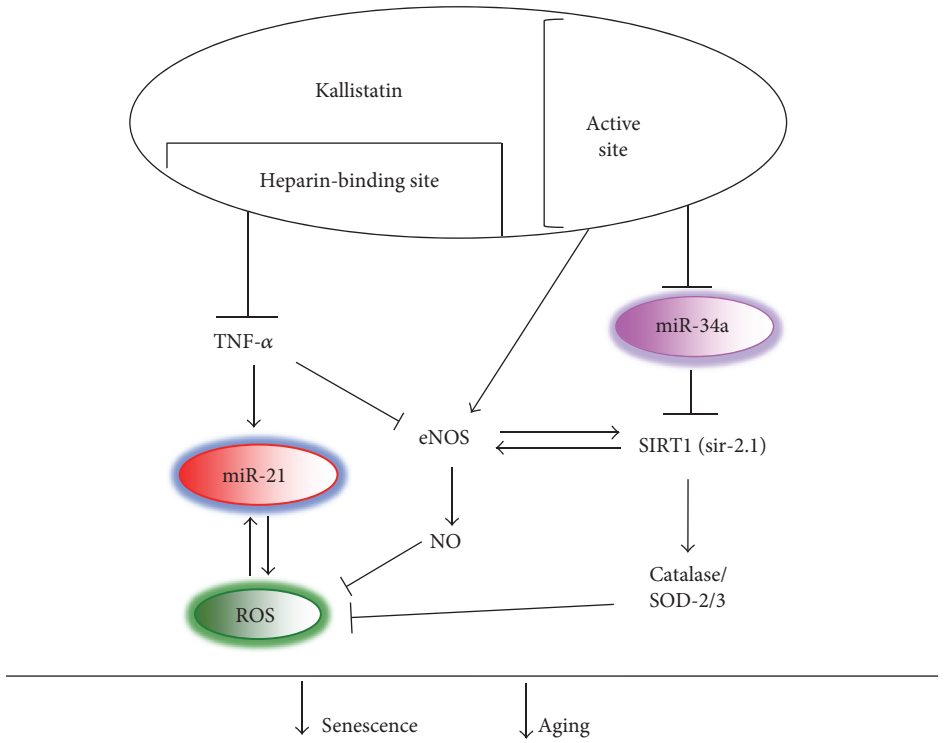

Figure 1: Signaling mechanism by which kallistatin inhibits senescence and aging through suppressing miR-34a expression and TNF-α-induced miR-21-ROS production and stimulating eNOS/SIRT1-NO levels in EPCs.

mediated insults [54, 55]. Therefore, prosenescent miR-34a and miR-21, as well as antioxidant enzymes, underlie the molecular basis for endothelial senescence and aging-associated diseases.

Kallistatin treatment significantly reduces TNF-α-induced senescence in EPCs, as indicated by reduced senescence-associated β-galactosidase activity and elevated telomerase activity. Telomerase prevents telomere attrition by synthesis of telomeric repeats onto the 3′ end of telomeres. Telomere shortening is observed during normal aging in humans and mice [56]. Circulatory kallistatin levels are positively associated with leucocyte telomere length in humans [57], indicating a potential role of kallistatin in maintaining telomere length and attenuating the aging process. In addition, kallistatin via its heparin-binding site antagonizes TNF-α-induced superoxide levels and miR-21 synthesis, as well as TNF-α-mediated inhibition of SIRT1, eNOS, and catalase synthesis in EPCs. Kallistatin via its active site inhibits miR-34a synthesis but stimulates the expression of antioxidant enzymes in EPCs. Overexpression of miR-34a abolishes kallistatin's effects on SIRT1 and eNOS and its antisenescence activity. Kallistatin administration attenuates aortic senescence, oxidative stress, and miR-34a and miR-21 synthesis, in association with elevated SIRT1, eNOS, and catalase levels in STZ-induced diabetic mice. Furthermore, human kallistatin treatment prolongs the lifespan of wild-type *C. elegans* under heat or oxidative stress conditions but has no effect on miR-34 or sir-2.1 (SIRT1 homolog) *C. elegans* mutants. Similar to diabetic mice, kallistatin inhibits miR-34 and superoxide formation but stimulates sir-2.1 synthesis in *C. elegans*. The signaling mechanism of kallistatin in senescence and aging by regulating miR-34a and miR-21 levels is shown in Figure 1. These combined findings provide significant insights into the novel role and mechanism of kallistatin in endothelial senescence and aging.

4. Kallistatin Inhibits EndMT via Suppressing TGF-β-Induced Oxidative Stress and miR-21 Expression

Endothelial-mesenchymal transition (EndMT) contributes greatly to organ fibrosis and tumor metastasis [58, 59]. Morphological changes in EndMT induced by TGF-β signaling cascades include loss of cell-cell junctions and endothelial markers, such as vascular endothelial- (VE-) cadherin and CD31, and gain of the mesenchymal marker α-smooth muscle actin (SMA). Moreover, miR-21 expression levels are highly elevated during EMT and EndMT [15, 60]. TGF-β-induced EndMT is partly mediated by upregulation of the miR-21-Akt pathway, as blockade of miR-21 can prevent EndMT and inhibit Akt activation [15]. Furthermore, ROS production further stimulates miR-21 synthesis in fibroblasts [61]. Therefore, miR-21 is a key mediator of EndMT, as well as EndMT-associated fibrosis and tumor development.

Human kallistatin delivery exerts beneficial effects on fibrosis by suppressing TGF-β synthesis in animal models [40, 62, 63]. Kallistatin treatment blocks TGF-β-induced EndMT in endothelial cells, as evidenced by morphological changes, increased endothelial markers (VE-cadherin and CD31), and reduced mesenchymal marker (α-SMA) [31]. Kallistatin prevents TGF-β-mediated activation of the miR-

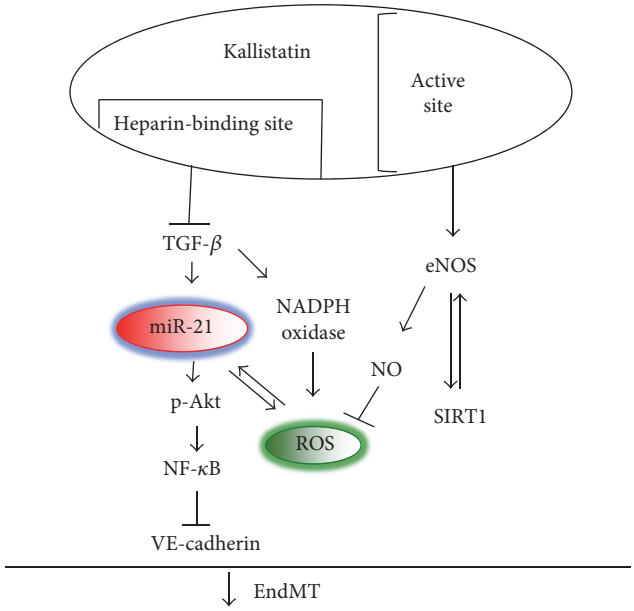

Figure 2: Signaling mechanism by which kallistatin inhibits EndMT by preventing the TGF-β-induced miR-21-Akt-NF-κB pathway and oxidative stress and stimulating eNOS/SIRT1 expression in endothelial cells.

21-phospho-Akt-NF-κB signaling pathway, as well as TGF-β-induced NADPH oxidase expression and activity, and ROS formation [31]. Kallistatin's heparin-binding site is crucial for inhibiting TGF-β-induced oxidative stress, while its active site is a key for stimulating expression of the antioxidant proteins eNOS and SIRT1 and production of NO. Moreover, kallistatin via the heparin-binding site blocks TGF-β-induced miR-21 expression, Akt phosphorylation, and NF-κB activation. Thus, kallistatin inhibits EndMT through suppressing the TGF-β-induced miR-21-Akt-NF-κB signaling pathway and stimulating antioxidant protein expression (Figure 2). These findings indicate that kallistatin attenuates fibrosis and cancer by suppressing TGF-β-induced EndMT.

5. Kallistatin Induces Cancer Cell Apoptosis by Stimulating miR-34a and Inhibiting miR-21 Expression

miRNAs are well categorized by their cancer-related functions, including tumor suppression, oncogene expression, epithelial-mesenchymal transition, apoptosis, and immune response [64]. miR-34a plays an important role as a tumor suppressor in many types of cancers [65]. Indeed, miR-34a levels are underexpressed in a variety of human tumors, and low levels of miR-34 have been related to poor clinical outcome of cancer patients [66, 67]. Moreover, miR-34a inhibits the proliferation, invasion, and migration of breast cancer cells and breast tumor growth in vivo by deactivating the Wnt/β-catenin signaling pathway [68]. On the other hand, miR-21, a well-recognized tumor inducer, is upregulated in a large range of human tumors, including gastric,

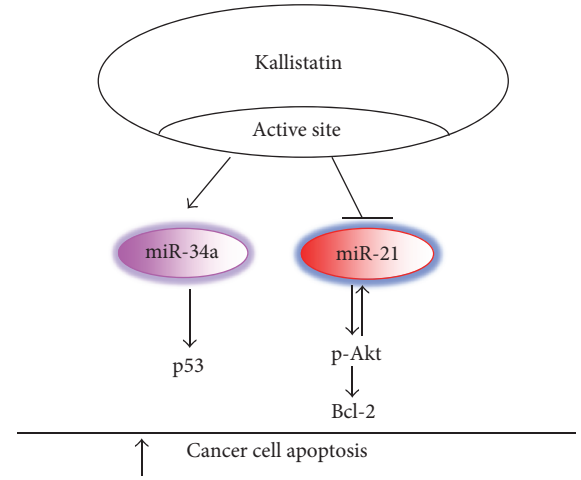

Figure 3: Signaling mechanism by which kallistatin induces apoptosis through upregulating miR-34a-p53 and downregulating miR-21-Akt-Bcl-2 pathways in breast cancer cells.

colorectal, lung, pancreatic, ovarian, and breast cancer [69–74]. In addition, high levels of miR-21 expression are strongly related to poor clinical prognosis of patients in pancreatic cancer [75]. The prosurvival protein Bcl-2, a key regulator of apoptosis in many types of human tumors, is positively regulated by miR-21, and an anti-miR-21 inhibitor downregulates Bcl-2 in breast cancer cells [76]. Moreover, resveratrol induces bladder cancer cell apoptosis by reducing miR-21 expression, Akt phosphorylation, and Bcl-2 levels [77]. Therefore, these findings indicate opposite effects of miR-34a and miR-21 in cancer development.

Kallistatin gene transfer has been reported to inhibit tumor growth and metastasis in several animal models [32, 78–82]. Local administration of human kallistatin reduces tumor growth and angiogenesis in nude mice via antagonizing VEGF-mediated proliferation, migration, and invasion of cultured endothelial cells [32, 78]. Moreover, kallistatin induces apoptotic cell death in human colorectal cancer cells [83]. Kallistatin via the active site stimulates miR-34a and suppresses miR-21 expression in breast cancer cells [44]. Kallistatin reduces cancer cell viability and induces apoptosis by increasing miR-34a and p53 expression but reducing miR-21 synthesis, Akt phosphorylation, and Bcl-2 expression in breast cancer cells [44]. Thus, kallistatin induces breast cancer cell apoptosis by stimulating miR-34a-p53 and suppressing miR-21-Akt-Bcl-2 signaling pathways (Figure 3). These findings indicate that kallistatin induces cancer cell death through upregulation of miR-34a and downregulation of miR-21 expression.

6. Conclusion

Kallistatin plays a protective role in accelerated aging and cancer development by regulation of miR-34a and miR-21. Kallistatin's antisenescence/aging effect is mainly attributed to suppression of oxidative stress and inflammation and downregulation of miR-34a and miR-21 synthesis. Kallistatin via its heparin-binding domain antagonizes TNF-α-induced ROS formation and miR-21 expression, while its active site

is crucial for inhibiting miR-34a synthesis in EPCs. Kallistatin protects against fibrosis and tumorigenesis by inhibiting EndMT. Kallistatin's heparin-binding site is critical for suppressing TGF-β-induced ROS formation and the miR-21-Akt-NF-κB signaling pathway in endothelial cells. However, kallistatin via its active site stimulates miR-34a and p53 synthesis and inhibits miR-21-Akt-Bcl-2 signaling, leading to apoptosis in breast cancer cells. As an endogenous protein, kallistatin treatment could improve human health during aging process and tumor progression with minimal side effects. This review article provides a new potential prospective in kallistatin-based therapeutic intervention in aging and cancer.

Conflicts of Interest

The authors declare that there is no conflict of interests regarding the publication of this paper.

Authors' Contributions

Julie Chao contributes to the writing, and Youming Guo, Pengfei Li, and Lee Chao contribute to the revision and citation of the paper.

Acknowledgments

This work was supported by the National Institutes of Health grant (HL118516).

References

[1] C. Lopez-Otin, M. A. Blasco, L. Partridge, M. Serrano, and G. Kroemer, "The hallmarks of aging," *Cell*, vol. 153, no. 6, pp. 1194–1217, 2013.

[2] P. Storz, "Reactive oxygen species in tumor progression," *Frontiers in Bioscience*, vol. 10, pp. 1881–1896, 2005.

[3] P. Davalli, T. Mitic, A. Caporali, A. Lauriola, and D. D'Arca, "ROS, cell senescence, and novel molecular mechanisms in aging and age-related diseases," *Oxidative Medicine and Cellular Longevity*, vol. 2016, Article ID 3565127, 18 pages, 2016.

[4] D. P. Bartel, "MicroRNAs: genomics, biogenesis, mechanism, and function," *Cell*, vol. 116, no. 2, pp. 281–297, 2004.

[5] F. Olivieri, M. R. Rippo, V. Monsurro et al., "MicroRNAs linking inflamm-aging, cellular senescence and cancer," *Ageing Research Reviews*, vol. 12, no. 4, pp. 1056–1068, 2013.

[6] B. Zhang, X. Pan, G. P. Cobb, and T. A. Anderson, "microRNAs as oncogenes and tumor suppressors," *Developmental Biology*, vol. 302, no. 1, pp. 1–12, 2007.

[7] P. Olson, J. Lu, H. Zhang et al., "MicroRNA dynamics in the stages of tumorigenesis correlate with hallmark capabilities of cancer," *Genes & Development*, vol. 23, no. 18, pp. 2152–2165, 2009.

[8] Y. Guo, S. Li, J. Qu et al., "MiR-34a inhibits lymphatic metastasis potential of mouse hepatoma cells," *Molecular and Cellular Biochemistry*, vol. 354, no. 1-2, pp. 275–282, 2011.

[9] L. Sun, Z. Wu, Y. Shao et al., "MicroRNA-34a suppresses cell proliferation and induces apoptosis in U87 glioma stem cells," *Technology in Cancer Research & Treatment*, vol. 11, no. 5, pp. 483–490, 2012.

[10] X. Zhang, W. L. Ng, P. Wang et al., "MicroRNA-21 modulates the levels of reactive oxygen species by targeting SOD3 and TNFalpha," *Cancer Research*, vol. 72, no. 18, pp. 4707–4713, 2012.

[11] G. Liu, A. Friggeri, Y. Yang et al., "miR-21 mediates fibrogenic activation of pulmonary fibroblasts and lung fibrosis," *The Journal of Experimental Medicine*, vol. 207, no. 8, pp. 1589–1597, 2010.

[12] T. Thum, N. Chau, B. Bhat et al., "Comparison of different miR-21 inhibitor chemistries in a cardiac disease model," *The Journal of Clinical Investigation*, vol. 121, no. 2, pp. 461-462, 2011, author reply 462-463.

[13] X. Zhong, A. C. Chung, H. Y. Chen, X. M. Meng, and H. Y. Lan, "Smad3-mediated upregulation of miR-21 promotes renal fibrosis," *Journal of the American Society of Nephrology*, vol. 22, no. 9, pp. 1668–1681, 2011.

[14] M. Fierro-Fernandez, V. Miguel, and S. Lamas, "Role of redox-imiRs in fibrogenesis," *Redox Biology*, vol. 7, pp. 58–67, 2016.

[15] R. Kumarswamy, I. Volkmann, V. Jazbutyte, S. Dangwal, D. H. Park, and T. Thum, "Transforming growth factor-beta-induced endothelial-to-mesenchymal transition is partly mediated by microRNA-21," *Arteriosclerosis, Thrombosis, and Vascular Biology*, vol. 32, no. 2, pp. 361–369, 2012.

[16] S. Zhu, S. Deng, Q. Ma et al., "MicroRNA-10A* and microRNA-21 modulate endothelial progenitor cell senescence via suppressing high-mobility group A2," *Circulation Research*, vol. 112, no. 1, pp. 152–164, 2013.

[17] H. Hermeking, "The miR-34 family in cancer and apoptosis," *Cell Death and Differentiation*, vol. 17, no. 2, pp. 193–199, 2010.

[18] T. Ito, S. Yagi, and M. Yamakuchi, "MicroRNA-34a regulation of endothelial senescence," *Biochemical and Biophysical Research Communications*, vol. 398, no. 4, pp. 735–740, 2010.

[19] X. Y. Bai, Y. Ma, R. Ding, B. Fu, S. Shi, and X. M. Chen, "miR-335 and miR-34a promote renal senescence by suppressing mitochondrial antioxidative enzymes," *Journal of the American Society of Nephrology*, vol. 22, no. 7, pp. 1252–1261, 2011.

[20] J. Chao, D. M. Tillman, M. Y. Wang, H. S. Margolius, and L. Chao, "Identification of a new tissue-kallikrein-binding protein," *The Biochemical Journal*, vol. 239, no. 2, pp. 325–331, 1986.

[21] M. Y. Wang, J. Day, L. Chao, and J. Chao, "Human kallistatin, a new tissue kallikrein-binding protein: purification and characterization," *Advances in Experimental Medicine and Biology*, vol. 247B, pp. 1–8, 1989.

[22] J. Chao, K. X. Chai, L. M. Chen et al., "Tissue kallikrein-binding protein is a serpin. I. Purification, characterization, and distribution in normotensive and spontaneously hypertensive rats," *The Journal of Biological Chemistry*, vol. 265, no. 27, pp. 16394–16401, 1990.

[23] G. X. Zhou, L. Chao, and J. Chao, "Kallistatin: a novel human tissue kallikrein inhibitor. Purification, characterization, and reactive center sequence," *The Journal of Biological Chemistry*, vol. 267, no. 36, pp. 25873–25880, 1992.

[24] J. Chao and L. Chao, "Biochemistry, regulation and potential function of kallistatin," *Biological Chemistry Hoppe-Seyler*, vol. 376, no. 12, pp. 705–713, 1995.

[25] L. M. Chen, Q. Song, L. Chao, and J. Chao, "Cellular localization of tissue kallikrein and kallistatin mRNAs in human kidney," *Kidney International*, vol. 48, no. 3, pp. 690–697, 1995.

[26] W. C. Wolf, R. A. Harley, D. Sluce, L. Chao, and J. Chao, "Localization and expression of tissue kallikrein and kallistatin in human blood vessels," *The Journal of Histochemistry and Cytochemistry*, vol. 47, no. 2, pp. 221–228, 1999.

[27] V. C. Chen, L. Chao, and J. Chao, "Reactive-site specificity of human kallistatin toward tissue kallikrein probed by site-directed mutagenesis," *Biochimica et Biophysica Acta*, vol. 1479, no. 1-2, pp. 237–246, 2000.

[28] V. C. Chen, L. Chao, and J. Chao, "Roles of the P1, P2, and P3 residues in determining inhibitory specificity of kallistatin toward human tissue kallikrein," *The Journal of Biological Chemistry*, vol. 275, no. 49, pp. 38457–38466, 2000.

[29] V. C. Chen, L. Chao, D. C. Pimenta, G. Bledsoe, L. Juliano, and J. Chao, "Identification of a major heparin-binding site in kallistatin," *The Journal of Biological Chemistry*, vol. 276, no. 2, pp. 1276–1284, 2001.

[30] V. C. Chen, L. Chao, and J. Chao, "A positively charged loop on the surface of kallistatin functions to enhance tissue kallikrein inhibition by acting as a secondary binding site for kallikrein," *The Journal of Biological Chemistry*, vol. 275, no. 51, pp. 40371–40377, 2000.

[31] Y. Guo, P. Li, G. Bledsoe, Z. R. Yang, L. Chao, and J. Chao, "Kallistatin inhibits TGF-beta-induced endothelial-mesenchymal transition by differential regulation of microRNA-21 and eNOS expression," *Experimental Cell Research*, vol. 337, no. 1, pp. 103–110, 2015.

[32] R. Q. Miao, V. Chen, L. Chao, and J. Chao, "Structural elements of kallistatin required for inhibition of angiogenesis," *American Journal of Physiology Cell Physiology*, vol. 284, no. 6, pp. C1604–C1613, 2003.

[33] H. Yin, L. Gao, B. Shen, L. Chao, and J. Chao, "Kallistatin inhibits vascular inflammation by antagonizing tumor necrosis factor-alpha-induced nuclear factor kappaB activation," *Hypertension*, vol. 56, no. 2, pp. 260–267, 2010.

[34] P. Li, G. Bledsoe, Z. R. Yang, H. Fan, L. Chao, and J. Chao, "Human kallistatin administration reduces organ injury and improves survival in a mouse model of polymicrobial sepsis," *Immunology*, vol. 142, no. 2, pp. 216–226, 2014.

[35] J. Chao, G. Bledsoe, and L. Chao, "Protective role of kallistatin in vascular and organ injury," *Hypertension*, vol. 68, no. 3, pp. 533–541, 2016.

[36] L. M. Chen, L. Chao, and J. Chao, "Adenovirus-mediated delivery of human kallistatin gene reduces blood pressure of spontaneously hypertensive rats," *Human Gene Therapy*, vol. 8, no. 3, pp. 341–347, 1997.

[37] C. R. Wang, S. Y. Chen, C. L. Wu et al., "Prophylactic adenovirus-mediated human kallistatin gene therapy suppresses rat arthritis by inhibiting angiogenesis and inflammation," *Arthritis and Rheumatism*, vol. 52, no. 4, pp. 1319–1324, 2005.

[38] J. Chao, H. Yin, Y. Y. Yao, B. Shen, R. S. Smith Jr., and L. Chao, "Novel role of kallistatin in protection against myocardial ischemia-reperfusion injury by preventing apoptosis and inflammation," *Human Gene Therapy*, vol. 17, no. 12, pp. 1201–1213, 2006.

[39] L. Gao, H. Yin, S. R. Smith Jr., L. Chao, and J. Chao, "Role of kallistatin in prevention of cardiac remodeling after chronic myocardial infarction," *Laboratory Investigation*, vol. 88, no. 11, pp. 1157–1166, 2008.

[40] B. Shen, M. Hagiwara, Y. Y. Yao, L. Chao, and J. Chao, "Salutary effect of kallistatin in salt-induced renal injury, inflammation, and fibrosis via antioxidative stress," *Hypertension*, vol. 51, no. 5, pp. 1358–1365, 2008.

[41] B. Shen, R. S. Smith Jr., Y. T. Hsu, L. Chao, and J. Chao, "Kruppel-like factor 4 is a novel mediator of kallistatin in inhibiting endothelial inflammation via increased endothelial nitric-oxide synthase expression," *The Journal of Biological Chemistry*, vol. 284, no. 51, pp. 35471–35478, 2009.

[42] B. Shen, L. Gao, Y. T. Hsu et al., "Kallistatin attenuates endothelial apoptosis through inhibition of oxidative stress and activation of Akt-eNOS signaling," *American Journal of Physiology Heart and Circulatory Physiology*, vol. 299, no. 5, pp. H1419–H1427, 2010.

[43] P. Li, Y. Guo, G. Bledsoe, Z. Yang, L. Chao, and J. Chao, "Kallistatin induces breast cancer cell apoptosis and autophagy by modulating Wnt signaling and microRNA synthesis," *Experimental Cell Research*, vol. 340, no. 2, pp. 305–314, 2016.

[44] J. Wu, S. Xia, B. Kalionis, W. Wan, and T. Sun, "The role of oxidative stress and inflammation in cardiovascular aging," *BioMed Research International*, vol. 2014, Article ID 615312, 13 pages, 2014.

[45] C. Soria-Valles, F. G. Osorio, A. Gutierrez-Fernandez et al., "NF-kappaB activation impairs somatic cell reprogramming in ageing," *Nature Cell Biology*, vol. 17, no. 8, pp. 1004–1013, 2015.

[46] S. Y. Khan, E. M. Awad, A. Oszwald et al., "Premature senescence of endothelial cells upon chronic exposure to TNFalpha can be prevented by N-acetyl cysteine and plumericin," *Scientific Reports*, vol. 7, article 39501, 2017.

[47] Y. Liu, G. Bledsoe, M. Hagiwara, B. Shen, L. Chao, and J. Chao, "Depletion of endogenous kallistatin exacerbates renal and cardiovascular oxidative stress, inflammation, and organ remodeling," *American Journal of Physiology Renal Physiology*, vol. 303, no. 8, pp. F1230–F1238, 2012.

[48] L. Gao, P. Li, J. Zhang et al., "Novel role of kallistatin in vascular repair by promoting mobility, viability, and function of endothelial progenitor cells," *Journal of the American Heart Association*, vol. 3, no. 5, article e001194, 2014.

[49] J. R. Matthews, C. H. Botting, M. Panico, H. R. Morris, and R. T. Hay, "Inhibition of NF-kappaB DNA binding by nitric oxide," *Nucleic Acids Research*, vol. 24, no. 12, pp. 2236–2242, 1996.

[50] S. Dimmeler and P. Nicotera, "MicroRNAs in age-related diseases," *EMBO Molecular Medicine*, vol. 5, no. 2, pp. 180–190, 2013.

[51] T. Zhao, J. Li, and A. F. Chen, "MicroRNA-34a induces endothelial progenitor cell senescence and impedes its angiogenesis via suppressing silent information regulator 1," *American Journal of Physiology Endocrinology and Metabolism*, vol. 299, no. 1, pp. E110–E116, 2010.

[52] X. Chen, B. T. Andresen, M. Hill, J. Zhang, F. Booth, and C. Zhang, "Role of reactive oxygen species in tumor necrosis factor-alpha induced endothelial dysfunction," *Current Hypertension Reviews*, vol. 4, no. 4, pp. 245–255, 2008.

[53] M. Kitada, Y. Ogura, and D. Koya, "The protective role of Sirt1 in vascular tissue: its relationship to vascular aging and atherosclerosis," *Aging*, vol. 8, no. 10, pp. 2290–2307, 2016.

[54] S. Wassmann, K. Wassmann, and G. Nickenig, "Modulation of oxidant and antioxidant enzyme expression and function in vascular cells," *Hypertension*, vol. 44, no. 4, pp. 381–386, 2004.

[55] H. Ota, M. Eto, S. Ogawa, K. Iijima, M. Akishita, and Y. Ouchi, "SIRT1/eNOS axis as a potential target against vascular

senescence, dysfunction and atherosclerosis," *Journal of Atherosclerosis and Thrombosis*, vol. 17, no. 5, pp. 431–435, 2010.

[56] M. A. Blasco, "Telomere length, stem cells and aging," *Nature Chemical Biology*, vol. 3, no. 10, pp. 640–649, 2007.

[57] H. Zhu, J. Chao, A. Raed et al., "Plasma kallistatin is associated with leukocyte telomere length in young African Americans," *The FASEB Journal*, vol. 30, no. 1, p. 625.1, 2016.

[58] E. M. Zeisberg, O. Tarnavski, M. Zeisberg et al., "Endothelial-to-mesenchymal transition contributes to cardiac fibrosis," *Nature Medicine*, vol. 13, no. 8, pp. 952–961, 2007.

[59] S. Potenta, E. Zeisberg, and R. Kalluri, "The role of endothelial-to-mesenchymal transition in cancer progression," *British Journal of Cancer*, vol. 99, no. 9, pp. 1375–1379, 2008.

[60] O. Bornachea, M. Santos, A. B. Martinez-Cruz et al., "EMT and induction of miR-21 mediate metastasis development in Trp53-deficient tumours," *Scientific Reports*, vol. 2, p. 434, 2012.

[61] M. Ling, Y. Li, Y. Xu et al., "Regulation of miRNA-21 by reactive oxygen species-activated ERK/NF-kappaB in arsenite-induced cell transformation," *Free Radical Biology & Medicine*, vol. 52, no. 9, pp. 1508–1518, 2012.

[62] X. Huang, X. Wang, Y. Lv, L. Xu, J. Lin, and Y. Diao, "Protection effect of kallistatin on carbon tetrachloride-induced liver fibrosis in rats via antioxidative stress," *PloS One*, vol. 9, no. 2, article e88498, 2014.

[63] W. H. Yiu, D. W. Wong, H. J. Wu et al., "Kallistatin protects against diabetic nephropathy in db/db mice by suppressing AGE-RAGE-induced oxidative stress," *Kidney International*, vol. 89, no. 2, pp. 386–398, 2016.

[64] C. Qiu, G. Chen, and Q. Cui, "Towards the understanding of microRNA and environmental factor interactions and their relationships to human diseases," *Scientific Reports*, vol. 2, p. 318, 2012.

[65] X. J. Li, Z. J. Ren, and J. H. Tang, "MicroRNA-34a: a potential therapeutic target in human cancer," *Cell Death & Disease*, vol. 5, article e1327, 2014.

[66] D. Kong, E. Heath, W. Chen et al., "Epigenetic silencing of miR-34a in human prostate cancer cells and tumor tissue specimens can be reversed by BR-DIM treatment," *American Journal of Translational Research*, vol. 4, no. 1, pp. 14–23, 2012.

[67] S. Roy, E. Levi, A. P. Majumdar, and F. H. Sarkar, "Expression of miR-34 is lost in colon cancer which can be re-expressed by a novel agent CDF," *Journal of Hematology & Oncology*, vol. 5, p. 58, 2012.

[68] W. Si, Y. Li, H. Shao et al., "miR-34a inhibits breast cancer proliferation and progression by targeting Wnt1 in Wnt/beta-catenin signaling pathway," *The American Journal of the Medical Sciences*, vol. 352, no. 2, pp. 191–199, 2016.

[69] S. H. Chan, C. W. Wu, A. F. Li, C. W. Chi, and W. C. Lin, "miR-21 microRNA expression in human gastric carcinomas and its clinical association," *Anticancer Research*, vol. 28, no. 2A, pp. 907–911, 2008.

[70] L. X. Yan, X. F. Huang, Q. Shao et al., "MicroRNA miR-21 overexpression in human breast cancer is associated with advanced clinical stage, lymph node metastasis and patient poor prognosis," *RNA*, vol. 14, no. 11, pp. 2348–2360, 2008.

[71] T. Moriyama, K. Ohuchida, K. Mizumoto et al., "MicroRNA-21 modulates biological functions of pancreatic cancer cells including their proliferation, invasion, and chemoresistance," *Molecular Cancer Therapeutics*, vol. 8, no. 5, pp. 1067–1074, 2009.

[72] Y. Lou, X. Yang, F. Wang, Z. Cui, and Y. Huang, "MicroRNA-21 promotes the cell proliferation, invasion and migration abilities in ovarian epithelial carcinomas through inhibiting the expression of PTEN protein," *International Journal of Molecular Medicine*, vol. 26, no. 6, pp. 819–827, 2010.

[73] X. Xia, B. Yang, X. Zhai et al., "Prognostic role of microRNA-21 in colorectal cancer: a meta-analysis," *PloS One*, vol. 8, no. 11, article e80426, 2013.

[74] L. F. Xu, Z. P. Wu, Y. Chen, Q. S. Zhu, S. Hamidi, and R. Navab, "MicroRNA-21 (miR-21) regulates cellular proliferation, invasion, migration, and apoptosis by targeting PTEN, RECK and Bcl-2 in lung squamous carcinoma, Gejiu City, China," *PloS One*, vol. 9, no. 8, article e103698, 2014.

[75] M. Dillhoff, J. Liu, W. Frankel, C. Croce, and M. Bloomston, "MicroRNA-21 is overexpressed in pancreatic cancer and a potential predictor of survival," *Journal of Gastrointestinal Surgery*, vol. 12, no. 12, pp. 2171–2176, 2008.

[76] J. Dong, Y. P. Zhao, L. Zhou, T. P. Zhang, and G. Chen, "Bcl-2 upregulation induced by miR-21 via a direct interaction is associated with apoptosis and chemoresistance in MIA PaCa-2 pancreatic cancer cells," *Archives of Medical Research*, vol. 42, no. 1, pp. 8–14, 2011.

[77] C. Zhou, J. Ding, and Y. Wu, "Resveratrol induces apoptosis of bladder cancer cells via miR21 regulation of the Akt/Bcl2 signaling pathway," *Molecular Medicine Reports*, vol. 9, no. 4, pp. 1467–1473, 2014.

[78] R. Q. Miao, J. Agata, L. Chao, and J. Chao, "Kallistatin is a new inhibitor of angiogenesis and tumor growth," *Blood*, vol. 100, no. 9, pp. 3245–3252, 2002.

[79] L. Lu, Z. Yang, B. Zhu et al., "Kallikrein-binding protein suppresses growth of hepatocellular carcinoma by anti-angiogenic activity," *Cancer Letters*, vol. 257, no. 1, pp. 97–106, 2007.

[80] B. Zhu, L. Lu, W. Cai et al., "Kallikrein-binding protein inhibits growth of gastric carcinoma by reducing vascular endothelial growth factor production and angiogenesis," *Molecular Cancer Therapeutics*, vol. 6, no. 12, Part 1, pp. 3297–3306, 2007.

[81] A. L. Shiau, M. L. Teo, S. Y. Chen et al., "Inhibition of experimental lung metastasis by systemic lentiviral delivery of kallistatin," *BMC Cancer*, vol. 10, p. 245, 2010.

[82] D. Jia, C. Zheng, J. Feng, J. Zou, and Y. Diao, "Plasmid mediated kallistain gene expression via intramuscular electroporation delivery in vivo for treatment of NCI-H446 subcutaneous xenograft tumor," *Pakistan Journal of Pharmaceutical Sciences*, vol. 27, 3 Supplement, pp. 633–636, 2014.

[83] Y. Yao, L. Li, X. Huang et al., "SERPINA3K induces apoptosis in human colorectal cancer cells via activating the Fas/FasL/caspase-8 signaling pathway," *The FEBS Journal*, vol. 280, no. 14, pp. 3244–3255, 2013.

Hindawi
Oxidative Medicine and Cellular Longevity
Volume 2017, Article ID 6051874, 10 pages
https://doi.org/10.1155/2017/6051874

Research Article

miR-Let7A Controls the Cell Death and Tight Junction Density of Brain Endothelial Cells under High Glucose Condition

Juhyun Song,[1] So Ra Yoon,[2] and Oh Yoen Kim[2]

[1]*Department of Biomedical Sciences, Center for Creative Biomedical Scientists at Chonnam National University, Gwangju 61469, Republic of Korea*
[2]*Department of Food Science and Nutrition, Dong-A University, Brain Busan 21 Project, Busan 49315, Republic of Korea*

Correspondence should be addressed to Oh Yoen Kim; oykim@dau.ac.kr

Received 27 January 2017; Revised 7 May 2017; Accepted 21 May 2017; Published 7 June 2017

Academic Editor: Savita Khanna

Hyperglycemia-induced stress in the brain of patients with diabetes triggers the disruption of blood-brain barrier (BBB), leading to diverse neurological diseases including stroke and dementia. Recently, the role of microRNA becomes an interest in the research for deciphering the mechanism of brain endothelial cell damage under hyperglycemia. Therefore, we investigated whether mircoRNA Let7A (miR-Let7A) controls the damage of brain endothelial (bEnd.3) cells against high glucose condition. Cell viability, cell death marker expressions (p-53, Bax, and cleaved poly ADP-ribose polymerase), the loss of tight junction proteins (ZO-1 and claudin-5), proinflammatory response (interleukin-6, tumor necrosis factor-α), inducible nitric oxide synthase, and nitrite production were confirmed using MTT, reverse transcription-PCR, quantitative-PCR, Western blotting, immunofluorescence, and Griess reagent assay. miR-Let7A overexpression significantly prevented cell death and loss of tight junction proteins and attenuated proinflammatory response and nitrite production in the bEnd.3 cells under high glucose condition. Taken together, we suggest that miR-Let7A may attenuate brain endothelial cell damage by controlling cell death signaling, loss of tight junction proteins, and proinflammatory response against high glucose stress. In the future, the manipulation of miR-Let7A may be a novel solution in controlling BBB disruption which leads to the central nervous system diseases.

1. Introduction

Blood-brain barrier (BBB) is a well-organized physiological structure composed of several cells such as brain endothelial cells, pericytes, and astrocytes from the central nervous system (CNS), which tightly controls the movement of cells and molecules between the blood and brain parenchyma [1]. Brain endothelial cells as a main component of BBB are linked together by the interactions between tight junction proteins such as claudins and occludin [2]. As an intact BBB is necessary for maintaining the microenvironment of the brain, the breakdown of BBB is associated with the occurrence of various diseases including stroke, dementia, and epilepsy [3, 4]. Several studies demonstrated that diabetes triggers the risk of neurological dysfunction due to the BBB disruption [5, 6]. High glucose condition in diabetes triggers the alteration of microvascular [7, 8] and neurovascular unit [6]. To control the microenvironment of BBB in diabetes, many researchers investigated how high glucose condition triggers the death of brain endothelial cells [9, 10] and the degradation of tight junction protein which is involved in the BBB permeability [11, 12].

MicroRNAs as nonprotein-coding RNAs with 21–25 nucleotides have been known to control various gene expressions at the posttranscriptional level by targeting with 3′-UTR of mRNA and play an important regulator of metabolic disease, thereby emerging as biomarkers and therapeutic targets [13, 14]. Among the microRNAs, microRNA-Let7A (miR-Let7A) is recently suggested as a therapeutic target for improvement of the pathological conditions related to metabolic diseases (i.e., cancer, diabetes, obesity, inflammation, vascular disease, etc.) [15–25]. It was known to be involved in cellular senescence, glucose metabolism, and inflammatory pathways [15–25]. In high glucose condition, miR-Let7A could control the cytokine production [21] and inflammatory mechanisms [25, 20]. However, the regulatory

effects of miR-Let7A on metabolic status in associated with hyperglycemic condition were different among the studies: some reported the protective properties of miR-Let7A, but the others presented the negative properties [15–26]. As mentioned above, recent studies reported the involvement of microRNAs in the control of BBB disruption, but the mechanism is not fully understood. Furthermore, there are few studies on the role of miR-Let7A in cerebrovascular system including BBB under hyperglycemic condition. Therefore, the present study aimed to investigate the role of miR-Let7A in brain endothelial cells, for example, apoptosis, tight junction protein expression, and inflammatory response under high glucose condition, which may suggest that the manipulation of miR-Let7A would be a crucial issue for the protection of BBB disruption.

2. Materials and Methods

2.1. Cell Culture. Mouse brain endothelial cells (bEnd.3 cells) (ATCC Manassas, VA, USA) were cultured in Dulbecco Modified Eagle Medium (DMEM) (Gibco, Grand Island, NY, USA) which contained 0.45% glucose, 0.37% $NaHCO_3$, 4 mM glutamine, 10% fetal bovine serum (FBS), 100 μg/ml penicillin, and 100 μg/ml streptomycin. bEnd.3 cells were cultured in a humidified incubator at 37°C with 5% CO_2. The cells were treated with D-glucose (Sigma-Aldrich, St. Louis, MO, USA) at various concentrations (100 μM, 10 mM, and 25 mM) for 24 hours.

2.2. 3-(4,5-Dimethylthiazol-2-yl)-2,5-diphenyltetrazolium Bromide (MTT) Assay. To examine the cell viability, we performed a 3-(4,5-dimethylthiazol-2-yl)-2,5-diphenyltetrazolium bromide (MTT) assay. After exposure to various concentrations of glucose, bEnd.3 cells (2×10^5 cells/ml) were rinsed three times with PBS. Next, the culture medium was replaced with a serum-free medium, and 100 μl of MTT (Sigma-Aldrich, St. Louis, MO, USA) solution (2 mg/ml in PBS) was treated to each well. After 1 hour 30 min of incubation, the medium was removed, and dimethyl sulfoxide (DMSO) 0.1% was added to form a solution with the formazan reaction product. The supernatant from each well was measured using an ELISA reader at a wavelength of 570 nm. All experiments were repeated three times. Cell viabilities are calculated relative to nontreated controls, whose cell viabilities are considered to be 100%.

2.3. MicroRNA Transfection. miR-Let7A was purchased from Ambion (Austin, TX, USA) and followed the manufacturer's protocol. Two kinds of miR-Let7A were used in this study; Let-7A mimic (catalogue number, 4464066; assay ID, MC10050) and Let-7A inhibitor (catalogue number, 4464084; assay ID, MH 10050). The expression and inhibition levels were validated with negative (catalogue number, 4464058) and positive control miRNA (catalogue number, 4464062). bEnd.3 cells were cultured for 2 days and were then treated with miR-Let-7A and miRNA negative control for each group.

2.4. Western Blot Analysis. bEnd.3 cells were washed with PBS and collected. The cell pellets were lysed with cold RIPA 20 min at 4°C to produce whole-cell extracts. Protein (25 μg) in cells was separated on a 12% SDS-polyacrylamide gel and transferred onto a polyvinylidene difluoride membrane. After blocking with skim milk prepared in tris-buffered saline—Tween (TBST) (20 nM tris, pH 7.2, 150 mM NaCl, 0.1% Tween 20) for 1 hour and 30 min at room temperature, immunoblots were incubated for 14 hours at 4°C with primary antibodies that detect cleaved poly ADP-ribose polymerase (PARP) (1 : 1000, Abcam, Cambridge, MA, USA), claudin 5 (CLD5) (1 : 1000, Cell Signaling, Danvers, MA, USA), or β-actin (1 : 1000; Millipore, Billerica, MA, USA). Blots were then incubated with specific secondary antibodies (Abcam, Cambridge, MA, USA) for 2 hours at room temperature. Blots were visualized by ECL solution (Millipore, Billerica, MA, USA).

2.5. Reverse Transcription Polymerase Chain Reaction (RT-PCR). RNA in bEnd.3 cells was extracted using Trizol Reagent (Gibco, Grand Island, NY, USA). Reverse transcription polymerase chain reaction (RT-PCR) was conducted by using Invitrogen One step III™ Reverse Transcription PCR kit (Invitrogen, Carlsbad, CA, USA). PCR was performed following thermal cycling conditions: 95°C for 10 min; 40 cycles of denaturing at 95°C for 15 seconds, annealing at 60.5°C for 30 seconds, and elongation at 72°C for 30 seconds; final extension at 72°C for 5 minutes; and holding at 4°C. PCR was performed using the following primers (5′ to 3′): tumor necrosis factor (TNF)-α (F); CGT CAG CCG ATT TGC TAT CT, (R); CGG ACT CCG CAA AGT CTA AG; interleukin (IL)-6 (F); GTT GCC TTC TTG GGA CTG AT, (R); CTG GCT TTG TCT TTC TTG TTA T; CLD5 (F); CTG CTG GTT CGC CAA CAT T, (R); TGC GAC ACG GGC ACA G; inducible nitric oxide synthase (iNOS) (F); GGG AAT CTT GGA GCG AGT TG, (R); GTG AGG GCT TGG CTG AGT GA, Bax (F); AAG AAG CTG AGC GAG TGT, (R); GGA GGA AGT CCA ATG TC, p-53 (F); GAG TGT TCC GTG TAT GGC AC, (R); GAT GCC TTG GAT GAT GGT C, ZO-1 CAG CCG GTC ACG ATC TCC T, (R); TCC GGA GAC TGC CAT TGC, GAPDH (F); GAC AAG CTT CCC GTT CTC AG, (R); GAG TCA ACG GAT TTG GTC GT. PCR products were electrophoresed in 1% agarose gels and stained with mango blue. All samples were normalized with GAPDH.

2.6. TaqMan Assay for miRNA. To analyze the level of miR-Let7A, reverse transcription was performed using the Taqman microRNA reverse transcription kit (Applied Biosystems, Waltham, Massachusetts, USA) with 10 g RNA. The PCR reactions were conducted as per the manufacturer's protocol to quantitate the level of miRNA Let7A using Taqman Universal PCR Master Mix, No Amp Erase UNG (Applied Biosystems, Waltham, Massachusetts, USA) and Taqman microRNA assay (Applied Biosystems, Waltham, Massachusetts, USA) for miR-Let7A. PCR amplification was conducted in Takara Real Time PCR (Takara, Tokyo, Japan) at 95°C for 10 minutes, followed by 40 cycles at 95°C for 15 seconds, and 60°C for 60 seconds. The PCR incubation profile was extended to 40 cycles for miR-Let7A. The differential level was calculated using the $\Delta\Delta$Ct method. The level

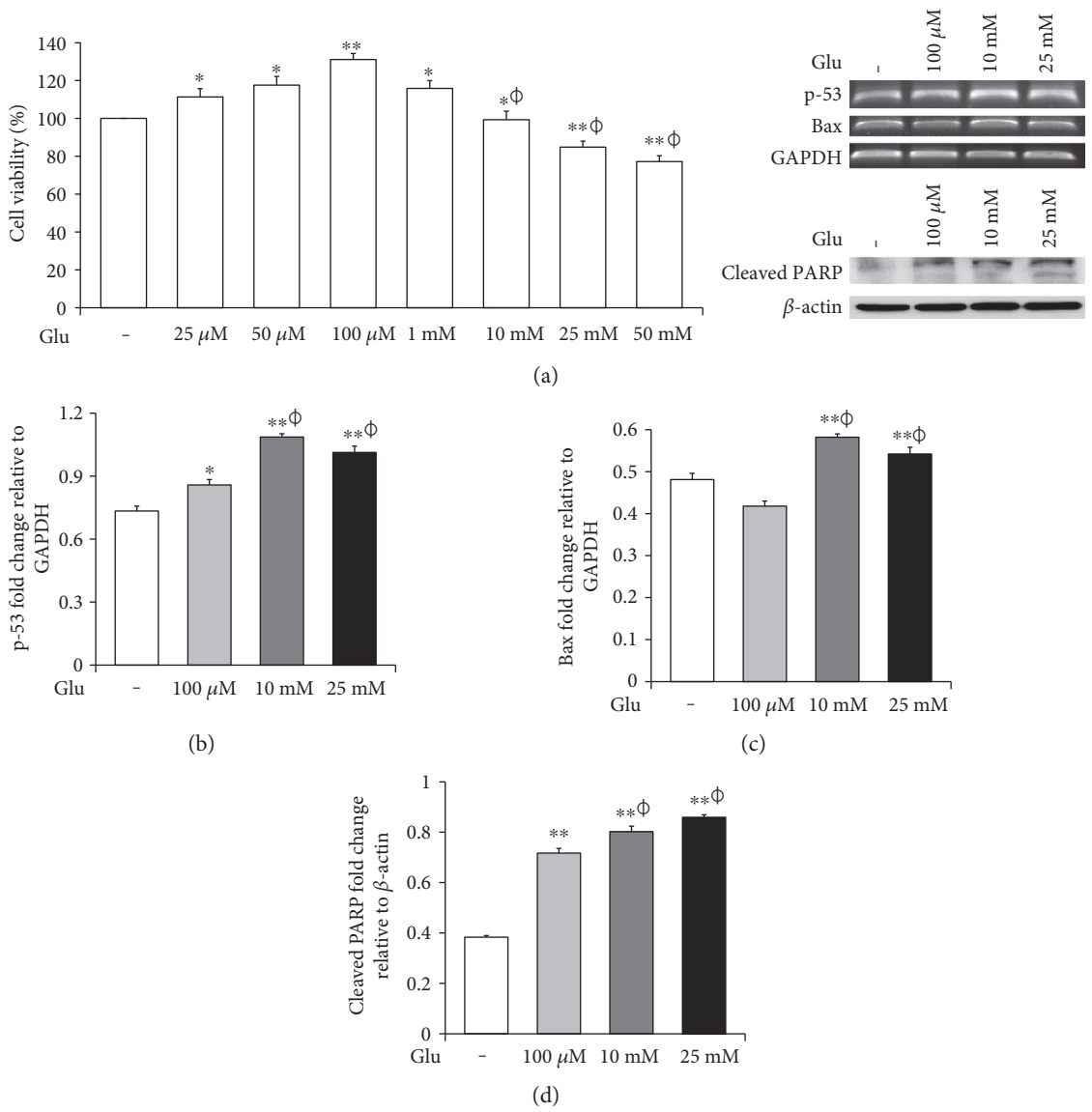

Figure 1: High glucose triggers cell death of bEnd.3 cells under high glucose in vitro condition. Cell viability was tested by the MTT assay (a). The mRNA levels of p-53 (a) and Bax (b) were measured by reverse transcription PCR, and protein levels of cleaved PARP (c) were measured by Western blot analysis. The results are expressed as the mean ± standard deviations (SD). Each experiment included at least 3 replicates per condition. $^{*}p < 0.05$ and $^{**}p < 0.001$ compared with nontreated control cells; $^{\phi}p < 0.05$ compared with 100 μM glucose-treated cells. Glu: D-glucose treatment for 24 hours; PARP: poly ADP-ribose polymerase.

of miRNA Let7A was represented as a relative quantity (RQ) normalized to U6. The PCR reactions were conducted three times.

2.7. Quantitative Real-Time PCR. Total cellular RNA was extracted from the cells using Trizol Reagent (Invitrogen, Carlsbad, CA, USA) according to the manufacturer's instructions. Poly (A) was added using poly (A) polymerase (Ambion, Austin, TX, USA). One Step SYBR® Prime Script™ RT-PCR Kit II (Takara, Japan) was used to conduct qPCR. PCR was performed using the following primers (5′ to 3′): ZO-1 CAG CCG GTC ACG ATC TCC T, (R); TCC GGA GAC TGC CAT TGC, TNF-α (F); CGT CAG CCG ATT TGC TAT CT, (R); CGG ACT CCG CAA AGT CTA AG, iNOS (F); GGG AAT CTT GGA GCG AGT TG, (R); GTG AGG GCT TGG CTG AGT GA. The expression of each factors was assessed using an ABI prism 7500 Real-Time PCR System (Life Technologies Corporation, CA, USA) and analyzed with comparative Ct quantification. β-actin was amplified as an internal control. The values were presented by relative quantity (RQ). All experiments were repeated three times.

2.8. Immunocytochemistry. bEnd.3 cells were washed thrice with PBS and were permeabilized for 20 minutes. bEnd.3 cells were incubated with the primary antibodies for 12 hours at 4°C. The following primary antibodies were used: anti-rabbit CLD5 (1 : 500, Cell Signaling, Danvers, MA, USA) and anti-rabbit cleaved PARP (1 : 500, Abcam, Cambridge, MA, USA). After 16 hours incubation, bEnd.3 cells were

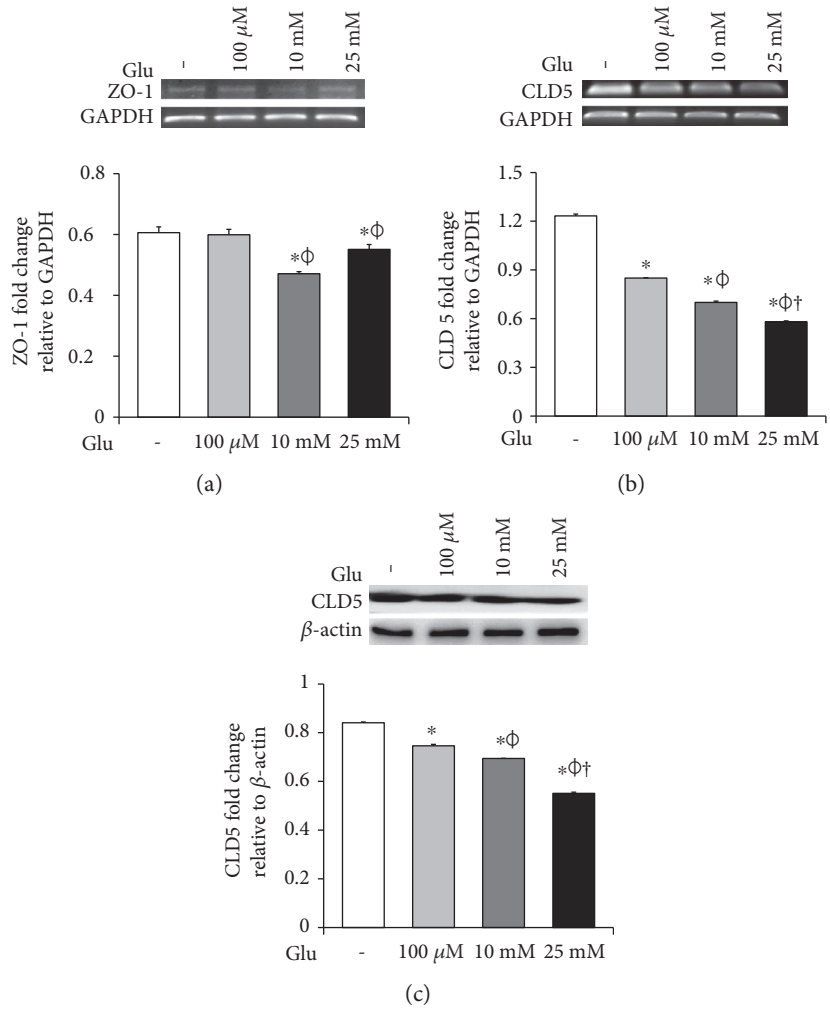

Figure 2: High glucose condition aggravates the loss of tight junction proteins in bEnd.3 cells. The mRNA levels of ZO-1 (a) and CLD5 (b) were measured by reverse transcription PCR, and protein levels of CLD5 (c) were measured by Western blot analysis. The results are expressed as the mean ± standard deviations (SD). Each experiment included at least 3 replicates per condition. $^{*}p < 0.05$ compared with nontreated control cells; $^{\phi}p < 0.05$ compared with 100 μM glucose-treated cells; $^{\dagger}p < 0.05$ compared with 10 mM glucose-treated cells. Glu: D-glucose treatment for 24 hours; CLD5: claudin 5.

washed three times with PBS and incubated with each specific secondary antibody for 1 hour at room temperature. bEnd.3 cells were counterstained with 1 μg/ml 4′,6-diamidino-2-phenylindole (DAPI, 1 : 100, Invitrogen, Carlsbad, CA, USA) for 5 minutes at room temperature. Images were obtained using confocal microscope (Carl Zeiss, Thornwood, NY, USA). Cells in three randomly selected fields were measured for immunodensity using ImageJ software (ImageJ, Madison, Wisconsin, USA).

2.9. Determination of Nitrite Production. bEnd.3 cells were seeded onto 96-well plates at density of 5×10^4 cells/well and pretreated with D-glucose (25 mM), Let7A mimic or Let7A inhibitor. The supernatants were collected and assessed for nitrite production using Griess reagent (Sigma-Aldrich, St. Louis, MO, USA). The Griess reagents (100 μl) were added and incubated for 30 minutes at room temperature. The absorbance of supernatants was measured at 540 nm using the ELISA reader (Versamax Molecular Devices, Hampton, NH, USA).

2.10. Statistical Analysis. Statistical analysis was conducted by SPSS 23.0 software (IBM Corp., Armonk, NY, USA). The results are expressed as the mean ± standard deviations (SD). Statistical analyses were performed using one-way analysis of variance (ANOVA) followed by Bonferroni post hoc multiple comparison. Each experiment included at least 3 replicates per condition. A P value less than 0.05 was considered statistically significant.

3. Results

3.1. High Glucose Condition Is Associated with Cell Death of bEnd.3 Cells under High Glucose In Vitro Condition. To assess the cell death of bEnd.3 cells under high glucose condition, we performed MTT (Figure 1(a)), RT-PCR (p-53 and Bax, Figures 1(b) and 1(c)) and Western blot (cleaved

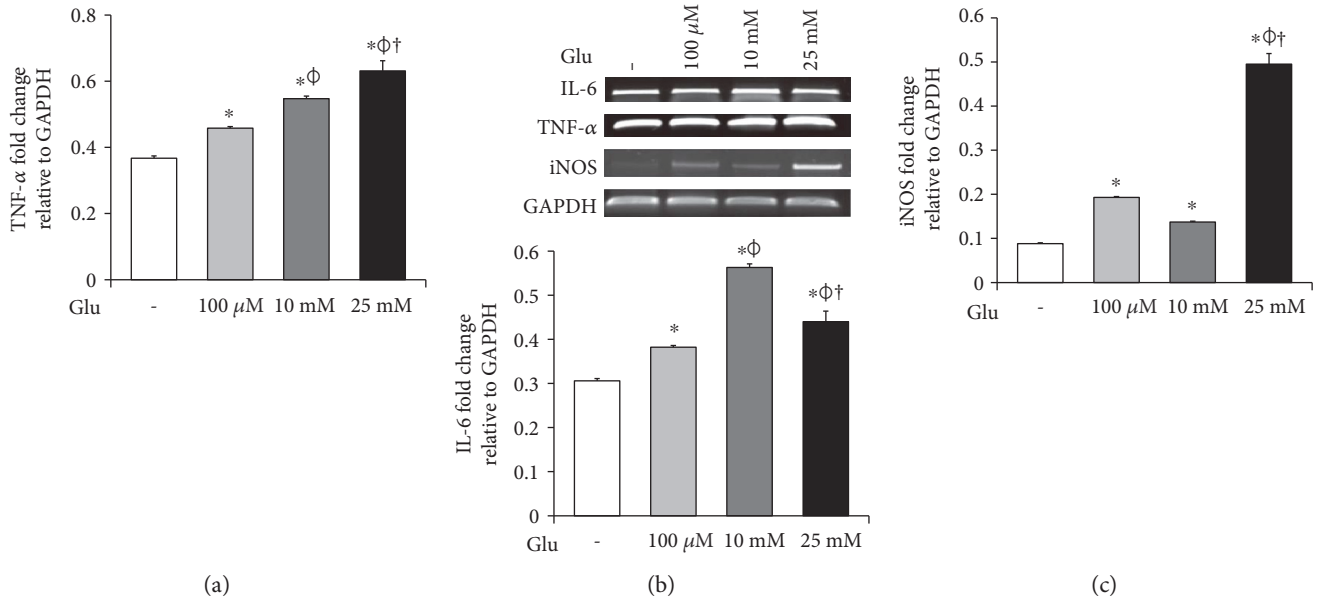

Figure 3: High glucose produces proinflammatory cytokines and iNOS in bEnd.3 cells. The mRNA levels of TNF-α (a), IL-6 (b), and iNOS (c) were measured by reverse transcription PCR. The results are expressed as the mean ± standard deviations (SD). Each experiment included at least 3 replicates per condition. $^{*}p < 0.05$ compared with nontreated control cells; $^{\phi}p < 0.05$ compared with 100 μM glucose-treated cells; $^{\dagger}p < 0.05$ compared with 10 mM glucose-treated cells. Glu: D-glucose treatment for 24 hours; IL-6: interleukin-6; iNOS: inducible nitric oxide synthase; TNF-α: tumor necrosis factor-α.

PARP, Figure 1(d)) analyses. The cell viability was dose dependently increased by 25, 50, and 100 μM of glucose and then gradually decreased at 10, 25, and 50 mM of glucose. Particularly, the cell viabilities exposed at 25 and 50 mM of glucose were significantly reduced than those of nontreated control cells (Figure 1(a)). Therefore, we selected 100 μM, 10 mM, and 25 mM of glucose for further experiment. mRNA levels of p-53 were significantly increased by glucose treatment (100 μM, 10 mM, and 25 mM) (Figure 1(b)), and those of Bax were also increased by glucose treatment particularly at concentrations of 10 mM and 25 mM (Figure 1(c)). In addition, cleaved PARP protein levels were significantly and gradually increased by glucose treatment (100 μM, 10 mM, and 25 mM) (Figure 1(d)).

3.2. High Glucose Condition Is Associated with the Loss of Tight Junction Integrity in bEnd.3 Cells. To examine the change of tight junction-related protein expression in bEnd.3 cells under high glucose condition, we conducted RT-PCR (ZO-1 and CLD5, Figures 2(a) and 2(b)) and Western blot analyses (CLD5, Figure 2(c)). The mRNA levels of ZO-1 in bEnd.3 cells were significantly attenuated by the treatment of glucose (10 mM and 25 mM) (Figure 2(a)). The mRNA levels of CLD5 were markedly and dose dependently decreased by glucose treatment (Figure 2(b)). In addition, protein levels of CLD5 were also dose dependently decreased by glucose treatment (Figure 2(c)).

3.3. High Glucose Condition Is Associated with Production of Proinflammatory Cytokines and iNOS in bEnd.3 Cells. To investigate the mRNA expression of proinflammatory cytokines and iNOS in the bEnd.3 cells under high glucose condition, we conducted RT-PCR (Figures 3(a), 3(b), and 3(c)).

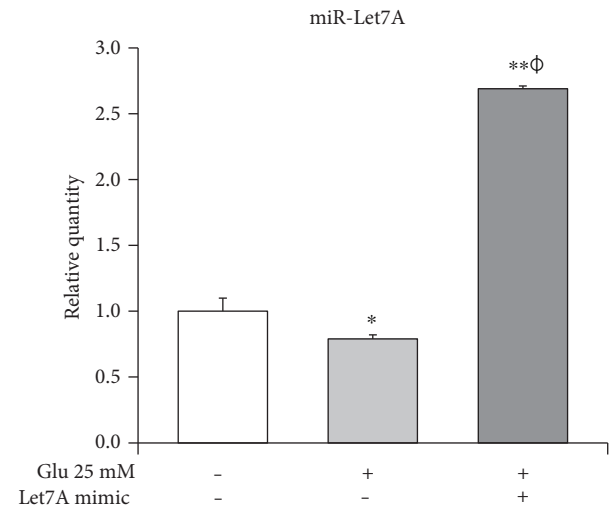

Figure 4: miR-Let-7A expression in the (bEnd.3) cells under high glucose condition. Expression of miR-Let7A was measured in all groups using TaqMan real-time PCR. The results are expressed as the mean ± standard deviations (SD). Each experiment included at least 3 replicates per condition. $^{*}p < 0.05$ and $^{**}p < 0.001$ compared with nontreated control cells; $^{\phi}p < 0.05$ compared with 25 mM glucose-treated cells.

The mRNA levels of TNF-α were dose dependently increased by the treatment of glucose (Figure 3(a)). IL-6 mRNA levels were also significantly increased by the glucose treatment (Figure 3(b)). In addition, mRNA levels of iNOS were significantly increased by the glucose treatment: particularly, marked increase was observed at 25 mM of glucose (Figure 3(c)).

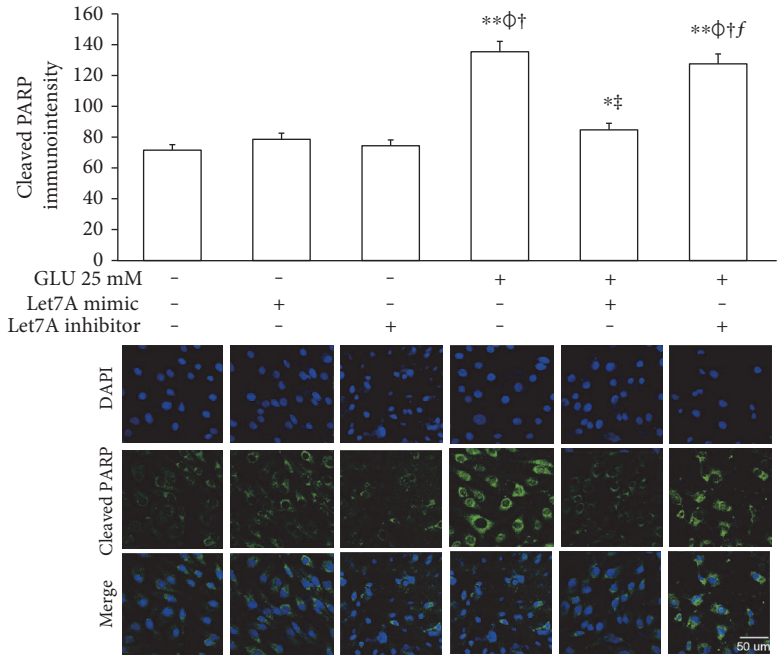

Figure 5: miR-Let7A attenuates the expression of cleaved PARP, a cell death marker in bEnd.3 cells under high glucose in vitro condition. To confirm the effect of miR-Let7A on the expression of cleaved PARP in high glucose-treated bEnd.3 cells, immunostaining was performed. Cells in three randomly selected fields were measured for immunodensity using ImageJ software (ImageJ, Madison, Wisconsin, USA). $^{*}p < 0.05$ and $^{**}p < 0.001$ compared with nontreated control cells; $^{\phi}p < 0.05$ compared with Let7A mimic overexpressed control cells; $^{\dagger}p < 0.05$ compared with Let7A inhibitor overexpressed control cells; $^{\ddagger}p < 0.05$ compared with 25 mM glucose-treated cells; $^{f}p < 0.05$ compared with 25 mM glucose-treated and Let7A-overexpressed cells. Scale bar: 50 μm, 4′,6-diamidino-2-phenylindole (DAPI): blue, cleaved PARP: green, Glu: D-glucose treatment for 24 hours, Let7A mimic: Let7A mimic pretreatment for 48 hrs, Let7A inhibitor: anti-Let7A pretreatment for 48 hrs, and PARP: poly ADP-ribose polymerase.

3.4. High Glucose Condition Is Involved in the Downregulation of miR-Let7A Expression in the (bEnd.3) Cells. Taqman assay was performed to compare the miR-Let7A expression level among the nontreated cells, 25 mM glucose only-treated cells, and Let7A mimic overexpressed and 25 mM glucose-treated cells. As shown in Figure 4, we found that miR-Let7A expression level in the 25 mM glucose only-treated cells was significantly lower than that in the nontreated cells. On the other hand, miR-Let7A expression level in the Let7A mimic overexpressed and 25 mM glucose-treated cells were markedly increased (more than 2.5-fold) compared with the nontreated cells or the 25 mM glucose only-treated cells. This result may show that miR-Let7A expression in the brain endothelial cells was downregulated under high glucose condition.

3.5. miR-Let7A Is Involved in the Regulation of Cell Death and Tight Junction Protein in bEnd.3 Cells under High Glucose In Vitro Condition. To confirm whether miR-Let7A is involved in the regulation of cell death and tight junction protein of bEnd.3 cells under high glucose condition, we performed immunofluorescence analysis for cleaved PARP and CLD5 with immunointensity calculation (Figures 5 and 6) and qPCR for ZO-1 mRNA expression (Figure 7(a)). Cleaved PARP was evidently increased by the treatment of 25 mM glucose. Interestingly, translocation of cleaved PARP into the nucleus was also observed in the glucose-treated bEnd.3 cells. On the other hand, miR-Let7A overexpression markedly attenuated the expression of cleaved PARP as well as its translocation into the nucleus in the glucose-treated bEnd.3 cells (Figure 5). Decreased CLD5 level under high glucose condition was significantly recovered by the overexpression of miR-Let7A (Figure 6). The mRNA levels of ZO-1 were significantly reduced by the treatment of 25 mM glucose compared with nontreated cells. The reduced mRNA levels of ZO-1 under high glucose condition were significantly recovered by the overexpression of miR-Let7A (Figure 7(a)). On the other hand, high glucose-induced alterations of cleaved PARP, CLD5, and ZO-1 were still retained when treated with miR-Let7A inhibitor (Figures 5 and 6).

3.6. miR-Let7A Attenuates the mRNA Expression of TNF-α, iNOS, and Nitrite Production in bEnd.3 Cells under High Glucose In Vitro Condition. To confirm whether miR-Let7A is involved in the regulation of proinflammatory cytokine and immune responses in the bEnd.3 cells under high glucose condition, we performed qPCR analysis for mRNA expressions of TNF-α, iNOS, and Griess reagent assay for nitrite production (Figures 7(b), 7(c), and 7(d)). mRNA levels of TNF-α were significantly increased under high glucose condition but significantly attenuated by miR-Let7A overexpression (Figure 7(b)). mRNA levels of iNOS was markedly

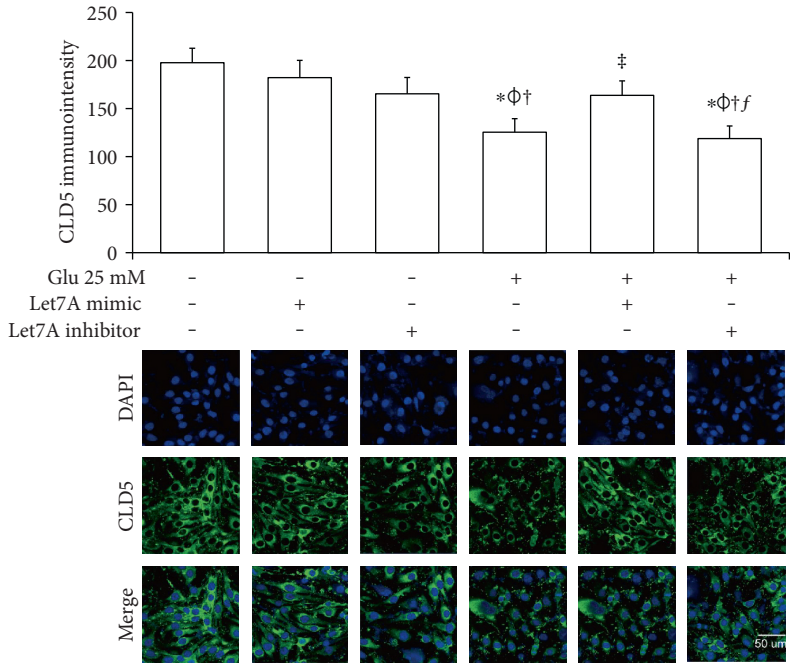

Figure 6: miR-Let7A ameliorates the expression of CLD5, a tight junction protein in bEnd.3 cells under high glucose in vitro condition. To confirm the effect of miR-Let7A on the expression of CLD5 in high glucose-treated bEnd.3 cells, immunostaining was performed. Cells in three randomly selected fields were measured for immunodensity using ImageJ software (ImageJ, Madison, Wisconsin, USA). $^{*}p < 0.05$ compared with nontreated control cells; $^{\phi}p < 0.05$ compared with Let7A mimic overexpressed control cells; $^{\dagger}p < 0.05$ compared with Let7A inhibitor overexpressed control cells; $^{\ddagger}p < 0.05$ compared with 25 mM glucose-treated cells; $^{f}p < 0.05$ compared with 25 mM glucose-treated and Let7A-overexpressed cells. Scale bar: 50 μm, 4′,6-diamidino-2-phenylindole (DAPI): blue, cleaved PARP: green, Glu: D-glucose treatment for 24 hours, Let7A mimic: Let7A mimic pretreatment for 48 hrs, Let7A inhibitor: anti-Let7A pretreatment for 48 hrs, and CLD5: claudin 5.

increased under high glucose condition but significantly and greatly attenuated by miR-Let7A overexpression (Figure 7(c)). On the other hand, high glucose-induced increases of TNF-α and iNOS were still retained when treated with miR-Let7A inhibitor (Figures 7(b) and 7(c)). Nitrite production in the cells treated with 25 mM glucose was about 2 times higher than that in the nontreated cells. On the other hand, increased production of nitrite in the glucose-treated bEnd.3 cell was significantly reduced by miR-Let7A overexpression but markedly increased by the treatment of Let7A inhibitor (Figure 7(d)).

4. Discussion

The present study shows that miR-Let7A significantly prevented cell death and loss of tight junction proteins and attenuated proinflammatory response in the bEnd.3 cells under high glucose in vitro condition. It suggests that the manipulation of miR-Let7A may be a novel solution in controlling BBB disruption which leads to the CNS diseases.

Brain endothelial cells are the main cellular element of BBB that is necessary for CNS homeostasis [27]. They constitute the multiple network of vessels which transport nutrients and gases throughout the brain [28] and form the metabolic barrier [27, 29]. Brain endothelial cells are interconnected by complicated tight junctions between lateral plasma membranes [30]. The integrity of tight junctions was reported to be responsible for the brain endothelial permeability [31]; thus, the loss of tight junction proteins may cause BBB disruption, leading to the various CNS diseases [32–34]. Especially, diabetes is emerging as a critical issue in BBB breakdown [35, 36], suggesting that high glucose could damage the cells and attenuate the integrity of tight junction [37–39]. In this present study, we confirmed that high glucose activates mRNA expressions of p-53 and Bax and protein expression of cleaved PARP which indicates the activation of cell death signaling [35, 40, 41]. We also observed reduced mRNA expressions of ZO-1 and CLD5 and protein expression of CLD5 which present the loss of tight junction proteins in brain endothelial cells [32, 33, 36, 42].

Recent studies suggested that posttranscriptional gene regulation via microRNAs in brain endothelial cells may alleviate neuropathology of CNS diseases [43–50]. Of these miRNAs, miR-Let7A was reported to remarkably downregulate proinflammatory cytokines in neuroinflammation conditions [50] and moreover to support brain endothelial barrier function including increases of monocyte cell adhesion and migration [50]. In the present study, we observed that miR-Let7A expression in the brain endothelial cells was downregulated under high glucose condition, but miR-Let7A overexpression significantly attenuated proinflammatory cytokine production (i.e., TNF-α) [23], suppressed the increased expression of cleaved PARP and its translocation into the nucleus which indicate cell death signaling [51], and recovered the loss of tight junction proteins

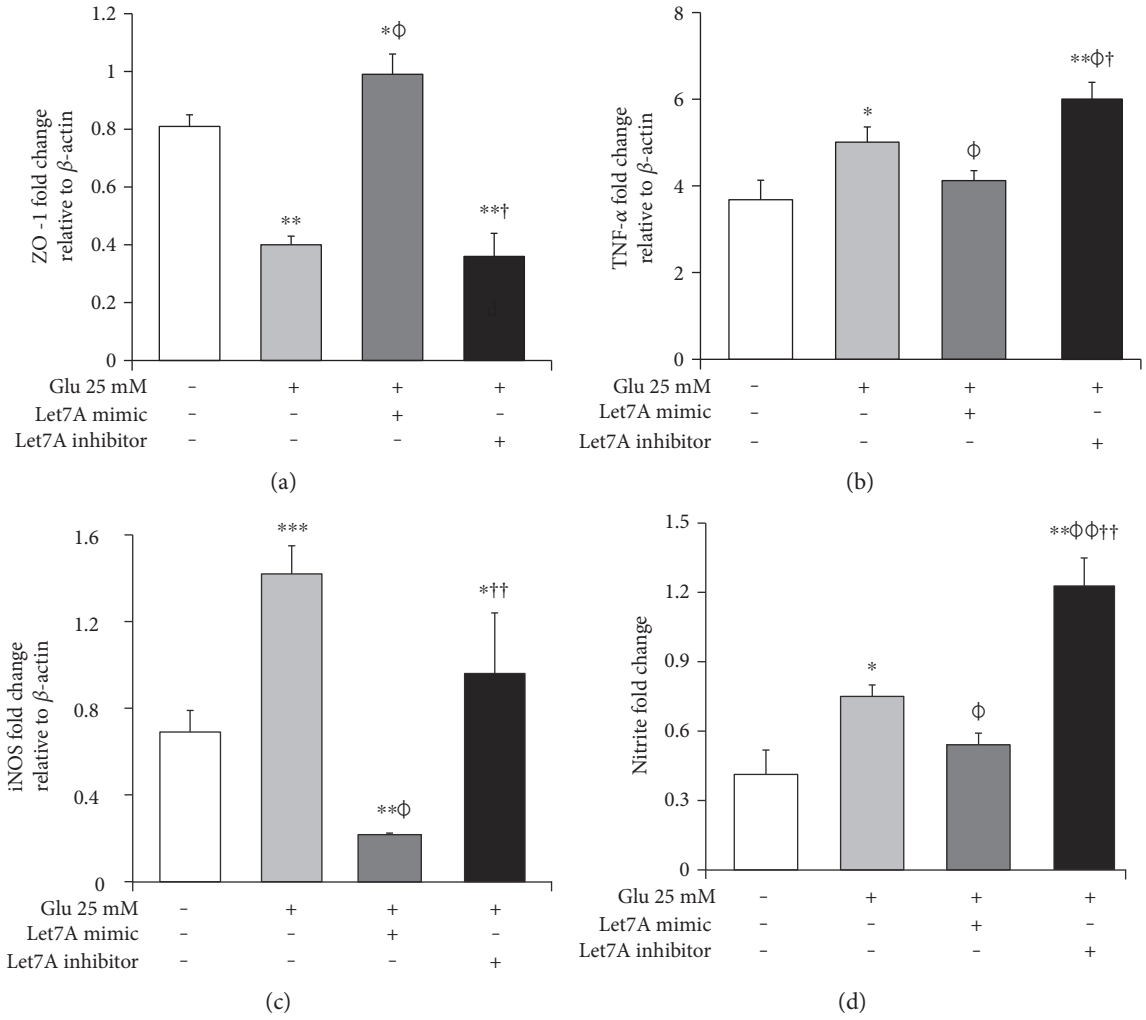

Figure 7: miR-Let7A modulates the expressions of ZO-1, TNF-α, and iNOS and nitrite production in bEnd.3 cells under high glucose in vitro condition. The mRNA levels of ZO-1 (a), TNF-α (b), and iNOS (b) were measured by quantitative real-time PCR. The production of nitrite (d) was detected by Griess reagent assay. The results are expressed as the mean ± standard deviations (SD). Each experiment included at least 3 replicates per condition. $^{*}p < 0.05$ and $^{**}p < 0.001$ compared with nontreated control cells; $^{\phi}p < 0.05$ compared with Let7A mimic overexpressed control cells; $^{\dagger}p < 0.05$ compared with Let7A inhibitor overexpressed control cells; $^{\ddagger}p < 0.05$ compared with 25 mM glucose-treated cells; $^{f}p < 0.05$ compared with 25 mM glucose-treated and Let7A-overexpressed cells. Glu: D-glucose treatment for 24 hours, Let7A mimic: Let7A mimic pretreatment for 48 hrs, Let7A inhibitor: anti-Let7A pretreatment for 48 hrs, iNOS: inducible nitric oxide synthase, and TNF-α: tumor necrosis factor-α.

(i.e., CLD5 and ZO-1) in bEnd.3 cells [32, 33, 36, 42] under high glucose condition. In addition, we found that nitrite production and iNOS mRNA expression under high glucose condition [52] were significantly suppressed by miR-Let7A overexpression. From these results, we assume that miR-Let7A significantly attenuated the disruption of BBB and the cell death of brain endothelial cells. It may indicate that miR-Let7A plays a beneficial role against the loss of tight junction proteins, cell death signaling, and proinflammatory response in the brain endothelial cells under high glycemic condition.

This study has limitations. Animal study (i.e., knockout or knockin mouse model for miR-Let7A) together with in vitro experiment would be more supportive for the conclusion. Further study with animal model is needed to elucidate the role of miR-Let7A in brain endothelial system under hyperglycemic condition. Second, this study used nontreated cells and high glucose-treated cells as "control" based on the previous reports [16, 21–24], but using control mimic (i.e., *C.* elegans miR-2 or any other unrelated miR) in the control cells would be meaningful to elucidate the sole effect of miR-Let7A on brain endothelial cells in the future.

Despite the study limitations, we highlight three points in this study. First, high glucose aggravates the loss of tight junction proteins and cell death. Second, miR-Let7A contributes to the maintenance of tight junction integrity in spite of high glucose stress. Finally, miR-Let7A alleviates the apoptosis of brain endothelial cells under high glucose in vitro condition. Thus, we suggest that the manipulation of miR-Let7A would ameliorate the disruption of BBB by protecting brain endothelial cells in hyperglycemia condition.

5. Conclusions

From this study, we suggest that miR-Let7A could attenuate the damage of brain endothelial cells by controlling cell death signaling, loss of tight junction proteins, and proinflammatory response against high glucose stress. Furthermore, the manipulation of miR-Let7A may be a novel solution in controlling BBB disruption which leads to the CNS diseases.

Conflicts of Interest

The authors declare that there are no conflicts of interest.

Authors' Contributions

Juhyun Song and Oh Yoen Kim designed the experiments and wrote the manuscript. Juhyun Song conducted the experiments. Juhyun Song, So Ra Yoon, and Oh Yoen Kim analyzed the data. Oh Yoen Kim revised the manuscript and provided the research funding. All authors reviewed and agreed on the final version of the manuscript.

Acknowledgments

This study was supported by the National Research Foundation of Korea Grant funded by the Korean Government (2016R1A2B4013627).

References

[1] M. H. Horani and A. D. Mooradian, "Effect of diabetes on the blood brain barrier," *Current Pharmaceutical Design*, vol. 9, no. 10, pp. 833–840, 2003.

[2] H. Wolburg and A. Lippoldt, "Tight junctions of the blood-brain barrier: development, composition and regulation," *Vascular Pharmacology*, vol. 38, no. 6, pp. 323–337, 2002.

[3] C. S. Abraham, N. Harada, M. A. Deli, and M. Niwa, "Transient forebrain ischemia increases the blood-brain barrier permeability for albumin in stroke-prone spontaneously hypertensive rats," *Cellular and Molecular Neurobiology*, vol. 22, no. 4, pp. 455–462, 2002.

[4] P. Mecocci, L. Parnetti, G. P. Reboldi et al., "Blood-brain-barrier in a geriatric population: barrier function in degenerative and vascular dementias," *Acta Neurologica Scandinavica*, vol. 84, no. 3, pp. 210–213, 1991.

[5] J. D. Huber, R. L. VanGilder, and K. A. Houser, "Streptozotocin-induced diabetes progressively increases blood-brain barrier permeability in specific brain regions in rats," *American Journal of Physiology. Heart and Circulatory Physiology*, vol. 291, no. 6, pp. H2660–H2668, 2006.

[6] M. R. Hayden, W. A. Banks, G. N. Shah, Z. Gu, and J. R. Sowers, "Cardiorenal metabolic syndrome and diabetic cognopathy," *Cardiorenal Medicine*, vol. 3, no. 4, pp. 265–282, 2013.

[7] C. Y. Cheung, Y. T. Ong, M. K. Ikram et al., "Microvascular network alterations in the retina of patients with Alzheimer's disease," *Alzheimers Dement*, vol. 10, no. 2, pp. 135–142, 2014.

[8] S. M. Manschot, A. M. Brands, J. van der Grond et al., "Brain magnetic resonance imaging correlates of impaired cognition in patients with type 2 diabetes," *Diabetes*, vol. 55, no. 4, pp. 1106–1113, 2006.

[9] J. Su, H. Zhou, Y. Tao et al., "G-CSF protects human brain vascular endothelial cells injury induced by high glucose, free fatty acids and hypoxia through MAPK and Akt signaling," *PloS One*, vol. 10, no. 4, article e0120707, 2015.

[10] K. Mishiro, T. Imai, S. Sugitani et al., "Diabetes mellitus aggravates hemorrhagic transformation after ischemic stroke via mitochondrial defects leading to endothelial apoptosis," *PloS One*, vol. 9, no. 8, article e103818, 2014.

[11] X. Ma, H. Zhang, Q. Pan et al., "Hypoxia/Aglycemia-induced endothelial barrier dysfunction and tight junction protein downregulation can be ameliorated by citicoline," *PloS One*, vol. 8, no. 12, article e82604, 2013.

[12] A. C. Chao, T. C. Lee, S. H. Juo, and D. I. Yang, "Hyperglycemia increases the production of amyloid beta-peptide leading to decreased endothelial tight junction," *CNS Neuroscience & Therapeutics*, vol. 22, no. 4, pp. 291–297, 2016.

[13] P. Skrha, J. Hajer, M. Andel, A. Horinek, and M. Korabecna, "miRNA as a new marker of diabetes mellitus and pancreatic carcinoma progression," *Casopis Lekaru Ceskych*, vol. 154, no. 3, pp. 122–126, 2015.

[14] J. A. Deiuliis, "MicroRNAs as regulators of metabolic disease: pathophysiologic significance and emerging role as biomarkers and therapeutics," *International Journal of Obesity*, vol. 40, pp. 88–101, 2016.

[15] T. Wang, G. Wang, D. Hao et al., "Aberrant regulation of the LIN28A/LIN28B and let-7 loop in human malignant tumors and its effects on the hallmarks of cancer," *Molecular Cancer*, vol. 14, p. 125, 2015.

[16] J. Song, K. J. Cho, Y. Oh, and J. E. Lee, "Let7a involves in neural stem cell differentiation relating with TLX level," *Biochemical and Biophysical Research Communications*, vol. 462, pp. 396–401, 2015.

[17] R. J. A. Frost and E. N. Olson, "Control of glucose homeostasis and insulin sensitivity by the *Let-7* family of microRNAs," *Proceedings of the National Academy of Sciences of the United States of America*, vol. 108, no. 52, pp. 21075–21080, 2011.

[18] L. Q. Jiang, N. Franck, B. Egan et al., "Autocrine role of interleukin-13 on skeletal muscle glucose metabolism in type 2 diabetic patients involves microRNA let-7," *American Journal of Physiology. Endocrinology and Metabolism*, vol. 305, pp. E1359–E1366, 2013.

[19] H. Zhu, N. Shyh-Chang, A. V. Segrè et al., "The Lin28/let-7 axis regulates glucose metabolism," *Cell*, vol. 147, no. 1, pp. 81–94, 2011.

[20] L. M. Perez, A. Bernal, N. San Martin, M. Lorenzo, S. Fernandez-Veledo, and B. G. Galvez, "Metabolic rescue of obese adipose-derived stem cells by Lin28/Let7 pathway," *Diabetes*, vol. 62, no. 7, pp. 2368–2379, 2013.

[21] J. Song and J. E. Lee, "ASK1 modulates the expression of microRNA Let7A in microglia under high glucose in vitro condition," *Frontiers in Cellular Neuroscience*, vol. 9, p. 198, 2015.

[22] J. Song, Y. Oh, and J. E. Lee, "miR-Let7A modulates autophagy induction in LPS-activated microglia," *Experimental Neurobiology*, vol. 24, no. 2, pp. 117–125, 2015.

[23] J. Song, M. Jun, M. R. Fahn, and O. Y. Kim, "Involvement of miR-Let7A in inflammatory response and cell survival/apoptosis regulated by resveratrol in THP-1 macrophage," *Nutrition Research and Practice*, vol. 10, no. 4, pp. 377–384, 2016.

[24] K. J. J. Song, Y. Cho, and J. E. L. Oh, "MicroRNA-Let-7a regulates the function of microglia in inflammation," *Molecular and Cellular Neurosciences*, vol. 68, pp. 167–176, 2015.

[25] D. Iliopoulos, H. A. Hirsch, and K. Struhl, "An epigenetic switch involving NF-kappaB, Lin28, Let-7 MicroRNA, and IL6 links inflammation to cell transformation," *Cell*, vol. 139, no. 4, pp. 693–706, 2009.

[26] D. Santovito, V. De Nardis, P. Marcantonio et al., "Plasma exosome microRNA profiling unravels a new potential modulator of adiponectin pathway in Diabetes: effect of glycemic control," *The Journal of Clinical Endocrinology and Metabolism*, vol. 99, pp. E1681–E1685, 2014.

[27] M. Chat, C. Bayol-Denizot, G. Suleman, F. Roux, and A. Minn, "Drug metabolizing enzyme activities and superoxide formation in primary and immortalized rat brain endothelial cells," *Life Sciences*, vol. 62, no. 2, pp. 151–163, 1998.

[28] S. Ge, L. Song, and J. S. Pachter, "Where is the blood-brain barrier …really?" *Journal of Neuroscience Research*, vol. 79, no. 4, pp. 421–427, 2005.

[29] S. M. Stamatovic, R. F. Keep, and A. V. Andjelkovic, "Brain endothelial cell-cell junctions: how to "open" the blood brain barrier," *Current Neuropharmacology*, vol. 6, no. 3, pp. 179–192, 2008.

[30] F. Joo, "Endothelial cells of the brain and other organ systems: some similarities and differences," *Progress in Neurobiology*, vol. 48, no. 3, pp. 255–273, 1996.

[31] W. Y. Liu, Z. B. Wang, L. C. Zhang, X. Wei, and L. Li, "Tight junction in blood-brain barrier: an overview of structure, regulation, and regulator substances," *CNS Neuroscience & Therapeutics*, vol. 18, no. 8, pp. 609–615, 2012.

[32] X. Zhang, Z. Fan, and T. Jin, "Crocin protects against cerebral-ischemia-induced damage in aged rats through maintaining the integrity of blood-brain barrier," *Restorative Neurology and Neuroscience*, vol. 35, 2017.

[33] Y. Zhang, F. Fan, G. Zeng et al., "Temporal analysis of blood-brain barrier disruption and cerebrospinal fluid matrix metalloproteinases in rhesus monkeys subjected to transient ischemic stroke," *Journal of Cerebral Blood Flow & Metabolism*, 2016.

[34] E. M. Weekman and D. M. Wilcock, "Matrix metalloproteinase in blood-brain barrier breakdown in dementia," *Journal of Alzheimer's Disease*, vol. 49, no. 4, pp. 893–903, 2016.

[35] Z. Xu, W. Zeng, J. Sun et al., "The quantification of blood-brain barrier disruption using dynamic contrast-enhanced magnetic resonance imaging in aging rhesus monkeys with spontaneous type 2 diabetes mellitus," *NeuroImage*, 2016.

[36] L. Zhang, M. Chopp, Y. Zhang et al., "Diabetes mellitus impairs cognitive function in middle-aged rats and neurological recovery in middle-aged rats after stroke," *Stroke*, vol. 47, no. 8, pp. 2112–2118, 2016.

[37] R. J. Ran, X. Y. Zheng, L. P. Du, X. D. Zhang, X. L. Chen, and S. Y. Zhu, "Upregulated inflammatory associated factors and blood-retinal barrier changes in the retina of type 2 diabetes mellitus model," *International Journal of Ophthalmology*, vol. 9, no. 11, pp. 1591–1597, 2016.

[38] T. O. Price, V. Eranki, W. A. Banks, N. Ercal, and G. N. Shah, "Topiramate treatment protects blood-brain barrier pericytes from hyperglycemia-induced oxidative damage in diabetic mice," *Endocrinology*, vol. 153, no. 1, pp. 362–372, 2012.

[39] M. Brownlee, "The pathobiology of diabetic complications: a unifying mechanism," *Diabetes*, vol. 54, no. 6, pp. 1615–1625, 2005.

[40] D. Soon, D. Tozer, D. Altmann, P. Tofts, and D. Miller, "Quantification of subtle blood-brain barrier disruption in non-enhancing lesions in multiple sclerosis: a study of disease and lesion subtypes," *Multiple Sclerosis*, vol. 13, no. 7, pp. 884–894, 2007.

[41] A. K. Bhattacharjee, T. Nagashima, T. Kondoh, and N. Tamaki, "Quantification of early blood-brain barrier disruption by in situ brain perfusion technique," *Brain Research. Brain Research Protocols*, vol. 8, no. 2, pp. 126–131, 2001.

[42] B. Zünkeler, R. E. Carson, J. Olson et al., "Quantification and pharmacokinetics of blood-brain barrier disruption in humans," *Journal of Neurosurgery*, vol. 85, no. 6, pp. 1056–1065, 1996.

[43] A. Reijerkerk, M. A. Lopez-Ramirez, B. van Het Hof et al., "MicroRNAs regulate human brain endothelial cell-barrier function in inflammation: implications for multiple sclerosis," *The Journal of Neuroscience*, vol. 33, no. 16, pp. 6857–6863, 2013.

[44] M. A. Lopez-Ramirez, D. Wu, G. Pryce et al., "MicroRNA-155 negatively affects blood-brain barrier function during neuroinflammation," *The FASEB Journal*, vol. 28, no. 6, pp. 2551–2565, 2014.

[45] J. Ma, Y. Yao, P. Wang et al., "MiR-181a regulates blood-tumor barrier permeability by targeting Kruppel-like factor 6," *Journal of Cerebral Blood Flow and Metabolism*, vol. 34, no. 11, pp. 1826–1836, 2014.

[46] W. Zhao, P. Wang, J. Ma et al., "MiR-34a regulates blood-tumor barrier function by targeting protein kinase Cepsilon," *Molecular Biology of the Cell*, vol. 26, no. 10, pp. 1786–1796, 2015.

[47] C. Cichon, H. Sabharwal, C. Ruter, and M. A. Schmidt, "MicroRNAs regulate tight junction proteins and modulate epithelial/endothelial barrier functions," *Tissue Barriers*, vol. 2, no. 4, article e944446, 2014.

[48] M. A. Lopez-Ramirez, R. Fischer, C. C. Torres-Badillo et al., "Role of caspases in cytokine-induced barrier breakdown in human brain endothelial cells," *Journal of Immunology*, vol. 189, no. 6, pp. 3130–3139, 2012.

[49] M. A. Lopez-Ramirez, D. K. Male, C. Wang, B. Sharrack, D. Wu, and I. A. Romero, "Cytokine-induced changes in the gene expression profile of a human cerebral microvascular endothelial cell-line, hCMEC/D3," *Fluids Barriers CNS*, vol. 10, no. 1, p. 27, 2013.

[50] S. Rom, H. Dykstra, V. Zuluaga-Ramirez, N. L. Reichenbach, and Y. Persidsky, "miR-98 and let-7g* protect the blood-brain barrier under neuroinflammatory conditions," *Journal of Cerebral Blood Flow and Metabolism*, vol. 35, no. 12, pp. 1957–1965, 2015.

[51] J. J. Boyle, "Vascular smooth muscle cell apoptosis in ahteroslceorsis," *International Journal of Experimental Pathology*, vol. 80, no. 4, pp. 197–203, 1999.

[52] M. P. Murphy, "Nitric oxide and cell death," *Biochimica et Biophysica Acta*, vol. 1411, pp. 401–414, 1999.

Hindawi
Oxidative Medicine and Cellular Longevity
Volume 2017, Article ID 4708516, 16 pages
https://doi.org/10.1155/2017/4708516

Research Article

miR-382 Contributes to Renal Tubulointerstitial Fibrosis by Downregulating HSPD1

Yi Fang,[1,2,3] Ting Xie,[1] Ning Xue,[1] Qing Kuang,[1] Zheng Wei,[4] Mingyu Liang,[5] and Xiaoqiang Ding[1,2,3]

[1]*Department of Nephrology, Zhongshan Hospital, Fudan University, Shanghai, China*
[2]*Shanghai Institute of Kidney and Dialysis, Shanghai, China*
[3]*Shanghai Key Laboratory of Kidney and Blood Purification, Shanghai, China*
[4]*Department of Hematology, Zhongshan Hospital, Fudan University, Shanghai, China*
[5]*Department of Physiology, Medical College of Wisconsin, Milwaukee, WI, USA*

Correspondence should be addressed to Mingyu Liang; mliang@mcw.edu and Xiaoqiang Ding; ding.xiaoqiang@zs-hospital.sh.cn

Received 2 February 2017; Revised 30 March 2017; Accepted 5 April 2017; Published 7 June 2017

Academic Editor: Jaideep Banerjee

Redox imbalance plays an important role in the pathogenesis of CKD progression. Previously, we demonstrated that microRNA-382 (miR-382) contributed to TGF-β1-induced loss of epithelial polarity in human kidney epithelial cells, but its role in the development of renal tubulointerstitial fibrosis remains unknown. In this study, we found that with 7 days of unilateral ureteral obstruction (UUO) in mice, the abundance of miR-382 in the obstructed kidney was significantly increased. Meanwhile, the protein expression of heat shock protein 60 (HSPD1), a predicted target of miR-382, was reduced after 7 days of UUO. Expression of 3-nitrotyrosine (3-NT) was upregulated, but expression of thioredoxin (Trx) was downregulated. Anti-miR-382 treatment suppressed the upregulation of miR-382, attenuated renal interstitial fibrosis in the obstructed kidney, and reversed the downregulation of HSPD1/Trx and upregulation of 3-NT after UUO. Furthermore, in vitro study revealed that overexpression of HSPD1 significantly restored Trx expression and reversed TGF-β1-induced loss of E-cadherin, while in vivo study found that direct siRNA-mediated suppression of HSPD1 in the UUO kidney promoted oxidative stress despite miR-382 blockade. Our clinical data showed that upregulation of miR-382/3-NT and downregulation of HSPD1/Trx were also observed in IgA nephropathy patients with renal interstitial fibrosis. These data supported a novel mechanism in which miR-382 targets HSPD1 and contributes to the redox imbalance in the development of renal fibrosis.

1. Introduction

Renal tubulointerstitial fibrosis (TIF) is a prominent pathological feature of chronic kidney disease (CKD) and the pathway leading to end-stage renal disease. It involves an excess accumulation of extracellular matrix proteins in the renal interstitium and is associated with inflammatory cell infiltration, tubular cell loss, and fibroblast accumulation [1–4]. In our previous study, we found that microRNA-382 (miR-382) contributed to TGF-β1-induced loss of epithelial characteristics in cultured human kidney epithelial (HK2) cells [5]. Proteomic and bioinformatic analyses revealed that heat shock protein 60 (HSPD60, HSPD1) was a target gene of miR-382 [5]. HSPD1 is a key protein that maintains mitochondrial integrity and cellular activity, thereby protecting the cell from oxidative stress by assisting in mitochondrial protein folding and inhibiting apoptosis [6–9]. Since enhanced oxidative stress or redox imbalance has been proved to correlate with renal dysfunction [10, 11], miR-382 or HSPD1 might potentially serve as a new target for therapy in advanced CKD. Therefore, the goals of this study mainly were to verify the complementary relationship between miR-382 and HSPD1, as well as to further explore the role of miR-382 in the development of renal tubulointerstitial fibrosis.

2. Materials and Methods

2.1. Cell Culture and Drug Treatments. Human kidney epithelial (HK2) cells were obtained from ATCC (Manassas, Virginia, USA). DMEM (Gibco), Opti-MEM I (Gibco), or other cell culture media were used according to the manufacturer's recommendations. HK2 cells at approximately 40% confluency were treated with recombinant human TGF-β1 (3 ng/ml) (R&D Systems) or the vehicle control in DMEM for the indicated time period. Pre-miR-382 or anti-miR-382 oligonucleotides were obtained from Ambion. HK2 cells were transfected with the oligonucleotides (100 nM) using Oligofectamine (Invitrogen).

2.2. Mouse Model of UUO. Laboratory animals: ICR mice (6–8 weeks, 23–26 g, male) were purchased from Shanghai SLRC Laboratory Animal Co. Ltd. (Shanghai, China). Animals were housed in temperature- and humidity-controlled cages, with free access to water and rodent food on a 12 h light/dark cycle. Experiments were completed at Fudan University, and all protocols were approved by the Institutional Animal Care and Use Committee of Fudan University, as well as adhered strictly to the NIH Guide for the Care and Use of Laboratory Animals. For mice which became severely ill or moribund during the experiment, euthanasia was performed according to euthanasia guidelines of animals issued by the Institutional Animal Care and Use Committee of Fudan University.

All surgeries were performed under intraperitoneal sodium pentobarbital anesthesia (80 mg/kg), intrarectal temperature of mice was maintained at 36.5°C–37.0°C with a heating pad during the surgeries, and efforts were made to minimize suffering and the number of mice used. Mice underwent unilateral ureteral obstruction (UUO) or sham operation of the left ureter. The obstruction was produced by ligation of the left ureter following midline laparotomy. The left ureter was isolated, but not ligated, in sham-operated controls. After UUO surgery, mice were transferred to the recovery cages, one cage each. Parameters like vital signs and time to wake up from anesthesia were monitored. Food intake was monitored every day and animals were weighed once every other day. Locked nucleic acid- (LNA-) modified anti-miR-382 oligonucleotides antiscrambled (Exiqon) were diluted in saline (5 mg/ml) and intravenously delivered via tail vein (10 mg/kg) within 30 mins prior to UUO, and the dosage was repeated 24 hours after the surgery. In vivo delivery of small interfering RNA (siRNA) designed against HSPD1 or negative control siRNA (10 μg, GenePharma) was performed by retrograde injection into the ureter proximal to the ligature, immediately following occlusion of the ureter. Mice were sacrificed by cervical dislocation 7 days after left ureteral obstruction. The kidneys were collected for evaluating the abundance of miR-382, HSPD1, thioredoxin (Trx), 3-nitrotyrosine (3-NT), VCAM-1, and CD3. The degree of renal fibrosis was graded according to Masson trichrome staining and Sirius red staining.

2.3. Patient Selection and Renal Morphologic Analysis. We studied 12 patients with primary IgA nephropathy between 2014 and 2015, and all diagnoses were confirmed by kidney biopsy at Zhongshan Hospital, Fudan University. Six patients had no tubulointerstitial fibrosis, and 6 patients exhibited moderate to severe tubulointerstitial fibrosis. Analysis of renal fibrosis was performed with 2 μm paraffin-embedded sections stained by Masson trichrome and Sirius red stain. The degree of renal fibrosis was scored by an experienced pathologist. For tubulointerstitial fibrosis, 10 microscopic fields were viewed at a magnification of ×400 and scored subjectively from 0 to 100% for each patient. The degree of tubulointerstitial fibrosis was graded on a scale of 0 to 4: grade 0 had no affected area (normal); grade 1 had an affected area of less than 10%; grade 2 had an affected area of 10 to 25%; grade 3 had an affected area of 25 to 75%; grade 4 had an affected area of greater than 75% [12]. The resulting index in each slide was expressed as a mean of all scores obtained. The same method was applied in the analysis of mouse renal pathology. The study was approved by the Clinical Research Ethical Committee of Zhongshan Hospital, Fudan University. All patients provided written informed consents. Clinical data including blood pressure, serum creatinine, and 24 h urine protein tests were recorded at the time of kidney biopsy.

2.4. RNA Isolation. Total RNA was extracted using TRIzol (Invitrogen) from cells or tissue sections as previously described [5, 13]. Total RNA from formalin-fixed and paraffin-embedded (FFPE) tissues was extracted by Recover-ALL total nucleic acid isolation kit (Ambion, Austin, Texas, USA) according to the manufacturer's protocol.

2.5. TaqMan Real-Time PCR. Expression levels of miR-382 were quantified by real-time reverse transcription-PCR with the TaqMan chemistry (Applied Biosystems) as previously described [5, 13]. The mRNA levels of HSPD1, α-SMA, E-cadherin, Vimentin, Trx, and GAPDH were quantified using SYBR Green as previously described [5, 13]. Total RNA samples were adopted in these analyses. 5S rRNA and GAPDH mRNA were used as normalization controls for miRNA and protein-coding genes, respectively. Relative changes in mRNA and miR-21 expression were determined using the $2^{-\Delta\Delta Ct}$ method. Relative gene levels were expressed as ratios to control. The sequences of primers are listed in Table 1.

2.6. Western Blot and Immunohistochemistry. The relative abundance of several proteins was analyzed using Western blot or immunohistochemistry (IHC) as previously described [5, 13]. Primary antibodies for HSPD1 (1 : 100; Enzo Life Sciences), E-cadherin (1 : 100; Abcam), Vimentin (1 : 100; Abcam), α-SMA (1 : 75; Sigma-Aldrich), 3-NT (1 : 100; Abcam), Trx (1 : 100; Abcam), VCAM-1 (1 : 10;0 Abcam), CD3 (1 : 50; Abcam), and Bax (1 : 100; Cell Signaling Tech) were applied according to the manufacturer's instructions. Secondary antibodies (1 : 1000; Jackson ImmunoResearch) were also applied according to the manufacturer's instructions. All immunohistochemistry staining and collagen staining were analyzed as the following steps: under a microscope (400x), we move the slices randomly and take 20–25 pictures per slice, then analyze by Image Pro-Plus 6.0 Software (Media Cybernetics, USA) to quantify the abundance of our

Table 1: Primers used in real-time PCR.

Target	Gene symbol	Sequence
Heat shock protein 1 (chaperonin) (mouse)	Hspd1	Sense:5- TTGCTAATGCTCATCGGAAG -3 Antisense:5- AGCGTGCTTAGAGCTTCTCC
Heat shock protein family D (Hsp60) member 1 (human)	HSPD1	Sense:5- AAATTGCACAGGTTGCTACG -3 Antisense:5- TGATGACACCCTTTCTTCCA -3
E-cadherin (human)	CDH1	Sense:5- TGCCAAGTGGGTGGTATAGAGG -3 Antisense:5- CAGTGGGATGGTGGGTGTAAGA -3
Glyceraldehyde-3-phosphate dehydrogenase (human)	GAPDH	Sense:5- CATCTTCTTTTGCGTCGCCA -3 Antisense:5- TTAAAAGCAGCCCTGGTGACC -3
Glyceraldehyde-3-phosphate dehydrogenase (mouse)	Gapdh	Sense:5- CGGAGTCAACGGATTTGGTCGTAT -3′ Antisense:5- AGCCTTCTCCATGGTGGTGAAGAC
α-Smooth muscle actin (human)	ACTA2	Sense:5- CTGTTCCAGCCATCCTTCAT -3 Antisense:5- TCATGATGCTGTTGTAGGTGGT -3
α-Smooth muscle actin (mouse)	Acta2	Sense:5- CTGACAGAGGCACCACTGAA -3 Antisense:5- CATCTCCAGAGTCCAGCACA -3
Vimentin (human)	VIM	Sense: 5- TACAGGAAGCTGCTGGAAGG -3 Antisense: 5- ACCAGAGGGAGTGAATCCAG -3
Vimentin (mouse)	Vim-	Sense:5- TGAAGGAAGATGGCTCGT -3 Antisense:5- TCCAGCAGCTTCCTGTAGGT -3
Thioredoxin (human)	TXN	Sense:5′- TTGGACGCTGCAGGTGATAAAC -3′ Antisense:5′- GGCATGCATTTGACTTCACACTC -3′

target protein/gene. Parameter of IOD (integrated optical density) was employed to do this work. To prove our assumption with a second method, we also quantified tyrosine-nitrosylated proteins by fluorescence immunoblotting of 3-NT (Abcam; 1 : 100). Secondary antibodies were species-specific FITC-conjugated IgG (1 : 500, Invitrogen).

2.7. 3′-Untranslated Region (UTR) Reporter Analysis. 3′-UTR reporter constructs were generated, and reporter activity was analyzed as previously described with minor modifications [5, 13]. Briefly, HeLa cells (80–90% confluency) were cotransfected with the following: a 3′-UTR reporter construct (100 ng per well), a pRL-TK internal control plasmid (50 ng per well), and control pre-miR-382 oligonucleotides (10 pmol per well, from Ambion). Cells were cotransfected using Lipofectamine 2000 (Invitrogen), following the manufacturer's protocol. Firefly and Renilla luciferase activities were measured in each well 24 h after the transfection using the Dual-Luciferase Reporter Assay System (Promega), following the manufacturer's protocol. Renilla luciferase activity was used as a normalization control for luciferase activity to measure transfection efficiency and cell density.

Site-directed mutagenesis was performed with the QuickChange II XL site-directed mutagenesis kit (Stratagene), following the manufacturer's protocol. Primers used for introducing point mutations for HSPD1 were as follows: forward primer, 5- CAAGGCAGTGTTCCTCACCAATA gaTTCAGAGAAGACAGTTG -3; reverse primer, 5- CAACTGTCTTCTCTGAAtcTATTGGTGAGGAACACTG CCTTG -3. Underlined nucleotides represent the mutations introduced, and these nucleotides are located in the core region of the predicted target site for miR-382.

2.8. miR-382 In Situ Hybridization. Expression of miR-382 was detected by in situ hybridization (ISH), following the protocol of "One-day microRNA ISH" suggested by Exiqon. The experimental conditions for renal tissues of IgA nephropathy patients were as follows: FFPE kidney tissues were cut into 2 μm thick sections, cleared in xylenes, rehydrated using an ethanol gradient, and then exposed to a 10 min proteinase K (15 mg/ml) treatment at 37°C. The probe was diluted in hybridization buffer (60 nM, 60 μl/tissue section) and preheated at 90°C for 4 min to linearize. The probe was then added to the slides and incubated for 90 min at 54°C. Sheep antidigoxigenin alkaline phosphatase (anti-DIG-AP) antibody was diluted (1 : 1000) and added to the slides, which were incubated at room temperature for 60 min. Slides were incubated in nitro blue tetrazolium/5-bromo-4-chloro-3-indolyl phosphate (NBT/BCIP; Roche) diluted with double-distilled H_2O at 32°C, and tissues were then mounted with neutral resin.

2.9. Plasmid Transfection. HSPD1 human cDNA ORF clone was obtained from KeyGentec. The clone expresses HSPD1 driven by a CMV promoter and tagged with C-terminal Myc-DDK. The clone was amplified and purified as previously described [5]. HK2 cells were transfected with HSPD1 plasmid or an empty vector using Lipofectamine 2000 with a working concentration of 2 μg for each 35 mm dish.

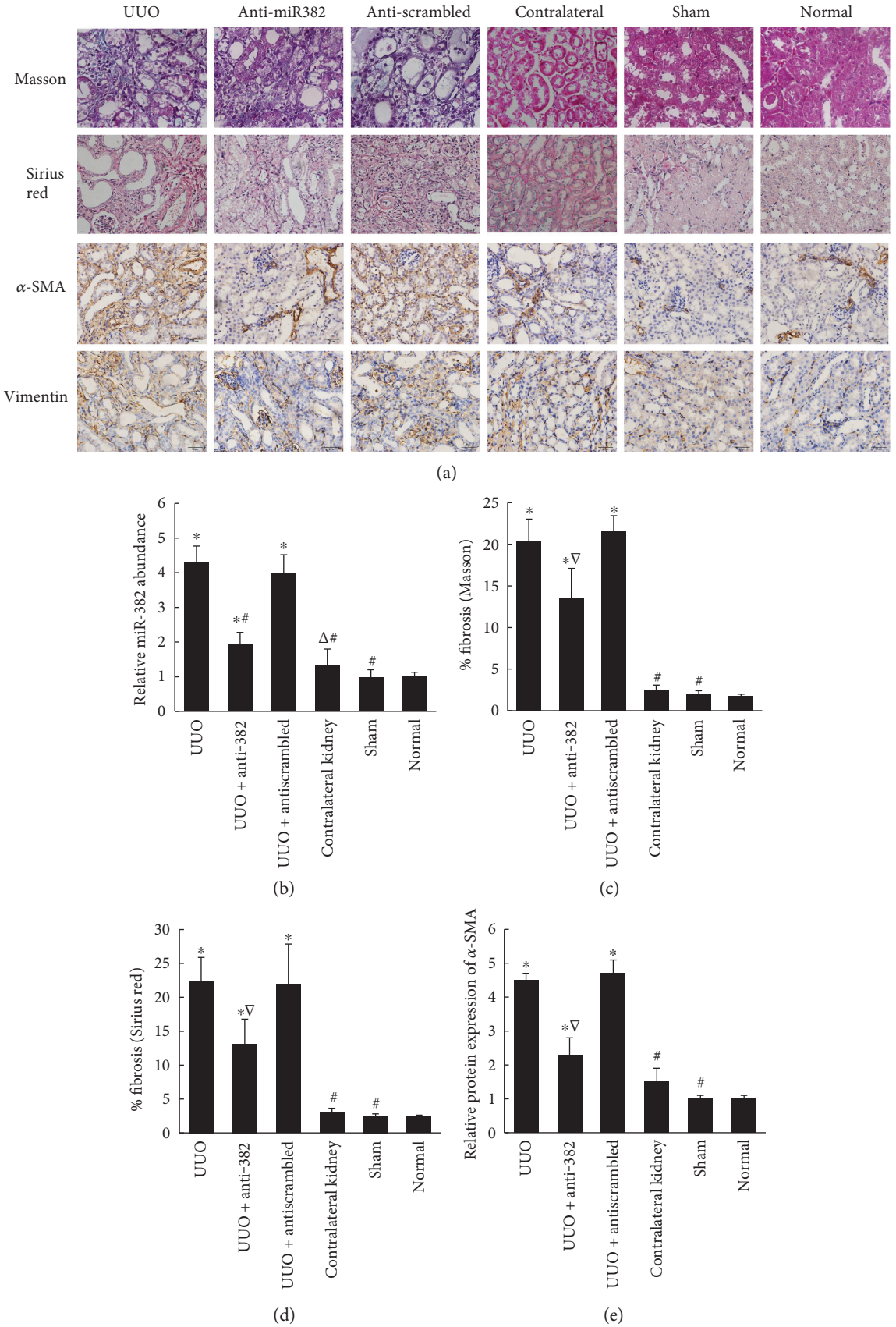

Figure 1: Continued.

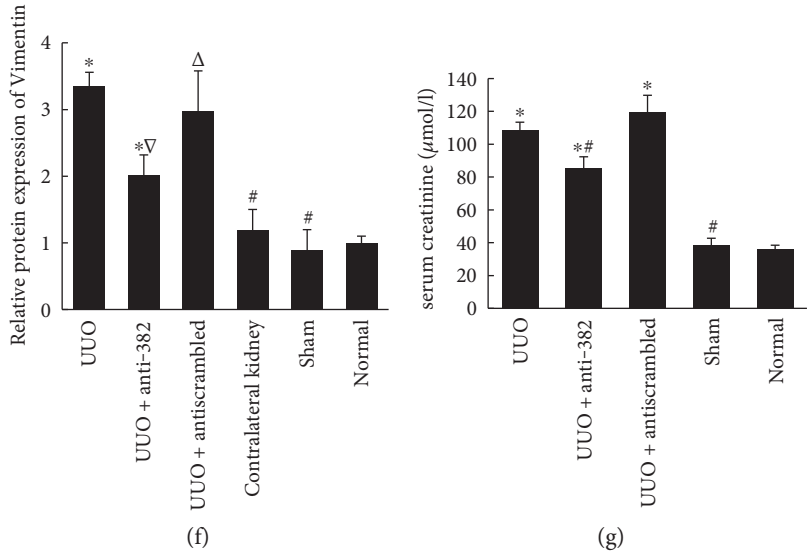

Figure 1: miR-382 contributed to the progression of renal tubulointerstitial fibrosis in UUO mice. (a) Staining of collagen, α-SMA, and Vimentin. (b) Relative abundance of miR-382. (c) The abundance of collagen was analyzed using Masson trichrome staining (Masson trichrome staining ×400, $n = 4$). (d) The abundance of collagen was analyzed using Sirius red staining (Sirius red staining ×400, $n = 4$). (e) Quantification of α-SMA staining. (f) Quantification of Vimentin staining. The abundance of collagen, α-SMA, or Vimentin was quantitatively measured using Image Pro-Plus 6.0 Software (Media Cybernetics, USA). Relative protein levels were expressed as ratios to control. (g) Serum creatinine concentration. Mice underwent unilateral ureteral obstruction or sham operation of the left ureter. Locked nucleic acid-modified anti-miR-382 oligonucleotides and antiscrambled were diluted in saline (5 mg/ml) and intravenously delivered via tail vein (10 mg/kg) within 30 min prior to UUO, and the dosage was repeated 24 hours after the surgery. $^{\Delta}P < 0.05$, $^{*}P < 0.01$ compared with the normal group; $^{\nabla}P < 0.05$, $^{\#}P < 0.01$ compared with the UUO group. UUO indicates unilateral ureteral obstruction. Normal indicates the normal control group.

2.10. Measurement of Cellular ROS Level. CM-H2DCFCA, a ROS-sensitive fluorescent dye, was used to measure ROS levels, as previously described [14]. HK-2 cells were incubated in 96-well plates. 5 mM CM-H2DCFCA was added to each well. Fluorescence intensities were measured using a microplate fluorescence reader.

2.11. Statistical Analysis. Data were expressed as mean ± SD. Differences among three or more groups were evaluated using one-way analysis of variance (ANOVA) with Bonferroni adjustment. SPSS software (version 19.0) was used for statistical analysis. A value of $P < 0.05$ was considered to be statistically significant.

3. Results

3.1. miR-382 Contributes to the Progression of Renal Tubulointerstitial Fibrosis in UUO Mice. Tubulointerstitial fibrosis developed after 7 days of UUO in the obstructed kidneys (Figure 1(a)), and the expression of miR-382 was higher in the UUO group (UUO versus control, 4.32 ± 0.45 versus 1.00 ± 0.13, resp., $P < 0.01$). Locked nucleic acid-(LNA-) modified anti-miR-382 (10 mg/kg) was delivered by tail vein injection 30 min prior to UUO, and the dosage was repeated 24 h after the surgery. In the anti-miR-382 group, the expression of miR-382 was significantly suppressed by 10 mg/kg LNA-anti-miR-382 treatment compared with the antiscrambled (10 mg/kg anti-382 versus antiscrambled, 1.95 ± 0.33 versus 3.98 ± 0.54, resp., $P < 0.05$) (Figure 1(a)). Renal histological analysis showed that blocking the expression of miR-382 could attenuate renal interstitial fibrosis (Figures 1(a), 1(c), and 1(d)) and the immunohistochemical staining indicated that the upregulation of α-SMA and Vimentin was partially reversed in obstructed kidneys after 10 mg/kg anti-miR-382 treatment (Figures 1(e) and 1(f)). Besides, anti-miR382 treatment also attenuated renal injury with less increased serum creatinine (Figure 1(f)) and blocked inflammatory cell infiltration in the obstructed kidney (Figure 2).

3.2. Identification of HSPD1 as a New Target of miR-382. According to our previously published data, we found that miR-382 targeted a cluster of oxidative-related genes including HSPD1 [5]. In this study, we found that transfecting HK2 cells with pre-miR-382 significantly suppressed the protein expression of HSPD1 (pre-382 versus pre-NC, 0.60 ± 0.04 versus 1.00 ± 0.04, resp., $P < 0.05$) (Figure 3(a)). Anti-miR-382 oligo treatment inhibited the upregulation of miR-382 and reversed the decrease of HSPD1 expression induced by TGF-β1 in cultured HK2 cells (Figure 3(b)). A 3′-UTR segment of HSPD1 was cloned into a gene expression vector with a luciferase reporter gene. Cotransfection with pre-miR-382 to the HeLa cells reduced the luciferase activity significantly. Mutations introduced into the predicted binding site of miR-382 within the 3′-UTR of HSPD1 prevented the suppression of HSPD1 by pre-miR-382 (Figure 3(c)).

3.3. Overexpression of miR-382 Reduces the Antioxidant Capacity of Renal Tissues by Downregulating HSPD1. The inverse relationship between miR-382 expression and renal

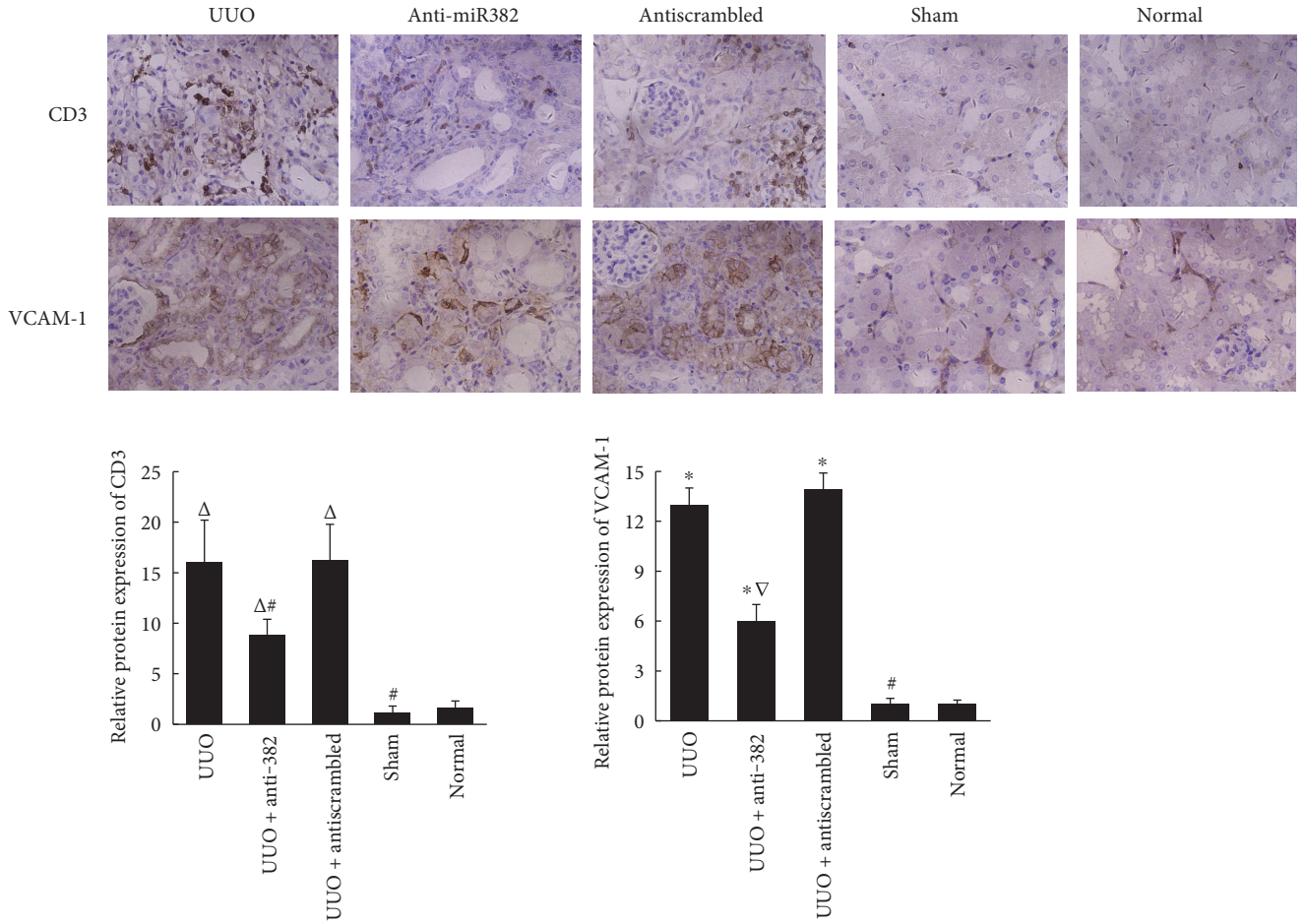

Figure 2: Expression of CD3 and VCAM-1 in the obstructed mouse kidneys. Treatment with 10 mg/kg anti-miR-382 reversed the upregulation of CD3 and VCAM-1. The positive stained area of VCAM-1 staining or CD3 was quantitatively measured by Image-Pro Plus, as described in Figure 1. $^{\Delta}P < 0.05$, $^{*}P < 0.01$ compared with the normal group; $^{\nabla}P < 0.05$, $^{\#}P < 0.01$ compared with the UUO group. UUO indicates unilateral ureteral obstruction. Normal indicates the normal control group ($n = 4$).

expression of HSPD1 also exists in the obstructed kidneys of UUO mice as well as in patients with chronic kidney disease. There was a lower protein expression of HSPD1 after 7 days of UUO in the obstructed murine kidney (UUO versus normal, 0.14 ± 0.04 versus 1.00 ± 0.11, resp., $P < 0.05$). Anti-miR-382 treatment with a dosage of 10 mg/kg suppressed the downregulation of HSPD1 in UUO mice (Figure 4). In the clinical setting, patients with IgA nephropathy (IgAN) were identified, and cases were selected based on whether the diagnosis was minimal or substantial renal interstitial fibrosis. In IgAN patients with TIF, miR-382 abundance was significantly upregulated compared to that in IgAN patients with no TIF (5.59 ± 0.79 versus 1.00 ± 0.23, $P < 0.01$, Figure 5(c)). Comparative protein abundance of E-cadherin was suppressed (TIF versus no TIF, 0.33 ± 0.18 versus 1.00 ± 0.47, resp., $P < 0.05$), while both α-SMA (TIF versus no TIF, 4.29 ± 1.72 versus 1.00 ± 0.20, resp., $P < 0.01$) and Vimentin (TIF versus no TIF, 4.60 ± 1.82 versus 1.00 ± 0.26, resp., $P < 0.05$) were augmented in the TIF group (Figure 6). There also existed an inverse relationship between HSPD1 and miR-382 abundance. The protein abundance (TIF versus no TIF, 0.12 ± 0.04 versus 1.00 ± 0.18, resp., $P < 0.05$) of HSPD1 was significantly reduced in patients with TIF (Figure 5(d)).

Immunohistochemical staining analysis showed that the comparative protein expression of thioredoxin (Trx), a marker of antioxidant capacity, was reduced in the obstructed kidneys (Figure 7). In contrast, the protein expression of 3-nitrotyrosine (3-NT), a marker of oxidative stress, was upregulated (Figure 7). LNA-anti-miR-382 treatment (10 mg/kg) significantly reversed the downregulation of Trx and suppressed the expression of 3-NT in mice subjected to UUO (10 mg/kg anti-382 group versus anti-NC group, Trx: 0.43 ± 0.13 versus 0.20 ± 0.06, $P < 0.05$; 3-NT: 2.11 ± 0.27 versus 4.52 ± 0.16, $P < 0.05$). Similar profiles of Trx and 3-NT expression were also detected in the renal biopsy tissues of IgAN patients (TIF versus no TIF, Trx: 0.35 ± 0.09 versus 1.00 ± 0.15, $P < 0.05$; 3-NT: 1.00 ± 0.24 versus 6.43 ± 0.69, $P < 0.05$) (Figure 6).

3.4. Overexpression of HSPD1 Restores Renal Antioxidant Capacity and Attenuates TGF-β1-Induced Loss of Cell Polarity In Vitro. The cellular ROS production induced by TGF-β1 in the TGF-β1+HSPD1 plasmid group was

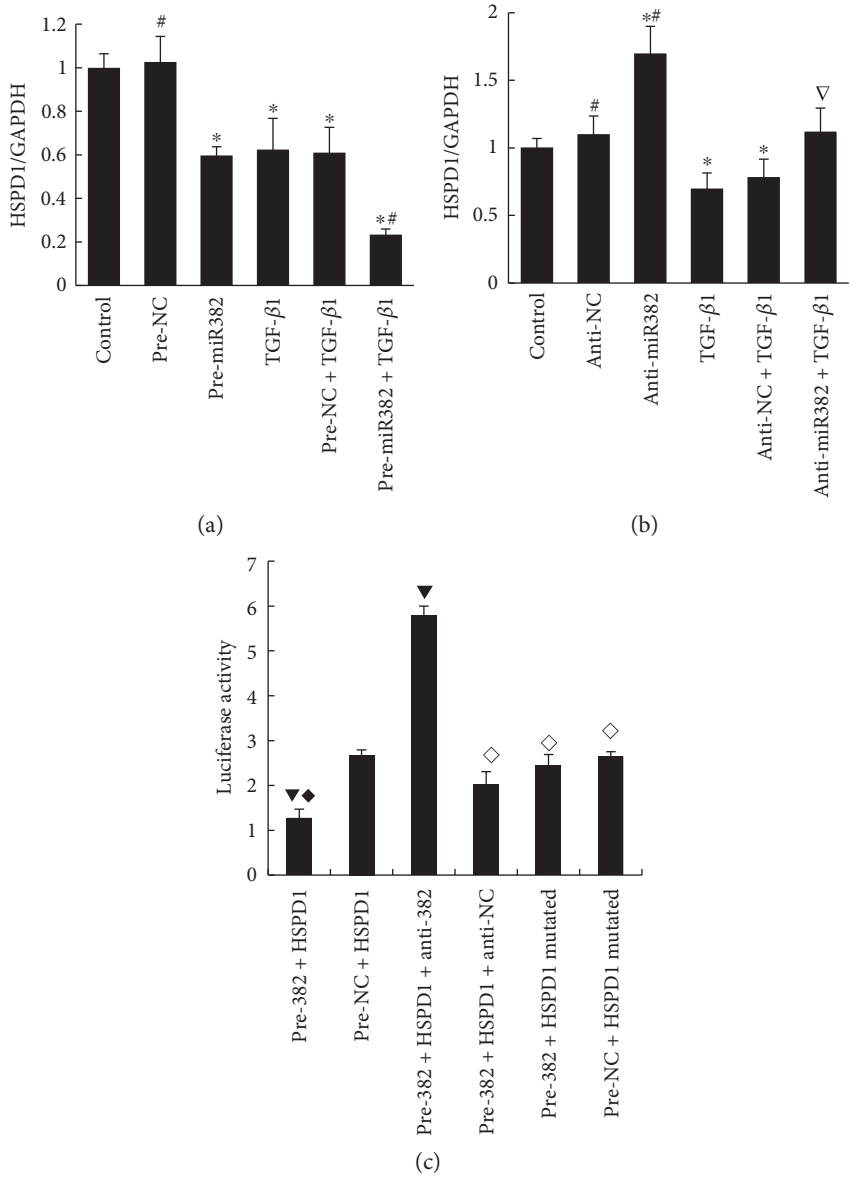

Figure 3: Interaction between miR-382 and HSPD1. (a) Both TGF-β1 and pre-miR-382 could repress the protein expression of HSPD1 in HK2 cells. (b) Anti-miR-382 treatment could partially reverse the downregulation of HSPD1 that is induced by TGF-β1 in HK2 cells. (c) MiR-382 interacted with the 3′-UTR of HSPD1. HeLa cells at ~80% confluency were cotransfected with a 3′-UTR segment of HSPD1 (marked with luciferase reporter gene), a pRL-TK internal control plasmid, and control pre-miR oligonucleotides or the miR-382. Luciferase activity was significantly decreased by pre-miR-382, while in the mutated group, pre-miR-382 did not have significant effect on luciferase activity. $^{*}P < 0.01$ compared with the control group; $^{\triangledown}P < 0.05$, $^{\#}P < 0.01$ compared with the TGF-β1 group. $^{\blacktriangledown}P < 0.05$ compared with the pre-NC+HSPD1 group; $^{\diamond}P < 0.05$, $^{\blacklozenge}P < 0.01$ compared with the pre-382 + HSPD1 + anti-382 group. NC indicates negative control. Anti-382 indicates the group treated with anti-miR-382 oligos. Pre-382 indicates the group treated with pre-miR-382 oligos. Anti-NC indicates antinegative control. Pre-NC indicates prenegative control. UUO indicates unilateral ureteral obstruction. (a, b) Western blot; (c) 3′-UTR luciferase reporter assay and site-directed mutagenesis ($n = 5$).

significantly lower than that in the TGF-β1+vehicle plasmid group (relative fluorescence units, 89.67 ± 14.15 versus 179.55 ± 16.32, $P < 0.05$) (Figure 8(a)). HK2 cells were quite resistant to TGF-β1 exposure with pretreatment of HSPD1 plasmid transfection, due to the similar levels both mRNA and protein of E-cadherin maintained compared to those of the control groups (Figures 8(b) and 8(c)). ELISA assay of the cell homogenate revealed that TGF-β1-induced downregulation of Trx was completely restored by HSPD1 transfection (TGF-β1 + HSPD1 plasmid group versus TGF-β1 + vehicle group, 122.99 ± 9.08 pg/ml versus 78.43 ± 1.21 pg/ml, resp., $P < 0.01$; TGF-β1 + HSPD1 plasmid group versus control group, 122.99 ± 9.08 pg/ml versus 103.24 ± 2.58 pg/ml, resp., $P > 0.05$), while the protein expression of 3-NT in HK2 cells, as a biomarker of oxidative stress and inadequate cellular antioxidant defenses, was attenuated after HSPD1 plasmid transfection (TGF-β1 + HSPD1 plasmid group versus TGF-β1 + vehicle plasmid group, 13.57 ± 0.24 ng/ml versus 18.28

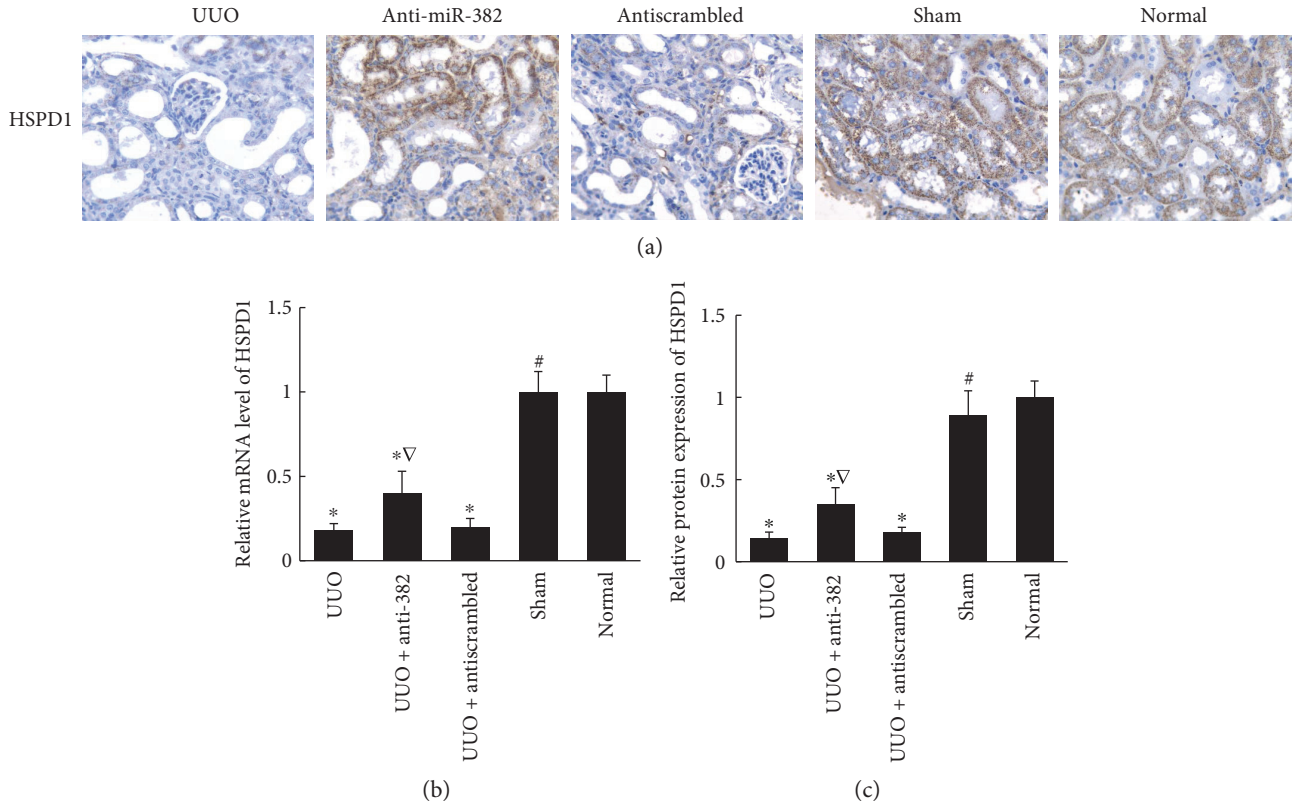

Figure 4: Expression of HSPD1 in obstructed mouse kidneys. (a) Immunohistochemical analysis of HSPD1 abundance in kidney specimens from mice. 10 mg/kg dosage of anti-miR-382 treatment suppressed the downregulation of HSPD1 in UUO mice. (b) Histogram represented the relative mRNA expression of HSPD1 in the mouse kidneys. (c) Quantification of HSPD1 staining. $^{*}P < 0.05$ compared with the normal group; $^{\nabla}P < 0.05$, $^{\#}P < 0.01$ compared with the UUO group. UUO indicates unilateral ureteral obstruction. Normal indicates the normal control group. ($n = 4$).

$\pm$ 0.66 ng/ml, resp., $P < 0.01$; TGF-β1 + HSPD1 plasmid group versus control group, 13.57 $\pm$ 0.24 ng/ml versus 13.08 $\pm$ 0.23 ng/ml, resp., $P > 0.05$) (Figures 8(e) and 8(f)). The above results suggested that overexpression of HSPD1 might protect renal epithelial cells from oxidative stress-induced loss of cell polarity.

3.5. Renal HSPD1 Mediates the Protective Effects of miR-382 Blockade against Renal Tubulointerstitial Fibrosis. In our in vivo animal study, mice that underwent UUO were treated with either anti-miR-382 or antiscrambled control. The ligated kidney was treated locally with HSPD1 siRNA or control siRNA by retrograde injection. By measuring the abundance of miR-382 by real-time PCR, the anti-miR-382 treatment was considered effective (67.86%–70.99% reduction in the level of miR-382, compared with that in the anti-scrambled group) (Figure 9(a)). Compared with that in the control siRNA group, protein expression of HSPD1 was significantly suppressed in the HSPD1 siRNA group, while the protein abundance of Bax, a proapoptosis marker, was significantly upregulated after HSPD1 siRNA treatment (Figures 9(b), 9(c), and 9(d)). Fibrosis quantification from Sirius red-stained tissues indicated that anti-miR-382-treated mice with renal knockdown of HSPD1 were not protected from developing tubulointerstitial fibrosis (Figures 9(f) and 9(g)). Meanwhile, the downregulation of Trx or the upregulation of Bax secondary to UUO was partially reversed after anti-miR-382 treatment but not reversed with anti-miR-382 treatment combined with HSPD1 siRNA treatment (Figures 9(b), 9(c), and 9(e)). Fluorescence immunoblotting test showed that the downregulation of 3-NT secondary to anti-miR-382 treatment was blocked by HSPD1 siRNA (Figures 9(f) and 9(h)).

4. Discussion

Renal tubulointerstitial fibrosis is a common pathological manifestation of a great variety of chronic kidney diseases (CKD), irrespective of the initial trigger or site of injury. Tubulointerstitial fibrosis (TIF) is also the final common pathway that drives advanced CKD to end-stage renal disease. It has been proven that the extent of TIF is predictive for declining renal function in animal models and humans [15, 16]. Therefore, blocking or even reversing the process of TIF might be one way to halt CKD progression.

The histopathological profiles of TIF is often characterized as excessive extracellular matrix deposition produced by myofibroblasts within the renal interstitium with inflammatory cellular infiltration, tubular atrophy, and capillary loss [17, 18]. The mechanism of epithelial-mesenchymal transition (EMT) was well known, in which injured renal tubular cells transform into mesenchymal cells during renal

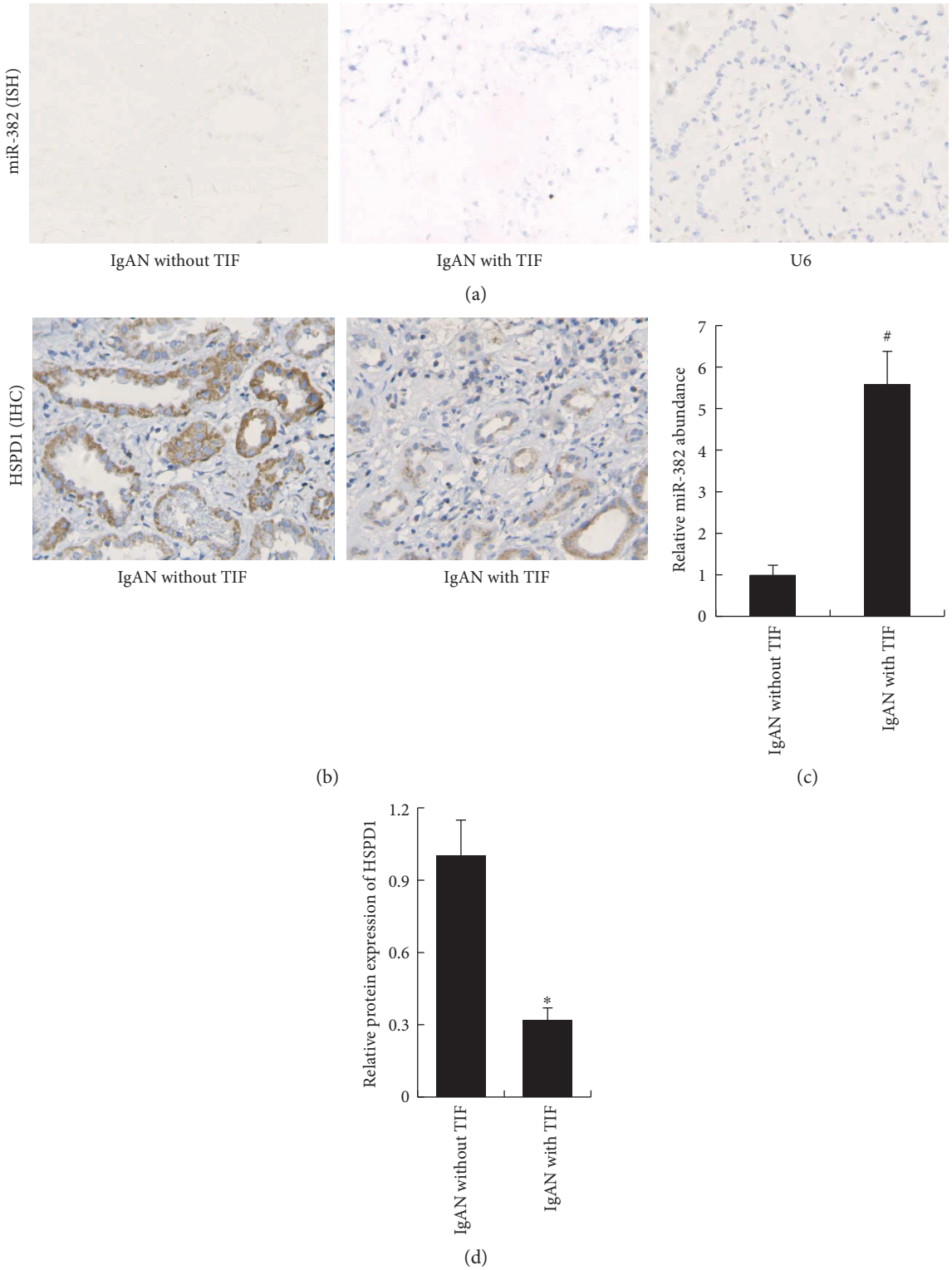

Figure 5: MiR-382 abundance and HSPD1 in patients with IgA nephropathy (IgAN). (a) Representative images of miR-382 expression in renal biopsy specimens from IgA nephropathy (IgAN) patients, obtained by in situ hybridization (ISH). (b) Immunohistochemical (IHC) analysis of HSPD1 abundance in renal biopsy specimens. (c) Histogram represented the TaqMan qPCR analysis of miR-382 abundance. Total RNA from formalin-fixed and paraffin-embedded tissue was extracted by using RecoverALL total nucleic acid isolation kit (Ambion, Austin, Texas, USA). (d) Histogram represented the relative protein expression of HSPD1 of renal biopsy specimens from IgAN patients. The positively stained area of HSPD1 protein was quantified as described in Figure 1. TIF indicates tubulointerstitial fibrosis. $^{*}P < 0.05$, $^{\#}P < 0.01$ compared with IgAN without TIF (IHC, $n = 6$; ISH, $n = 6$).

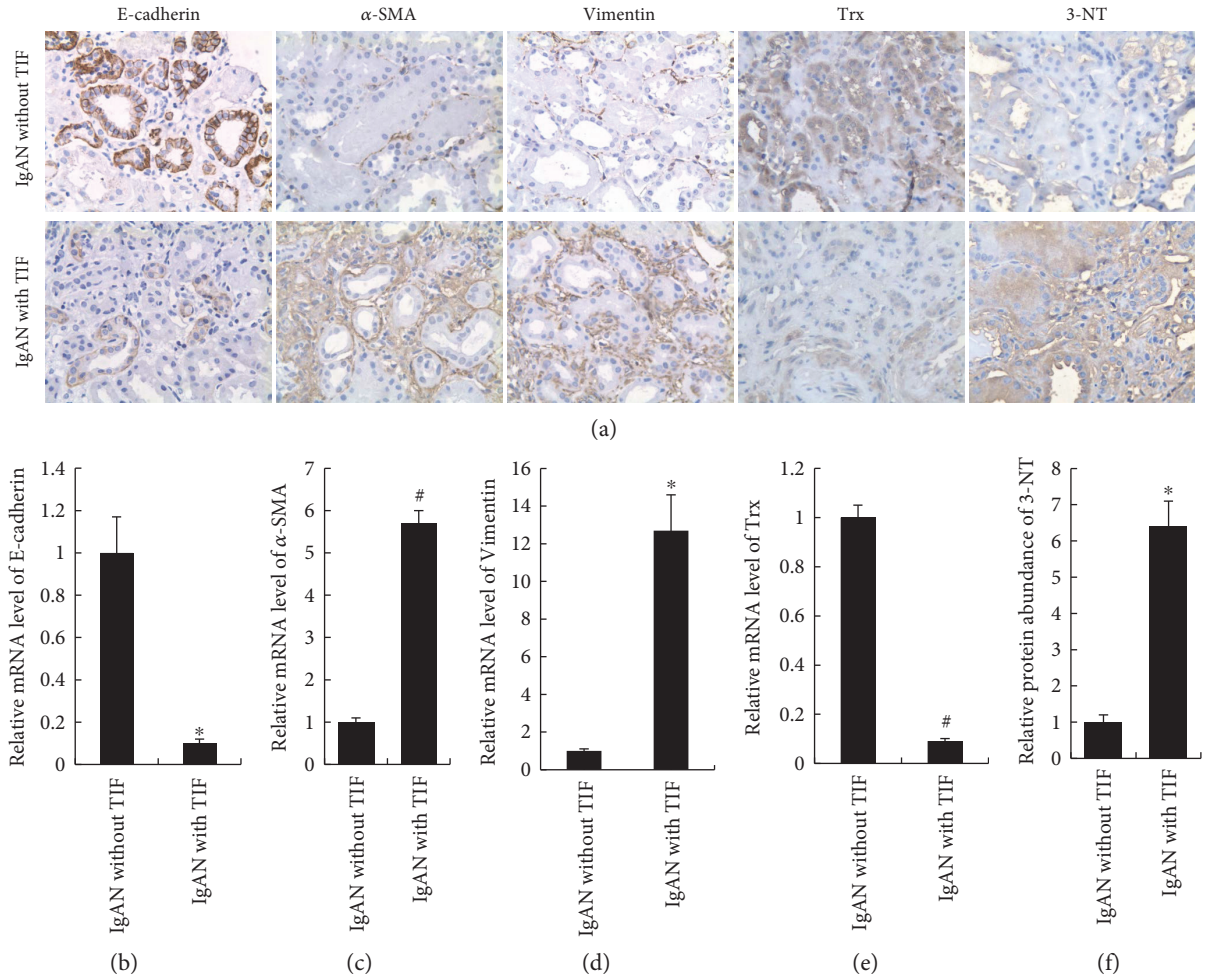

Figure 6: Expression of EMT markers (E-cadherin, α-SMA, and Vimentin) and oxidative stress-related markers (Trx, 3-NT) in patients with IgAN. (a) Representative images of protein expression of E-cadherin, α-SMA, Vimentin, thioredoxin (Trx), and 3-nitrotyrosine (3-NT) in renal biopsy specimens from IgA nephropathy (IgAN) patients. Immunohistochemical analysis was performed between patients with and without tubulointerstitial fibrosis (TIF). Histograms (b–e) represented the relative mRNA expression of E-cadherin, α-SMA, Vimentin, and Trx. (f) Histogram represents the relative protein abundance of 3-NT. The positively stained area of 3-NT protein was quantified as described in Figure 1. $^{*}P < 0.05$, $^{\#}P < 0.01$ compared with IgAN without TIF (IHC, $n = 6$; qPCR, $n = 6$).

fibrogenesis [19–22]. Based on the results from our previous study, EMT participated in the pathogenesis of CKD progression in vivo, and in certain conditions, it was reversible, even with the increasing doubts about the existence of EMT in vivo [23]. In this study, a loss of epithelial marker E-cadherin and an increase in extracellular matrix markers (α-SMA and Vimentin) were observed in the obstructed kidneys of UUO mice and IgAN patients with TIF.

MicroRNAs (miRNAs) are small, endogenously expressed, noncoding RNA molecules (21–25 nucleotides) founded in plants, animals, and some viruses. MiRNAs regulate gene expression at the posttranslation level through translation inhibition or mRNA degradation, presenting a reciprocal relationship between miRNA and its targeted genes in most cases [24–26]. In our previous study, the abundance of miR-382 in HK2 cells was upregulated with the development of EMT induced by TGF-β1. Treatment with anti-miR-382 oligos significantly reversed TGF-β1-induced suppression of E-cadherin expression and augmentation of α-SMA expression [5]. In the mouse UUO model, we found that the progression of TIF was accompanied with an increased abundance of miR-382 in the obstructed kidneys. Intravenous injection of LNA-anti-miR-382 oligonucleotides (10 mg/kg) significantly alleviated the pathological damage in the obstructed kidneys and suppressed the protein expression of Vimentin and α-SMA. Recently, Xu et al. reported miR-382 as an inhibitor of metastasis and EMT in osteosarcoma, which was contradictory to our results from renal tissue [27]. Owing to only a subset of target genes of a miRNA being expressed in a tissue, limited tissue-specific functional roles of the miR-382 can be expected. Therefore, the role of miR-382 could be different in different subtypes of EMT [22].

MiRNAs achieve their biological effects, mostly by repressing translation or decreasing the abundance of their target mRNAs [28, 29]. Kriegel AJ, a member of our research group, had demonstrated that Kalliken5 (KLK5), a (chymo) trypsin-like proteinase that mediates degradation of many extracellular matrix proteins, was a target of miR-382 in the mouse UUO model. Her study revealed that the upregulation

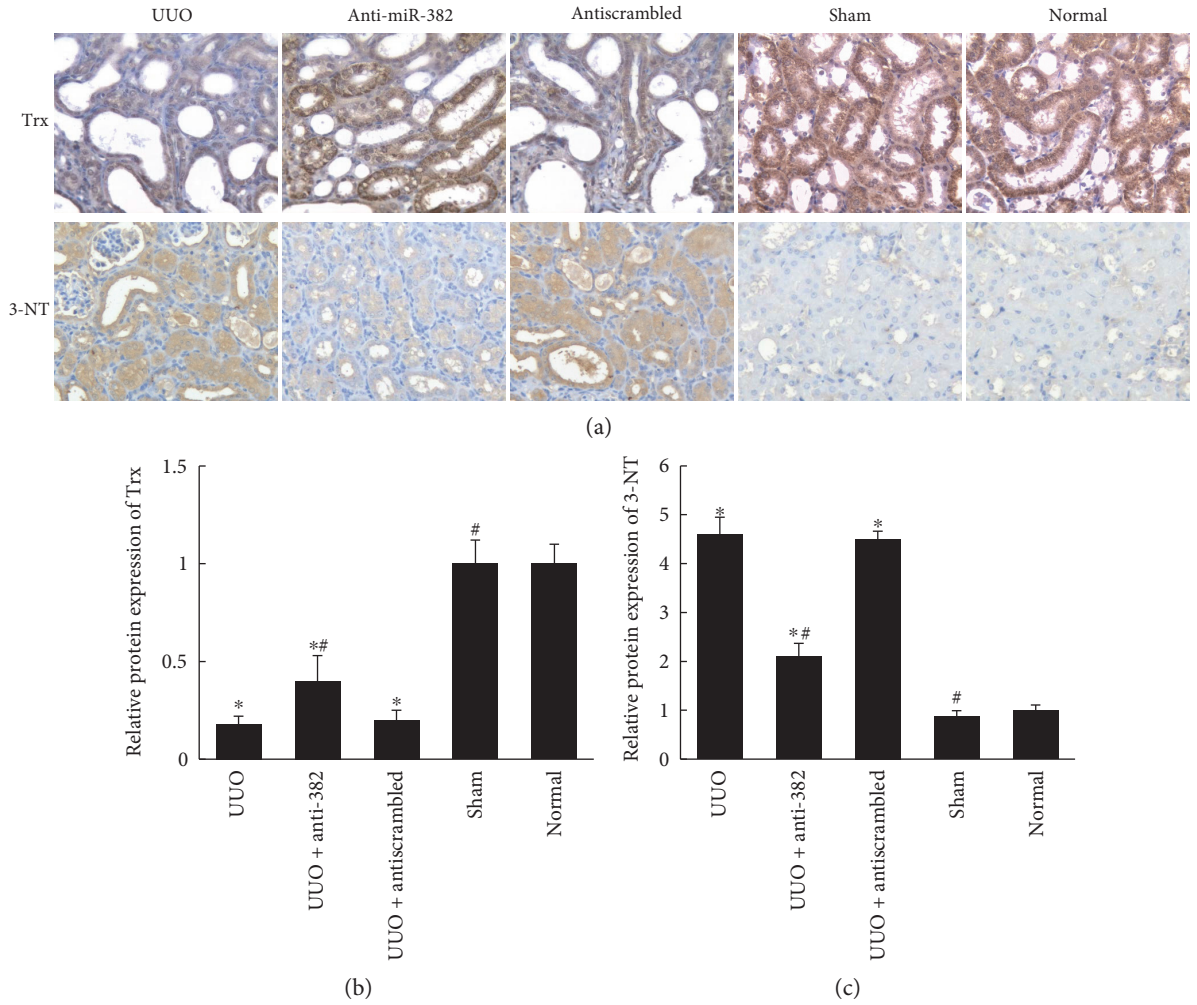

Figure 7: Expression of oxidative stress-related markers (Trx, 3-NT) in obstructed mouse kidneys. Treatment with 10 mg/kg anti-miR-382 reversed the downregulation of thioredoxin (Trx) and upregulation of 3-nitrotyrosine (3-NT) in UUO mice. (a) Representative images of Trx and 3-NT expression in mouse kidneys from all treatment groups. (b, c) Histogram represents the quantification of Trx and 3-NT staining in mouse kidneys. The positively stained area of 3-NT or Trx was quantified as described in Figure 1. $^{*}P < 0.05$ compared with the normal group; $^{\#}P < 0.05$ compared with the UUO group. UUO indicates unilateral ureteral obstruction. Normal indicates normal control ($n = 4$).

of miR-382 contributed to the inner medullary interstitial fibrosis in mice, partially mediated by targeting of KLK5 [30]. Besides ECM genes, a cluster of mitochondrial proteins including HSPD1 was identified as new predicted target genes of miR-382, suggesting that the contribution of miR-382 in the development of TIF could be mediated by pathways of different mechanisms [5].

HSPD1, also called heat shock 60 kDa protein 1, serves as an important molecular chaperone for mitochondrial proteins. HSPD1 was reported to maintain mitochondrial integrity and protect against oxidative stress [8–10]. In vitro experiments revealed that the mRNA expression of HSPD1 was significantly suppressed by pre-miR-382 in HK2 cells, whereas anti-miR-382 treatment significantly reversed the decrease of HSPD1 mRNA. We also found that anti-miR-382 treatment alone could, to some extent, induce HSPD1 expression independently of TGF-β1. It is possible that miR-382 may serve as either the downstream of TGF-β1 or being in parallel to TGF-β1. Besides, the endogenous abundance of miR-382 in HK2 cells should be taken into account. Similarly, HSPD1 expression was upregulated and TIF in the obstructed kidneys was alleviated after LNA-anti-miR-382 (10 mg/kg) treatment. The interaction between miR-382 and HSPD1 was also observed in a clinical study. In situ hybridization, immunohistochemical staining as well as q-PCR measurement revealed the reciprocal relationship between miR-382 and HSPD1 in IgAN patients with TIF. Therefore, HSPD1 serves as one of the target genes of miR-382, which was further verified by site-directed mutagenesis. Since HSPD1 participated in oxidative stress [8, 9], we selected Trx as a marker of antioxidant capacity [31–33] and 3-NT as a marker of oxidative stress [34–36]. Downregulation of HSPD1 was accompanied with a decrease in Trx and an increase in 3-NT, both in UUO mice and in IgAN patients with TIF. Inhibiting the expression of miR-382 with anti-miR-382 led to an increased expression of Trx, as well as a decreased expression of 3-NT in UUO mice. We have also shown that overexpression of HSPD1 is protective against TGFβ1-induced loss of epithelial characteristics and oxidative stress in vitro. In addition, in vivo study found that the renal

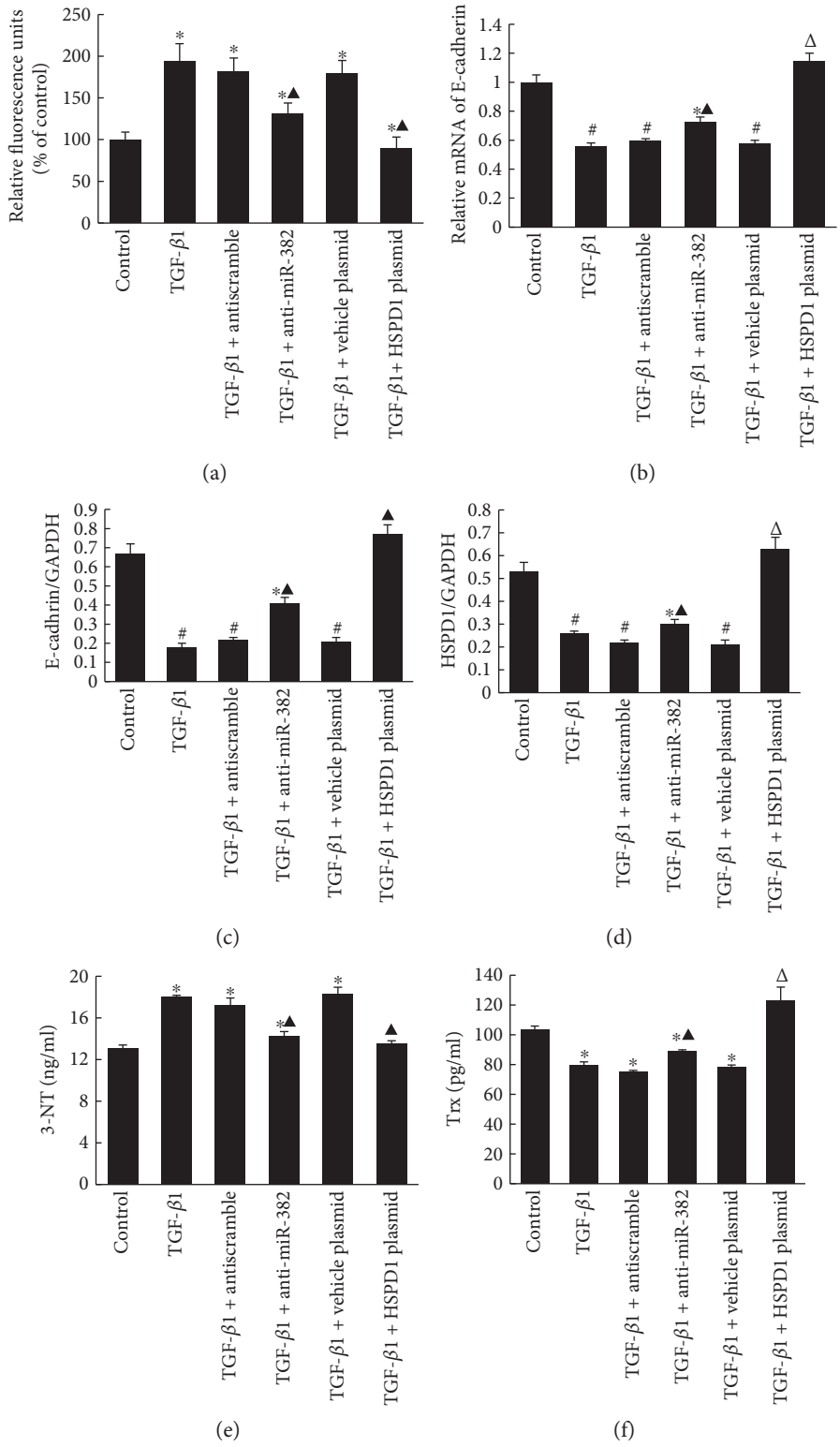

Figure 8: Overexpression of HSPD1 restored renal antioxidant capacity and attenuated TGF-β1-induced loss of cell polarity in vitro. HK2 cells were not transfected or were transfected with Myc-DDK-tagged plasmid (pHSPD1) or an empty vector. Cells without plasmid transfection were transfected with LNA-anti-miR382/anti-scramble oligos. (a) Effects of anti-382 treatment or HSPD1 overexpression on ROS levels in HK2 cells under TGF-β1 exposure. Fluorescence intensity was measured at an excitation wavelength of 485 nm and an emission wavelength of 535 nm. (b) Relative mRNA level of E-cadherin. (c, d) Relative protein abundance of E-cadherin and HSPD1, examined by Western blot analysis. (e) ELISA assay of 3-NT (Abcam) with the cell homogenate. (f) ELISA assay of Trx (BioVendor R&D) with the cell homogenate. 3-NT indicates 3-nitrotyrosine; Trx indicates thioredoxin. $^{*}P < 0.05$, $^{\#}P < 0.01$ compared with the control group; $^{\blacktriangle}P < 0.05$, $^{\Delta}P < 0.01$ compared with the TGF-β1 group ($n = 5$).

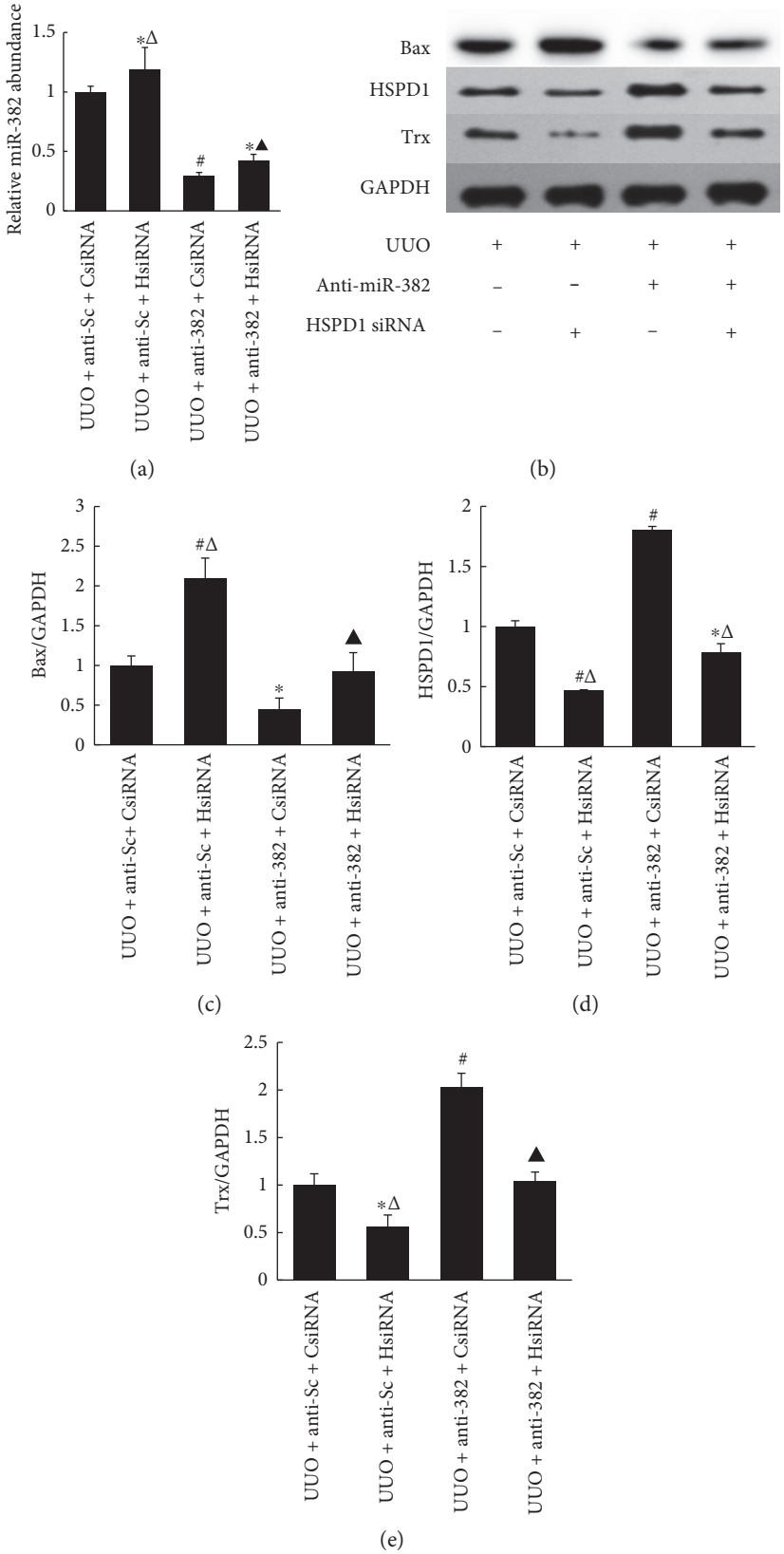

Figure 9: Continued.

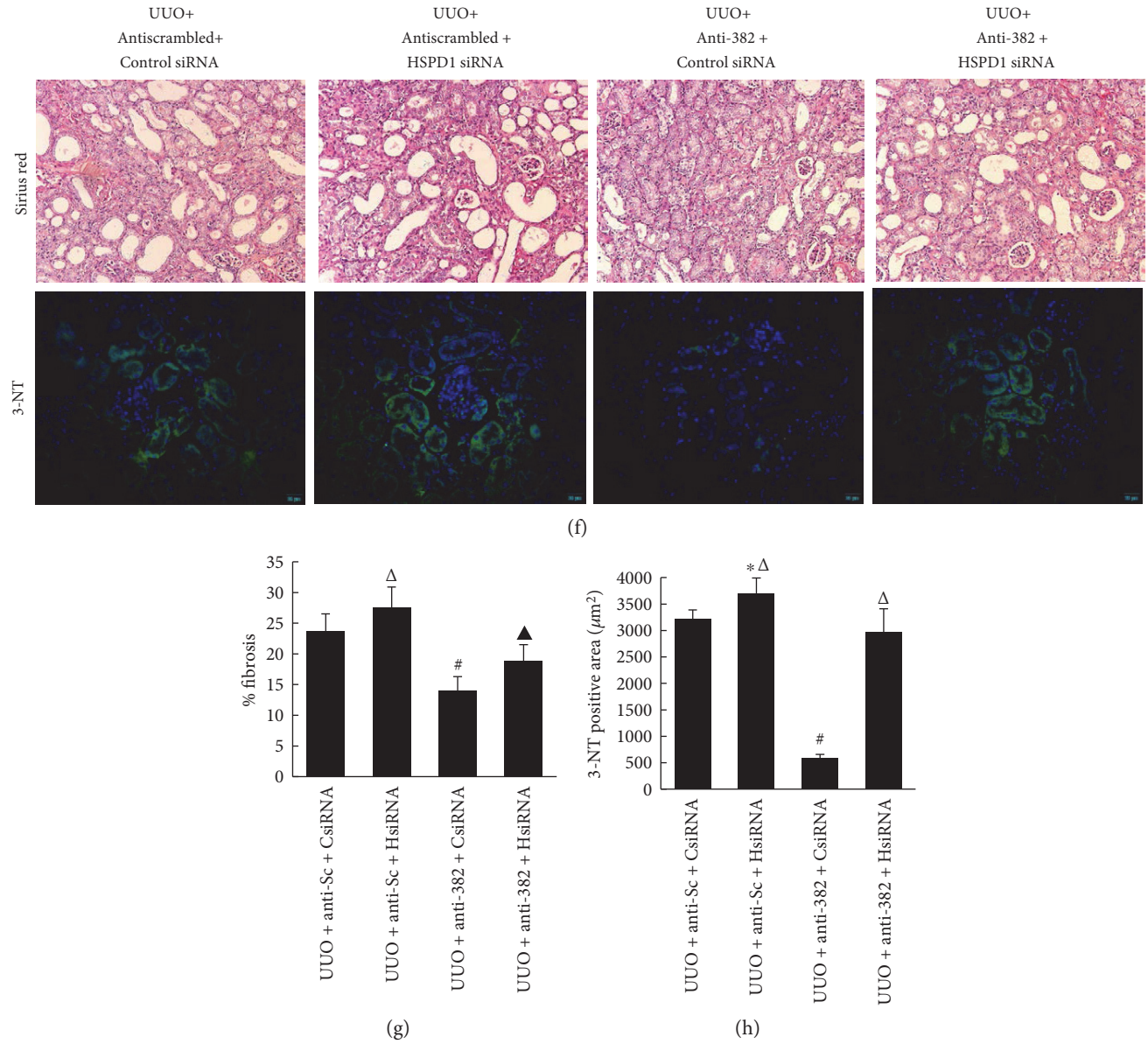

Figure 9: Direct siRNA-mediated suppression of HSPD1 in the UUO kidney promoted oxidative stress despite miR-382 blockade. (a) MiR-382 abundance determined by real-time PCR measurement of the whole kidney RNA from the obstructed mouse kidneys. (b–e) Protein expression of Bax, HSPD1, and Trx was normalized to GAPDH in the obstructed kidneys treated with anti-miR and siRNA from the experiment above. (f) Representative images of kidney tissue with Sirius red staining and 3-NT immunofluorescence from animals undergoing UUO surgery and receiving a combination of HSPD1 or control siRNA (ureteral delivery) and anti-miR-382 or control anti-miR (intravenous delivery). 3-NT (green) and DAPI (blue) immunofluorescence from control and anti-miR382/HSPD1 siRNA-treated mice are displayed (scale = 20 μm). (g) The relative abundance of collagen was analyzed using Sirius red staining. (h) The positive-stained area of 3-NT was quantitatively measured using a computer-aided image system (IMS) (ShentengIT Co., Shanghai, China) on digitalized images that were transformed from analogue images taken by a video camera (Panasonic, MV-CP410, Japan). Each field was 72,800 μm^2, magnification ×200. $^{*}P < 0.05$, $^{\#}P < 0.01$ compared with the antiscrambled + control siRNA group; $^{\blacktriangle}P < 0.05$, $^{\Delta}P < 0.01$ compared with the anti-382 + control siRNA group. Trx indicates thioredoxin; 3-NT indicates 3-nitrotyrosine. UUO + anti-Sc + CsiRNA indicates UUO mice treated with scrambled anti-miR and control siRNA; UUO + anti-Sc + HsiRNA indicates UUO mice treated with scrambled anti-miR and HSPD1 siRNA; UUO + anti-382 + CsiRNA indicates UUO mice treated with anti-miR-382 and control siRNA; UUO + anti-382 + HsiRNA indicates UUO mice treated with anti-miR-382 and HSPD1 siRNA ($n = 4$).

protective effects of miR-382 blockade against fibrosis, apoptosis, and redox imbalance of the obstructed kidneys were abolished by renal knockdown of HSPD1, which further proved our hypothesis that miR-382 might contribute to renal interstitial fibrosis by oxidative stress-induced apoptosis secondary to the inhibition of HSPD1.

These results suggested that downregulation of HSPD1 may lead to a decrease in the protective antioxidative capacity

within renal tissue. As excessive oxidative stress contribute to the development of TIF, therefore, inhibiting the antioxidative capacity of renal tissue may be one of the important mechanisms in which miR-382 promotes renal tubular interstitial fibrosis.

5. Conclusions

In this study, we explored the role of miR-382 in the development of renal fibrosis and its possible mechanism. We proved that miR-382-targeted HSPD1 participated in the setting of renal tubulointerstitial fibrosis. The antioxidative capacity of renal tissue declined when HSPD1 expression was downregulated, which suggested that excessive oxidative stress may be an important mechanism whereby miR-382 participates in renal fibrosis. The current study suggests that upregulation of miR-382, which targets antioxidative stress genes and HSPD1, may partially contribute to the development of renal tubulointerstitial fibrosis. More work is needed to examine, and miR-382 is a potential therapeutic candidate for prevention or treatment of renal tubulointerstitial fibrosis in combination with others.

Conflicts of Interest

No conflicts of interest, financial or otherwise, are declared by the authors.

Authors' Contributions

Yi Fang and Ting Xie contributed equally to this work.

Acknowledgments

This work was supported by the National Natural Science Foundation of China (81200557) and the Science and Technology Commission of Shanghai Municipality (14DZ2260200, the project of Shanghai Key Laboratory of Kidney and Blood Purification).

References

[1] P. J. Stahl and D. Felsen, "Transforming growth factor-β, basement membrane, and epithelial-mesenchymal transdifferentiation: implications for fibrosis in kidney disease," *The American Journal of Pathology*, vol. 159, no. 4, pp. 1187–1192, 2001.

[2] M. Iwano and E. G. Neilson, "Mechanisms of tubulointerstitial fibrosis," *Current Opinion in Nephrology and Hypertension*, vol. 13, no. 3, pp. 279–284, 2004.

[3] M. Iwano, D. Plieth, T. M. Danoff, C. Xue, H. Okada, and E. G. Neilson, "Evidence that fibroblasts derive from epithelium during tissue fibrosis," *The Journal of Clinical Investigation*, vol. 110, no. 3, pp. 341–350, 2002.

[4] T. D. Hewitson, "Renal tubulointerstitial fibrosis: common but never simple," *American Journal of Physiology. Renal Physiology*, vol. 296, no. 6, pp. F1239–F1244, 2009.

[5] A. J. Kriegel, Y. Fang, Y. Liu et al., "MicroRNA-target pairs in human renal epithelial cells treated with transforming growth factor β1: a novel role of miR-382," *Nucleic Acids Research*, vol. 38, no. 22, pp. 8338–8347, 2010.

[6] D. S. Reading, R. L. Hallberg, and A. M. Myers, "Characterization of the yeast HSP60 gene coding for a mitochondrial assembly factor," *Nature*, vol. 337, no. 6208, pp. 655–659, 1989.

[7] H. Tang, E. Tian, C. Liu, Q. Wang, and H. Deng, "Oxidative stress induces monocyte necrosis with enrichment of cell-bound albumin and overexpression of endoplasmic reticulum and mitochondrial chaperones," *PloS One*, vol. 8, no. 3, article e59610, 2013.

[8] E. Cabiscol, G. Belli, J. Tamarit, P. Echave, E. Herrero, and J. Ros, "Mitochondrial Hsp60, resistance to oxidative stress, and the labile iron pool are closely connected in *Saccharomyces cerevisiae*," *The Journal of Biological Chemistry*, vol. 277, no. 46, pp. 44531–44538, 2002.

[9] M. Y. Cheng, F. U. Hartl, J. Martin et al., "Mitochondrial heat-shock protein hsp60 is essential for assembly of proteins imported into yeast mitochondria," *Nature*, vol. 337, no. 6208, pp. 620–625, 1989.

[10] K. P. Poulianiti, A. Kaltsatou, G. I. Mitrou et al., "Redox imbalance in chronic kidney disease: a systematic review," *Oxidative Medicine and Cellular Longevity*, vol. 2016, Article ID 8598253, 19 pages, 2006.

[11] H. Terawaki, K. Yoshimura, T. Hasegawa et al., "Oxidative stress is enhanced in correlation with renal dysfunction: examination with the redox state of albumin," *Kidney International*, vol. 66, no. 5, pp. 1988–1993, 2004.

[12] C. Maric, K. Sandberg, and C. Hinojosa-Laborde, "Glomerulosclerosis and tubulointerstitial fibrosis are attenuated with 17β-estradiol in the aging Dahl salt sensitive rat," *Journal of the American Society of Nephrology*, vol. 15, no. 6, pp. 1546–1556, 2004.

[13] Y. Fang, X. Yu, Y. Liu et al., "MiR-29c is down-regulated in renal interstitial fibrosis in humans and rats and restored by HIF- activation," *American Journal of Physiology. Renal Physiology*, vol. 304, no. 10, pp. F1274–F1282, 2013.

[14] L. Tongqiang, L. Shaopeng, Y. Xiaofang et al., "Salvianolic acid B prevents iodinated contrast media-induced acute renal injury in rats via the PI3K/AKT/Nrf2 pathway," *Oxidative Medicine and Cellular Longevity*, vol. 2016, Article ID 7079487, 11 pages, 2016.

[15] A. A. Eddy, "Molecular insights into renal interstitial fibrosis," *Journal of the American Society of Nephrology*, vol. 7, no. 12, pp. 2495–2508, 1996.

[16] E. Healy and H. R. Brady, "Role of tubule epithelial cells in the pathogenesis of tubulointerstitial fibrosis induced by glomerular disease," *Current Opinion in Nephrology and Hypertension*, vol. 7, no. 5, pp. 525–530, 1998.

[17] A. Bohle, H. Christ, K. E. Grund, and S. Mackensen, "The role of the interstitium of the renal cortex in renal disease," *Contributions to Nephrology*, vol. 16, pp. 109–114, 1979.

[18] G. Greenburg and E. D. Hay, "Epithelia suspended in collagen gels can lose polarity and express characteristics of migrating mesenchymal cells," *The Journal of Cell Biology*, vol. 95, no. 1, pp. 333–339, 1982.

[19] W. Kriz, B. Kaissling, and M. Le Hir, "Epithelial-mesenchymal transition (EMT) in kidney fibrosis: fact or fantasy?" *The Journal of Clinical Investigation*, vol. 121, no. 2, pp. 468–474, 2011.

[20] M. Zeisberg and J. S. Duffield, "Resolved: EMT produces fibroblasts in the kidney," *Journal of the American Society of Nephrology*, vol. 21, no. 8, pp. 1247–1253, 2010.

[21] R. Kalluri, "EMT: when epithelial cells decide to become mesenchymal-like cells," *The Journal of Clinical Investigation*, vol. 119, no. 6, pp. 1417–1419, 2009.

[22] M. Zeisberg and E. G. Neilson, "Mechanisms of tubulointerstitial fibrosis," *Journal of the American Society of Nephrology*, vol. 21, no. 11, pp. 1819–1834, 2010.

[23] X. Yu, Y. Fang, X. Ding et al., "Transient hypoxia-inducible factor activation in rat renal ablation and reduced fibrosis with L-mimosine," *Nephrology (Carlton, Vic.)*, vol. 17, no. 1, pp. 58–67, 2012.

[24] M. Liang, Y. Liu, D. Mladinov et al., "MicroRNA: a new frontier in kidney and blood pressure research," *American Journal of Physiology. Renal Physiology*, vol. 297, no. 3, pp. F553–F558, 2009.

[25] J. Winter, S. Jung, S. Keller, R. I. Gregory, and S. Diederichs, "Many roads to maturity: microRNA biogenesis pathways and their regulation," *Nature Cell Biology*, vol. 11, no. 3, pp. 228–234, 2009.

[26] J. Krol, I. Loedige, and W. Filipowicz, "The widespread regulation of microRNA biogenesis, function and decay," *Nature Reviews. Genetics*, vol. 11, no. 9, pp. 597–610, 2010.

[27] M. Xu, H. Jin, C. X. Xu et al., "miR-382 inhibits osteosarcoma metastasis and relapse by targeting Y box-binding protein 1," *Molecular Therapy*, vol. 23, no. 1, pp. 89–98, 2015.

[28] G. Meister, "miRNAs get an early start on translational silencing," *Cell*, vol. 131, no. 1, pp. 25–28, 2007.

[29] L. P. Lim, N. C. Lau, A. Grimson et al., "Microarray analysis shows that some microRNAs downregulate large numbers of target mRNAs," *Nature*, vol. 433, no. 7027, pp. 769–773, 2005.

[30] A. J. Kriegel, Y. Liu, B. Cohen, Y. Liu, and M. Liang, "MiR-382 targeting of kallikrein 5 contributes to renal inner medullary interstitial fibrosis," *Physiological Genomics*, vol. 44, no. 4, pp. 259–267, 2012.

[31] R. Sengupta and A. Holmgren, "Thioredoxin and glutaredoxin-mediated redox regulation of ribonucleotide reductase," *World Journal of Biological Chemistry*, vol. 5, no. 1, pp. 68–74, 2014.

[32] E. M. Hanschmann, J. R. Godoy, C. Berndt, C. Hudemann, and C. H. Lillig, "Thioredoxins, glutaredoxins, and peroxiredoxins-molecular mechanisms and health significance: from cofactors to antioxidants to redox signaling," *Antioxidants & Redox Signaling*, vol. 19, no. 13, pp. 1539–1605, 2013.

[33] J. Lu and A. Holmgren, "The thioredoxin antioxidant system," *Free Radical Biology & Medicine*, vol. 66, pp. 75–87, 2014.

[34] F. Yamakura, H. Taka, T. Fujimura, and K. Murayama, "Inactivation of human manganese-superoxide dismutase by peroxynitrite is caused by exclusive nitration of tyrosine 34 to 3-nitrotyrosine," *The Journal of Biological Chemistry*, vol. 273, no. 23, pp. 14085–14089, 1998.

[35] M. F. Beal, R. J. Ferrante, S. E. Browne, R. T. Matthews, N. W. Kowall, and R. H. Brown Jr., "Increased 3-nitrotyrosine in both sporadic and familial amyotrophic lateral sclerosis," *Annals of Neurology*, vol. 42, no. 4, pp. 644–654, 1997.

[36] A. Ceriello, F. Mercuri, L. Quagliaro et al., "Detection of nitrotyrosine in the diabetic plasma: evidence of oxidative stress," *Diabetologia*, vol. 44, no. 7, pp. 834–838, 2001.

Hindawi
Oxidative Medicine and Cellular Longevity
Volume 2017, Article ID 7038789, 14 pages
https://doi.org/10.1155/2017/7038789

Clinical Study

Actinidia chinensis Planch. Improves the Indices of Antioxidant and Anti-Inflammation Status of Type 2 Diabetes Mellitus by Activating Keap1 and Nrf2 via the Upregulation of MicroRNA-424

Longfeng Sun,[1] Xiaofei Li,[2] Gang Li,[3] Bing Dai,[1] and Wei Tan[1]

[1]*Department of Geriatrics, The First Affiliated Hospital of China Medical University, Shenyang 110001, China*
[2]*Department of Emergency Medicine, The First Affiliated Hospital of China Medical University, Shenyang 110001, China*
[3]*Department of Urology, Liaoning Cancer Hospital and Institute, Shenyang 110042, China*

Correspondence should be addressed to Longfeng Sun; sunlf1012@yeah.net

Received 24 December 2016; Revised 24 February 2017; Accepted 19 March 2017; Published 31 May 2017

Academic Editor: Jaideep Banerjee

The fruit juice of *Actinidia chinensis* Planch. has antioxidant and anti-inflammation properties on patients with type 2 diabetes mellitus (T2DM), but the molecular mechanism was unclear. The patients took the juice and the serum level of antioxidant miR-424, Kelch-like ECH-associated protein 1 (Keap1), erythroid-derived 2-like 2 (Nrf2), and biochemical indices were measured. The juice increased the levels of serum microRNA-424, Keap1, and Nrf2 and reduced the levels of interleukin-1 (IL-1) beta and IL-6 in T2DM patients. The levels of SOD and GSH were higher while the levels of ALT and AST were lower in the patients consuming the juice when compared to the patients without taking the juice. The Spearman rank correlation analysis showed that the serum levels of miR-424 were positively related to Keap1 and Nrf2 levels while Keap1 and Nrf2 levels were positively related to the levels of SOD and GSH and negatively related to IL-1 beta and IL-6. Thus, FJACP improves the indices of antioxidant and anti-inflammation status by activating Keap1 and Nrf2 via the upregulation of miR-424 in the patients with T2DM. This trial is registered with ChiCTR-ONC-17011087 on 04/07/2017.

1. Introduction

Type 2 diabetes mellitus (T2DM) is increasingly prevalent in the elderly and has become a major public health issue. The nutrients of different foods will affect physiological activities and their imbalance may contribute to the development of T2DM. Thus, different diets will affect the risk of T2DM. The food is rich with fruits, vegetables, grains, and fish and low-level meat and fat may be beneficial to reduce the progression of T2DM [1]. Most diabetic patients cannot meet the demanded food and nutrients for a healthy person. For instance, some fruits are very important to health, but they cannot be used by most T2DM patients because most fruits have high-level sugar. The uptake of some vegetables and fruits has been found to be related to a low incidence of diabetes. However, fruit juice consumption can be harmful to increase the risk of diabetes in women [2].

Kiwi fruit (*Actinidia chinensis* Planch.) as a food with significant effects on human health, including antioxidant and anti-inflammatory activity, can inhibit the development and deterioration of the disorders caused by oxidative stress [3]. Lacking vitamin C is an important risk for the development of diabetes [4]. The vitamin C in *Actinidia chinensis* Planch. can reach up to 380 mg/100 g [5]. The daily uptake of vitamin C at a high level has been found to increase antisenescence and antiatherosclerotic activity by improving biochemical indices via antioxidant and antiglycation activities [6]. The risk of type 2 diabetes mellitus (T2DM) is often associated with muscle atrophy while inflammatory status will aggravate the symptoms. Clinical trial shows that vitamin C

consumption has preventative and therapeutic functions for inflammatory symptoms in patients [7]. FJACP (fruit juice of *Actinidia chinensis* Planch.) has been found to improve physiological functions in the patients with neuropathy disorders [8]. More importantly, the main characters of FJACP are with low-level sugar content [9]. Thus, it may be useful for preventing the progression of T2DM. However, the related molecular mechanisms for the functions of FJACP on T2DM patients remain widely unknown.

Obesity patients with chronic low-grade inflammation have more chances to get heart disorders and T2DM. The etiology of this obesity-related proinflammatory is more focused on adipose tissue dysfunctions and/or insulin resistance in skeletal muscles [10]. Furthermore, inflammation has also been found to be associated with the development of insulin resistance in T2DM patients [11]. On the other hand, oxidative stress is also an important factor in the pathogenesis of T2DM complications. Alloxan-induced diabetes can cause an imbalance in an antioxidative system in the skeletal muscles of an animal model. Controlling the damage from oxidation stresses is also a potential therapeutic approach to prevent T2DM development [12]. These results suggest that inflammatory and oxidant stresses are the two main reasons for causing the impairment in T2DM patients. MicroRNAs (miRNAs), small, noncoding RNA, have been found to regulate protein expression and multiple cellular physiological activities, including antioxidant activities [13, 14]. Studies have shown that miR-424 plays a critical role in the antioxidant activity by suppressing oxidant stress. MiR-424 therapy prevents infarct volume and neuronal apoptosis, reduces the levels of reactive oxygen species (ROS) and malondialdehyde (MAD), and enhances the activities of the antioxidant enzyme SOD. All the results suggest that miR-424 has protective effects against oxidative stress [15]. On the other hand, the nuclear factor, erythroid-derived 2-like 2 (Nrf2), is a redox-sensitive transcription factor and related with inflammatory disease [16, 17]. Nrf2 can combine with Kelch-like ECH-associated protein 1 (Keap1) to form an important complex to increase the levels of antioxidant molecules [18]. However, the relationship between the serum level of miR-424 and antioxidants Keap1 and Nrf2 remains unclear. Therefore, we want to explore the effects of FJACP on Keap1 and Nrf2 in T2DM patients by investigating the serum levels of miR-424.

2. Materials and Methods

2.1. Participants. All protocols were approved by the Ethical Committee of The First Affiliated Hospital of China Medical University (Shenyang, China), and the study was carried out according to the principles described in the World Medical Association Declaration of Helsinki [19]. A total of 122 patients, at the age of 50–70, were recruited from our hospital and diagnosed with T2DM.

2.2. Including Criteria. The following including criteria were used: (1) the patients seldom consumed fruits daily; (2) the patients had normal work and spouse; (3) they wanted to join our research, such as receiving FJACP treatment; (4) the patients were diagnosed with T2DM; (5) the patients had a body mass index (BMI) more than 25 and less than 39 kg/m^2; and (6) their weight were stable within three months before the present experiment.

2.3. Excluding Criteria. The following excluding criteria were performed: (1) the patients had senile dementia, such as Parkinson's disease (PD), Alzheimer's disease (AD), and brain injury; (2) the patients suffered from cardiac disorder, hypertension, dizziness, and related disorders; (3) the patients had the obstacle for limb movement; and (4) the patients had obvious abnormal clinical findings.

2.4. Study Design. After the selection by using the including criteria and excluding criteria, 122 patients were evenly and randomly assigned into a FJACP group (FJACPG, received 10 ml FJACP daily) and a control group (CG, received 10 ml liquid placebo daily) (Figure 1). The whole period was nine months. Exercise (each person walks about 1.5 to 2 miles per day) was considered for both groups at the same level. Fifteen patients (6 patients from FJACPG and 9 patients from CG) dropped out at the end of the experiment. Among the patients, six patients dropped out of FJACPG and nine patients dropped out of CG. Thus, 55 and 52 patients from FJACPG and CG finished the whole experiment.

2.5. Biochemical Analysis. All the patients had a random capillary glucose level more than 6.1 mM and regarded as higher risk of diabetes [20] and needed further examination. The concentrations of glucose and HbAlc were tested after a 2-hour 75-gram oral glucose intake. Glucose concentrations were measured by using YSI 2700 Select Biochemical Analyzer (YSI, Yellow Springs, OH, USA). HbA1c levels were measured by BIO-RAD D-10 HPLC (Hercules, CA, USA). High- and low-density lipoprotein-cholesterol was measured by using HDL and LDL/VLDL Cholesterol Assay Kit (Cat. number ab65390, Abcam Shanghai office launch, Shanghai, China). Triglyceride levels were measured by using a Triglyceride Quantification Assay Kit (ab65336). Basal blood glucose (BG) and fasting blood glucose (FBG) levels were measured by ABL800 FLEX blood gas analyzer (Midland, ON, Canada). Serum basal insulin (BINS) and fasting insulin (FINS) were tested by radioimmunoassay (Linco, Seaford, DE, USA). Insulin resistance ($\mathrm{HOMA-IR} = \mathrm{FBG} \times \mathrm{FINS}/22.5$) and insulin secretory function ($\mathrm{HOMA-IS} = 20 \times \mathrm{FINS}/(\mathrm{FBG} - 3.5)$) were calculated.

2.6. Analysis of Enzyme Activities. Diabetes is associated with increased oxidative stress [21, 22]. SOD [23, 24], AST [25, 26], ALT [27, 28], and GSH are associated with oxidative stress [29–34]. Here, the levels of SOD, AST, ALT, and GSH were measured. AST and ALT were measured by an automated clinical chemistry analyzer (Indianapolis, IN, USA). The activity of SOD was measured by Superoxide Dismutase Activity Assay Kit (Cat. number ab65354 from Abcam). GSH was measured by Glutathione Detection Assay Kit (Cat. number ab65322 from Abcam).

2.7. Measurement of Lipid Pattern Indexes. The serum lipid pattern, including total triglycerides (TG), total cholesterol

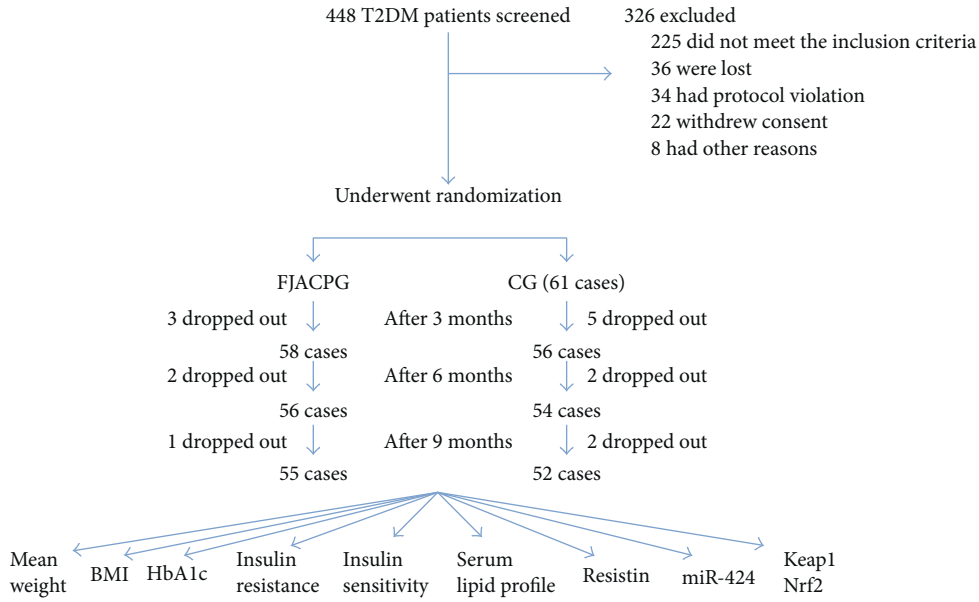

Figure 1: The flowchart of the present study. FJACPG: FJACP group; CG: placebo group. The whole period of the follow-up was nine months.

(TC), high-density lipoprotein-cholesterol (HDL-C), and low-density lipoprotein-cholesterol (LDL-C), was measured by FACA-401 Fully Automatic Biochemistry Analyzer (Labomed Inc., Los Angeles, CA, USA). Malondialdehyde (MDA) level was measured by using a Lipid Peroxidation (MDA) Assay Kit (Sigma, St. Louis, MO, USA). Lipid indexes were measured before and after 3 months of the present experiment.

2.8. Measurement of Inflammatory Cytokines. The pathology of diabetes is closely associated with interleukin-1 (IL-1) beta and IL-6. 5 ml blood samples were obtained from all participants before the experiment, and after 3-, 6-, and 9-month exercises. Thus, the levels of these cytokines were measured by using human ELISA kits for IL-1 beta (Cat. number ab100562) and IL-6 (Cat. number ab46042) and Nrf2 Transcription Factor Assay Kit (ab207223) from Abcam (Shanghai) Ltd. (Shanghai, China).

Serum inflammatory cytokines were measured before and after 3, 6, and 9 months of the present experiment.

2.9. Quantitative Real-Time RT-PCR (qRT-PCR). RNA was isolated from blood samples by a RNA purification kit (Thermo Fisher Scientific, Waltham, MA, USA). cDNA was synthesized by cDNA Synthesis Kits from Thermo Fisher Scientific. SYBR Green Real-Time PCR Master Mixes (Thermo Fisher Scientific) was used for qRT-PCR. The following primers were synthesized: miR-424, F: 5′-cga ggggatacagcagcaat-3′, R: 5′- ccccaccttctaccttcc (98 bp); Keap1, F: 5′-gaggtgacgccctcccagca-3′, R: 5′-catggccttgaagacagggc-3′ (210 bp); Nrf2, F: 5′- agtggatctgccaactactc-3′, R: 5′-agt gactgaaacgtagccga-A3′ (140 bp); and GAPDH, F: 5′-GG AAAGCFJACPGFJACPGGCGFJACPGAT-3′, R: 5′-AAG GFJACPGGAAGAAFJACPGGGAGTT-3′. The values of cycle time for the interest genes were normalized with GAPDH.

2.10. Western Blot Analysis. Total proteins were extracted by using a total protein isolation kit (ITSI-Biosciences, Johnstown, PA, USA). Total proteins were separated by SDS-PAGE and transferred to a polyvinylidene difluoride (PVDF) (RTP Company, Winona, MN, USA). The PVDF was incubated with rabbit polyclonal Keap1 antibody (ab139729, Abcam), rabbit polyclonal anti-Nrf2 antibody (ab137550, Abcam), and rabbit polyclonal GAPDH antibody (ab37168, Abcam) overnight at 4°C. Subsequently, the sample was incubated with peroxidase and peroxidase-conjugated goat anti-rabbit IgG (ab97051, Abcam). The immunoreactive bands were visualized with DAB (Sigma-Aldrich Chemicals, St. Louis, MO, USA) and densitometry was quantified by ImageJ software (National Institutes of Health, Bethesda, MD, USA).

2.11. Statistical Analysis. SPSS20.0 was used to process the data. Adopt t to detect when comparing the measurement data. Spearman's rank correlation was used for the comparison of two variables. Results were presented as the mean ± SD. In the case of $P < 0.05$, there were significantly statistical differences.

3. Results

3.1. Baseline Characters. Table 1 showed the clinical characters were similar between the two groups. All the patients were at the age of 56.1 ± 14.4 in FJACPG and 57.5 ± 12.3 in CG. The ratio of males and females was 37/24 and 39/22 in FJACPG and CG, respectively. There was no significantly statistical difference for baseline demographic and metabolic characteristics of the patients between the two groups ($P > 0.05$).

3.2. The Changes for Biochemical Indexes between the Two Groups. Table 2 showed FJACPG and CG could not improve insulin resistance and insulin secretory function.

Table 1: Baseline demographic and metabolic characteristics of T2DM subjects.

Characteristics of patients	FJACPG ($n = 61$)	CG ($n = 61$)	t/χ^2	P value
Age (years)	56.1 ± 14.4	57.5 ± 12.3	0.24	0.65[a]
Males/females	37/24	39/22	0.14	0.71[b]
Smoker/nonsmoker	18/43	20/41	0.15	0.70[b]
Drinker/nondrinker	24/37	23/38	0.04	0.85[b]
Race, n (%)				
Han Zhu	50	48	0.26	0.61[b]
Manchu	8	10	0.26	0.61[b]
Mongolians	2	2	0.26	0.61[b]
Tibetans	1	1	0.51	0.48[b]
Weight (kg)	81.6 ± 17.5	82.8 ± 17.1	0.24	0.51[a]
BMI (kg/m^2)	29.3 ± 3.6	30.1 ± 2.9	0.64	0.65[a]
HbA1c (%)	8.9 ± 1.6	8.7 ± 1.8	0.71	0.48[a]
FBG (mmol/l)	8.4 ± 1.2	8.7 ± 1.5	0.85	0.32[a]
2hPG (mmol/l)	14.9 ± 2.6	14.1 ± 3.7	0.64	0.56[a]
FJACPG (mmol/l)	2.9 ± 1.2	2.9 ± 1.4	0.13	0.87[a]
TC (mmol/l)	5.8 ± 1.4	5.9 ± 1.6	0.27	0.40[a]
HDL (mmol/l)	1.3 ± 0.3	1.5 ± 0.5	0.24	0.56[a]
LDL (mmol/l)	3.8 ± 1.0	4.0 ± 1.2	0.28	0.71[a]
Resistin (ng/ml)	15.3 ± 4.6	15.5 ± 3.7	1.29	0.14[a]
HOMA-IR	6.4 ± 3.4	6.6 ± 3.5	1.98	0.27[a]
HOMA-IS	66.2 ± 36.7	68.4 ± 27.4	1.58	0.20[a]

Note: [a]t-test and [b]chi-square test. There was no significantly statistical difference at $P > 0.05$.

Table 2: Parameters changes in both groups.

Parameters	FJACPG ($n = 55$)			CG ($n = 52$)			P values after 9 months
	Before	After 9 months	P values	Before	After 9 months	P values	(FJACPG via CG)
Weight (kg)	81.6 ± 17.5	80.5 ± 15.4	0.25	82.8 ± 17.1	80.6 ± 15.3	0.42	0.54
BMI (kg/m^2)	29.3 ± 3.6	27.1 ± 3.9	0.16	30.1 ± 2.9	28.1 ± 2.6	0.34	0.46
FBG (mmol/l)	8.4 ± 1.2	8.0 ± 1.3	0.21	8.7 ± 1.5	8.3 ± 1.2	0.28	0.39
2hPG (mmol/l)	14.9 ± 2.6	14.0 ± 3.2	0.18	14.1 ± 3.7	13.9 ± 3.4	0.29	0.32
HbAlc (%)	8.9 ± 1.6	8.4 ± 1.9	0.08	8.7 ± 1.8	8.5 ± 1.6	0.43	0.38
FJACPG (mmol/l)	2.9 ± 1.2	2.4 ± 1.4	0.04	2.9 ± 1.4	2.7 ± 1.8	0.31	0.07
TC (mmol/l)	5.8 ± 1.4	5.0 ± 1.1	0.02	5.9 ± 1.6	5.5 ± 2.2	0.04	0.02
HDL (mmol/l)	1.3 ± 0.3	1.6 ± 0.5	0.01	1.5 ± 0.5	1.7 ± 0.2	0. 24	0.17
LDL (mmol/l)	3.8 ± 1.0	3.3 ± 1.2	0.03	4.0 ± 1.2	3.2 ± 1.6	0.01	0.14
Resistin (ng/ml)	15.3 ± 4.6	14.1 ± 3.7	0.27	15.5 ± 3.7	14.5 ± 4.1	0.18	0.35
HOMA-IR	6.4 ± 3.4	6.2 ± 3.9	0.35	6.6 ± 3.5	6.4 ± 2.9	0.14	0.44
HOMA-IS	66.2 ± 36.7	69.4 ± 21.3	0.11	68.4 ± 27.4	70.34 ± 14.2	0.29	0.54

Note: there is no significantly statistical difference at $P > 0.05$.

FJACP increased the level of HDL and reduced the levels of TG, TC, and LDL-C ($P < 0.05$). There were significant statistical differences in these parameters between the two groups ($P < 0.05$).

3.3. Biochemical Parameters of Enzyme Activities. The levels of SOD, AST, ALT, and GSH were measured. As showed in Table 3, FJACP and control groups increased SOD and GSH levels after 3 months when compared with the levels before this study ($P < 0.05$). There was no significant statistical difference for these parameters between the two groups after 3-month therapy ($P > 0.05$). The levels of SOD and GSH were higher in FJACPG than in CG after 6-month therapy ($P < 0.05$). Similarly, the levels of SOD and GSH

Table 3: Biochemical parameters of enzyme activities.

		SOD (U/ml)	GSH (ng/ml)	ALT (U/ml)	AST (U/ml)
Before	CG	25.34 ± 3.17	26.89 ± 4.19	46.88 ± 12.24	112.34 ± 25.26
	FJACPG	22.78 ± 3.02	25.65 ± 4.04	48.31 ± 11.38	114.18 ± 22.39
	P value	0.23	0.56	0.14	0.40
3-month	CG	26.38 ± 2.90	27.45 ± 4.27	45.84 ± 15.23	106.35 ± 28.43
	FJACPG	25.31 ± 3.24	29.36 ± 4.78	43.22 ± 16.51	101.48 ± 27.55
	P value	0.64	0.12	0.08	0.17
6-month	CG	25.44 ± 2.37	26.99 ± 4.91	43.24 ± 16.98	102.48 ± 29.36
	FJACPG	30.32 ± 3.24	35.38 ± 4.56	38.46 ± 17.25	96.23 ± 26.22
	P value	0.02*	0.04*	0.04*	0.11
9-month	CG	29.49 ± 2.93	32.11 ± 5.27	40.35 ± 18.29	98.40 ± 27.44
	FJACPG	46.39 ± 3.89	39.71 ± 4.56	30.28 ± 19.16	91.95 ± 28.32
	P value	0.01*	0.02*	0.01*	0.07

Note: FJACPG: the group treated with the fruit juice of *Actinidia chinensis* Planch.; CG: control group. *$p < 0.05$ versus CG. Note: *t*-test and chi-square test. There is no significantly statistical difference at $P > 0.05$.

Table 4: Comparison of lipid pattern in T2DM patients before and after therapy.

		TG (mmol/l)	TC (mmol/l)	HDL-C (mmol/l)	LDL-C (mmol/l)	MDA (mmol/l)
Before	FJACPG	2.8 ± 1.2	5.7 ± 1.2	1.3 ± 0.3	3.8 ± 1.0	1.7 ± 0.3
	CG	2.7 ± 1.1	5.6 ± 1.2	1.2 ± 0.2	4.0 ± 1.1	1.6 ± 0.2
	P value	0.73	0.86	0.64	0.76	0.89
3-month	FJACPG	2.6 ± 1.3	5.5 ± 1.1	1.4 ± 0.2	3.5 ± 1.1	1.5 ± 0.2
	CG	2.7 ± 1.3	5.7 ± 1.1	1.3 ± 0.2	3.9 ± 1.1	1.7 ± 0.3
	P value	0.34	0.22	0.18	0.26	0.27
6-month	FJACPG	2.2 ± 1.3	5.1 ± 1.1	1.6 ± 0.2	3.2 ± 1.1	1.3 ± 0.2
	CG	2.8 ± 1.3	5.8 ± 1.1	1.3 ± 0.2	4.0 ± 1.2	1.8 ± 0.3
	P value	0.02*	0.04*	0.04*	0.03*	0.02*
9-month	FJACPG	1.8 ± 1.1	4.6 ± 1.4	1.6 ± 0.3	3.0 ± 1.1	0.9 ± 0.1
	CG	2.6 ± 1.3	5.5 ± 1.1	1.2 ± 0.2	3.9 ± 1.2	1.6 ± 0.3
	P value	0.01*	0.02*	0.01*	0.01*	0.01*

Note: *$P < 0.05$ via CG.

were higher in FJACPG than in CG after 9-month therapy ($P < 0.05$). In contrast, the levels of ALT were lower in FJACPG than CG after 9 month therapy ($P < 0.05$). The results suggested that long-term FJACP consumption showed better results for antioxidant activities when compared with CG.

3.4. Comparison of Lipid Pattern. Table 4 showed that the serum levels of TG, TC, LDL-C, and MDA were reduced while the level of HDL-C was increased in FJACPG after 3-month therapy, but there was no statistical significance of difference between the two groups ($P > 0.05$). Lipid pattern was improved further in FJACPG after 6-month therapy, and there was statistical significance of differences between the two groups ($P < 0.05$). Similarly, lipid pattern was improved significantly in FJACPG after 9 months, and there was statistical significance of difference between the two groups ($P < 0.05$). All the results suggested that FJACP significantly improved lipid patterns in T2DM patients.

3.5. Long-Term FJACP Significantly Reduces the Levels of IL-1 Beta and IL-6. As Figure 2 showed, before this study, there was no significant statistical difference in blood concentrations of IL-1 beta and IL-6 between the two groups ($P > 0.05$). Comparatively, the levels of IL-1 beta and IL-6 were reduced in both groups ($P < 0.05$), but there was still no significantly statistical difference in blood concentrations of IL-1 beta and IL-6 between the two groups after 3-month therapy ($P > 0.05$). The levels of IL-1 beta and IL-6 were further reduced in both groups ($P < 0.05$), and there were significant statistical differences in blood concentrations of IL-1 beta between the two groups after 6- and 9-month therapy (Figure 2(a), $P < 0.05$). There were significant statistical differences for blood concentrations of IL-6 between the two groups after and 9-month therapy (Figure 2(b), $P < 0.05$). The results suggest that long-term FJACP significantly reduces the levels of IL-1 beta and IL-6.

3.6. Long-Term FJACP Consumption Increased the Levels of Serum miR-424, Keap1, and Nrf2. As Figure 3 showed, before

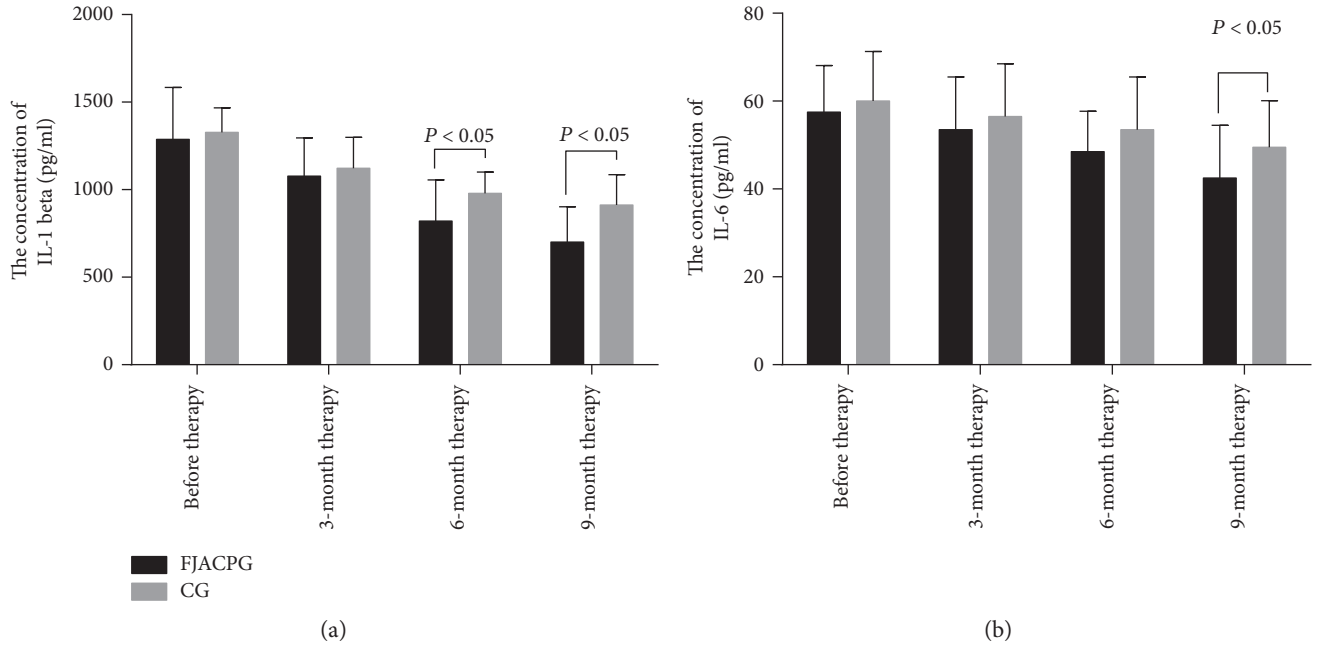

Figure 2: Measurement of the concentrations of IL-1 beta and IL-6 by ELISA in blood samples. (a) The concentration of IL-1 beta. (b) The concentration of IL-6. FJACPG: FJACP group; CG: placebo group. All data were presented as mean values ± SD.

this study, there was no significant statistical difference for mRNA levels of serum miR-424, Keap1, and Nrf2 between the two groups ($P > 0.05$). Comparatively, mRNA levels of serum miR-424, Keap1, and Nrf2 were increased in both groups ($P < 0.05$), but there were significantly statistical differences for mRNA levels of Nrf2 between the two groups after 3 months ($P < 0.05$). The mRNA levels of serum miR-424, Keap1, and Nrf2 were further increased in both groups ($P < 0.05$), and there were significant statistical differences in mRNA levels of Keap1 and Nrf2 between the two groups since 6 months (Figure 3, $P < 0.05$). Much difference for mRNA levels of serum miR-424, Keap1, and Nrf2 was observed between the two groups after and 9 months (Figures 3(a), 3(b), and 3(c), $P < 0.05$). The results suggest that long-term FJACP consumption significantly increases mRNA levels of Keap1 and Nrf2.

3.7. Long-Term FJACP Consumption Increased Protein Levels of Keap1 and Nrf2. As Figure 4 showed, before this study, there was no significantly statistical difference for protein levels of Keap1 and Nrf2 between the two groups ($P > 0.05$). Comparatively, the protein levels of Keap1 and Nrf2 were increased in both groups ($P < 0.05$), but there were only significant statistical differences for the protein levels of Nrf2 between the two groups after 3-month therapy ($P < 0.05$). The protein levels of Keap1 and Nrf2 were further increased in both groups ($P < 0.05$), and there were significant statistical differences in the protein levels of Keap1 and Nrf2 between the two groups since 6-month therapy (Figure 4, $P < 0.05$). Much difference for the protein levels of Keap1 and Nrf2 was observed between the two groups after and 9-month therapy (Figures 4(a) and 4(b), $P < 0.05$). The results suggest that long-term FJACP significantly increases protein levels of Keap1 and Nrf2.

3.8. The Association of the Levels between miR-424 and Inflammatory Cytokines. Spearman's rank correlation analysis showed that the levels of IL-1 beta (Figure 5(a)) and IL-6 (Figure 5(b)) were reduced when the level of miR-424 was increased. There was a negative relationship between the level of miR-424 and the level of IL-1 beta or IL-6 ($P < 0.05$). The results suggest that a higher level of Nrf2 will result in lower levels of IL-1 beta and IL-6.

3.9. The Association of the Levels between miR-424 and Biomarkers of Antioxidant Factors. Spearman's rank correlation analysis showed that the levels of SOD (Figure 6(a)) and GSH (Figure 6(b)) were increased when the level of miR-424 was increased. There was a positive relationship between the levels of miR-424 and the levels of IL-1 beta or IL-6 ($P < 0.05$). In contrast, the levels of ALT (Figure 6(c)) and AST (Figure 6(d)) were reduced when the level of miR-424 was increased. The results suggest that a higher level of miR-424 will promote antioxidant activities of T2DM patients.

3.10. The Association of the Protein Levels between Nrf2 and Inflammatory Cytokines. Spearman's rank correlation analysis showed that the levels of IL-1 beta (Figure 7(a)) and IL-6 (Figure 7(b)) were reduced when the level of Nrf2 was increased. There were a negative relationship between the level of Nrf2 and the level of IL-1 beta or IL-6 ($P < 0.05$). The results suggest that a higher level of Nrf2 will result in lower levels of IL-1 beta and IL-6.

3.11. The Association of the Protein Levels between Nrf-2 and Biomarkers of Antioxidant Factors. Spearman's rank correlation analysis showed that the levels of SOD (Figure 8(a)) and GSH (Figure 8(b)) were increased when

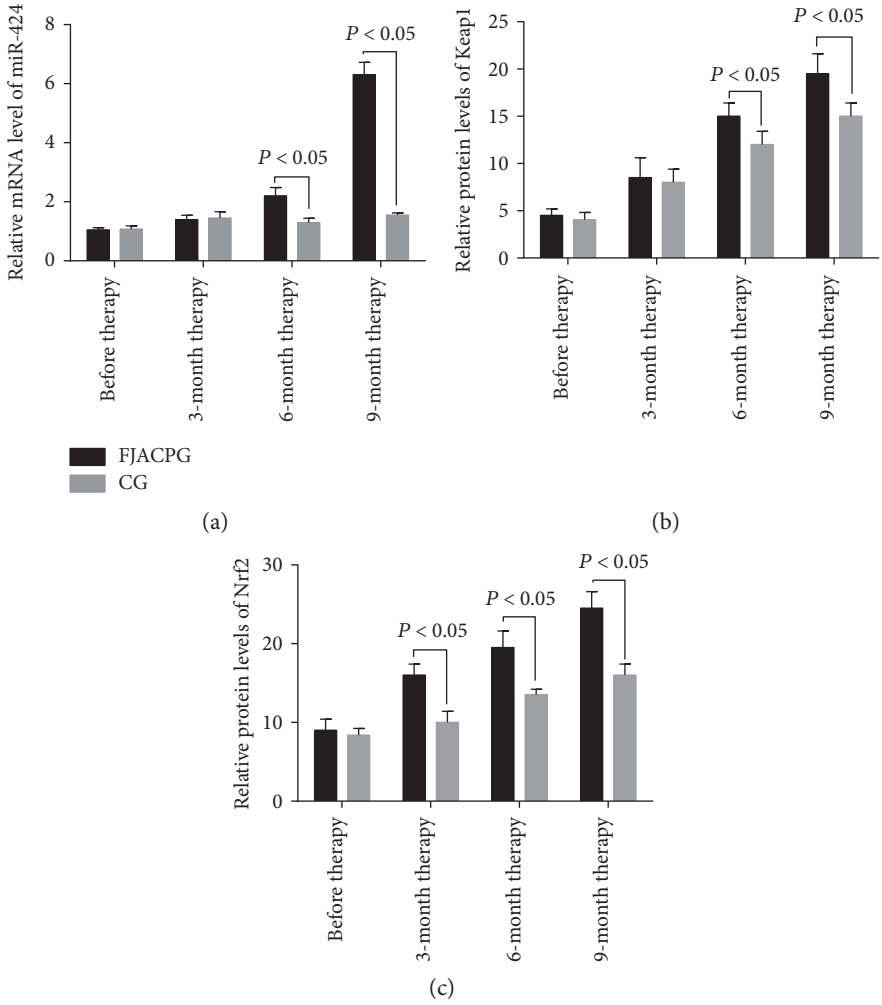

Figure 3: qRT-PCR analysis of relative mRNA levels. (a) Relative mRNA levels of serum miR-424. (b) Relative mRNA levels of Keap1. (c) Relative mRNA levels of Nrf2. FJACPG: FJACP group; CG: placebo group. All data were presented as mean values ± SD.

the level of Nrf2 was increased. There was positive relationship between the level of Nrf2 and the level of IL-1 beta or IL-6 ($P < 0.05$). In contrast, the levels of ALT (Figure 8(c)) and AST (Figure 8(d)) were reduced when the level of Nrf2 was increased. The results suggest that a higher level of Nrf2 will promote antioxidant activities of T2DM patients.

3.12. The Association of the Levels between miR-424 and Nrf2. Spearman's rank correlation analysis showed that the levels of Keap1 (Figure 9(a)) and Nrf2 (Figure 9(b)) were increased when the level of miR-424 was increased. There was a positive relationship between the level of miR-424 and the level of Keap1 or Nrf2 ($P < 0.05$). The results suggest that a higher level of miR-424 will increase the levels of Keap1 and Nrf2.

4. Discussion

The changes of physical indexes indicated that both the control group and the FJACP group improved the antioxidant activities of T2DM. Notably, long-term FJACP showed a better result after 3-month therapy. For the most elderly, the ability of movement begins to decline and the strength of the skeletal muscles of the lower limbs plays a critical role in the activity. In the population cohort with difficult walking, higher risk of diabetic complications will be developed [35]. In contrast, long-term consumption of FJACP significantly ameliorates diabetes, including the improvement of general well-being and the decrease of the levels of HbA1c, FBG, and BMI [36]. Similarly, FJACP also has been reported to have the functions for reducing the levels of BMI [37] and blood glucose [38].

Present comparing study showed physical condition was improved in both groups after 3 months. Furthermore, the knee extension strength and balance function in FJACPG were improved obviously (data was not shown). The results might be caused by the normal exercise (walking daily) which could be maintained. The exercise was kept at the same level (each person walks about 1.5 to 2 miles per day) between the two groups. The exercise function was not explored in detail. The general improvement in the patients from FJACPG was better than those from CG. After 6 months, there were significant statistical differences between FJACPG and CG. The results suggest that FJACP may have some benefits on

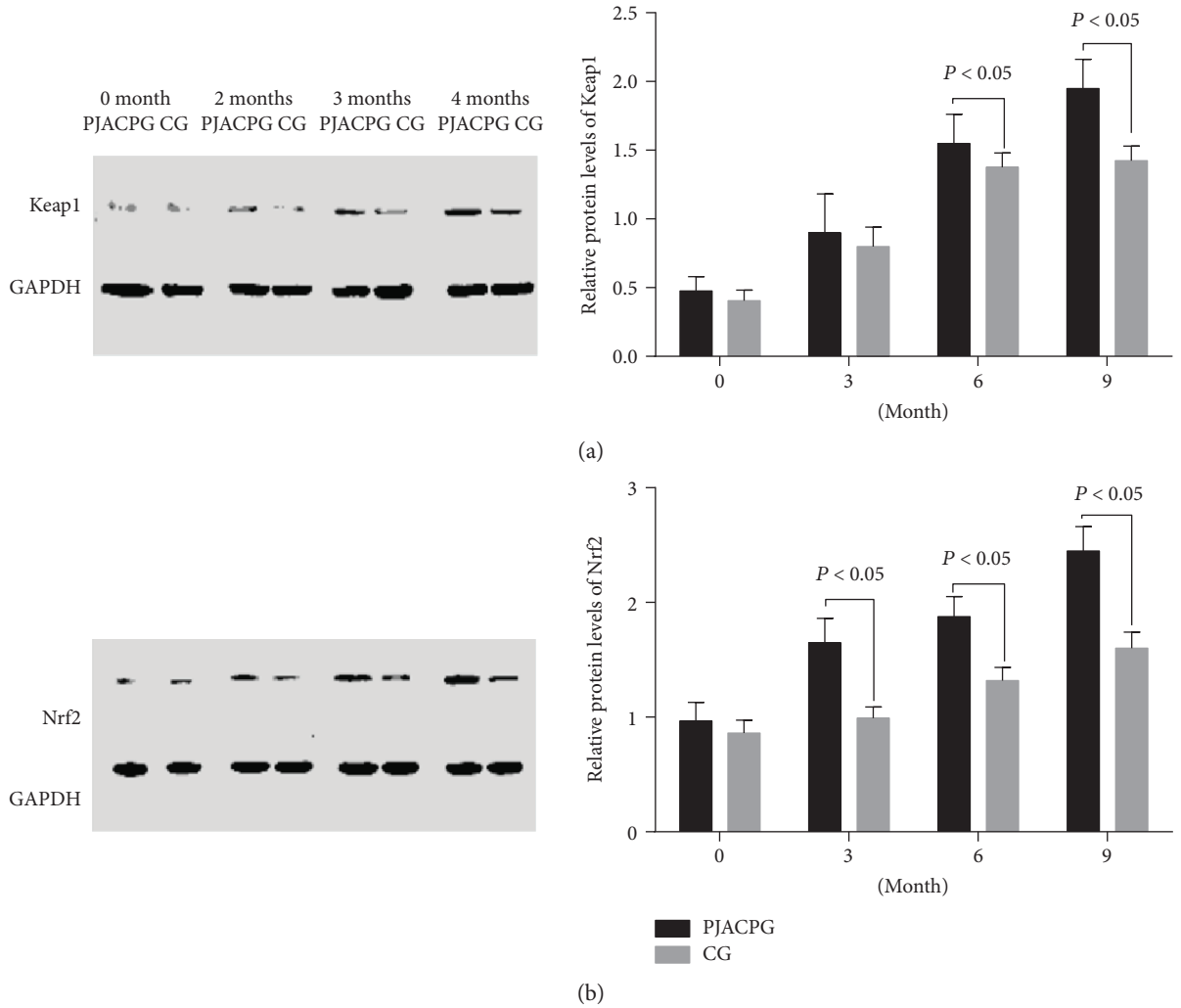

Figure 4: Western blot analysis of relative protein levels of Keap1 and Nrf2. (a) Relative protein levels of Keap1. (b) Relative protein levels of Nrf2. FJACPG: FJACP group; CG: placebo group. All data were presented as mean values ± SD.

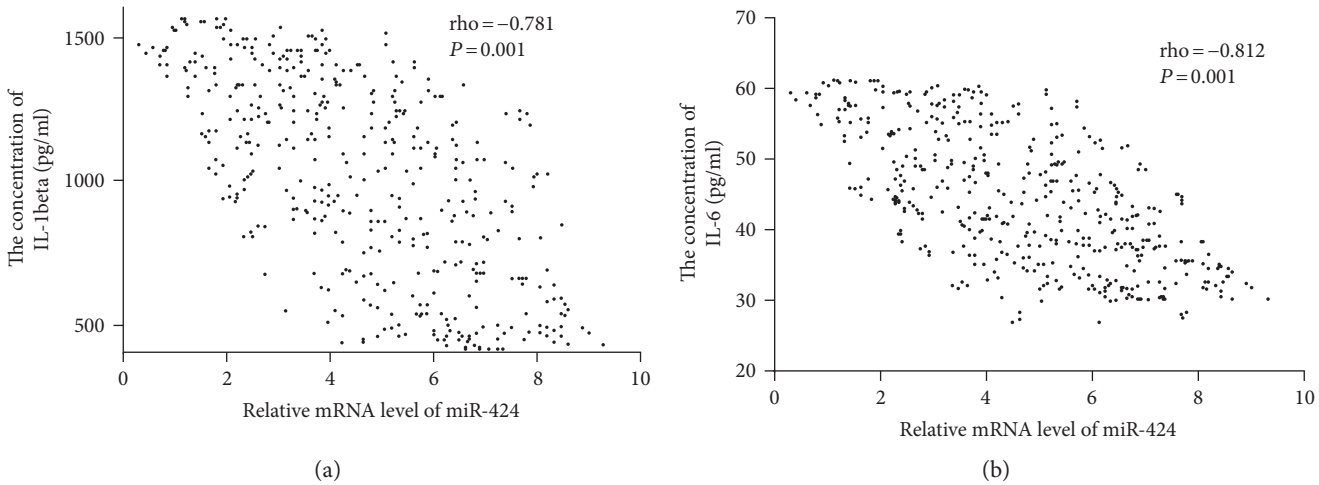

Figure 5: The relationship between the level of miR-424 and the levels of proinflammatory cytokines. (a) The relationship between the level of miR-424 and the level of IL-1 beta. (b) The relationship between the level of miR-424 and the level of IL-6. Spearman's rank correlation test was performed to compare two variables. There is a strong negative association if the value of rho falls between −1 and −0.5.

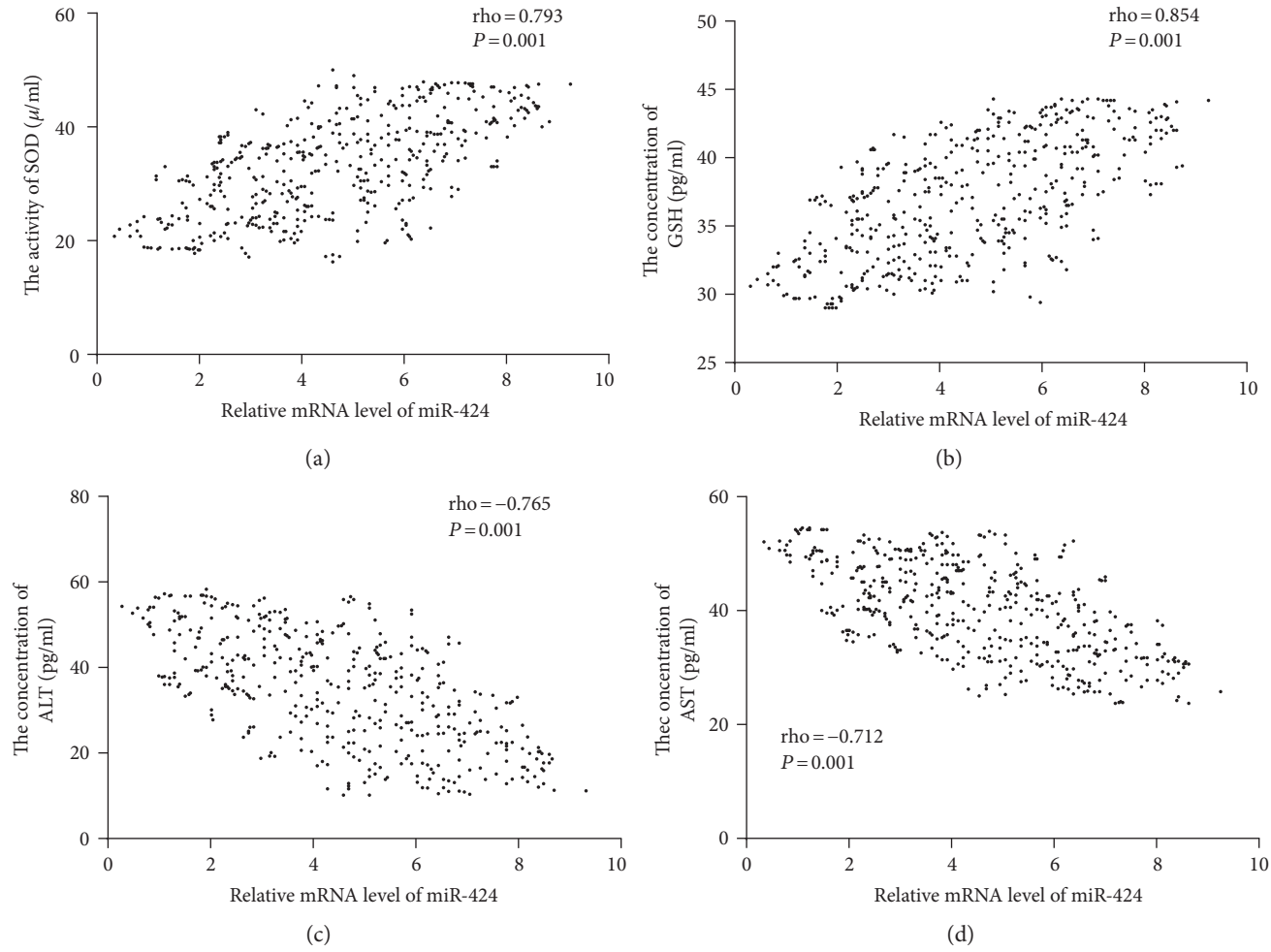

Figure 6: The relationship between the level of miR-424 and the levels of biomarkers of antioxidant factors. (a) The relationship between the level of miR-424 and the level of SOD. (b) The relationship between the level of miR-424 and the level of GSH. (c) The relationship between the level of miR-424 and the level of ALT. (d) The relationship between the level of miR-424 and the level of AST. Spearman's rank correlation test was performed to compare two variables. There is a strong negative association if the value of rho falls between −1 and −0.5. There is a strong positive association if the value of rho falls between 0.5 and 1.

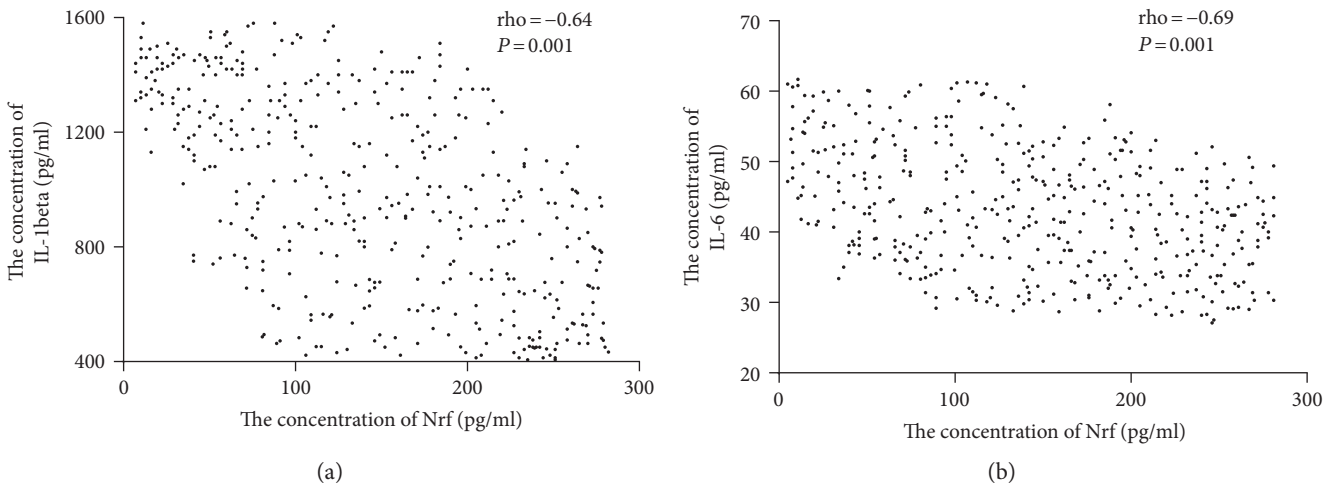

Figure 7: The relationship between the level of Nrf2 and the levels of proinflammatory cytokines. (a) The relationship between the level of Nrf2 and the level of IL-1 beta. (b) The relationship between the level of Nrf2 and the level of IL-6. Spearman's rank correlation test was performed to compare two variables. There is a strong negative association if the value of rho falls between −1 and −0.5.

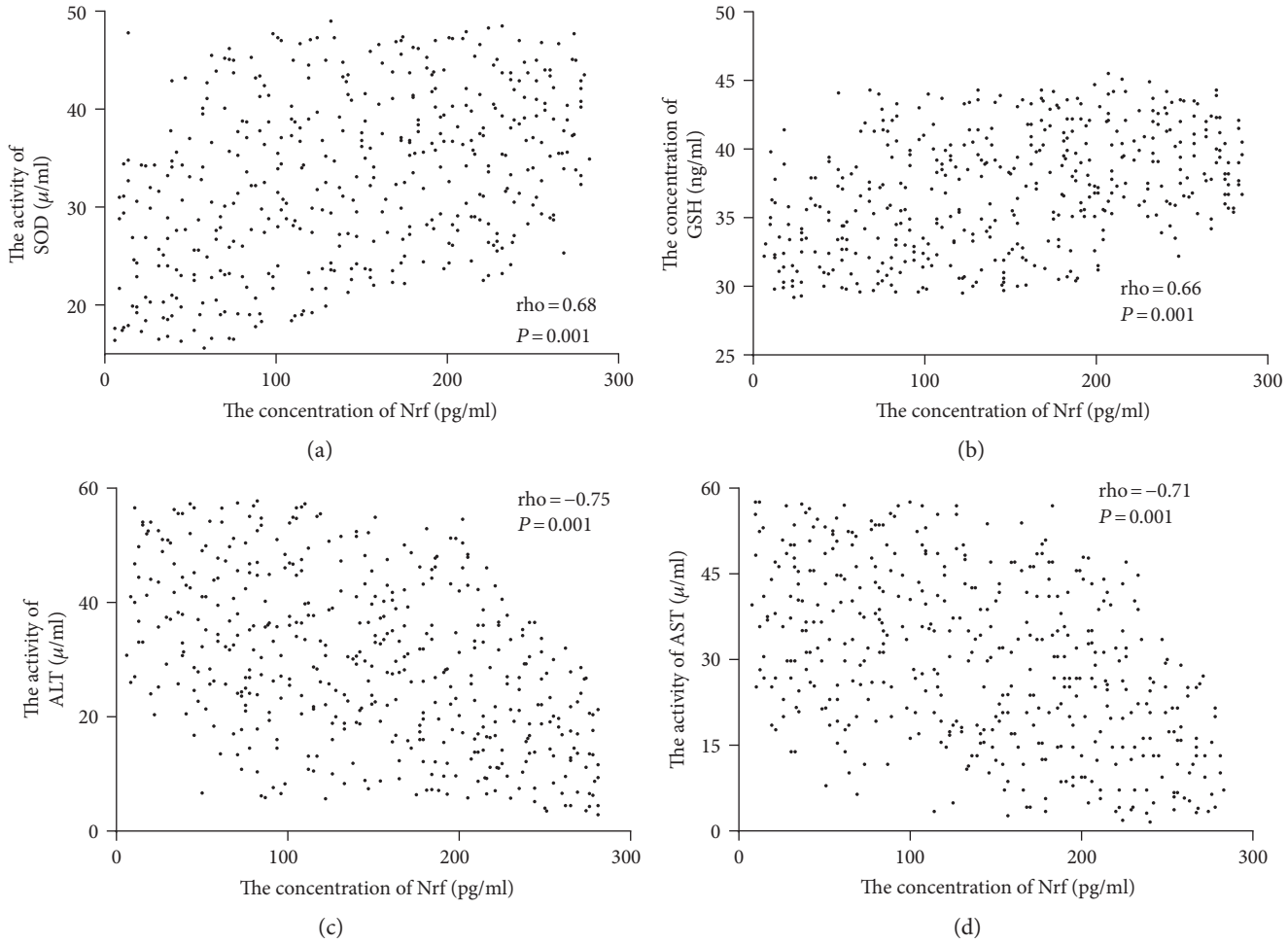

Figure 8: The relationship between the level of Nrf2 and the levels of biomarkers of antioxidant factors. (a) The relationship between the level of Nrf2 and the level of SOD. (b) The relationship between the level of Nrf2 and the level of GSH. (c) The relationship between the level of Nrf2 and the level of ALT. (d) The relationship between the level of Nrf2 and the level of AST. Spearman's rank correlation test was performed to compare two variables. There is a strong negative association if the value of rho falls between −1 and −0.5. There is a strong positive association if the value of rho falls between 0.5 and 1.

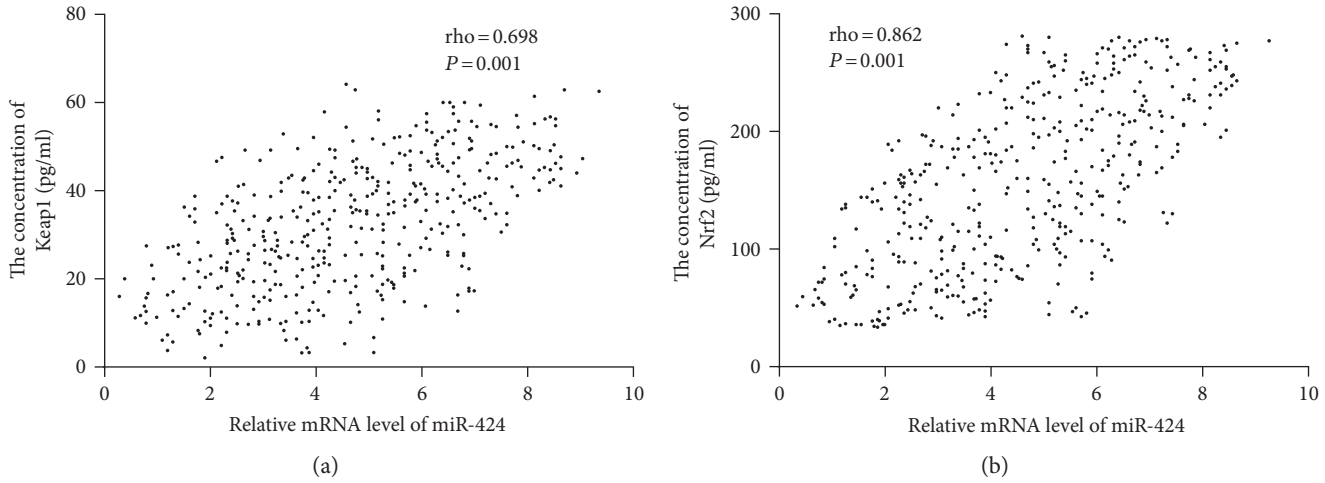

Figure 9: The relationship between the level of miR-424 and the levels of Keap1 or Nrf2. (a) The relationship between the level of miR-424 and the level of Keap1. (b) The relationship between the level of miR-424 and the level of Nrf2. Spearman's rank correlation test was performed to compare two variables. There is a strong negative association if the value of rho falls between −1 and −0.5. There is a strong positive association if the value of rho falls between 0.5 and 1.

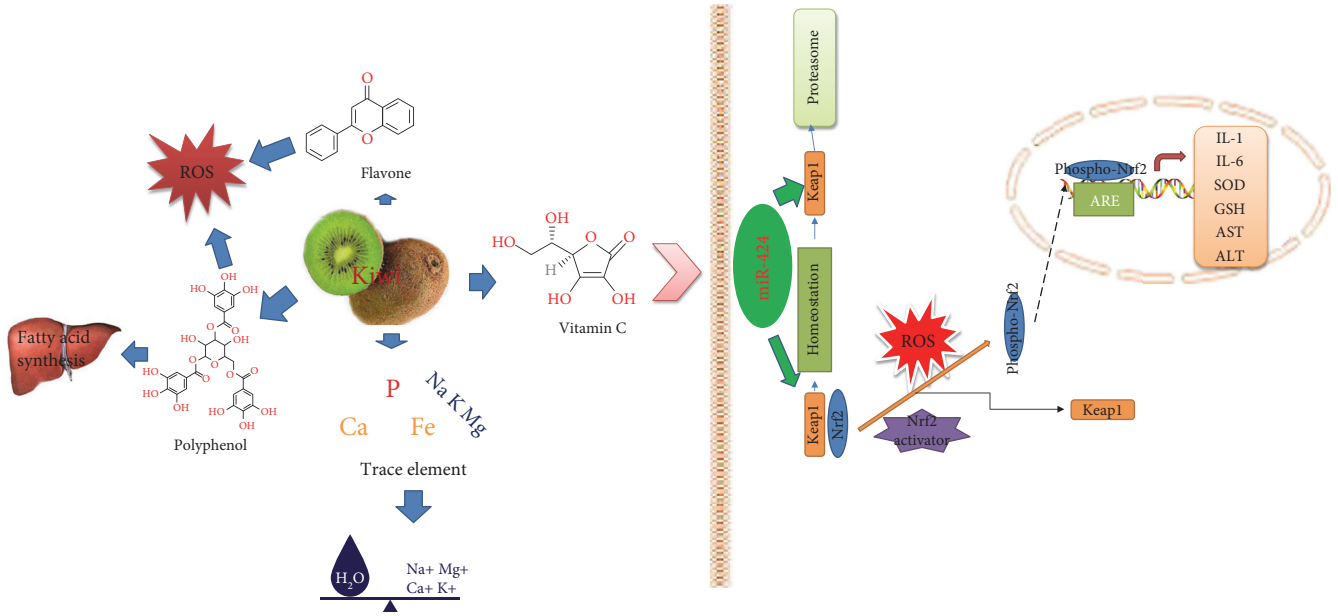

Figure 10: The multiple functions of FJACP on T2DM patients.

general well-being. The work is not the focus of the present study, but it is very important and will be performed in the future to confirm the conclusion.

FJACP improves the indices of antioxidant and anti-inflammation status by affecting Keap1 and Nrf2 in the patients with T2DM. Keap1 and Nrf2 play an important role in preventing the risk and development of T2DM. It can reduce the levels of proinflammatory cytokines and increase the level of antioxidant molecules. T2DM is characterized by inflammatory [39, 40] and oxidant status [41, 42]. The disease is closely associated with kidney disorder [43, 44] and peripheral neuropathy [45, 46]. T2DM is also the main cause for cardiovascular disorder [47, 48]. The levels of Nrf2 and Keap1 were significantly decreased in T2DM patients. To make sure the interaction between Nrf2 and Keap1, and these molecules, is present, much work is needed to be done in future work.

The reasons for the functions of FJACP are complex (Figure 10). The reasons for the functions of FJACP are complex (Figure 10). FJACP contains a large number of antioxidants such as polyphenols and vitamins [49]. Polyphenols show strong antioxidant activities as ROS scavengers [50]. Polyphenols as an important bioactive compound have been reported to have anticancer effects by upregulating the level of miR-1 [51]. Other reports also show that polyphenol exhibits its biological functions by affecting miRNA-mediated regulation [52]. Thus, FJACP may also affect the level of serum miR-424.

Vitamin C is rich in FJACP which may affect serum levels of microRNAs. Vitamin C is regarded as a reprogramming enhancer for inducing a blastocyst state in embryo cells. Vitamin C demethylates gene promoters by affecting epigenetic modifiers, which activates pluripotency genes and miRNAs of embryo cells [53]. Then, differentiation and development genes are repressed by ESC-enriched miRNAs, which maintain the stem cell state. MicroRNA-expressing profiles have been reported to be affected by vitamin C [54]. Present findings showed that FJACP increased the levels of microRNA-424, which downregulated the activities of Nrf2 and Keap1. The results improved the indices of antioxidant and anti-inflammatory situation of T2DM patients.

According to Chinese theory, FJACP can transfer the strength between deficiency and excess from different parts of the human body, including the upper and lower limbs, the internal organs, and environment. Full body and cooperation among the different organs are the main ideas of FJACP. The limitation of FJACP is that it must be understood well and performed exactly as its central ideas. Overconsumption of FJACP will cause harmful effects on human health since it contains much vitamin C. More trouble, incorrect of FJACP consumption may result in stomach pain.

There were some limitations to the present study. The function of FJACP should be performed in a larger population since it shows fewer side effects. The detail molecular mechanism for the association between proinflammatory cytokines and Keap1and Nrf2 remains unclear. Although FJACP is rich with polyphenols and vitamin C, the relationship between miR-424 and polyphenols or vitamin C remains unknown. To make sure the functional role of FJACP on T2DM is present, much work is still needed to be done in the future.

5. Conclusions

Beneficial effects of FJACP were proven here, and the long-term FJACP would be beneficial for improving the symptoms of T2DM. The rehabilitant functions of FJACP might be associated with the increase in the activities and levels of SOD and GSH and the decrease in the levels of ALT and AST, which further increased the level of HDL-c and

decreased the level of FJACPG, TC, and LDL-c. All the results decreased oxidative stress in T2DM. Furthermore, FJACP activated Keap1 and Nrf2 via the upregulation of miR-424, which plays an important role in antioxidant and anti-inflammatory activities in T2DM patients. FJACP as a nonpharmaceutical intervention should be developed as a potential way for preventing the risk or development of T2DM.

Conflicts of Interest

The authors declare that they have no conflict of interests.

References

[1] D. A. Schoenaker, G. D. Mishra, L. K. Callaway, and S. S. Soedamah-Muthu, "The role of energy, nutrients, foods, and dietary patterns in the development of gestational diabetes mellitus: a systematic review of observational studies," *Diabetes Care*, vol. 39, no. 1, pp. 16–23, 2016.

[2] L. A. Bazzano, T. Y. Li, K. J. Joshipura, and F. B. Hu, "Intake of fruit, vegetables, and fruit juices and risk of diabetes in women," *Diabetes Care*, vol. 31, no. 7, pp. 1311–1317, 2008.

[3] H. Iwasawa, E. Morita, S. Yui, and M. Yamazaki, "Anti-oxidant effects of kiwi fruit in vitro and in vivo," *Biological & Pharmaceutical Bulletin*, vol. 34, no. 1, pp. 128–134, 2011.

[4] K. E. Sarji, J. Kleinfelder, P. Brewington, J. Gonzalez, H. Hempling, and J. A. Colwell, "Decreased platelet vitamin C in diabetes mellitus: possible role in hyperaggregation," *Thrombosis Research*, vol. 15, no. 5-6, pp. 639–650, 1979.

[5] E. H. Soufleros, I. Pissa, D. Petridis et al., "Instrumental analysis of volatile and other compounds of Greek kiwi wine; sensory evaluation and optimisation of its composition," *Food Chemistry*, vol. 75, no. 4, pp. 487–500, 2001.

[6] S. M. Kim, S. M. Lim, J. A. Yoo, M. J. Woo, and K. H. Cho, "Consumption of high-dose vitamin C (1250 mg per day) enhances functional and structural properties of serum lipoprotein to improve anti-oxidant, anti-atherosclerotic, and anti-aging effects via regulation of anti-inflammatory microRNA," *Food & Function*, vol. 6, no. 11, pp. 3604–3612, 2015.

[7] N. Mikirova, J. Casciari, N. Riordan, and R. Hunninghake, "Clinical experience with intravenous administration of ascorbic acid: achievable levels in blood for different states of inflammation and disease in cancer patients," *Journal of Translational Medicine*, vol. 11, no. 1, p. 1, 2013.

[8] G. Mohajeri, M. Safaee, and M. H. Sanei, "Effects of topical kiwifruit on healing of neuropathic diabetic foot ulcer," *Journal of Research in Medical Sciences*, vol. 19, no. 6, pp. 520–524, 2014.

[9] M. Esti, M. C. Messia, P. Bertocchi et al., "Chemical compounds and sensory assessment of kiwifruit (*Actinidia chinensis* (Planch.) var. *chinensis*): electrochemical and multivariate analyses," *Food Chemistry*, vol. 61, no. 3, pp. 293–300, 1998.

[10] C. Bleau, A. D. Karelis, D. H. St-Pierre, and L. Lamontagne, "Crosstalk between intestinal microbiota, adipose tissue and skeletal muscle as an early event in systemic low-grade inflammation and the development of obesity and diabetes," *Diabetes/Metabolism Research and Reviews*, vol. 31, no. 6, pp. 545–561, 2015.

[11] J. Boon, A. J. Hoy, R. Stark et al., "Ceramides contained in LDL are elevated in type 2 diabetes and promote inflammation and skeletal muscle insulin resistance," *Diabetes*, vol. 62, no. 2, pp. 401–410, 2013.

[12] A. Gumieniczek, H. Hopkala, Z. Wojtowicz, and M. Nieradko, "Differences in antioxidant status in skeletal muscle tissue in experimental diabetes," *Clinica Chimica Acta*, vol. 314, no. 1-2, pp. 39–45, 2001.

[13] Y. F. Chen, C. C. Yang, S. Y. Kao, C. J. Liu, S. C. Lin, and K. W. Chang, "MicroRNA-211 enhances the oncogenicity of carcinogen-induced oral carcinoma by repressing TCF12 and increasing antioxidant activity," *Cancer Research*, vol. 76, no. 16, pp. 4872–4886, 2016.

[14] K. M. Lim, S. An, O. K. Lee et al., "Analysis of changes in microRNA expression profiles in response to the troxerutin-mediated antioxidant effect in human dermal papilla cells," *Molecular Medicine Reports*, vol. 12, no. 2, pp. 2650–2660, 2015.

[15] P. Liu, H. Zhao, R. Wang et al., "MicroRNA-424 protects against focal cerebral ischemia and reperfusion injury in mice by suppressing oxidative stress," *Stroke*, vol. 46, no. 2, pp. 513–519, 2015.

[16] T. Yan, X. Yu, X. Sun, D. Meng, and J. M. Jia, "A new steroidal saponin, furotrilliumoside from Trillium tschonoskii inhibits lipopolysaccharide-induced inflammation in Raw264.7 cells by targeting PI3K/Akt, MARK and Nrf2/HO-1 pathways," *Fitoterapia*, vol. 115, pp. 37–45, 2016.

[17] X. Zhao, L. Wen, M. Dong, and X. Lu, "Sulforaphane activates the cerebral vascular Nrf2-ARE pathway and suppresses inflammation to attenuate cerebral vasospasm in rat with subarachnoid hemorrhage," *Brain Research*, vol. 1653, pp. 1–7, 2016.

[18] M. Danilenko and G. P. Studzinski, "Keep harm at bay: oxidative phosphorylation induces Nrf2-driven antioxidant response via ERK5/MEF2/miR-23a signaling to Keap-1," *eBioMedicine*, vol. 3, pp. 4–5, 2016.

[19] A. General Assembly of the World Medical, "World Medical Association Declaration of Helsinki: ethical principles for medical research involving human subjects," *The Journal of the American College of Dentists*, vol. 81, no. 3, pp. 14–18, 2014.

[20] M. M. Engelgau, T. J. Thompson, W. H. Herman et al., "Comparison of fasting and 2-hour glucose and HbA1c levels for diagnosing diabetes. Diagnostic criteria and performance revisited," *Diabetes Care*, vol. 20, no. 5, pp. 785–791, 1997.

[21] F. Santilli, R. Liani, P. Di Fulvio et al., "Increased circulating resistin is associated with insulin resistance, oxidative stress and platelet activation in type 2 diabetes mellitus," *Thrombosis and Haemostasis*, vol. 116, no. 6, 2016.

[22] C. R. Wietzycoski, J. C. Marchesini, S. Al-Themyat, F. S. Meyer, and M. R. Trindade, "Improvement in oxidative stress after duodenojejunostomy in an experimental model of type 2 diabetes mellitus," *Arquivos Brasileiros de Cirurgia Digestiva*, vol. 29, Supplement 1, pp. 3–7, 2016.

[23] T. G. Araujo, A. G. Oliveira, J. F. Vecina et al., "Treatment with *Parkinsonia aculeata* combats insulin resistance-induced oxidative stress through the increase in PPARγ/CuZn-SOD axis expression in diet-induced obesity mice," *Molecular and Cellular Biochemistry*, vol. 419, no. 1-2, pp. 93–101, 2016.

[24] J. Wan, L. Deng, C. Zhang et al., "Chikusetsu saponin V attenuates H_2O_2-induced oxidative stress in human neuroblastoma SH-SY5Y cells through Sirt1/PGC-1α/Mn-SOD signaling pathways," *Canadian Journal of Physiology and Pharmacology*, vol. 94, no. 9, pp. 919–928, 2016.

[25] H. Fujii, Y. Yonekura, Y. Yamashita et al., "Anti-oxidative effect of AST-120 on kidney injury after myocardial infarction," *British Journal of Pharmacology*, vol. 173, no. 8, pp. 1302–1313, 2016.

[26] S. Yamamoto, J. J. Kazama, K. Omori et al., "Continuous reduction of protein-bound uraemic toxins with improved oxidative stress by using the oral charcoal adsorbent AST-120 in haemodialysis patients," *Scientific Reports*, vol. 5, p. 14381, 2015.

[27] G. Vendemiale, I. Grattagliano, P. Portincasa, G. Serviddio, G. Palasciamo, and E. Altomare, "Oxidative stress in symptom-free HCV carriers: relation with ALT flare-up," *European Journal of Clinical Investigation*, vol. 31, no. 1, pp. 54–63, 2001.

[28] E. Jansen, P. Beekhof, D. Viezeliene, V. Muzakova, and J. Skalicky, "Long-term stability of cancer biomarkers in human serum: biomarkers of oxidative stress and redox status, homocysteine, CRP and the enzymes ALT and GGT," *Biomarkers in Medicine*, vol. 9, no. 5, pp. 425–432, 2015.

[29] X. Dong, D. Li, H. Liu, and Y. Zhao, "SOD3 and eNOS genotypes are associated with SOD activity and NO," *Experimental and Therapeutic Medicine*, vol. 8, no. 1, pp. 328–334, 2014.

[30] S. Su, Q. Li, Y. Liu et al., "Sesamin ameliorates doxorubicin-induced cardiotoxicity: involvement of Sirt1 and Mn-SOD pathway," *Toxicology Letters*, vol. 224, no. 2, pp. 257–263, 2014.

[31] S. M. Kumar, K. Swaminathan, D. L. Clemens, and A. Dey, "GSH protects against oxidative stress and toxicity in VL-17A cells exposed to high glucose," *European Journal of Nutrition*, vol. 54, no. 2, pp. 223–234, 2014.

[32] S. Jung, O. Y. Kim, M. Kim, J. Song, S. H. Lee, and J. H. Lee, "Age-related increase in alanine aminotransferase correlates with elevated levels of plasma amino acids, decanoylcarnitine, Lp-PLA(2) activity, oxidative stress, and arterial stiffness," *Journal of Proteome Research*, vol. 13, no. 7, pp. 3467–3475, 2014.

[33] J. Yamada, H. Tomiyama, M. Yambe, and A. Yamashina, "Elevated serum alanine aminotransferase is a marker of inflammation and oxidative stress associated with the metabolic syndrome," *Journal of Hypertension*, vol. 24, p. 193, 2006.

[34] H. H. Mansour, S. Ismael Nel, and H. F. Hafez, "Ameliorative effect of septilin, an ayurvedic preparation against gamma-irradiation-induced oxidative stress and tissue injury in rats," *Indian Journal of Biochemistry & Biophysics*, vol. 51, no. 2, pp. 135–141, 2014.

[35] G. A. Hawker, R. Croxford, A. S. Bierman et al., "Osteoarthritis-related difficulty walking and risk for diabetes complications," *Osteoarthritis and Cartilage*, vol. 25, no. 1, pp. 67–75, 2017.

[36] S. Shenoy, R. Guglani, and J. S. Sandhu, "Effectiveness of an aerobic walking program using heart rate monitor and pedometer on the parameters of diabetes control in Asian Indians with type 2 diabetes," *Primary Care Diabetes*, vol. 4, no. 1, pp. 41–45, 2010.

[37] R. W. Geib, H. Li, E. Oggeo et al., "Using computerized posturography to explore the connection between bmi and postural stability in long-term tai chi practitioners - biomed 2011," *Biomedical Sciences Instrumentation*, vol. 47, pp. 288–293, 2011.

[38] X. Liu, Y. D. Miller, N. W. Burton, J. H. Chang, and W. J. Brown, "The effect of tai chi on health-related quality of life in people with elevated blood glucose or diabetes: a randomized controlled trial," *Quality of Life Research*, vol. 22, no. 7, pp. 1783–1786, 2013.

[39] K. Singh, N. K. Agrawal, S. K. Gupta, P. Sinha, and K. Singh, "Increased expression of TLR9 associated with pro-inflammatory S100A8 and IL-8 in diabetic wounds could lead to unresolved inflammation in type 2 diabetes mellitus (T2DM) cases with impaired wound healing," *Journal of Diabetes and Its Complications*, vol. 30, no. 1, pp. 99–108, 2016.

[40] L. van Beek, M. A. Lips, A. Visser et al., "Increased systemic and adipose tissue inflammation differentiates obese women with T2DM from obese women with normal glucose tolerance," *Metabolism*, vol. 63, no. 4, pp. 492–501, 2014.

[41] E. M. Zakaria, N. N. El-Maraghy, A. F. Ahmed, A. A. Ali, and H. M. El-Bassossy, "PARP inhibition ameliorates nephropathy in an animal model of type 2 diabetes: focus on oxidative stress, inflammation, and fibrosis," *Naunyn-Schmiedeberg's Archives of Pharmacology*, pp. 1–11, 2017.

[42] E. Aboualizadeh, M. Ranji, C. M. Sorenson, R. Sepehr, N. Sheibani, and C. J. Hirschmugl, "Retinal oxidative stress at the onset of diabetes determined by synchrotron FTIR widefield imaging: towards diabetes pathogenesis," *Analyst*, vol. 142, no. 7, pp. 1061–1072, 2017.

[43] P. A. Bittle, "Use of dipeptidyl peptidase-4 inhibitors in patients with type 2 diabetes and chronic kidney disease," *The Nurse Practitioner*, 2017, Epub ahead of print.

[44] E. M. Miller, "Elements for success in managing type 2 diabetes with SGLT-2 inhibitors: role of the kidney in glucose homeostasis: implications for SGLT-2 inhibition in the treatment of type 2 diabetes mellitus," *The Journal of Family Practice*, vol. 66, 2 Supplement, pp. S3–S5, 2017.

[45] A. Marzban, J. Kiani, M. Hajilooi, H. Rezaei, Z. Kahramfar, and G. Solgi, "HLA class II alleles and risk for peripheral neuropathy in type 2 diabetes patients," *Neural Regeneration Research*, vol. 11, no. 11, pp. 1839–1844, 2016.

[46] D. Wang, J. X. Zhai, and D. W. Liu, "Serum folate, vitamin B12 levels and diabetic peripheral neuropathy in type 2 diabetes: a meta-analysis," *Molecular and Cellular Endocrinology*, vol. 443, pp. 72–79, 2017.

[47] S. Ou and N. Behzad, "Prevalence of microalbuminuria and its utility as an early predictive marker for cardiovascular damage in T2DM," *The Journal of the Association of Physicians of India*, vol. 64, no. 1, pp. 84–85, 2016.

[48] M. Kumar, K. D. Singh, and M. Indurkar, "Cardiovascular risk evaluation in T2DM patients with normal resting ECG with special reference to echocardiography and TMT," *The Journal of the Association of Physicians of India*, vol. 64, no. 1, p. 40, 2016.

[49] A. K. Duttaroy and A. Jorgensen, "Effects of kiwi fruit consumption on platelet aggregation and plasma lipids in healthy human volunteers," *Platelets*, vol. 15, no. 5, pp. 287–292, 2004.

[50] H. Wang, D. Li, Z. Hu, S. Zhao, Z. Zheng, and W. Li, "Protective effects of green tea polyphenol against renal injury through ROS-mediated JNK-MAPK pathway in lead exposed rats," *Molecules and Cells*, vol. 39, no. 6, pp. 508–513, 2016.

[51] K. Zhu and W. Wang, "Green tea polyphenol EGCG suppresses osteosarcoma cell growth through upregulating miR-1," *Tumour Biology*, vol. 37, no. 4, pp. 4373–4382, 2016.

[52] H. Zhou, J. X. Chen, C. S. Yang, M. Q. Yang, Y. Deng, and H. Wang, "Gene regulation mediated by microRNAs in response to green tea polyphenol EGCG in mouse lung cancer," *BMC Genomics*, vol. 15, Supplement 11, p. S3, 2014.

[53] Y. Gao, Z. Han, Q. Li et al., "Vitamin C induces a pluripotent state in mouse embryonic stem cells by modulating microRNA expression," *The FEBS Journal*, vol. 282, no. 4, pp. 685–699, 2015.

[54] Y. J. Kim, S. Y. Ku, Z. Rosenwaks et al., "MicroRNA expression profiles are altered by gonadotropins and vitamin C status during in vitro follicular growth," *Reproductive Sciences*, vol. 17, no. 12, pp. 1081–1089, 2010.

Hindawi
Oxidative Medicine and Cellular Longevity
Volume 2017, Article ID 9397631, 11 pages
https://doi.org/10.1155/2017/9397631

Research Article

NPC-EXs Alleviate Endothelial Oxidative Stress and Dysfunction through the miR-210 Downstream Nox2 and VEGFR2 Pathways

Hua Liu,[1] Jinju Wang,[2] Yusen Chen,[3] Yanfang Chen,[2] Xiaotang Ma,[3] Ji C. Bihl,[2] and Yi Yang[1]

[1]*College of Health Science, Wuhan Sports University, Wuhan 430079, China*
[2]*Department of Pharmacology & Toxicology, Boonshoft School of Medicine, Wright State University, Dayton, OH 45435, USA*
[3]*Guangdong Key Laboratory of Age-Related Cardiac and Cerebral Diseases, Institute of Neurology, Affiliated Hospital of Guangdong Medical University, Zhanjiang 524000, China*

Correspondence should be addressed to Ji C. Bihl; ji.bihl@wright.edu and Yi Yang; yangyi999999@yahoo.com

Received 27 January 2017; Revised 12 April 2017; Accepted 20 April 2017; Published 28 May 2017

Academic Editor: Jaideep Banerjee

We have demonstrated that neural progenitor cells (NPCs) protect endothelial cells (ECs) from oxidative stress. Since exosomes (EXs) can convey the benefit of parent cells through their carried microRNAs (miRs) and miR-210 is ubiquitously expressed with versatile functions, we investigated the role of miR-210 in the effects of NPC-EXs on oxidative stress and dysfunction in ECs. NPCs were transfected with control and miR-210 scramble/inhibitor/mimic to generate NPC-EXs^{con}, NPC-EXs^{sc}, NPC-EXs$^{anti\text{-}miR\text{-}210}$, and NPC-EXs$^{miR\text{-}210}$. The effects of various NPC-EXs on angiotensin II- (Ang II-) induced reactive oxygen species (ROS) overproduction, apoptosis, and dysfunction, as well as dysregulation of Nox2, ephrin A3, VEGF, and p-VEGFR2/VEGFR2 in ECs were evaluated. Results showed (1) Ang II-induced ROS overproduction, increase in apoptosis, and decrease in tube formation ability, accompanied with Nox2 upregulation and reduction of p-VEGFR2/VEGFR2 in ECs. (2) Compared to NPC-EXs^{con} or NPC-EXs^{sc}, NPC-EXs$^{anti\text{-}miR\text{-}210}$ were less whereas NPC-EXs$^{miR\text{-}210}$ were more effective on attenuating these detrimental effects induced by Ang II in ECs. (3) These effects of NPC-EXs$^{anti\text{-}miR\text{-}210}$ and NPC-EXs$^{miR\text{-}210}$ were associated with the changes of miR-210, ephrin A3, VEGF, and p-VEGFR2/VEGFR2 ratio in ECs. Altogether, the protective effects of NPC-EXs on Ang II-induced endothelial injury through miR-210 which controls Nox2/ROS and VEGF/VEGFR2 signals were studied.

1. Introduction

Oxidative stress is well-known to play a critical role in a diverse array of cardiovascular disorders including hypertension, diabetic vasculopathy, hypercholesterolemia, and atherosclerosis [1–3]. Indeed, overproduction of reactive oxygen species (ROS) has been shown to induce dysfunction, proinflammatory, and apoptotic death of endothelial cells (ECs) [4–6]. Therefore, an efficient antioxidant defense system to prevent endothelial dysfunction is critical in the protection of vasculature.

Recently, neural crest stem cells have been reported to promote the survival of neurons under normal and oxidative stress conditions in a superoxide dismutase 2 mutant neuron cell line [7]. As one type of stem cells in the brain, neural progenitor cells (NPCs) residing in the subventricular zone contact the blood vessels and directly juxtapose to ECs [8]. The two types of cells could interact with each other through direct physical contact or through paracrine mechanisms with potentially different biological effects. As showed in our previous study [9], NPCs can decrease hypoxia/reoxygenation-induced ROS overproduction on ECs. However, the exact mechanism of NPCs against oxidative stress remains unclear. Exosomes (EXs), small vesicles secreted by most cells, are emerging as mediators for cell-cell communications. They can transfer the carried cargoes such as microRNAs (miRs) and proteins to distant/nearby cells and thereby modulate the recipient cell function [10–12]. Stem cell-derived EXs have been shown to convey the benefits of their parent cells [13–17]. For example, endothelial progenitor cell-derived vesicles can protect ECs against hypoxia/reoxygenation injury [16]. Mesenchymal stem cell-derived EXs can promote functional recovery and neurovascular plasticity after stroke in rats through miR-133 [13] and enhance cell survival in kidney

injury [17]. More recently, our group demonstrated that endothelial progenitor cell-derived vesicles from healthy controls have protective effects on the function of endothelial progenitor cells from diabetic patients through their carried miR-126 [14]. In order to explore the mechanism of NPCs protecting ECs from oxidative stress, we investigated whether EXs released from NPCs (NPC-EXs) can protect ECs from oxidative stress and dysfunction in an Ang II-induced injury model.

miR-210 is ubiquitously expressed in a wide range of cells, such as inducible pluripotent stem cells and bone marrow stem cells, and has versatile functions [18]. It is reported that miR-210 is a crucial element of ECs in response to hypoxia which considerably influences the endothelial angiogenic capability [19]. More studies have demonstrated that miR-210 not only influences cell survival by targeting apoptotic genes [20–22] but also displays antioxidant effect by reducing mitochondrial ROS production [23–25]. Recently, Wang et al. reported that EXs derived from inducible pluripotent stem cells can deliver miR-210 to the cardiomyocytes and protect the cardiomyocytes against H_2O_2-induced oxidative stress [15]. Nevertheless, there is no study investigating whether miR-210 is involved in the protective effects of NPC-EXs on ECs against oxidative stress.

In this study, we illustrated whether miR-210 participates in the protective effects of NPC-EXs on attenuating Ang II-induced ROS overproduction and dysfunction in ECs.

2. Materials and Methods

2.1. Cell Culture of NPCs and ECs. Human NPCs were purchased from ATCC® (ATCC-BYS012; Manassas, VA, USA) and cultured according to the manufacturer's protocol. Briefly, NPCs were cultured in complete growth medium which includes DMEM/F12 supplemented with the growth kit for NPC expansion (ATCC ACS-3003; Manassas, VA, USA). Medium was changed every other day. Human brain ECs were purchased from Cell Systems (Kirkland, WA, USA) and cultured with CSC complete medium (Cell Systems) containing 10% serum, 2% human recombinant growth factors, and 0.2% antibiotic solution under standard cell culture conditions (5% CO2, 37°C). Medium was changed twice a week.

2.2. Overexpression of miR-210 in NPCs. NPCs were expanded and used for transfection to up- or downregulate of miR-210 [19]. Briefly, the NPCs were cultured to 60–70% confluence and transfected with miR-210 mimic, miR-210 inhibitor, or the scramble control (SC) (40 nM, Exiqon, Woburn, MA) by using lipofectamine 2000 (Invitrogen, Carlsbad, CA) for 24 hrs according to the manufacturer's instruction. NPCs transfected with miR-210 SC, inhibitor, or mimic were denoted as $NPCs^{sc}$, $NPCs^{anti\text{-}miR\text{-}210}$, or $NPCs^{miR\text{-}210}$, respectively. NPCs cultured in complete culture medium served as control ($NPCs^{con}$). The three types of NPCs were used for producing corresponding EXs. All transfections were carried out in triplicate.

2.3. Preparation and Collection of EXs Released from NPCs. The protocol for collecting EXs from serum-free culture medium has been reported in our previous study [26]. Briefly, $NPCs^{con}$, $NPCs^{sc}$, $NPCs^{anti\text{-}miR\text{-}210}$, or $NPCs^{miR\text{-}210}$ were cultured in serum-free culture medium to release EXs which were denoted as $NPC\text{-}EXs^{con}$, $NPC\text{-}EXs^{sc}$, $NPC\text{-}EXs^{anti\text{-}miR\text{-}210}$, and $NPC\text{-}EXs^{miR\text{-}210}$. After 24 hrs, the medium was collected and centrifuged at $300g$ for 15 mins to remove dead cells. The supernatants were centrifuged at $2000g$ for 30 mins to remove cell debris, followed by centrifugation at $20{,}000g$ for 70 mins and ultracentrifugation at $170{,}000g$ for 90 mins to pellet EXs. The pelleted $NPC\text{-}EXs^{con}$, $NPC\text{-}EXs^{sc}$, $NPC\text{-}EXs^{anti\text{-}miR\text{-}210}$, or $NPC\text{-}EXs^{miR\text{-}210}$ were resuspended with phosphate-buffered saline (PBS) and aliquoted for nanoparticle tracking analysis (NTA) and coculture experiments. PBS was filtered through 20 nm filter (Whatman, Pittsburgh, PA).

2.4. Nanoparticle Tracking Analysis of NPC-EXs. The NanoSight NS300 (Malvern Instruments, Malvern, UK) was used to detect EXs as we previously reported [26]. Briefly, 700 μl diluted suspensions containing NPC-EXs were loaded into the sample chamber and the camera level was maintained at 10 for light scatter mode for sample analysis. Three videos of typically 30-second duration were taken, with a frame rate of 30 frames per second. Data was analyzed by NTA 3.0 software (Malvern Instruments, Malvern, UK) on a frame-by-frame basis. The experiment was repeated four times.

2.5. Labeling of NPC-EXs. NPC-EXs were labeled with a red fluorescence dye PKH26 (Sigma Aldrich, St. Louis, MO) as we previously reported [16]. In brief, NPC-EXs were incubated with 2 μM PKH26 dye in PBS for 5 mins at RT. An equal volume of FBS was added to stop staining. Then, NPC-EXs were pelleted by ultracentrifugation and resuspended with culture medium for coculture experiments.

2.6. Ang II Injury Model in ECs. ECs were seeded in 12-well plates (5×10^4 cells/well) during the logarithmic growth phase. When 70–80% confluent was reached, the cells were incubated with Ang II (0 or 10^{-6} M; Sigma-Aldrich, St. Louis, MO) for 24 hrs [27]. After coincubation, the medium was replaced with fresh culture medium. ECs were then used for coculture experiments or collected for various analyses.

2.7. Coculture of NPC-EXs with ECs. To further elucidate the effects NPC-EXs on ECs, ECs were divided into five coculture groups: vehicle (coculture medium only), $NPC\text{-}EXs^{con}$, $NPC\text{-}EXs^{sc}$, $NPC\text{-}EXs^{anti\text{-}miR\text{-}210}$, or $NPC\text{-}EXs^{miR\text{-}210}$. Briefly, the NPC-EXs labeled with PKH 26 were resuspended with CSC medium and added to the culture medium of ECs subjected to Ang II injury. The concentration of NPC-EXs (50 μg/ml) was determined based on our previous study [16]. After 24 hr coculture, the incorporation of NPC-EXs into ECs was observed by fluorescence microscopy (EVOS; Thermo Fisher Scientific). The level of cellular fluorescence intensity was analyzed by ImageJ (NIH) according to the instruction and a previous report [28]. The culture medium of ECs was collected for measuring the concentration of VEGF by ELISA. ECs were used for apoptosis, tube formation, and ROS production assays. The levels of miR-210, ephrin A3, Nox2, and p-VEGFR2/VEGFR2 in ECs were analyzed by quantitative RT-PCR and Western blot, respectively. ECs

cultured under normal condition were used as controls. The experiment was repeated for four times.

2.8. Apoptosis Assay of ECs. After coculture, ECs were detached for apoptosis assay by using the FITC Annexin V apoptosis detection kit (BD Biosciences, CA) [9]. Briefly, cells were washed with PBS, resuspended with 100 μL 1x annexin-binding buffer, incubated with 5 μL FITC-conjugated annexin V and 5 μL propidium iodide (PI) for 15 mins in the dark, and then analyzed by flow cytometry. The apoptotic cells were defined as annexin V+/PI− cells. The percentage of apoptotic cells was calculated as the following: annexin V+/PI− cells/total cells × 100%. The experiment was repeated four times.

2.9. Measurement of ROS. Intracellular ROS production was determined by dihydroethidium (DHE) (Sigma) staining. Briefly, cells were incubated with 2 μM DHE solution at 37°C for 2 hrs. Cells were then washed twice with PBS, and images were taken under a fluorescence microscope (EVOS, Life Sciences). The level of cellular fluorescence intensity was analyzed by ImageJ (NIH, Bethesda, MD) according to a previous report [29]. Data are expressed as fold of fluorescence compared with the control. ECs cultured with CSC medium were used as control.

2.10. Quantitative RT-PCR Analysis. After transfection, cells were washed twice with PBS. The miRs from NPCs and their released EXs, as well as the ECs cocultured with various NPC-EXs were extracted using mirVana miRNA isolation kit (Qiagen, Hilden, Germany). For detecting miR-210 level, reverse transcription (RT) reactions were performed by using mirVana qRT-PCR miRNA detection kit and hsa-miR-210 qRT-PCR primer set from Ambion. The RT primer was 5′-GTCGTATCCAGTGCAGGGTCCGAGGTATTCGCACTG GATACGACGACTGT-3′. The forward primer of miR-210 was 5′-CACGCAGTCGTA TCCAGTGCAGG-3′. The reverse primer of miR-210 was 5′-CCAGTGCAGGGTCCG AGG TA-3′. The expression of U6 was used as endogenous control for each sample. The forward primer of U6 was 5′-CT CGCTTCGGCAGCACA-3′, and the reverse primer of U6 was 5′-AACGCTTCACGAATTTGCGT-3′. Relative expression level of each gene was normalized to U6 and calculated using the $2^{-\Delta\Delta CT}$ method. The experiment was repeated four times.

2.11. Enzyme-Linked Immunosorbent Assay. The level of VEGF in the culture medium of ECs cocultured with NPC-EXs^{con}, NPC-EXs^{sc}, NPC-EXs$^{anti\text{-}miR\text{-}210}$, or NPC-EXs$^{miR\text{-}210}$ were measured by enzyme-linked immunosorbent assay (ELISA) according to the manufacturer's instructions (R&D Systems, Minneapolis, MN, USA). The concentration of VEGF was calculated as pg/ml of culture medium. Each group was triplicated. The experiment was repeated four times.

2.12. The Tube Formation Assay for ECs. The tube formation assay was conducted by using in vitro angiogenesis assay kit (Chemicon, Rosemont, IL). First, the ECMatrix solution was thawed and mixed with the ECMatrix diluent. Then, the ECMatrix mixture was placed in a 96-well tissue culture plate at 37°C for 1 hr to allow the matrix solution to solidify. ECs (1×10^4 cells/well) were seeded onto the solidified matrix and incubated at regular cell culture conditions (5% CO2, 37°C). After 24 hr post-seeding, 2 μg/ml calcein (Fisher Scientific, Hampton, NH) was directly added to the culture well and incubated for 20 mins prior to imaging under an inverted fluorescence microscope. Tubes were defined as a tube structure exhibiting a length 4 times of its width [30]. The number of tubes per field was determined. Five random microscopic fields were assessed in each well. The average number from the five fields represents a group.

Table 1: NTA analysis of the size and concentration of various NPC-EXs.

EX type	Size range (nm)	Concentration ($\times 10^6$ particles/ml)
NPC-EXs^{con}	102 ± 30	5.67 ± 0.07
NPC-EXs^{sc}	104 ± 43	5.58 ± 0.11
NPC-EXs$^{anti\text{-}miR\text{-}210}$	100 ± 51	5.69 ± 0.18
NPC-EXs$^{miR\text{-}210}$	105 ± 62	5.74 ± 0.08

NPC-EXs^{con}, NPC-EXs^{sc}, NPC-EXs$^{anti\text{-}miR\text{-}210}$, and NPC-EXs$^{miR\text{-}210}$ represent EXs released from NPCs cultured in culture medium (control) and transfected with scramble control, miR-210 inhibitor, or miR-210 mimic. Data are expressed as mean ± SEM. $N = 4$/group.

2.13. Western Blot Analysis. After 24 hr treatments, proteins of ECs in different groups were extracted with cell lysis buffer (Thermo Fisher Scientific, Waltham, MA) supplemented with complete mini protease inhibitor tablet (Roche, Basel, Switzerland). Then, the protein lysates were electrophoresed through SDS-PAGE gel and transferred onto PVDF membranes. The membranes were blocked with 5% nonfat milk for 1 hr at room temperature and incubated with primary antibody against ephrin A3 (1 : 500; Abcam, Cambridge, MA), Nox2 (1 : 1000; Abcam, Cambridge, MA), VEGFR2 (1 : 1000; Abcam, Cambridge, MA), p-VEGFR2 (p-Flk1; 1 : 1000; Abcam, Cambridge, MA), or β-actin (1 : 4000; Sigma, St. Louis, MO) at 4°C overnight. On the next day, membranes were washed and incubated with horseradish-peroxidase-conjugated anti-rabbit or anti-mouse IgG (1 : 40,000; Jackson Immuno Research Lab, West Grove, PA) for 1 hr at room temperature. Blots were developed with enhanced chemiluminescence developing solutions, and images were quantified under ImageJ software. The experiment was repeated four times.

2.14. Statistical Analysis. All experiments were repeated for four times. Data are expressed as mean ± SEM. Multiple comparisons were analyzed by one- or two-way ANOVA followed by LSD post hoc test. SPSS 17.0 statistical software was used for analyzing the data. For all measurements, a $p < 0.05$ was considered statistically significant.

3. Results

3.1. Transfection of miR-210 Mimic and Inhibitor Altered the Level of miR-210 in NPCs and NPC-EXs. Upon the results obtained from NTA analysis (Table 1), modulation

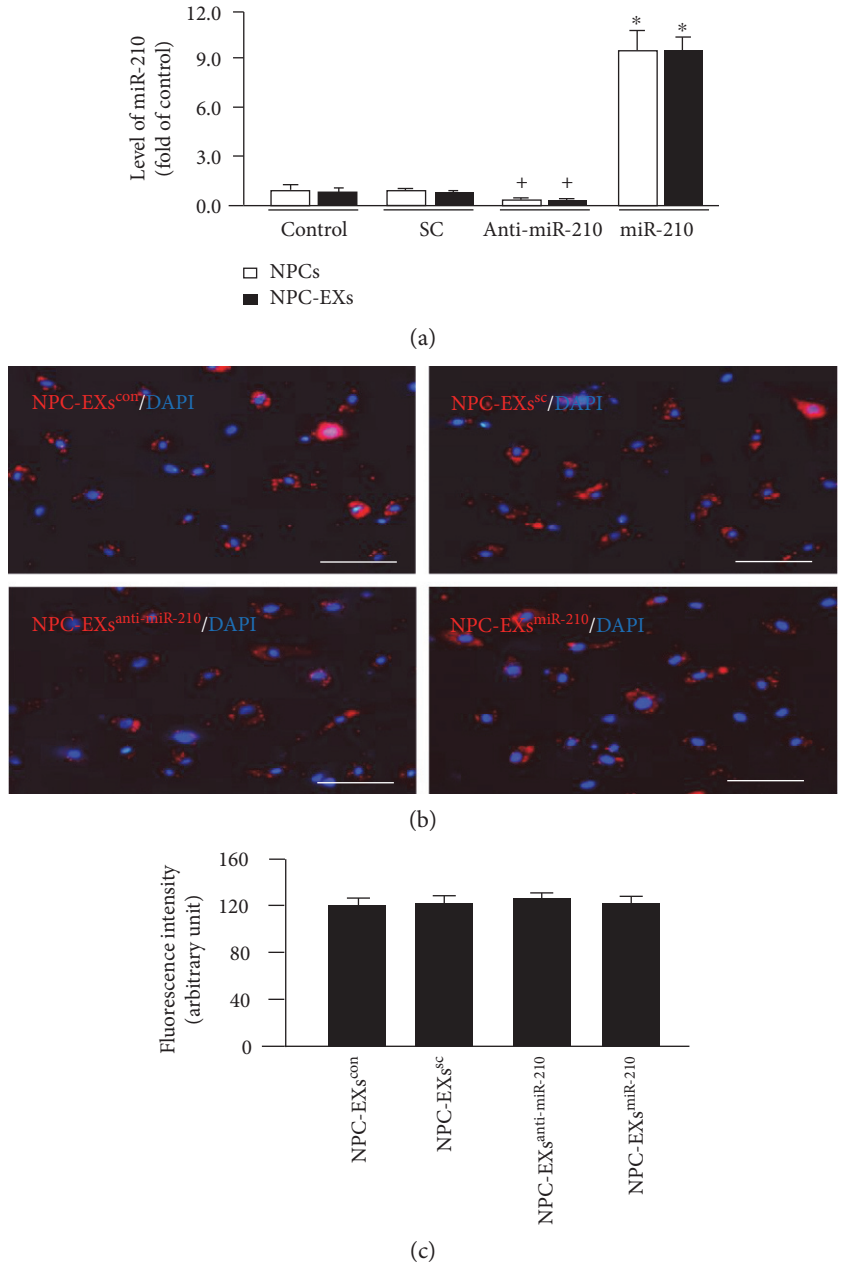

Figure 1: The levels of miR-210 in NPCs and their released NPC-EXs were changed by miR-210 mimic or inhibitor. (a) Summarized data showing the levels of miR-210 in NPCs and NPC-EXs. $^{*}p < 0.05$ versus control or SC or anti-miR-210; $^{+}p < 0.05$ versus control or SC. SC: scramble control of miR-210. (b) Representative images showing the incorporation of NPC-EXs into the cytoplasm of ECs. (c) Summarized data showing the fluorescence intensity in ECs. Data are expressed as mean ± SEM. $N = 4$/group.

of miR-210 did not change the size and the concentration of EXs released from NPCs (versus NPC-EXs^{con} or NPC-EXs^{sc}, $p > 0.05$). As shown in Figure 1(a), transfection of the miR-210 mimic significantly increased miR-210 level in NPCs. As expected, miR-210 level was higher in NPC-EXs$^{miR\text{-}210}$ than that in NPC-EXs^{con} and NPC-EXs^{sc}. On the contrary, miR-210 inhibitor significantly decreased the level of miR-210 in NPCs and their released EXs.

3.2. NPC-EXs$^{miR\text{-}210}$ Significantly Upregulated the Level of miR-210 and Downregulated Ephrin A3 Level in ECs. As shown in Figures 1(b) and 1(c), PKH26-labeled NPC-EXs were observed in the cytoplasm of ECs after 24 hr of coculture, indicating EXs were uptaken by ECs. There was no significant difference of the fluorescence intensity among different groups.

In order to evaluate whether coculture with NPC-EXs can alter the level of miR-210 in ECs, we conducted quantitative RT-PCR to determine the level of miR-210 in ECs after different treatments. As shown in Figure 2(a), Ang II downregulated the level of miR-210 in ECs (versus control, $p < 0.05$). In the treatment groups, coculture with NPC-EXs^{con} or NPC-EXs^{sc} alone significantly upregulated miR-210 level in ECs (versus vehicle, $p < 0.05$). NPC-EXs$^{anti\text{-}miR\text{-}210}$ did not

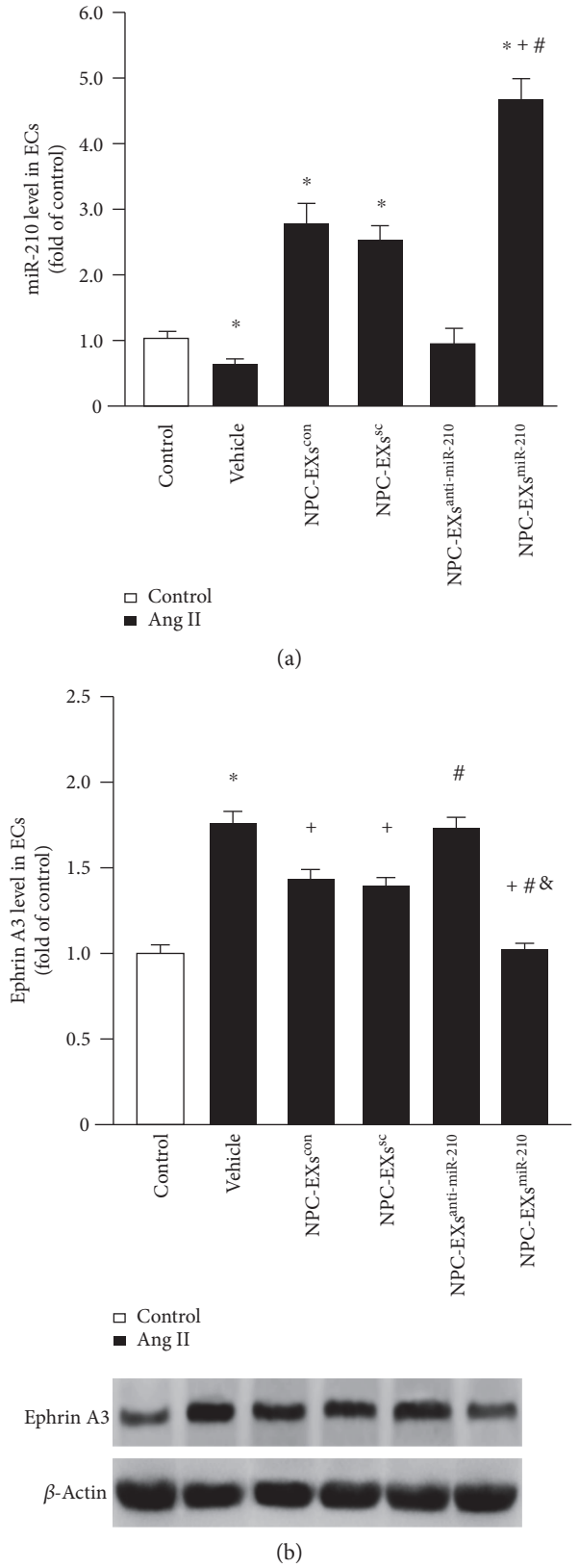

Figure 2: Up- or downregulation of miR-210 affected the effects of NPC-EXs on the levels of miR-210 and its target gene ephrin A3. (a) The level of miR-210 in ECs treated with various NPC-EXs. (b) Summarized data and representative bands showing the protein level of ephrin A3 in ECs treated with various NPC-EXs. $^{*}p < 0.05$ versus control; $^{+}p < 0.05$ versus vehicle; $^{\#}p < 0.05$ versus NPC-EXs^{con} or NPC-EXs^{sc}; $^{\&}p < 0.05$ versus NPC-EXs$^{anti\text{-}miR\text{-}210}$. EXs released from NPCs^{con}, NPCs^{sc}, NPC-EXs$^{anti\text{-}miR\text{-}210}$, or NPCs$^{miR\text{-}210}$ were denoted as NPC-EXs^{con}, NPC-EXs^{sc}, NPC-EXs$^{anti\text{-}miR\text{-}210}$, or NPC-EXs$^{miR\text{-}210}$. Data are expressed as mean ± SEM. $N = 4$/group.

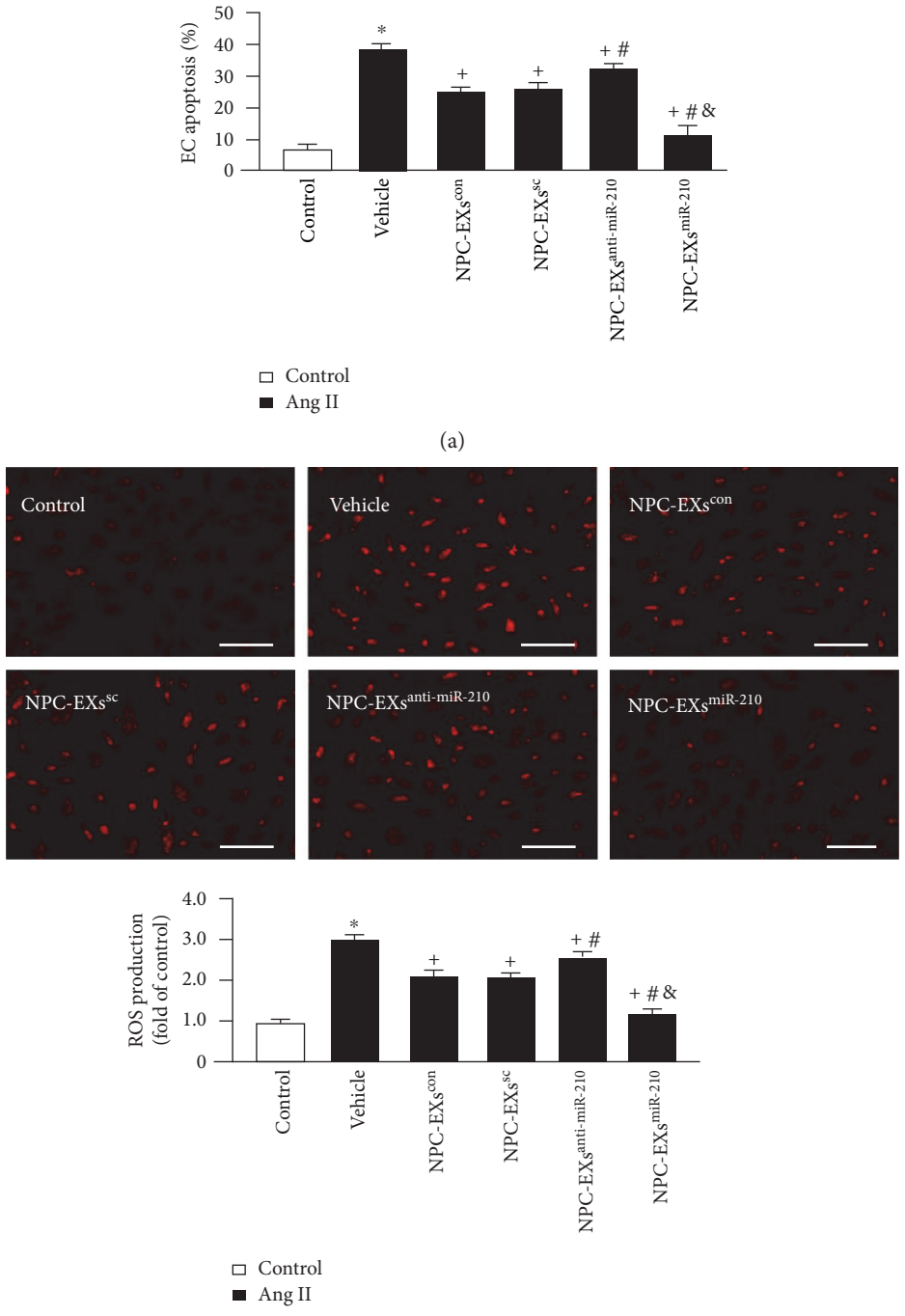

Figure 3: Up- or downregulation of miR-210 modulated the effects of NPC-EXs on reducing Ang II-induced apoptosis and ROS overproduction in ECs. (a) The apoptotic rate of ECs treated with different NPC-EXs. (b) Up: representative images showing DHE staining of ECs treated with different NPC-EXs; bar: 100 μm; bottom: summarized data; $^{*}p < 0.05$ versus con; $^{+}p < 0.05$ versus vehicle; $^{\#}p < 0.05$ versus NPC-EXs^{con} or NPC-EXs^{sc}; $^{\&}p < 0.05$ versus NPC-EXs$^{anti\text{-}miR\text{-}210}$. EXs released from NPCs^{con}, NPCs^{sc}, NPC-EXs$^{anti\text{-}miR\text{-}210}$, or NPCs$^{miR\text{-}210}$ were denoted as NPC-EXs^{con}, NPC-EXs^{sc}, NPC-EXs$^{anti\text{-}miR\text{-}210}$, or NPC-EXs$^{miR\text{-}210}$. Data are expressed as mean ± SEM. $N = 4$/group.

significantly alter the level of miR-210 in Ang II-injured ECs (versus vehicle, $p > 0.05$), whereas, NPC-EXs$^{miR\text{-}210}$ remarkably raised the level of miR-210 in ECs (versus NPC-EXs^{con} or NPC-EXs^{sc} or NPC-EXs$^{anti\text{-}miR\text{-}210}$, $p < 0.05$). These data suggest that NPC-EXs can deliver miR-210 into ECs in vitro.

We also determined the protein level of ephrin A3, a target gene of miR-210, in ECs after coculture. Our data (Figure 2(b)) showed that the ephrin A3 level was upregulated in Ang II-injured ECs (versus control, $p < 0.05$), which was downregulated by NPC-EXs^{con} or NPC-EXs^{sc}

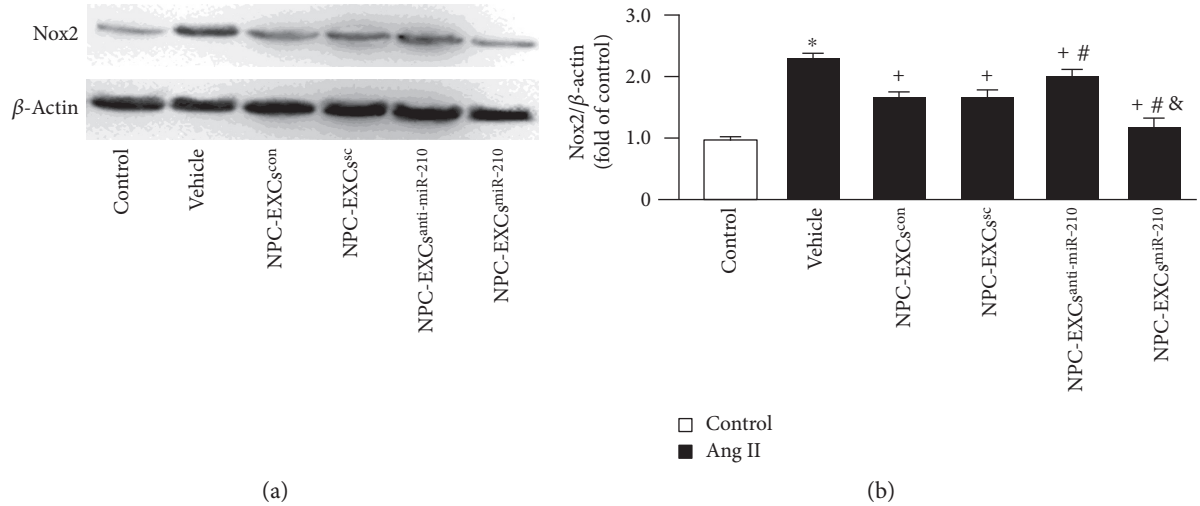

(a) (b)

Figure 4: Manipulation of miR-210 with inhibitor or mimic altered the effect of NPC-EXs on reducing Ang II-induced Nox2 expression. (a) Representative Western blot bands. (b) Summarized data showing the expression of Nox2 in ECs treated with different NPC-EXs; $^{*}p < 0.05$ versus con; $^{+}p < 0.05$ versus vehicle; $^{\#}p < 0.05$ versus NPC-EXs^{con} or NPC-EXs^{sc}; $^{\&}p < 0.05$ versus NPC-EXs$^{anti\text{-}miR\text{-}210}$. EXs released from NPCs^{con}, NPCs^{sc}, NPC-EXs$^{anti\text{-}miR\text{-}210}$, or NPCs$^{miR\text{-}210}$ were denoted as NPC-EXs^{con}, NPC-EXs^{sc}, NPC-EXs$^{anti\text{-}miR\text{-}210}$, or NPC-EXs$^{miR\text{-}210}$. Data are expressed as mean ± SEM. $N = 4$/group.

coculture (versus vehicle, $p < 0.05$). NPC-EXs$^{anti\text{-}miR\text{-}210}$ did not significantly affect, while NPC-EXs$^{miR\text{-}210}$ upregulated the level of ephrin A3 in Ang II-injured ECs. These findings reflect that NPC-EXs and NPC-EXs$^{miR\text{-}210}$ could transfer miR-210 to ECs and modulate the expression of its target gene, ephrin A3, in ECs.

3.3. NPC-EXs$^{anti\text{-}miR\text{-}210}$ Were Less, Whereas NPC-EXs$^{miR\text{-}210}$ Were More Effective on Reducing Ang II-Induced Apoptosis, ROS Overproduction, and Nox2 Upregulation on ECs. To verify the model of Ang II-induced EC injury, we conducted flow cytometry and DHE staining to evaluate the apoptotic rate and ROS production, respectively. Our results (Figure 3) showed that Ang II significantly increased the percentage of ECs in the early apoptosis phase and the level of ROS production (versus control, $p < 0.05$).

To determine the effects of NPC-EXs on ECs against Ang II-induced oxidative stress injury, we cocultured Ang II-injured ECs with various NPC-EXs. Our data showed that coculture with NPC-EXs^{con} or NPC-EXs^{sc} alone can reduce Ang II-induced apoptosis and ROS overproduction (versus vehicle, $p < 0.05$). NPC-EXs$^{anti\text{-}miR\text{-}210}$ can decrease these detrimental effects of Ang II, but was less than NPC-EXs^{con} and NPC-EXs^{sc} did (versus NPC-EXs^{con} or NPC-EXs^{sc}, $p < 0.05$). NPC-EXs$^{miR\text{-}210}$ had the most effects on decreasing Ang II-induced apoptosis and ROS production of ECs among the four types of NPC-EXs.

In addition, we analyzed the expression of Nox2 in ECs after cocultured with different NPC-EXs. Our Western blot results (Figure 4) showed that Ang II upregulated Nox2 expression in ECs (versus control, $p < 0.05$). Coculture with NPC-EXs^{con} or NPC-EXs^{sc} alone significantly downregulated Nox2 expression (versus vehicle, $p < 0.05$). NPC-EXs$^{anti\text{-}miR\text{-}210}$ can downregulate Nox2 expression, but had much less effect than NPC-EXs^{con} and NPC-EXs^{sc} had (versus NPC-EXs^{con} or NPC-EXs^{sc}, $p < 0.05$). Similarly, NPC-EXs$^{miR\text{-}210}$ had the most effect on decreasing Ang II-induced Nox2 expression in ECs.

Collectively, this data suggests that miR-210 plays a role in the protective effects of NPC-EXs on ECs against Ang II-induced oxidative stress, and exogenous miR-210 can boost the antioxidant and antiapoptosis effects elicited by NPC-EXs.

3.4. NPC-EXs$^{anti\text{-}miR\text{-}210}$ Were Less, Whereas NPC-EXs$^{miR\text{-}210}$ Were More Effective on Increasing VEGF Secretion and Improving the Tube Formation Ability of ECs. In order to assess whether NPC-EXs can improve the endothelial angiogenic function compromised by Ang II, we analyzed VEGF level in the culture medium and the tube formation ability of ECs. Our data showed that the level of VEGF in the culture medium was decreased in ECs injured by Ang II (versus control, $p < 0.05$). In the treatment groups, coculture with NPC-EXs^{con} and NPC-EXs^{sc} increased the VEGF level (versus vehicle, $p < 0.05$), whereas NPC-EXs$^{anti\text{-}miR\text{-}210}$ had less effect than NPC-EXs^{con} and NPC-EXs^{sc} had (versus NPC-EXs^{con} or NPC-EXs^{sc}, $p < 0.05$). Similarly, NPC-EXs$^{miR\text{-}210}$ had the most effect on upregulating VEGF secretion of ECs among the four types of NPC-EXs (Figure 5(a)).

Similarly, the tube formation ability of ECs was compromised by Ang II (versus control, $p < 0.05$). Coculture with NPC-EXs^{con} or NPC-EXs^{sc} alone significantly improved the tube formation ability of ECs subjected to Ang II (versus vehicle, $p < 0.05$). NPC-EXs$^{anti\text{-}miR\text{-}210}$ displayed less effect than NPC-EXs^{con} or NPC-EXs^{sc} did. Likely, NPC-EXs$^{miR\text{-}210}$ had the most effect on promoting tube formation (Figure 5(b)). Taken together, these results indicate that miR-210 is involved in the effect elicited by NPC-EXs on improving the angiogenic function of Ang II-injured ECs.

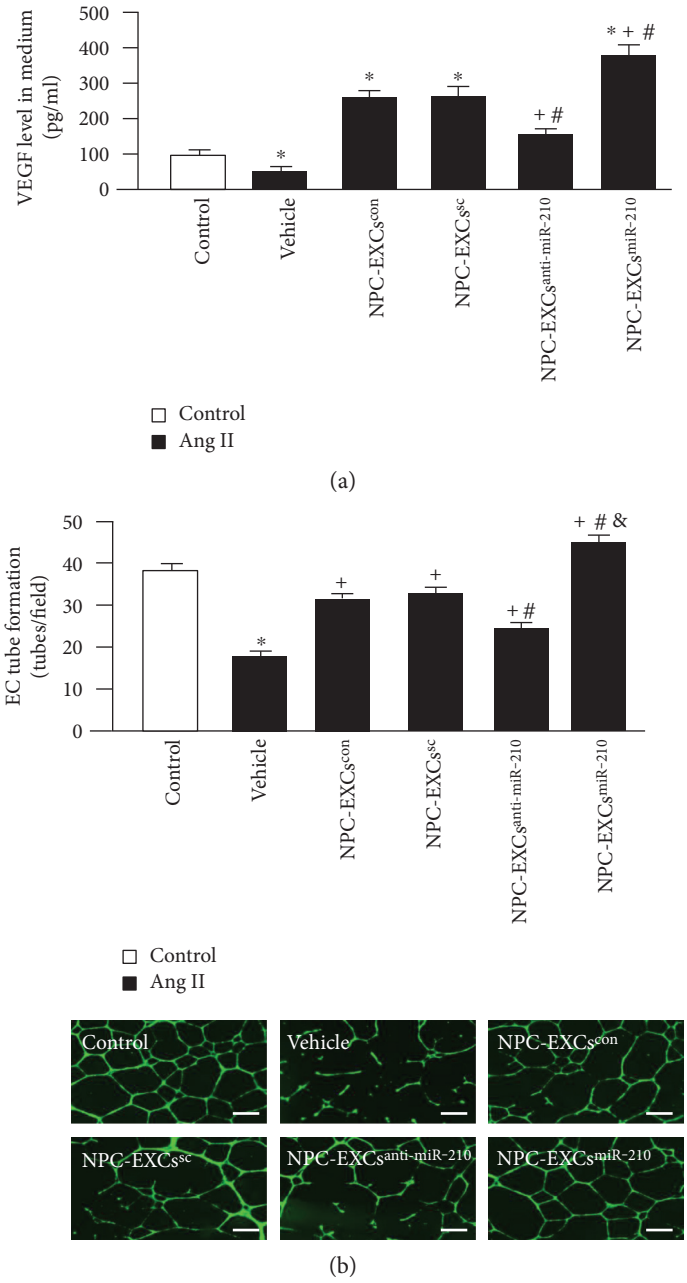

Figure 5: Modulation of miR-210 altered the effect of NPC-EXs on improving the VEGF secretion and tube formation ability of ECs. (a) VEGF level in the culture medium of ECs treated with various NPC-EXs. (b) Summarized data of tube formation and representative images showing the tube formation of ECs treated by various NPC-EXs; bar: 500 μm. $^{*}p < 0.05$ versus control; $^{+}p < 0.05$ versus vehicle; $^{\#}p < 0.05$ versus NPC-EXs^{con} or NPC-EXs^{sc}; $^{\&}p < 0.05$, versus NPC-EXs$^{anti\text{-}miR\text{-}210}$. Data are expressed as mean ± SEM. $N = 4$/group.

3.5. NPC-EXs$^{anti\text{-}miR\text{-}210}$ Were Less, Whereas NPC-EXs$^{miR\text{-}210}$ Were More Effective on Upregulating the Expression of p-VEGFR2/VEGFR2 in ECs. As shown in Figure 6, the ratio of p-VEGFR2/VEGFR2 in ECs was decreased by Ang II (versus control, $p < 0.05$). In the treatment groups, coculture with NPC-EXs^{con} or NPC-EXs^{sc} increased the phosphorylation of VEGFR2 (versus control or vehicle, $p < 0.05$). NPC-EXs$^{anti\text{-}miR\text{-}210}$ also raised the expression ratio of p-VEGFR2/VEGFR2, but the effect was less than NPC-EXs^{con} or NPC-EXs^{sc} had (versus NPC-EXs^{con} or NPC-EXs^{sc}, $p < 0.05$). Similarly, NPC-EXs$^{miR\text{-}210}$ had the strongest effect on upregulating the ratio of p-VEGFR2/VEGFR2 in ECs subjected to Ang II injury (versus NPC-EXs^{con}, NPC-EXs^{sc}, or NPC-EXs$^{anti\text{-}miR\text{-}210}$, $p < 0.05$).

4. Discussion

In the present study, we have demonstrated that NPC-EXs have protective effects against Ang II-induced oxidative stress, cell death, and angiogenic dysfunction in ECs, which

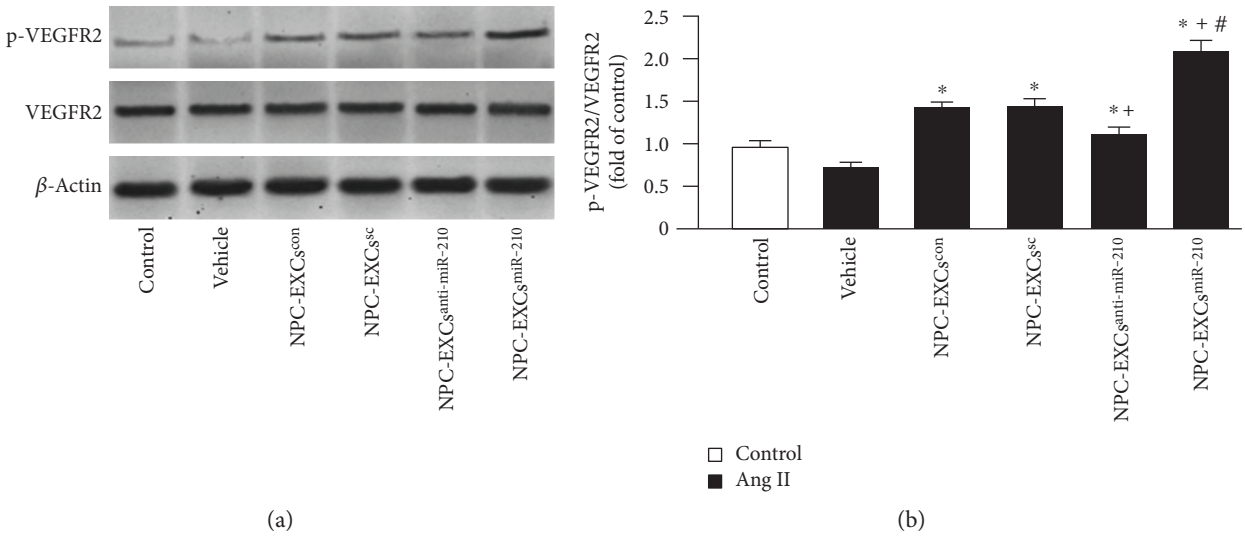

Figure 6: Up- and downregulation of miR-210 altered the effect of NPC-EXs on the expression of p-VEGFR2/VEGFR2 in ECs. (a) Representative western blot bands. (b) Summarized data. $^{*}p < 0.05$ versus vehicle; $^{+}p < 0.05$ versus NPC-EXs^{con} or NPC-EXs^{sc}; $^{\#}p < 0.05$ versus NPC-EXs$^{anti\text{-}miR\text{-}210}$. Data are expressed as mean ± SEM. $N = 4$/group.

are at least partly through Nox2/ROS and VEGF/VEGFR2 signaling pathways modulated by miR-210.

Oxidative stress is the major cause of endothelial dysfunction which is implicated in various vascular diseases [31]. Ang II has been well documented to trigger ROS overproduction and decrease the production/bioavailability of nitric oxide of ECs, which consequently contribute to endothelial dysfunction [32, 33]. In this study, we used Ang II to construct an EC oxidative stress model. As agreed with previous reports [27, 34], Ang II resulted in increasing of apoptosis, overproduction of ROS, and impairment of angiogenic function (tube formation ability and VEGF secretion), along with the upregulation of Nox2 level and downregulation of the ratio of p-VEGFR2/VEGFR2 in ECs.

We previously demonstrated that NPCs could decrease apoptosis and ROS overproduction on hypoxia/reoxygenation-injured ECs [9]. Our study is supported by a recent report showing that neural crest-derived stem cells promote the survival of neurons under normal and oxidative stress conditions in a mutant neuron cell line [7]. However, the underlying mechanism requires further investigation. Currently, EXs are emerging as cell-cell communicators. Mounting evidence shows that stem cell-derived EXs harbor the benefits of their parent cells and can alter the function of recipient cells [13, 16, 17]. For instance, mesenchymal stem cell-derived extracellular vesicles can enhance cell survival in kidney injury [17] and promote functional recovery and neurovascular plasticity after stroke in rats [13]. We have demonstrated that endothelial progenitor cell-derived vesicles can protect ECs against hypoxia/reoxygenation [16]. In this study, we investigated whether NPC-EXs could rescue injured ECs following direct oxidative stress by using the Ang II injury model. In order to test our hypothesis, we cocultured NPC-EXs^{con} with Ang II-injured ECs and found that NPC-EXs^{con} could be uptaken by ECs and can attenuate Ang II-induced apoptosis, ROS overproduction, and Nox2 upregulation. In addition, the tube formation capacity and VEGF secretion capacities compromised by Ang II were also rescued by NPC-EXs^{con}. All of these findings suggest that NPC-EXs can protect ECs against Ang II, associated with the suppression of Nox2 expression and subsequently inhibiting ROS overproduction.

Interestingly, we also found that the level of miR-210 was increased in ECs after coincubation with NPC-EXs. This raised the hypothesis that the protective effects of NPC-EXs on Ang II-induced ECs might be related with miR-210. Previous studies have demonstrated that miR-210 is ubiquitously expressed in a wide range of cells and displays versatile functions such as antioxidative stress [15, 25, 35, 36] and apoptosis defense [20–22]. Blockade of miR-210 in myoblasts greatly increases myoblast cell sensitivity to oxidative stress and mitochondrial dysfunction [25]. Overexpression of miR-210 enhances the survival of mesenchymal stem cells in an oxidative stress environment [35] and reduces ROS overproduction as well as cardiomyocyte death in response to hypoxia-reoxygenation [36]. Recently, Wang et al. reported that EXs derived from inducible pluripotent stem cells can deliver miR-210 to cardiomyocytes and protect them against H_2O_2-induced oxidative stress [15]. In order to investigate the potential mechanisms, we tested our hypothesis that miR-210 modulates the beneficial effects exhibited by NPC-EXs on Ang II-injured ECs. First, we up- or downregulated miR-210 in NPCs and found that the miR-210 level was parallelly raised or reduced in their corresponding EXs, NPC-EXs$^{miR\text{-}210}$, and NPC-EXs$^{anti\text{-}miR\text{-}210}$. This suggests that NPCs carried by miR-210 was packaged into NPC-EXs. Next, we cocultured NPC-EXs$^{miR\text{-}210}$, NPC-EXs$^{anti\text{-}miR\text{-}210}$, and their controls (NPC-EXs^{sc}) with Ang II-injured ECs. Our data showed that both NPC-EXs^{sc} and NPC-EXs$^{miR\text{-}210}$ increased the miR-210 level in ECs. Meanwhile, we found that the protein level of ephrin A3, a target gene of miR-210 [19], was significantly downregulated by NPC-EXs$^{miR\text{-}210}$ in Ang II-injured ECs. These results reflect

that NPC-EXs can deliver miR-210 into ECs. Besides, we found that NPC-EXs$^{miR\text{-}210}$ had the strongest effects on decreasing Ang II-induced apoptosis and ROS production, indicating miR-210 can boost the protection effects of NPC-EXs on ECs. As one of the most prominent sources of vascular ROS [37], Nox2 level was also evaluated. We found the Nox2 level in ECs was remarkably decreased by NPC-EXs$^{miR\text{-}210}$, suggesting that the antioxidant effect of NPC-EXs might be associated with the Nox2/ROS signal. In contrast, NPC-EXs$^{anti\text{-}miR\text{-}210}$ partially reduced the protective effects of NPC-EXs, which further confirmed the important role of miR-210 in NPC-EXs for protecting ECs from Ang II-induced injury. This data also suggests that other cargoes such as proteins and cytokines carried by NPC-EXs might also participate in the protection event.

As we know, VEGF is a proangiogenic factor [38] which could be modulated by ephrin A3 [39]. In the present study, our data indicated that NPC-EXs$^{miR\text{-}210}$ could decrease ephrin A3 level whereas increase VEGF level in the culture medium of ECs, suggesting that ephrin A3 is connecting miR-210 and VEGF in ECs. The result showing the increase of VEGF level is coherent with that NPC-EXs$^{miR\text{-}210}$ improved tube formation ability of ECs compromised by Ang II. VEGFR2 is responsible for most downstream angiogenic effects of VEGF [40]. Binding of VEGF to VEGFR2 can activate downstream survival and migration pathways involving PI3-kinase/Akt and focal adhesion kinase, respectively [41]. In order to determine whether the increased level of VEGF can activate VEGFR2 signal, we used Western blots to evaluate the changes in the signaling proteins VEGFR2 and its phosphorylation. We found the total expression of VEGFR2 in ECs was not changed after NPC-EX treatment, while the expression of p-VEGFR2 was remarkably increased by NPC-EXs$^{miR\text{-}210}$, indicating the activation of the VEGF/VEGFR2 signal. Meanwhile, our data indicated that NPC-EXs$^{anti\text{-}miR\text{-}210}$ also upregulated the phosphorylating VEGFR2, though at a less extent as compared to that of NPC-EXs^{con} or NPC-EXs^{sc} had. This effect could be resulted from other cargoes such as proteins and cytokines carried by NPC-EXs$^{anti\text{-}miR\text{-}210}$. Collectively, these data reflect that miR-210 can modulate the effect of NPC-EXs on ECs subjected to Ang II injury by activating the VEGF/VEGFR2 signal.

5. Conclusion

Our results demonstrate that miR-210 can modulate the effects of NPC-EXs on protecting ECs from Ang II-induced oxidative stress, majorly through the Nox2/ROS and VEGF/VEGFR2 signals.

Conflicts of Interest

There is no conflict of interests.

Authors' Contributions

Hua Liu, Jinju Wang, and Yusen Chen contributed equally to this work.

Acknowledgments

This work was supported by the American Heart Association (16SDG26420078), the Natural Science Foundation of Hubei Province (2015CFA084), the Outstanding Young Scientific and Technological Innovation Team in the Colleges and Universities of Hubei Province, China (T201523), and the Scientific Research Project supported by the Wuhan Sports University (2014QZ07, 2016XH24).

References

[1] Y. Ohara, T. E. Peterson, and D. G. Harrison, "Hypercholesterolemia increases endothelial superoxide anion production," *The Journal of Clinical Investigation*, vol. 91, no. 6, pp. 2546–2551, 1993.

[2] S. Grunfeld, C. A. Hamilton, S. Mesaros et al., "Role of superoxide in the depressed nitric oxide production by the endothelium of genetically hypertensive rats," *Hypertension*, vol. 26, no. 6 Part 1, pp. 854–857, 1995.

[3] S. Rajagopalan, X. P. Meng, S. Ramasamy, D. G. Harrison, and Z. S. Galis, "Reactive oxygen species produced by macrophage-derived foam cells regulate the activity of vascular matrix metalloproteinases in vitro. Implications for atherosclerotic plaque stability," *The Journal of Clinical Investigation*, vol. 98, no. 11, pp. 2572–2579, 1996.

[4] J. Bauersachs, A. Bouloumie, D. Fraccarollo, K. Hu, R. Busse, and G. Ertl, "Endothelial dysfunction in chronic myocardial infarction despite increased vascular endothelial nitric oxide synthase and soluble guanylate cyclase expression: role of enhanced vascular superoxide production," *Circulation*, vol. 100, no. 3, pp. 292–298, 1999.

[5] M. Aoki, T. Nata, R. Morishita et al., "Endothelial apoptosis induced by oxidative stress through activation of NF-κB: antiapoptotic effect of antioxidant agents on endothelial cells," *Hypertension*, vol. 38, no. 1, pp. 48–55, 2001.

[6] N. Marui, M. K. Offermann, R. Swerlick et al., "Vascular cell adhesion molecule-1 (VCAM-1) gene transcription and expression are regulated through an antioxidant-sensitive mechanism in human vascular endothelial cells," *The Journal of Clinical Investigation*, vol. 92, no. 4, pp. 1866–1874, 1993.

[7] T. Aggarwal, J. Hoeber, P. Ivert, S. Vasylovska, and E. N. Kozlova, "Boundary cap neural crest stem cells promote survival of mutant SOD1 motor neurons," *Neurotherapeutics*, vol. 9, pp. 1–11, 2017.

[8] M. Tavazoie, L. Van der Veken, V. Silva-Vargas et al., "A specialized vascular niche for adult neural stem cells," *Cell Stem Cell*, vol. 3, no. 3, pp. 279–288, 2008.

[9] J. Wang, Y. Chen, Y. Yang et al., "Endothelial progenitor cells and neural progenitor cells synergistically protect cerebral endothelial cells from hypoxia/reoxygenation-induced injury via activating the PI3K/Akt pathway," *Molecular Brain*, vol. 9, no. 1, p. 12, 2016.

[10] Y. Shao, Y. Shen, T. Chen, F. Xu, X. Chen, and S. Zheng, "The functions and clinical applications of tumor-derived exosomes," *Oncotarget*, vol. 7, no. 37, pp. 60736–60751, 2016.

[11] Y. Chen, Y. Tang, W. Long, and C. Zhang, "Stem cell-released microvesicles and exosomes as novel biomarkers and treatments of diseases," *Stem Cells International*, vol. 2016, Article ID 2417268, 2 pages, 2016.

[12] N. Tang, B. Sun, A. Gupta, H. Rempel, and L. Pulliam, "Monocyte exosomes induce adhesion molecules and cytokines via activation of NF-κB in endothelial cells," *The FASEB Journal*, vol. 30, no. 9, pp. 3097–3106, 2016.

[13] H. Xin, Y. Li, Z. Liu et al., "miR-133b promotes neural plasticity and functional recovery after treatment of stroke with multipotent mesenchymal stromal cells in rats via transfer of exosome-enriched extracellular particles," *Stem Cells*, vol. 31, no. 12, pp. 2737–2746, 2013.

[14] K. Wu, Y. Yang, Y. Zhong et al., "The effects of microvesicles on endothelial progenitor cells are compromised in type 2 diabetic patients via downregulation of the miR-126/VEGFR2 pathway," *American Journal of Physiology. Endocrinology and Metabolism*, vol. 310, no. 10, pp. E828–E837, 2016.

[15] Y. Wang, L. Zhang, Y. Li et al., "Exosomes/microvesicles from induced pluripotent stem cells deliver cardioprotective miRNAs and prevent cardiomyocyte apoptosis in the ischemic myocardium," *International Journal of Cardiology*, vol. 192, pp. 61–69, 2015.

[16] J. Wang, S. Chen, X. Ma et al., "Effects of endothelial progenitor cell-derived microvesicles on hypoxia/reoxygenation-induced endothelial dysfunction and apoptosis," *Oxidative Medicine and Cellular Longevity*, vol. 2013, Article ID 572729, 9 pages, 2013.

[17] S. Bruno, C. Grange, F. Collino et al., "Microvesicles derived from mesenchymal stem cells enhance survival in a lethal model of acute kidney injury," *PloS One*, vol. 7, no. 3, article e33115, 2012.

[18] Y. Gong, F. Xu, L. Zhang et al., "MicroRNA expression signature for Satb2-induced osteogenic differentiation in bone marrow stromal cells," *Molecular and Cellular Biochemistry*, vol. 387, no. 1-2, pp. 227–239, 2014.

[19] P. Fasanaro, Y. D'Alessandra, V. Di Stefano et al., "MicroRNA-210 modulates endothelial cell response to hypoxia and inhibits the receptor tyrosine kinase ligand ephrin-A3," *The Journal of Biological Chemistry*, vol. 283, no. 23, pp. 15878–15883, 2008.

[20] H. W. Kim, H. K. Haider, S. Jiang, and M. Ashraf, "Ischemic preconditioning augments survival of stem cells via miR-210 expression by targeting caspase-8-associated protein 2," *The Journal of Biological Chemistry*, vol. 284, no. 48, pp. 33161–33168, 2009.

[21] S. Y. Chan and J. Loscalzo, "MicroRNA-210: a unique and pleiotropic hypoxamir," *Cell Cycle*, vol. 9, no. 6, pp. 1072–1083, 2010.

[22] C. Devlin, S. Greco, F. Martelli, and M. Ivan, "miR-210: more than a silent player in hypoxia," *IUBMB Life*, vol. 63, no. 2, pp. 94–100, 2011.

[23] Y. Jiang, L. Li, X. Tan, B. Liu, Y. Zhang, and C. Li, "miR-210 mediates vagus nerve stimulation-induced antioxidant stress and anti-apoptosis reactions following cerebral ischemia/reperfusion injury in rats," *Journal of Neurochemistry*, vol. 134, no. 1, pp. 173–181, 2015.

[24] J. H. Kim, S. G. Park, S. Y. Song, J. K. Kim, and J. H. Sung, "Reactive oxygen species-responsive miR-210 regulates proliferation and migration of adipose-derived stem cells via PTPN2," *Cell Death & Disease*, vol. 4, no. 4, p. e588, 2013.

[25] L. Cicchillitti, V. Di Stefano, E. Isaia et al., "Hypoxia-inducible factor 1-alpha induces miR-210 in normoxic differentiating myoblasts," *The Journal of Biological Chemistry*, vol. 287, no. 53, pp. 44761–44771, 2012.

[26] J. Wang, R. Guo, Y. Yang et al., "The novel methods for analysis of exosomes released from endothelial cells and endothelial progenitor cells," *Stem Cells International*, vol. 2016, Article ID 2639728, 12 pages, 2016.

[27] X. Xiao, C. Zhang, X. Ma et al., "Angiotensin-(1-7) counteracts angiotensin II-induced dysfunction in cerebral endothelial cells via modulating Nox2/ROS and PI3K/NO pathways," *Experimental Cell Research*, vol. 336, no. 1, pp. 58–65, 2015.

[28] E. C. Jensen, "Quantitative analysis of histological staining and fluorescence using ImageJ," *The Anatomical Record*, vol. 296, no. 3, pp. 378–381, 2013.

[29] H. Xia, S. Suda, S. Bindom et al., "ACE2-mediated reduction of oxidative stress in the central nervous system is associated with improvement of autonomic function," *One*, vol. 6, no. 7, article e22682, 2011.

[30] T. G. Chen, J. Z. Chen, and X. X. Wang, "Effects of rapamycin on number activity and eNOS of endothelial progenitor cells from peripheral blood," *Cell Proliferation*, vol. 39, no. 2, pp. 117–125, 2006.

[31] H. Ogita and J. Liao, "Endothelial function and oxidative stress," *Endothelium*, vol. 11, no. 2, pp. 123–132, 2004.

[32] M. Sata and D. Fukuda, "Crucial role of renin-angiotensin system in the pathogenesis of atherosclerosis," *The Journal of Medical Investigation*, vol. 57, no. 1-2, pp. 12–25, 2010.

[33] C. E. Murdoch, S. P. Alom-Ruiz, M. Wang et al., "Role of endothelial Nox2 NADPH oxidase in angiotensin II-induced hypertension and vasomotor dysfunction," *Basic Research in Cardiology*, vol. 106, no. 4, pp. 527–538, 2011.

[34] S. Sivasinprasasn, R. Pantan, S. Thummayot, J. Tocharus, A. Suksamrarn, and C. Tocharus, "Cyanidin-3-glucoside attenuates angiotensin II-induced oxidative stress and inflammation in vascular endothelial cells," *Chemico-Biological Interactions*, vol. 28, 2016.

[35] J. Xu, Z. Huang, L. Lin et al., "miR-210 over-expression enhances mesenchymal stem cell survival in an oxidative stress environment through antioxidation and c-Met pathway activation," *Science China. Life Sciences*, vol. 57, no. 10, pp. 989–997, 2014.

[36] R. K. Mutharasan, V. Nagpal, Y. Ichikawa, and H. Ardehali, "MicroRNA-210 is upregulated in hypoxic cardiomyocytes through Akt- and p53-dependent pathways and exerts cytoprotective effects," *American Journal of Physiology. Heart and Circulatory Physiology*, vol. 301, no. 4, pp. H1519–H1530, 2011.

[37] R. P. Brandes, N. Weissmann, and K. Schroder, "NADPH oxidases in cardiovascular disease," *Free Radical Biology & Medicine*, vol. 49, no. 5, pp. 687–706, 2010.

[38] J. Skog, T. Wurdinger, S. Van Rijn et al., "Glioblastoma microvesicles transport RNA and proteins that promote tumour growth and provide diagnostic biomarkers," *Nature Cell Biology*, vol. 10, no. 12, pp. 1470–1476, 2008.

[39] Z. Wang, Z. Liu, B. Liu, G. Liu, and S. Wu, "Dissecting the roles of ephrin-A3 in malignant peripheral nerve sheath tumor by TALENs," *Oncology Reports*, vol. 34, no. 1, pp. 391–398, 2015.

[40] T. Sakurai and M. Kudo, "Signaling pathways governing tumor angiogenesis," *Oncology*, vol. 81, Supplement 1, pp. 24–29, 2011.

[41] G. Taraboletti, S. D'Ascenzo, I. Giusti et al., "Bioavailability of VEGF in tumor-shed vesicles depends on vesicle burst induced by acidic pH," *Neoplasia*, vol. 8, no. 2, pp. 96–103, 2006.

Hindawi
Oxidative Medicine and Cellular Longevity
Volume 2017, Article ID 2398696, 12 pages
https://doi.org/10.1155/2017/2398696

Review Article

MicroRNA Regulation of Oxidative Stress-Induced Cellular Senescence

Huaije Bu, Sophia Wedel, Maria Cavinato, and Pidder Jansen-Dürr

Institute for Biomedical Aging Research and Center for Molecular Biosciences Innsbruck (CMBI), Universität Innsbruck, Innsbruck, Austria

Correspondence should be addressed to Huaije Bu; huajie.bu@uibk.ac.at

Received 1 February 2017; Revised 31 March 2017; Accepted 11 April 2017; Published 16 May 2017

Academic Editor: Jaideep Banerjee

Aging is a time-related process of functional deterioration at cellular, tissue, organelle, and organismal level that ultimately brings life to end. Cellular senescence, a state of permanent cell growth arrest in response to cellular stress, is believed to be the driver of the aging process and age-related disorders. The free radical theory of aging, referred to as oxidative stress (OS) theory below, is one of the most studied aging promoting mechanisms. In addition, genetics and epigenetics also play large roles in accelerating and/or delaying the onset of aging and aging-related diseases. Among various epigenetic events, microRNAs (miRNAs) turned out to be important players in controlling OS, aging, and cellular senescence. miRNAs can generate rapid and reversible responses and, therefore, are ideal players for mediating an adaptive response against stress through their capacity to fine-tune gene expression. However, the importance of miRNAs in regulating OS in the context of aging and cellular senescence is largely unknown. The purpose of our article is to highlight recent advancements in the regulatory role of miRNAs in OS-induced cellular senescence.

1. Introduction

Cellular senescence, a state of permanent cell growth arrest in response to cellular stress, is characterized by morphological transformations, expression of senescence-associated β-galactosidase (SA-β-gal), accumulation of the cyclin-dependent kinase (CDK) inhibitor $p16^{INK4a}$, senescence-associated secretory phenotype (SASP), senescence-associated heterochromatin foci (SAHF), telomere shortening, and concomitant-persistent DNA damage response (DDR) [1]. Senescence-inducing stimuli include a variety of intracellular and extracellular stressors. Telomere shortening is found to cause replicative senescence in vitro, although its relevance to human aging remains unclear [2]. Other factors like oncogene activation, tumor suppressor loss, DNA damage, and oxidative stress (OS) are responsible for stress-induced premature cellular senescence [3]. The halting of damaged cells from proliferation has been initially considered as a tumor suppressor mechanism [4], although recent studies showed that the physiological role of senescence also extends to development, tissue repair, inflammation associated with tumor promotion, and aging [1]. Aging is a time-related process of functional deterioration at cellular, tissue, organelle, and organismal level that ultimately brings life to end. Senescent cells accumulate in multiple tissues with age [5], and removal of these cells delays tumorigenesis and age-related disorders in different tissues [6] as well as prolongs lifespan in vivo [7]. It is generally believed that cellular senescence is the driver of the aging process and age-related disorders [3, 8].

The signaling networks and molecular mechanisms underlying the induction and maintenance of cellular senescence are being unraveled. In response to DNA damage and reactive oxygen species (ROS), DDR is activated, in which ATR or ATM kinase blocks cell-cycle progression through stabilization of p53 and transactivation of the CDK inhibitor $p21^{Waf1/Cip1}$ [3]. Other stressors trigger senescence in DDR-dependent or DDR-independent way through activating $p19^{Arf}$, $p16^{Ink4a}$, and pRb [3]. Senescence is a multistep evolving process, in which the cells evolve from early to full senescence [3]. p53/p21 or p16/pRb signaling are important for the early phase of senescence, in which the cells

transit from temporal to persistent cell-cycle arrest, whereas extensive changes in chromatin structure and chromosome organization are required in order to progress to full senescence [3, 9]. Alterations in chromatin structure greatly affect the transcriptional program [3], including the upregulation of a group of secreted proteins, such as growth factors, proteases, and proinflammatory cytokines and chemokines, collectively referred to as the senescence-associated secretory phenotype (SASP). SASP is one of the key characteristics that distinguishes senescent cells from quiescent or terminally differentiated cells [1]. Of note, unlike quiescent cells that are metabolically inactive, senescent cells are highly metabolically active. New findings reveal key roles of changes in cell metabolism in the establishment and control of senescent phenotypes [10]. For example, a significant shift to more glycolytic metabolism but also less energetic state was observed as fibroblasts undergo replicative senescence [11]. In line with these findings, mitochondria, the cellular powerhouse, play a key role in pathophysiology of aging, and mitochondrial dysfunction is a major contributor to aging and aging-related diseases [12]. Thus, cellular senescence, as both evolving and static phenotype, is induced and maintained by a complex signaling network, in which genomic surveillance pathways, transcription program, and cellular metabolism are coordinated.

2. OS, Cellular Senescence, and Aging

The free radical theory of aging [13] describes one of the most studied mechanisms of aging and aging-related pathologies such as diabetes, cardiovascular diseases, and neurodegenerative diseases. It explains aging at a molecular level by cellular accumulation of oxidative damage to macromolecules, like DNA, proteins, and lipids, and results from failure to maintain antioxidant defenses, mitochondrial function, genomic integrity, metabolic homeostasis, and immune function [14]. ROS are produced from inefficient electron transfer in the mitochondrial respiratory chain and can be enhanced by a number of pathophysiological stimuli like tobacco smoking, UV radiation, and inflammation [15]. In the aging process, increased ROS generation results from mitochondrial dysfunction characterized by accumulation of mitochondrial DNA mutations, impairment of oxidative phosphorylation, impairment of antioxidant defenses [16], and other regulatory inputs. The function of ROS in controlling cellular senescence, aging, and age-associated diseases, as well as its regulation mechanisms, has been recently reviewed [14, 17, 18]. ROS causes senescence associated cell-cycle arrest by triggering DDR pathway to stabilize p53 and transactivate p21 gene expression [19]. In case of persistent DNA damage, p16 is activated via p38/MAPK pathway and nuclear lamin B1 is downregulated, triggering chromatin remodeling coupled with the formation of highly condensed chromatin regions referred to as senescence-associated heterochromatin foci (SAHF) [9]. SASP, the senescence-specific proinflammatory secretome, is closely linked to SAHF and reinforces senescence by coupling with a persistent DDR as a positive feedback loop with the ROS stimulation [20]. Stem cells, a group of self-renewable cells responsible for maintenance of tissue homeostasis and whose dysfunction leads to accelerated aging, age-associated pathologies, or cancer, are also sensitive to ROS level [17]. High levels of ROS impair the function of hematopoietic and neural stem cells, while physiological levels of ROS are required for both their proliferation and their differentiation [17]. Collectively, ROS that trigger aging are referred to as aging-inducing ROS (AIROS) below.

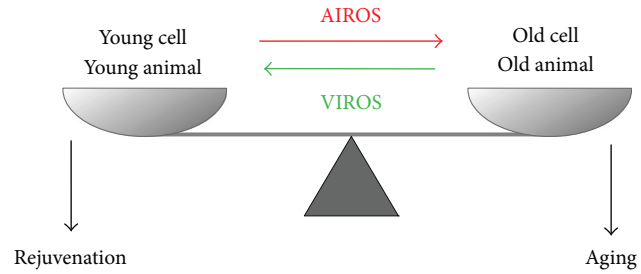

Figure 1: Role of ROS in aging and youthful physiology.

Although widely accepted, the OS theory of aging has been recently challenged due to (1) failure of evidence from increasing antioxidant capacity to prolong lifespan and (2) the fact that several longevity-promoting interventions, for example, caloric restriction or inhibition of target of rapamycin (TOR), in animal models converge by causing activation of mitochondrial oxygen consumption and, sometimes, increased ROS production [21]. In fact, nontoxic levels of ROS, referred to as vitality-associated ROS (VIROS) below, are suggested to promote metabolic health and longevity [21]. An increasing body of evidence shows that besides inducing OS, ROS are able to act as signaling molecules in the maintenance of physiological functions—a process termed redox biology. In contrast to high level of ROS that results in damage to macromolecules, redox biology refers to modulation of ROS levels that activates signaling pathways to initiate biological processes, like proliferation, inflammation, and aging [17]. Depending on ROS concentration, subcellular localization, and species, the cellular response can be either OS-induced damage or redox signaling [17]. For instance, increasing mitochondrial superoxide level extends lifespan, while cytosolic ROS shortens lifespan in *C. elegans* [22]. The function of mitochondrial ROS in increasing immunity to various pathogens suggests a possible link between ROS, immunity, and longevity [23]. In the case of UVB-induced senescence of human diploid fibroblasts (HDFs), ROS is essential for autophagy activation and inhibition of ROS production by antioxidant treatment leads to cell death [24]. The different functions of ROS in aging and senescence are depicted in Figure 1.

In young animals and young cells, youthful physiology and vitality are assured by physiological levels of reactive oxygen species (ROS), referred to as VIROS, which are essential for a plethora of signaling pathways. During aging, increased levels of ROS, probably in combination with an altered spectrum of ROS chemistry and ROS subcellular localization, collectively referred to as AIROS, lead to the

accumulation of damage to biological macromolecules contributing to aging.

Taken together, these studies suggest a reorientation of the initial view of ROS as promoter of cellular senescence and aging by causing cumulative damage; instead, ROS act as signaling molecules which are able to elicit either beneficial or detrimental effects depending on intracellular and environmental factors.

3. p53, OS, Cellular Senescence, and Aging

p53 plays key and complex roles in cellular response to OS. p53 as a cellular gatekeeper on one side is able to decrease ROS level in order to control OS and repair DNA damage; and on the other side, it can also promote ROS production and induce apoptosis or senescence when the damage is irreversible. In response to physiological OS, p53 reduces intracellular ROS level by inducing antioxidants and regulating metabolism [25]. In this context, antioxidant enzymes including MnSOD, Sestrins, and GP x 1 are involved [25, 26]; other metabolic enzymes like TIGAR, GLS2, and ALDH4 decrease ROS production by either slowing down glycolysis and promoting NAPDH production or strengthening mitochondrial function [25, 26]. In response to high levels of OS, p53 exacerbates OS and executes cellular apoptosis by targeting pro-oxidants including NADPH oxidase, members of pro-oxidant family PIG1–13 (p53-inducible genes 1–13), and proapoptotic molecules BAX and PUMA, as well as inhibiting expression of antioxidants [25, 26].

p53 is also a longevity assurance gene through tumor-suppressing function and a regulator of aging and cellular senescence. In mouse models, altered p53 activity may either suppress longevity and accelerate aging phenotypes or enhance longevity [27–32]. p53 mutant mice with consistent active p53 showed diminished stress tolerance and reduced lifespan [27, 28], while mouse with increased but otherwise normally regulated p53 showed a normal aging [29, 30]. Interestingly, modest and regulated increase of both p53 and Ink4/Arf significantly prolonged longevity and delayed organismal aging [31, 32]. At cellular level, p53 is induced in HDFs when cells are challenged by senescence stimuli, that is, OS, irradiation, or oncogene activation, leading to mitosis skip and subsequent senescence induction [33]. Transient activation of p53 at G2 phase was found to be sufficient for senescence induction [33, 34]. Interestingly, downregulation of p53 by SCF^{Fbxo22} was reported to be crucial for the induction of p16 and SASP [35]. In case of moderate stress challenge, p53 is activated to halt the cell cycle and trigger the repair mechanisms. The reversion of cell cycle arrest after the repair response requires p53 degradation in an ubiquitylation-dependent way [36]. mTOR is identified as a key molecule in determining the outcome of p53 signal to either induce reversible quiescence or irreversible senescence; while maximal activation of p53 blocked mTOR and led to quiescence, partial p53 activation preserved mTOR activity and induced senescence [37]. Other players in decision of cell fates in response to p53 pathway have been reviewed recently [38].

4. Changes in Gene Expression during Cellular Senescence

Senescence is a multistep dynamic process with acquired phenotypes. Changes in gene expression profiles have been proposed to be implicated in the process [39]. A time series transcriptome study in replicative senescence revealed changes in the expression of genes related to growth arrest and metabolism during the early onset of senescence and to genes involved in inflammation and immune function-related and growth regulation in the late stage of senescence [39]. Inflammation and the immune function are also found to be common pathways in both replicative and stress-induced premature senescence models [40]. As mentioned previously, in addition to p53/p21 and pRb/p16 signaling, epigenetic modifications including DNA methylation, histone modifications, and chromatin remodeling also play an important role in defining and maintaining the senescence state through regulating gene expression [9, 41]. For instance, both in vivo and in vitro studies show that aging and cellular senescence are associated with genome-wide DNA hypomethylation and focal DNA hypermethylation [42]. Loss of the active chromatin histone marker H3K4me3 at cell-cycle regulatory genes, due to proteolysis, facilitates transcriptional silencing and promotes senescence [43].

5. Changes of miRNA Biogenesis during Aging and Cellular Senescence

In the past years, microRNAs (miRNAs) turned out to be important players in controlling aging and cellular senescence [44–46] by regulating gene expression either by translational repression or by mRNA degradation [47]. For example, one of the best characterized aging-associated pathways in *C. elegans*, the IGF signaling pathway, is regulated by lin-4 and its target lin-14. Of note, a global decrease in miRNAs abundance was found in aging of different model organisms, suggesting aging-associated alteration of miRNAs biogenesis [44]. In fact, aging-induced dysregulation of miRNAs biogenesis proteins is reported to promote aging and aging-associated pathologies. Among them, ribonuclease Dicer is most studied and a reduced level was reported in tissues of aged mice and rats, as well as in senescent cells [48–50]. Downregulation of Dicer and multiple miRNAs in adipose tissue is associated with accelerated aging, reduced life span, and stress defense in different model organisms from *C. elegans* to mice and also in humans [48]. A similar phenotype was also observed in primary cerebromicrovascular endothelial cells, where aging-induced downregulation of Dicer1 resulted in altered miRNA profiles and vascular cognitive impairment [50]. Interestingly, longevity-promoting interventions, for example, caloric restriction and metformin supplementation [51], prevent age-related decline of Dicer and miRNA processing and exert Dicer-dependent antisenescence effect [48, 52], while senescence-inducing stimuli, like OS or UV radiation, decrease Dicer expression [48]. Knockdown or knockout of Dicer1 in cells resulted in increased DNA damage and p19Arf-p53 activity [53] and premature senescence

[48, 53, 54]. Dicer1 knockout mice showed a shift in metabolism from oxidative phosphorylation to aerobic glycolysis, hypersensitivity to OS, and cell senescence phenotype in vivo [48, 53, 55]. In comparison to Dicer, the role of proteins of microprocessor complex in cellular senescence is less studied. Although several studies pointed to an antisenescence role of DGCR8, the function of Drosha remains to be unraveled [56–60]. Loss of miRNA synthesis through blocking DGCR8 expression in adult *C. elegans* showed accelerated aging and reduced lifespan [57]. Knockdown of DGCR8 triggered a dramatic antiproliferative response and consequently senescence phenotype characterized by upregulation of p21 in primary fibroblasts of human and mouse origin [58]. In addition, several senescence regulating proteins are reported to regulate DGCR8. Among them, p63, an essential transcription factor for epidermal function and an antiaging molecule, directly promotes the transcription of DGCR8 and Dicer [60]; ING proteins (inhibitor of growth), a family of tumor suppressors and senescence promoters, repress DGCR8 expression [56, 59]. Drosha mRNA was reported to be moderately reduced in adipose tissue of aged mice [48] and the protein level was downregulated in replicative senescent WI-38 fibroblasts [61]. Although knockdown of Drosha in IMR90 human primary fibroblasts showed an antiproliferative effect [58], its downregulation in WI-38 fibroblast, however, revealed no effects on cellular senescence [61]. Further efforts are needed to clarify the role of Drosha in aging and cellular senescence.

6. miRNA Stability in Cellular Senescence

Although the mechanisms of miRNA biogenesis have been intensively investigated since the last years, processes regulating miRNA stability remain to be explored. miRNAs have been generally considered as stable molecules with half-life of days long [62, 63], while some miRNAs, for example, brain-enriched miRNA-9, miRNA-125b, are actually short lived with half-life of no more than few hours [64]. It is now clear that the absolute levels of mature miRNAs are also controlled by *cis*- and *trans*-acting factors that directly affect stability [65]. Under them, the association of mature miRNAs with Argonaute (AGO) is critical for miRNA stability [66], probably due to protection from degradation by ribonuclease. GW182, a downstream effector of AGO and an AGO-interacting partner essential for gene silencing is also important for stability of miRNAs [67]. In addition, the stability or degradation of mature miRNAs seems to be miRNA and modification specific. For example, 3′ adenylation of specific miRNAs like miR-122, miR-145, and Let-7d by PAPD4, a noncannonical poly(A) RNA polymerase, stabilized them [68], while PAPD5-mediated 3′ adenylation of miR-21 leads to its degradation [69]. The exonuclease XRN-2 also shows selectivity on degradation of its miRNAs substrates [70, 71]. Further efforts are needed to elucidate the mechanisms of altered miRNA stability in the context of miRNA modification and selectivity of miRNA stabilization and/or degradation enzymes.

If miRNA stability changes during cellular senescence is so far, to our knowledge, not known. In *Drosophila*, 2′-O-methylation of miRNAs, a modification occurs on nearly all small RNAs in plants to protect them from degradation [72, 73], was reported to be increased in aged animals [74]. An increased loading of these miRNAs to AGO2 and stabilizing was found to underlie the age-associated alteration and lack of 2′-O-methylation of miRNAs results in accelerated neurodegeneration and shorter life span [74]. Further researches on miRNA stability and degradation mechanisms in cellular senescence and aging are needed to identify its impact on age-associated process and may provide potential new targets to interfere the process.

7. miRNA Biomarkers of Senescence and Aging

A number of miRNAs, including miR-106b, miR-125b, miR-126, miR-146a, miR-21, miR-22, miR-29, miR-210, miR-34a, miR-449a, miR-494, and miR-17-92 cluster and miR-200 family, have been found to be differentially expressed in senescent cells or aged tissues and play a role in cellular senescence [75–77]. Recently, miRNAs have been found extracellularly and function in intercellular communication upon taken up by recipient cells [78]. The fact that circulating miRNAs are packed in the form of microvesicles, proteins including AGO2 or lipoprotein protects them from degradation [79]. The stability of miRNAs in the circulation and in body fluids, their tissue and disease specificity, and the easy and reliable quantification methods make them feasible as potential biomarkers [78]. Several miRNAs including miR-126, miR-130a, miR-142, miR-21, and miR-93 detected in blood samples have been found in several studies to be associated with human aging [80]. Furthermore, circulating miRNAs can also help to define healthy aging by comparing nonagenarians, centenarians and their offspring to patients with age-related diseases [80]. For example, miR-21 level is increased with aging process, aging associated diseases, and cancers but decreased in subjects older than 80 years and in centenarians, implying that low levels of miR-21 are beneficial for longevity and could be a promising biomarker candidate of healthy aging [80]. A miRNA profiling of serum samples collected longitudinally at the ages of 50, 55, and 60 from individuals with documented lifespans was recently analyzed [81]. When the participants were subdivided into long-lived and short-lived subgroups, a multiplex of aging biomarker with the expression of miR-211-5p, miR-374a-5p, miR-340-3p, miR-376c-3p, miR-5095, and miR-1225-3p was proposed to be significantly differentially expressed and correlated with lifespan, providing a basis for investigating miRNAs as potential longevity predictors and regulators of aging process [81]. Circulating miRNAs from blood samples have been also investigated as biomarkers of aging-associated diseases, like cardiovascular diseases, neurodegenerative diseases, type 2 diabetes mellitus, and bone diseases [78, 82, 83]. Body fluids other than blood samples are also a reservoir of miRNA biomarkers. For example, a pilot study on exosomal miRNAs in saliva suggests that miR-24 may be potential biomarkers for aging [84]. The levels of miR-34a, miR-125b, and miR-146a in cerebrospinal fluid of patients with Alzheimer's disease were lower compared with those of control subjects, implying a possibility to use

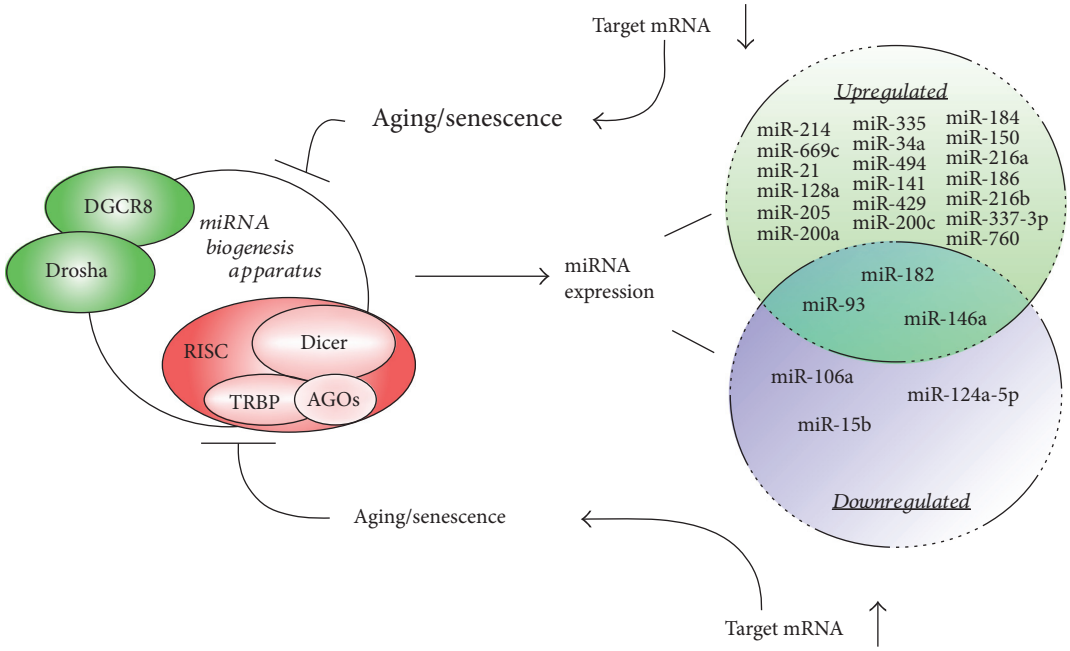

Figure 2: Role and regulation of micro-RNAs in aging and senescence.

miRNAs detected in cerebrospinal fluid as biomarkers for neurodegenerative diseases [85]. Further efforts are needed to identify consensus miRNA biomarkers not only as indicators of aging process and aging-associated disease but also as longevity predictors and eventually therapeutic approaches to modulate the aging process.

8. miRNAs Regulating OS in Cellular Senescence

OS can regulate miRNA-mediated gene silencing in senescence induction, by either affecting the miRNA producing organelle (Figure 2) or regulating (upregulation or downregulation) the expression of certain specific miRNAs (see below, Figure 3).

The function of miRNA biosynthesis apparatus is compromised during organismic aging and in cellular senescence, leading to a general decline of microRNA availability with age. On the other hand, cellular pathways regulating OS are fine-tuned by specific microRNAs (up- or downregulated) which alter the expression of cellular target genes with the final result to induce and/or enforce senescence and aging.

In a study of RAS-induced premature senescence of fibroblasts, AGO2 was found to be a substrate of protein tyrosine phosphatase 1B (PTP1B), a major target of RAS-induced ROS [86]. Inactivation of PTP1B and consequently phosphorylation of AGO2, which inhibits loading and function of miRNAs, were necessary and sufficient for RAS-induced senescence, implying the importance of OS-mediated inhibition of miRNA function in senescence induction [86]. On the other hand, miRNAs can generate rapid and reversible responses and, therefore, are ideal players for mediating adaptive responses against stress through their capacity to fine-tune gene expression [87]. In the following section, we will summarize and categorize the miRNAs that regulate OS in cellular senescence according to their targets (Figure 3).

8.1. Redox Homeostasis. miR-93, miR-214, and miR-669c were found to be overexpressed in aged mouse livers [88]. Through proteomics approach, glutathione S-transferases, such as microsomal glutathione S-transferase 1 (MGST1), glutathione S-transferase zeta 1 (GSTZ1), glutathione S-transferase mu 1 (GSTM1), and glutathione S-transferase theta-1 (GSTT1), were identified as targets of these miRNAs, implying the decline of oxidative defense mechanisms through miRNAs in aging liver [88]; miR-93 was also reported to be upregulated in aged rat liver where Sirtuin1 (SIRT1), in addition to MGST1, was identified as its target [89]. SIRT1 is a nicotinamide adenine dinucleotide-(NAD^+-) dependent deacetylase that regulates crucial cellular functions and is associated with aging and longevity. It mediates stress resistance and its expression levels decline in aging organisms, where OS occurs [90]. A variety of miRNAs regulate SIRT1 expression [90]. Of note, miR-34a was found to induce cellular senescence by targeting SIRT1 in different tissues [89, 91–93]. miR-217 was reported to induce a premature senescence-like phenotype and impaired angiogenesis in endothelial cells through directly targeting SIRT1 and modulating its deacetylase activity [94]. miR-92a was found to exacerbate endothelial dysfunction in response to OS through targeting SIRT1, Krüppel-like factor 2, and Krüppel-like factor 4, which are key molecules in endothelial cell homeostasis [95].

miR-34a was also reported to target genes in the antioxidant pathway other than SIRT1 to contribute to OS-mediated cellular senescence. Together with miR-335, miR-34a was found to be upregulated in aged rat kidney having superoxide

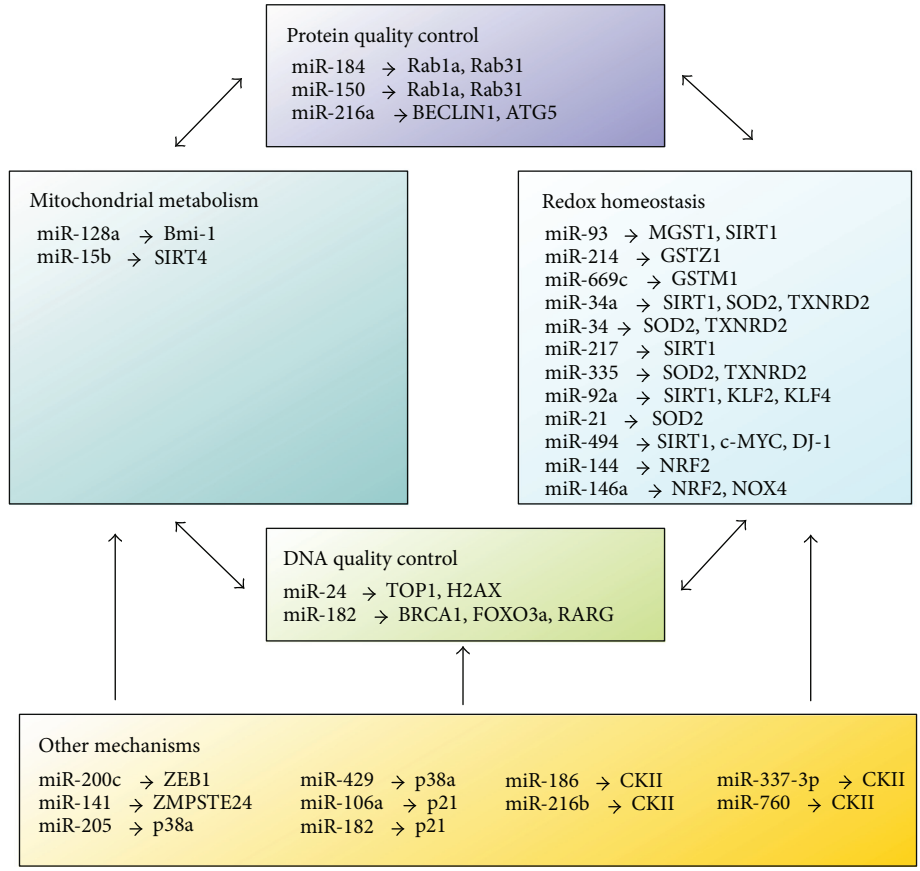

Figure 3: MicroRNAs and their mRNA targets as modulators of redox biology, mitochondrial metabolism, and quality control of DNA and proteins. The maintenance of DNA and protein quality is crucial for the preservation of youthful physiology in animals. Accordingly, mechanisms of DNA and protein quality control (QC) were identified as key targets for cellular senescence and aging. The performance of both QC mechanisms is affected by both mitochondrial and cytosolic ROS. Depicted here are known functions of microRNAs as mediators between ROS production and QC mechanisms. The final outcome of this regulatory circuit is further modulated by other (additional) mechanisms which are currently incompletely understood.

dismutase 2 (SOD2) and thioredoxin reductase 2 (TXNRD2) as their targets, respectively [96]. Overexpression of miR-335 and miR-34a induced premature senescence of young mesangial cells via suppression of both antioxidative enzymes with a concomitant increase in ROS [96]. SOD2 is also a target of miR-21 in human angiogenic progenitor cells (APCs). Reversed correlation of miR-21 and SOD expression was seen in APCs from patients with coronary artery disease. Upregulation of this miRNA increased cellular ROS generation and impaired migratory capacity of APCs [97].

miR-494 was observed to be overexpressed in both replicative senescence and OS-induced premature senescence of HDFs. Its overexpression also promoted a senescent phenotype, as well as enhanced DNA damage and intracellular ROS generation [98]. In line with this, several OS regulators were found to be miR-494 targets. For instance, both c-MYC and SIRT1 were identified as direct targets in pancreatic cancer cells and tissues, where miR-494 is often found to be downregulated. Overexpression of miR-494 could inhibit proliferation of pancreatic cancer cells through induction of apoptosis, G1-phase arrest, and senescence [99]. DJ-1, an oxidative sensor and molecular chaperone, whose dysfunction contributes to Parkinson's disease, was also found to be posttranslationally repressed by miR-494. This miRNA reversely correlated with DJ-1 level in vivo and rendered cells more susceptible to OS, resulting in loss of dopaminergic neurons in mice [100].

Caloric restriction (CR) is a well-accepted lifespan prolongation intervention method described for most model organisms from worms to primates. In a study conducted to elucidate the mechanism protective of moderate CR on cerebrovascular cells of aged rats, age-related increase in OS was found to be positively correlated with miR-144 and negatively correlated with miRNA target transcription factor of antioxidant gene *Nrf2*. CR significantly decreased miR-144 levels and restored NRF2 expression, indicating that CR confers antioxidative effects through regulating miR-144-NRF2 axis [101]. Actually, as master regulator of redox biology through induction of antioxidant defense, NRF2 is targeted by various miRNAs in order to "fine-tune" the redox homeostasis, and these miRNAs have been reviewed elsewhere [102]. In a recent miRNA profiling study addressing age-related changes in NRF2 protein homeostasis using rat hepatocytes, miR-146a was found to be significantly upregulated in aged liver and identified as a new NRF2-targeting miRNA [103]. Interestingly, the effect of miR-146a in modulating

redox biology seems to be tissue dependent. During replicative senescence of human endothelial cells, this miRNA is continuously decreased in higher passage cells and its overexpression was found to delay the appearance of the senescence-like phenotype through direct targeting of NADPH oxidase 4 (NOX4) protein, a major ROS generator in HUVEC cells [104, 105].

8.2. DNA Quality Control. miR-24 was previously found by us to exacerbate OS induced cellular senescence through directly targeting DNA topoisomerase I (TOP1) [106]. Since TOP1 plays a role in genomic stability [107], we suggested that in the OS-induced premature senescence model of HDFs, TOP1 attenuates cellular senescence potentially due to its physiological function to maintain genomic stability. miR-24 was also reported by others to target H2AX, a key double-strand break repair protein, in terminally differentiated hematopoietic cell lines and to render cells hypersensitive to DNA damage [108]. In highly differentiated CD8+ T cells, miR-24 was found to be upregulated upon etoposide treatment and to sensitize them to apoptotic cell death [109].

Excess intracellular ROS in normal human fallopian tube epithelial cells upregulates miR-182. miR-182 overexpression triggers significant cellular senescence in a p53/p21-dependant way. However, in cells with p53 mutations, miR-182 overexpression no longer increases p21 expression but functions as an "Onco-miR" to enhance senescence bypass in cells exposed to OS or DNA damage in vitro and in vivo [110]. Since miR-182 is reported to target DNA repair genes, BRCA1 and FOXO3a [111], a role of slowing down DNA damage repair by miR-182 in cells with dysfunctional p53 is suggested underlying miR-182-mediated tumorigenesis [110].

8.3. Protein Quality Control. Major cellular mechanisms controlling protein quality control during aging are autophagy and the 20S proteasome. Autophagy activation has been considered as part of the cellular responses to excessive OS, eliminating unwanted, damaged, or oxidative structures, thus favoring antiaging mechanism [112]. Alteration of the cellular quality control mechanism contribute to aging and aging-associated pathology [113]. miR-184 and miR-150 were found to be upregulated in aged rat kidney. Autophagy-associated proteins Rab1a and Rab31 were identified as targets of both miRNAs. Transfection of kidney cells with mimics of miR-184 and miR-150 suppressed the expression of both proteins and consequently lowered autophagy activity, increasing cellular oxidative products that lead to cellular senescence [114]. miR-216a is induced during endothelial aging and is reported to repress oxidized low-density lipoprotein- (ox-LDL-) induced autophagy. Two autophagy-related genes, Beclin1 (BECN1) and ATG5 are putative targets of miR-216a, whose expression reversely correlated with putative targets in vitro and in vivo. BECN1 was identified as a direct target of miR-216a, implying that miR-216a controls OS induced autophagy in HUVECs by regulating intracellular levels of BECN1 and may have a relevant role in aging-associated cardiovascular disorders [115].

8.4. Mitochondrial Metabolism. In a search of a tumor-suppressive role of miRNAs in medulloblastoma, miR-128a, which is downregulated in this type of tumor, was found to inhibit cancer cell growth by promoting senescence, through increased ROS production, upregulation of p16 protein level, and increased number of SA-β-Gal positive cells [116]. Bmi-1 oncogene, which is important for mitochondrial function and redox homeostasis [117], was identified as a direct target of miR-128a, indicating novel regulation of ROS by miR-128a via the specific inhibition of the Bmi-1 oncogene [116]. SIRT4, a member of sirtuin family exclusively localized in mitochondria, plays an important role in mitochondrial metabolism [118]. Upregulation of SIRT4 was found to be inversely associated with miR-15b in replicative, stress-induced cellular senescence and photoaged human skin in vivo. SIRT4 was identified as a direct target of miR-15b, whose inhibition promotes mitochondrial ROS generation and mitochondrial dysfunction in a SIRT4-dependent manner, linking the miR-15b-SIRT4 axis to senescence-associated mitochondrial dysfunction [119]. In addition, miR-15 was also found to be downregulated in UVB-induced senescence of human dermal fibroblasts [120].

8.5. Other Mechanisms. miR-200 family members are often reported to be associated with cellular senescence. For instance, miR-141 is overexpressed in replicative and HDAC-inhibitor-induced senescence of human mesenchymal stem cells [121]. ZMPSTE24, an enzyme involved in the posttranslational maturation of lamin A and responsible for the prelamin A accumulation related to cellular senescence, is found to be a direct target of miR-141 [121]. miR-200 family members, especially miR-200c and miR-141, are upregulated in OS-induced HUVEC cells [122]. Similar to hydrogen peroxide treatment, miR-200c overexpression also induced growth arrest, apoptosis, and senescence in HUVEC cells. E-cadherin transcriptional repressor zinc finger E-box-binding homeobox 1 (ZEB1), a molecule downregulated by OS, was identified as a target of miR-200c. Downregulation of ZEB1 was required for miR-200c-mediated effects [122]. miR-200 family members have been previously reported to target p38α, modulate OS response and chemosensitize cancer cells [123]. A similar mechanism was proposed in a ROS-dependent chemotherapeutic drug-induced senescent model of HDFs, where metformin was found to sensitize the doxorubicin-treated cells to senescence through upregulation of miR-205, together with miR-200 family members miR-200a, miR-141, and miR-429 [124].

In a screen of OS-induced premature senescence in primary cultures of HDFs and human trabecular meshwork (HTM) cells, miR-106a was found to be downregulated in both models and p21 was identified as its target [125]. miR-106a was also downregulated in several human models of cellular aging in vitro and in vivo [46]. Among the upregulated miRNAs, miR-182 was found to target retinoic acid receptor gamma (RARG), whose level is downregulated in both senescent models [125]. The function of RARG in cellular senescence requires more study. Protein kinase CKII is a ubiquitous serine/threonine kinase that catalyzes the phosphorylation of a large number of cytoplasmic and nuclear

proteins. Its downregulation is found to induce cellular senescence in both HDFs [126] and human colon cancer cells in p53/p21-dependent way [127]. In a search of CKII targeting miRNAs, miR-186, miR-216b, miR-337-3p, and miR-760 were identified. Overexpression of these miRNAs altogether increased cellular senescence and ROS production, which could be antagonized by CKII overexpression [128]. miR-125a-5p was downregulated in human brain microvessel endothelial cells by ox-LDL, a risk factor for vascular diseases by inducing proinflammatory and proatherogenic responses [129]. Overexpression of this miRNA increased nitric oxide production and decreased ROS production, consequently reducing senescence and apoptosis. miR-125a-5p also improved endothelial cell function and decreased cell adhesion to leukocytes, indicating an anti-inflammatory role by decreasing leukocyte recruitment [129].

9. Conclusions

Although a relatively new field of research, miRNAs add substantial complexity to the regulation of aging processes and cellular senescence. On one side, a single miRNA can regulate the expression of hundreds of genes from different signaling pathways, which means the whole signaling network could be reset by modulating the expression of one single miRNA. In contrast, miRNAs as players of adaptive stress response could act both as promoters and inhibitors of senescence, depending on the type of stress, the cell or tissue where they are located, and the molecular context in which they play a role. Further efforts are needed to explore the modulatory role of additional miRNAs in OS- and stress-induced cellular senescence. Especially important is to distinguish the function of specific miRNAs in specific cell or tissue types, where the knowledge gained on cell culture level will be applied to the organismal level.

Conflicts of Interest

The authors declare that they have no conflicts of interest.

Acknowledgments

The work in Pidder Jansen-Dürr's laboratory is supported by the Austrian Research Promotion Agency (FFG). The research leading to these results has also received funding from the European Union's Seventh Framework Programme (FP7/2007-2013) under Grant Agreement no. 305483, FRAILOMIC Project. Huaije Bu is supported by a grant from the Tiroler Wissenschaftsfonds (TWF). Maria Cavinato was supported by a Ph.D. fellowship from CNPqb (Brazil).

References

[1] F. Rodier and J. Campisi, "Four faces of cellular senescence," *The Journal of Cell Biology*, vol. 192, no. 4, pp. 547–556, 2011.

[2] K. A. Mather, A. F. Jorm, R. A. Parslow, and H. Christensen, "Is telomere length a biomarker of aging? A review," *The Journals of Gerontology. Series A, Biological Sciences and Medical Sciences*, vol. 66, no. 2, pp. 202–213, 2011.

[3] J. M. van Deursen, "The role of senescent cells in ageing," *Nature*, vol. 509, no. 7501, pp. 439–446, 2014.

[4] M. Serrano, A. W. Lin, M. E. McCurrach, D. Beach, and S. W. Lowe, "Oncogenic ras provokes premature cell senescence associated with accumulation of p53 and p16INK4a," *Cell*, vol. 88, no. 5, pp. 593–602, 1997.

[5] J. C. Jeyapalan and J. M. Sedivy, "Cellular senescence and organismal aging," *Mechanisms of Ageing and Development*, vol. 129, no. 7, pp. 467–474, 2008.

[6] D. J. Baker, T. Wijshake, T. Tchkonia et al., "Clearance of p16Ink4a-positive senescent cells delays ageing-associated disorders," *Nature*, vol. 479, no. 7372, pp. 232–236, 2011.

[7] D. J. Baker, B. G. Childs, M. Durik et al., "Naturally occurring p16(Ink4a)-positive cells shorten healthy lifespan," *Nature*, vol. 530, no. 7589, pp. 184–189, 2016.

[8] N. Bhatia-Dey, R. R. Kanherkar, S. E. Stair, E. O. Makarev, and A. B. Csoka, "Cellular senescence as the causal nexus of aging," *Frontiers in Genetics*, vol. 7, p. 13, 2016.

[9] S. W. Criscione, Y. V. Teo, and N. Neretti, "The chromatin landscape of cellular senescence," *Trends in Genetics*, vol. 32, no. 11, pp. 751–761, 2016.

[10] C. D. Wiley and J. Campisi, "From ancient pathways to aging cells-connecting metabolism and cellular senescence," *Cell Metabolism*, vol. 23, no. 6, pp. 1013–1021, 2016.

[11] W. Zwerschke, S. Mazurek, P. Stockl, E. Hutter, E. Eigenbrodt, and P. Jansen-Durr, "Metabolic analysis of senescent human fibroblasts reveals a role for AMP in cellular senescence," *The Biochemical Journal*, vol. 376, no. 2, pp. 403–411, 2003.

[12] M. Gonzalez-Freire, R. de Cabo, M. Bernier et al., "Reconsidering the role of mitochondria in aging," *The Journals of Gerontology. Series A, Biological Sciences and Medical Sciences*, vol. 70, no. 11, pp. 1334–1342, 2015.

[13] D. Harman, "Aging: a theory based on free radical and radiation chemistry," *Journal of Gerontology*, vol. 11, no. 3, pp. 298–300, 1956.

[14] A. Chandrasekaran, M. D. Idelchik, and J. A. Melendez, "Redox control of senescence and age-related disease," *Redox Biology*, vol. 11, pp. 91–102, 2016.

[15] S. Mena, A. Ortega, and J. M. Estrela, "Oxidative stress in environmental-induced carcinogenesis," *Mutation Research*, vol. 674, no. 1-2, pp. 36–44, 2009.

[16] C. H. Wang, S. B. Wu, Y. T. Wu, and Y. H. Wei, "Oxidative stress response elicited by mitochondrial dysfunction: implication in the pathophysiology of aging," *Experimental Biology and Medicine (Maywood, N.J.)*, vol. 238, no. 5, pp. 450–460, 2013.

[17] M. Schieber and N. S. Chandel, "ROS function in redox signaling and oxidative stress," *Current Biology*, vol. 24, no. 10, pp. R453–R462, 2014.

[18] P. Davalli, T. Mitic, A. Caporali, A. Lauriola, and D. D'Arca, "ROS, cell senescence, and novel molecular mechanisms in aging and age-related diseases," *Oxidative Medicine and Cellular Longevity*, vol. 2016, Article ID 3565127, p. 18, 2016.

[19] T. von Zglinicki, "Oxidative stress shortens telomeres," *Trends in Biochemical Sciences*, vol. 27, no. 7, pp. 339–344, 2002.

[20] A. R. Young, M. Narita, and M. Narita, "Cell senescence as both a dynamic and a static phenotype," *Methods in Molecular Biology*, vol. 965, pp. 1–13, 2013.

[21] M. Ristow and S. Schmeisser, "Extending life span by increasing oxidative stress," *Free Radical Biology & Medicine*, vol. 51, no. 2, pp. 327–336, 2011.

[22] C. E. Schaar, D. J. Dues, K. K. Spielbauer et al., "Mitochondrial and cytoplasmic ROS have opposing effects on lifespan," *PLoS Genetics*, vol. 11, no. 12 article e1004972, 2015.

[23] A. B. Hwang, E. A. Ryu, M. Artan et al., "Feedback regulation via AMPK and HIF-1 mediates ROS-dependent longevity in Caenorhabditis elegans," *Proceedings of the National Academy of Sciences of the United States of America*, vol. 111, no. 42, pp. E4458–E4467, 2014.

[24] M. Cavinato, R. Koziel, N. Romani et al., "UVB-induced senescence of human dermal fibroblasts involves impairment of proteasome and enhanced autophagic activity," *The Journals of Gerontology. Series A, Biological Sciences and Medical Sciences*, vol. 72, no. 5, pp. 632–639, 2017.

[25] D. Liu and Y. Xu, "p53, oxidative stress, and aging," *Antioxidants & Redox Signaling*, vol. 15, no. 6, pp. 1669–1678, 2011.

[26] A. V. Budanov, "The role of tumor suppressor p53 in the antioxidant defense and metabolism," *Sub-Cellular Biochemistry*, vol. 85, pp. 337–358, 2014.

[27] S. D. Tyner, S. Venkatachalam, J. Choi et al., "p53 mutant mice that display early ageing-associated phenotypes," *Nature*, vol. 415, no. 6867, pp. 45–53, 2002.

[28] B. Maier, W. Gluba, B. Bernier et al., "Modulation of mammalian life span by the short isoform of p53," *Genes & Development*, vol. 18, no. 3, pp. 306–319, 2004.

[29] I. Garcia-Cao, M. Garcia-Cao, J. Martin-Caballero et al., ""Super p53" mice exhibit enhanced DNA damage response, are tumor resistant and age normally," *The EMBO Journal*, vol. 21, no. 22, pp. 6225–6235, 2002.

[30] S. M. Mendrysa, K. A. O'Leary, M. K. McElwee et al., "Tumor suppression and normal aging in mice with constitutively high p53 activity," *Genes & Development*, vol. 20, no. 1, pp. 16–21, 2006.

[31] A. Matheu, A. Maraver, P. Klatt et al., "Delayed ageing through damage protection by the Arf/p53 pathway," *Nature*, vol. 448, no. 7151, pp. 375–379, 2007.

[32] A. Matheu, A. Maraver, M. Collado et al., "Anti-aging activity of the Ink4/Arf locus," *Aging Cell*, vol. 8, no. 2, pp. 152–161, 2009.

[33] Y. Johmura, M. Shimada, T. Misaki et al., "Necessary and sufficient role for a mitosis skip in senescence induction," *Molecular Cell*, vol. 55, no. 1, pp. 73–84, 2014.

[34] L. Krenning, F. M. Feringa, I. A. Shaltiel, J. van den Berg, and R. H. Medema, "Transient activation of p53 in G2 phase is sufficient to induce senescence," *Molecular Cell*, vol. 55, no. 1, pp. 59–72, 2014.

[35] Y. Johmura, J. Sun, K. Kitagawa et al., "SCF(Fbxo22)-KDM4A targets methylated p53 for degradation and regulates senescence," *Nature Communications*, vol. 7, p. 10574, 2016.

[36] P. A. Lazo, "Reverting p53 activation after recovery of cellular stress to resume with cell cycle progression," *Cellular Signalling*, vol. 33, pp. 49–58, 2017.

[37] O. V. Leontieva, Z. N. Demidenko, A. V. Gudkov, and M. V. Blagosklonny, "Elimination of proliferating cells unmasks the shift from senescence to quiescence caused by rapamycin," *PloS One*, vol. 6, no. 10, article e26126, 2011.

[38] M. Y. Terzi, M. Izmirli, and B. Gogebakan, "The cell fate: senescence or quiescence," *Molecular Biology Reports*, vol. 43, no. 11, pp. 1213–1220, 2016.

[39] Y. M. Kim, H. O. Byun, B. A. Jee et al., "Implications of time-series gene expression profiles of replicative senescence," *Aging Cell*, vol. 12, no. 4, pp. 622–634, 2013.

[40] M. Purcell, A. Kruger, and M. A. Tainsky, "Gene expression profiling of replicative and induced senescence," *Cell Cycle*, vol. 13, no. 24, pp. 3927–3937, 2014.

[41] R. A. Veitia, D. R. Govindaraju, S. Bottani, and J. A. Birchler, "Aging: somatic mutations, epigenetic drift and gene dosage imbalance," *Trends in Cell Biology*, vol. 27, no. 4, pp. 299–310, 2016.

[42] A. A. Johnson, K. Akman, S. R. Calimport, D. Wuttke, A. Stolzing, and J. P. de Magalhaes, "The role of DNA methylation in aging, rejuvenation, and age-related disease," *Rejuvenation Research*, vol. 15, no. 5, pp. 483–494, 2012.

[43] L. F. Duarte, A. R. Young, Z. Wang et al., "Histone H3.3 and its proteolytically processed form drive a cellular senescence programme," *Nature Communications*, vol. 5, p. 5210, 2014.

[44] S. Inukai and F. Slack, "MicroRNAs and the genetic network in aging," *Journal of Molecular Biology*, vol. 425, no. 19, pp. 3601–3608, 2013.

[45] F. Pourrajab, A. Vakili Zarch, S. Hekmatimoghaddam, and M. R. Zare-Khormizi, "The master switchers in the aging of cardiovascular system, reverse senescence by microRNA signatures; as highly conserved molecules," *Progress in Biophysics and Molecular Biology*, vol. 119, no. 2, pp. 111–128, 2015.

[46] M. Hackl, S. Brunner, K. Fortschegger et al., "miR-17, miR-19b, miR-20a, and miR-106a are down-regulated in human aging," *Aging Cell*, vol. 9, no. 2, pp. 291–296, 2010.

[47] V. Ambros, "The functions of animal microRNAs," *Nature*, vol. 431, no. 7006, pp. 350–355, 2004.

[48] M. A. Mori, P. Raghavan, T. Thomou et al., "Role of microRNA processing in adipose tissue in stress defense and longevity," *Cell Metabolism*, vol. 16, no. 3, pp. 336–347, 2012.

[49] L. S. Nidadavolu, L. J. Niedernhofer, and S. A. Khan, "Identification of microRNAs dysregulated in cellular senescence driven by endogenous genotoxic stress," *Aging (Albany NY)*, vol. 5, no. 6, pp. 460–473, 2013.

[50] Z. Ungvari, Z. Tucsek, D. Sosnowska et al., "Aging-induced dysregulation of dicer1-dependent microRNA expression impairs angiogenic capacity of rat cerebromicrovascular endothelial cells," *The Journals of Gerontology. Series A, Biological Sciences and Medical Sciences*, vol. 68, no. 8, pp. 877–891, 2013.

[51] A. Martin-Montalvo, E. M. Mercken, S. J. Mitchell et al., "Metformin improves healthspan and lifespan in mice," *Nature Communications*, vol. 4, p. 2192, 2013.

[52] N. Noren Hooten, A. Martin-Montalvo, D. F. Dluzen et al., "Metformin-mediated increase in DICER1 regulates microRNA expression and cellular senescence," *Aging Cell*, vol. 15, no. 3, pp. 572–581, 2016.

[53] R. Mudhasani, Z. Zhu, G. Hutvagner et al., "Loss of miRNA biogenesis induces p19Arf-p53 signaling and senescence in primary cells," *The Journal of Cell Biology*, vol. 181, no. 7, pp. 1055–1063, 2008.

[54] Y. Zhao, D. Wu, C. Fei et al., "Down-regulation of Dicer1 promotes cellular senescence and decreases the differentiation and stem cell-supporting capacities of mesenchymal stromal cells in patients with myelodysplastic syndrome," *Haematologica*, vol. 100, no. 2, pp. 194–204, 2015.

[55] F. C. Reis, J. L. Branquinho, B. B. Brandao et al., "Fat-specific Dicer deficiency accelerates aging and mitigates several effects of dietary restriction in mice," *Aging (Albany NY)*, vol. 8, no. 6, pp. 1201–1222, 2016.

[56] D. Gomez-Cabello, S. Callejas, A. Benguria, A. Moreno, J. Alonso, and I. Palmero, "Regulation of the microRNA processor DGCR8 by the tumor suppressor ING1," *Cancer Research*, vol. 70, no. 5, pp. 1866–1874, 2010.

[57] N. J. Lehrbach, C. Castro, K. J. Murfitt, C. Abreu-Goodger, J. L. Griffin, and E. A. Miska, "Post-developmental microRNA expression is required for normal physiology, and regulates aging in parallel to insulin/IGF-1 signaling in C. elegans," *RNA*, vol. 18, no. 12, pp. 2220–2235, 2012.

[58] D. Gomez-Cabello, I. Adrados, D. Gamarra et al., "DGCR8-mediated disruption of miRNA biogenesis induces cellular senescence in primary fibroblasts," *Aging Cell*, vol. 12, no. 5, pp. 923–931, 2013.

[59] S. Satpathy, C. Guerillon, T. S. Kim et al., "SUMOylation of the ING1b tumor suppressor regulates gene transcription," *Carcinogenesis*, vol. 35, no. 10, pp. 2214–2223, 2014.

[60] E. Candi, I. Amelio, M. Agostini, and G. Melino, "MicroRNAs and p63 in epithelial stemness," *Cell Death and Differentiation*, vol. 22, no. 1, pp. 12–21, 2015.

[61] S. Srikantan, B. S. Marasa, K. G. Becker, M. Gorospe, and K. Abdelmohsen, "Paradoxical microRNAs: individual gene repressors, global translation enhancers," *Cell Cycle*, vol. 10, no. 5, pp. 751–759, 2011.

[62] D. Gatfield, G. Le Martelot, C. E. Vejnar et al., "Integration of microRNA miR-122 in hepatic circadian gene expression," *Genes & Development*, vol. 23, no. 11, pp. 1313–1326, 2009.

[63] S. Bail, M. Swerdel, H. Liu et al., "Differential regulation of microRNA stability," *RNA*, vol. 16, no. 5, pp. 1032–1039, 2010.

[64] P. Sethi and W. J. Lukiw, "Micro-RNA abundance and stability in human brain: specific alterations in Alzheimer's disease temporal lobe neocortex," *Neuroscience Letters*, vol. 459, no. 2, pp. 100–104, 2009.

[65] Z. S. Kai and A. E. Pasquinelli, "MicroRNA assassins: factors that regulate the disappearance of miRNAs," *Nature Structural & Molecular Biology*, vol. 17, no. 1, pp. 5–10, 2010.

[66] J. Winter and S. Diederichs, "Argonaute proteins regulate microRNA stability: increased microRNA abundance by Argonaute proteins is due to microRNA stabilization," *RNA Biology*, vol. 8, no. 6, pp. 1149–1157, 2011.

[67] B. Yao, L. B. La, Y. C. Chen, L. J. Chang, and E. K. L. Chan, "Defining a new role of GW182 in maintaining miRNA stability," *Embo Reports.*, vol. 13, no. 12, pp. 1102–1108, 2012.

[68] A. D'Ambrogio, W. Gu, T. Udagawa, C. C. Mello, and J. D. Richter, "Specific miRNA stabilization by Gld2-catalyzed monoadenylation," *Cell Reports*, vol. 2, no. 6, pp. 1537–1545, 2012.

[69] J. Boele, H. Persson, J. W. Shin et al., "PAPD5-mediated 3′ adenylation and subsequent degradation of miR-21 is disrupted in proliferative disease," *Proceedings of the National Academy of Sciences of the United States of America*, vol. 111, no. 31, pp. 11467–11472, 2014.

[70] S. Chatterjee and H. Grosshans, "Active turnover modulates mature microRNA activity in Caenorhabditis elegans," *Nature*, vol. 461, no. 7263, pp. 546–549, 2009.

[71] T. S. Miki, S. Ruegger, D. Gaidatzis, M. B. Stadler, and H. Grosshans, "Engineering of a conditional allele reveals multiple roles of XRN2 in Caenorhabditis elegans development and substrate specificity in microRNA turnover," *Nucleic Acids Research*, vol. 42, no. 6, pp. 4056–4067, 2014.

[72] B. Yu, Z. Yang, J. Li et al., "Methylation as a crucial step in plant microRNA biogenesis," *Science*, vol. 307, no. 5711, pp. 932–935, 2005.

[73] Y. Zhao, Y. Yu, J. Zhai et al., "The Arabidopsis nucleotidyl transferase HESO1 uridylates unmethylated small RNAs to trigger their degradation," *Current Biology*, vol. 22, no. 8, pp. 689–694, 2012.

[74] M. Abe, A. Naqvi, G. J. Hendriks et al., "Impact of age-associated increase in 2′-O-methylation of miRNAs on aging and neurodegeneration in Drosophila," *Genes & Development*, vol. 28, no. 1, pp. 44–57, 2014.

[75] S. Weilner, R. Grillari-Voglauer, H. Redl, J. Grillari, and T. Nau, "The role of microRNAs in cellular senescence and age-related conditions of cartilage and bone," *Acta Orthopaedica*, vol. 86, no. 1, pp. 92–99, 2015.

[76] A. Carnero, "Markers of cellular senescence," *Methods in Molecular Biology*, vol. 965, pp. 63–81, 2013.

[77] J. Williams, F. Smith, S. Kumar, M. Vijayan, and P. H. Reddy, "Are microRNAs true sensors of ageing and cellular senescence?" *Ageing Research Reviews*, vol. 35, pp. 350–363, 2017.

[78] H. J. Jung and Y. Suh, "Circulating miRNAs in ageing and ageing-related diseases," *Journal of Genetics and Genomics*, vol. 41, no. 9, pp. 465–472, 2014.

[79] E. E. Creemers, A. J. Tijsen, and Y. M. Pinto, "Circulating microRNAs: novel biomarkers and extracellular communicators in cardiovascular disease?" *Circulation Research*, vol. 110, no. 3, pp. 483–495, 2012.

[80] F. Olivieri, M. Capri, M. Bonafe et al., "Circulating miRNAs and miRNA shuttles as biomarkers: perspective trajectories of healthy and unhealthy aging," *Mechanisms of Ageing and Development*, 2016.

[81] T. Smith-Vikos, Z. Liu, C. Parsons et al., "A serum miRNA profile of human longevity: findings from the Baltimore Longitudinal Study of Aging (BLSA)," *Aging (Albany NY)*, vol. 8, no. 11, pp. 2971–2987, 2016.

[82] G. Mushtaq, N. H. Greig, F. Anwar et al., "miRNAs as circulating biomarkers for Alzheimer's disease and Parkinson's disease," *Medicinal Chemistry*, vol. 12, no. 3, pp. 217–225, 2016.

[83] M. Hackl, U. Heilmeier, S. Weilner, and J. Grillari, "Circulating microRNAs as novel biomarkers for bone diseases - complex signatures for multifactorial diseases?" *Molecular and Cellular Endocrinology*, vol. 432, pp. 83–95, 2016.

[84] T. Machida, T. Tomofuji, D. Ekuni et al., "MicroRNAs in salivary exosome as potential biomarkers of aging," *International Journal of Molecular Sciences*, vol. 16, no. 9, pp. 21294–21309, 2015.

[85] T. Kiko, K. Nakagawa, T. Tsuduki, K. Furukawa, H. Arai, and T. Miyazawa, "MicroRNAs in plasma and cerebrospinal fluid as potential markers for Alzheimer's disease," *Journal of Alzheimer's Disease*, vol. 39, no. 2, pp. 253–259, 2014.

[86] M. Yang, A. D. Haase, F. K. Huang et al., "Dephosphorylation of tyrosine 393 in argonaute 2 by protein tyrosine phosphatase 1B regulates gene silencing in oncogenic RAS-induced senescence," *Molecular Cell*, vol. 55, no. 5, pp. 782–790, 2014.

[87] J. T. Mendell and E. N. Olson, "MicroRNAs in stress signaling and human disease," *Cell*, vol. 148, no. 6, pp. 1172–1187, 2012.

[88] O. C. Maes, J. An, H. Sarojini, and E. Wang, "Murine microRNAs implicated in liver functions and aging process," *Mechanisms of Ageing and Development*, vol. 129, no. 9, pp. 534–541, 2008.

[89] N. Li, S. Muthusamy, R. Liang, H. Sarojini, and E. Wang, "Increased expression of miR-34a and miR-93 in rat liver during aging, and their impact on the expression of Mgst1 and Sirt1," *Mechanisms of Ageing and Development*, vol. 132, no. 3, pp. 75–85, 2011.

[90] M. Buler, U. Andersson, and J. Hakkola, "Who watches the watchmen? Regulation of the expression and activity of sirtuins," *The FASEB Journal*, vol. 30, no. 12, pp. 3942–3960, 2016.

[91] T. Ito, S. Yagi, and M. Yamakuchi, "MicroRNA-34a regulation of endothelial senescence," *Biochemical and Biophysical Research Communications*, vol. 398, no. 4, pp. 735–740, 2010.

[92] T. Tabuchi, M. Satoh, T. Itoh, and M. Nakamura, "MicroRNA-34a regulates the longevity-associated protein SIRT1 in coronary artery disease: effect of statins on SIRT1 and microRNA-34a expression," *Clinical Science (London, England)*, vol. 123, no. 3, pp. 161–171, 2012.

[93] F. Lamoke, S. Shaw, J. Yuan et al., "Increased oxidative and nitrative stress accelerates aging of the retinal vasculature in the diabetic retina," *PloS One*, vol. 10, no. 10, article e0139664, 2015.

[94] R. Menghini, V. Casagrande, M. Cardellini et al., "MicroRNA 217 modulates endothelial cell senescence via silent information regulator 1," *Circulation*, vol. 120, no. 16, pp. 1524–1532, 2009.

[95] Z. Chen, L. Wen, M. Martin et al., "Oxidative stress activates endothelial innate immunity via sterol regulatory element binding protein 2 (SREBP2) transactivation of microRNA-92a," *Circulation*, vol. 131, no. 19, pp. 805–814, 2015.

[96] X. Y. Bai, Y. Ma, R. Ding, B. Fu, S. Shi, and X. M. Chen, "miR-335 and miR-34a promote renal senescence by suppressing mitochondrial antioxidative enzymes," *Journal of the American Society of Nephrology*, vol. 22, no. 7, pp. 1252–1261, 2011.

[97] F. Fleissner, V. Jazbutyte, J. Fiedler et al., "Short communication: asymmetric dimethylarginine impairs angiogenic progenitor cell function in patients with coronary artery disease through a microRNA-21-dependent mechanism," *Circulation Research*, vol. 107, no. 1, pp. 138–143, 2010.

[98] R. Faraonio, P. Salerno, F. Passaro et al., "A set of miRNAs participates in the cellular senescence program in human diploid fibroblasts," *Cell Death and Differentiation*, vol. 19, no. 4, pp. 713–721, 2012.

[99] Y. Liu, X. Li, S. Zhu et al., "Ectopic expression of miR-494 inhibited the proliferation, invasion and chemoresistance of pancreatic cancer by regulating SIRT1 and c-Myc," *Gene Therapy*, vol. 22, no. 9, pp. 729–738, 2015.

[100] R. Xiong, Z. Wang, Z. Zhao et al., "MicroRNA-494 reduces DJ-1 expression and exacerbates neurodegeneration," *Neurobiology of Aging*, vol. 35, no. 3, pp. 705–714, 2014.

[101] A. Csiszar, T. Gautam, D. Sosnowska et al., "Caloric restriction confers persistent anti-oxidative, pro-angiogenic, and anti-inflammatory effects and promotes anti-aging miRNA expression profile in cerebromicrovascular endothelial cells of aged rats," *American Journal of Physiology. Heart and Circulatory Physiology*, vol. 307, no. 3, pp. H292–H306, 2014.

[102] X. Cheng, C. H. Ku, and R. C. Siow, "Regulation of the Nrf2 antioxidant pathway by microRNAs: new players in micromanaging redox homeostasis," *Free Radical Biology & Medicine*, vol. 64, pp. 4–11, 2013.

[103] E. J. Smith, K. P. Shay, N. O. Thomas, J. A. Butler, L. F. Finlay, and T. M. Hagen, "Age-related loss of hepatic Nrf2 protein homeostasis: potential role for heightened expression of miR-146a," *Free Radical Biology & Medicine*, vol. 89, pp. 1184–1191, 2015.

[104] M. Vasa-Nicotera, H. Chen, P. Tucci et al., "miR-146a is modulated in human endothelial cell with aging," *Atherosclerosis*, vol. 217, no. 2, pp. 326–330, 2011.

[105] H. Xu, C. Goettsch, N. Xia et al., "Differential roles of PKCalpha and PKCepsilon in controlling the gene expression of Nox4 in human endothelial cells," *Free Radical Biology & Medicine*, vol. 44, no. 8, pp. 1656–1667, 2008.

[106] H. Bu, G. Baraldo, G. Lepperdinger, and P. Jansen-Durr, "mir-24 activity propagates stress-induced senescence by down regulating DNA topoisomerase 1," *Experimental Gerontology*, vol. 75, pp. 48–52, 2016.

[107] S. Tuduri, L. Crabbe, C. Conti et al., "Topoisomerase I suppresses genomic instability by preventing interference between replication and transcription," *Nature Cell Biology*, vol. 11, no. 11, pp. 1315–1324, 2009.

[108] A. Lal, Y. Pan, F. Navarro et al., "miR-24-mediated downregulation of H2AX suppresses DNA repair in terminally differentiated blood cells," *Nature Structural & Molecular Biology*, vol. 16, no. 5, pp. 492–498, 2009.

[109] S. Brunner, D. Herndler-Brandstetter, C. R. Arnold et al., "Upregulation of miR-24 is associated with a decreased DNA damage response upon etoposide treatment in highly differentiated CD8(+) T cells sensitizing them to apoptotic cell death," *Aging Cell*, vol. 11, no. 4, pp. 579–587, 2012.

[110] Y. Liu, W. Qiang, X. Xu et al., "Role of miR-182 in response to oxidative stress in the cell fate of human fallopian tube epithelial cells," *Oncotarget*, vol. 6, no. 36, pp. 38983–38998, 2015.

[111] Z. Liu, J. Liu, M. F. Segura et al., "MiR-182 overexpression in tumourigenesis of high-grade serous ovarian carcinoma," *The Journal of Pathology*, vol. 228, no. 2, pp. 204–215, 2012.

[112] B. Caballero and A. Coto-Montes, "An insight into the role of autophagy in cell responses in the aging and neurodegenerative brain," *Histology and Histopathology*, vol. 27, no. 3, pp. 263–275, 2012.

[113] S. E. Wohlgemuth, R. Calvani, and E. Marzetti, "The interplay between autophagy and mitochondrial dysfunction in oxidative stress-induced cardiac aging and pathology," *Journal of Molecular and Cellular Cardiology*, vol. 71, pp. 62–70, 2014.

[114] X. Liu, B. Fu, D. Chen et al., "miR-184 and miR-150 promote renal glomerular mesangial cell aging by targeting Rab1a and Rab31," *Experimental Cell Research*, vol. 336, no. 2, pp. 192–203, 2015.

[115] R. Menghini, V. Casagrande, A. Marino et al., "MiR-216a: a link between endothelial dysfunction and autophagy," *Cell Death & Disease*, vol. 5, no. 1, article e1029, 2014.

[116] S. Venkataraman, I. Alimova, R. Fan, P. Harris, N. Foreman, and R. Vibhakar, "MicroRNA 128a increases intracellular ROS level by targeting Bmi-1 and inhibits medulloblastoma cancer cell growth by promoting senescence," *PloS One*, vol. 5, no. 5, article e10748, 2010.

[117] J. Liu, L. Cao, J. Chen et al., "Bmi1 regulates mitochondrial function and the DNA damage response pathway," *Nature*, vol. 459, no. 7245, pp. 387–392, 2009.

[118] Y. Zhu, Y. Yan, D. R. Principe, X. Zou, A. Vassilopoulos, and D. Gius, "SIRT3 and SIRT4 are mitochondrial tumor suppressor proteins that connect mitochondrial metabolism and carcinogenesis," *Cancer and Metabolism*, vol. 2, p. 15, 2014.

[119] A. Lang, S. Grether-Beck, M. Singh et al., "MicroRNA-15b regulates mitochondrial ROS production and the senescence-associated secretory phenotype through sirtuin 4/SIRT4," *Aging (Albany NY)*, vol. 8, no. 3, pp. 484–505, 2016.

[120] R. Greussing, M. Hackl, P. Charoentong et al., "Identification of microRNA-mRNA functional interactions in UVB-induced senescence of human diploid fibroblasts," *BMC Genomics*, vol. 14, p. 224, 2013.

[121] K. R. Yu, S. Lee, J. W. Jung et al., "MicroRNA-141-3p plays a role in human mesenchymal stem cell aging by directly targeting ZMPSTE24," *Journal of Cell Science*, vol. 126, Part 23, pp. 5422–5431, 2013.

[122] A. Magenta, C. Cencioni, P. Fasanaro et al., "miR-200c is upregulated by oxidative stress and induces endothelial cell apoptosis and senescence via ZEB1 inhibition," *Cell Death and Differentiation*, vol. 18, no. 10, pp. 1628–1639, 2011.

[123] B. Mateescu, L. Batista, M. Cardon et al., "miR-141 and miR-200a act on ovarian tumorigenesis by controlling oxidative stress response," *Nature Medicine*, vol. 17, no. 12, pp. 1627–1635, 2011.

[124] S. Cufi, A. Vazquez-Martin, C. Oliveras-Ferraros et al., "Metformin lowers the threshold for stress-induced senescence: a role for the microRNA-200 family and miR-205," *Cell Cycle*, vol. 11, no. 16, pp. 1235–1246, 2012.

[125] G. Li, C. Luna, J. Qiu, D. L. Epstein, and P. Gonzalez, "Alterations in microRNA expression in stress-induced cellular senescence," *Mechanisms of Ageing and Development*, vol. 130, no. 11-12, pp. 731–741, 2009.

[126] S. W. Ryu, J. H. Woo, Y. H. Kim, Y. S. Lee, J. W. Park, and Y. S. Bae, "Downregulation of protein kinase CKII is associated with cellular senescence," *FEBS Letters*, vol. 580, no. 3, pp. 988–994, 2006.

[127] J. Y. Kang, J. J. Kim, S. Y. Jang, and Y. S. Bae, "The p53-p21(Cip1/WAF1) pathway is necessary for cellular senescence induced by the inhibition of protein kinase CKII in human colon cancer cells," *Molecules and Cells*, vol. 28, no. 5, pp. 489–494, 2009.

[128] S. Y. Kim, Y. H. Lee, and Y. S. Bae, "MiR-186, miR-216b, miR-337-3p, and miR-760 cooperatively induce cellular senescence by targeting alpha subunit of protein kinase CKII in human colorectal cancer cells," *Biochemical and Biophysical Research Communications*, vol. 429, no. 3-4, pp. 173–179, 2012.

[129] Q. Pan, X. Liao, H. Liu et al., "MicroRNA-125a-5p alleviates the deleterious effects of ox-LDL on multiple functions of human brain microvessel endothelial cells," *American Journal of Physiology. Cell Physiology*, vol. 312, no. 2, pp. C119–C130, 2017.

Hindawi
Oxidative Medicine and Cellular Longevity
Volume 2017, Article ID 7968905, 9 pages
https://doi.org/10.1155/2017/7968905

Research Article

Inhibition of miR-302 Suppresses Hypoxia-Reoxygenation-Induced H9c2 Cardiomyocyte Death by Regulating Mcl-1 Expression

Yao-Ching Fang[1] and Chi-Hsiao Yeh[1,2]

[1]*Department of Thoracic and Cardiovascular Surgery, Chang Gung Memorial Hospital, Keelung, Taiwan*
[2]*College of Medicine, Chang Gung University, Taoyuan, Taiwan*

Correspondence should be addressed to Chi-Hsiao Yeh; yehccl@cgmh.org.tw

Received 10 November 2016; Revised 30 January 2017; Accepted 7 March 2017; Published 11 April 2017

Academic Editor: Jaideep Banerjee

MicroRNAs play important roles in cell proliferation, differentiation, and apoptosis, and their expression influences cardiomyocyte apoptosis resulting from ischemia-induced myocardial infarction. Here, we determined the role of miR expression in cardiomyocyte apoptosis during hypoxia and reoxygenation. The rat cardiomyocyte cell line H9c2 was incubated for 3 h in normal or hypoxia medium, followed by reoxygenation for 24 h and transfection with a miR-302 mimic or antagomir. The effect of miR-302 on myeloid leukemia cell-differentiation protein-1 (Mcl-1) expression was determined by western blot, real-time polymerase chain reaction, and luciferase reporter assays, with cell viability assays. We observed that miR-302 expression was elevated by hypoxia/reoxygenation injury and increased further or decreased by transfection of the miR-302 mimic or miR-302 antagomir, respectively. Additionally, elevated miR-302 levels increased apoptosis-related protein levels and cardiomyocyte apoptosis, and luciferase reporter assays revealed miR-302 binding to the Mcl-1 mRNA 3′ untranslated region. Our findings suggested that miR-302 overexpression aggravated hypoxia/reoxygenation-mediated cardiomyocyte apoptosis by inhibiting antiapoptotic Mcl-1 expression, thereby activating proapoptotic molecules. Furthermore, results indicating cardiomyocyte rescue from hypoxia/reoxygenation injury following treatment with miR-302 antagomir suggested that miR-302 inhibition might constitute a therapeutic strategy for protection against cardiomyocyte apoptosis during hypoxia/reoxygenation injury.

1. Introduction

MicroRNAs (miRs) are a group of noncoding RNAs (~20–25 nucleotides in length) that downregulate mRNA expression through binding to their 3′ untranslated region (3′UTR) [1]. Over 1000 miRs have been discovered in human beings [2], and several mechanisms of miR-induced target suppression have been described [3]. Moreover, miRs regulate cell proliferation, differentiation, apoptosis, autophagy, and development by upregulating or downregulating mRNA expression [4–8].

Cardiomyocyte apoptosis occurs when cardiac tissue is exposed to a stressor, such as ischemia and/or reperfusion, during myocardial infarction, which is a major cause of morbidity and mortality worldwide [9]. Our previous study revealed that upon cardiomyocyte hypoxia/reoxygenation (H/R) injury, alterations in miR expression occur, causing disturbances in downstream mRNA expression and apoptotic pathway regulation [10]. Other studies reported that certain diseases, such as myocardial infarction, ischemia-reperfusion, and arrhythmia, can be treated or prevented by pharmacological (mimics or antagomirs) or genetic approaches to alter miR expression [2, 11–15]. miRs can also regulate mRNA expression to mitigate H/R injury. Cheng et al. [2] reported that miR-21 inhibits cell death under H/R conditions by regulating expression of the programmed cell death 4 (*PDCD4*) gene, which is also targeted by miR-499 [2]. Additionally, they found that miR-499 mitigates lipopolysaccharide-induced cardiac cell death by inhibiting the translation of *PDCD4* and *sex-determining region* Y- (SRY-) box *6* mRNA [15]. miR-20a also inhibits expression of the apoptotic factor Egl

nine homolog 3 to protect cardiomyocytes from H/R injury [11]. Furthermore, several miRs, including miR-210 (which regulates angiogenesis) [14], miR-199a (which modulates hypoxia-inducible factor-1α (HIF-1α) expression) [16], and miR-494 (which upregulates p-Akt, HIF-1α, and heme oxygenase-1 expression) [17], protect cells from hypoxia- or ischemia-induced damage.

During cardiomyocyte H/R injury, pro- and antiapoptotic proteins of the B-cell lymphoma 2 (Bcl-2) family are in disequilibrium in the mitochondrial membrane, leading to changes in membrane potential, leakage of cytochrome *c* from the mitochondrion, and subsequent activation and binding of caspase-9 to form apoptosomes, which ultimately activate caspase-3 and induce apoptosis [18]. The binding of myeloid leukemia cell-differentiation protein-1 (Mcl-1), an antiapoptotic protein of the Bcl-2 family, to proapoptotic proteins, such as Bas, Bid, or Bak, inhibits apoptosis [19]. miRs regulate gene expression posttranscriptionally by direct endonucleolytic cleavage or slicer-independent decay of mRNAs and posttranslationally by decreasing the rate of translation [20]. The binding of the seed sequence in miRs to a complementary sequence in the mRNA 3′UTR promotes mRNA degradation, whereas failure to bind due to the sequences not being complementary can result in translation inhibition [21]. miR-302 transcriptionally regulates gene expression and methylation [22] and supports reprogramming in stem cells during hypoxia [23, 24]. As a putative upstream regulator of Mcl-1 expression, the role of miR-302 in protecting cardiomyocytes from H/R remains unknown. Here, we investigated whether miR-302 binds to the 3′UTR of Mcl-1 mRNA and the effects of that binding activity on protecting H9c2 cardiomyocytes from H/R injury.

2. Materials and Methods

2.1. Cell Culture. The rat cardiomyocyte cell line H9c2 was cultured in Dulbecco's modified Eagle medium (Thermo Fisher Scientific, Waltham, MA, USA) containing 10% fetal bovine serum at 37°C in a humidified atmosphere containing 95% air and 5% CO_2. Cells were rendered quiescent by serum starvation for 24 h before all experiments. H/R injury was induced by hypoxia for 3 h (i.e., incubation in oxygen and glucose deprivation medium containing 2.3 mM $CaCl_2$, 5.6 mM KCl, 154 mM NaCl, 5 mM Hepes, and 3.6 mM $NaHCO_3$ (pH 7.4) and under an atmosphere of 5% CO_2, 85% N_2, 10% H_2, and <0.1% O_2), followed by the addition of glucose (4500 mg/L) to the medium and reoxygenation for 24 h in a humidified atmosphere (95% air and 5% CO_2) at 37°C. Control cells were incubated at 37°C under 95% air and 5% CO_2 for 27 h. To upregulate and downregulate miR-302 expression, an miR-302 mimic (m302; 50 or 100 nM; Thermo Fisher Scientific) or antagomir (i302; 50–100 nM; Thermo Fisher Scientific) was transfected into cells using Lipofectamine 2000 (Invitrogen, Carlsbad, CA, USA) according to manufacturer instructions. Nonsense control (NC) miR (100 nM) was also used as an internal control. The sequences of the nonsense miR, miR-302 mimic, and miR-302 antagomir were as follows: NC, 5′-UCACAACCUCCUAGAAAGAGUAGA-3′; miR-302 mimic, 5′-UAAGUGCUUCCAUGUUUUGGUGA-3′; and miR-302 antagomir, 5′-AUUCACGAAGGUACAAAAC CACU-3′.

2.2. Luciferase Reporter Assay. The Mcl-1 3′UTR sequences (three repeats of 5′-TCTCTAAGGACCTAAAAGCACTTT-3′) were synthesized and subcloned into a PsiCheck2 vector (psi-Mcl-1; Promega, Madison, WI, USA). The PsiCheck2 vector without the Mcl-1 3′UTR was used as a control. Cells were cotransfected with 200 ng of plasmids containing 3′ UTR or nonsense sequences and 100 nM miR mimic or a 100 nM NC miR (Thermo Fisher Scientific) according to manufacturer instructions using Lipofectamine 2000 reagent (Thermo Fisher Scientific). Experiments were performed in triplicate. After 48 h, cells were harvested and their luciferase activities were measured using the Luciferase dual-reporter kit (Promega) according to manufacturer instructions.

2.3. Real-Time Quantitative Polymerase Chain Reaction (qPCR). The expression of Mcl-1 and miR-302 was examined by real-time qPCR using glyceraldehyde-3-phosphate dehydrogenase (GAPDH) or U6 as internal controls, respectively. A poly-A tail was added to the extracted total RNA, which was then reverse transcribed into cDNA, to extend RNA length. Mcl-1 and miR-302 expression was quantified following cDNA annealing using the following real-time PCR primers: Mcl-1 forward, 5′-TGCTTCGGAAACTGGACAT TAAA-3′ and Mcl-1 reverse, 5′-ATGGGTCATCACTCG AGAAAAAG-3′; miR-302 forward, 5′-TAAGTGCTTCCA TGTTTTGGTGA-3′ and miR-302 reverse, 5′-GAACATG TCTGCGTATCTCAGACTTC-3′; GAPDH forward, 5′-AT GACTCTACCCACGGCAAG-3′ and GAPDH reverse, 5′-GGAAGATGGTGATGGGTTTC-3′; U6 forward, 5′-GCTT CGGCAGCACATATA-3′ and U6 reverse, 5′-AACGCTTC ACGAATTTGCGT-3′.

2.4. Western Blot Analysis. Proteins were resolved based on molecular weight via electrophoresis on 8%, 10%, and 12% polyacrylamide gels, followed by transfer to a polyvinylidene difluoride membrane. The membrane was blocked and incubated with antibodies for cleaved caspase-3, cleaved caspase-9, poly ADP ribose polymerase (PARP; Cell Signaling Technology, Danvers, MA, USA), β-actin (Sigma-Aldrich, St. Louis, MO, USA), and Mcl-1 (Abcam, Cambridge, MA, USA). Protein levels were analyzed using an enhanced chemiluminescence detection kit (GE Healthcare, Wauwatosa, WI, USA).

2.5. 3-(4,5-Dimethylthiazol-2-yl)-2,5-diphenyltetrazolium Bromide (MTT). Following incubation and treatment with different miRs under control or H/R conditions for 27 h, cell viability was tested by incubation with MTT reagent (Sigma-Aldrich) at a final concentration of 0.5 mg/mL and a temperature of 37°C for 4 h. The optical density of the purple MTT formazan product was measured at 570 nm using an enzyme-linked immunosorbent assay (ELISA) reader. The absorbance of cells transfected with NC was regarded as indicating 100% viability.

3′ aguGGUU-UUGUACCUUCGUGAAu 5′ miR-302
3′ ucuCUAAGGACCUAAAAGCACUUu 3′ Mcl-1 3′UTR (2209–2232)

(a) Sequence matching between 3′UTR of Mcl-1 gene and miR-302 binding site

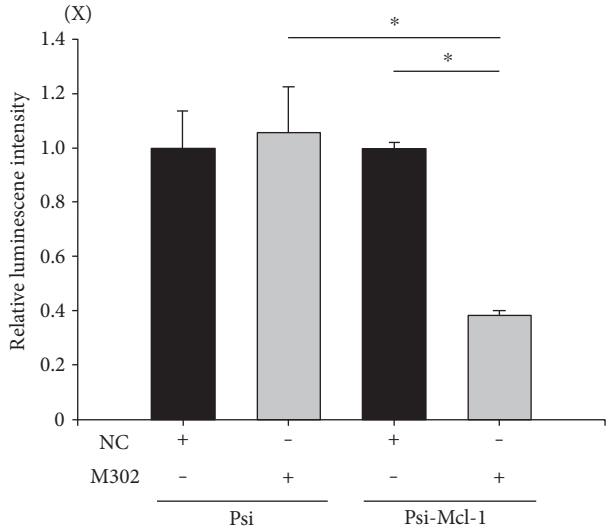

(b) Dual-luciferase reporter assay

Figure 1: miR-302 regulates the transcriptional activity of *Mcl-1* by targeting its 3′UTR. (a) The 3′UTR sequence (2209–2232) of *Mcl-1* contains a miR-302a-binding site as predicted by miRanda (http://microRNA.org). (b) Mcl-1 is a miR-302 target based on dual-luciferase reporter results. Luciferase activity was evaluated in H9c2 cells transfected with the PsiCheck2 vector only or with PsiCheck2 vectors containing the Mcl-1 3′UTR with nonsense control (NC) or a miR-302 mimic (m302). Data are presented as the mean ± STD of six experiments. $^*p < 0.05$.

2.6. Lactate Dehydrogenase (LDH) Release Assay. H9c2 cells were incubated in 96-well plates under hypoxic conditions, followed by reoxygenation, and LDH released to the medium from damaged cells was measured using an LDH cytotoxicity kit (Roche, Indianapolis, IN, USA) and ELISA reader to measure the change in absorbance at 490 nm. The absorbance of cells treated with Triton X-100 (Sigma-Aldrich) was regarded as indicating 100% cytotoxicity.

2.7. Flow Cytometry. H9c2 cells (1×10^6) were collected, washed with cold phosphate buffer, and resuspended with 1x binding buffer containing Annexin V-FITC and propidium iodide (PI; Sigma-Aldrich) for double staining according to manufacturer instructions (BD Bioscience, San Jose, CA, USA). The collected samples were analyzed by flow cytometry (Beckman Coulter, San Diego, CA, USA), and the percentage of living cells, apoptotic cells, and necrotic cells was calculated using Kaluza software (Beckman Coulter).

2.8. Statistical Analysis. All data are expressed as the mean ± standard deviation (STD), and a $p < 0.05$ was regarded as significant. A two-tailed unpaired Student's *t*-test or analysis of variance (ANOVA) was used to compare two or more than three groups, respectively. ANOVA with a post hoc Scheffe's test was used to evaluate the statistical significance of differences between groups.

3. Results

3.1. miR-302 Binds to the Mcl-1 mRNA 3′UTR. To determine whether miR-302 binds to Mcl-1 mRNA, we utilized a reporter gene (luciferase) conjugated to the Mcl-1 3′UTR inserted into a PsiCheck2 vector. We predicted that upon miR-302 binding to the Mcl-1 3′UTR (Figure 1(b), mirSVR score: −1.094; http://www.microrna.org/), reporter-gene expression would decrease. miRs exhibiting a mirSVR score of ≤−1.0 represent the top 7% of predictions and exhibit a >35% probability of having a (Z-transformed) log expression change of at least −1 concerning downregulation of the predicted gene [24]. Cells were transfected with the following vector combinations: (1) luciferase vector not containing the Mcl-1 3′UTR (PsiCheck2), (2) luciferase vector containing the Mcl-1 3′UTR (psi-Mcl-1) and the NC vector, (3) PsiCheck2 and the vector containing m302, (4) psi-Mcl-1 and the NC vector, or (5) psi-Mcl-1 and the vector containing m302. Transfection with psi-Mcl-1 and m302, but not psi-Mcl-1 and NC, PsiCheck2 and m302, or PsiCheck2 and NC decreased luciferase activity (Figure 1(b)). These results indicated that miR-302 binds to the target sequence in the Mcl-1 3′UTR.

3.2. Transfection of the miR-302 Mimic and Antagomir Upregulates and Downregulates miR-302 Expression, Respectively, in an H/R Injury Model. We examined the

effects of H/R injury on miR-302 expression in H9c2 cardiomyocytes following transfection with NC, m302, and i302. Results of qPCR analysis (Figure 2) showed that miR-302 expression increased significantly in H9c2 cells transfected with m302 or i302 as compared with cells transfected with NC following H/R injury, respectively.

3.3. miR-302 Regulates Mcl-1 mRNA and Protein Levels in H/R-Injured Cardiomyocytes. qPCR analysis showed that transfection with m302 or i302 (compared with transfection with NC) significantly decreased and increased Mcl-l mRNA levels in H9c2 cardiomyocytes following H/R injury, respectively, as compared with levels observed in NC-transfected controls (Figure 3(a)). Mcl-1 mRNA levels in H9c2 cardiomyocytes cotransfected with m302 and i302 prior to H/R injury were significantly higher and lower, respectively, than those observed in cells transfected with either m302 or i302 alone. Western blot analyses showed that patterns of Mcl-1 protein expression following H/R injury in H9c2 cardiomyocytes transfected with either NC, m302, or i302 matched levels of Mcl-1 mRNA expression (Figure 3(b)); however, Mcl-1 mRNA levels were lower in cells cotransfected with m302 and i302 as compared with levels in cells transfected with i302 alone; although, the difference was not significant.

3.4. miR-302 Induces Cardiomyocyte Injury. To examine the possible damage attributable to miR-302 expression during H/R injury, H9c2 cardiomyocyte viability was evaluated by MTT and LDH assays. We observed that LDH levels increased significantly in cells transfected with m302 (50 nM: 132.7 ± 7.9%; or 100 nM: 184.5 ± 26.4%) versus NC (50 nM: 103.2 ± 12.9%; or 100 nM: 100 ± 21.9%; $p < 0.05$ for both groups ($n = 6$)) (Figure 4(b)). Our results showed that LDH levels increased along with higher concentrations of transfected m302 ($p = 0.047$; $n = 6$). Additionally, the amount of LDH released from cardiomyocytes following H/R injury was reduced by decreasing the expression of miR-302 following i302 transfection and by elevating Mcl-1 expression. Cotransfection of m302 (50 nM) and i320 (50 nM and 100 nM) also significantly decreased the amount of LDH released (50 nM m302: 125.3 ± 18.2%; and 50 nM i302: 101.0 ± 12.8%) during H/R injury, and cotransfection with the higher concentration of i302 decreased LDH release to an even greater extent ($p = 0.048$).

However, during H/R injury, m302 transfection (50 nM: 92.3 ± 7.2%; and 100 nM: 81.2 ± 5.2%) decreased cell viability, whereas i302 transfection increased cell viability (50 nM: 107.9 ± 1.5%; and 100 nM: 116.2 ± 7.8%) according to MTT assay results (Figure 4(a)). The increases and decreases in viability were more pronounced in cells transfected with higher concentrations (50 nM versus 100 nM) of m302 ($p = 0.02$) or i302 ($p = 0.03$). These results indicated that cotransfection with i302 and m302 increased cell viability as compared with levels observed following m302 transfection alone.

3.5. i302 Transfection Decreases Cell Apoptosis and Necrosis in H/R-Injured Cardiomyocytes. Levels of apoptosis and necrosis can be elevated by stress. Flow cytometry with Annexin V and PI staining were used to determine levels of

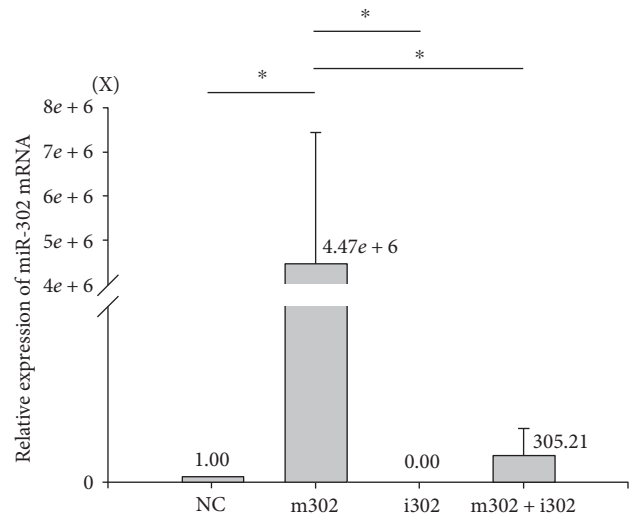

Figure 2: Assessment of miR302 expression and transfection efficiency as determined by real-time qPCR analysis in H9c2 cells exposed to H/R injury. Data are presented as the mean ± STD of six experiments. $^*p < 0.05$. NC: nonsense control; m302: miR-302 mimic; i302: miR-302 antagomir.

cardiomyocyte apoptosis or necrosis during H/R injury and whether changes in apoptosis and necrosis are aggravated or mitigated by miR-302 expression. Cells not stained by either Annexin V or PI were considered healthy. The number of PI-stained cells (necrotic) and PI + Annexin V costained cells (late apoptotic) was calculated as a percentage of the total number of cardiomyocyte nuclei (Figure 5). Following H/R injury, the percentage of apoptotic H9c2 cardiomyocytes was significantly higher following m302 transfection (30.4 ± 2.2%) as compared with that observed following NC transfection (17.5 ± 0.7%; $p = 0.0012$). Additionally, the percentage of apoptotic H9c2 cardiomyocytes was significantly lower following i302 transfection (13.2 ± 1.0%; $p = 0.014$) and i302 and m302 cotransfection (9.1 ± 0.8%; $p = 0.0003$) as compared with percentages accompanying NC transfection.

3.6. miR-302 Regulates the Expression and Activation of Apoptosis-Related Proteins. To determine whether the underlying mechanism of apoptotic suppression involves inhibition of miR-302 expression, levels of apoptosis-related proteins were evaluated by western blot analysis in cells transfected with NC, m302, i302, or m302 + i302 (Figure 6). Consistent with previous data, H9c2 cells transfected with m302 and exhibiting elevated miR-302 expression and reduced Mcl-1 expression also exhibited significantly increased levels of activated caspase-3 and -9 (both $p < 0.05$), which significantly increased the expression of cleaved PARP (both $p < 0.05$). However, cells transfected with i302 or cotransfected with m302 + i302 exhibited significantly reduced levels of activated caspase-3 and -9 and cleaved PARP.

4. Discussion

miRs are critical regulators of cell function [25] and influence a myriad of cell characteristics, including stem cell

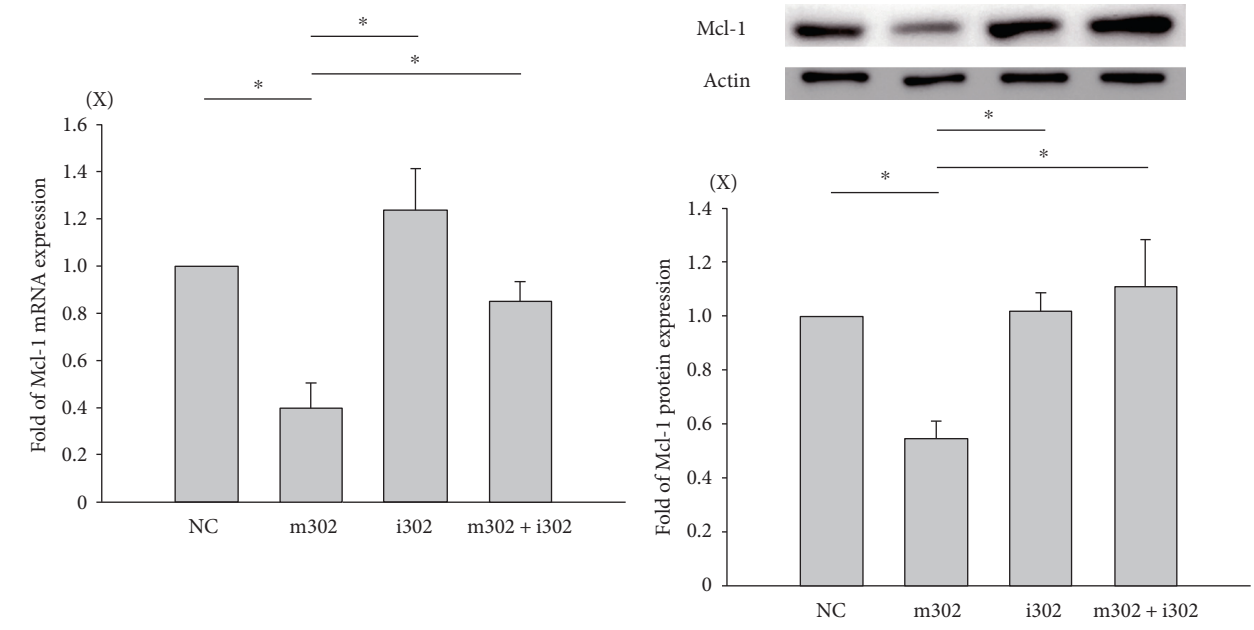

(a) Expression of Mcl-1 mRNA (b) Expression of Mcl-1 protein

FIGURE 3: H9c2 cardiomyocytes subjected to H/R injury in the presence of different concentrations of nonsense control (NC), miR-302 mimic (m302), and/or miR-302 antagomir (i302). Mcl-1 expression was assessed by (a) real-time qPCR and (b) western blot analysis. β-actin was used as an internal control. Data are presented as the mean ± STD of six experiments. $^{*}p < 0.05$ between two groups.

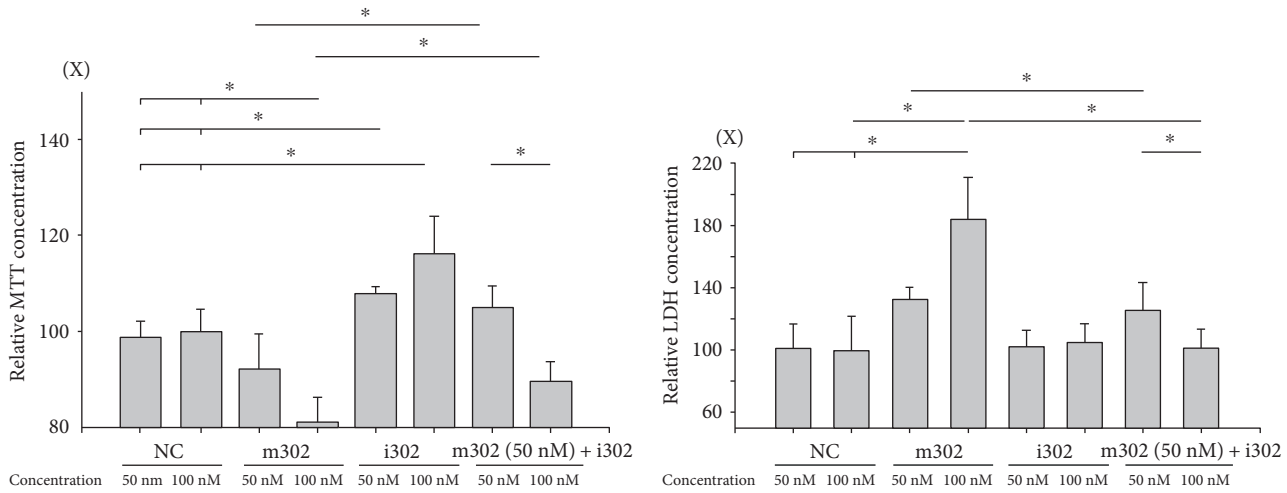

(a) MTT assay (b) LDH assay

FIGURE 4: H9c2 cardiomyocytes were subjected to H/R injury in the presence of different concentrations of miR-302 mimic (m302) and/or miR-302 antagomir (i302). Relative viability was assessed by (a) MTT and (b) LDH assays. Data are presented as the mean ± STD of six experiments. $^{*}p < 0.05$ compared with the group transfected with nonsense control (NC).

reprogramming, cardiac differentiation, and hypertrophy [5]. Successful manipulation of miRs can improve outcomes of cardiovascular disease and constitutes a new cardiovascular therapeutic strategy [26, 27]. In this study, we showed that decreasing miR-302 expression by transfection of a miR-302 antagonist elevated the expression of the antiapoptotic protein Mcl-1, decreased the activation of caspase-3 and -9, and reduced cardiomyocyte injury and death during H/R injury.

The antiapoptotic Mcl-1 protein is a member of the Bcl-2 family, a suppressor of apoptosis, and enhances cell viability during H/R [28]. Here, we confirmed that the Mcl-1 3′UTR is a miR-302 target. miR-302 plays a role in preventing cell death resulting from oxidant-induced damage [4] and affects the reprogramming of stem cells and somatic cells [29]. Additionally, miR-302-transfected cells can be used to repair heart damage [30], and another study found that miR-302 can inhibit the expression of transformation-related genes

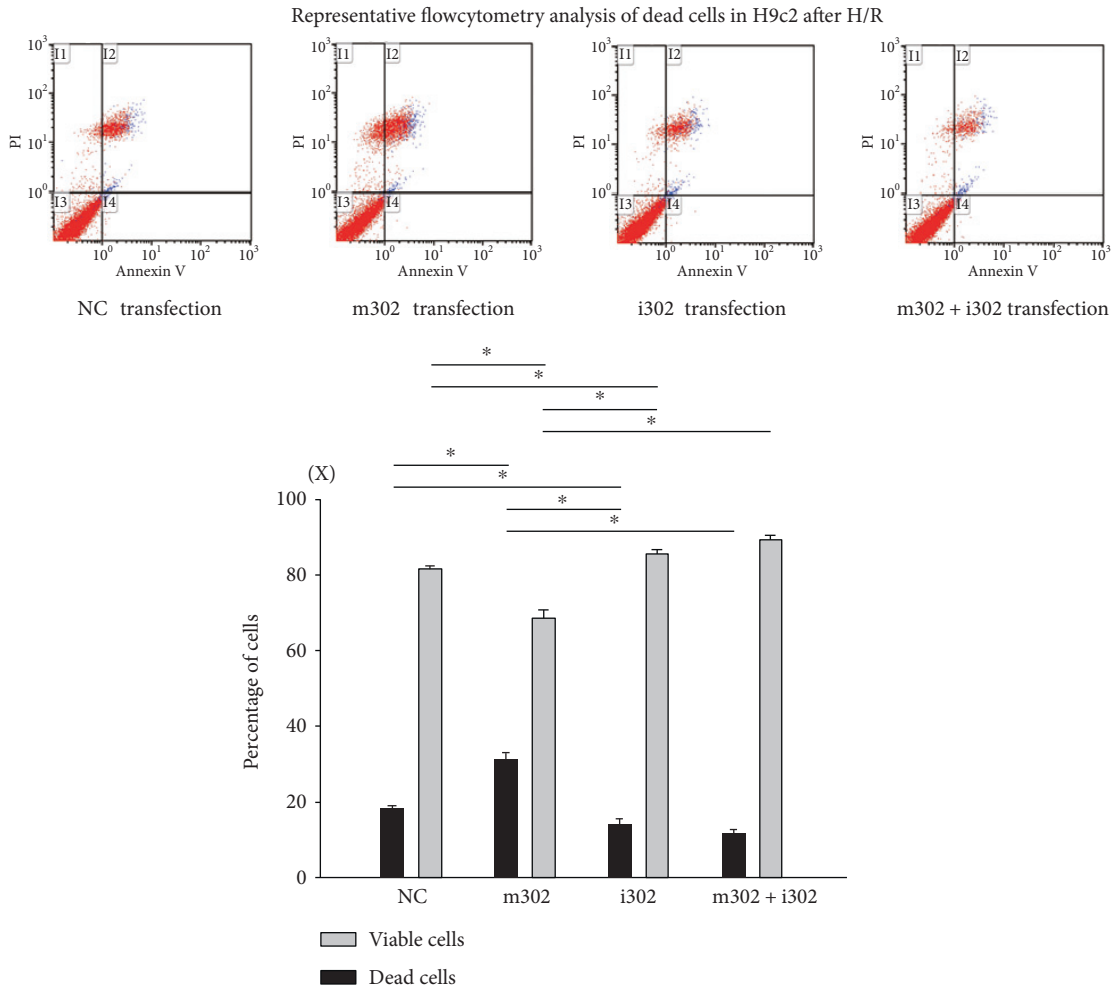

Figure 5: Flow cytometry analysis of cells subjected to H/R injury and transfection with nonsense control (NC), miR-302 mimic (m302; 100 nM), miR-302 antagomir (i302; 100 nM), or m302 + i302 (100 nM). The percentage of viable and apoptotic cardiomyocytes was analyzed in different groups. Data are presented as the mean ± STD of six experiments. $^{*}p < 0.05$ between two groups.

and exhibit a deprogramming effect on glioblastoma cells, implying that miR-302 could also be a cancer therapeutic target [31]. Regarding the effects of miR-302 on cell proliferation and reprogramming, Kuppusamy et al. [5] reported that miR-302 plays an important role in cardiomyocyte differentiation and maturation, especially after myocardial infarction [5]. However, the possible differential effects associated with miR-302 on cardiomyocytes under H/R injury had not been previously studied. According to our hypothesis, miR-302 downregulation would result in elevation of Mcl-1 expression and reductions in cardiomyocyte death. We found that H/R-induced cell death was potentiated by miR-302 overexpression following m302 transfection, whereas decreased miR-302 expression via its antagomir (i302) protected cells from H/R injury. Moreover, cotransfection of i302 with m302 mitigated H/R-induced cell injury. Our results showed for the first time that elevated miR-302 expression was harmful to H/R-injured cardiomyocytes.

Additionally, we confirmed that miR-302 binds to the Mcl-1 3′UTR and decreases Mcl-1 mRNA and protein levels according to luciferase reporter results. Mcl-1 is capable of inhibiting the activation of proapoptotic proteins, such as Bax, Bak, or Bid, and the release of cytochrome *c* from mitochondria, thereby preventing apoptosis during H/R [19]. In H9c2 cells, m302 transfection elevated miR-302 expression, resulting in decreased Mcl-1 mRNA and protein levels during H/R, whereas i302 transfection in the presence or absence of m302 transfection attenuated H/R-induced miR-302 expression, rescued Mcl-1 mRNA and protein levels, and decreased cell injury. These results indicated that Mcl-1 expression was inhibited by miR-302 during H/R injury. Analysis of the percentage of cells undergoing apoptosis by Annexin V/PI double staining revealed that m302 transfection increased rates of cell death following H/R, whereas cotransfection with i302 significantly decreased the percentage of apoptotic cells. Therefore, inhibition of miR-302 expression decreased cytotoxicity, increased viability, and decreased apoptosis during H/R by promoting increased Mcl-1 protein levels.

Our results showed that the effects of m302 could be reversed by i302 cotransfection. miR-302 levels following m302 transfection were elevated as compared with those observed in other groups (Figure 2). Additionally, Mcl-1 mRNA levels were significantly decreased only in the m302-

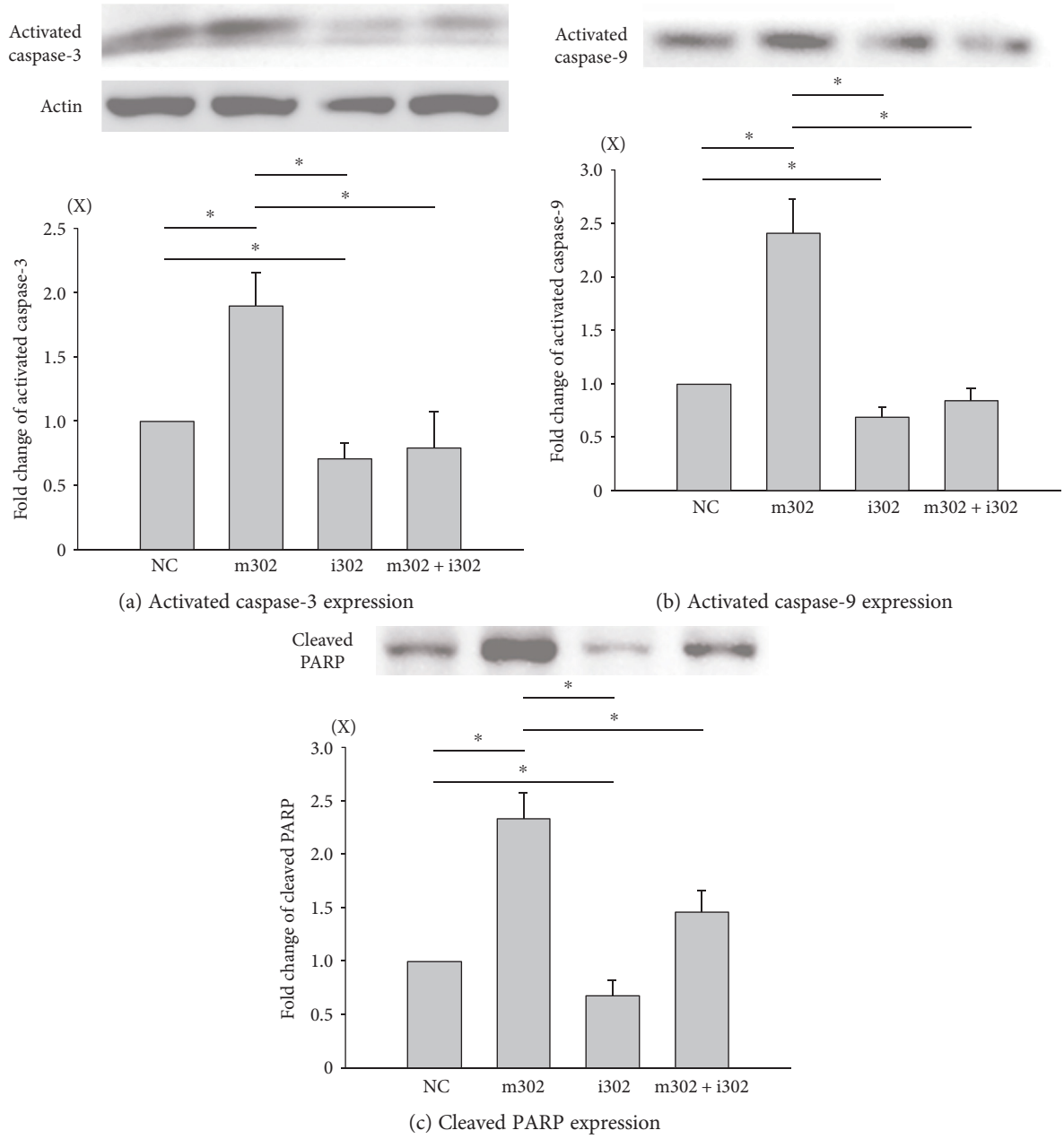

Figure 6: H9c2 cardiomyocytes subjected to H/R injury in the presence of different concentrations of nonsense control (NC), miR-302 mimic (m302), and/or miR-302 antagomir (i302). (a) Activated caspase-3, (b) activated caspase-9, and (c) cleaved PARP in different groups were analyzed by western blot. *B*-actin was used as an internal control. Data are presented as the mean ± STD of six analyses. $^*p < 0.05$ between two groups.

transfected group, indicating that high levels of miR-302 were capable of attenuating Mcl-1 levels. This finding verified our hypothesis that miR-302 was induced in cardiomyocyte H/R injury and subsequently inhibited the expression of Mcl-1 mRNA and protein.

Cardiomyocyte apoptosis is a key cellular event in cardiac ischemia/reperfusion injury [32]. Changes in Mcl-1 expression, as well as that of other key elements of the apoptosis pathway, such as phosphoinositide 3-kinase, Bcl-2, heat-shock protein 60, heat-shock protein 70, PDCD4, and Fas ligand, alter cellular response to ischemia-reperfusion injury [33]. Mcl-1 is involved in cardiomyocyte loss and contributes to a variety of cardiac pathologies, including heart failure and ischemia/reperfusion injury [34, 35]. Additionally, Mcl-1 is known to function as an upstream antagonist of the intrinsic death activators caspase-3 and -9, thereby inhibiting apoptosis while also being essential for maintaining cardiac mitochondrial homeostasis and inducing autophagy in the heart [34]. Wang et al. [35] found that Mcl-1 ablation results in a loss of cardiac contractility, followed by fatal cardiomyopathy [35]. Similar to our findings concerning miR-302, Zou et al. [8] reported that miR-153 targets Mcl-1 to modulate apoptosis and autophagy, thereby regulating the survival of cardiomyocytes during oxidative

stress [8]. Here, miR-302 overexpression or knockdown alone was shown to decrease and increase Mcl-1 protein levels, respectively.

Restoration of blood flow or reoxygenation produces free radicals that harm cells and tissues. In developing countries, myocardial infarction is a primary cause of death, because therapies to restore blood circulation are not always available. Therefore, maintenance of cardiomyocyte function to improve heart contraction is a potential therapeutic approach. According to recent studies, miRs regulate cells or tissues exposed to myocardial infarction or ischemia, with reports finding that miR-21 protects hearts from ischemic injury via PDCD4 expression [2], miR-361 transfected into rat hearts causes mitochondrial fission and myocardial ischemic injury [36], and miR-30b protects cardiomyocytes by inhibiting cyclophilin D [3]. Embryonic stem cells express high levels of the miR-302/367 cluster, with this expression regulated by the binding of transcription factors, such as octamer-binding transcription factor 3/4, SRY-box 2, and Nanog, to miR-302/367-cluster promoter regions. The miR-302/367 cluster subsequently increases stem cell self-renewal capacity, pluripotency, and maintenance of stemness [37]. miR-302 inhibits differentiation by inhibiting the differentiation factors Lefty1 and Lefty2 to maintain embryonic stem cell proliferation [37]. Furthermore, increases in hydrogen peroxide in quiescent fibroblasts lead to miR-302-mediated regulation of the cell cycle regulatory factor AT-rich interaction domain 4A and chemokine (C-C motif) ligand-5 mRNA levels [38]. Other cell-signaling pathways, such those related to bone morphogenetic protein signaling and the tumor necrosis factor-β/Nodal/Smad-2/3 pathway, are also regulated by the miR-302/367 cluster [39]. Here, our data showed that miR-302 increased cardiomyocyte apoptosis and regulated Mcl-1 mRNA and protein levels, resulting in elevated levels of Mcl-1 preventing cell death or tissue damage and decreased levels promoting apoptosis. Because miR-302 transfection preserves stem cell stemness, cells transfected with miR-302 and transplanted into the heart have been used to explore their ability to promote cell proliferation and the repair of cardiomyocytes damaged by myocardial infection. Similarly, we examined the effect of miR-302 transfection on H/R-injured cardiomyocytes, revealing that elevated miR-302 levels were detrimental to cells, whereas decreased miR-302 levels were beneficial according to an H/R model. These findings suggested that reducing miR-302 levels in cardiomyocytes during H/R might constitute an effective therapeutic intervention.

5. Conclusions

We found that miR-302 mediates H/R-induced cardiomyocyte death by regulating Mcl-1 expression. Therefore, miR-302 inhibition might offer an effective therapeutic strategy for the treatment of myocardial infarction or ischemia-related diseases.

Conflicts of Interest

The authors declare no conflicts of interest.

Acknowledgments

Chi-Hsiao Yeh was supported by the Grant NSC 104-2314-B-182A-133 from the National Science Council, Taiwan, Republic of China, and by the Grants CMRPG 2A0203 and 2A0213 from Chang Gung Memorial Hospital, Taiwan, Republic of China. Yao-Ching Fang was supported by the Grants CMRPG 2D0022 and 2D0023 from Chang Gung Memorial Hospital, Taiwan, Republic of China.

References

[1] R. D. Mortensen, M. Serra, J. A. Steitz, and S. Vasudevan, "Posttranscriptional activation of gene expression in *Xenopus laevis* oocytes by microRNA-protein complexes (microRNPs)," *Proceedings of the National Academy of Sciences of the United States of America*, vol. 108, no. 20, pp. 8281–8286, 2011.

[2] Y. Cheng, P. Zhu, J. Yang et al., "Ischaemic preconditioning-regulated mir-21 protects heart against ischaemia/reperfusion injury via anti-apoptosis through its target pdcd4," *Cardiovascular Research*, vol. 87, no. 3, pp. 431–439, 2010.

[3] K. Wang, T. An, L. Y. Zhou et al., "E2F1-regulated miR-30b suppresses cyclophilin D and protects heart from ischemia/reperfusion injury and necrotic cell death," *Cell Death and Differentiation*, vol. 22, no. 5, pp. 743–754, 2014.

[4] J. Y. Kim, K. K. Shin, A. L. Lee et al., "MicroRNA-302 induces proliferation and inhibits oxidant-induced cell death in human adipose tissue-derived mesenchymal stem cells," *Cell Death & Disease*, vol. 5, no. 8, article e1385, 2014.

[5] K. T. Kuppusamy, H. Sperber, and H. Ruohola-Baker, "MicroRNA regulation and role in stem cell maintenance, cardiac differentiation and hypertrophy," *Current Molecular Medicine*, vol. 13, no. 5, pp. 757–764, 2013.

[6] Y. Zhang, N. Fisher, S. E. Newey et al., "The impact of proliferative potential of umbilical cord-derived endothelial progenitor cells and hypoxia on vascular tubule formation in vitro," *Stem Cells and Development*, vol. 18, no. 2, pp. 359–375, 2009.

[7] J. Zhou, X. Dong, Q. Zhou et al., "microRNA expression profiling of heart tissue during fetal development," *International Journal of Molecular Medicine*, vol. 33, no. 5, pp. 1250–1260, 2014.

[8] Y. Zou, W. Liu, J. Zhang, and D. Xiang, "miR-153 regulates apoptosis and autophagy of cardiomyocytes by targeting Mcl-1," *Molecular Medicine Reports*, vol. 14, no. 1, pp. 1033–1039, 2016.

[9] H. D. White, P. E. Aylward, Z. Huang et al., "Mortality and morbidity remain high despite captopril and/or valsartan therapy in elderly patients with left ventricular systolic dysfunction, heart failure, or both after acute myocardial infarction: results from the valsartan in acute myocardial infarction trial (VALIANT)," *Circulation*, vol. 112, no. 22, pp. 3391–3399, 2005.

[10] C. H. Yeh, T. P. Chen, Y. C. Wang, Y. M. Lin, and S. W. Fang, "MicroRNA-27a regulates cardiomyocytic apoptosis during cardioplegia-induced cardiac arrest by targeting interleukin 10–related pathways," *Shock*, vol. 38, no. 6, pp. 607–614, 2012.

[11] D. Frank, J. Gantenberg, I. Boomgaarden et al., "MicroRNA-20a inhibits stress-induced cardiomyocyte apoptosis involving its novel target egln3/phd3," *Journal of Molecular and Cellular Cardiology*, vol. 52, no. 3, pp. 711–717, 2011.

[12] J. Gong, J. P. Zhang, B. Li et al., "MicroRNA-125b promotes apoptosis by regulating the expression of Mcl-1, Bcl-w and IL-6R," *Oncogene*, vol. 32, no. 25, pp. 3071–3079, 2012.

[13] P. L. Hedley, A. L. Carlsen, K. M. Christiansen et al., "MicroRNAs in cardiac arrhythmia: DNA sequence variation of MiR-1 and MiR-133A in long QT syndrome," *Scandinavian Journal of Clinical and Laboratory Investigation*, vol. 74, no. 6, pp. 485–491, 2014.

[14] S. Hu, M. Huang, Z. Li et al., "MicroRNA-210 as a novel therapy for treatment of ischemic heart disease," *Circulation*, vol. 122, Supplement 11, pp. S124–S131, 2010.

[15] Z. Jia, J. Wang, Q. Shi et al., "SOX6 and PDCD4 enhance cardiomyocyte apoptosis through LPS-induced miR-499 inhibition," *Apoptosis*, vol. 21, no. 2, pp. 174–183, 2015.

[16] S. Rane, M. He, D. Sayed et al., "Downregulation of miR-199a derepresses hypoxia-inducible factor-1alpha and sirtuin 1 and recapitulates hypoxia preconditioning in cardiac myocytes," *Circulation Research*, vol. 104, no. 7, pp. 879–886, 2009.

[17] G. Sun, Y. Zhou, H. Li et al., "Over-expression of microRNA-494 up-regulates hypoxia-inducible factor-1 alpha expression via pi3k/akt pathway and protects against hypoxia-induced apoptosis," *Journal of Biomedical Science*, vol. 20, no. 1, p. 100, 2013.

[18] H. Zou, R. Yang, J. Hao et al., "Regulation of the Apaf-1/caspase-9 apoptosome by caspase-3 and XIAP," *The Journal of Biological Chemistry*, vol. 278, no. 10, pp. 8091–8098, 2003.

[19] B. A. Croker, J. A. O'Donnell, C. J. Nowell et al., "Fas-mediated neutrophil apoptosis is accelerated by Bid, Bak, and Bax and inhibited by Bcl-2 and Mcl-1," *Proceedings of the National Academy of Sciences of the United States of America*, vol. 108, no. 32, pp. 13135–13140, 2011.

[20] M. A. Valencia-Sanchez, J. Liu, G. J. Hannon, and R. Parker, "Control of translation and mRNA degradation by miRNAs and siRNAs," *Genes & Development*, vol. 20, no. 5, pp. 515–524, 2006.

[21] D. W. Thomson, C. P. Bracken, and G. J. Goodall, "Experimental strategies for microRNA target identification," *Nucleic Acids Research*, vol. 39, no. 16, pp. 6845–6853, 2011.

[22] S. Foja, M. Jung, B. Harwardt, D. Riemann, O. Pelz-Ackermann, and I. S. Schroeder, "Hypoxia supports reprogramming of mesenchymal stromal cells via induction of embryonic stem cell-specific microRNA-302 cluster and pluripotency-associated genes," *Cellular Reprogramming*, vol. 15, no. 1, pp. 68–79, 2013.

[23] K. E. Hawkins, T. V. Sharp, and T. R. McKay, "The role of hypoxia in stem cell potency and differentiation," *Regenerative Medicine*, vol. 8, no. 6, pp. 771–782, 2013.

[24] D. Betel, A. Koppal, P. Agius, C. Sander, and C. Leslie, "Comprehensive modeling of microRNA targets predicts functional non-conserved and non-canonical sites," *Genome Biology*, vol. 11, no. 8, p. R90, 2010.

[25] B. Liao, X. Bao, L. Liu et al., "MicroRNA cluster 302-367 enhances somatic cell reprogramming by accelerating a mesenchymal-to-epithelial transition," *The Journal of Biological Chemistry*, vol. 286, no. 19, pp. 17359–17364, 2011.

[26] R. L. Montgomery and E. van Rooij, "MicroRNA regulation as a therapeutic strategy for cardiovascular disease," *Current Drug Targets*, vol. 11, no. 8, pp. 936–942, 2010.

[27] C. L. Song, B. Liu, H. Y. Diao et al., "Downregulation of microRNA-320 suppresses cardiomyocyte apoptosis and protects against myocardial ischemia and reperfusion injury by targeting IGF-1," *Oncotarget*, vol. 7, no. 26, pp. 39740–39757, 2016.

[28] M. Li, P. Gao, and J. Zhang, "Crosstalk between autophagy and apoptosis: potential and emerging therapeutic targets for cardiac diseases," *International Journal of Molecular Sciences*, vol. 17, no. 3, p. 332, 2016.

[29] K. Takahashi and S. Yamanaka, "Induction of pluripotent stem cells from mouse embryonic and adult fibroblast cultures by defined factors," *Cell*, vol. 126, no. 4, pp. 663–676, 2006.

[30] Y. Tian, Y. Liu, T. Wang et al., "A microRNA-Hippo pathway that promotes cardiomyocyte proliferation and cardiac regeneration in mice," *Science Translational Medicine*, vol. 7, no. 279, p. 279ra38, 2015.

[31] C. M. Yang, T. Chiba, B. Brill et al., "Expression of the miR-302/367 cluster in glioblastoma cells suppresses tumorigenic gene expression patterns and abolishes transformation related phenotypes," *International Journal of Cancer*, vol. 137, no. 10, pp. 2296–22309, 2015.

[32] A. Abbate, R. Bussani, M. S. Amin, G. W. Vetrovec, and A. Baldi, "Acute myocardial infarction and heart failure: role of apoptosis," *The International Journal of Biochemistry & Cell Biology*, vol. 38, no. 11, pp. 1834–1840, 2006.

[33] Y. Ye, J. R. Perez-Polo, J. Qian, and Y. Birnbaum, "The role of microRNA in modulating myocardial ischemia-reperfusion injury," *Physiological Genomics*, vol. 43, no. 10, pp. 534–542, 2011.

[34] R. L. Thomas, D. J. Roberts, D. A. Kubli et al., "Loss of MCL-1 leads to impaired autophagy and rapid development of heart failure," *Genes & Development*, vol. 27, no. 12, pp. 1365–13677, 2013.

[35] X. Wang, M. Bathina, J. Lynch et al., "Deletion of MCL-1 causes lethal cardiac failure and mitochondrial dysfunction," *Genes & Development*, vol. 27, no. 12, pp. 1351–1364, 2013.

[36] K. Wang, C. Y. Liu, X. J. Zhang et al., "miR-361-regulated prohibitin inhibits mitochondrial fission and apoptosis and protects heart from ischemia injury," *Cell Death and Differentiation*, vol. 22, no. 6, pp. 1058–1068, 2014.

[37] A. Barroso-delJesus, C. Romero-Lopez, G. Lucena-Aguilar et al., "Embryonic stem cell-specific miR302-367 cluster: human gene structure and functional characterization of its core promoter," *Molecular and Cellular Biology*, vol. 28, no. 21, pp. 6609–6619, 2008.

[38] M. G. Kumar, N. M. Patel, A. M. Nicholson, A. L. Kalen, E. H. Sarsour, and P. C. Goswami, "Reactive oxygen species mediate microRNA-302 regulation of AT-rich interacting domain 4a and C-C motif ligand 5 expression during transitions between quiescence and proliferation," *Free Radical Biology & Medicine*, vol. 53, no. 4, pp. 974–982, 2012.

[39] Z. Gao, X. Zhu, and Y. Dou, "The miR-302/367 cluster: a comprehensive update on its evolution and functions," *Open Biology*, vol. 5, no. 12, p. 150138, 2015.

Hindawi
Oxidative Medicine and Cellular Longevity
Volume 2017, Article ID 2696071, 8 pages
https://doi.org/10.1155/2017/2696071

Research Article

Redox Regulating Enzymes and Connected MicroRNA Regulators Have Prognostic Value in Classical Hodgkin Lymphomas

Peeter Karihtala,[1] Katja Porvari,[2] Ylermi Soini,[2] and Kirsi-Maria Haapasaari[2]

[1]*Department of Oncology and Radiotherapy, Medical Research Center Oulu, Oulu University Hospital and University of Oulu, Oulu, Finland*
[2]*Department of Pathology, Medical Research Center Oulu, Oulu University Hospital and University of Oulu, Oulu, Finland*

Correspondence should be addressed to Peeter Karihtala; peeter.karihtala@oulu.fi

Received 19 December 2016; Accepted 9 February 2017; Published 9 March 2017

Academic Editor: Jaideep Banerjee

There are no previous studies assessing the microRNAs that regulate antioxidant enzymes in Hodgkin lymphomas (HLs). We determined the mRNA levels of redox regulating enzymes peroxiredoxins (PRDXs) I–III, manganese superoxide dismutase (MnSOD), nuclear factor erythroid-derived 2-like 2 (Nrf2), and Kelch-like ECH-associated protein 1 (Keap1) from a carefully collected set of 41 classical HL patients before receiving any treatments. The levels of redoxmiRs, miRNAs known to regulate the above-mentioned enzymes, were also assessed, along with CD3, CD20, and CD30 protein expression. RNAs were isolated from freshly frozen lymph node samples and the expression levels were analyzed by qPCR. mir23b correlated inversely with CD3 and CD20 expressions ($p = 0.00076$; $r = -0.523$ and $p = 0.0012$; $r = -0.507$) and miR144 with CD3, CD20, and CD30 ($p = 0.030$; $r = -0.352$, $p = 0.041$; $r = -0.333$ and $p = 0.0032$; $r = -0.47$, resp.). High MnSOD mRNA levels associated with poor HL-specific outcome in the patients with advanced disease ($p = 0.045$) and high miR-122 levels associated with worse HL-specific survival in the whole patient population ($p = 0.015$). When standardized according to the CD30 expression, high miR212 and miR510 predicted worse relapse-free survival ($p = 0.049$ and $p = 0.0058$, resp.). In conclusion, several redoxmiRs and redox regulating enzyme mRNA levels associate with aggressive disease outcome and may also produce prognostic information in classical HL.

1. Introduction

Although modern polychemotherapy has significantly improved Hodgkin lymphoma (HL) survival rates, relapsed and refractory HL have still poor prognosis [1]. There are prognostic risk factor scores separately both in limited (IA–IIA) and in advanced (IIB–IV) stages of HL to guide the treatment selection. Nevertheless, prognosis varies considerably inside these classes and it would be of utmost importance to find novel prognostic and predictive biomarkers to help to select the patients at the highest risk for relapse.

We recently demonstrated a potential prognostic role of the protein expression of several cellular redox state regulating enzymes [2]. Since reactive oxygen species (ROS), especially superoxide anions, are produced primarily in mitochondria, mitochondrially located manganese superoxide dismutase (MnSOD or SOD2) is in the first-line defense by dismutating superoxide to the less harmful hydrogen peroxide (H_2O_2) and oxygen. H_2O_2 is further catalyzed to water and oxygen by peroxiredoxins (PRDXs), glutathione peroxidases, and catalase. PRDXs are a peroxidase family having multiple subcellular locations such as cytosol (PRDXs I, II, III, V, and VI), peroxisomes (PRDXs IV and V), lysosomes (PRDXs IV and VI), endoplasmic reticulum, extracellular space, Golgi apparatus (PRDX IV), and also mitochondria (PRDXs III) [3–6]. Their structure is conserved from bacteria to mammals and knockdown mice with PRDX I or II deficiency are susceptible to early aging and carcinogenesis [7–9]. PRDXs are involved in a variety of activities where

H_2O_2 is generated, including cellular metabolism, growth, differentiation, inflammation, and proliferation [10].

Nuclear factor erythroid-derived 2-like 2 (Nrf2) is considered as the main cellular redox state regulator. It is a transcription factor able to regulate the expression of genes for antioxidant enzymes, metal-binding proteins, drug-metabolizing enzymes, drug transporters, and molecular chaperones. Under basal conditions, Nrf2 is bound to a cytoplasmic complex with its inhibitor Kelch-like ECH-associated protein 1 (Keap1). During oxidative stress Nrf2 is released and moves to the nucleus where it complexes with a small maf proteins and consequently upregulates the above-mentioned genes [11, 12].

MicroRNAs are small, single-stranded, noncoding RNAs that are essential posttranscriptional regulators of gene expression. The knowledge of miRNA in the regulation of redox state regulating enzymes ("redoxmiRs") is rapidly increasing [13]. Although miRNAs are recognized as essential cellular homeostasis regulators, there is only limited amount of data on their role in the pathogenesis of HL with no existing literature on the impact of redoxmiRs in HL.

Cluster of differentiation proteins CD3, CD20, and CD30 are typically used as cell type markers of lymphocytes. Interestingly, they are membrane proteins with important physiological functions and likely to interact in oxidative stress also: CD3 is a coreceptor of T cell receptor, responsible for ligand-dependent initiation of intracellular signaling [14]. CD20 is a potential mediator of apoptosis through its interaction with membrane microdomains rich in src-family kinases [15], while CD30 is a member of tumor necrosis factor receptor superfamily [16].

Based on the results of our previous work assessing antioxidant protein expression in HL [2], we aimed here to clarify whether major redox regulator mRNA levels or miRNAs regulating them would associate with traditional prognostic factors of HL or chemoresistance or if they could serve as potential novel prognostic factors in classical HLs. We also compared their expression with CD30, a marker to detect Hodgkin's cells in classical Hodgkin's lymphoma, to CD20, a marker for B cell lineage, and CD3, a marker for T cell lineage.

2. Materials and Methods

2.1. Cases. The cohort consisted of 41 previously untreated classical Hodgkin lymphomas [17]. The samples were collected from the archives of Department of Pathology of Oulu University Hospital and they dated from the year 2000 until the year 2011. Freshly frozen lymph node samples were stored at −80°C. Clinical data of the patients were retrospectively collected from the patient records of Oulu University Hospital. Median follow-up of patients was 77.0 months and 6 patients had a relapse during the follow-up. Patients' characteristics are described in Table 1.

Table 1: Patient characteristics.

Male	20 (48.8%)
Limited stage	17 (41.5%)
Limited stage risk factors	8 (47.1%)[1]
International Prognostic Score > 2	9 (37.5%)[1]
B-symptoms	18 (43.9%)
WHO performance status ≥ 1	31.3%
Radiotherapy	21 (51.2%)
Relapsed	6 (14.6%)
CR with 1st-line ABVD	34 (82.9%)

[1]Percentage from the patients with limited stage and advanced stage, respectively.

2.2. CD3, CD20, and CD30 Immunohistochemistry. Sections of 4 μm thickness were cut from samples which had been routinely fixed in formalin and embedded in paraffin. The paraffin tissue sections were deparaffinized in xylene (5 min, 2 times) and rehydrated through graded ethanol. Antigen retrieval was performed by immersing sections in 10 mM sodium citrate buffer (pH 6.0) and boiling by microwave (95°C, 30 min). After boiling the sections were allowed to cool at room temperature and washed by PBS (5 min, 3 times). The sections were incubated in 3% hydrogen peroxidase for 10 min to inactivate endogenous peroxidases. After washing by PBS (5 min, 3 times), sections were incubated with the primary antibodies for 30 minutes at room temperature with a dilution of 1 : 300 for CD30 (code K5007, Dako, Dakopatts, Denmark), 1 : 1000 for CD20 (clone L26, Dako), and 1 : 50 for CD3 (clone PS1, Novocastra Biosystems Newcastle Ltd., Newcastle upon Tyne, UK). The following day, sections were washed repeatedly by PBS and incubated with Dako REALTM EnVision™/HRP, Rabbit/Mouse (Dako REAL EnVision Detection System: Dako, code K5007) for 1 h at room temperature. After washing repeatedly by PBS, the labelled secondary antibody was visualized by adding Dako REAL Substrate Buffer (Dako REAL EnVision Detection System: Dako, code K5007) containing Dako REAL DAB+ Chromogen (Dako REAL EnVision Detection System: Dako, code K5007). Sections were then counterstained with hematoxylin, dehydrated, and mounted. The data was evaluated by assessing the percentage of positive cells in the section for each antibody.

2.3. RNA Isolation and qPCR Analyses. Total RNA was extracted from lymph nodes using miRNeasy Mini Kit (Qiagen, Hilden, Germany). RNA quality was checked by electrophoresis. cDNA synthesis was done with miScript II Reverse Transcription Kit (Qiagen). miScript SYBR Green PCR Kit (Qiagen) was used for cDNA amplification by Rotor-Gene Q real-time quantitative PCR equipment (Qiagen). The following gene-specific primers were used for amplification; Keap1 (NM_203500.1): F (forward primer): 5′-GGTCCCCTACAGCCAAGGT-3′ and R: (reverse primer) 5′-CTGCATGGGGTTCCAGAAGAT-3′; Nrf2 (S74017.1): F: 5′-GCAGGACATGGATTTGATTGACA-3′ and R: 5′-TCATACTCTTTCCGTCGCTGA-3′; PRDX1 (NM_002574.3): F: 5′-CACTGACAAACATGGGGAAGT-3′ and R: 5′-TGCTCTTTTGGACATCAGGCT-3′; PRDX2 (NM_005809.5): F: 5′-GTCCAGGCCTTCCAGTACAC-3′ and R: 5′-TGTCATCCACGTTGGGCTTA-3′; PRDX3 (NM_006793.3): F: 5′-TTAAACATGGTTAGTTGCTAGTACAAGGA-3′ and

Table 2: Associations between CD3, CD20, and CD30 protein levels and redoxmRNAs and miRNAs regulating them.

	CD3	CD20	CD30
CD3			
CD20	$p = 0.000040$; $r = 0.615$		
CD30	NS	NS	NS
PRDX I mRNA	$p = 0.037$; $r = -0.339$	NS	NS
PRDX II mRNA			
PRDX III mRNA		$p = 0.046$; $r = -0.326$	
Nrf2 mRNA			
Keap1 mRNA		$p = 0.050$; $r = -0.320$	
SOD2 mRNA			
miR23b	$p = 0.00076$; $r = -0.523$	$p = 0.0012$; $r = -0.507$	
miR28	$p = 0.022$; $r = -0.370$	$p = 0.011$; $r = -0.409$	
miR93		$p = 0.031$; $r = -0.351$	
miR122			
miR144	$p = 0.030$; $r = -0.352$	$p = 0.041$; $r = -0.333$	$p = 0.0032$; $r = -0.471$
miR200a			
miR212			
miR383			
miR510			

R: 5′-TTGAGACATGATCTAAGAATAGCCTTCTA-3′; MnSOD (NM_000636.2): F: 5′-GGACACTTACAAATTGCTGCTT-3′ and R: 5′-CCACACATCAATCCCCAGCA-3′. GAPD (BC029618; F: 5-TGGAAGGACTCATGACCACA-3′ and R: 5-CCATCACGCCACAGTTT-3′) was used as reference gene for normalization of qPCR results in mRNA studies. For miRNA quantification, the following commercial miScript Primer Assays (Qiagen) were used: MIR23B, MIR28, MIR93, MIR122, MIR144, MIR200A, MIR212, MIR383, and MIR510. miScript Primer Assay for RNU6B was used for normalization of qPCR results in miRNA studies. Cycling was carried out as recommended in the PCR Kit with annealing temperatures of 60–68 or 55°C for mRNA and miRNA, respectively. Fluorescence signals were measured continuously during repetitive cycles in order to detect Ct values for target RNA and reference (GAPD or RNU6B) in the samples. Relative expression levels of mRNA or miRNA targets were calculated using $2^{-\Delta\Delta Ct}$ method [18], where $\Delta\Delta Ct = (Ct_{\text{target RNA}} - Ct_{\text{GAPD or RNU6B}})_{\text{sample}} - (Ct_{\text{target RNA}} - Ct_{\text{GAPD or RNU6B}})_{\text{reference sample}}$.

2.4. Statistical Analyses. Statistical analyses were performed by using IBM SPSS Statistics software, v. 22.0.0.0 (IBM Corporation, Armonk, NY, USA). The significance of associations was defined by using Mann–Whitney U test and Spearman's rho test with correlation coefficient. Kaplan–Meier curves with the log-rank test were applied in survival analysis. In survival analyses, median mRNA and miRNA levels were used as a cut-off for two-classed variable. Disease-specific survival (DSS) was calculated from the time of diagnosis to the time of confirmed Hodgkin lymphoma-related death and relapse-free survival (RFS) from the time of diagnosis to the confirmed relapse. Values of p of less than 0.05 were considered significant.

The ethical committee of the Northern Ostrobothnia Hospital District approved the study design. During the data collection and management, the principles of the Declaration of Helsinki were followed.

3. Results

CD3, CD20, and CD30 immunohistochemistry were applied to 37 (90.2%) samples. The median expressions of CD3, CD20, and CD30 were 65%, 35%, and 7%, and the ranges of expression were 30–95%, 5–80%, and 1–55%, respectively.

CD3 expression correlated with CD20 expression highly significantly ($p = 0.000040$; $r = 0.615$). mir23b correlated inversely with CD3 and CD20 expressions ($p = 0.00076$; $r = -0.523$ and $p = 0.0012$; $r = -0.507$) and miR144 with CD3, CD20, and CD30 ($p = 0.030$; $r = -0.352$, $p = 0.041$; $r = -0.333$ and $p = 0.0032$; $r = -0.47$, resp.). These and other correlations between CD3, CD20, and CD30 and redoxmiRs and mRNAs are presented in Table 2.

Higher redox regulator mRNA levels associated consistently with the traditional factors of poor prognosis (Table 3). PRDX I mRNA expression associated with the presence of limited stage risk factors ($p = 0.027$) and was the most highly expressed in nodular sclerosis subtype, following mixed cell histology, and the least expressed in the tumors with classical lymphocyte-rich subtype ($p = 0.008$). MnSOD mRNA expression associated with the presence of B-symptoms ($p = 0.006$) and higher Nrf2 mRNA levels with the presence of risk factors of limited disease ($p = 0.027$). Nrf2 and Keap1 mRNA expressions correlated strongly with each other ($p = 1.09 \times 10^{-9}$, $r = 0.787$).

Table 3: Two-sided p values < 0.05 when the clinicopathological parameters are set against mRNA and miRNA expression. ↑ and ↓ indicate the direction of the correlation.

Expression of mRNA or miRNA	Histology	Stage		B-symptoms	Risk factors		Disease-specific survival	
		Limited	Advanced		Limited disease	Advanced disease	Limited disease	Advanced disease
PRDX I	0.008[1]				0.027			
miR-510								
PRDX II								
miR-122↑				0.037			0.015	
PRDX III								
miR-23b↑			0.021	0.025				
miR-383↑	0.019[1]		0.014	0.013	0.015			
MnSOD↑				0.006				0.045
miR-212↑			0.047					
Nrf2↑					0.027			
miR-28↑			0.036					
miR-93								
miR-144								
Keap1								
miR-200a↑	0.044[1]							

[1] Most frequently expressed in nodular sclerosis subtype followed by mixed cell histology and least expressed in lymphocyte-rich subtype.

miR-383 ($p = 0.019$) and miR-200a ($p = 0.044$) were the most frequently expressed in the tumors with nodular sclerosis histology, following mixed cell histology. It was least expressed in the tumors with classical lymphocyte-rich subtype. miR-383 also associated with the presence of advanced disease ($p = 0.014$) and B-symptoms at the time of diagnosis ($p = 0.013$). Likewise, miR-23b associated with advanced stage ($p = 0.021$) and B-symptoms ($p = 0.025$). miR-212 and miR-28 levels were elevated in advanced stage tumors (p values 0.047 and 0.036, resp.). High miR-122 expression associated with the presence of B-symptoms.

Higher MnSOD mRNA levels associated with shorter disease-specific survival (DSS), but only in the patients with advanced disease ($p = 0.045$). miR-122 levels over median were also in association with poor DSS ($p = 0.015$) in the whole patient population.

When the results were standardized according to the CD30 expression (miRNA or mRNA variable divided by CD30 expression), there were no significant associations with stage, histology, chemotherapy response, or risk factors. Instead, higher miR212 and miR510 levels predicted worse RFS ($p = 0.049$ and $p = 0.0058$, resp.) (Figure 1).

4. Discussion

We report here a potential role of high mitochondrial antioxidant enzyme MnSOD mRNA levels in predicting worse prognosis of patients with untreated classical HL. This is in line with our previous study assessing MnSOD protein expression in HL [2] and may be related to the role of MnSOD in chemoresistance. In addition, miR510, PRDX I suppressing redoxmiR, was a highly significant predictor of dismal RFS when miR510 level was related to CD30 protein expression.

The most common first-line treatment of classical HL is ABVD, consisting of intensive dosing of doxorubicin, bleomycin, vinblastine, and dacarbazine. The mechanism of action of these drugs is closely linked to ROS generation, especially in the case of bleomycin. Although doxorubicin and vinblastine have other mechanisms of action, they also induce ROS generation leading to enhanced oxidative stress and eventually apoptosis [19, 20]. Dacarbazine produces also toxic amounts of ROS contributing to cell lysis [21]. Increasing evidence suggests that antioxidant enzyme levels may confer to chemoresistance in solid tumors, although evidence is still scarce in lymphomas [22, 23] and almost absent in HLs. We previously reported that stronger immunohistochemical MnSOD expression is a predictor of worse RFS in classical HLs. Consistently, in the current material MnSOD mRNA levels associated with poor DSS rates. This was observed only with the patients with advanced disease, among the patient group most eagerly requiring novel prognostic and predictive factors to guide treatment intensification. miR-212 has been identified to interact with MnSOD mRNA and miR-212 downregulation is able to promote colorectal cancer metastasis growth in animal models [24]. This effect seems to be cancer-specific since in the current material increased miR-212 level was associated with advanced rather than limited stage. High miR212 levels also predicted worse RFS, when the expression was related to CD30 expression.

Both plasma miRNA levels and specific miRNA signatures have been demonstrated to have prognostic significance in classical HL [25, 26]. Although there are no previous publications on the miRNA regulation of redox status in HL, there is a plenty of data on the impact of miRNAs to redox regulators in other cancers. miR-28, miR-144, and miR-93 have been shown to directly repress the major antioxidant

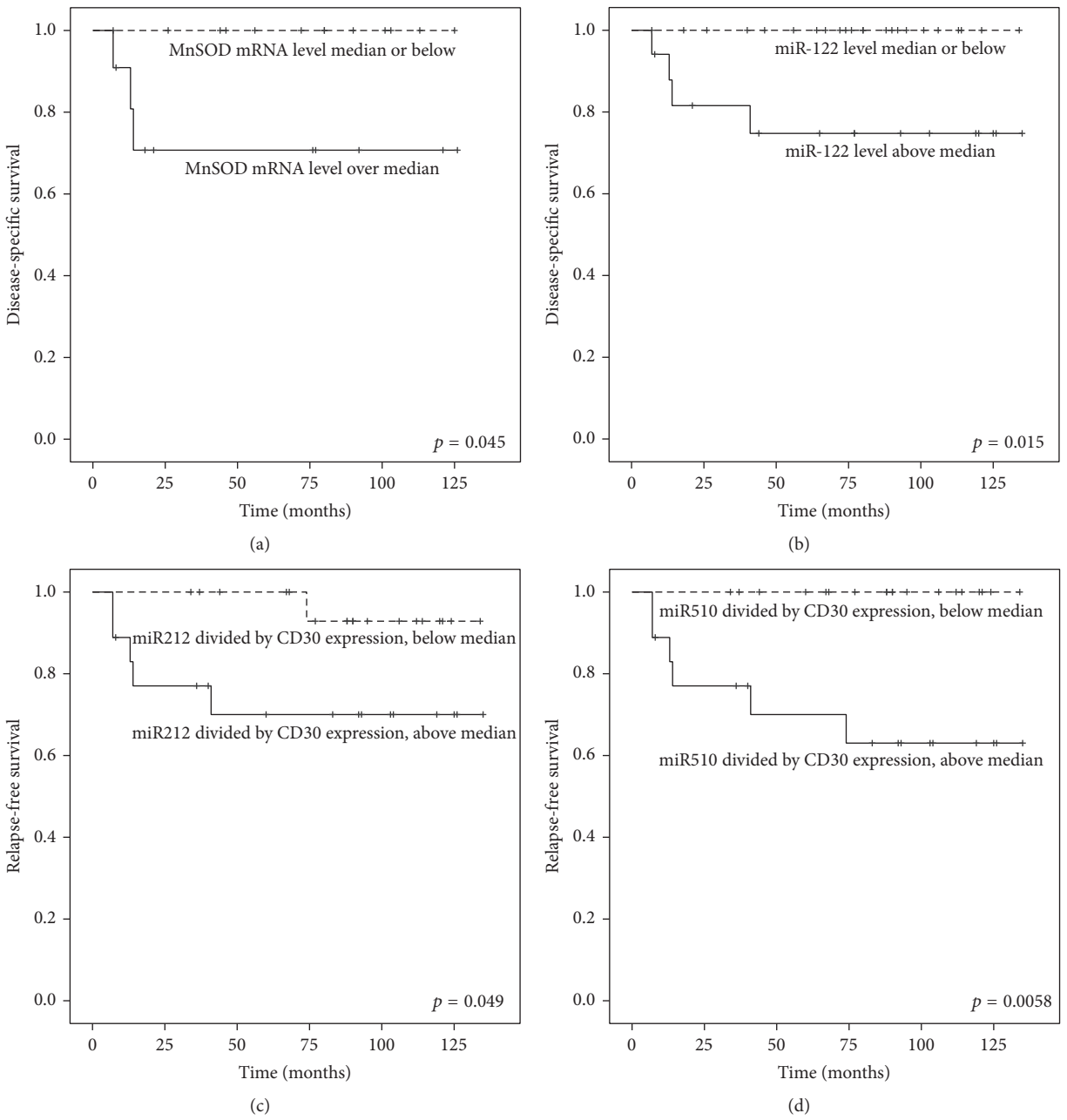

Figure 1: Kaplan–Meier curve of disease-specific survival according to MnSOD mRNA level only in patients with advanced stage (a) and miR-122 level in the whole patient population (b). Relapse-free survival is demonstrated when miR212 (c) and miR510 (d) are standardized according to the CD30 expression.

response inducer Nrf2 mRNA [27]. On the other hand, there is emerging evidence that Nrf2 can regulate the expression of various miRNAs [28]. Nrf2 has emerged as a prognostic factor in multiple solid carcinomas [29–31] and the blockage of Nrf2 by siRNA leads to the inhibition of tumor growth and increased chemosensitivity [32]. We found that Nrf2 mRNA levels associated with the presence of traditional risk factors of limited stage HL and miR-28 was clearly overexpressed in the advanced disease. Although the results with miR-28 are more difficult to explain with the current knowledge of its function, our data suggests that Nrf2 may accelerate HL lymphomagenesis. This would be in line with multiple solid carcinomas, but, to confirm this hypothesis, more mechanistic approach should be adopted in further studies. In addition, we noted that Keap1 and Nrf2 mRNA levels had extremely significant correlation. Although this seems logical based on the inhibitory function of Keap1 against Nrf2 activation, to the best of our knowledge this correlation has been previously reported only at protein level, but not at mRNA level [33].

In solid tumors PRDX overexpression has been connected to chemoresistance and radiotherapy resistance, the

best data being available from PRDX II [34, 35]. There is increasing evidence from in vitro studies that PRDX II may block especially doxorubicin-mediated cell death [36, 37]. PRDX I and II overexpression have also been connected to poorer prognostic factors in several carcinomas [36, 38–40]. In the present study PRDX I associated with more aggressive histological subtypes of classical HL and the presence of risk factors in limited stage patients. Although these are surrogates to aggressive disease course in general, no link between PRDX I mRNA expression and survival or chemoresistance was observed. miR510 has been proposed as PRDX I 3′UTR binding, tumor growth promoting oncomiR in breast cancer [41, 42], while in ovarian cancer high miR510 expression levels associate with better outcome [43]. When we standardized miR510 expression with CD30 expression, none of the patients with low mir510 expression had relapse during the follow-up, compared to the dismal RFS of 63% at 6 years in those with high mir510 levels. Furthermore, high levels of PRDX II mRNA targeting miRNA, miR-122 [44], associated with the dismal outcome in the current material. The prognostic role of miR-122 has been previously quite extensively studied especially in hepatocellular carcinoma with both worse and better survival being reported [45–47].

miR-23b and miR-383 have been recognized to downregulate the mitochondrial isoform of PRDX family, PRDX III [48, 49]. miR-23b and miR-383 were linked to advanced stage and B-symptoms and miR-383 associated also with poor risk factor profile of limited disease and to more aggressive histological subtype. miR-23b is a well characterized miRNA of aggressive features of several solid carcinomas ("oncomiR") and may induce tumor survival, accelerate glioma invasion, and promote prostate cancer cell proliferation by regulating PTEN and its downstream signaling [50, 51]. In gastric cancer miR-23b associated with unfavorable survival [52]. The existing evidence from miR-383 suggests its tumor-suppressing role in vitro, for example, hepatocellular, pancreatic, and esophageal carcinomas [53–55]. This is in contradiction with our results, which suggested both miR-23b and miR-383 act clearly oncogenic in Hodgkin lymphomas.

CD30 is a well-known marker for Hodgkin's cells in classical Hodgkin's lymphoma. Hodgkin's lymphoma is a type of neoplastic disease where the tissue contains abundant reactive elements. Of lymphocytes T cells are overwhelmingly present but B cells and macrophages constitute also a significant part of the reactive elements in tumor tissue. No reports have been published on CD30 and miRNAs studied here. In ALK negative large anaplastic lymphomas there was a high miR-155 expression [56]. Interestingly, miR-155 is also highly expressed in Hodgkin lymphoma cell lines, but CD30 is not a target for this miRNA even though anaplastic large cell lymphoma and Hodgkin lymphoma both share its expression [57]. Additionally, miR-155 is elevated in all B cell lymphomas except Burkitt's lymphoma [58].

CD3 complex mediates activation of the T cell receptor across the plasma membrane [59]. Since T cells are most abundantly expressed in Hodgkin lymphoma low miR-23b or miR-144 expression would be expected to be due to low miRNA synthesis in these cells. In scanning miRNA levels from blood cells these miRNAs were not, however, found to be present among the most over- or underexpressed miRNAs in CD3 or CD19 positive cells [60]. miR-23b or miR-144 are not either targets against CD3 gene complex [61]. The miRNAs studied here, however, are regulating the Nrf2/Keap1 axis in these cells, and in activated T or B cells their expression may change. The inverse association of CD3 as well as CD20 with miR-23b or miR-144 thus suggests a promotion of Nrf2 related antioxidative response in the lymphatic elements. In line with this, high miR-144 levels have been shown to reduce Nrf2 levels [62]. miR23, on the other hand, has an impact on Keap1 synthesis [63]. All in all, the associations between CD30, CD3, CD20, and the miRNAs shown in this study most likely reflects the activation of the oxidative defense system in stromal lymphocytes and Hodgkin cells.

5. Conclusions

This study gives support to the previous evidence that MnSOD expression could have prognostic impact in untreated advanced HL. It is possible that MnSOD mRNA levels could also be used as predictive factor, but this has to be assessed in future studies. Several redoxmiRs, especially miR510, also appear as potentially interesting indicators of aggressive disease course and should be validated in larger cohort of HLs, the most optimally with microdissection technique enabling assessing different tumor compartments separately.

Competing Interests

The authors declare that there is no conflict of interests regarding the publication of this paper.

References

[1] J. Kuruvilla, A. Keating, and M. Crump, "How I treat relapsed and refractory Hodgkin lymphoma," *Blood*, vol. 117, no. 16, pp. 4208–4217, 2011.

[2] H. Bur, K.-M. Haapasaari, T. Turpeenniemi-Hujanen et al., "Oxidative stress markers and mitochondrial antioxidant enzyme expression are increased in aggressive Hodgkin lymphomas," *Histopathology*, vol. 65, no. 3, pp. 319–327, 2014.

[3] A. Okado-Matsumoto, A. Matsumoto, J. Fujii, and N. Taniguchi, "Peroxiredoxin IV is a secretable protein with heparin-binding properties under reduced conditions," *The Journal of Biochemistry*, vol. 127, no. 3, pp. 493–501, 2000.

[4] J.-P. Declercq, C. Evrard, A. Clippe, D. V. Stricht, A. Bernard, and B. Knoops, "Crystal structure of human peroxiredoxin 5, a novel type of mammalian peroxiredoxin at 1.5 Å resolution," *Journal of Molecular Biology*, vol. 311, no. 4, pp. 751–759, 2001.

[5] V. L. Kinnula, S. Lehtonen, R. Sormunen et al., "Overexpression of peroxiredoxins I, II, III, V, and VI in malignant mesothelioma," *Journal of Pathology*, vol. 196, no. 3, pp. 316–323, 2002.

[6] S. W. Kang, I. C. Baines, and S. G. Rhee, "Characterization of a mammalian peroxiredoxin that contains one conserved cysteine," *Journal of Biological Chemistry*, vol. 273, no. 11, pp. 6303–6311, 1998.

[7] V. Rani, C. A. Neumann, C. Shao, and J. A. Tischfield, "Prdx1 deficiency in mice promotes tissue specific loss of heterozygosity mediated by deficiency in DNA repair and increased oxidative stress," *Mutation Research—Fundamental and Molecular Mechanisms of Mutagenesis*, vol. 735, no. 1-2, pp. 39–45, 2012.

[8] J. Cao, J. Schulte, A. Knight et al., "Prdx1 inhibits tumorigenesis via regulating PTEN/AKT activity," *EMBO Journal*, vol. 28, no. 10, pp. 1505–1517, 2009.

[9] Y.-H. Han, H.-S. Kim, J.-M. Kim, S.-K. Kim, D.-Y. Yu, and E.-Y. Moon, "Inhibitory role of peroxiredoxin II (Prx II) on cellular senescence," *FEBS Letters*, vol. 579, no. 21, pp. 4897–4902, 2005.

[10] P. Karihtala and Y. Soini, "Reactive oxygen species and antioxidant mechanisms in human tissues and their relation to malignancies," *APMIS*, vol. 115, no. 2, pp. 81–103, 2007.

[11] K. Itoh, J. Mimura, and M. Yamamoto, "Discovery of the negative regulator of Nrf2, keap1: a historical overview," *Antioxidants and Redox Signaling*, vol. 13, no. 11, pp. 1665–1678, 2010.

[12] R. Hu, C. L.-L. Saw, R. Yu, and A.-N. T. Kong, "Regulation of NF-E2-related factor 2 signaling for cancer chemoprevention: antioxidant coupled with antiinflammatory," *Antioxidants and Redox Signaling*, vol. 13, no. 11, pp. 1679–1698, 2010.

[13] X. Cheng, C.-H. Ku, and R. C. M. Siow, "Regulation of the Nrf2 antioxidant pathway by microRNAs: new players in micromanaging redox homeostasis," *Free Radical Biology and Medicine*, vol. 64, pp. 4–11, 2013.

[14] L. A. Pitcher and N. S. C. Van Oers, "T-cell receptor signal transmission: who gives an ITAM?" *Trends in Immunology*, vol. 24, no. 10, pp. 554–560, 2003.

[15] J. P. Deans, H. Li, and M. J. Polyak, "CD20-mediated apoptosis: signalling through lipid rafts," *Immunology*, vol. 107, no. 2, pp. 176–182, 2002.

[16] C. Schneider and G. Hübinger, "Pleiotropic signal transduction mediated by human CD30: a member of the tumor necrosis factor receptor (TNFR) family," *Leukemia and Lymphoma*, vol. 43, no. 7, pp. 1355–1366, 2002.

[17] S. H. Swerdlow, E. Campo, N. L. Harris et al., "Mature B-cell neoplasms," in *WHO Classification of Tumours of Hematopoietic and Lymphoid Tissues*, pp. 179–268, IARC Press, Lyon, France, 4th edition, 2008.

[18] K. J. Livak and T. D. Schmittgen, "Analysis of relative gene expression data using real-time quantitative PCR and the 2(-Delta Delta C(T)) Method," *Methods*, vol. 25, pp. 402–408, 2001.

[19] R. T. Dorr, "Bleomycin pharmacology: mechanism of action and resistance, and clinical pharmacokinetics," *Seminars in Oncology*, vol. 19, no. 2, pp. 3–8, 1992.

[20] J. Fang, H. Nakamura, and A. K. Iyer, "Tumor-targeted induction of oxystress for cancer therapy," *Journal of Drug Targeting*, vol. 15, no. 7-8, pp. 475–486, 2007.

[21] J. Pourahmad, M. Amirmostofian, F. Kobarfard, and J. Shahraki, "Biological reactive intermediates that mediate dacarbazine cytotoxicity," *Cancer Chemotherapy and Pharmacology*, vol. 65, no. 1, pp. 89–96, 2009.

[22] M. E. Tome, J. B. Frye, D. L. Coyle et al., "Lymphoma cells with increased anti-oxidant defenses acquire chemoresistance," *Experimental and Therapeutic Medicine*, vol. 3, no. 5, pp. 845–852, 2012.

[23] M. E. L. Kuusisto, K.-M. Haapasaari, T. Turpeenniemi-Hujanen et al., "High intensity of cytoplasmic peroxiredoxin VI expression is associated with adverse outcome in diffuse large B-cell lymphoma independently of International Prognostic Index," *Journal of Clinical Pathology*, vol. 68, no. 7, pp. 552–556, 2015.

[24] X. Meng, J. Wu, C. Pan et al., "Genetic and epigenetic down-regulation of MicroRNA-212 promotes colorectal tumor metastasis via dysregulation of MnSOD," *Gastroenterology*, vol. 145, no. 2, pp. 426–436, 2013.

[25] B. Sánchez-Espiridión, A. M. Martín-Moreno, C. Montalbán et al., "MicroRNA signatures and treatment response in patients with advanced classical Hodgkin lymphoma," *British Journal of Haematology*, vol. 162, no. 3, pp. 336–347, 2013.

[26] K. Jones, J. P. Nourse, C. Keane, A. Bhatnagar, and M. K. Gandhi, "Plasma microRNA are disease response biomarkers in classical hodgkin lymphoma," *Clinical Cancer Research*, vol. 20, no. 1, pp. 253–264, 2014.

[27] M. Yang, Y. Yao, G. Eades, Y. Zhang, and Q. Zhou, "MiR-28 regulates Nrf2 expression through a Keap1-independent mechanism," *Breast Cancer Research and Treatment*, vol. 129, no. 3, pp. 983–991, 2011.

[28] N. M. Shah, S. A. Rushworth, M. Y. Murray, K. M. Bowles, and D. J. MacEwan, "Understanding the role of NRF2-regulated miRNAs in human malignancies," *Oncotarget*, vol. 4, no. 8, pp. 1130–1142, 2013.

[29] L. M. Solis, C. Behrens, W. Dong et al., "Nrf2 and Keap1 abnormalities in non-small cell lung carcinoma and association with clinicopathologic features," *Clinical Cancer Research*, vol. 16, no. 14, pp. 3743–3753, 2010.

[30] Y. Soini, M. Eskelinen, P. Juvonen et al., "Nuclear Nrf2 expression is related to a poor survival in pancreatic adenocarcinoma," *Pathology Research and Practice*, vol. 210, no. 1, pp. 35–39, 2014.

[31] J. M. Hartikainen, M. Tengström, V.-M. Kosma, V. L. Kinnula, A. Mannermaa, and Y. Soini, "Genetic polymorphisms and protein expression of NRF2 and sulfiredoxin predict survival outcomes in breast cancer," *Cancer Research*, vol. 72, no. 21, pp. 5537–5546, 2012.

[32] A. Singh, S. Boldin-Adamsky, R. K. Thimmulappa et al., "RNAi-mediated silencing of nuclear factor erythroid-2-related factor 2 gene expression in non-small cell lung cancer inhibits tumor growth and increases efficacy of chemotherapy," *Cancer Research*, vol. 68, no. 19, pp. 7975–7984, 2008.

[33] C.-F. Huang, L. Zhang, S.-R. Ma et al., "Clinical significance of keap1 and Nrf2 in oral squamous cell carcinoma," *PLOS ONE*, vol. 8, no. 12, Article ID e83479, 2013.

[34] T. Wang, A. J. G. Diaz, and Y. Yen, "The role of peroxiredoxin II in chemoresistance of breast cancer cells," *Breast Cancer: Targets and Therapy*, vol. 6, pp. 73–80, 2014.

[35] P. S. Smith-Pearson, M. Kooshki, D. R. Spitz, L. B. Poole, W. Zhao, and M. E. Robbins, "Decreasing peroxiredoxin II expression decreases glutathione, alters cell cycle distribution, and sensitizes glioma cells to ionizing radiation and H_2O_2," *Free Radical Biology and Medicine*, vol. 45, no. 8, pp. 1178–1189, 2008.

[36] D. Kubota, K. Mukaihara, A. Yoshida, H. Tsuda, A. Kawai, and T. Kondo, "Proteomics study of open biopsy samples identifies peroxiredoxin 2 as a predictive biomarker of response to induction chemotherapy in osteosarcoma," *Journal of Proteomics*, vol. 91, pp. 393–404, 2013.

[37] C. McDonald, J. Muhlbauer, G. Perlmutter, K. Taparra, and S. A. Phelan, "Peroxiredoxin proteins protect MCF-7 breast cancer cells from doxorubicin-induced toxicity," *International Journal of Oncology*, vol. 45, no. 1, pp. 219–226, 2014.

[38] S. Suenaga, Y. Kuramitsu, Y. Wang et al., "Human pancreatic cancer cells with acquired gemcitabine resistance exhibit significant up-regulation of peroxiredoxin-2 compared to sensitive parental cells," *Anticancer Research*, vol. 33, no. 11, pp. 4821–4826, 2013.

[39] Q.-K. Sun, J.-Y. Zhu, W. Wang et al., "Diagnostic and prognostic significance of peroxiredoxin 1 expression in human hepatocellular carcinoma," *Medical Oncology*, vol. 31, no. 1, article no. 786, 2014.

[40] E. V. Kalinina, T. T. Berezov, A. A. Shtil' et al., "Expression of peroxiredoxin 1, 2, 3, and 6 genes in cancer cells during drug resistance formation," *Bulletin of Experimental Biology and Medicine*, vol. 153, no. 6, pp. 879–882, 2012.

[41] Q. J. Guo, J. N. Mills, S. G. Bandurraga et al., "MicroRNA-510 promotes cell and tumor growth by targeting peroxiredoxin1 in breast cancer," *Breast Cancer Research*, vol. 15, no. 4, article no. R70, 2013.

[42] P. Gaj and R. Zagozdzon, "In silico analysis of microRNA-510 as a potential oncomir in human breast cancer," *Breast Cancer Research*, vol. 16, no. 2, article 403, 2014.

[43] X. Zhang, G. Guo, G. Wang et al., "Profile of differentially expressed miRNAs in high-grade serous carcinoma and clear cell ovarian carcinoma, and the expression of miR-510 in ovarian carcinoma," *Molecular Medicine Reports*, vol. 12, no. 6, pp. 8021–8031, 2015.

[44] S. Diao, J.-F. Zhang, H. Wang et al., "Proteomic identification of microRNA-122a target proteins in hepatocellular carcinoma," *Proteomics*, vol. 10, no. 20, pp. 3723–3731, 2010.

[45] H. J. Cho, J. K. Kim, J. S. Nam et al., "High circulating microRNA-122 expression is a poor prognostic marker in patients with hepatitis B virus-related hepatocellular carcinoma who undergo radiofrequency ablation," *Clinical Biochemistry*, vol. 48, no. 16-17, pp. 1073–1078, 2015.

[46] Y. Xu, X. Bu, C. Dai, and C. Shang, "High serum microRNA-122 level is independently associated with higher overall survival rate in hepatocellular carcinoma patients," *Tumor Biology*, vol. 36, no. 6, pp. 4773–4776, 2015.

[47] V. Köberle, B. Kronenberger, T. Pleli et al., "Serum microRNA-1 and microRNA-122 are prognostic markers in patients with hepatocellular carcinoma," *European Journal of Cancer*, vol. 49, no. 16, pp. 3442–3449, 2013.

[48] K. K. Li, J. C. Pang, K. M. Lau et al., "MiR-383 is downregulated in medulloblastoma and targets peroxiredoxin 3 (PRDX3)," *Brain Pathology*, vol. 23, no. 4, pp. 413–425, 2013.

[49] H.-C. He, J.-G. Zhu, X.-B. Chen et al., "MicroRNA-23b downregulates peroxiredoxin III in human prostate cancer," *FEBS Letters*, vol. 586, no. 16, pp. 2451–2458, 2012.

[50] L. Tian, Y.-X. Fang, J.-L. Xue, and J.-Z. Chen, "Four microRNAs promote prostate cell proliferation with regulation of PTEN and its downstream signals in vitro," *PlOS one*, vol. 8, no. 9, Article ID e75885, 2013.

[51] L. Chen, L. Han, K. Zhang et al., "VHL regulates the effects of miR-23b on glioma survival and invasion via suppression of HIF-1α/VEGF and β-catenin/Tcf-4 signaling," *Neuro-Oncology*, vol. 14, no. 8, pp. 1026–1036, 2012.

[52] G. Ma, W. Dai, A. Sang, X. Yang, and C. Gao, "Upregulation of microRNA-23a/b promotes tumor progression and confers poor prognosis in patients with gastric cancer," *International Journal of Clinical and Experimental Pathology*, vol. 7, no. 12, pp. 8833–8840, 2014.

[53] S. Han, C. Cao, T. Tang et al., "ROBO3 promotes growth and metastasis of pancreatic carcinoma," *Cancer Letters*, vol. 366, no. 1, pp. 61–70, 2015.

[54] X. Wang, Y. Ren, Z. Wang et al., "Down-regulation of 5S rRNA by miR-150 and miR-383 enhances c-Myc-rpL11 interaction and inhibits proliferation of esophageal squamous carcinoma cells," *FEBS Letters*, vol. 589, no. 24, pp. 3989–3997, 2015.

[55] L. Chen, H. Guan, C. Gu, Y. Cao, J. Shao, and F. Wang, "miR-383 inhibits hepatocellular carcinoma cell proliferation via targeting APRIL," *Tumor Biology*, vol. 37, no. 2, pp. 2497–2507, 2016.

[56] O. Merkel, F. Hamacher, R. Griessl et al., "Oncogenic role of MIR-155 in anaplastic large cell lymphoma lacking the t(2;5) translocation," *The Journal of Pathology*, vol. 236, no. 4, pp. 445–456, 2015.

[57] J. H. Gibcus, L. P. Tan, G. Harms et al., "Hodgkin lymphoma cell lines are characterized by a specific miRNA expression profile," *Neoplasia*, vol. 11, no. 2, pp. 167–176, 2009.

[58] I. Slezak-Prochazka, J. Kluiver, D. D. Jong et al., "Inhibition of the miR-155 target NIAM phenocopies the growth promoting effect of miR-155 in B-cell lymphoma," *Oncotarget*, vol. 7, no. 3, pp. 2391–2400, 2016.

[59] U. D'Oro, I. Munitic, G. Chacko, T. Karpova, J. McNally, and J. D. Ashwell, "Regulation of constitutive TCR internalization by the ζ-chain," *Journal of Immunology*, vol. 169, no. 11, pp. 6269–6278, 2002.

[60] P. Leidinger, C. Backes, B. Meder, E. Meese, and A. Keller, "The human miRNA repertoire of different blood compounds," *BMC Genomics*, vol. 15, article 474, 2014.

[61] F. A. Alashti and Z. Minuchehr, "MiRNAs which target CD3 subunits could be potential biomarkers for cancers," *PLOS ONE*, vol. 8, no. 11, Article ID e78790, 2013.

[62] C. Sangokoya, M. J. Telen, and J.-T. Chi, "microRNA miR-144 modulates oxidative stress tolerance and associates with anemia severity in sickle cell disease," *Blood*, vol. 116, no. 20, pp. 4338–4348, 2010.

[63] A. U. Khan, M. G. Rathore, N. Allende-Vega et al., "Human leukemic cells performing oxidative phosphorylation (OXPHOS) generate an antioxidant response independently of reactive oxygen species (ROS) production," *EBioMedicine*, vol. 3, pp. 43–53, 2016.

Hindawi
Oxidative Medicine and Cellular Longevity
Volume 2017, Article ID 3565613, 11 pages
https://doi.org/10.1155/2017/3565613

Research Article

Protection of Human Umbilical Vein Endothelial Cells against Oxidative Stress by MicroRNA-210

Tianyi Li, Xianjing Song, Jichang Zhang, Lei Zhao, Yongfeng Shi, Zhibo Li, Jia Liu, Ning Liu, Youyou Yan, Yanlong Xiao, Xin Tian, Wei Sun, Yinuo Guan, and Bin Liu

Department of Cardiology, The Second Hospital of Jilin University, Changchun, Jilin, China

Correspondence should be addressed to Bin Liu; liubin3333@vip.sina.com

Received 4 November 2016; Revised 12 January 2017; Accepted 9 February 2017; Published 7 March 2017

Academic Editor: Jaideep Banerjee

Oxidative stress induces endothelial cell apoptosis and promotes atherosclerosis development. MicroRNA-210 (miR-210) is linked with apoptosis in different cell types. This study aimed to investigate the role of miR-210 in human umbilical vein endothelial cells (HUVECs) under oxidative stress and to determine the underlying mechanism. HUVECs were treated with different concentrations of hydrogen peroxide (H_2O_2), and cell viability was evaluated using the 3-(4,5-dimethylthiazol-2-yl)-2,5-diphenyltetrazolium bromide assay and ATP assay. To evaluate the role of miR-210 in H_2O_2-mediated apoptosis, gain-and-loss-of-function approaches were used, and the effects on apoptosis and reactive oxygen species (ROS) level were assayed using flow cytometry. Moreover, miR-210 expression was detected by quantitative reverse transcriptase polymerase chain reaction (qRT-PCR), and expression of the following apoptosis-related genes was assessed by qRT-PCR and Western blot at the RNA and protein level, respectively: caspase-8-associated protein 2 (CASP8AP2), caspase-8, and caspase-3. The results showed that H_2O_2 induced apoptosis in HUVECs in a dose-dependent manner and increased miR-210 expression. Overexpression of miR-210 inhibited apoptosis and reduced ROS level in HUVECs treated with H_2O_2. Furthermore, miR-210 downregulated CASP8AP2 and related downstream caspases at protein level. Thus, under oxidative stress, miR-210 has a prosurvival and antiapoptotic effect on HUVECs by reducing ROS generation and downregulating the CASP8AP2 pathway.

1. Introduction

Atherosclerosis is the leading cause of coronary heart disease, with high mortality and morbidity rates [1]. Under oxidative stress, excessive reactive oxygen species- (ROS-) induced endothelial cell apoptosis plays a crucial role in atherosclerosis development [2]. Therefore, reduction of endothelial apoptosis is vital in atherosclerosis prevention.

The association of microRNAs (miRNAs), which are involved closely in various cell processes through post-transcriptional downregulation of their target mRNAs, with apoptosis has drawn much attention [3–6]. In particular, expression of miRNA-210 (miR-210) has been considered a general response to hypoxia [7], and miR-210 has been reported to be participated in various cellular processes, including cell cycle arrest [8], angiogenesis [6], and cell survival [5] in various cell types, including endothelial cells [6]. Besides hypoxia, miR-210 is involved in oxidative stress-induced injury. Our previous study has revealed that miR-210 protects cardiomyoblasts against apoptosis under oxidative stress [9]. However, the role of miR-210 in cell apoptosis apparently varies with cell types and stimuli [10–13]. It has been reported that miR-210 protects cardiomyocytes against apoptosis under hypoxic conditions [10] and protects stem cells against oxidative stress [11]. However, some studies identified miR-210 as a proapoptotic component in human pulmonary artery epithelial cells [12] and in a human lung cancer cell line [13]. Therefore, the role of miR-210 in apoptosis in different cell types and under different conditions needs further investigation.

Some studies have indicated that miR-210 exerts anti-apoptosis action by downregulating caspase-8-associated protein 2 (CASP8AP2) in stem cells under hypoxic conditions [5]. CASP8AP2 (or FLICE-associated huge protein), a 1,962-amino acid-long protein, takes part in several cellular processes, such as mRNA processing, cell cycle, apoptosis, and transcriptional control [14]. CASP8AP2 was identified

as a proapoptosis member that acts via binding the death effector domains of procaspase-8, which activates caspase-8 and its downstream caspases, including caspase-3, thereby participating in the extrinsic apoptosis pathway mediated by CD95 [15, 16].

However, the effect of miR-210 on endothelial cells under oxidative stress remains unclear. In this study, we investigated the effects of miR-210 on apoptosis and the underlying mechanism in human umbilical vein endothelial cells (HUVECs) treated with hydrogen peroxide (H_2O_2), which has been commonly used to induce oxidative stress in in vitro models [17]. We found that miR-210 protected HUVECs against oxidative stress by reducing ROS generation and downregulating the CASP8AP2 pathway.

2. Materials and Methods

2.1. Cell Culture. HUVECs were obtained from the Department of Cardiology of The Second Hospital of Jilin University and cultured in a humidified incubator at 5% CO_2 and 37°C. The complete growth medium for this cell line consisted of the vascular cell basal medium (ATCC, USA) with the endothelial cell growth kit-BBE (ATCC, USA) and contained the following components: 2% fetal bovine serum, 0.2% bovine brain extract, 10 mmol/L L-glutamine, 1 μg/mL hydrocortisone hemisuccinate, 5 ng/mL rhEGF, 50 μg/mL ascorbic acid, and 0.75 units/mL heparin sulfate.

2.2. Lentivirus Infection of HUVECs. A replication-deficient lentivirus was purchased from Sangon Biotech (Shanghai, China), encoding the human miR-210 precursor (pre-210), miR-210 inhibitor (anti-miR-210), or miR-scramble (miR-Scr, without miR-210 as a control) labeled with green fluorescent protein. 5 μL of lentiviral vectors was added per well for transduction of HUVECs in 6-well plates (1×10^5 cells/well) for 12 h. Fresh complete growth medium was subsequently added to replace the medium. To eliminate nontransduced cells, puromycin (Sigma-Aldrich, USA) was added to the medium at a final concentration of 4 μg/mL [18], and the medium was incubated for at least 72 h. The transduced cells were then stained with DAPI and observed with a fluorescence microscope. The Image J software was used to quantitate the transduction efficiency.

2.3. DAPI Staining. After transduction with the lentivirus, cells were stained with DAPI to visualize the nucleus. Cells were cultured in a 6-well plate and fixed in 4% paraformaldehyde for 25 min at room temperature (25°C). Subsequently, cells were incubated with DAPI for 10 min and washed with PBS thrice.

2.4. Transfection. HUVECs were transfected in 6-well plates using Lipofectamine 2000 Reagent (Invitrogen, Carlsbad, CA, USA) according to the manufacturer's instructions. HUVECs were transfected with miR-210 mimics, miR-210 inhibitor, or negative control (NC) (GenePharma, Shanghai, China) at approximately 80% confluence.

2.5. 3-(4,5-Dimethylthiazol-2-yl)-2,5-diphenyltetrazolium Bromide (MTT) Detection. MTT detection was used to evaluate the viability of HUVECs treated with different concentrations of H_2O_2 and the effect of miR-210 on cell viability. Cells in a 96-well plate (1×10^4 cells/well) were treated with different concentrations of H_2O_2 (0, 0.1, 0.2, 0.5, 1.0, 1.5, and 2.0 mmol/L) for 24 h. MTT (Biosharp, China) was added to each well, and the wells were incubated for 4 h at 37°C. Subsequently, the medium was removed, and dimethyl sulfoxide (Sigma-Aldrich, USA) was added (150 μL/well) to solubilize the formazan crystals. Optical density was measured at 570 nm with a Varioskan Flash microplate reader (Thermo Scientific, USA), and cell viability was calculated as a percentage of the control optical density.

2.6. ATP Assay. To further evaluate cell viability, a luminescent ATP assay kit, CellTiter-Glo® Luminescent Cell Viability Assay (Promega, USA), was employed. Cells were treated with different concentrations of H_2O_2 (0, 0.1, 0.2, 0.5, 1.0, 1.5, and 2.0 mmol/L) for 24 h in a white 96-well plate (1×10^4 cells/well). After the treatment, 100 μL of CellTiter-Glo Reagent was added per well. The luminescence was then detected with a Varioskan Flash microplate reader (Thermo Scientific, USA). Cell viability was calculated as a percentage normalized to the control group.

2.7. Flow Cytometry. To detect apoptosis and determine ROS level of HUVECs treated with different concentrations of H_2O_2 and to assess the effect of miR-210, flow cytometry experiments were performed with the FACSCalibur system (BD Biosciences, USA). After treatment with different concentrations of H_2O_2 (0, 0.5, and 1.0 mmol/L), PE Annexin V Apoptosis Detection kit I (BD Biosciences, USA) was used following the protocol for apoptosis detection. After transfection with miR-210 mimics, miR-210 inhibitor, or negative control, cells were dealt with H_2O_2 (0.5 mmol/L). A Reactive Oxygen Species Assay Kit (Beyotime, China) was used following the protocol for ROS detection.

2.8. Quantitative PCR. Total RNA was extracted using Eastep® Super Total RNA Extraction Kit (Promega, USA) following the protocol. The quality of the extracted RNA was evaluated with a NanoDrop 2000 Spectrophotometer (Thermo Scientific, USA). To detect miR-210 expression levels, RNA was reverse-transcribed into cDNA by using the miRcute miRNA First-Strand cDNA Synthesis Kit (TIANGEN Biotech, China) according to the protocol. To determine expression profiles of apoptosis-related genes, RNA was reverse-transcribed into cDNA by using the TransScript One-Step gDNA Removal and cDNA Synthesis SuperMix Kit (TransGen Biotech, China) following the manufacturer's instructions. Thereafter, qRT-PCR was performed in the LightCycler 480 system (Roche, Switzerland) with TransStart Green qPCR SuperMix (TransGen Biotech, China). U6 was selected as the reference gene. qRT-PCR conditions were set as follows: 95°C for 1 min followed by 40 cycles of 95°C for 20 s and 61°C for 31 s. All primers were purchased from Sangon Biotech, China.

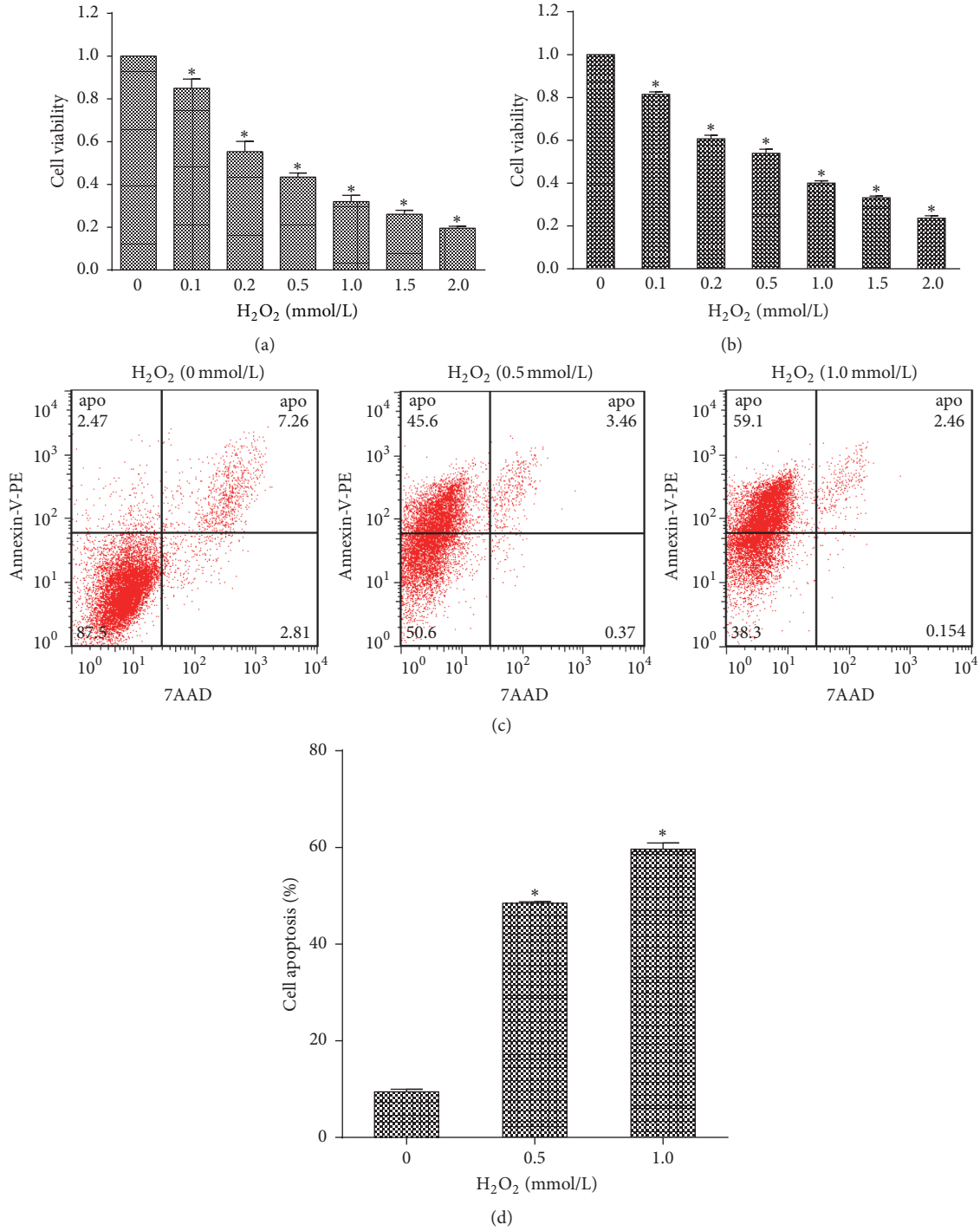

FIGURE 1: H_2O_2 induces cell death in a dose-dependent manner. (a) The effect of H_2O_2 on HUVECs viability compared to untreated control cells shown by the MTT assay. (b) Evaluation of HUVECs viability under H_2O_2 treatment using the ATP assay. (c) HUVECs were treated with 0, 0.5, or 1.0 mmol/L H_2O_2 for 24 h, and apoptosis was assessed by flow cytometry. (d) Flow cytometry analysis showed that H_2O_2 induced HUVEC apoptosis in a dose-dependent manner. All $n = 3$, $^*p < 0.05$.

2.9. Western Blot. After 24 h of treatment with H_2O_2 (0 or 0.5 mmol/L), HUVECs were lysed using the radioimmunoprecipitation assay buffer with protease inhibitors, 1 mM phenylmethylsulfonyl fluoride, and mercaptoethanol. The homogenate was centrifuged for 15 min at 4,500 rpm at 4°C, and the supernatant was used for sodium dodecyl sulfate polyacrylamide gel electrophoresis at 20 μg of total protein per lane, followed by transfer to a polyvinylidene fluoride membrane. The membranes were blocked with nonfat dry milk for 90 min at room temperature and incubated with primary monoclonal rabbit anti-CASP8AP2 (1 : 200; Santa Cruz Biotechnology, USA), monoclonal rabbit anti-caspase-8

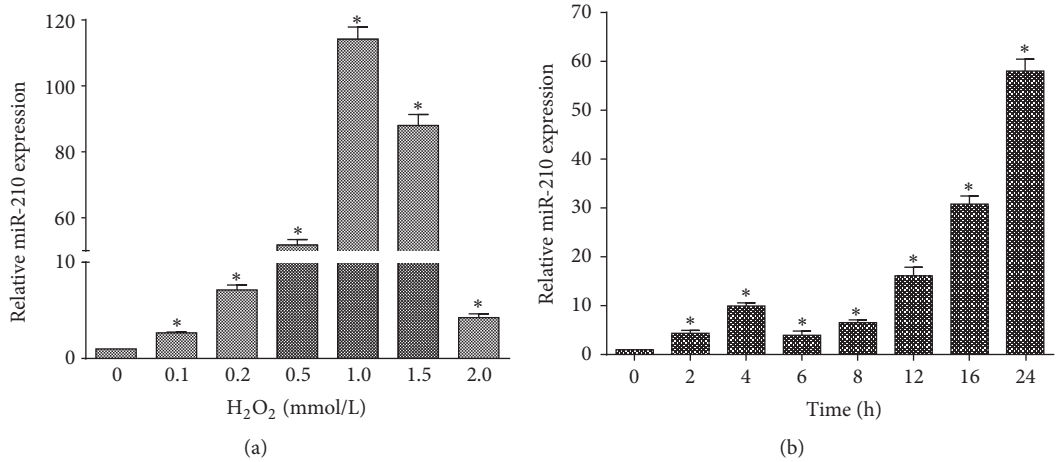

FIGURE 2: H_2O_2 increased miR-210 expression. (a) Incubation with H_2O_2 at different concentrations (0.1, 0.2, 0.5, 1.0, 1.5, and 2.0 mmol/L) for 24 h increased miR-210 expression compared that in untreated control cells. miR-210 expression was highest at 1.0 mmol/L. (b) HUVECs were treated with H_2O_2 at 0.5 mmol/L for 2, 4, 6, 8, 12, 16, and 24 h. miR-210 expression increased in all cases compared to that in untreated control cells. All $n = 3$, $^*p < 0.05$.

(1 : 1000; Cell Signaling Technology, USA), monoclonal rabbit anti-caspase-3 (1 : 1000; Cell Signaling Technology, USA), and monoclonal mouse anti-β-actin (1 : 2000; Proteintech, USA) antibodies, followed by incubation with a secondary horseradish peroxidase-conjugated anti-rabbit IgG antibody or anti-mouse IgG antibody (1 : 1000; Beyotime, China). The blots were visualized using the SuperSignal West Pico kit (Thermo Scientific, USA). The relative expression level of each protein was normalized to that of β-actin.

2.10. Statistical Analysis. Data are reported as means ± SE. Statistical analysis was performed using SPSS13.0 (IBM, USA). For all experiments, Student's t-test was employed to assess statistical significance, and the threshold was set at $p = 0.05$.

3. Results

3.1. The Effect of H_2O_2 on Cell Viability and miR-210 Expression in HUVECs. HUVECs were treated with different concentrations of H_2O_2 (0, 0.1, 0.2, 0.5, 1.0, 1.5, and 2.0 mmol/L), and cell viability was tested using the MTT assay and ATP assay. As shown in Figures 1(a) and 1(b), the viability of HUVECs was reduced with increasing H_2O_2 concentrations compared with that of control cells ($p < 0.05$). Apoptosis of HUVECs treated with different concentrations of H_2O_2 (0, 0.5, and 1.0 mmol/L) was evaluated by performing flow cytometry to determine whether H_2O_2-induced apoptosis contributed to cell viability variation (Figures 1(c) and 1(d)). The results demonstrated that H_2O_2 induced apoptosis in a dose-dependent manner ($p < 0.05$).

We then tested the expression of miR-210 in HUVECs with qPCR in response to stimulation with H_2O_2 at different concentrations (0, 0.1, 0.2, 0.5, 1.0, 1.5, and 2.0 mmol/L). miR-210 expression increased ($p < 0.05$; Figure 2(a)), with the highest value observed at 1.0 mmol/L. In addition, we investigated the dependence of miR-210 expression on duration of H_2O_2 stimulation. In HUVECs treated with H_2O_2 at 0.5 mmol/L for 0, 2, 4, 6, 8, 16, and 24 h, miR-210 expression increased ($p < 0.05$; Figure 2(b)). These results indicated that miR-210 was involved in HUVEC apoptosis induced by H_2O_2.

3.2. The Effect of miR-210 on HUVEC Apoptosis in Response to H_2O_2. Since miR-210 expression increased in HUVECs treated with H_2O_2, we tested the effect of miR-210 on HUVECs apoptosis upon H_2O_2 treatment using gain-and-loss-of-function approaches. HUVECs were transduced with lentiviral vectors and observed under a fluorescence microscope (Figure 3(a)). The Image J software was used to quantitate the transduction efficiency (Figure 3(b)). The mean transduction efficiency of miR-Scr, pre-210, and anti-miR-210 was 0.88, 0.89, and 0.86, respectively. qRT-PCR showed that miR-210 expression levels were increased in the pre-210 cell line and decreased in the anti-miR-210 cell line compared with that in normal HUVECs (all $p < 0.05$). The level of miR-210 in the control cell line transfected with miR-Scr did not differ from that in normal HUVECs (Figure 3(b)). Moreover, during H_2O_2 stimulation (0.5 mmol/L, 24 h), miR-210 expression increased in the pre-210 cells and decreased in the anti-miR-210 cells compared with the miR-Scr cells (Figures 3(c) and 3(d)) (all $p < 0.05$).

We then investigated the effect of miR-210 on survival by treating HUVECs transduced with pre-210, anti-miR-210, and miR-Scr with H_2O_2 at different concentrations. The MTT assay showed that the cell viability ratio increased in pre-210 HUVECs at all H_2O_2 concentrations and decreased in anti-miR-210 HUVECs treated with H_2O_2 at 0.2, 0.5, 1.0, and 1.5 mmol/L compared with miR-Scr HUVECs (Figures 4(a) and 4(b)). Similar results were obtained with the ATP assay. Under H_2O_2 treatment, cell viability also increased in pre-210 HUVECs at all concentrations and decreased in anti-miR-210 HUVECs at 0.1, 0.2, 0.5 and 1.0 mmol/L compared with miR-Scr HUVECs (Figures 4(c) and 4(d)). In agreement, flow

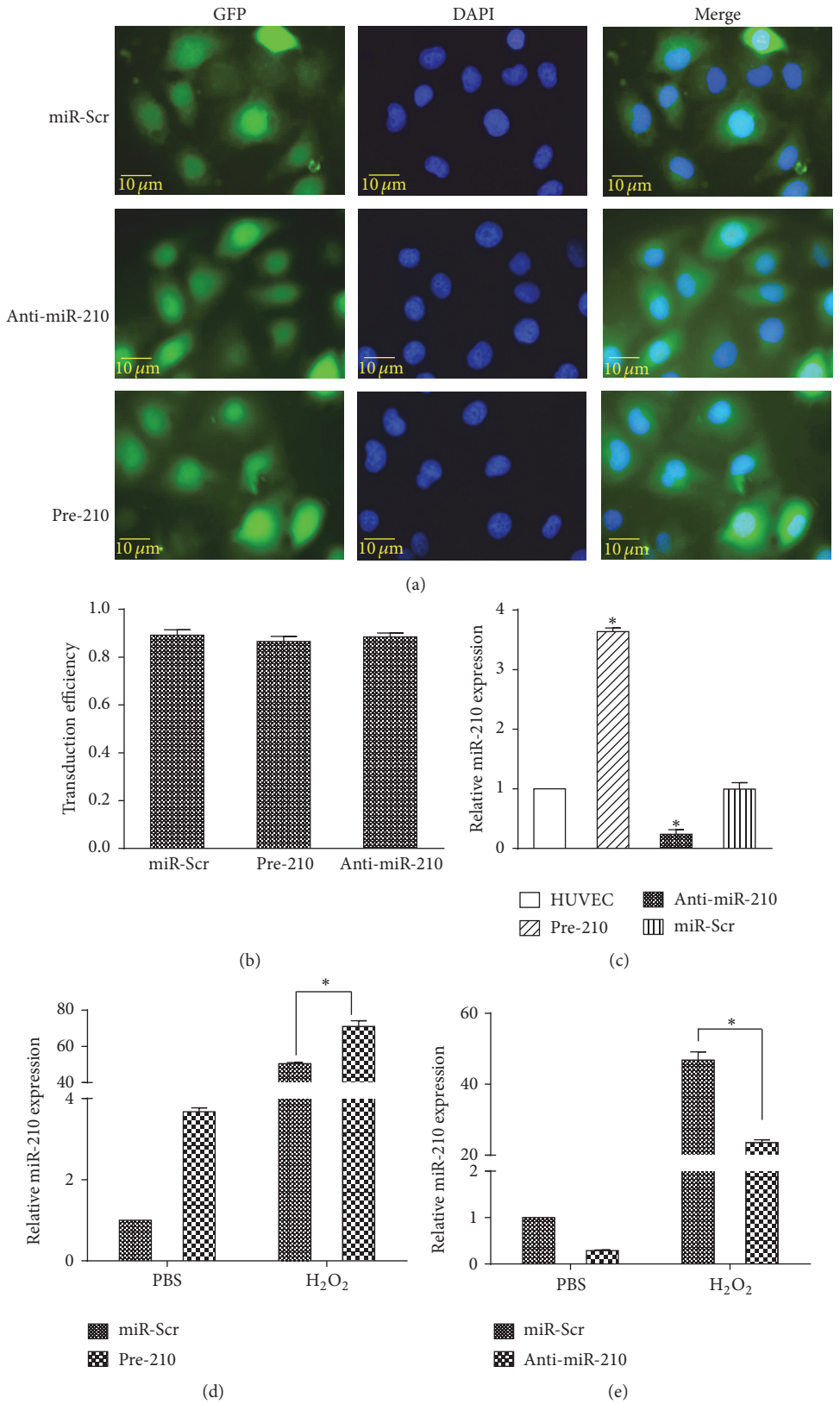

Figure 3: miR-210 expression variation in HUVECs transduced with lentivirus. (a) DAPI staining of HUVECs transduced with pre-210, anti-miR-210, and miR-Scr. (b) Quantification of transduction efficiency using the Image J software. (c) qRT-PCR results showing transgenic expression of miR-210 in HUVECs transduced with the lentivirus. (d) qRT-PCR results showing increased relative miR-210 expression in pre-210 HUVECs compared with miR-Scr HUVECs upon H_2O_2 treatment. (e) qRT-PCR results showing decreased relative miR-210 expression in anti-miR-210 HUVECs compared with miR-Scr HUVECs upon H_2O_2 treatment. All $n = 3$, $^*p < 0.05$.

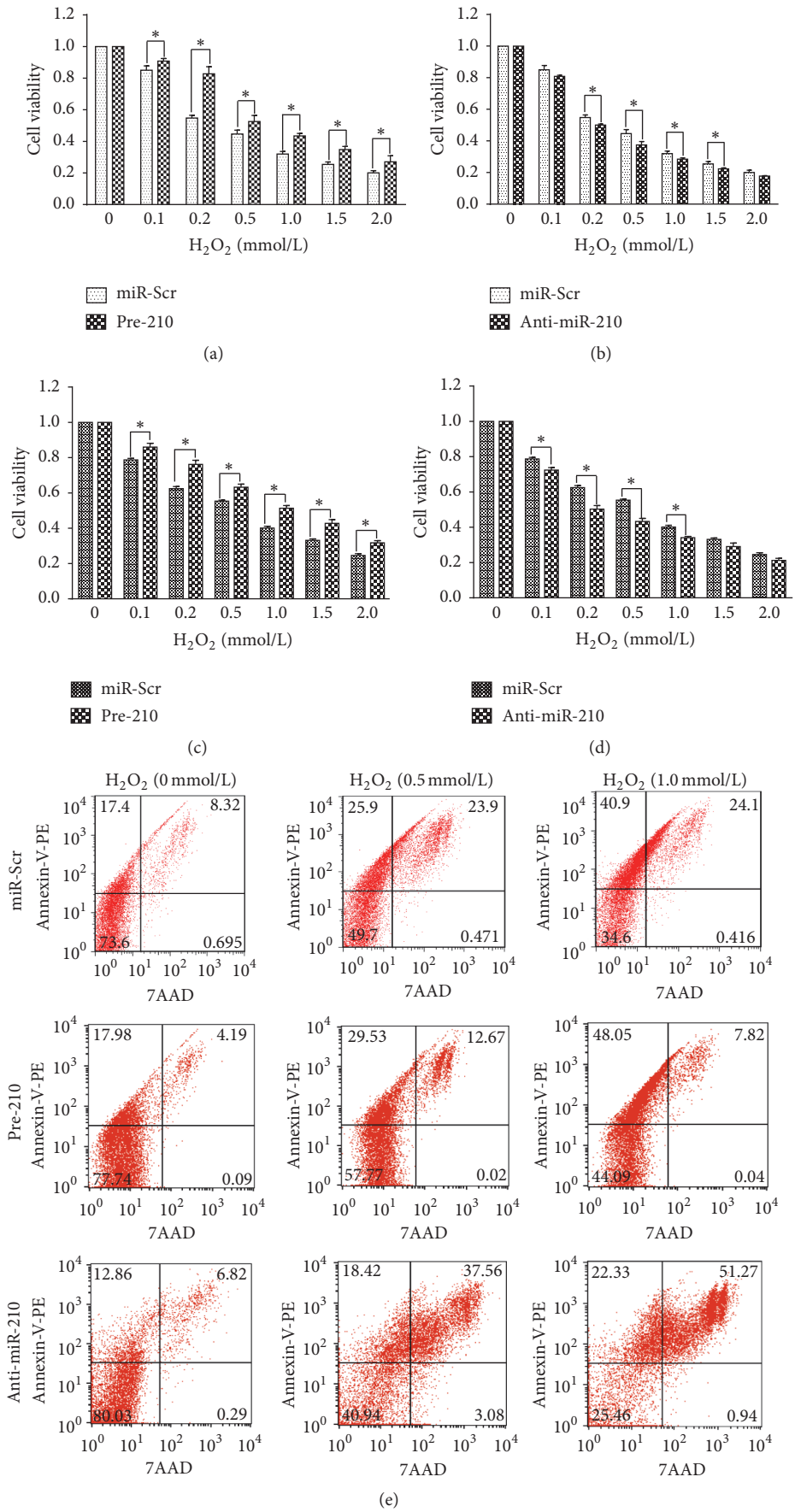

Figure 4: Continued.

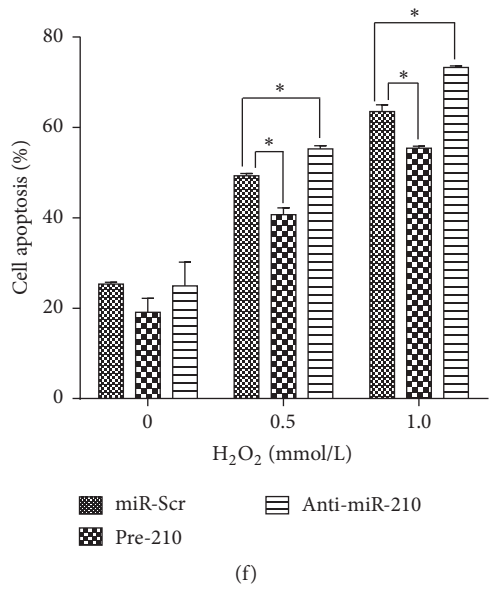

Figure 4: miR-210 reduced cell death in HUVECS treated with H_2O_2. (a) MTT assay results showing that miR-210 overexpression increased cell viability compared with that of miR-Scr HUVECs upon H_2O_2 treatment. (b) MTT assay results showing that miR-210 inhibition decreased cell viability compared with that of miR-Scr HUVECs upon H_2O_2 treatment. (c) ATP assay showing that miR-210 overexpression increased cell viability compared with that of miR-Scr HUVECs upon H_2O_2 treatment. (d) ATP assay showing that miR-210 inhibition decreased cell viability compared with that of miR-Scr HUVECs upon H_2O_2 treatment (e) Flow cytometry of the three transduced lines of HUVECs treated with H_2O_2 (0.5 mmol/L, 24 h). (f) Flow cytometry analysis showing that miR-210 protected HUVECs from apoptosis during H_2O_2 treatment. All $n = 3$, $^* p < 0.05$.

cytometry showed that the cell apoptosis ratio decreased in pre-miR-210 cells and increased in anti-miR-210 cells upon treating with H_2O_2 at 0.5 and 1.0 mmol/L ($p < 0.05$; Figures 4(c) and 4(d)).

3.3. The Effect of miR-210 on ROS Generation in HUVECs in Response to H_2O_2. To investigate the effect of miR-210 on ROS generation, the cells were transfected with miR-210 mimics, miR-210 inhibitor, or NC, and ROS levels were determined after H_2O_2 treatment (0, 0.5 mmol/L, 24 h). Based on the results of qPCR (see S1 Fig in Supplementary Material available online at https://doi.org/10.1155/2017/3565613), miR-210 expression increased after transfection with miR-210 mimics and decreased after transfection with the miR-210 inhibitor compared with that of untransfected HUVECs. No difference was found between untransfected HUVECs and those transfected with the NC. ROS levels (Figure 5) increased in the NC group and were higher in the miR-210 inhibitor-transfected cells upon H_2O_2 treatment. Overexpression of miR-210 decreased the ROS levels during H_2O_2 treatment when compared with cells transfected with the NC.

3.4. H_2O_2 Effect on Relative Expression of Genes of the CASP8AP2 Pathway in HUVECs. Since the CASP8AP2 pathway plays an important role in apoptosis, we investigated its contribution to the H_2O_2-induced apoptosis in HUVECs. The miR-Scr cells were treated with H_2O_2 at 0 or 0.5 mmol/L for 24 h, and expression of genes of the CASP8AP2 pathway was detected. There were no differences in mRNA expression after the H_2O_2 treatment (S2 Fig). However, Western blot results showed that, at protein level, CASP8AP2 expression increased after H_2O_2 treatment compared to the control ($p < 0.05$). In agreement, the cleaved caspase-8/caspase-8 and cleaved caspase-3/caspase-3 ratios were also increased (all $p < 0.05$) (Figures 6(a)–6(c)). These results indicated that the CASP8AP2 pathway was involved in HUVEC apoptosis during H_2O_2 treatment.

3.5. The Effect of miR-210 on the Expressions of CASP8AP2 Apoptosis Pathway-Related Genes in HUVECs Stimulated with H_2O_2. Since the CASP8AP2 pathway was involved in H_2O_2-mediated apoptosis, we investigated whether an association of the anti-apoptotic effect of miR-210 with CASP8AP2 pathway regulation existed. In HUVECs transduced with pre-210, anti-miR-210, and miR-Scr under H_2O_2 treatment (0 and 0.5 mmol/L, 24 h), no differences were found in the mRNA expression of CASP8AP2, caspase-8, or caspase-3 (S2 Fig). Nevertheless, protein expression of these genes differed in the three cell lines. CASP8AP2 expression was decreased in the pre-210 cells and increased in the anti-miR-210 cells compared with the miR-Scr cells (in cells both treated and not treated with H_2O_2, all $p < 0.05$; Figures 6(a) and 6(d)). Without H_2O_2 treatment, there were no differences in the caspase-8 cleavage or caspase-3 cleavage in the pre-210, anti-miR-210, and miR-Scr cells. However, under H_2O_2 stimulation, both caspase-8 cleavage and caspase-3 cleavage decreased in the pre-210 cells and increased in the anti-miR-210 cells versus the miR-Scr cells (all $p < 0.05$; Figures 6(b), 6(c), 6(e), and 6(f)). These results revealed that miR-210 downregulated the expression of CASP8AP2 pathway-related proteins.

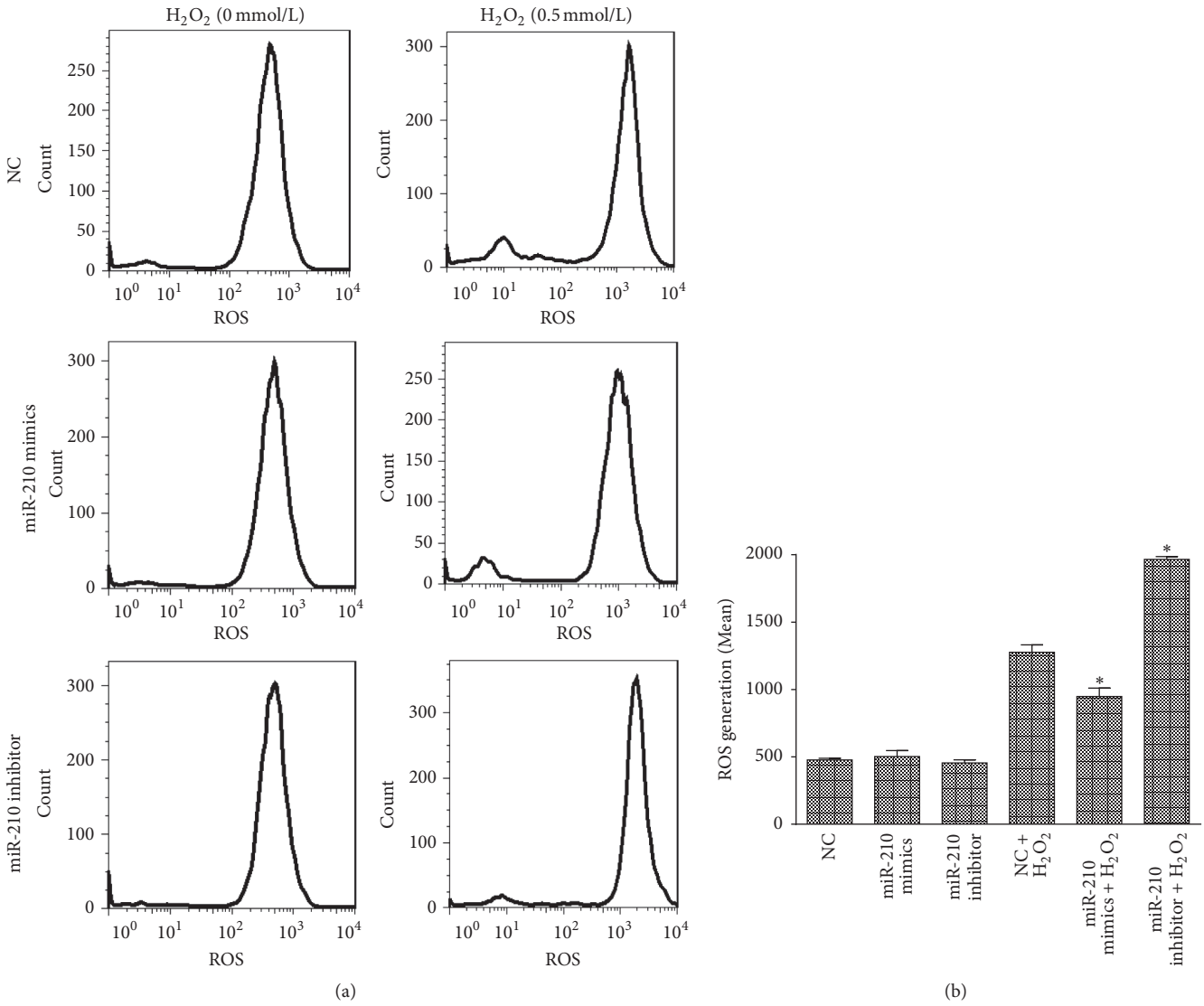

FIGURE 5: miR-210 reduced ROS generation in HUVECS treated with H_2O_2. (a) HUVECs were transfected with miR-210 mimics, miR-210 inhibitor, or NC and subsequently treated with H_2O_2 for 24 h (0, 0.5 mmol/L). Cells were collected and incubated with 10 μM DCFH-DA for 20 minutes according to the manufacturer's instructions. After the incubation, the cells were washed with warm PBS, and ROS levels were analyzed by flow cytometry. (b) Quantification of mean fluorescent intensity in each group. Stars above bars refer to p values between NC-transfected cells treated with H_2O_2 and the corresponding group. All $n = 3$, $^*p < 0.05$.

4. Discussion

Endothelial cell apoptosis under oxidative stress plays a critical role in the initiation and progression of atherosclerosis [17]. In this study, we found that H_2O_2 induced HUVEC apoptosis through CASP8AP2 pathway activation. In addition, H_2O_2 stimulation upregulated the expression of miR-210, which protected HUVECs against H_2O_2-induced apoptosis by reducing ROS generation and affecting the CASP8AP2 pathway.

We found that H_2O_2 induced HUVEC apoptosis in a dose-dependent manner. In addition, CASP8AP2 pathway-related proteins were upregulated by the H_2O_2 treatment, which further contributed to the process of apoptosis. CASP8AP2 is a member of the apoptosis signaling complex that activates caspase-8, which results in the activation of caspase-3, eventually leading to apoptosis [5, 19]. In agreement, our results showed that the CASP8AP2 protein expression level increased in miR-Scr HUVECs treated with H_2O_2. Furthermore, we found that the cleaved caspase-8/caspase-8 and cleaved caspase-3/caspase-3 ratios increased, reflecting elevated activation of the initiator and effector caspases (caspase-8 and caspase-3, resp.) that intensified apoptosis. Therefore, activation of the CASP8AP2 pathway leads to apoptosis in HUVECs under oxidative stress.

Moreover, miR-210 was upregulated in HUVECs during H_2O_2 stimulation. Some studies, including our previous work, showed that miR-210 upregulation had an antiapoptotic effect in the rat H9C2 cell line [9], human mesenchymal stem cells [20], and mouse myoblast C2C12 cell line [21].

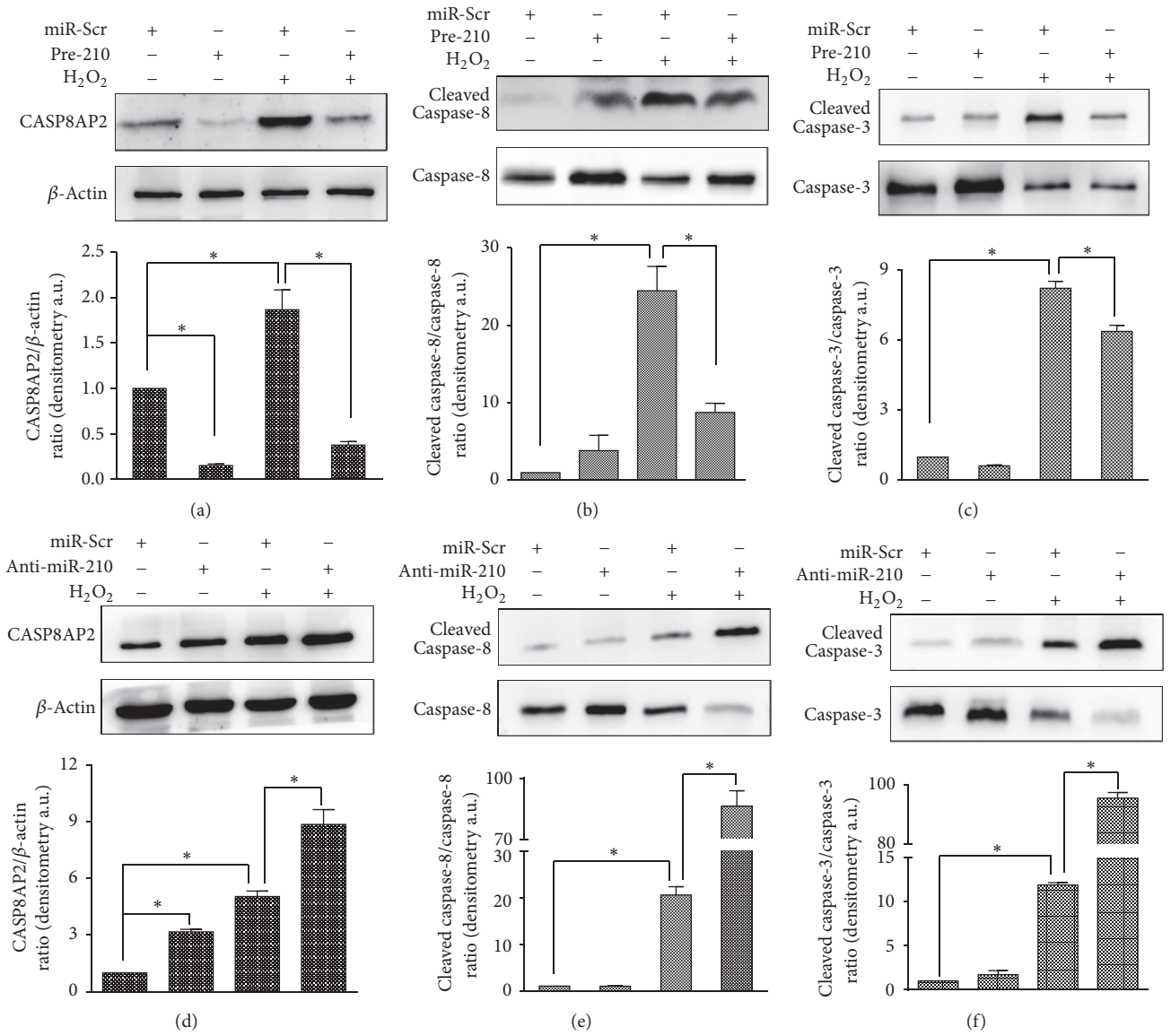

Figure 6: miR-210 downregulated CASP8AP2 pathway-related genes at the level of protein expression. (a) A Western blot showing that CASP8AP2 protein levels increased upon H_2O_2 treatment. miR-210 overexpression decreased the expression of CASP8AP2 in both H_2O_2-treated and untreated cells. (b) A Western blot showing that the cleaved caspase-8/caspase-8 ratio increased upon H_2O_2 treatment. miR-210 overexpression decreased the cleaved caspase-8/caspase-8 ratio upon H_2O_2 treatment. (c) A Western blot showing that the cleaved caspase-3/caspase-3 ratio increased upon H_2O_2 treatment. miR-210 overexpression decreased the cleaved caspase-3/caspase-3 ratio upon H_2O_2 treatment. (d) A Western blot showing that miR-210 inhibition increased CASP8AP2 protein levels in both the treated and untreated groups. (e) A Western blot showing that miR-210 inhibition increased the cleaved caspase-8/caspase-8 ratio upon H_2O_2 treatment. (f) A Western blot showing that miR-210 inhibition increased the cleaved caspase-3/caspase-3 ratio upon H_2O_2 treatment. All $n = 3$, $^*p < 0.05$.

However, other studies showed that miR-210 had a proapoptotic effect in pulmonary artery epithelial cells [12], human lung cancer cell line [13], and esophageal cancer cell line [22]. Of interest, previous study demonstrated that miR-210 played different roles in HCT116 and MCF7 cells at different conditions [23]. In particular, miR-210 played a proapoptotic role at normal oxygen levels and an antiapoptotic role under hypoxia [23]. Our study found that miR-210 protected HUVECs against H_2O_2-induced apoptosis. In line with our results, Fasanaro et al. reported that miR-210 also had a prosurvival effect on HUVECs under hypoxia [6].

Furthermore, we found a negative correlation between miR-210 level and ROS generation upon H_2O_2 treatment. Increased ROS production is known to accelerate cell impairment. Our results indicated that miR-210 protected cells against apoptosis, which could be attributed to reduced ROS production under oxidative stress. Similar results were found in cardiomyocytes [4], mesenchymal stem cells [11], and ischemic hindlimbs [21]. However, contrasting results were obtained in colorectal cancer cells [24] and adipose-derived stem cells [25]. These differences could be due to the different cellular contexts. The underlying molecular mechanism of

the reduced ROS generation could be related to the regulation of the c-Met pathway [11] and the expression of iron-sulfur cluster scaffold homolog [23].

We found that the antiapoptotic effect of miR-210 was also associated with the CASP8AP2 pathway. Overexpression of miR-210 inhibited the protein expression level of CASP8AP2 and thus decreased the cleaved caspase-8/caspase-8 ratio during H_2O_2 treatment, while miR-210 inhibition led to the opposite effect. These results suggested that miR-210 downregulated the CASP8AP2 pathway under oxidative stress.

Although CASP8AP2 was identified as a target of miR-210 in bone marrow-derived mesenchymal stem cells under anoxia [5], Barile et al. found no association between miR-210 and CASP8AP2 in HL-1 cells [26], which indicates that the target genes of miR-210 may vary with different cell types and conditions. Moreover, numerous studies identified several other target genes of miR-210, including *Efna3* [27], neuronal pentraxin 1 [28], *E2f3* [29], *PTPN2* [30], and *ptp1b* [10], suggesting that miR-210 has diverse roles in angiogenesis, DNA repair, cell cycle, migration, and apoptosis. Further studies on the association between miR-210 and other potential target genes in HUVECs under oxidative stress need to be conducted.

Of note, we found no differences in mRNA expression of CASP8AP2, caspase-8, and caspase-3 during H_2O_2 treatment versus control cells. It is possible that alterations in mRNA expression occurred prior to the changes in protein levels. Our results indicate that miR-210 protects HUVECs against oxidative stress in in vitro models. However, further research is needed to investigate the role of miR-210 in in vivo models and determine the underlying mechanisms.

5. Conclusions

We observed that miR-210 expression increased in HUVECs treated with H_2O_2. Moreover, miR-210 played a prosurvival and antiapoptotic role in HUVECs under oxidative stress by reducing ROS generation and downregulating the CASP8AP2 pathway. However, apoptosis-related pathways other than the CASP8AP2 pathway are known to exist. Further research on the relationship between miR-210 and these pathways is warranted. Our result may potentially lead to a new strategy for protecting against endothelial injury in atherosclerosis.

Competing Interests

The authors declare that there is no conflict of interests regarding the publication of this paper.

Acknowledgments

This study was supported by grants from the National Natural Science Foundation of China (no. 81570250), Jilin Province Department of Finance, China (no. 2014520), and the National Clinical Key Specialty Project.

References

[1] D. Mozaffarian, E. J. Benjamin, A. S. Go et al., "Executive summary: heart disease and stroke statistics—2016 update: a report from the American Heart Association," *Circulation*, vol. 133, no. 4, pp. 447–454, 2016.

[2] L. Ma, X. Guo, and W. Chen, "Inhibitory effects of oleoylethanolamide (OEA) on H_2O_2-induced human umbilical vein endothelial cell (HUVEC) injury and apolipoprotein E knockout (ApoE-/-) atherosclerotic mice," *International Journal of Clinical and Experimental Pathology*, vol. 8, no. 6, pp. 6301–6311, 2015.

[3] D. Gou, R. Ramchandran, X. Peng et al., "miR-210 has an antiapoptotic effect in pulmonary artery smooth muscle cells during hypoxia," *AJP: Lung Cellular and Molecular Physiology*, vol. 303, no. 8, pp. L682–L691, 2012.

[4] R. K. Mutharasan, V. Nagpal, Y. Ichikawa, and H. Ardehali, "microRNA-210 is upregulated in hypoxic cardiomyocytes through Akt- and p53-dependent pathways and exerts cytoprotective effects," *American Journal of Physiology—Heart and Circulatory Physiology*, vol. 301, no. 4, pp. H1519–H1530, 2011.

[5] H. W. Kim, H. K. Haider, S. Jiang, and M. Ashraf, "Ischemic preconditioning augments survival of stem cells via miR-210 expression by targeting caspase-8-associated protein 2," *Journal of Biological Chemistry*, vol. 284, no. 48, pp. 33161–33168, 2009.

[6] P. Fasanaro, Y. D'Alessandra, V. Di Stefano et al., "MicroRNA-210 modulates endothelial cell response to hypoxia and inhibits the receptor tyrosine kinase ligand ephrin-A3," *Journal of Biological Chemistry*, vol. 283, no. 23, pp. 15878–15883, 2008.

[7] H. W. Kim, S. Jiang, M. Ashraf, and K. H. Haider, "Stem cell-based delivery of Hypoxamir-210 to the infarcted heart: implications on stem cell survival and preservation of infarcted heart function," *Journal of Molecular Medicine*, vol. 90, no. 9, pp. 997–1010, 2012.

[8] Z. Zhang, H. Sun, H. Dai et al., "MicroRNA miR-210 modulates cellular response to hypoxia through the MYC antagonist MNT," *Cell Cycle*, vol. 8, no. 17, pp. 2756–2768, 2009.

[9] Y.-F. Shi, N. Liu, Y.-X. Li et al., "Insulin protects H9c2 rat cardiomyoblast cells against hydrogen peroxide-induced injury through upregulation of microRNA-210," *Free Radical Research*, vol. 49, no. 9, pp. 1147–1155, 2015.

[10] S. Hu, M. Huang, Z. Li et al., "MicroRNA-210 as a novel therapy for treatment of ischemic heart disease," *Circulation*, vol. 122, no. 11, pp. S124–S131, 2010.

[11] J. Xu, Z. Huang, L. Lin et al., "miR-210 over-expression enhances mesenchymal stem cell survival in an oxidative stress environment through antioxidation and c-Met pathway activation," *Science China Life Sciences*, vol. 57, no. 10, pp. 989–997, 2014.

[12] S. Y. Chan, Y.-Y. Zhang, C. Hemann, C. E. Mahoney, J. L. Zweier, and J. Loscalzo, "MicroRNA-210 controls mitochondrial metabolism during hypoxia by repressing the iron-sulfur cluster assembly proteins ISCU1/2," *Cell Metabolism*, vol. 10, no. 4, pp. 273–284, 2009.

[13] M.-P. Puisségur, N. M. Mazure, T. Bertero et al., "MiR-210 is overexpressed in late stages of lung cancer and mediates mitochondrial alterations associated with modulation of HIF-1 activity," *Cell Death & Differentiation*, vol. 18, no. 3, pp. 465–478, 2011.

[14] A. Vennemann and T. G. Hofmann, "SUMO regulates proteasome-dependent degradation of FLASH/Casp8AP2," *Cell Cycle*, vol. 12, no. 12, pp. 1914–1921, 2013.

[15] X.-C. Yang, B. D. Burch, Y. Yan, W. F. Marzluff, and Z. Dominski, "FLASH, a Proapoptotic Protein Involved in Activation of Caspase-8, Is Essential for 3′ End Processing of Histone Pre-mRNAs," *Molecular Cell*, vol. 36, no. 2, pp. 267–278, 2009.

[16] K. Milovic-Holm, E. Krieghoff, K. Jensen, H. Will, and T. G. Hofmann, "FLASH links the CD95 signaling pathway to the cell nucleus and nuclear bodies," *EMBO Journal*, vol. 26, no. 2, pp. 391–401, 2007.

[17] S. Liu, R. Luo, Q. Xiang, X. Xu, L. Qiu, and J. Pang, "Design and synthesis of novel xyloketal derivatives and their protective activities against H_2O_2-induced huvec injury," *Marine Drugs*, vol. 13, no. 2, pp. 948–973, 2015.

[18] Y. Duan, S. Liu, J. Tao et al., "Cellular repressor of E1A stimulated genes enhances endothelial monolayer integrity," *Molecular Biology Reports*, vol. 40, no. 6, pp. 3891–3900, 2013.

[19] Y. Imai, T. Kimura, A. Murakami, N. Yajima, K. Sakamaki, and S. Yonehara, "The CED-4-homologous protein FLASH is involved in Fas-mediated activation of caspase-8 during apoptosis," *Nature*, vol. 398, pp. 777–785, 1999.

[20] W. Chang, C. Y. Lee, J.-H. Park et al., "Survival of hypoxic human mesenchymal stem cells is enhanced by a positive feedback loop involving mir-210 and hypoxia-inducible factor 1," *Journal of Veterinary Science*, vol. 14, no. 1, pp. 69–76, 2013.

[21] G. Zaccagnini, B. Maimone, V. Di Stefano et al., "Hypoxia-induced miR-210 modulates tissue response to acute peripheral ischemia," *Antioxidants and Redox Signaling*, vol. 21, no. 8, pp. 1177–1188, 2014.

[22] S. Tsuchiya, T. Fujiwara, F. Sato et al., "MicroRNA-210 regulates cancer cell proliferation through targeting fibroblast growth factor receptor-like 1 (FGFRL1)," *Journal of Biological Chemistry*, vol. 286, no. 1, pp. 420–428, 2011.

[23] E. Favaro, A. Ramachandran, R. McCormick et al., "MicroRNA-210 regulates mitochondrial free radical response to hypoxia and krebs cycle in cancer cells by targeting iron sulfur cluster protein ISCU," *PLOS ONE*, vol. 5, no. 4, Article ID e10345, 2010.

[24] K. E. Tagscherer, A. Fassl, T. Sinkovic et al., "MicroRNA-210 induces apoptosis in colorectal cancer via induction of reactive oxygen," *Cancer Cell International*, vol. 16, no. 1, article 42, 2016.

[25] S. Kang, S.-M. Kim, and J.-H. Sung, "Cellular and molecular stimulation of adipose-derived stem cells under hypoxia," *Cell Biology International*, vol. 38, no. 5, pp. 553–562, 2014.

[26] L. Barile, V. Lionetti, E. Cervio et al., "Extracellular vesicles from human cardiac progenitor cells inhibit cardiomyocyte apoptosis and improve cardiac function after myocardial infarction," *Cardiovascular Research*, vol. 103, no. 4, pp. 530–541, 2014.

[27] S. Ujigo, N. Kamei, H. Hadoush et al., "Administration of microRNA-210 promotes spinal cord regeneration in mice," *Spine*, vol. 39, no. 14, pp. 1099–1107, 2014.

[28] K. Pulkkinen, T. Malm, M. Turunen, J. Koistinaho, and S. Ylä-Herttuala, "Hypoxia induces microRNA miR-210 in vitro and in vivo," *FEBS Letters*, vol. 582, no. 16, pp. 2397–2401, 2008.

[29] A. Giannakakis, R. Sandaltzopoulos, J. Greshock et al., "miR-210 links hypoxia with cell cycle regulation and is deleted in human epithelial ovarian cancer," *Cancer Biology and Therapy*, vol. 7, no. 2, pp. 255–264, 2008.

[30] J. H. Kim, S. G. Park, S.-Y. Song, J. K. Kim, and J.-H. Sung, "Reactive oxygen species-responsive miR-210 regulates proliferation and migration of adipose-derived stem cells via PTPN2," *Cell Death and Disease*, vol. 4, 2013.